

Constraints from geotemporal evolution of all-cause mortality on the hypothesis of disease spread during Covid

Joseph Hickey,^{1,2,*} PhD ; Denis G. Rancourt,¹ PhD ; Christian Linard,^{1,2} PhD

¹ Correlation Research in the Public Interest (correlation-canada.org)

² Université du Québec à Trois-Rivières (uqtr.ca/PagePerso/Christian.Linard)

* joseph.hickey@alumni.ucalgary.ca

This Correlation report is posted on several websites, including:

<https://correlation-canada.org/research/> <https://www.preprints.org/manuscript/202506.1240/v1>
<https://denisrancourt.ca/> <https://denisrancourt.substack.com/> https://archive.org/details/@dgr_legal_docs
<https://www.researchgate.net/profile/Joseph-Hickey>

All Correlation reports are here: <https://correlation-canada.org/research/>

Citation: Hickey J, Rancourt DG, Linard C. Constraints from geotemporal evolution of all-cause mortality on the hypothesis of disease spread during Covid. CORRELATION Research in the Public Interest, Report, 13 June 2025. <https://correlation-canada.org/constraints-on-hypothesis-of-disease-spread-during-Covid/>.

Abstract

Large peaks of excess all-cause mortality occurred immediately following the World Health Organization (WHO)'s March 11, 2020 COVID-19 pandemic declaration, in March-May 2020, in several jurisdictions in the Northern Hemisphere. The said large excess-mortality peaks are usually assumed to be due to a novel and virulent virus (SARS-CoV-2) that spreads by person-to-person contact, and are often referred to as resulting from the so-called first wave of infections.

We tested the presumption of this viral spread paradigm using high-resolution spatial and temporal variations of all-cause mortality in Europe and the USA.

We studied excess all-cause mortality for subnational regions in the USA (states and counties) and Europe (NUTS statistical regions at levels 0-3) during March-May 2020, which we call the “first-peak period”, and also during June-September 2020, which we call the “summer-peak period”.

The data reveal several definitive features that are incompatible with the viral spread hypothesis (in comparison with qualified predictions of the leading spatiotemporal epidemic models):

- **Geographic heterogeneity of first-peak period excess mortality:** There was a high degree of geographic heterogeneity in excess mortality in the USA and Europe, with a handful of geographic regions having essentially synchronous (within weeks of each other) large peaks of first-peak period excess mortality (“F-peaks”) and all other regions having low or negligible excess mortality in the said first-peak period. This includes vastly different F-peak sizes (up to a factor of 10 or more) for subnational regions on either side of an international border, such as Germany’s NUTS1 regions on its western border (small F-peaks) compared to the NUTS1 regions on the other side of the international border in the Netherlands, Belgium and France (large F-peaks), despite significant documented cross-border traffic volumes between the regions.
- **Temporal synchrony of first-peak period excess mortality:** F-peaks for USA states and European countries were almost all positioned within three or four weeks of one another and never earlier than the week of the WHO’s pandemic declaration. For a given large-F-peak European country, the F-peaks for all subnational regions rose and fell in lockstep synchrony but showed large variation in peak height and total integrated excess mortality. A similar result was seen for the counties of large-F-peak USA states.
- **Large differences in first-peak period excess mortality for comparable cities with large airports in the same countries:** We compare mortality results for Rome vs Milan in Italy, and Los Angeles and San Francisco vs New York City in the USA, and show that there was a dramatic difference in first-peak period excess mortality between the compared cities, despite their having similar demographics, health care systems, and international air travel traffic, including from China and East Asia.

We also examined data concerning the location of death (whether in hospital, at home, in a nursing home, etc.) and socioeconomic vulnerability (poverty, minority status, crowded living conditions, etc.) at high geographic resolutions, which support an alternative hypothesis that excess mortality in jurisdictions with large F-peaks was caused by the application of dangerous medical treatments (in particular, invasive mechanical ventilation and pharmaceutical

treatments) and pneumonia induced by biological stress due to treatment and lockdown measures.

Exceptionally large F-peaks occurred in areas with large publicly-funded hospitals serving poor or socioeconomically frail communities, in regions where poor neighbourhoods are situated in proximity to wealthy neighbourhoods, such as the case of The Bronx in New York City, and the boroughs of Brent and Westminster in London, UK.

Taken together, our study represents strong evidence that the patterns of excess mortality observed for the USA and Europe in March-May 2020 could not have been caused by a spreading respiratory virus, and instead were due to the medical and government interventions that were applied and mostly killed elderly and poor individuals.

Table of Contents

Abstract.....	1
1. Introduction.....	6
2. Data and Methods.....	8
2.1 Data sources.....	8
2.2 Technical points about mortality data.....	9
2.3 Method for calculating excess mortality.....	10
3. Results.....	11
3.1 Excess mortality at the continental scale in the USA and Europe in 2020	11
3.2 Maps of excess mortality in March-May 2020 in the USA and Europe at different subnational geographic scales	13
3.2.1 Europe excess mortality by country (NUTS0 regions)	14
3.2.2 Europe excess mortality by NUTS1 region.....	16
3.2.3 Europe excess mortality by NUTS2 region.....	17
3.2.4 Europe excess mortality by NUTS3 region.....	19
3.2.5 USA excess mortality by state.....	21
3.2.6 USA excess mortality by county.....	23
3.3 Timing of F-peaks at different geographic scales	31
3.3.1 Europe – national level (NUTS0).....	31
3.3.2 Europe – NUTS1 level subnational regions.....	33
3.3.3 Europe – NUTS2 level subnational regions.....	43

3.3.4	Europe – international border regions (NUTS1 level)	52
3.3.5	USA states	63
3.3.6	USA counties	70
3.4	Differing excess mortalities between regions with large international airports	85
3.4.1	The case of Rome vs Milan in Italy.....	85
3.4.2	The case of New York City vs Los Angeles and San Francisco in the USA.....	88
3.5	Deaths by institutional location for USA states and counties.....	90
3.6	Excess mortality P-scores vs socioeconomic variables	104
3.6.1	USA counties	104
3.6.2	European subnational regions	184
4.	Discussion	210
4.1	Overview of the Discussion	210
4.1.1	Summary of main features of the Results	210
4.1.2	Large-scale spatial epidemic models and their caveats	211
4.1.3	Incompatibility of first-peak period excess mortality outcomes with the paradigm of infectious disease spread, and alternative hypothesis of iatrogenic cause of excess mortality	214
4.2	Geographic heterogeneity of first-peak period excess mortality is incompatible with the paradigm of infectious respiratory disease spread	215
4.2.1	National-level (Europe) and state-level (USA) heterogeneity of excess mortality 215	
4.2.2	Subnational (Europe) and county-level (USA) excess mortality.....	218
4.3	Temporal synchronicity of F-peaks across jurisdictions is incompatible with the paradigm of infectious respiratory disease spread.....	221
4.3.1	Near synchronous timing of F-peaks across Europe and the USA.....	221
4.3.2	Simultaneous rise and fall of F-peaks for subnational regions within a given European country and for counties of a given USA state	222
4.3.3	Staggering in time of F-peaks of different countries in Europe linked to date of first national lockdown	229
4.4	Deadly medical treatments were prevalent in first-peak period mortality hotspots..	233
4.4.1	Italy.....	233
4.4.2	USA.....	237
4.4.3	Other European countries	239

4.5	Socioeconomic characteristics of first-peak period mortality hotspots	243
4.5.1	Integrated first-peak period P-scores vs socioeconomic variables for USA counties 243	
4.5.2	Integrated summer-peak period P-score vs socioeconomic variables for USA counties 244	
4.5.3	Correlation between P-scores and degree of interaction with the medical system 245	
4.5.4	The Bronx	246
4.5.5	The role of large “safety net” hospital complexes in regions with high inequality 248	
4.6	Pneumonia induced by biological stress of lockdown measures	249
5.	Conclusion	250
6.	References	252
A.	Additional graphs pertaining to section 3.3	281
A.1	Europe, weekly P-scores for national-level (NUTS0) jurisdictions, all countries, geographic subsets.....	281
A.2	USA, weekly P-scores for all states, organized geographically by census division	289
A.3	USA, weekly P-scores for each state, for the year 2020	302
B.	Additional graphs pertaining to section 3.5	319
C.	Tables of European regions by NUTS level, ordered by integrated first-peak period P-score 337	
C.1	NUTS0 level (countries).....	337
C.2	NUTS1 level	338
C.3	NUTS2 level	341
C.4	NUTS3 level	348
D.	Tables of USA regions (states and counties), ordered by integrated first-peak period P-score 376	
D.1	USA states.....	376
D.2	USA counties	377

1. Introduction

All-cause mortality by time and by administrative jurisdiction is arguably the most reliable data for detecting and epidemiologically characterizing events causing death, and for gauging the population-level impact of any surge or collapse in deaths from any cause. Such data can be collected by national or state jurisdiction or subdivision, by age, by sex, by location of death, and so on. It is not susceptible to reporting bias or to any bias in attributing causes of death in the mortality itself (see many references in Rancourt et al., 2023a).

Many researchers have examined all-cause mortality during the Covid period (from the WHO's March 11, 2020 pandemic declaration (WHO, 2020) to the WHO's May 5, 2023 declaration of the end of the public health emergency (WHO, 2023)) in countries around the world.

Representative references are as follows:

Bilinski & Emanuel, 2020; Bustos Sierra et al., 2020; Félix-Cardoso et al., 2020; Fouillet et al., 2020; Kontis et al., 2020; Mannucci et al., 2020; Mills et al., 2020; Olson et al., 2020; Piccininni et al., 2020; Sinnathamby et al., 2020; Tadbiri et al., 2020; Vestergaard et al., 2020; Villani et al., 2020; Achilleos et al., 2021; Al Wahaibi et al., 2021; Anand et al., 2021; Böttcher et al., 2021; Chan et al., 2021; Dahal et al., 2021; Das-Munshi et al., 2021; Deshmukh et al., 2021; Faust et al., 2021; Gallo et al., 2021; Islam, et al., 2021a, 2021b; Jacobson & Jokela, 2021; Jdanov et al., 2021; Joffe, 2021; Karlinsky & Kobak, 2021; Kobak, 2021; Kontopantelis et al., 2021a, 2021b; Kung et al., 2021a, 2021b; Liu et al., 2021; Locatelli & Rousson, 2021; Miller et al., 2021; Nørgaard et al., 2021; Panagiotou et al., 2021; Pilkington et al., 2021; Polyakova et al., 2021; 2021b; Rossen et al., 2021; Sanmarchi et al., 2021; Sempé et al., 2021; Soneji et al. 2021; Stein et al., 2021; Stokes et al., 2021; Vila-Corcoles et al., 2021; Wilcox et al., 2021; Woolf et al., 2021a, 2021b; Yorifuji et al., 2021; Ackley et al., 2022; Acosta et al., 2022; Engler, 2022; Faust et al., 2022; Ghaznavi et al., 2022; Gobiņa et al., 2022; He et al., 2022; Henry et al., 2022; Jha et al., 2022; Juul et al., 2022; Kontis et al., 2022; Kontopantelis et al., 2022; Lee et al., 2022; Leffler et al., 2022; Lewnard et al., 2022; McGrail, 2022; Neil et al., 2022; Neil & Fenton, 2022; Pálincás & Sándor, 2022; Ramírez-Soto & Ortega-Cáceres, 2022; Razak et al., 2022; Redert, 2022a, 2022b; Rossen et al., 2022; Safavi-Naini et al., 2022; Schöley et al., 2022; Thoma & Declercq, 2022; Wang et al., 2022; Aarstad & Kvitastein, 2023; Bilinski et al., 2023; de Boer et al., 2023; de Gier et al., 2023; Demetriou et al., 2023; Alessandria et al., 2025; Haugen, 2023; Jones & Ponomarenko, 2023; Kuhbandner & Reitzner, 2023; Masselot et al., 2023; Matveeva & Shabalina, 2023; Neil & Fenton, 2023; Paglino et al., 2023; Redert, 2023; Schellekens, 2023; Scherb & Hayashi, 2023; Šorli et al., 2023; Woolf et al., 2023; Rancourt et al., 2024; Rancourt & Hickey, 2023; Rancourt et al., 2023a; Rancourt et al., 2023b; Rancourt et al., 2022a; Rancourt, 2022; Rancourt et al., 2022b; Rancourt et al., 2022c; Rancourt, 2021; Rancourt et al., 2021a; Rancourt et al., 2021b; Rancourt et al., 2020; Rancourt, 2020; Johnson &

Rancourt, 2022; Aune et al., 2023; Bonnet et al., 2024; Faisant et al., 2024; Foster et al., 2024; Korsgaard, 2024; Léger & Rizzi, 2024; Matthes et al., 2024; Mostert et al., 2024; Nørgaard et al., 2024; Paganuzzi et al., 2024; Paglino et al., 2024; Pallari et al., 2024; Pulido et al., 2024; Zawisza et al., 2024; Zou et al., 2024.

Rancourt (2020), in an article dated June 2, 2020, was the first to analyze all-cause mortality for several countries and states for the time period immediately following the WHO's March 11, 2020 pandemic declaration. He argued that several features of the peaks of all-cause mortality that immediately follow the pandemic declaration were inconsistent with mortality that would result according to the paradigm of a novel spreading respiratory virus, in particular:

- the sharpness of the peaks, with full-width at half-maxima of approximately 4 weeks
- the timing of the peaks, being late in the winter season, surging after week 11 of 2020, which is unprecedented for any large sharp-peak feature in all-cause mortality data
- the synchronicity of the onset of the surge in all-cause mortality, across continents and immediately following the WHO's pandemic declaration
- the state-to-state (USA) absence or presence of the mortality peaks, being correlated with nursing home events and government public health measures.

Here we extend Rancourt (2020)'s analysis using high-resolution geotemporal all-cause mortality data for the USA and Europe. We use data at the level of states and counties in the USA and at levels 0-3 of the "NUTS" territorial statistics nomenclature (*Nomenclature des unités territoriales statistiques*) in Europe. We focus primarily on the period March-May 2020, which we call the "first-peak period".

Our results confirm and expand on the observations of Rancourt (2020), showing high synchronicity of onset of first-peak period excess mortality, and a high degree of geographic heterogeneity in magnitude and in presence or absence of first-peak period excess mortality. There are many locations with low or negligible excess mortality, including in places that neighbour jurisdictions with very large excess mortality. There are also comparable cities with large airports in the same country that have very different excess mortality outcomes, but which are predicted to have similar infection prevalence at the same time shortly prior to the pandemic declaration by epidemic spread models.

We propose that the said observations of geographic heterogeneity and temporal synchronicity of first-peak period excess mortality, which cannot be explained by the paradigm of a spreading respiratory virus, were caused by region-specific application of first-peak period lockdown policies and dangerous medical-system treatments, including invasive mechanical ventilation. We argue, following Rancourt (2024), that pneumonia induced by biological stress of lockdowns and medical-system intervention was ultimately responsible for the very large first-peak period excess mortality that occurred in hotspots such as New York City, Lombardy, Madrid, and London, UK.

Furthermore, researchers have shown strong correlations between Covid-period excess all-cause mortality and socioeconomic variables (Rancourt et al., 2021a; Ioannidis et al., 2023; Rancourt et al., 2024). Here, we do an in-depth examination of how first-peak period P-scores (number of excess deaths for a given time period, divided by expected number of deaths for the same time period, expressed as a percent) at high geographic resolutions correlate with socioeconomic variables and variables indicating the population's degree of interaction with the medical system.

We discuss how our observations regarding all-cause mortality data compare with the predictions of large-scale spatial epidemic spread models. We find that the empirical results are incompatible with the model predictions. The empirical results place stringent constraints on any application of epidemic spread modeling for the first-peak period (March-May 2020).

2. Data and Methods

2.1 Data sources

Our data for European countries and subnational regions are from Eurostat, as follows: all-cause mortality (Eurostat, 2024a), population in 2019 and 2020 (Eurostat, 2024b), population density in 2018 (Eurostat, 2024c), percentage of the population at-risk-of-poverty in 2019 (Eurostat, 2024d), volumes of road cargo transported between pairs of countries for 2017 to 2021 (Eurostat, 2024e, 2024f).

Data sources for the Italian regions examined in section 3.4.1 are as follows: number of hospital beds in 2020 (Eurostat, 2024g), number of Intensive Care Unit (ICU) beds in 2017 (Pecoraro et al., 2020), air traffic volumes to and from Italian airports (ENAC, 2017, 2018, 2019).

Data on socioeconomic variables for subnational regions of the UK (section 3.6.2) are from the following sources: gross disposable household income per capita in 2019 for the NUTS3 regions of the UK (ONS, 2024), population and population density for the NUTS3 regions of London, UK in 2019 (Greater London Authority, 2023), percent of the population of the NUTS3 regions of London, UK in 2021 that were non-white (ONS, 2022a), that were born outside the UK (ONS, 2022b), and that were living in poverty (pooled data from five years of survey data for the financial years 2017/18 to 2022/23, excluding 2020/21 due to data quality concerns) (Trust for London, 2024).

Mortality data for the United States are from the Centers for Disease Control and Prevention (CDC), as follows: weekly all-cause mortality by state (CDC, 2024a), monthly all-cause mortality by county, by state, and by institutional location of death (CDC, 2024b).

Population data for the United States are from the United States Census Bureau, as follows: population estimates for USA counties for 2019 (US Census Bureau, 2024a), population density estimates for USA counties (from the 5-Year American Community Survey for the years 2017-2021) (US Census Bureau, 2024b), and population of USA urban areas in 2020 (US Census Bureau, 2024c).

Data on number of international air passengers served by major USA airports (section 3.4.2) are from the United States Department of Transportation (Department of Transportation, 2020) and data on flights arriving from China at major USA airports from Eder et al. (2020).

Data on the following socioeconomic variables for USA counties (section 3.6.1) are from the 2014-2018 five-year American Community Survey, via the Agency for Toxic Substances and Disease Registry (ATSDR)'s socioeconomic vulnerability index website (ATSDR, 2024): per capita income, % living in poverty, % unemployed, Gini coefficient, % households with no vehicle available, % households with more people than rooms, % living in housing structures with 10+ units, % of population that speaks English "less than well", % minority, % aged 25+ with no high school diploma, % aged 65+, % aged 17 and under, % households that are single-parent households, and % with a disability.

Additional data on socioeconomic variables for USA counties (section 3.6.1) are from the following sources: diabetes rates for 2018 (CDC, 2024c), obesity rates for 2018 (RHHub, 2024), presidential election voting results in 2016 (MIT Election Data Science Lab, 2018), prescription drug claims in 2017 (HHS, 2024), COVID-19 vaccination doses received up to December 31, 2021 (CDC, 2025), ICU beds (Schulte et al., 2020).

2.2 Technical points about mortality data

All mortality data used in this article is for all causes of death combined ("all-cause mortality").

We use weekly mortality data for all European countries and subnational regions examined in this article. The data provider (Eurostat) reports mortality data for weeks consisting of the seven days beginning on Monday and ending on Sunday, per the International Organization for Standardization (ISO) week date system. Data points in all graphs in this article showing weekly data for European jurisdictions are placed at the date of the Monday (first day) of the ISO week.

For the USA, the data provider (CDC) reports mortality data for weeks consisting of the seven days beginning on Sunday and ending on Saturday, following the CDC format. Data points in all graphs in this article showing weekly data for USA states are placed on the Sunday (first day) of the CDC week.

For USA counties, data was suppressed by the CDC if the number of recorded deaths for the time interval and the county was less than 10. We use monthly data for USA counties to reduce

the number of instances of data suppression, and only use counties in our analyses that had no month with suppressed data within the time period 2015-2020. There are 1806 counties with sufficient data when one does not stratify by institutional location of death (in-hospital, at-home, in nursing home, etc.), whereas more counties are affected by data suppression when one considers only those deaths occurring in particular institutional locations. The county-level maps included in the Results section show which counties had sufficient data for the various analyses in this article.

2.3 Method for calculating excess mortality

Excess all-cause mortality by time (week or month) and its one-standard-deviation uncertainty are calculated as follows. We first applied this method in Rancourt & Hickey (2023). We believe that this simple and direct method is itself a significant advance in the methodology of analyzing all-cause mortality data, which does not introduce uncertainty from arbitrary choices or tenuous extrapolation algorithms.

The excess all-cause mortality at a given time (week or month) is the difference (positive or negative) between the reported all-cause mortality for the given time and the expected all-cause mortality for the given time, which is ascertained from the historic all-cause mortality in a reference period immediately preceding the Covid period (prior to the March 11, 2020 World Health Organization declaration of a pandemic).

Our reference period is 2015 through 2019. We least-squares fit a straight line to the same week or month in each of the five reference years as the week or month of interest, where the slope of this fitted line is constrained to always (for every week or month of interest) be equal to the slope of a least-squares fitted line to all of the all-cause mortality data (all weeks or months) in the full 5-year reference period, for each given jurisdiction.

The thus obtained fitted line is used (by extrapolation) to predict the expected all-cause mortality. The one-standard-deviation (1σ) uncertainty in the expected all-cause mortality is estimated as $\sqrt{\pi/2}$ times the average magnitude of the 5 deviations in the 2015-2019 reference period, for each particular week or month of interest. This simple relation is exact in the limit of a large sampling number, for a normally distributed uncertainty.

Finally, the one-standard-deviation uncertainty of the excess mortality is the combined error that includes the 1σ uncertainty in the expected value and the independent statistical (1σ) error in the all-cause mortality (\sqrt{N}).

We use the P-score as our measure of excess mortality, throughout this paper. The P-score is the excess mortality scaled by the predicted mortality. We express the P-score as a percentage

throughout the paper. The P-score is thus equivalent to the percent increase in mortality above (positive) or below (negative) the predicted mortality for a given time period. The time period of interest can be as short as the highest time-resolution unit of the data, namely the week or month (“weekly P-score” or “monthly P-score”), or can be expressed for a longer integration period, such as over several months. When the latter integration of weekly or monthly data is used, the P-score is equal to the total excess mortality over the integration period, divided by the total predicted mortality for the integration period, expressed as a percent.

Because the P-score measures the relative increase (or decrease) in mortality for a population compared to the predicted mortality for the population, it is inherently “adjusted” for the age structure and health frailty of the population. This makes the P-score a useful measure for comparing the effect or intensity of excess mortality events occurring in different countries or jurisdictions with different age structures or degrees of frailty.

3. Results

3.1 Excess mortality at the continental scale in the USA and Europe in 2020

We begin by examining how excess mortality evolved in the USA and Europe at the lowest (continental-scale) geographic resolution in 2020. We use the P-score (equivalently, “% increase mortality”), which is excess mortality expressed as a percentage of the predicted baseline mortality. The P-score is naturally adjusted for population age-structure and health-status, as described in section 2.

The top panel of Figure 1 shows the continental USA (blue) and the thirty-five European countries used in this paper (red). The bottom panel of Figure 1 shows the weekly P-score for the USA and Europe as a function of time. The vertical grey line in the bottom panel of Figure 1 indicates March 9, 2020, which is the Monday of the week of the WHO’s declaration of the COVID-19 pandemic (declaration of March 11, 2020).

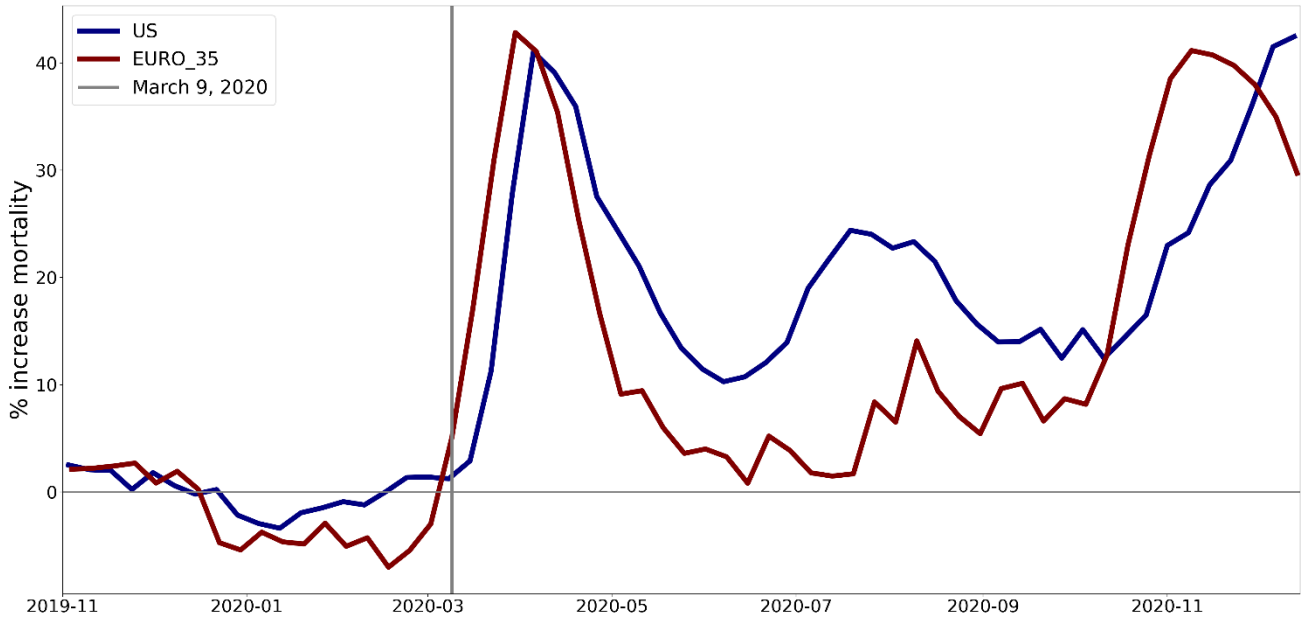
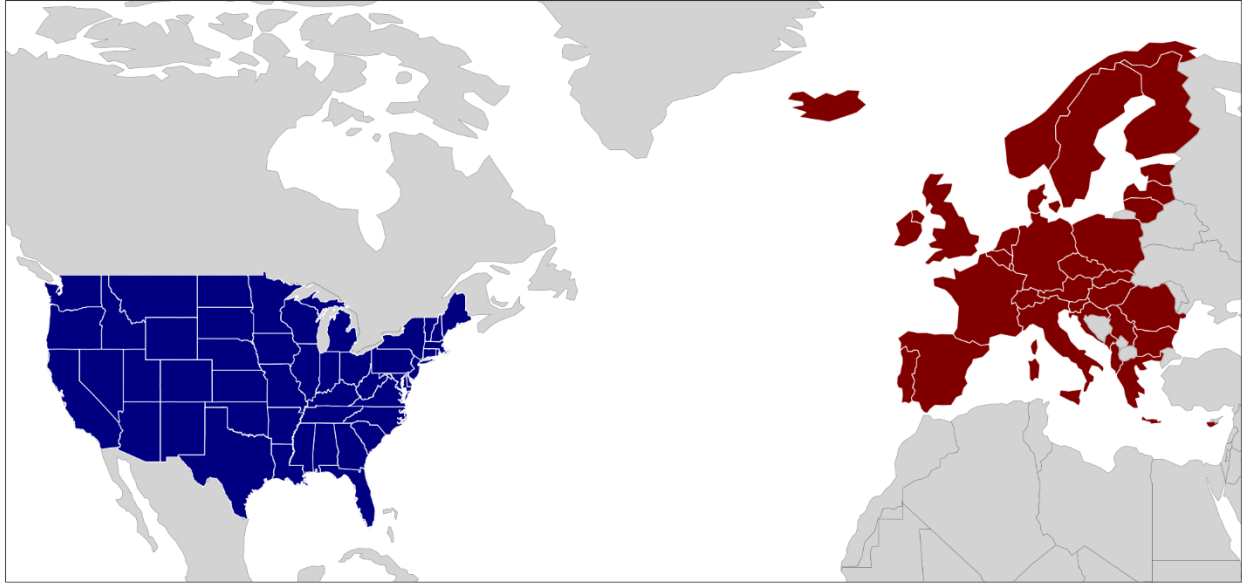


Figure 1. Top: Map showing the continental USA and its states (blue) and the European countries examined in this paper (red). Bottom: Excess all-cause mortality per week, expressed as a percentage of the predicted weekly baseline mortality (weekly P-score) for the USA and the European countries shown in the top panel. The vertical grey line in the bottom panel indicates the week of the WHO's declaration of the COVID-19 pandemic (declaration of March 11, 2020).

As can be seen (bottom panel of Figure 1), both Europe and the USA had non-positive (negative or indistinguishable from zero) weekly P-scores in the first two months of 2020. The weekly P-score for Europe became positive in the week of pandemic declaration, and rapidly increased to a maximum of about 43% three weeks later (week of March 30, 2020) before decreasing throughout April and May to reach a value near zero in mid-June (P-score of 0.8% in the week of June 15, 2020). The weekly P-score for the USA similarly increased shortly after the pandemic

declaration, reaching a maximum of about 41% four weeks later (week of April 5, 2020), and then decreased throughout April and May to a minimum of about 10% in mid-June (week of June 7, 2020).

We call the excess mortality peaks beginning at or slightly after the pandemic declaration “first peaks” or, for brevity, “F-peaks”. We use a nominal “first-peak period” spanning from the beginning of March 2020 to the end of May 2020, to avoid interference from subsequent excess mortality increases occurring in the summer of 2020, as can be seen in Figure 1.

To compare the timing of the excess mortality peaks in USA and Europe, we use the date at which the weekly P-score first obtains a value equal to half of its maximum. For Europe, this “rise-side half-maximum date” occurred about one week after the week of the pandemic declaration, and for the USA, the rise-side half-maximum date occurred about two weeks after the week of the declaration. Europe’s first-peak period excess mortality peak (“F-peak”) was thus positioned approximately one week earlier in time than that of the USA.

The bottom panel of Figure 1 also shows that significant excess mortality occurred in the USA and Europe throughout the second half of 2020. Notably, the USA’s weekly P-score never dropped below 10% for the remainder of 2020. Instead, the USA experienced a large summer peak of mortality, before having its weekly P-score dramatically increase to a level slightly above its first-peak period maximum value (above 40%) at the end of 2020. While the weekly P-score in Europe was close to zero in mid-June and July of 2020, Europe experienced a summer peak in August and September, followed by a dramatic increase excess mortality in the autumn of the year.

We stress that these continental-scale excess-mortality behaviours (Figure 1), in the continental USA and in Europe, should not be interpreted as uniform behaviours. In fact, there is large intra-continental heterogeneity on every geographic scale studied, and large east-west and north-south variations, as detailed below.

3.2 Maps of excess mortality in March-May 2020 in the USA and Europe at different subnational geographic scales

In this section we examine the F-peaks in Europe and the USA at different national (Europe) and subnational (Europe and USA) geographic scales. We use heatmaps of excess mortality (P-scores) integrated over our nominal first-peak period. When using weekly data (all geographic scales in Europe; USA states) we use a time period of 2020-02-24 to 2020-05-31 for Europe and 2020-03-01 to 2020-05-30 in the USA. When using monthly data (USA counties) we use the months of March-May 2020.

The national and subnational geographic regions that we use in Europe correspond to the Nomenclature of Territorial Units for Statistics (*Nomenclature des unités territoriales*

statistiques, in French), abbreviated as NUTS. The lowest geographic resolution in the NUTS system is the national level (NUTS0), and the highest geographic resolution is NUTS3. We consider the four geographic resolutions NUTS0, NUTS1, NUTS2 and NUTS3 in this section (Eurostat, 2025).

For several of the geographic scales considered below, we include two versions of the same heatmap: one version in which the maximum value of the color scale for the heatmap is equal to the maximum integrated first-peak period P-score value for the regions shown on the map; and a separate version for which the maximum value of the color scale for the heatmap is equal to a value lower than (typically half of) the maximum P-score value for the regions shown on the map. The second version therefore has a saturated color scale, in order to facilitate visualization of hotspots of excess mortality that would otherwise be hidden by the dominance of the hottest (highest P-score) regions.

3.2.1 Europe excess mortality by country (NUTS0 regions)

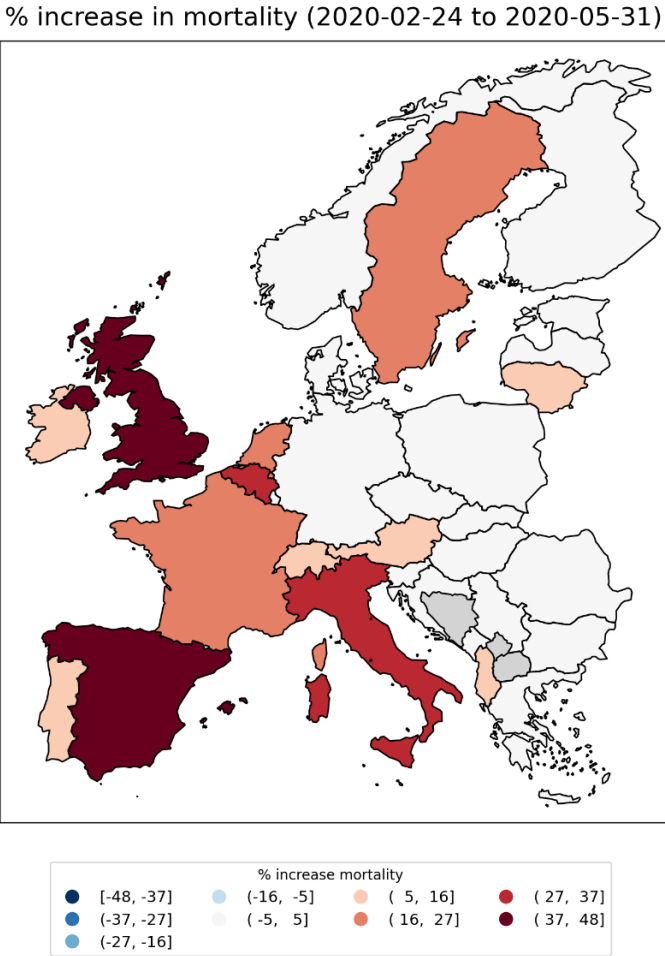


Figure 2: Integrated first-peak period P-scores in European NUTS0 (national-level) regions. Color range extends to maximum value. Dark grey indicates countries for which data was unavailable.

Figure 2 shows the integrated first-peak period P-scores for European countries. Iceland and Cyprus are omitted from the map for better visualization. The highest P-score (48%) is for Spain, followed by the UK (41%), Italy (34%), Belgium (31%) and Sweden (24%). As can be seen, first-peak period excess mortality was almost entirely confined to western European countries, with many countries in eastern, central and northern Europe having essentially no excess mortality during the first-peak period. Furthermore, there is a high degree of heterogeneity in P-scores among the western European countries, including among bordering countries such as Portugal (P-score of 12%) and Spain, Spain and France (P-score of 16%), France and Belgium, and France, Belgium, and the Netherlands (P-score of 22%) compared to Germany (P-score of 2%). The degree of region-to-region heterogeneity in P-score is amplified as one examines the data using higher geographic resolutions, as we show in the following sections.

The table in Appendix C.1 lists the integrated first-peak period P-scores, with their error values, for the NUTS0 regions shown in Figure 2, by order of decreasing P-score.

3.2.2 Europe excess mortality by NUTS1 region

Figure 3 shows integrated first-peak period P-scores for the NUTS1 regions of Europe. NUTS1 is the lowest geographic resolution for subnational regions in Europe, corresponding to states in Germany and regions in France, for example. For some smaller countries (e.g. Switzerland, Czechia, Slovakia), the NUTS1 region is equivalent to the national-level (NUTS0) region.

% increase in mortality (2020-02-24 to 2020-05-31) % increase in mortality (2020-02-24 to 2020-05-31)

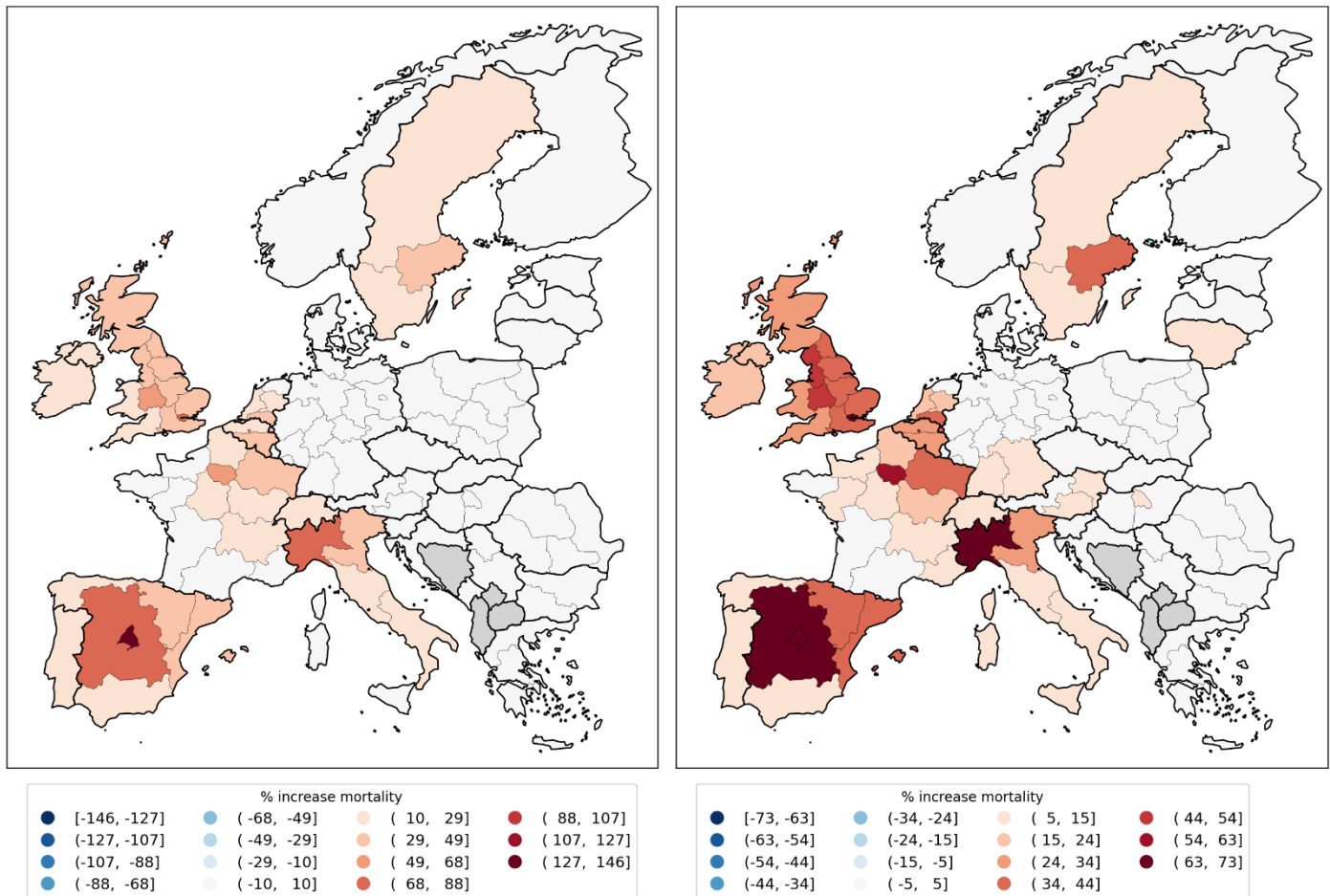


Figure 3: Integrated first-peak period P-scores for European NUTS1 regions. Left panel: color range extends to maximum value; Right panel: color range capped at half the maximum value. Dark grey indicates countries for which data was unavailable.

In the left panel of Figure 3, the maximum value of the heatmap color scale is set equal to the P-score of the NUTS1 region with the largest integrated first-peak period P-score, which was ES3 (Comunidad de Madrid, Spain), with a value of 146%. In the right panel of Figure 3, the heatmap is saturated at a value of 73%. From both panels, it is clear that there was essentially no excess mortality during the first-peak period in eastern, central and northern (except Sweden) Europe when viewed at the NUTS1 geographic resolution.

In western Europe and Sweden, the largest excess mortality occurred in a relatively small set of NUTS1 regions, especially in central and northeastern Spain, northeastern France, northern Italy, the area around Stockholm, Sweden, and most of the UK, Belgium and the Netherlands.

Large areas of southern and western France had essentially no excess mortality, while southern Italy and southern and northwestern Spain had much lower P-scores than the highest P-score regions in those countries.

The table in Appendix C.2 lists the integrated first-peak period P-scores, with their error values, for all the NUTS1 regions shown in Figure 3, by order of decreasing P-score.

Figure 4 shows the population density for the European NUTS2 regions in 2018, useful in examining higher-resolution P-score maps in the following section.

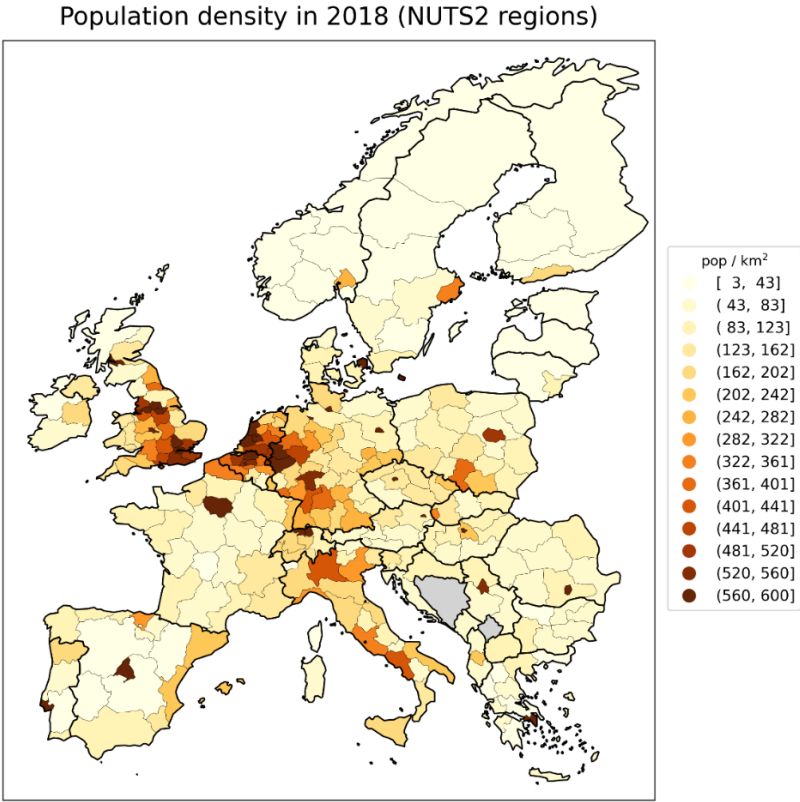


Figure 4: Number of persons per km² per European NUTS2 region in 2018 (Eurostat, 2024c). Color range saturated at a value of 600 km⁻² to aid visualization. Figure 144 and Figure 145 have, respectively, unsaturated linear and logarithmic scale versions of this figure, for comparison. Dark grey indicates countries for which data was unavailable.

3.2.3 Europe excess mortality by NUTS2 region

Figure 5 shows integrated first-peak period P-scores for the NUTS2 regions of Europe. The region Comunidad de Madrid, which had the highest P-score in Figure 3, again occurs as a

NUTS2 region, and has the highest P-score (146%) among all NUTS2 regions. The color scale for the right panel is saturated at a value of 73%. The regions with highest integrated first-peak period P-scores at the NUTS2 level were in central Spain (around Madrid); northeastern Spain (around Barcelona); the area around Paris and Alsace, in France; Lombardy in Northern Italy; the area around Stockholm, Sweden; and several areas in Belgium, the Netherlands and the UK, including the area around London, UK.

Mortality data was unavailable at higher geographic resolutions than NUTS1 for Germany, therefore we have used the NUTS1 results from Figure 3 for Germany in Figure 5.

% increase in mortality (2020-02-24 to 2020-05-31) % increase in mortality (2020-02-24 to 2020-05-31)

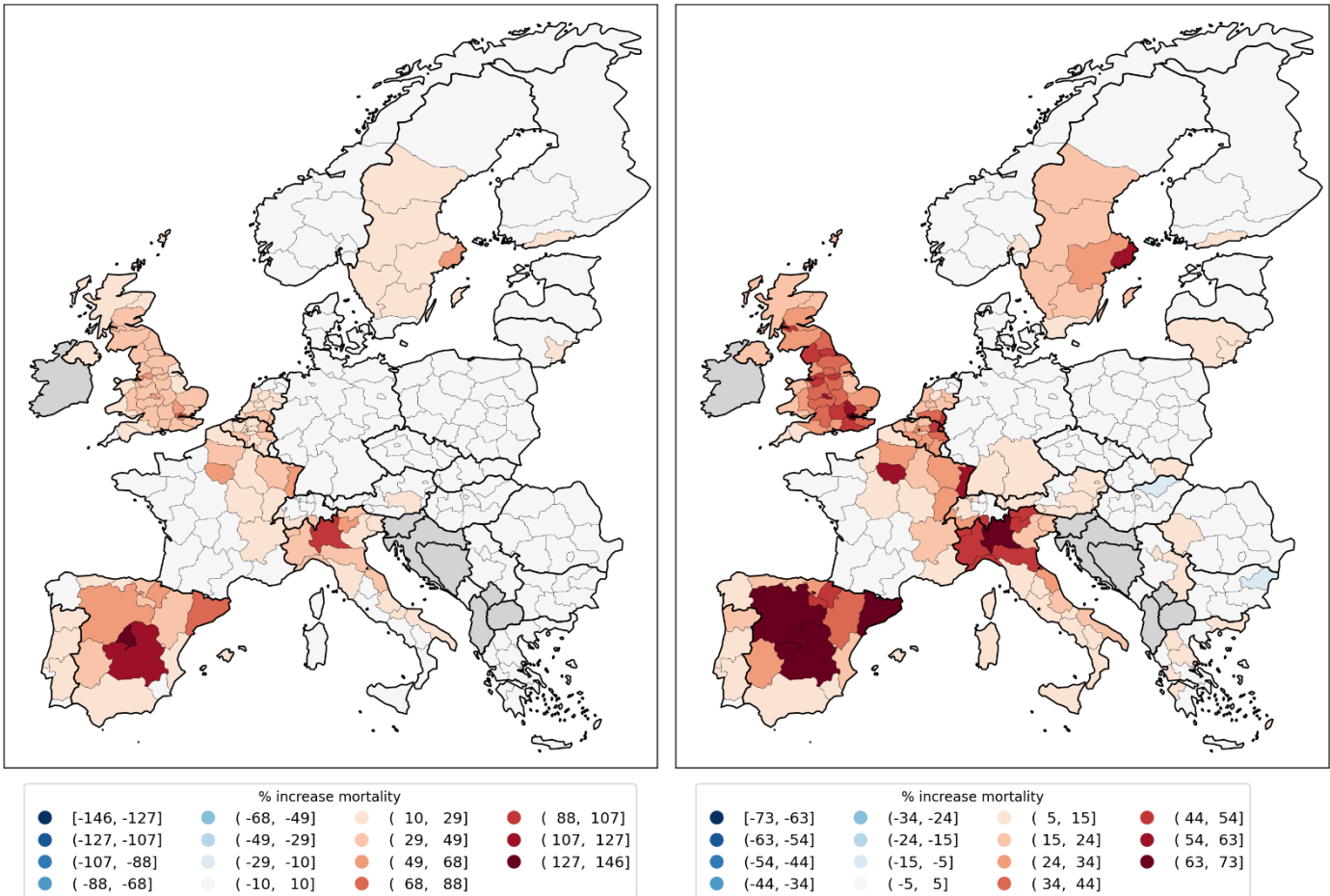


Figure 5: Integrated first-peak period P-scores for European NUTS2 regions. Left panel: color range extends to maximum value; Right panel: color range capped at half the maximum value. NUTS1 data is shown for Germany in this figure, as NUTS2 data was unavailable. Dark grey indicates countries (other than Germany) for which data was unavailable.

Figure 6 shows a blow-up of the results from Figure 5 for the NUTS2 regions of England and Wales, UK, for better visualization. The color scale in Figure 6 extends to the maximum value for UK NUTS2 regions (P-score = 87.3% for Inner London – East).

% increase in mortality (2020-02-24 to 2020-05-31)

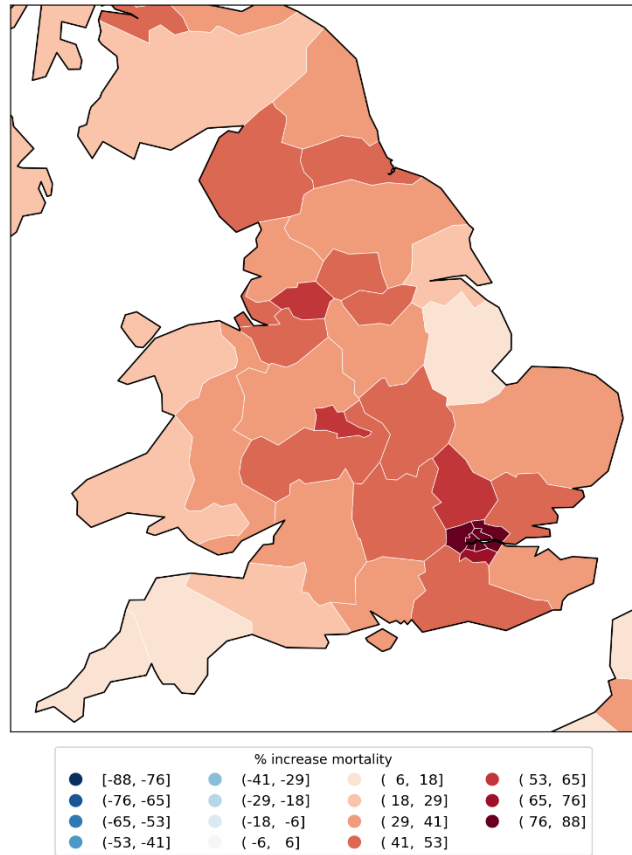


Figure 6: Integrated first-peak period P-scores for NUTS2 regions in England and Wales (UK). Color range extends to maximum value for UK NUTS2 regions.

The table in Appendix C.3 lists the integrated first-peak period P-scores, with their error values, for all the NUTS2 regions shown in Figure 5, by order of decreasing P-score.

3.2.4 Europe excess mortality by NUTS3 region

Figure 7 shows integrated first-peak period P-scores for the NUTS3 regions of Europe. This is the highest level of geographic resolution in our data, corresponding to the departments of France, for example.

At the NUTS3 level, the region with the largest integrated first-peak period P-score was ITC46 (Bergamo, Italy) with a value of 241%. As can be seen, excess mortality during the first-peak period was concentrated into a small number of hotspots, most intensely in Lombardy, Italy, and the areas around Madrid in Spain.

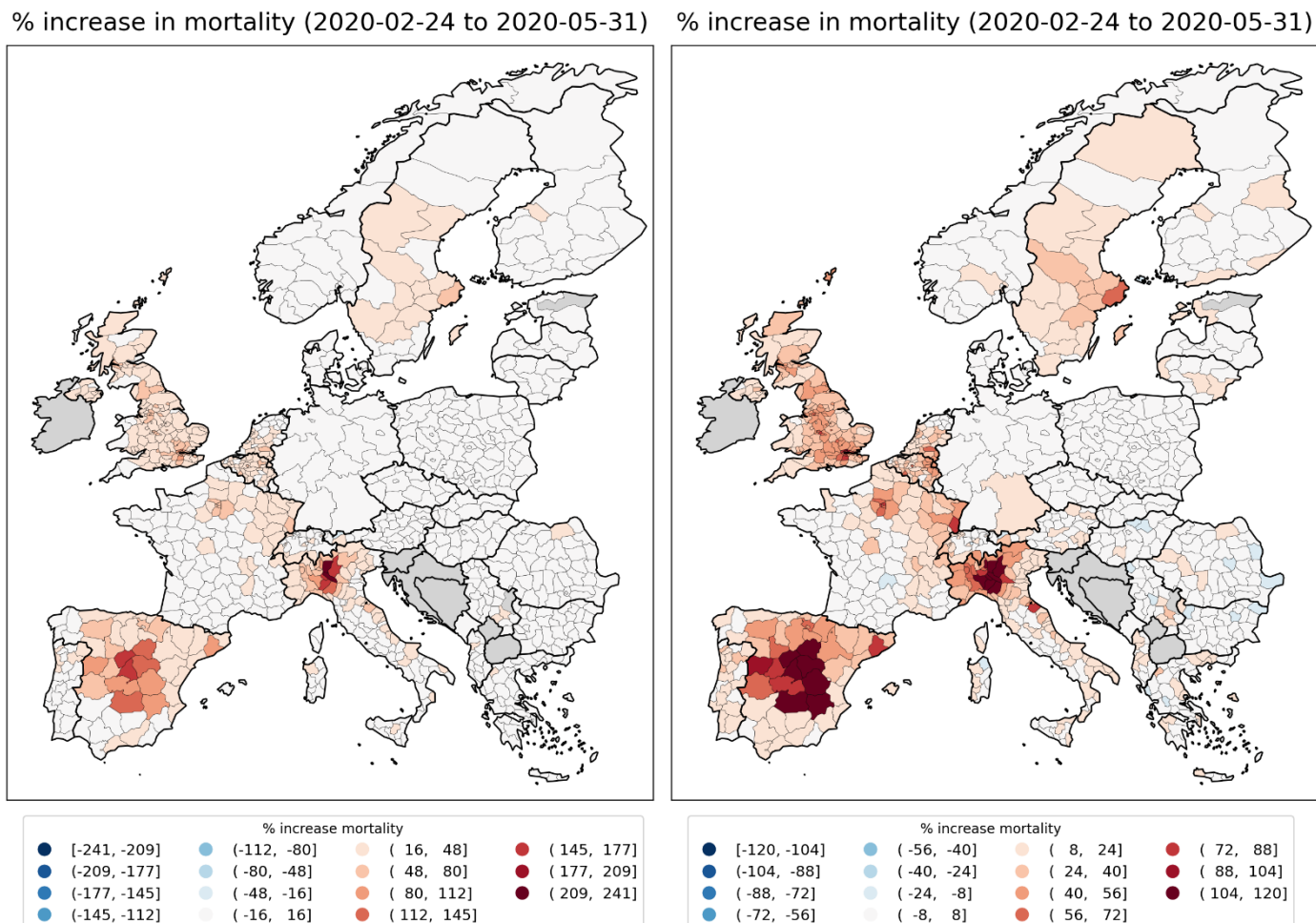


Figure 7: Integrated first-peak period P-scores for European NUTS3 regions. Left panel: color range extends to maximum value; Right panel: color range capped at half the maximum value. NUTS1 data is shown for Germany in this figure, as NUTS3 data was unavailable. Dark grey indicates countries (other than Germany) for which data was unavailable.

The table in Appendix C.4 lists the integrated first-peak period P-scores, with their error values, for the NUTS3 regions shown in Figure 7, by order of decreasing P-score. Among the ten NUTS3 regions with highest integrated first-peak period P-scores, nine were in Italy or Spain and the tenth was in the United Kingdom (the London borough of Brent); among the top thirty NUTS3 regions by first-peak period P-score, 8 were in Italy, 10 were in Spain and 12 were in the United Kingdom (all in the London area except for the region with the twenty-ninth highest P-score, East Surrey, which is on the outskirts of London).

The London, UK regions are difficult to see on the map in Figure 7 due to their small geographic sizes, but can be seen in the blow-up in Figure 8. The color scale in Figure 8 extends to the maximum value for UK NUTS3 regions (P-score = 120% for Brent).

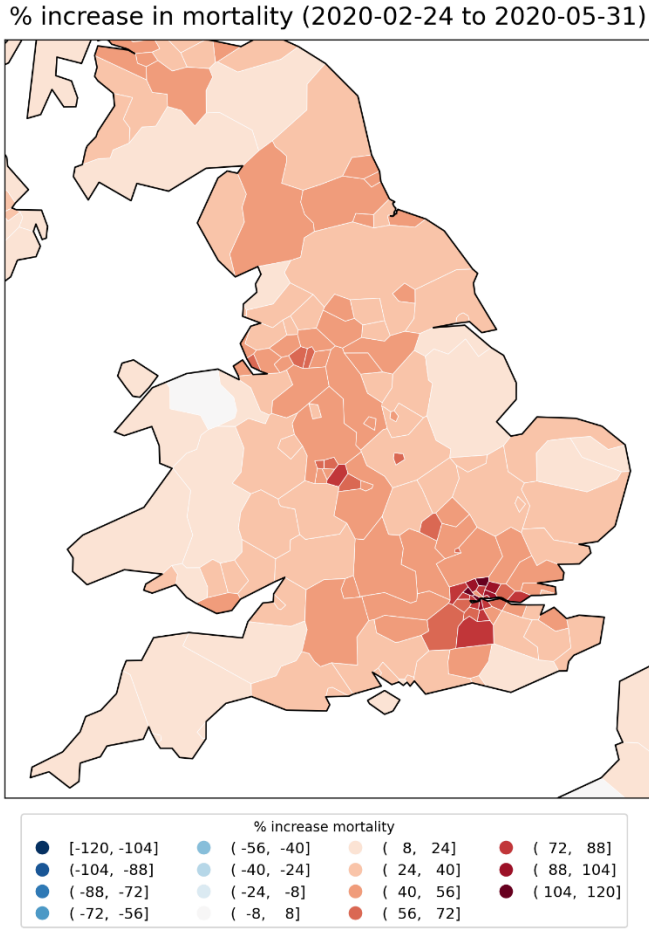


Figure 8: Integrated first-peak period P-scores for NUTS3 regions in England and Wales (UK). Color range extends to maximum value for UK NUTS3 regions.

3.2.5 USA excess mortality by state

Figure 9 shows the integrated first-peak period (March-May 2020) P-scores for the states of the contiguous USA.

As can be seen, the states of New York (P-score = 102%) and New Jersey (P-score = 90%) had the highest integrated first-peak period P-scores, followed by Connecticut (P-score = 54%) and Massachusetts (52%). Many states had near zero first-peak period excess mortality, while many others had moderate excess mortality. There is thus a high degree of heterogeneity in first-peak period excess mortality for the USA states, including among bordering pairs of states such as Louisiana (P-score = 31%) and Texas (P-score = 6.8%), Illinois (P-score = 29%) and Wisconsin (6.7%), and New Jersey (P-score = 90%) and Pennsylvania (P-score = 21%).

% increase mortality (2020-03-01 to 2020-05-30)

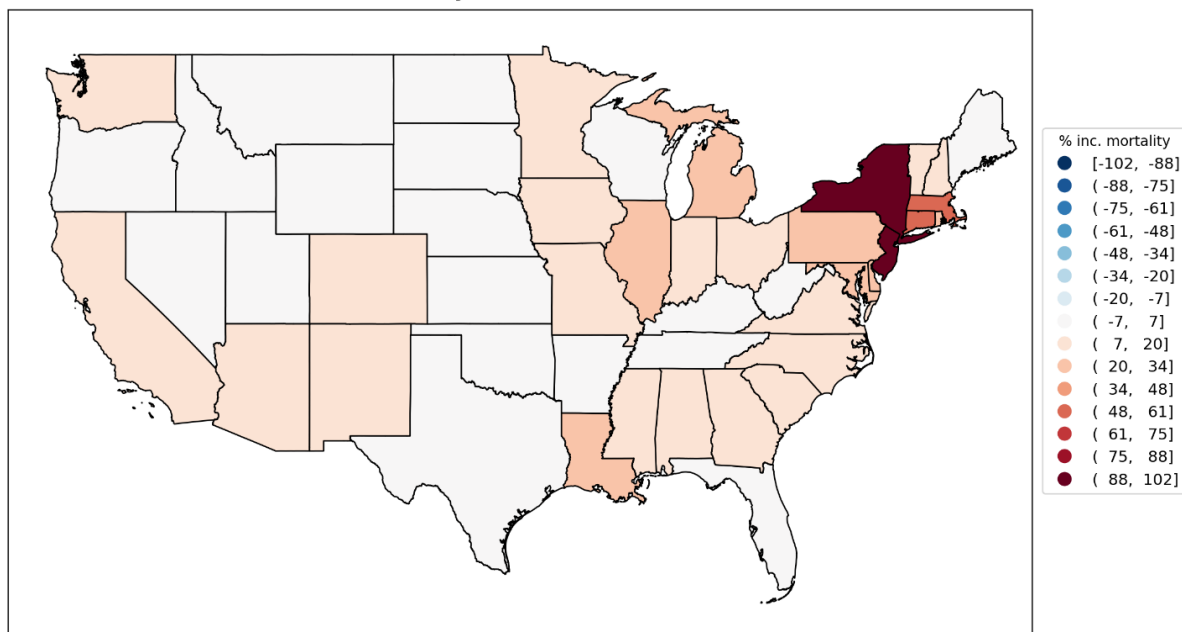


Figure 9: Integrated first-peak period P-scores in the states of the contiguous USA.

Figure 10 shows the logarithm of population density at the county level in the USA (estimates from the 5-Year American Community Survey for the years 2017-2021), which is useful in examining higher-resolution P-score maps in the following section.

$\log_{10}[\text{Pop. density (km}^{-2}\text{)}]$

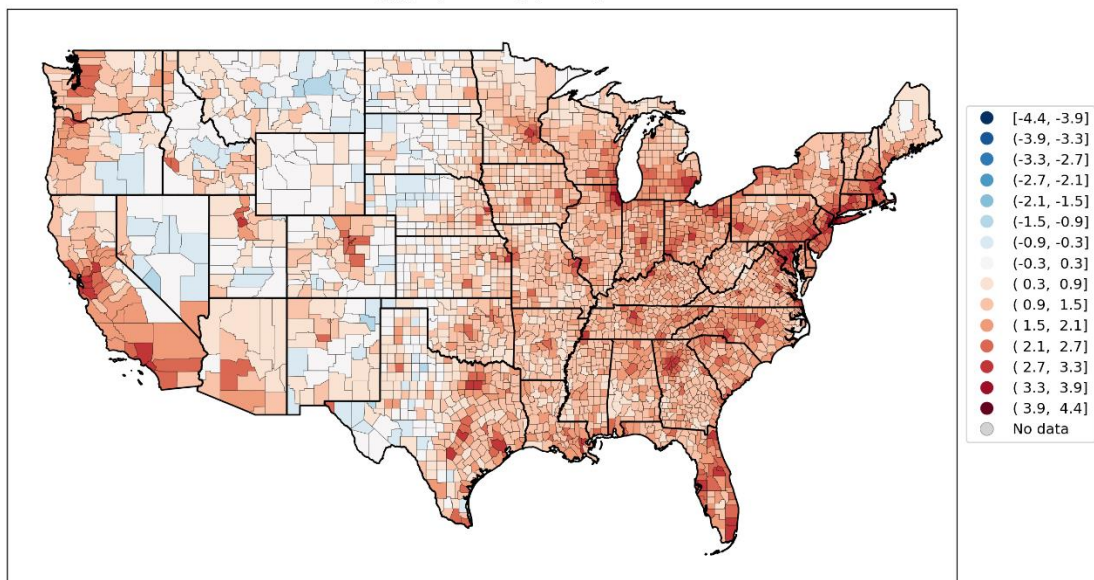


Figure 10: Logarithm of population density for counties of the contiguous USA (estimates from the 5-Year American Community Survey for the years 2017-2021).

The table in Appendix D.1 lists the integrated first-peak period P-scores and their uncertainty values for the USA states, by order of decreasing P-score.

3.2.6 USA excess mortality by county

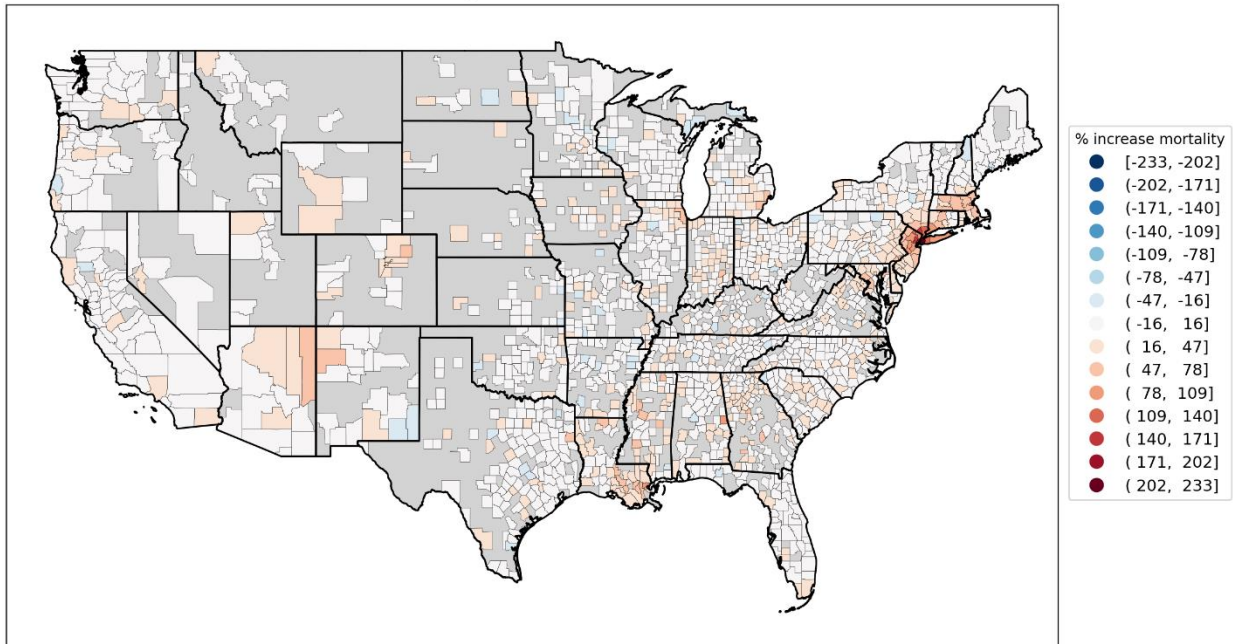
In this section, we examine excess mortality at the county level in the USA. USA mortality data is suppressed by the data provider if the number of deaths in the jurisdiction of interest and in the time period of interest is fewer than 10. We use monthly (rather than weekly) data to minimize the number of counties with suppressed data, and only use counties that had no month with suppressed data within the time period 2015-2020. We thus obtain 1806 counties (out of a total of 3143) with sufficient data for our purposes.

Figure 11 shows the integrated first-peak period (months of March-May 2020) P-scores for the counties of the contiguous USA. Counties with insufficient data are colored grey in the map. In the top panel of Figure 11, the color range extends to the maximum value for all USA counties (Bronx County, NY; P-score = 233%). Here, it can be seen that counties in the New York City urban area dominate, reflecting the very high integrated first-peak period P-scores observed at the state level for New York and New Jersey in Figure 9.

In the bottom panel of Figure 11, the color range is saturated at the maximum P-score among all counties outside of the states of New York and New Jersey, which is Chambers County, Alabama (P-score = 94%). Several hotspots outside of New York City can be seen in the bottom panel of Figure 11, especially in Detroit, Michigan, the Boston area of Massachusetts, and in Louisiana.

The table in Appendix D.2 lists the integrated first-peak period P-scores and their uncertainty values, for all 1806 counties with sufficient data, by order of decreasing P-score.

% increase in mortality for 2020-03-01 to 2020-05-31



% increase in mortality for 2020-03-01 to 2020-05-31

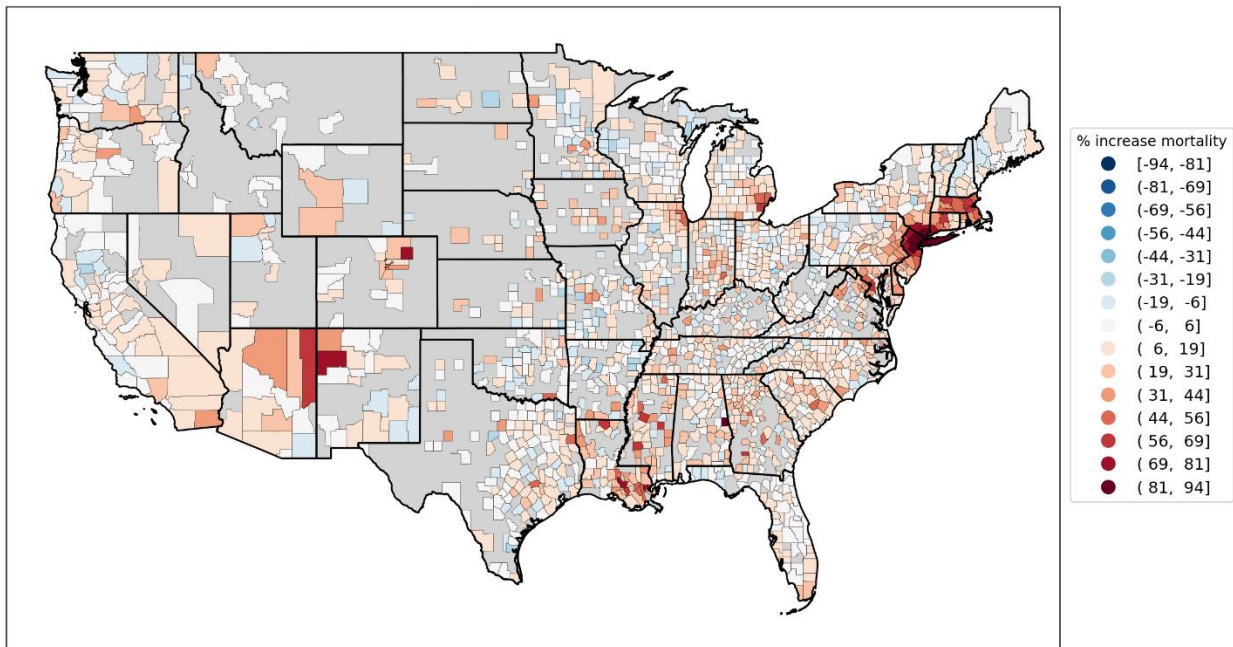


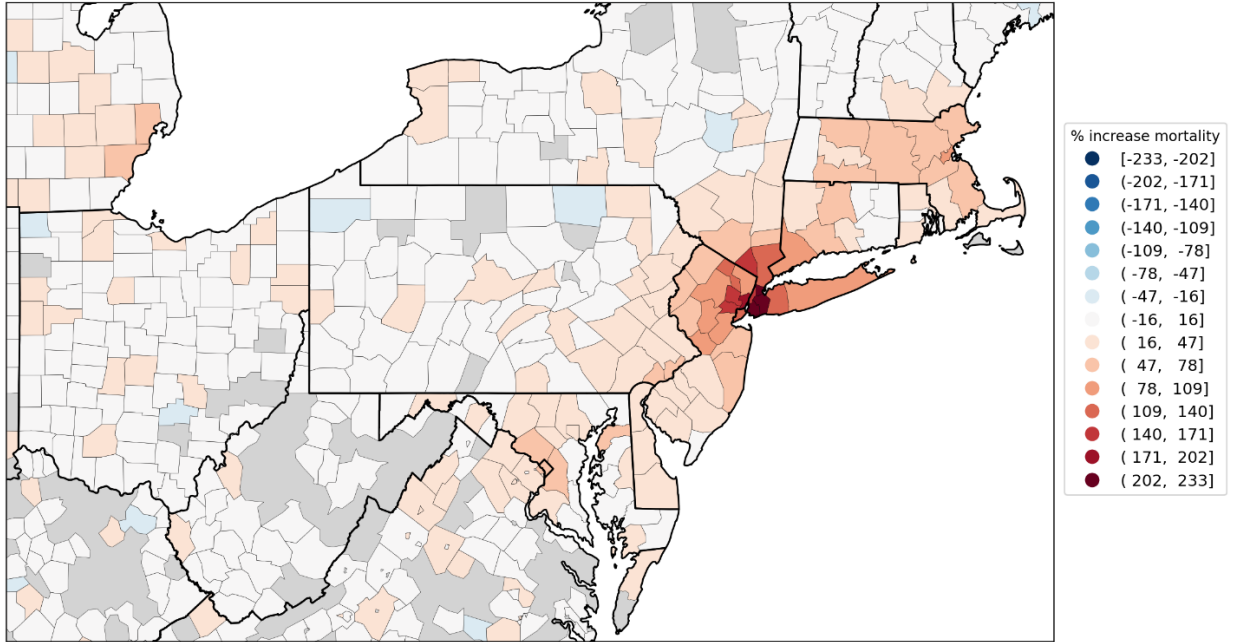
Figure 11: Integrated first-peak period P-scores in the counties of the contiguous USA. Top panel: color range extends to maximum value for all counties (Bronx County, NY; value = 233%); Bottom panel: color range capped at the maximum value for a county outside of the states of New York and New Jersey (Chambers County, Alabama; value = 94%). Dark grey indicates counties for which data was unavailable.

Figure 12 shows a blow-up of the northeastern USA, including the New York City urban area. In the top panel of Figure 12, the color scale extends to the maximum P-score value (Bronx County, NY). In the bottom panel of Figure 12, the color scale is saturated at the highest P-score value on the map for a county located outside of the states of New York and New Jersey, which is Suffolk County, Massachusetts (containing the city of Boston), with a P-score of 86%.

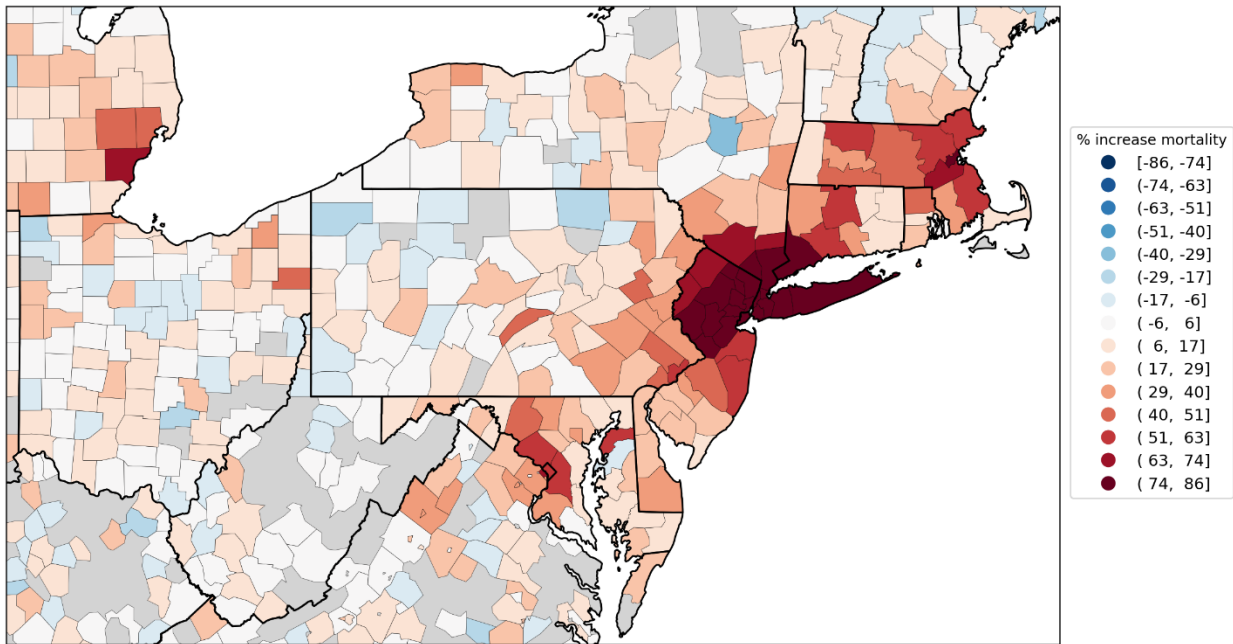
In addition to the intense hotspot in the New York City urban area, the bottom panel of Figure 12 shows hotspots for Detroit, Michigan (top-left corner of the bottom panel of Figure 12); Washington D.C. and surrounding counties in the state of Maryland; Philadelphia, Pennsylvania; and Boston, Massachusetts.

Outside of the hotspots, there were many counties in the northeastern USA with low or moderate first-peak period P-scores. This includes counties with sizeable urban populations such as Allegheny County, Pennsylvania (containing Pittsburgh), Franklin County, Ohio (containing Columbus), Cuyahoga County, Ohio (containing Cleveland) and Hamilton County, Ohio (containing Cincinnati). Figure 12 thus demonstrates the high degree of heterogeneity in integrated first-peak period P-scores across northeastern USA counties.

% increase in mortality for 2020-03-01 to 2020-05-31



% increase in mortality for 2020-03-01 to 2020-05-31



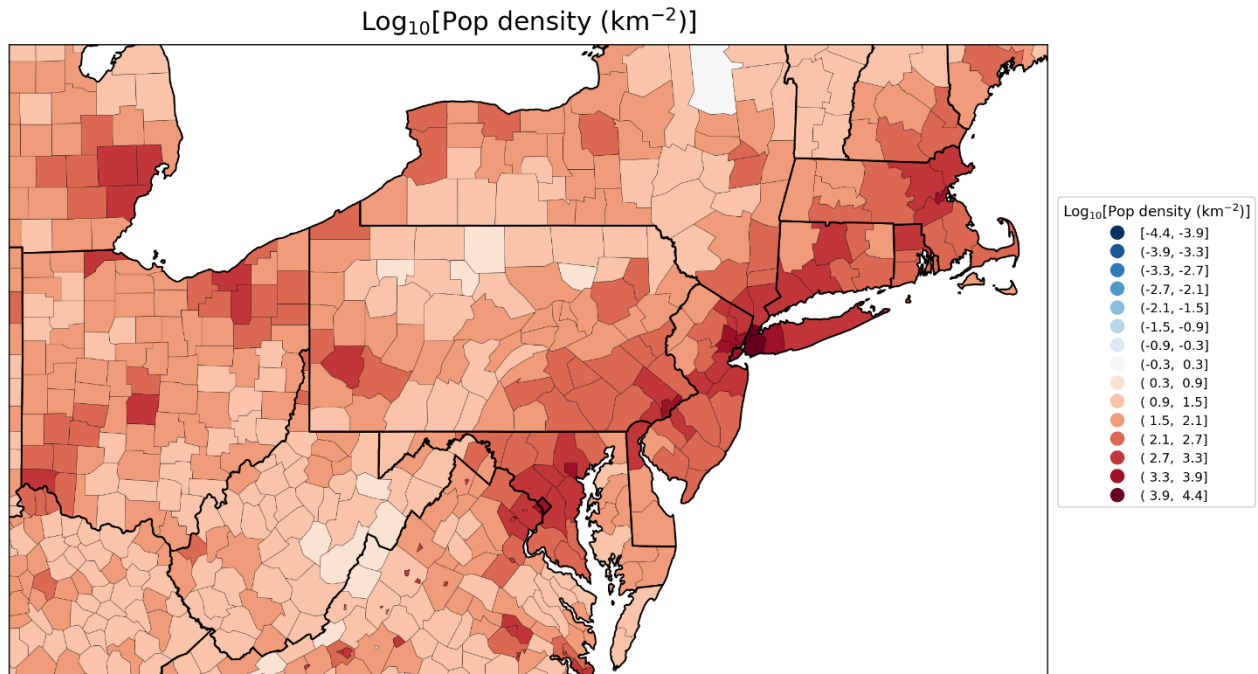


Figure 12: Top and middle panels: Integrated first-peak period P-scores in northeastern USA counties. Top: color range extends to maximum value (Bronx County, NY; value = 233%); Middle: color range capped at the maximum value for a county on the map in a state other than NY or NJ (Suffolk County, MA; value = 86%). Bottom panel: logarithm of population density by county (estimates from the 5-Year American Community Survey for the years 2017-2021). Dark grey indicates counties for which data was unavailable.

Figure 13 shows a blow-up of the mid-western USA. Here, the color scale is saturated at the highest P-score for a county on the map (Wayne County, Michigan; P-score = 67%). In addition to the Detroit, Michigan area (which includes Wayne County), the area around Chicago, Illinois also appears as a hotspot.

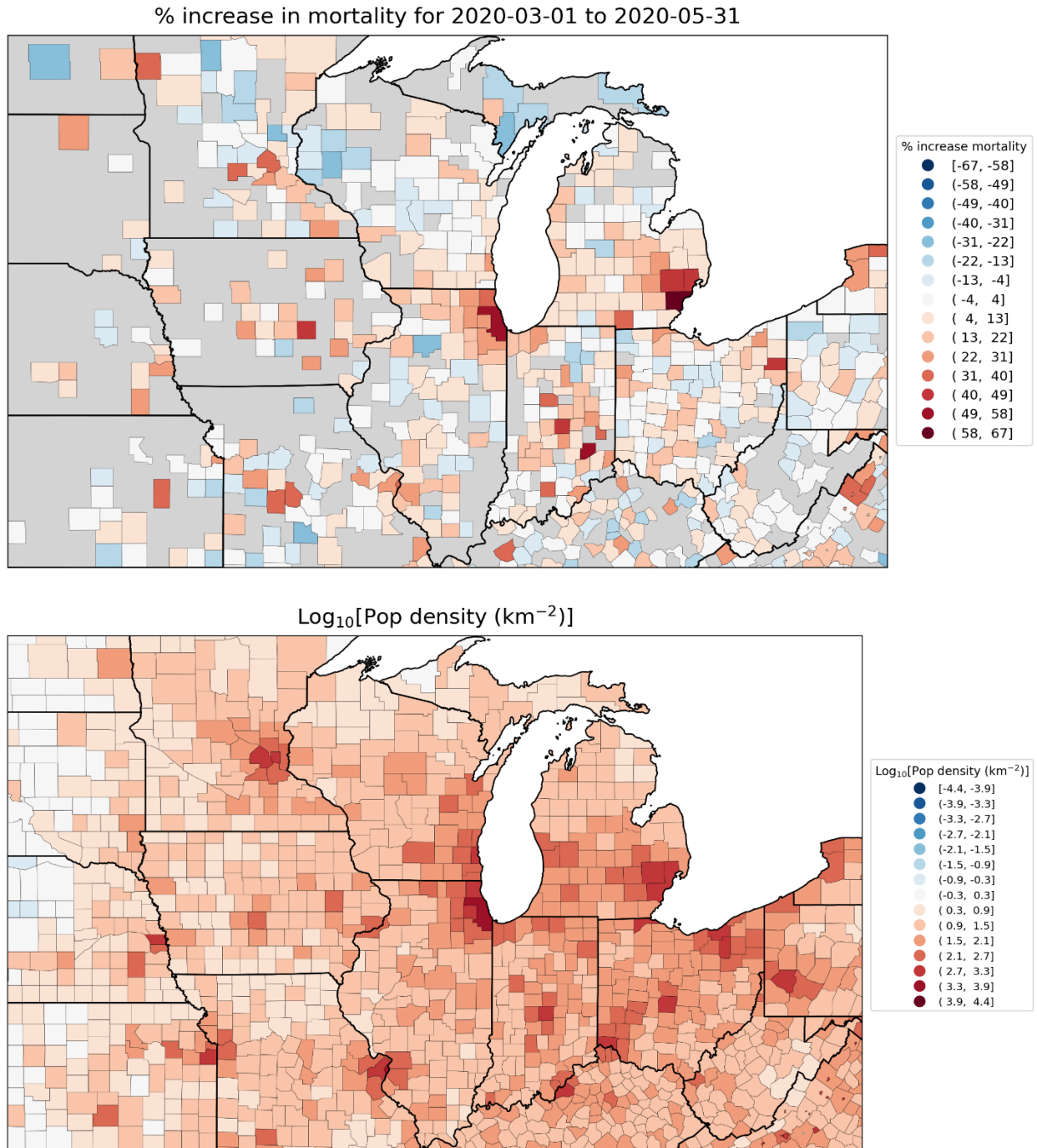


Figure 13: Top panel: Integrated first-peak period P-scores for Midwestern USA counties. Wayne County, Michigan (containing part of the Detroit metropolitan area) has the largest value (67%). Bottom panel: Logarithm of population density by county (estimates from the 5-Year American Community Survey for the years 2017-2021). Dark grey indicates counties for which data was unavailable.

Figure 14 shows a blow-up of the southern USA. Here, the color scale is saturated at the highest P-score for a county on the map (Chambers County, Alabama; P-score = 94%). The main hotspots are in Louisiana, around New Orleans and Baton Rouge.

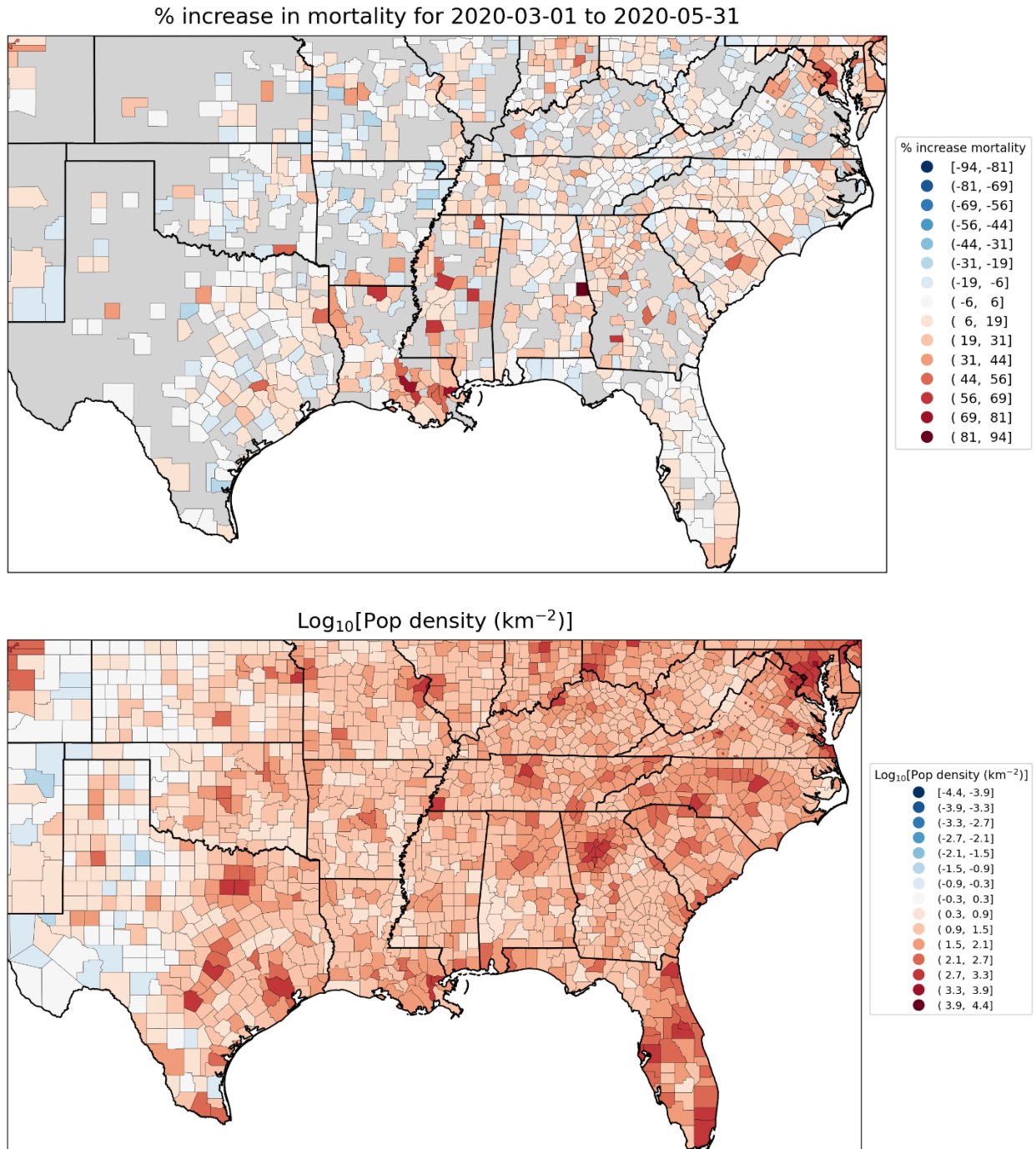


Figure 14: Top panel: Integrated first-peak period P-scores for southern USA counties. Chambers County, Alabama has the largest value (93.6%). Bottom panel: Logarithm of population density by county (estimates from the 5-Year American Community Survey for the years 2017-2021). Dark grey indicates counties for which data was unavailable.

A further blow-up showing Louisiana and parts of Texas and Mississippi is shown in Figure 15, with the color scale saturated at the P-score of the county with the highest value on the map, which is Orleans Parish, Louisiana (containing New Orleans), with a P-score of 79%.

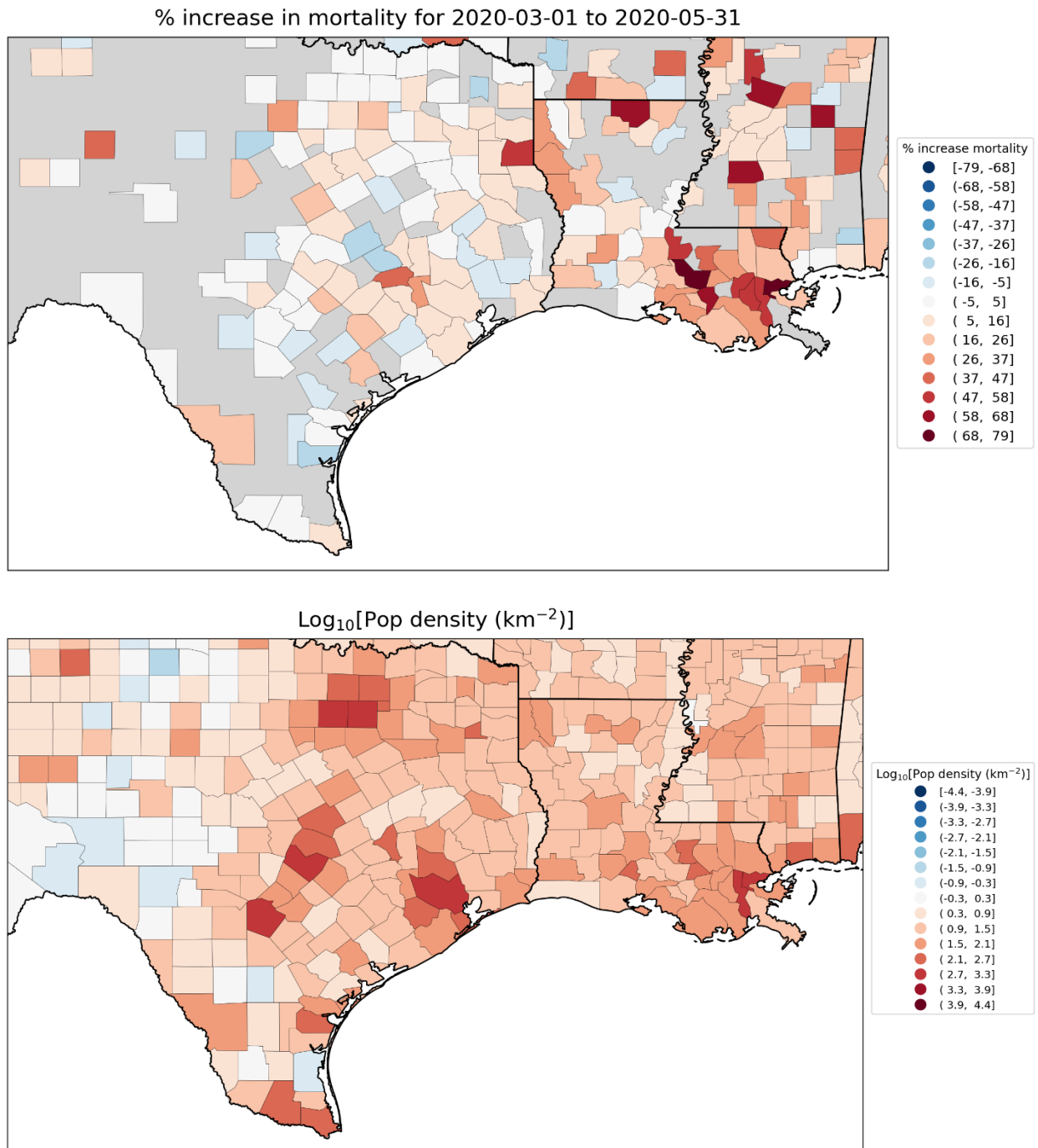


Figure 15: Top panel: Integrated first-peak period P-scores for counties in Texas and Louisiana. Orleans Parish, Louisiana (containing New Orleans) has the largest value (78.6%). Bottom panel: Logarithm of population density by county (estimates from the 5-Year American Community Survey for the years 2017-2021). Dark grey indicates counties for which data was unavailable.

3.3 Timing of F-peaks at different geographic scales

In this section, we examine how the timing of F-peaks compared between jurisdictions. To do this, we make two types of plots. The first type of plot shows the weekly (or monthly, for USA counties) P-scores for multiple jurisdictions during the first-peak period in the spring of 2020. The second type of plot shows the same data as the first plot type, with the curve for each jurisdiction scaled by its maximum value during the first-peak period. The latter scaling facilitates a comparison of the positioning in time of the F-peak, across jurisdictions with large differences in F-peak height and in total first-peak period excess mortality.

3.3.1 Europe – national level (NUTS0)

We begin with the national level in Europe. Figure 16 shows (top panel) the weekly P-scores for the seven countries with the largest F-peaks (Spain, the UK, Italy, Belgium, Sweden, the Netherlands and France) plus Germany. Germany is included as a large country with a small but present F-peak. The vertical grey line in Figure 16 indicates the Monday (March 9, 2020) of the week of the WHO's March 11, 2020 COVID-19 pandemic declaration.

European countries ES, UK, BE, SE, NL, FR, DE, IT

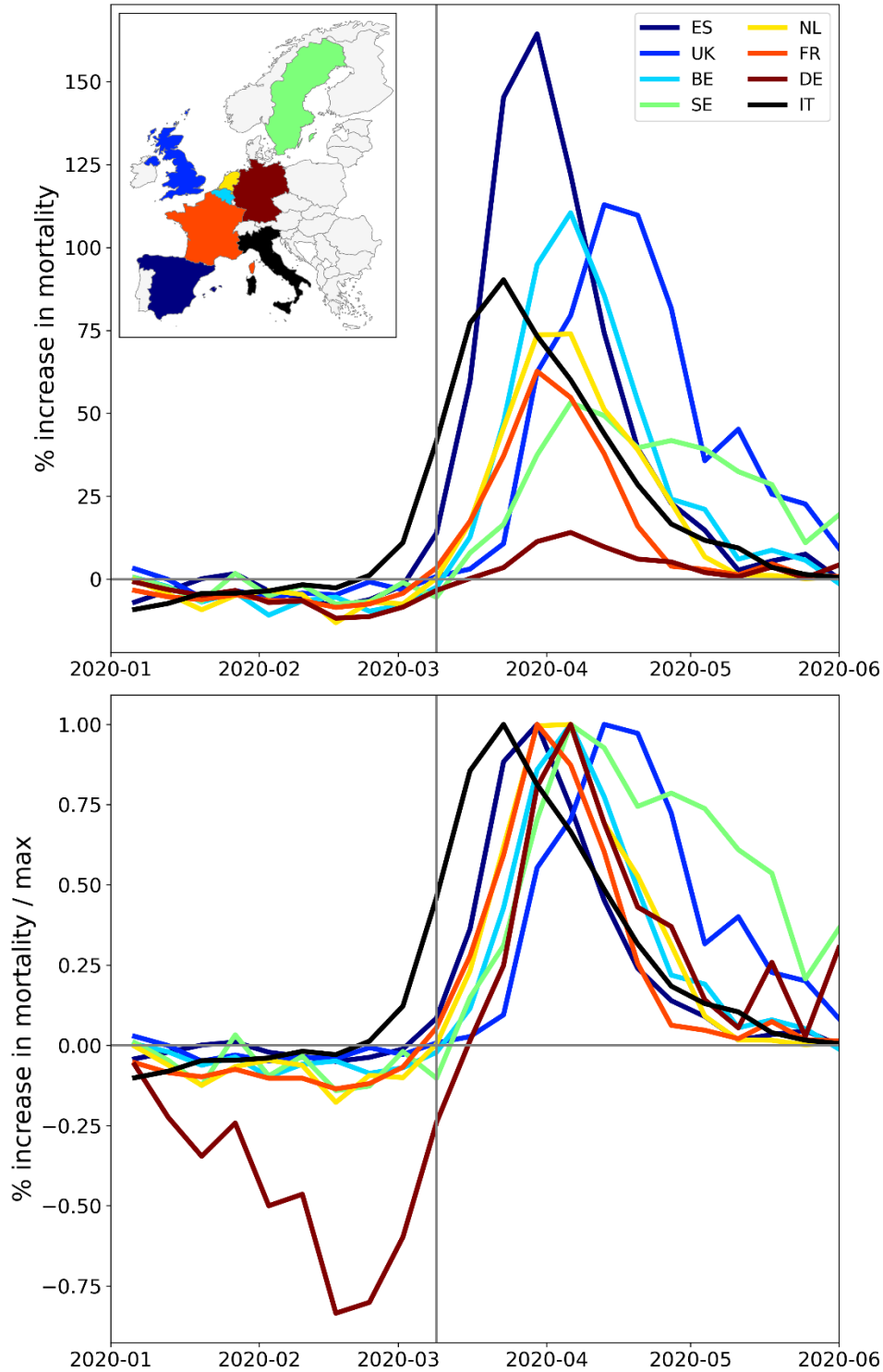


Figure 16: Top panel: weekly P-scores during the first-peak period for European countries Spain, UK, Belgium, Sweden, the Netherlands, France, Germany and Italy. Bottom panel: same as top panel, with each curve scaled by its maximum. The vertical grey lines indicate the week of the WHO's declaration of the COVID-19 pandemic (declaration of March 11, 2020).

The top panel of Figure 16 shows a large range of peak heights, with Spain topping out at a maximum weekly P-score of 164% in the week beginning on March 30, 2020, and Germany peaking at a maximum weekly P-score of 14% in the following week, for example.

The top panel of Figure 16 also shows that some peaks are located earlier in time (Italy, Spain) and others later in time (UK), and that there was essentially no excess mortality in these countries prior to the WHO's pandemic declaration. However, attempting to compare the timing of F-peaks using the top panel of Figure 16 can be difficult or misleading. To better ascertain the location in time of each peak, we use the graph in the bottom panel of Figure 16, where each curve has been scaled by its maximum weekly P-score during the first-peak period.

The bottom panel of Figure 16 thus allows for an ascertainment of each curve's rise-side half-maximum date (the date at which the weekly P-score first obtains a value equal to half of its maximum). For Italy, the rise-side half-maximum date occurred roughly during the week of the pandemic declaration. The rise-side half-maximum date for Spain is roughly one week after the week of the pandemic declaration, and the UK's rise-side half-maximum date is about three weeks after the week of the declaration. The other countries in Figure 16 with large F-peaks (France, the Netherlands, Belgium and Sweden) have rise-side half-maximum dates between those of Spain and the UK, that is, between one and three weeks after the declaration of the pandemic. Prior to the pandemic declaration, Germany had strongly negative weekly P-scores relative to its F-peak height (lower panel of Figure 16), such that its rise-side half-maximum date has a lower limit of roughly one week after week of the pandemic declaration and an upper limit of roughly three weeks after the week of the pandemic declaration. The bottom panel of Figure 16 thus shows that the national-level F-peaks in Europe, while occurring close to the date of the pandemic declaration, were offset from one another by up to three weeks.

Appendix A.1 contains additional figures showing the time-evolution of national-level weekly P-scores for the other European countries shown in the heatmaps in Figure 2. The figures in Appendix A.1 show that, among European countries that had F-peaks, all peaks occurred with rise-side half-maximum dates later than that of Italy and earlier than that of the UK.

Despite the differences in the timing of national-level F-peaks, when one examines the subnational regions within any particular European country that had an F-peak, it becomes apparent that all of the peaks in the country's subnational regions occurred in virtually complete synchrony with one another. This is shown in the next section.

3.3.2 Europe – NUTS1 level subnational regions

Figure 17 shows (top panel) the weekly P-scores for the NUTS1 subnational regions of Italy. The bottom panel of Figure 17 shows the same data as the top panel, with each curve scaled by its maximum value.

Italy (NUTS1 regions)

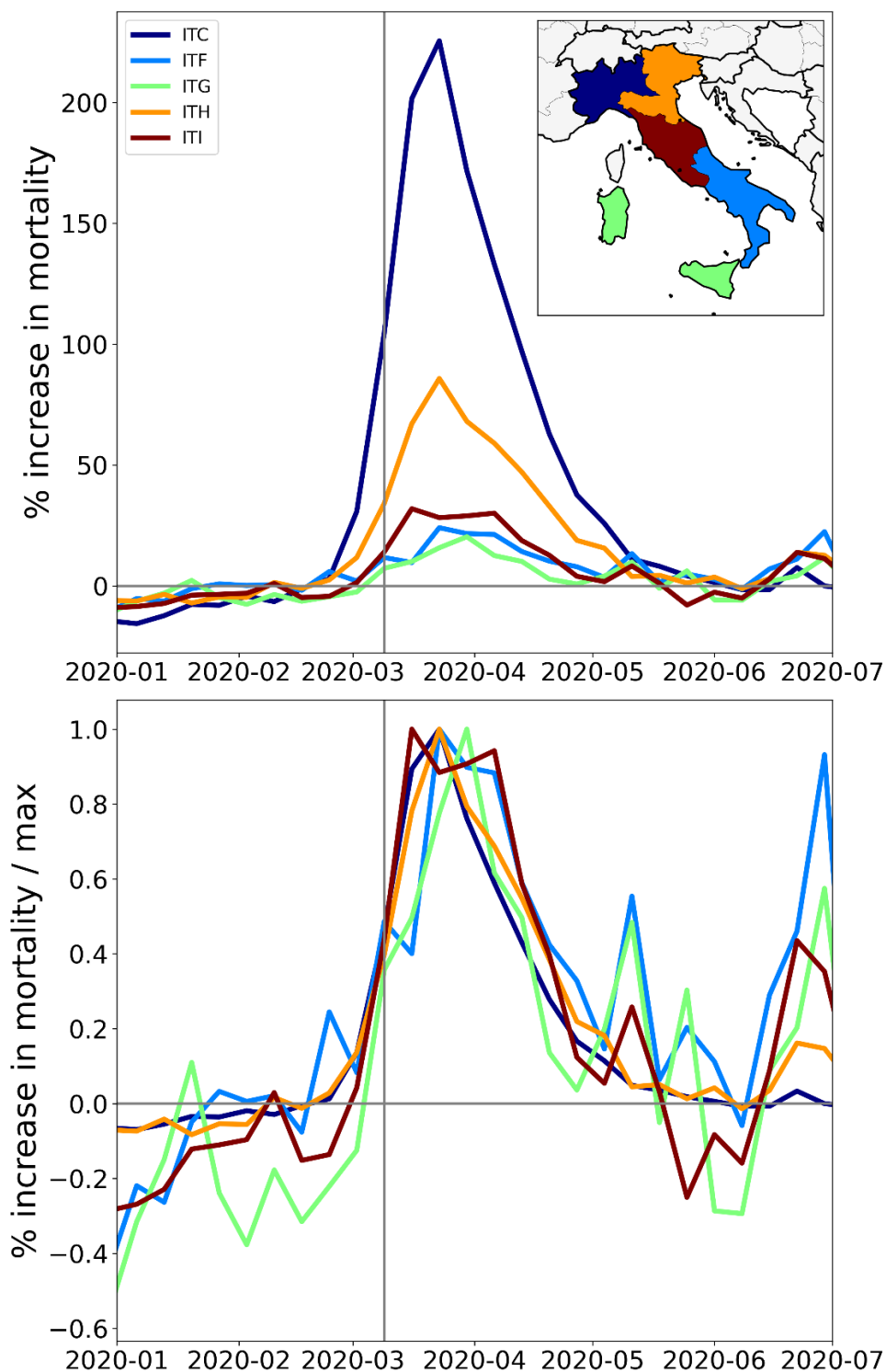


Figure 17: Top panel: weekly P-scores during the first-peak period for the NUTS1 regions of Italy, color coded as per the map in the inset. Bottom panel: same as top panel, with each curve scaled by its maximum. Vertical grey lines indicate the week of the WHO's pandemic declaration of 2020-03-11.

As can be seen in the top panel of Figure 17, there is a large variation in peak height, ranging from maximum first-peak period weekly P-scores of 20% (ITG = Insular Italy), 24% (ITF = South Italy) and 32% (ITI = Central Italy) to 225% (ITC = Northwest Italy). The Northwest Italy (ITC) NUTS1 region contains the smaller NUTS2 region of Lombardy (ITC4), which was the Italian NUTS2 region with the highest integrated first-peak period P-score. Lombardy is examined in more detail in sections 3.3.3, 3.3.4 and 3.4.

Despite the large variation in peak heights, the bottom panel of Figure 17 shows that the F-peaks for the Italian NUTS1 regions rose and fell in synchrony within measurement uncertainty, with rise-side half-maximum dates approximately equal to the week of the pandemic declaration, the same as for Italy at the national level (see section 3.3.1). In particular, the rise-side half-maximum dates for Central Italy (ITI, containing Rome) and Northwest Italy (ITC, containing the Lombardy region and the city of Milan) were both equal to the week of the pandemic declaration, while there was a 7-fold difference in peak heights across the two regions. The integrated first-peak period P-scores (heatmaps in Figure 3) for Northwest Italy (ITC) and Central Italy (ITI) were 81% and 12%, respectively, also a 7-fold difference. These two regions are examined and compared in more detail in section 3.4.1.

An even more striking result is seen for Spain (Figure 18). Here, the peak heights range by a factor of 13, from 39% (ES6 = Southern Spain and ES1 = Northwestern Spain) to 491% (ES3 = Comunidad de Madrid), and the rise-side half-maximum dates for all regions were equal to the week after the week of the pandemic declaration.

The same pattern of large variation in peak heights, with essentially synchronous peak timing and essentially the same peak widths can be seen in France, Belgium, the Netherlands, the UK, Sweden and Germany in Figure 19 to Figure 24.

Spain (NUTS1 regions)

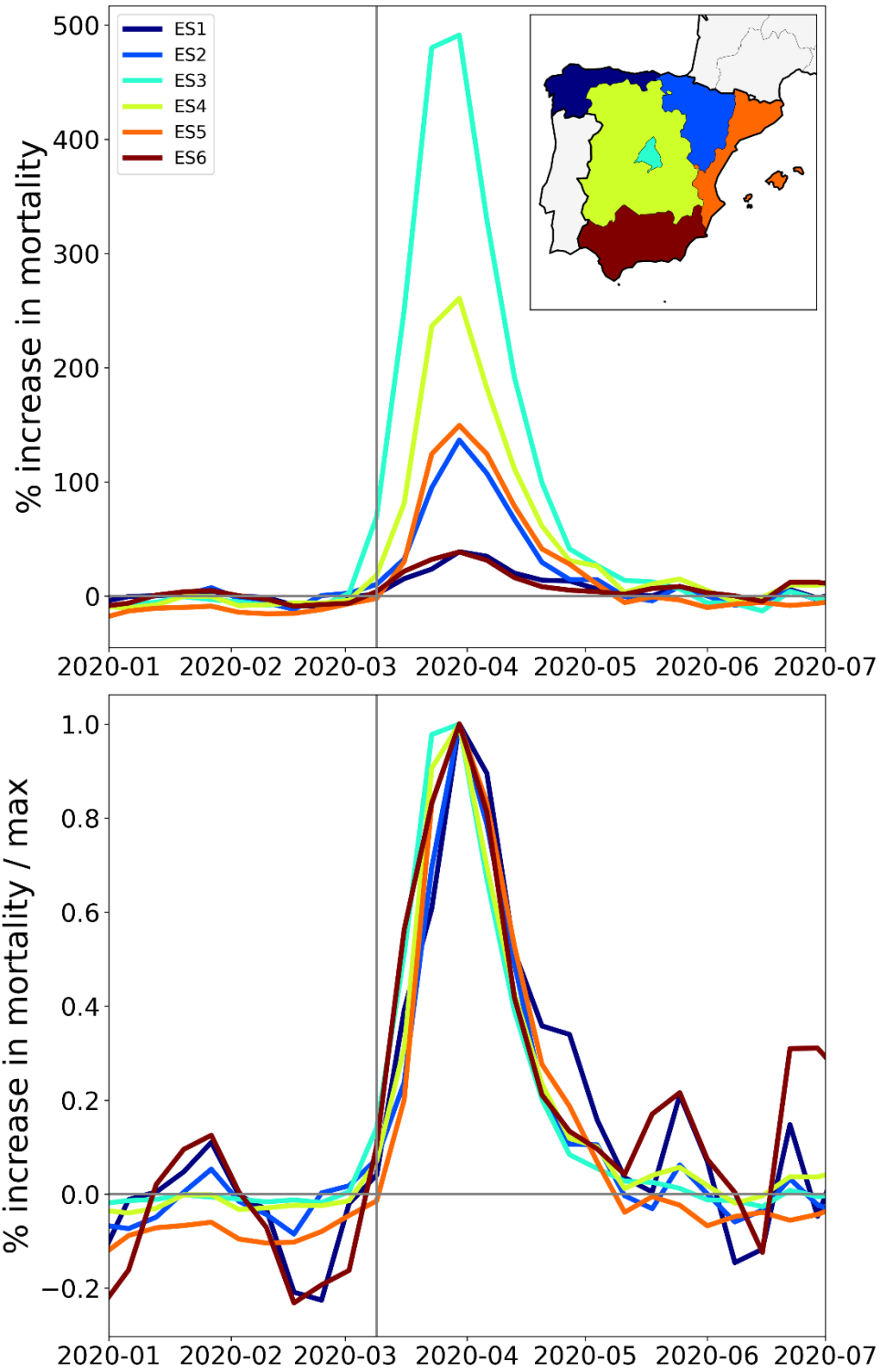


Figure 18: Top panel: weekly P-scores during the first-peak period for the NUTS1 regions of Spain, color coded as per the map in the inset. Bottom panel: same as top panel, with each curve scaled by its maximum. Vertical grey lines indicate the week of the WHO's pandemic declaration of 2020-03-11.

France (NUTS1 regions)

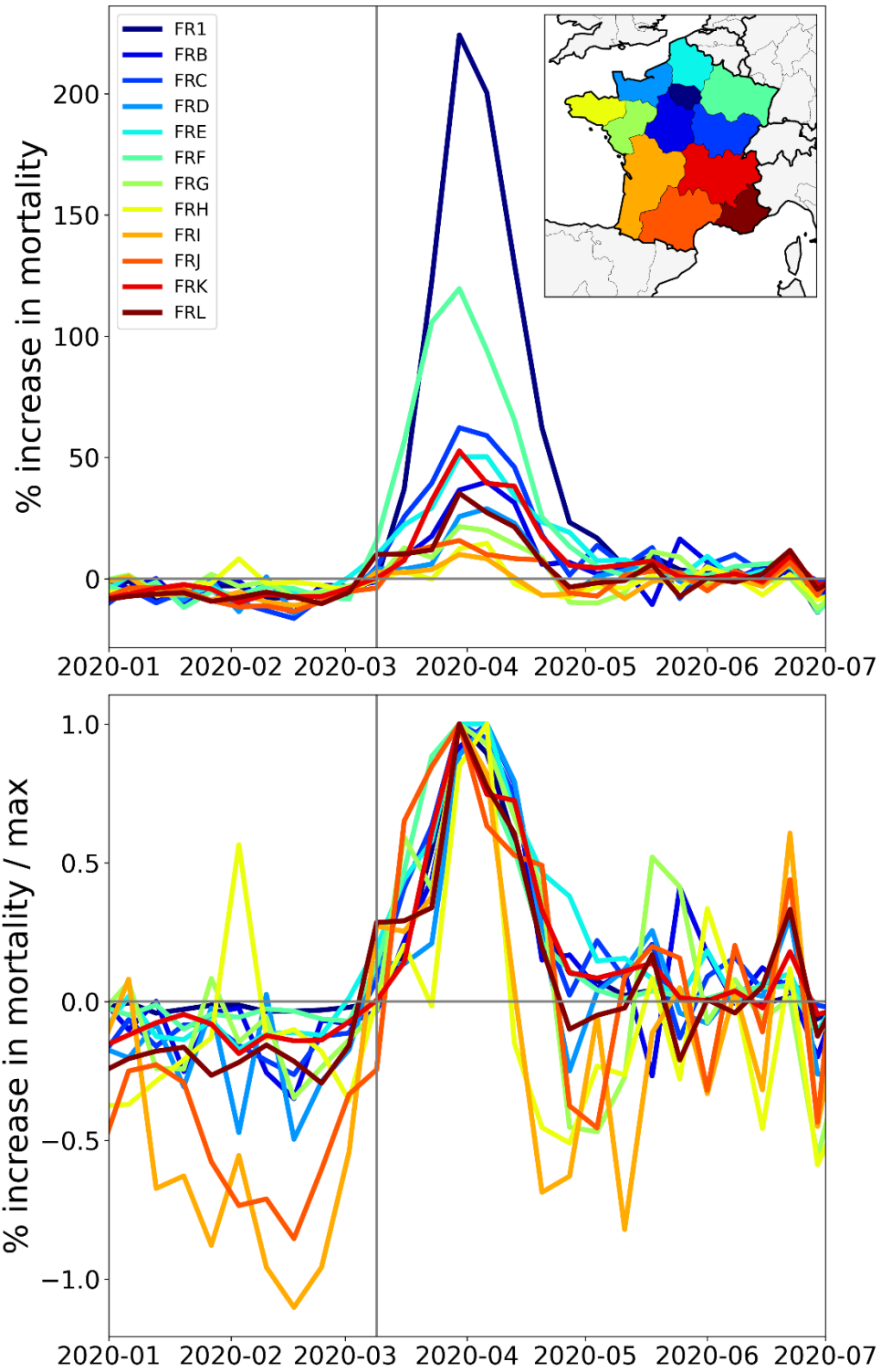


Figure 19: Top panel: weekly P-scores during the first-peak period for the NUTS1 regions of France, color coded as per the map in the inset. Bottom panel: same as top panel, with each curve scaled by its maximum. Vertical grey lines indicate the week of the WHO's pandemic declaration of 2020-03-11.

Belgium (NUTS1 regions)

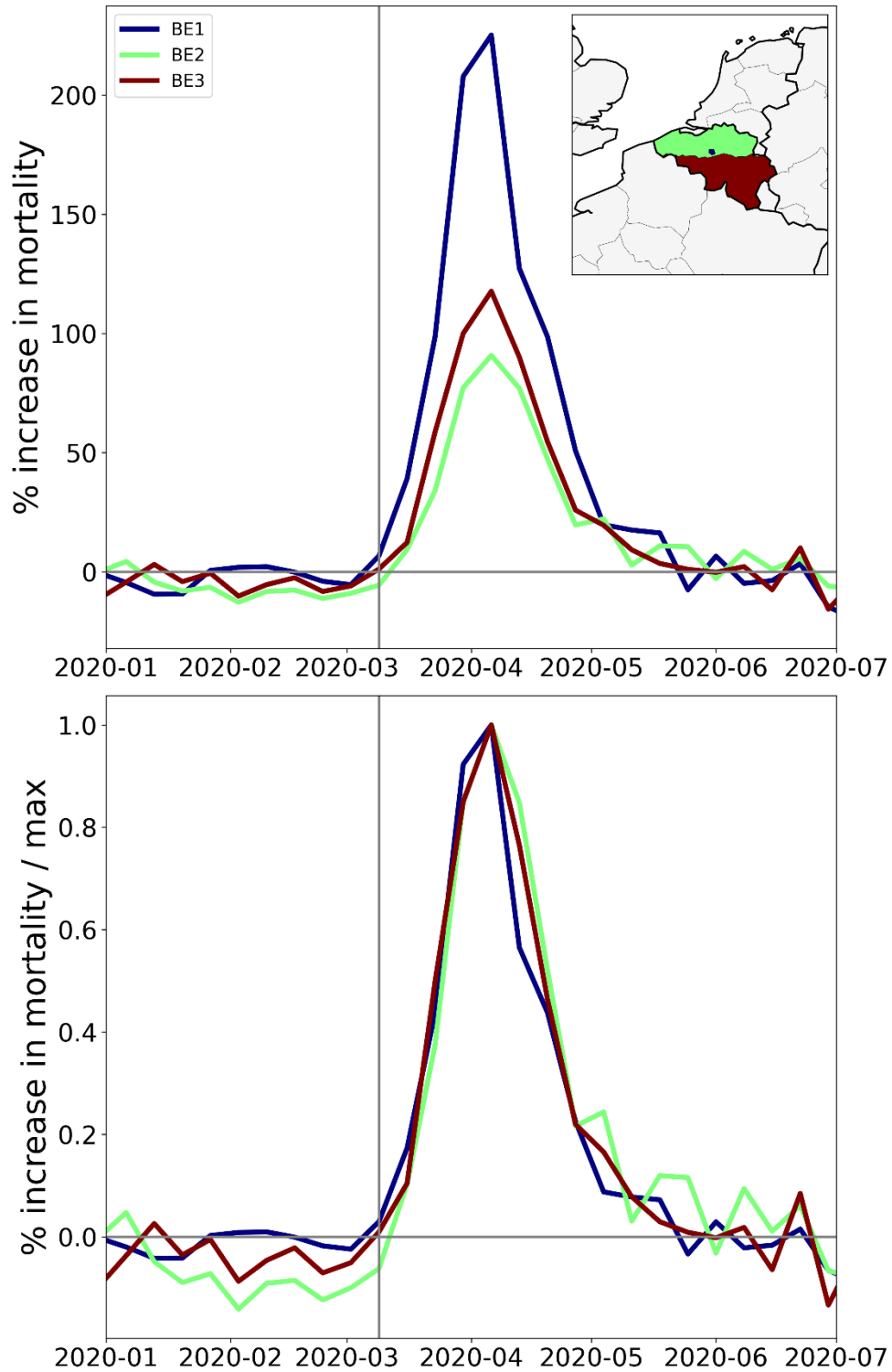


Figure 20: Top panel: weekly P-scores during the first-peak period for the NUTS1 regions of Belgium, color coded as per the map in the inset. Bottom panel: same as top panel, with each curve scaled by its maximum. Vertical grey lines indicate the week of the WHO's pandemic declaration of 2020-03-11.

Netherlands (NUTS1 regions)

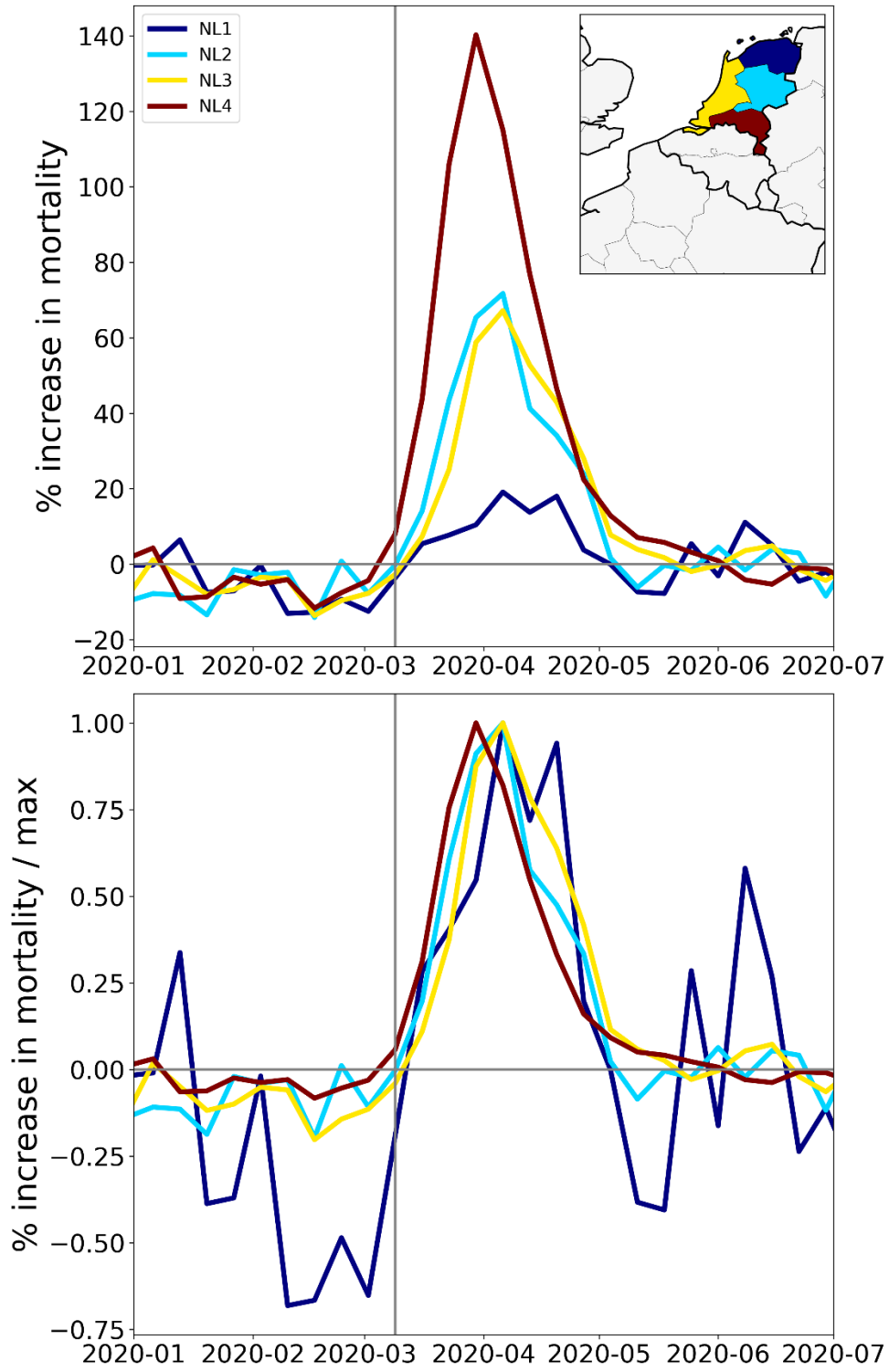


Figure 21: Top panel: weekly P-scores during the first-peak period for the NUTS1 regions of the Netherlands, color coded as per the map in the inset. Bottom panel: same as top panel, with each curve scaled by its maximum. Vertical grey lines indicate the week of the WHO pandemic declaration.

United Kingdom (NUTS1 regions)

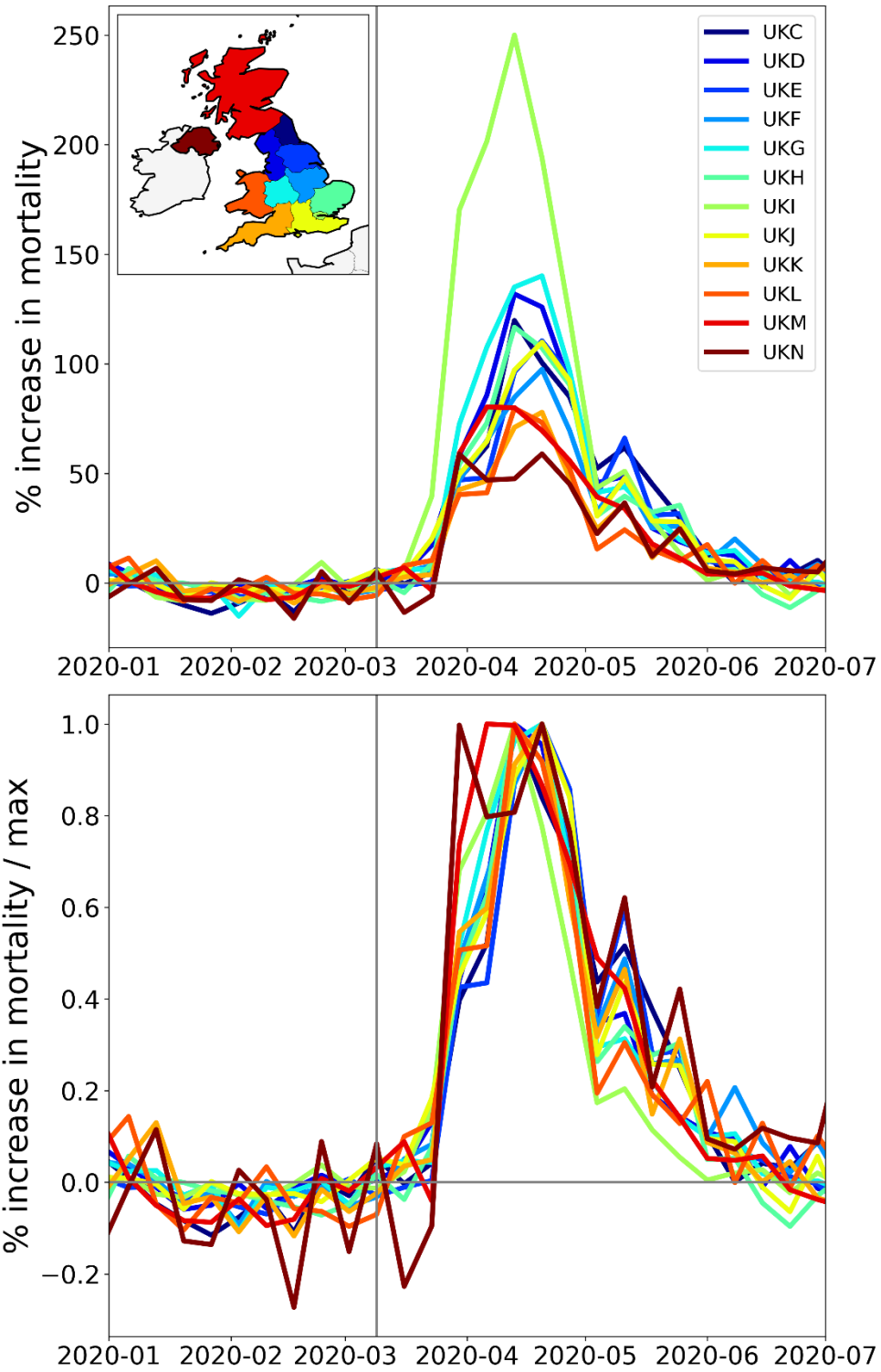


Figure 22: Top panel: weekly P-scores during the first-peak period for the NUTS1 regions of the UK, color coded as per the map in the inset. Bottom panel: same as top panel, with each curve scaled by its maximum. Vertical grey lines indicate the week of the WHO's pandemic declaration of 2020-03-11.

Sweden (NUTS1 regions)

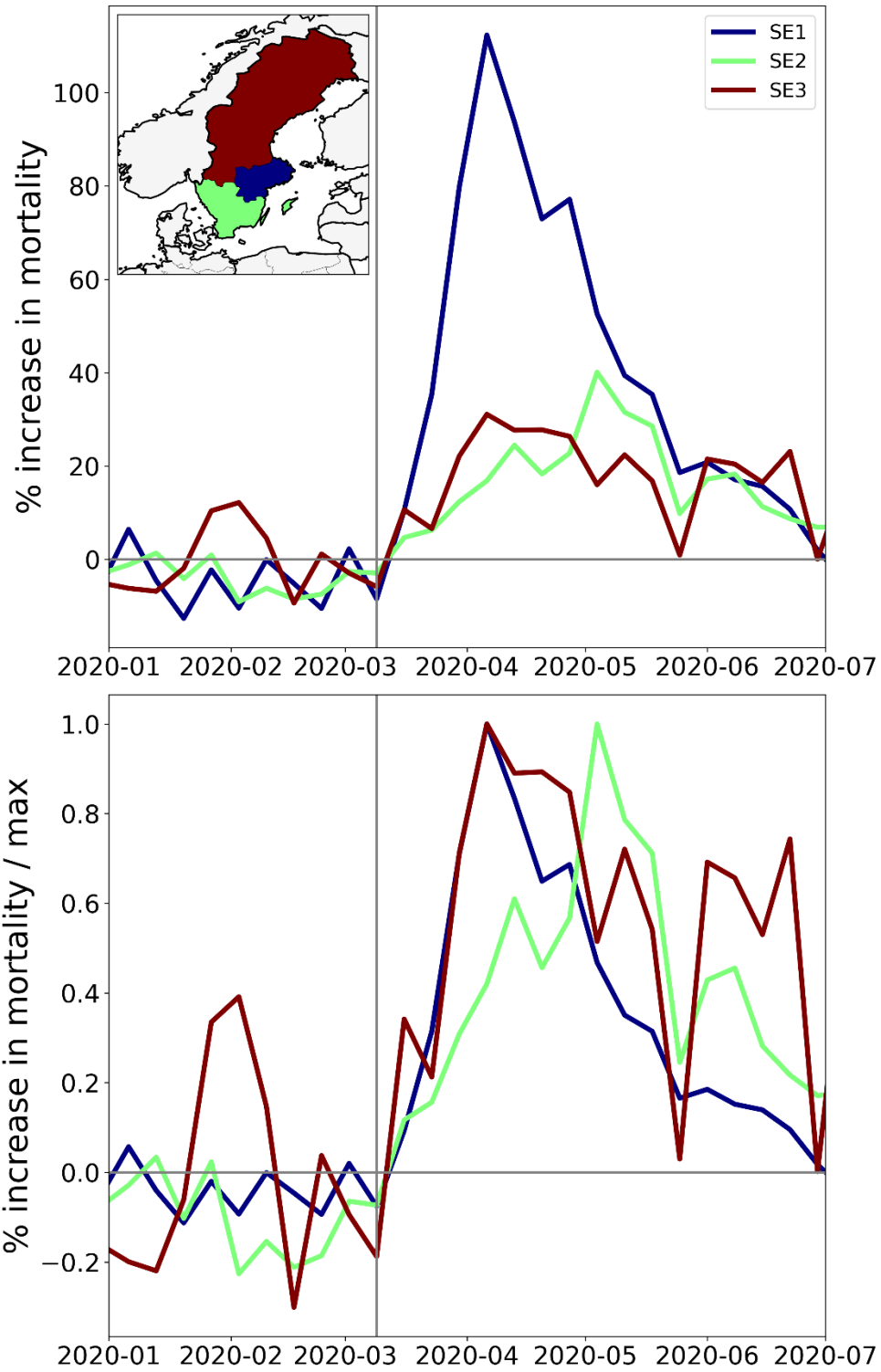


Figure 23: Top panel: weekly P-scores during the first-peak period for the NUTS1 regions of Sweden, color coded as per the map in the inset. Bottom panel: same as top panel, with each curve scaled by its maximum. Vertical grey lines indicate the week of the WHO's pandemic declaration of 2020-03-11.

Germany (NUTS1 regions)

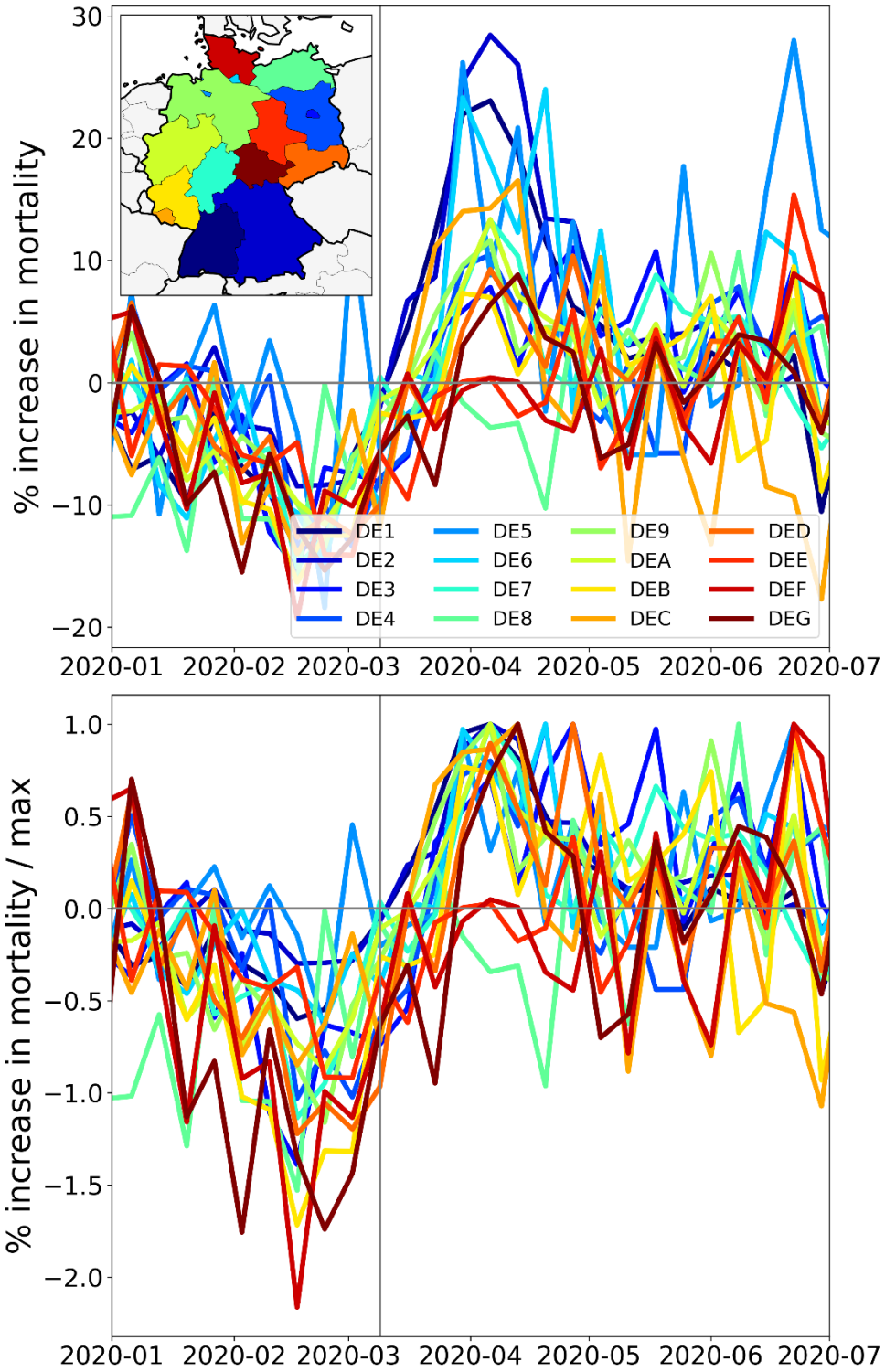


Figure 24: Top panel: weekly P-scores during the first-peak period for the NUTS1 regions of Germany, color coded as per the map in the inset. Bottom panel: same as top panel, with each curve scaled by its maximum. Vertical grey lines indicate the week of the WHO's pandemic declaration of 2020-03-11.

3.3.3 Europe – NUTS2 level subnational regions

The features of the F-peaks described in section 3.3.2 for the NUTS1 regions of particular European countries — large variation in peak height combined with essentially synchronous peak timing and essentially the same peak widths — are also observed at the finer NUTS2 geographic resolution. This is shown in Figure 25 to Figure 32.

In this section, we include a figure for Switzerland (Figure 32) in place of Germany, since we do not have data for the NUTS2 regions of Germany, and since Switzerland has a prominent F-peak.

Italy (NUTS2 regions)

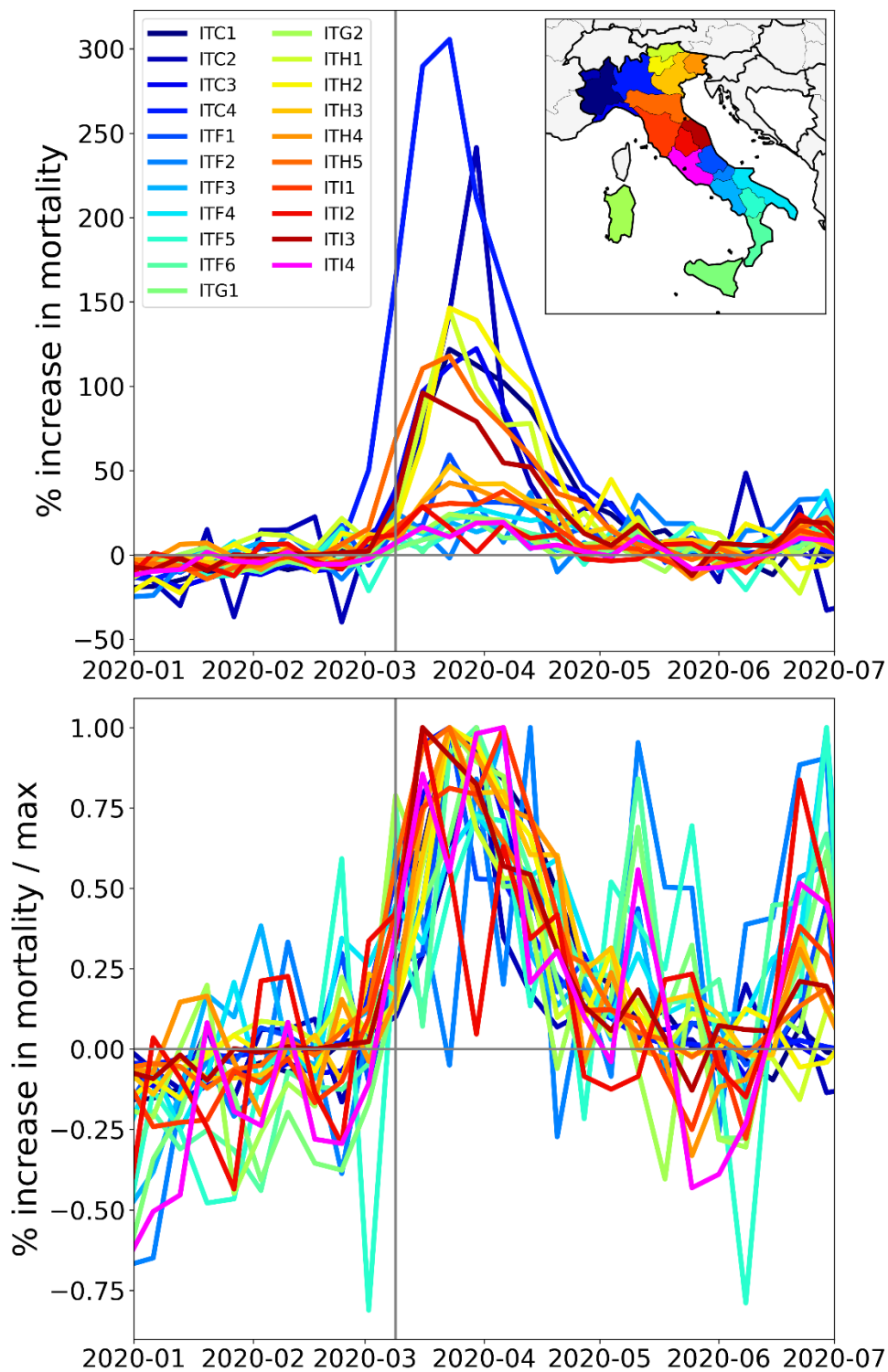


Figure 25: Top panel: weekly P-scores during the first-peak period for the NUTS2 regions of Italy, color coded as per the map in the inset. Bottom panel: same as top panel, with each curve scaled by its maximum. Vertical grey lines indicate the week of the WHO’s pandemic declaration of 2020-03-11.

Spain (NUTS2 regions)

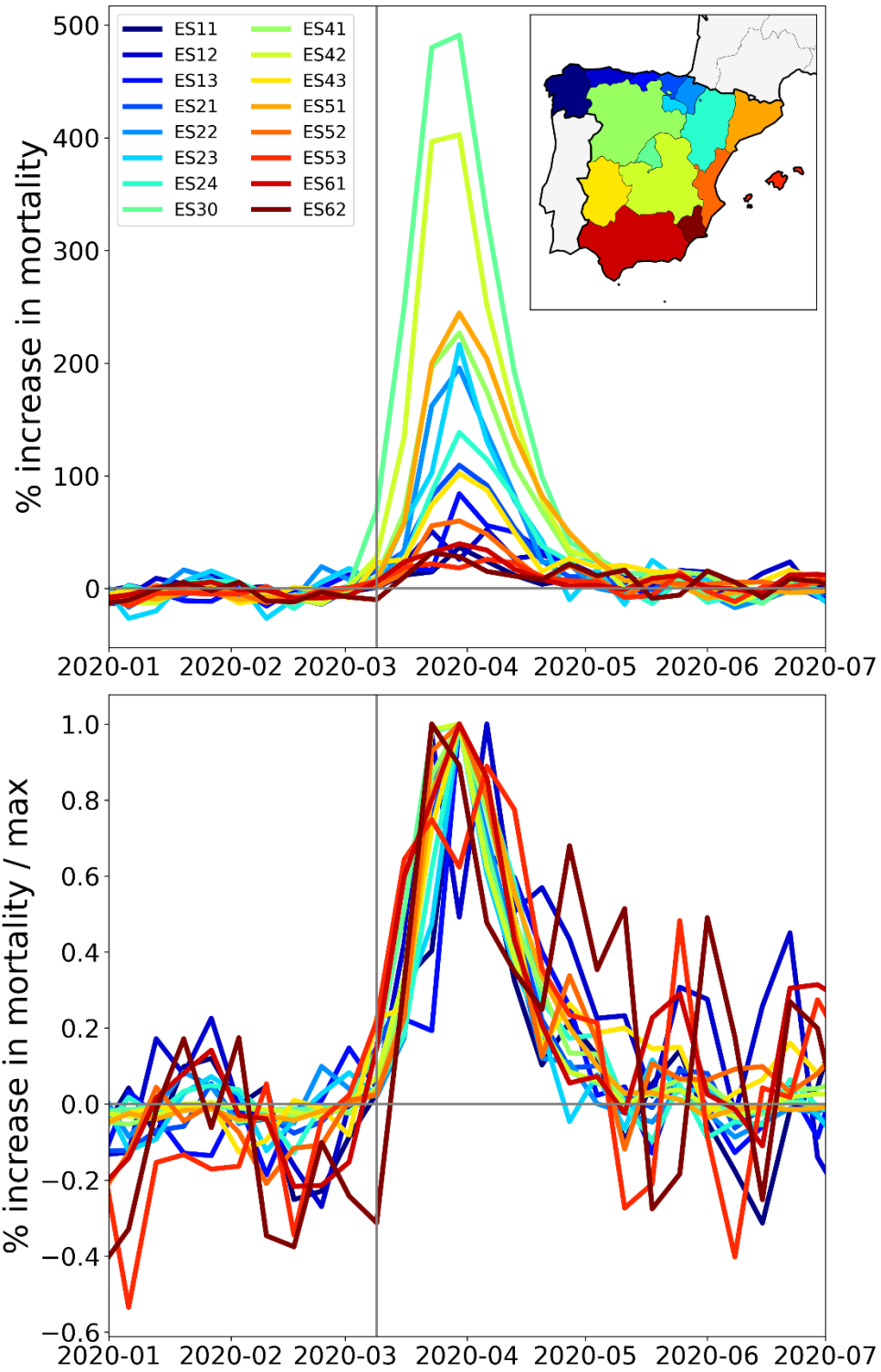


Figure 26: Top panel: weekly P-scores during the first-peak period for the NUTS2 regions of Spain, color coded as per the map in the inset. Bottom panel: same as top panel, with each curve scaled by its maximum. Vertical grey lines indicate the week of the WHO's pandemic declaration of 2020-03-11.

France (NUTS2 regions)

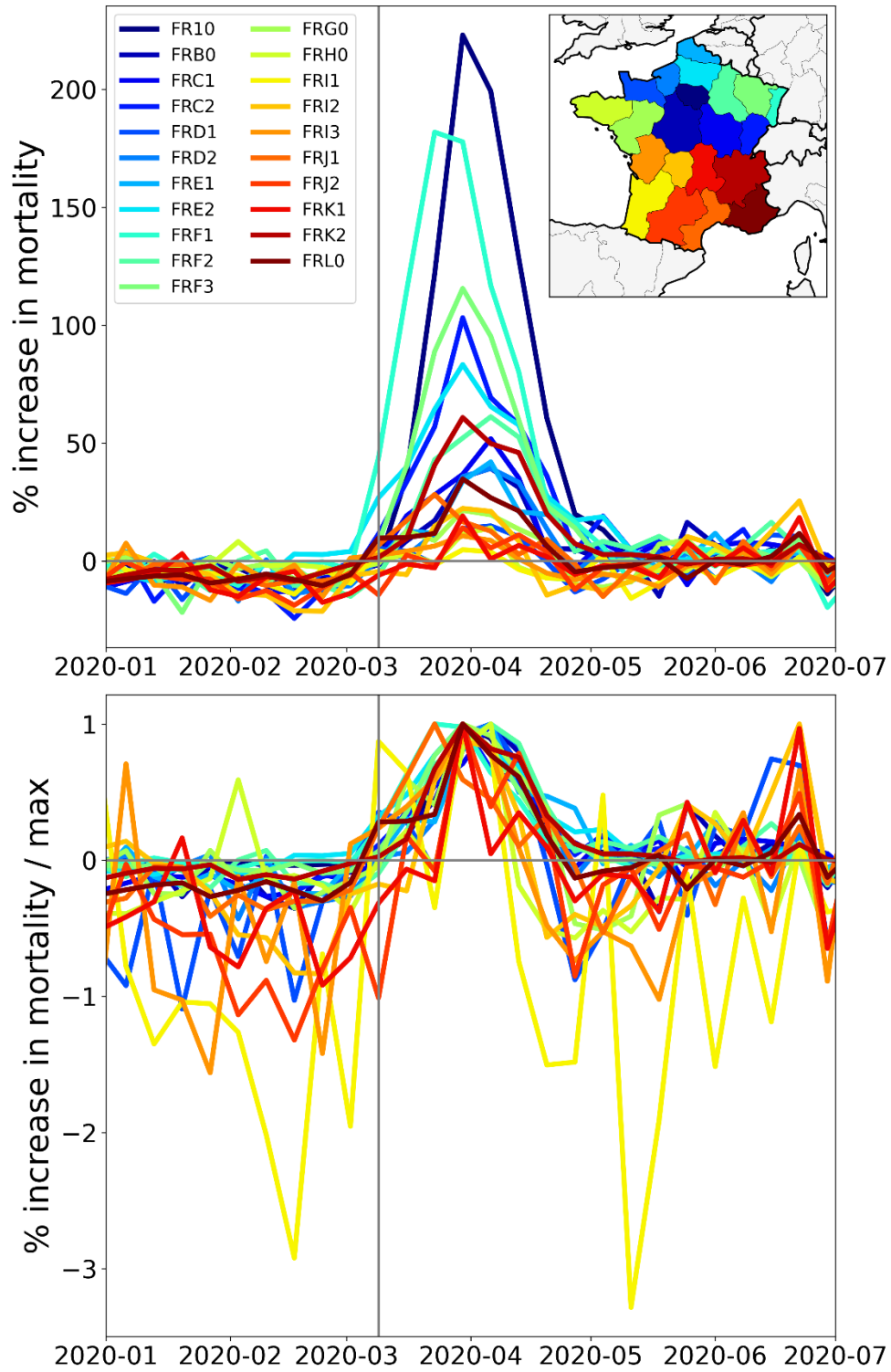


Figure 27: Top panel: weekly P-scores during the first-peak period for the NUTS2 regions of France, color coded as per the map in the inset. Bottom panel: same as top panel, with each curve scaled by its maximum. Vertical grey lines indicate the week of the WHO's pandemic declaration of 2020-03-11.

Belgium (NUTS2 regions)

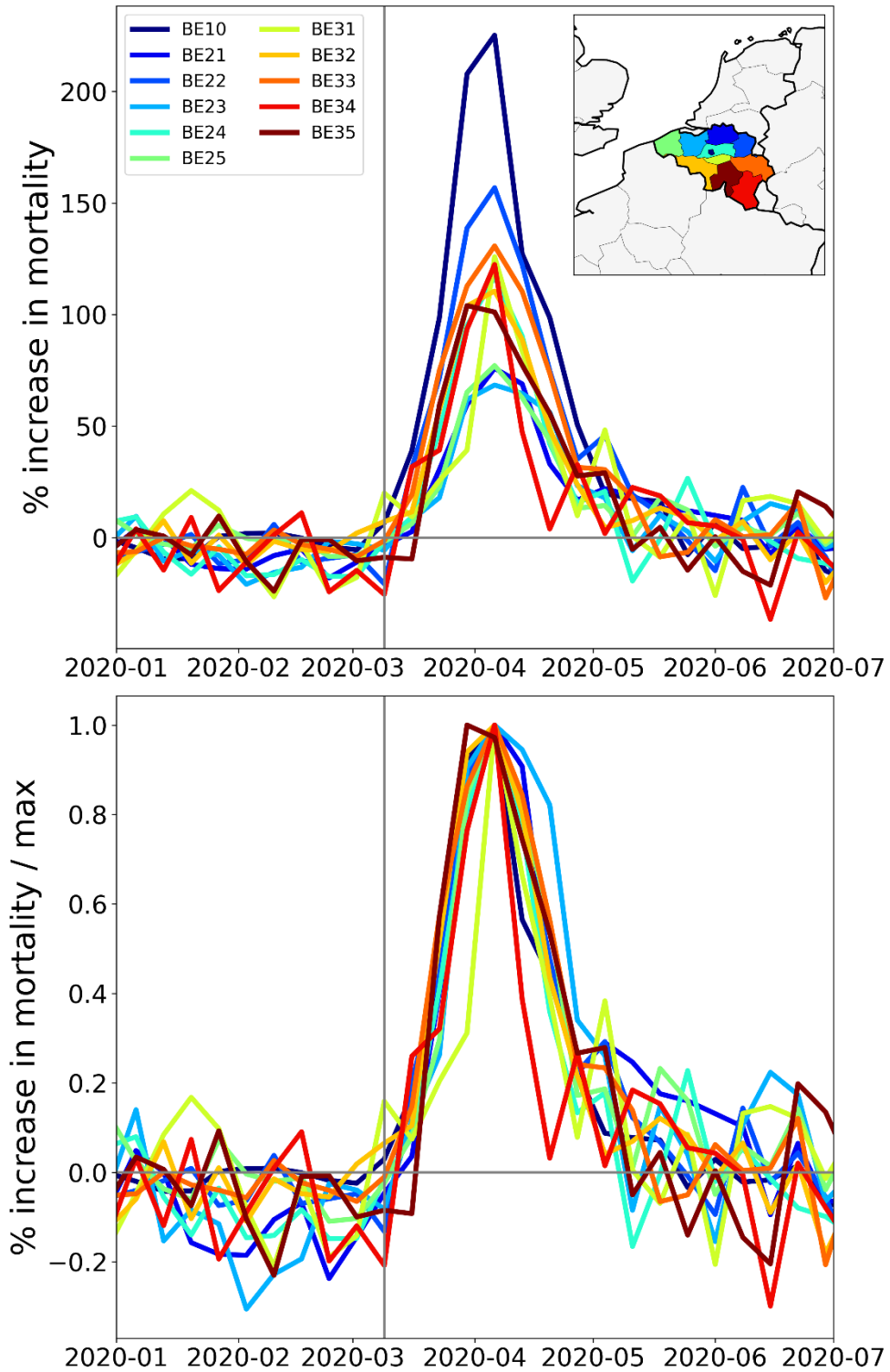


Figure 28: Top panel: weekly P-scores during the first-peak period for the NUTS2 regions of Belgium, color coded as per the map in the inset. Bottom panel: same as top panel, with each curve scaled by its maximum. Vertical grey lines indicate the week of the WHO's pandemic declaration of 2020-03-11.

Netherlands (NUTS2 regions)

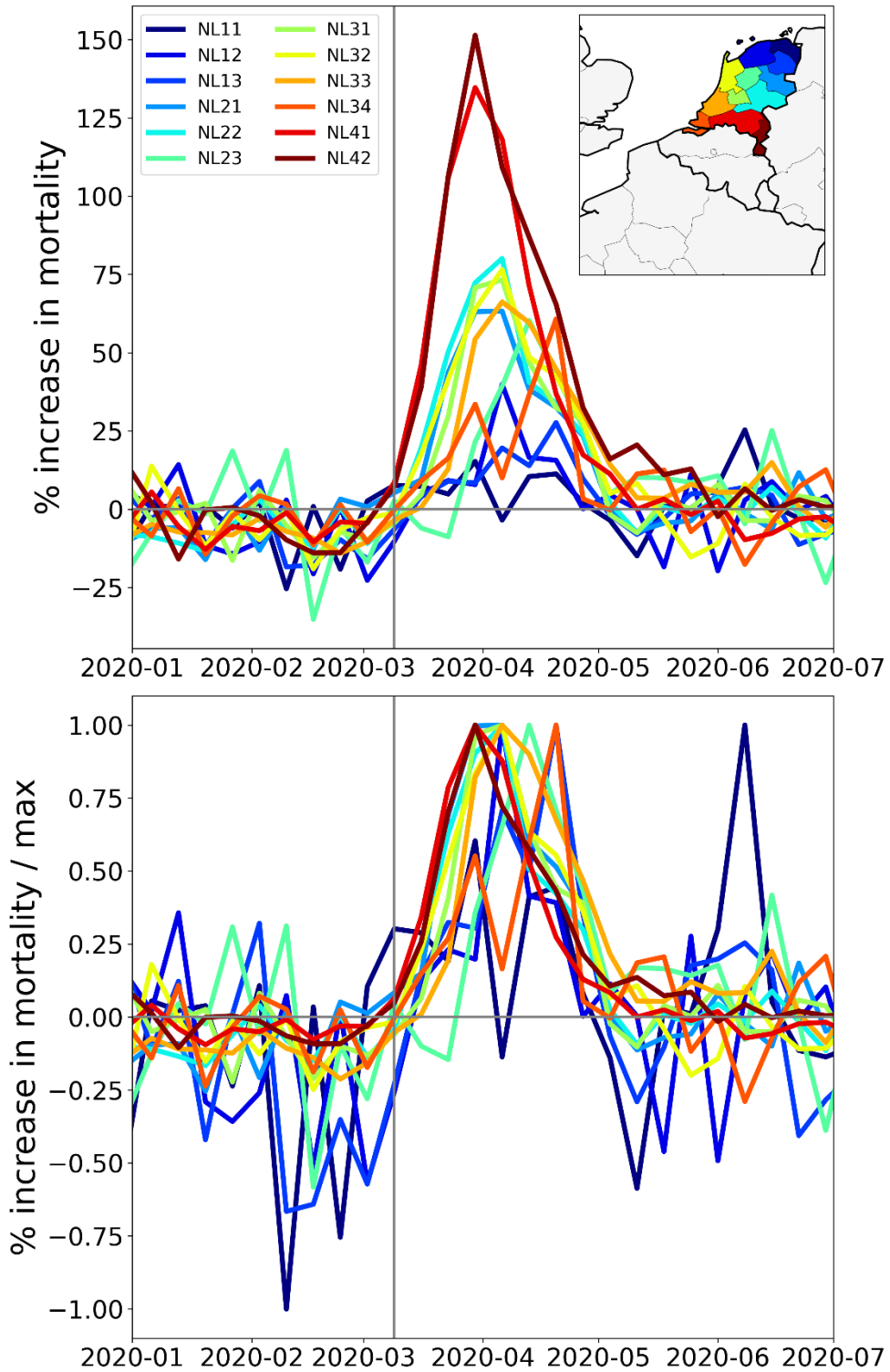


Figure 29: Top panel: weekly P-scores during the first-peak period for the NUTS2 regions of the Netherlands, color coded as per the map in the inset. Bottom panel: same as top panel, with each curve scaled by its maximum. Vertical grey lines indicate the week of the WHO pandemic declaration.

United Kingdom (NUTS2 regions)

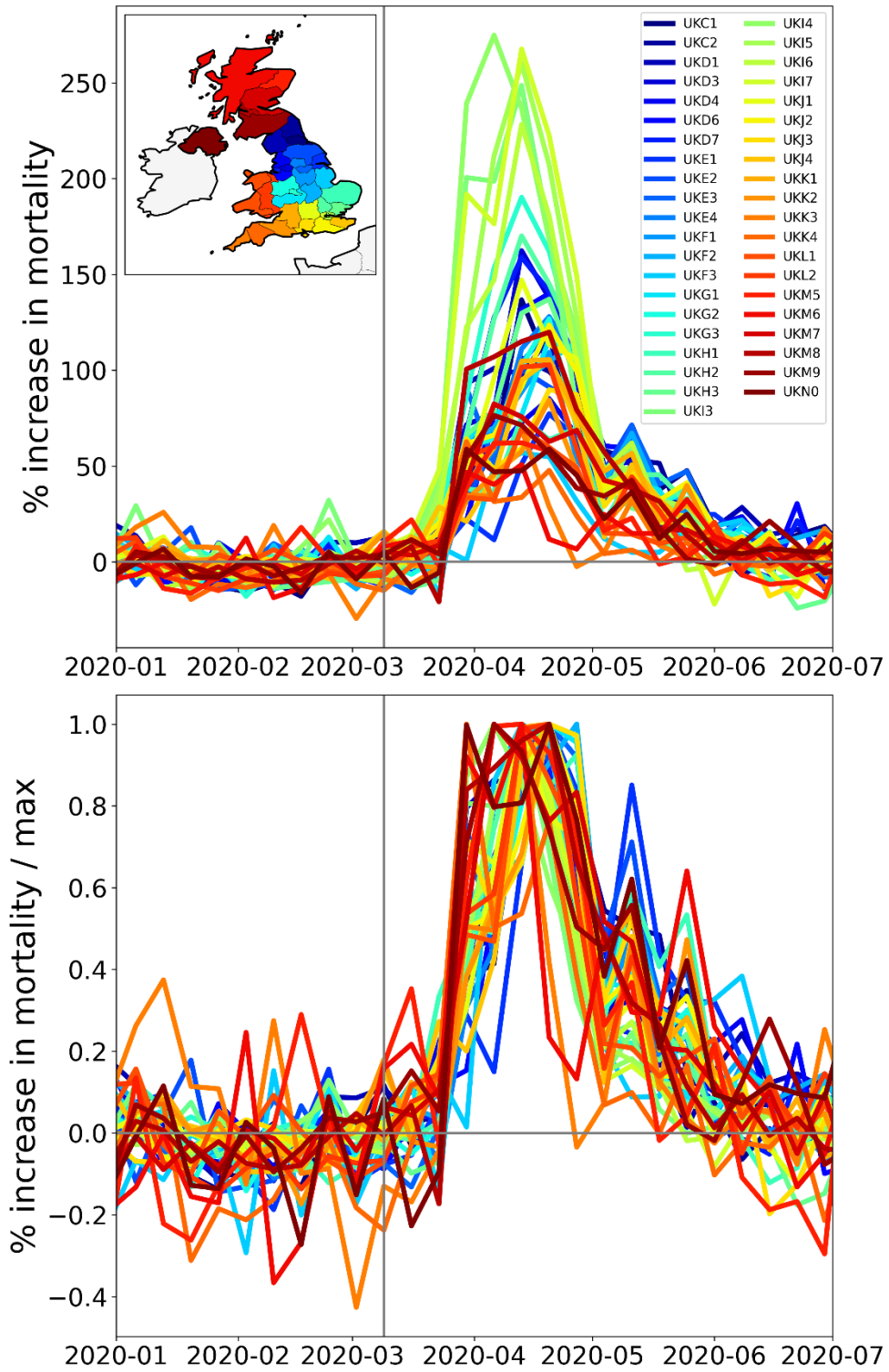


Figure 30: Top panel: weekly P-scores during the first-peak period for the NUTS2 regions of the UK, color coded as per the map in the inset. Bottom panel: same as top panel, with each curve scaled by its maximum. Vertical grey lines indicate the week of the WHO's pandemic declaration of 2020-03-11.

Sweden (NUTS2 regions)

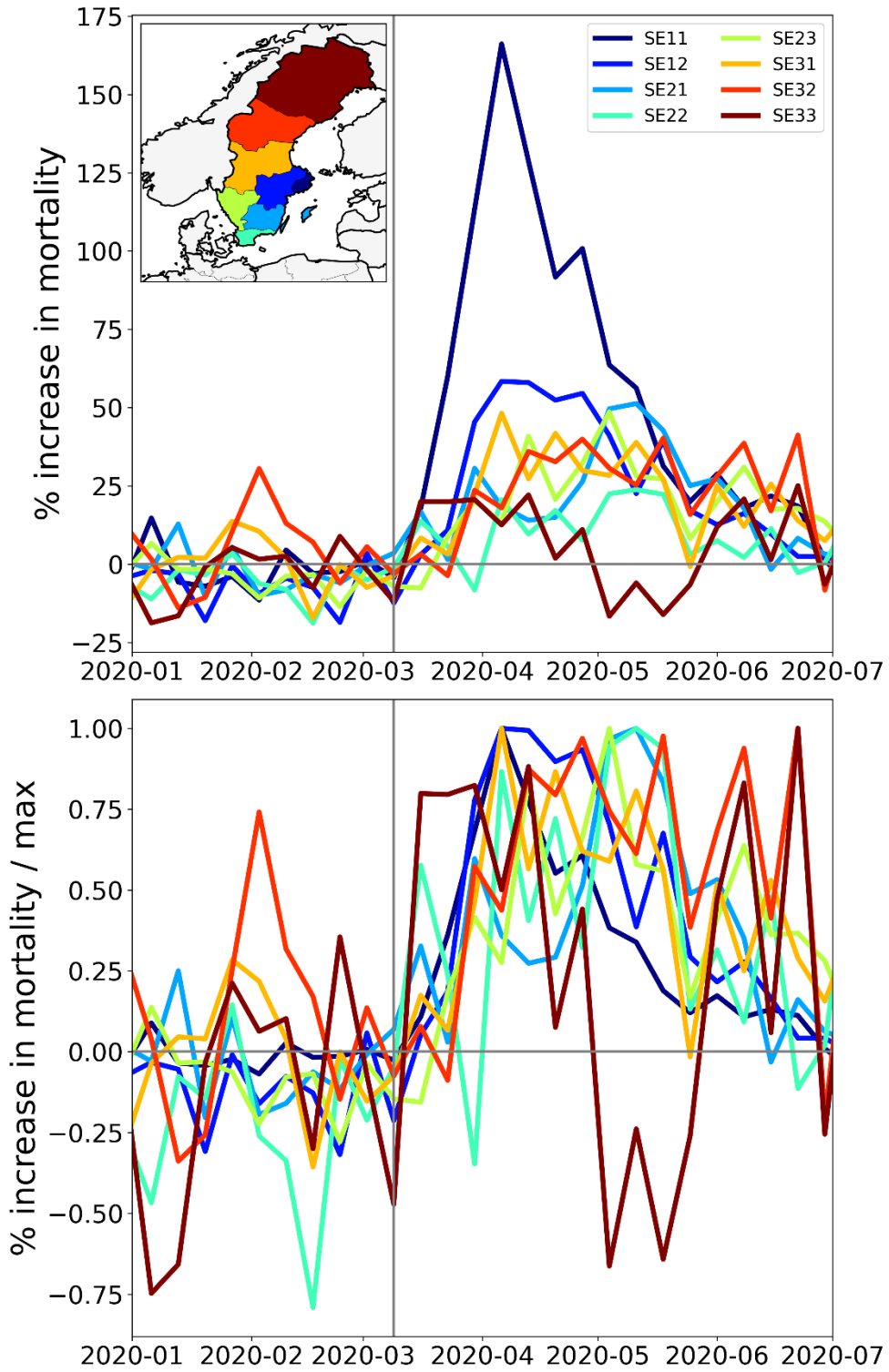


Figure 31: Top panel: weekly P-scores during the first-peak period for the NUTS2 regions of Sweden, color coded as per the map in the inset. Bottom panel: same as top panel, with each curve scaled by its maximum. Vertical grey lines indicate the week of the WHO's pandemic declaration of 2020-03-11.

Switzerland (NUTS2 regions)

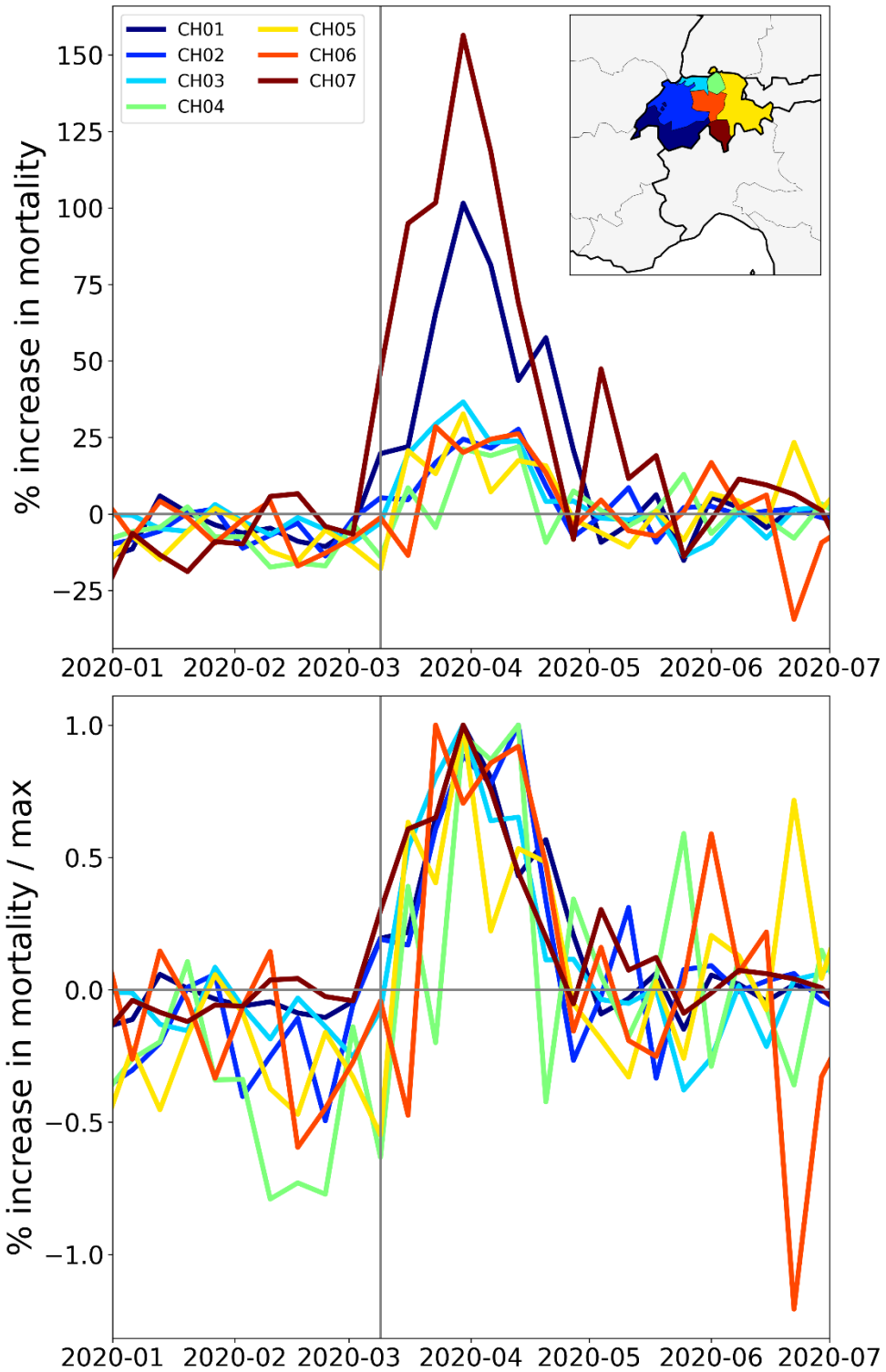


Figure 32: Top panel: weekly P-scores during the first-peak period for the NUTS2 regions of Switzerland, color coded as per the map in the inset. Bottom panel: same as top panel, with each curve scaled by its maximum. Vertical grey lines indicate the week of the WHO pandemic declaration.

3.3.4 Europe – international border regions (NUTS1 level)

In addition to examining how the size and timing of F-peaks compare for different subnational regions within a particular country, it is also interesting to compare subnational regions that are in different countries but which border one another.

We therefore make plots of the type used in sections 3.3.1, 3.3.2, and 3.3.3 for the NUTS1 subnational regions on both sides of Germany's borders with the Netherlands, Belgium, Luxembourg, and France (Figure 33), on Spain's borders with Portugal (Figure 35) and with France (Figure 36), and on Italy's borders with France, Switzerland, Austria, and Slovenia (Figure 38).

The top panel of Figure 33 has a map with the NUTS1 regions along Germany's western border (black and grey), and the NUTS1 regions in France (blue), Luxembourg (light blue), Belgium (yellow), and the Netherlands (red) that share an international border with the western German states.

At the national (NUTS0) level, Germany had low first-peak period excess mortality (see Figure 2). This is also true for Germany's NUTS1 regions on its western border, as can be seen from the graphs of weekly P-scores in the middle panel of Figure 33 (black and grey curves). In contrast, bordering NUTS1 regions in the Netherlands, Belgium and France had large F-peaks, with peak heights reaching to more than a factor of five times larger (NL4 = South Netherlands) than the peak height of the German western border state with the largest F-peak height (DE1 = Baden-Wurtemberg).

DE borders with FR, LU, BE and NL (NUTS1 regions)

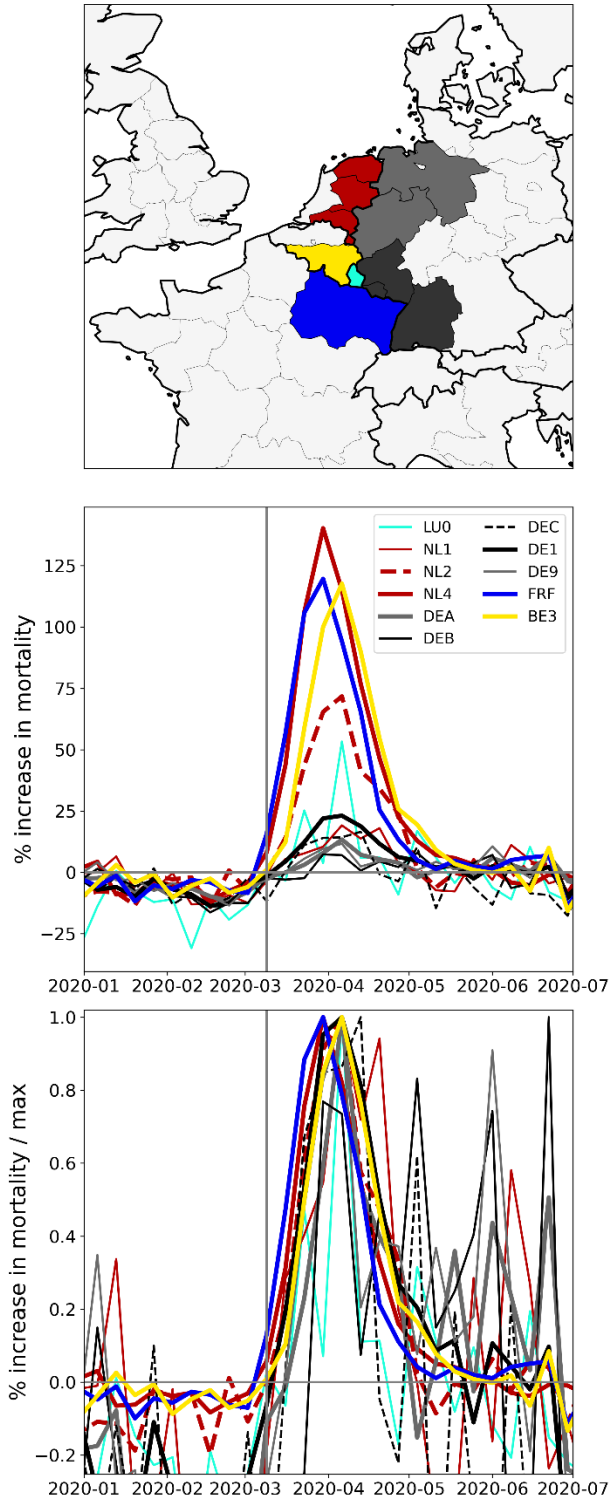


Figure 33: Top panel: Map of the bordering NUTS1 regions in Germany (black and grey), France (blue), Luxembourg (light blue), Belgium (yellow) and the Netherlands (red). Middle panel: weekly P-scores during the first-peak period for the regions shown in the top panel. Lower panel: same as middle

panel, with each curve scaled by its maximum. Vertical grey lines in the lower two panels indicate the week of the WHO's pandemic declaration of 2020-03-11.

The bottom panel of Figure 33 shows the same data as the middle panel, with each curve scaled by its maximum. As can be seen, the F-peak in the French region FRF (Grand Est) slightly preceded the peaks of the other regions shown in the figure. The rise-side half-maximum date for FRF is equal to one week after the week of the pandemic declaration, while the rise-side half-maximum date for the Belgian NUTS1 border region BE3 (Wallonia) is equal to two weeks after the week of the pandemic declaration. The F-peaks in the German regions DE1 (thick solid black lines in middle and bottom panels, most southwestern black-shaded state in the top panel of Figure 33), DEC (dashed black lines, smallest black-shaded state), and DE9 (thin grey lines, northern grey-shaded state) had rise-side half-maximum dates equal to the rise-side half-maximum dates of the Belgian region BE3. The German NUTS1 region DEB arguably did not have an F-peak (thin solid black line in the middle panel of Figure 33, northernmost black-shaded state), and the rise-side half-maximum date for the German NUTS1 region DEA (thick grey line, southern grey-shaded state) is equal to about three weeks after the week of the pandemic declaration.

The widths (FWHM) of the peaks for FRF, BE3, NL1, NL2, NL4, DE1 and DEC are all equal to about four weeks, while the FWHM for DEA and DE9 are equal to about three weeks. The data for LU0 is too noisy to make a reliable measurement of the FWHM and DEB arguably did not have an F-peak.

Main striking observations from Figure 33 include:

- All the western border regions of Germany had small first-peak period excess mortality. No border regions of Germany had large excess mortality peaks during the first-peak period.
- The German NUTS1 region DEB (Rhineland-Palatinate: thin solid black lines in middle and bottom panels, northern black-shaded region in top panel) essentially did not have an F-peak, whereas bordering NUTS1 regions in France (FRF) and Belgium (BE3) had large F-peaks and large integrated first-peak period P-scores (see Figure 3)
- The other four German NUTS1 regions had F-peaks with the same or nearly the same widths as, but with significantly smaller (up to more than five times smaller) peak heights than, the regions that share borders with them in France, Belgium, and the Netherlands. The Dutch NUTS1 region NL1 (North Netherlands: thin red lines, northernmost red-shaded region) is similar to the German regions in that it had a small F-peak height, whereas the other two Dutch NUTS1 border regions NL2 (East Netherlands: dashed red lines, middle red-shaded region) — which shares an internal border with NL1 — and NL4 (South Netherlands: thick solid red lines, southernmost red-shaded region) had large peak heights.

- The F-peaks in the bordering regions of the four countries France, Belgium, the Netherlands, and Germany all had essentially the same width (FWHM) while having significantly different peak heights.

The area of Europe covered by the shaded NUTS1 regions in the top panel of Figure 33 is the most densely-populated multi-national region on the European mainland, as can be seen from the map of NUTS2-region population densities in Figure 4. There are no mountain ranges or significant geographic barriers separating the countries in this area, all countries are in the Schengen zone (no passport controls when crossing the border) and a high volume of cross-international-border traffic normally occurs on a daily basis including daily commuters across the international borders (Eurostat, 2021).

During the first-peak period (March-May of 2020), border control measures were put in place. For example, Germany limited road travel into and out of the country to only essential travel such as for employment or commercial transportation (Amaro, 2020). The control measures at Germany's border with the Netherlands were voluntary, due to the critical importance of avoiding delays in goods transport from the Netherlands to Germany, and the volume of cross-border vehicular traffic decreased to about half its pre-COVID (January and February 2020) level in March-May of 2020, according to monitoring of cross-border traffic by the Dutch province of Gelderland, which is located in the NL2 ("East Netherlands") NUTS2 region (van der Velde et al., 2021).

A study using Facebook data on daily international border crossings in Europe showed that traffic across Luxembourg's borders with each of Belgium, France and Germany decreased by 75% compared to its pre-COVID level, during the first-peak period of 2020 (Docquier et al., 2022).

The volume of road freight transport loaded in each of the Netherlands, Belgium, Luxembourg or France and unloaded in Germany was essentially the same in the first two quarters of 2020 as in the first two quarters of 2019, as shown in Figure 34.

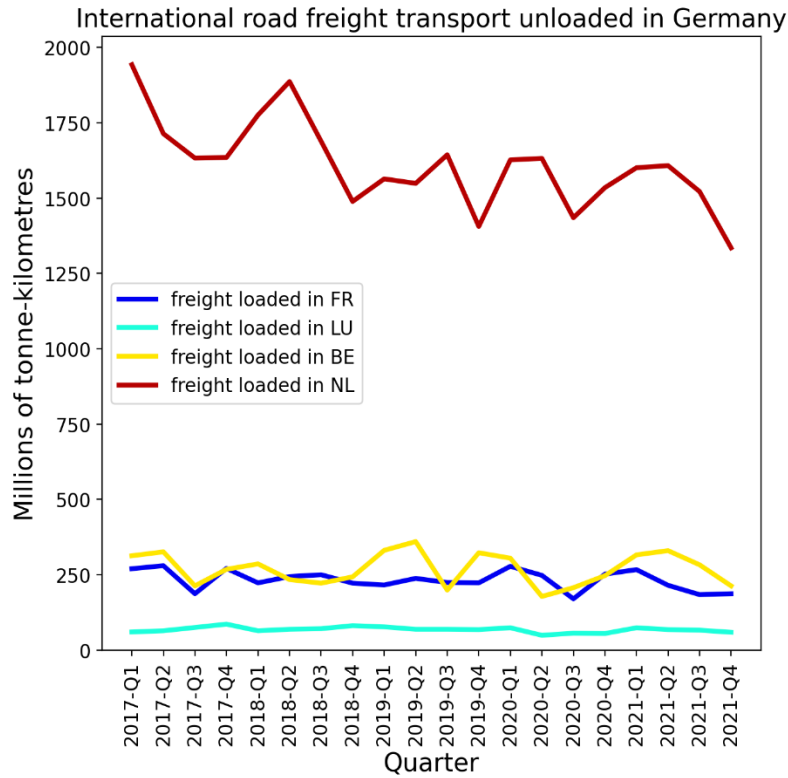


Figure 34: Millions of tonnes-kilometres of international road freight transport loaded in each of the Netherlands, Belgium, France, and Luxembourg and unloaded in Germany, by economic quarter. Data from Eurostat (2024e).

There was thus a significant volume of traffic that entered Germany via its northwest borders during the first-peak period of 2020.

Figure 35 shows results for the NUTS1 regions on Spain’s border with Portugal.

ES-PT border (NUTS1 regions)

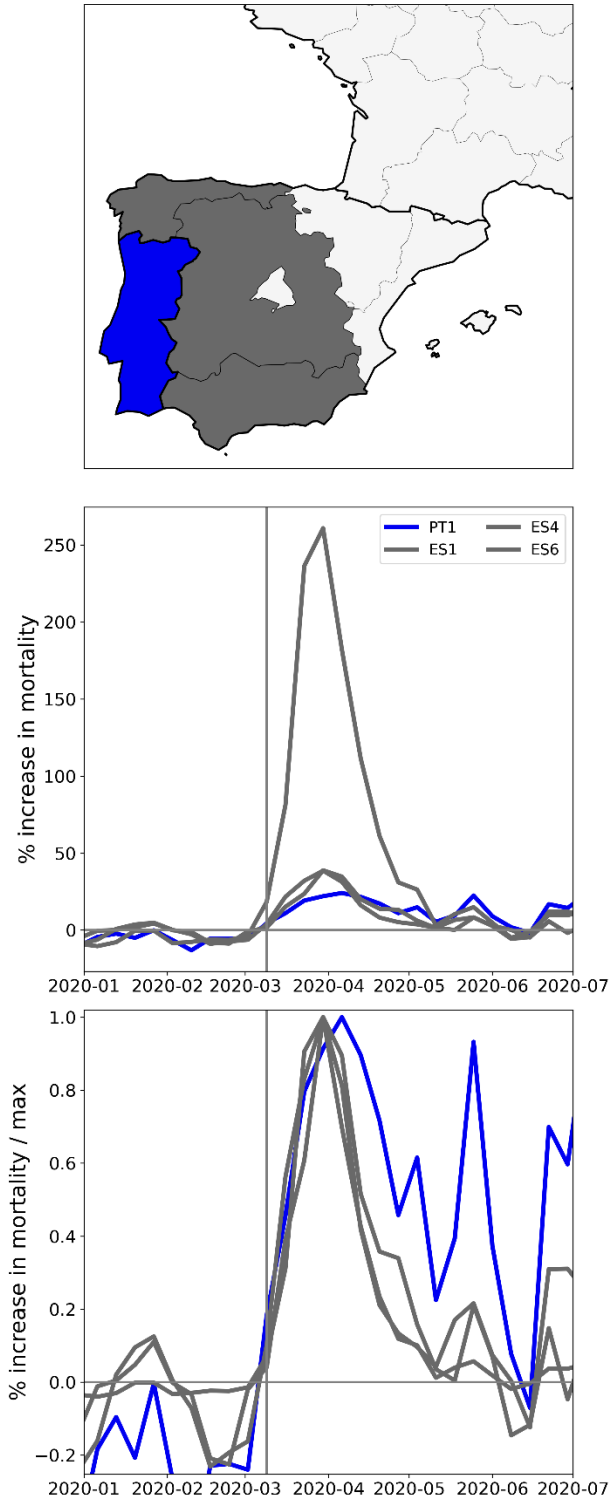


Figure 35: Top panel: Map of the bordering NUTS1 regions in Spain (grey) and Portugal (blue). Middle panel: weekly P-scores during the first-peak period for the regions shown in the top panel. Lower panel: same as middle panel, with each curve scaled by its maximum. Vertical grey lines in the lower two panels indicate the week of the WHO's pandemic declaration of 2020-03-11.

The peak for Spain's ES4 region (central grey-shaded region in the top panel of Figure 35) towers over the peaks for the other two Spanish regions and continental Portugal (PT1). The rise-side half-maximum dates for all four regions were equal to the week after the week of the pandemic declaration, showing a synchronous emergence of the peaks. While the FWHM was essentially the same for the three Spanish NUTS1 regions (between three and four weeks), the FWHM for the bordering Portuguese NUTS1 region was larger, between six and seven weeks long.

Figure 36 shows results for the NUTS1 regions on Spain's border with France. Here, the two Spanish NUTS1 regions have large F-peaks, whereas the two bordering regions in southwestern France had relatively very small (almost negligible) peaks.

ES-FR border (NUTS1 regions)

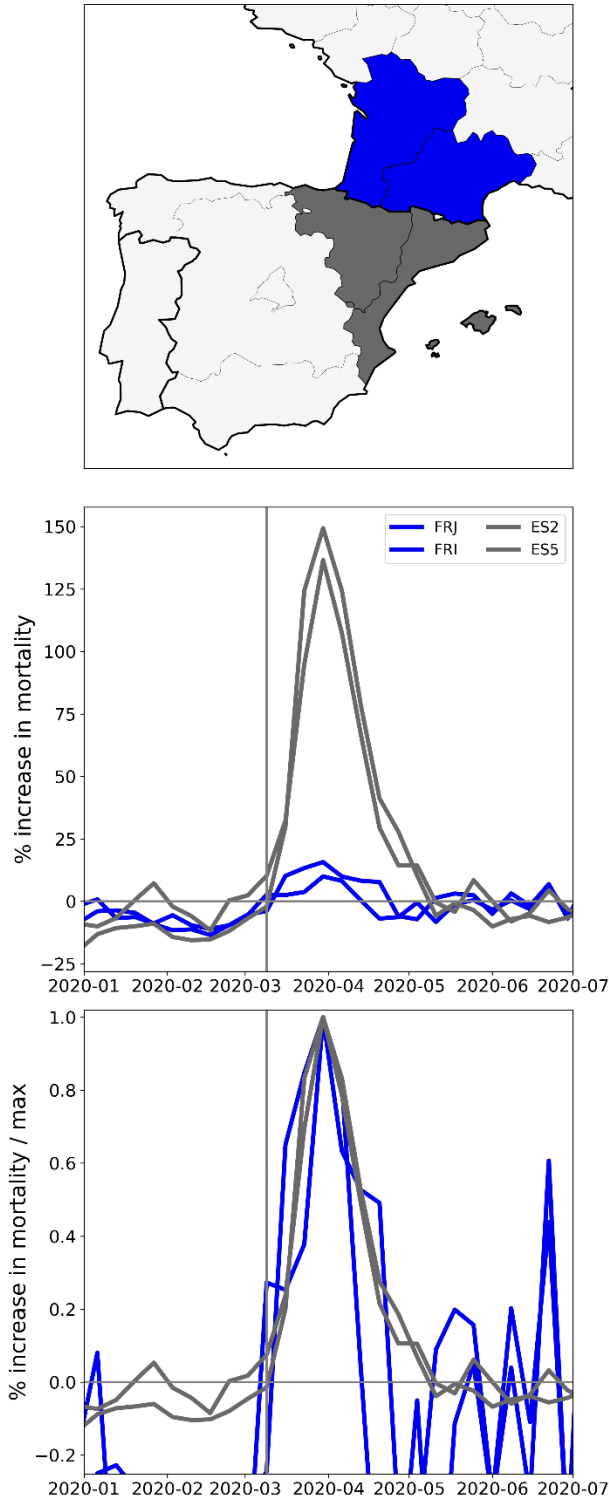


Figure 36: Top panel: Map of the bordering NUTS1 regions in Spain (grey) and France (blue). Middle panel: weekly P-scores during the first-peak period for the regions shown in the top panel. Bottom panel: same as middle panel, with each curve scaled by its maximum. Vertical grey lines in the lower two panels indicate the week of the WHO's pandemic declaration of 2020-03-11.

Despite strict mobility measures applied in Spain, the volume of traffic across Spain’s international borders remained well above zero during March-May of 2020. For example, the volume of road freight transport loaded in Spain and unloaded in France was not substantially decreased in the first and second quarters of 2020 compared to the same time period in 2019 and 2018, whereas the volume of road freight transport loaded in Spain and unloaded in Portugal decreased by about 50% in the first two quarters of 2020 compared to the first two quarters of 2018 and 2019 (see Figure 37).

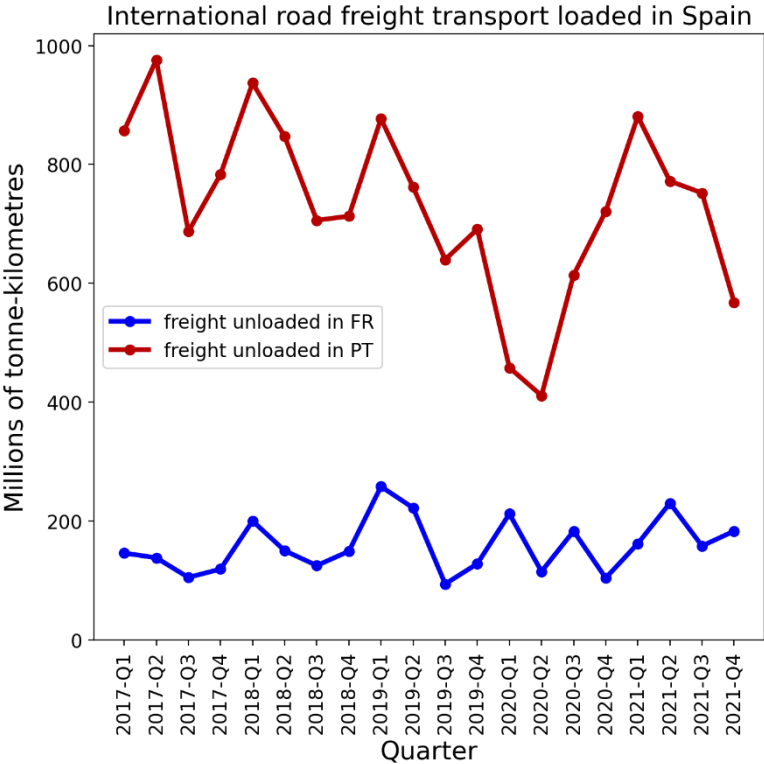


Figure 37: Millions of tonnes-kilometres of international road freight transport loaded in Spain and unloaded in each of Portugal and France, by economic quarter. Data from Eurostat (2024f).

Figure 38 shows the NUTS1 regions along Italy’s northern border with France, Switzerland, Austria, and Slovenia. Here (bottom panel) we can see that the large peaks in Italy’s two northern NUTS1 regions preceded the F-peaks in the bordering regions in France and Switzerland. However, the same cannot be said about the Austrian border regions, which had relatively small F-peaks, with rise-side half-maximum dates occurring less than one week after that of the Italian regions. Slovenia, which borders Italy to the northeast, did not have an F-peak (the NUTS1 region for Slovenia, SI0, covers the entire country).

IT borders with FR, CH, AT and SI (NUTS1 regions)

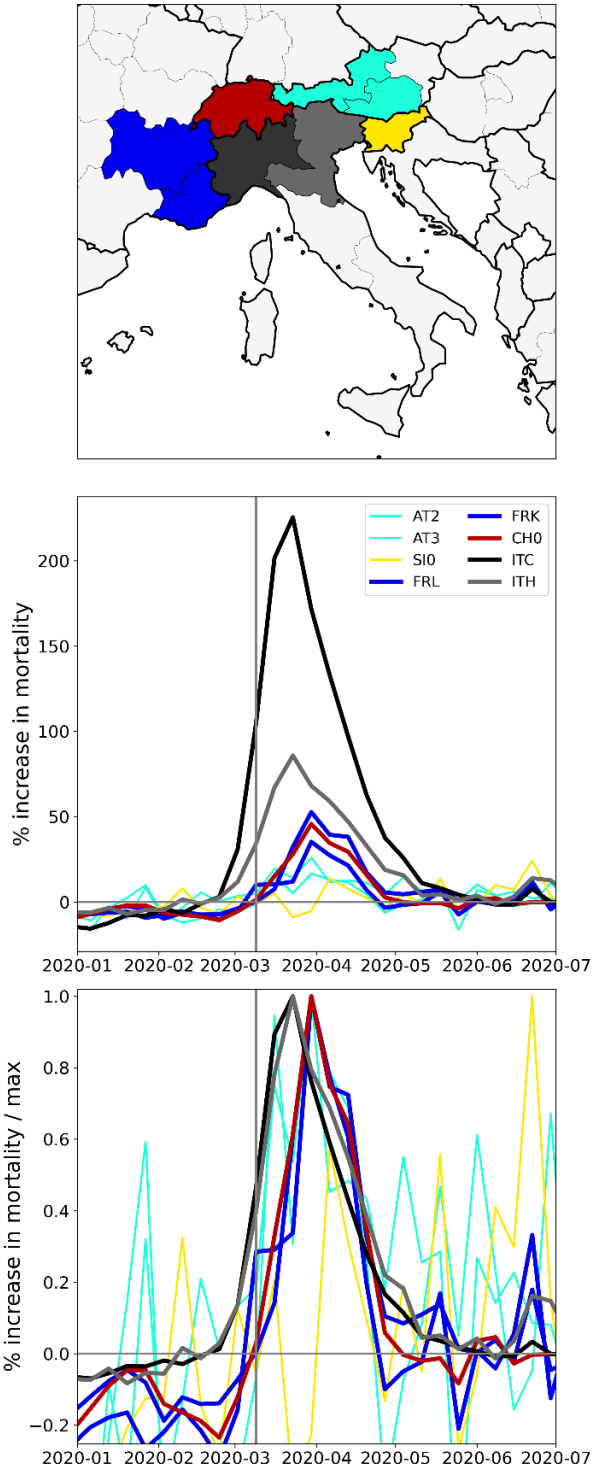


Figure 38: Top panel: Map of the bordering NUTS1 regions in Italy (black and grey) and France (blue), Switzerland (red), Austria (light blue), and Slovenia (yellow). Middle panel: weekly P-scores during the first-peak period for the regions shown in the top panel. Lower panel: same as middle panel, with each curve scaled by its maximum. Vertical grey lines in the lower two panels indicate the week of the WHO's pandemic declaration of 2020-03-11.

A study using Facebook data on daily border crossings showed that traffic across Italy’s borders with each of France, Switzerland, Austria, and Slovenia decreased by 75% compared to its pre-COVID level, during the first-peak period of 2020 (Docquier et al., 2022).

The volume of road freight traffic loaded in Italy and unloaded in each of France, Switzerland, Austria, and Slovenia was not substantially reduced during the first-peak period of 2020 (see Figure 39).

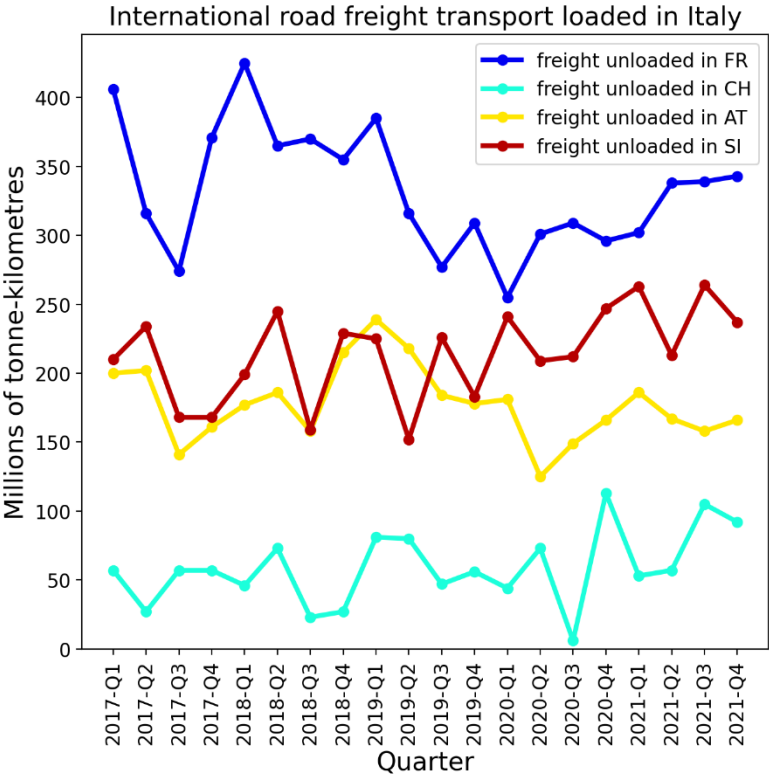


Figure 39: Millions of tonnes-kilometres of international road freight transport loaded in Italy and unloaded in each of France, Switzerland, Austria, and Slovenia, by economic quarter. Data from Eurostat (2024f).

There were thus large differences in excess mortality between the northern regions of Italy and those they border in France, Switzerland, Austria, and Slovenia, despite significant cross-border traffic during the first-peak period of 2020.

A more detailed examination of differences in excess mortality within large-population subnational regions within Italy, including Lombardy in the north and Lazio in the south, is contained in section 3.4.1.

Before addressing Italy in more detail, we first examine the timing of F-peaks in the United States, at the state and county level, in sections 3.3.5 and 3.3.6.

3.3.5 USA states

There is large heterogeneity in integrated first-peak period P-score values across USA states, as is shown in the heatmap in Figure 9. In this section, we compare the timing of the F-peaks in different states using graphs of weekly P-scores during the first-peak period.

Figure 40 shows the weekly P-scores for the four states with the highest integrated first-peak period P-scores: New York, New Jersey, Connecticut, and Massachusetts. The figure additionally includes Pennsylvania, which neighbours New York and New Jersey and had relatively moderate first-peak period excess mortality.

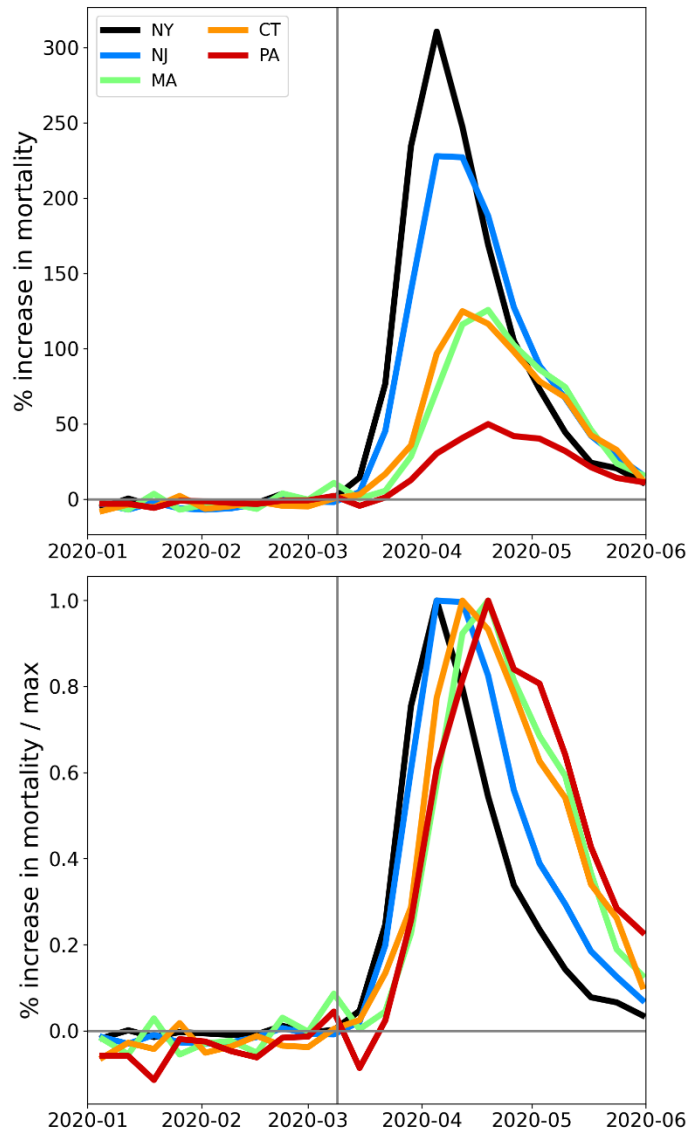
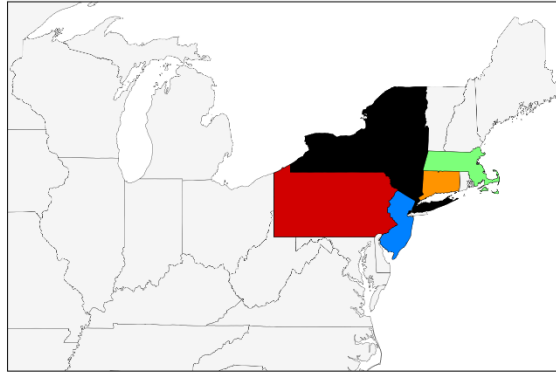


Figure 40: Top panel: Map of New York and four of its neighbouring states: New Jersey, Massachusetts, Connecticut, and Pennsylvania. Middle panel: weekly P-scores during the first-peak period. Lower panel: same as middle panel, with each curve scaled by its maximum. Vertical grey lines in the lower two panels indicate the week of the WHO's pandemic declaration of March 11, 2020.

The rise-side half-maximum date for New York and New Jersey is approximately two weeks after the week of the March 11, 2020 pandemic declaration, and the rise-side half-maximum date for Connecticut, Massachusetts, and Pennsylvania is approximately three weeks after the week of the March 11, 2020 pandemic declaration.

The FWHM for New York is about 4 weeks, for New Jersey it is about 5 weeks, and for Connecticut, Massachusetts, and Pennsylvania the FWHM is almost 6 weeks long.

Figure 41 shows the same thing as Figure 40, with Pennsylvania replaced by the District of Columbia (DC) and Rhode Island. Figure 41 thus shows the six states with the largest first-peak period integrated P-scores.

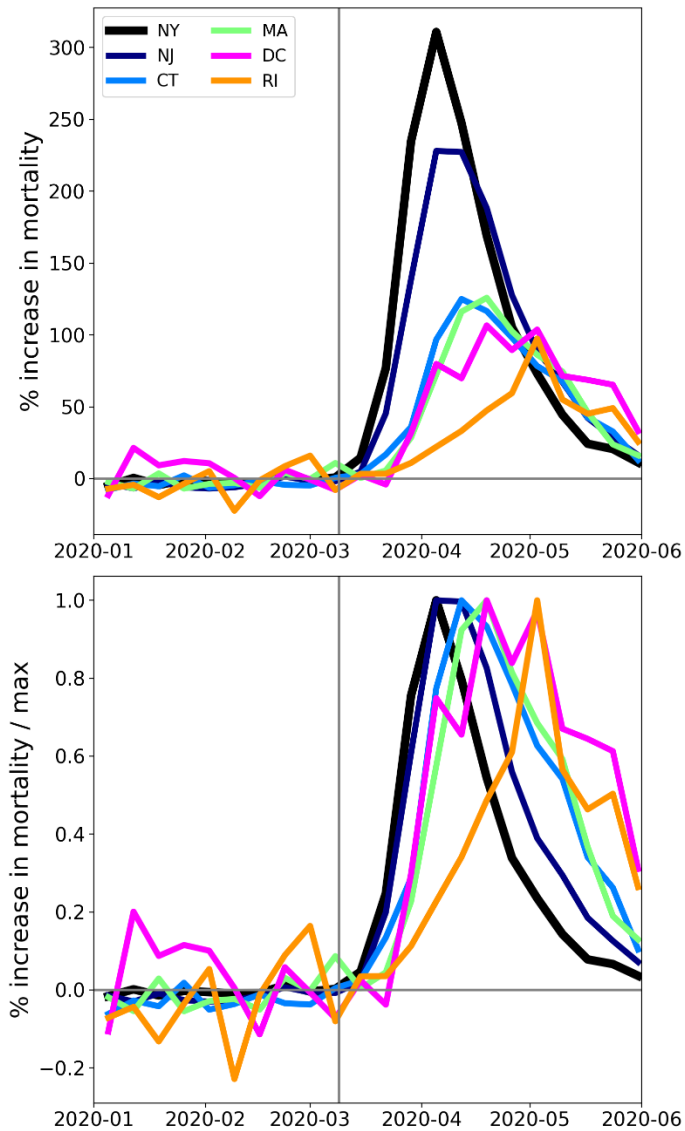
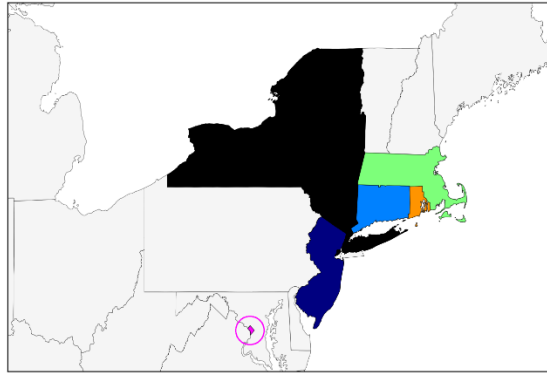


Figure 41: Top panel: Map of the six USA states with the largest integrated first-peak period P-scores: New York, New Jersey, Connecticut, Massachusetts, District of Columbia (inside the small pink circle), and Rhode Island. Middle panel: weekly P-scores during the first-peak period. Lower panel: same as

middle panel, with each curve scaled by its maximum. Vertical grey lines in the lower two panels indicate the week of the WHO's pandemic declaration of March 11, 2020.

As can be seen in Figure 41, the rise-side half-maximum date for DC is about three weeks after the week of the pandemic declaration (as for Connecticut and Massachusetts) and the rise-side half-maximum date for Rhode Island is about five weeks after the week of the pandemic declaration.

The FWHM for DC is about 7 weeks, and the FWHM for Rhode Island is about 4 weeks.

Figure 40 and Figure 41 therefore show that there were some differences in the timing and width of F-peaks in states with large integrated first-peak period P-scores, similar to the case of the European countries examined in section 3.3.1.

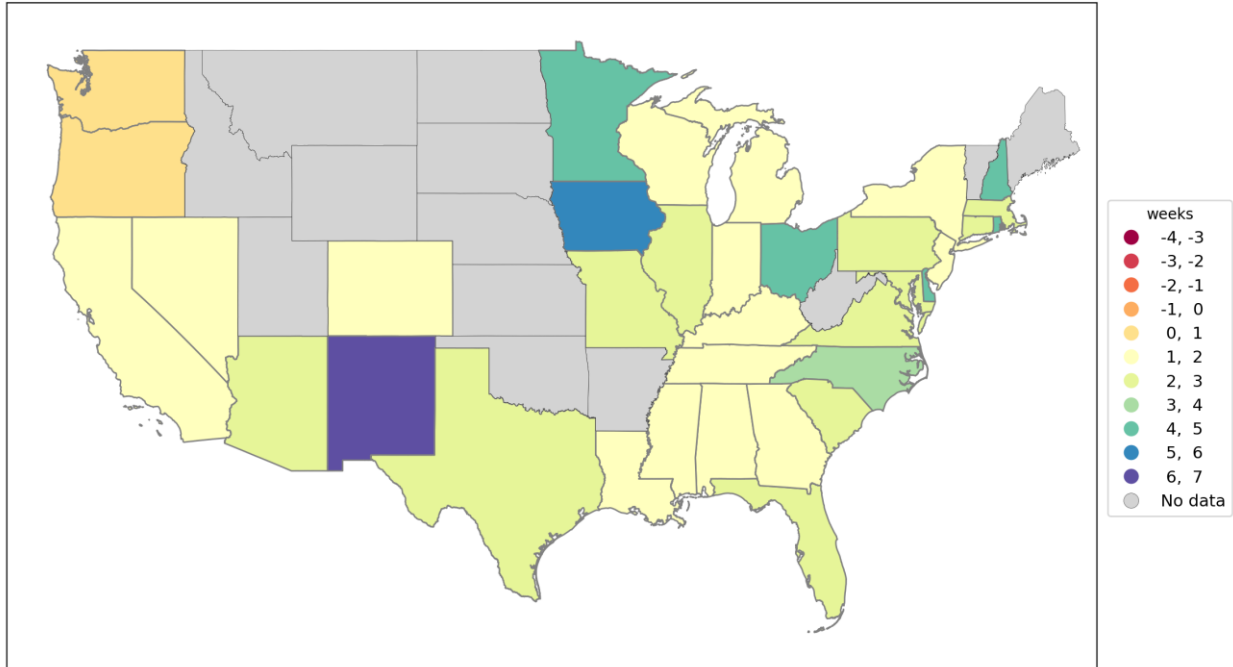
The timing of F-peaks for USA states is summarized in the map in the top panel of Figure 42, which shows the rise-side half-maximum dates for USA states with discernible F-peaks.

A state's F-peak was considered discernible if the state's integrated first-peak period P-score divided by its (1σ) error had a value of 3 or greater. A table of integrated first-peak period P-scores, 1σ error values, P-score / error ratios and rise-side half-maximum dates is included in Appendix D.1, and graphs showing weekly P-scores and weekly scaled P-scores for all USA states are included in Appendix A.2.

As can be seen from Figure 42, the majority of states with discernable F-peaks (28 of 36 = 78%) had rise-side half-maximum dates within one week of that of New York, i.e. within 1-3 weeks of the week of the pandemic declaration.

As can also be seen from Figure 42, the 13 states with identical rise-side half-maximum dates to New York, have a wide range of integrated first-peak period P-score values (bottom panel of Figure 42), extending from barely discernible to very large (New Jersey). Most of these states are far from New York. For example, Figure 43 shows a selection of four USA states that are geographically distant but which had identically-timed F-peaks: New York, Michigan, Louisiana and California.

Rise-side half-maximum date
(weeks since March 8-14, 2020)



% increase mortality (2020-03-01 to 2020-05-30)

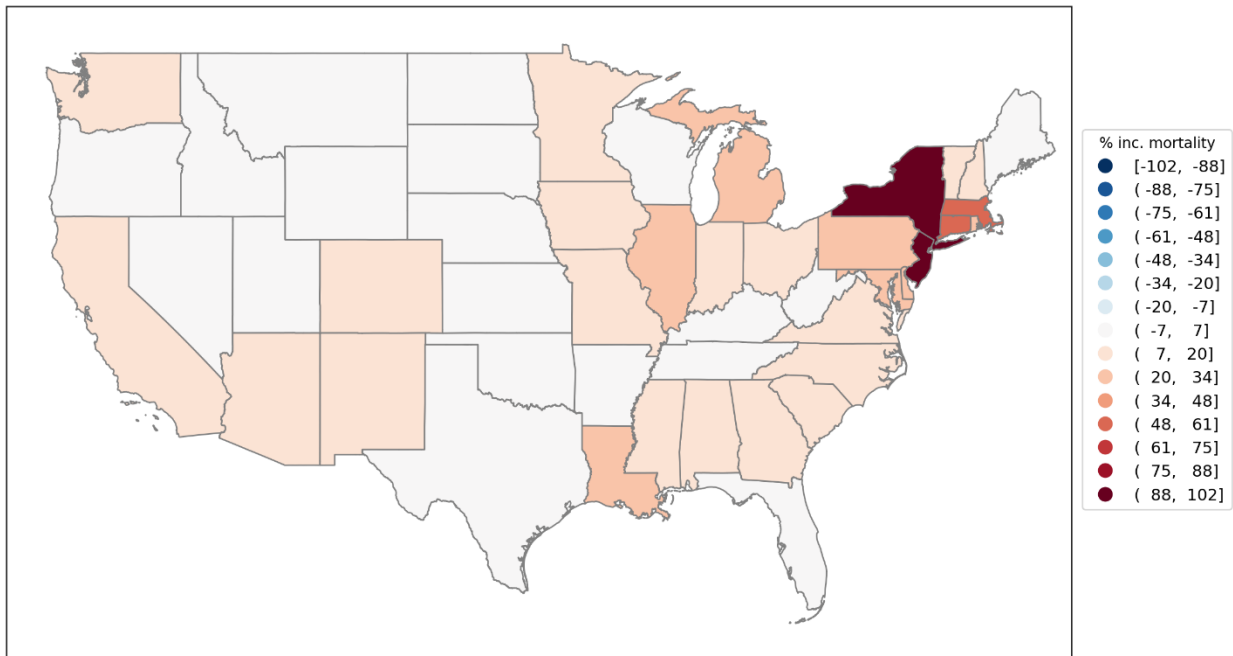


Figure 42: Top panel: Map of rise-side half-maximum dates for the F-peaks of USA states. Bottom panel: integrated first-peak period P-scores (%) for USA states (copy of Figure 9, for convenience). F-peaks for Hawaii and Alaska were indiscernible.

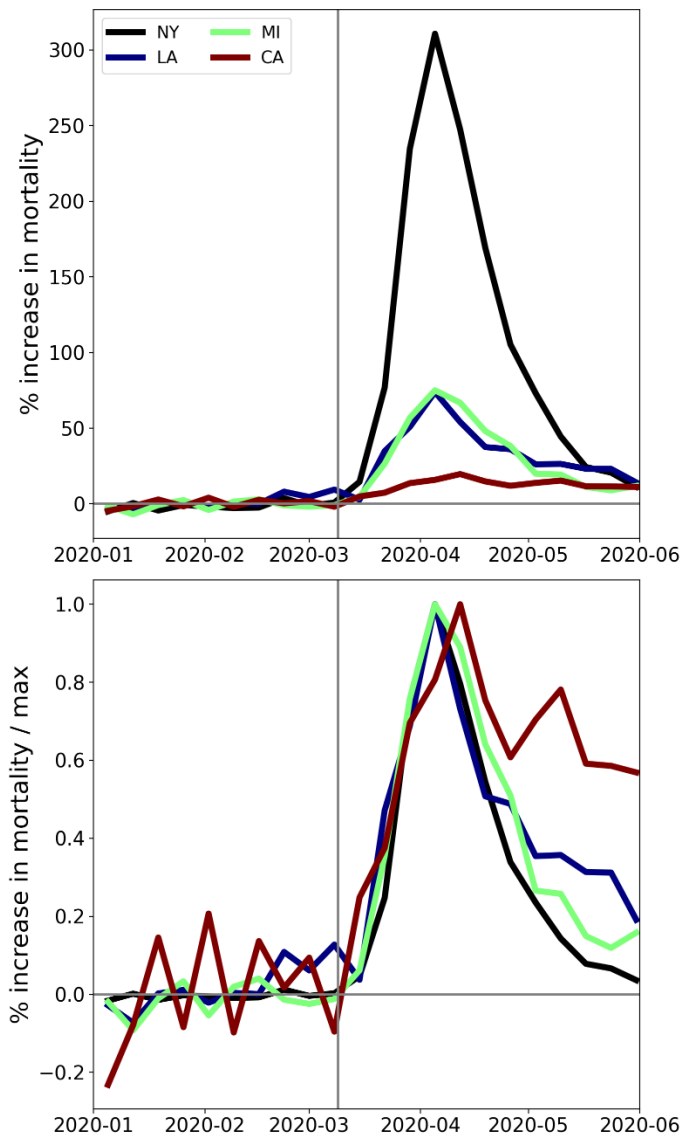
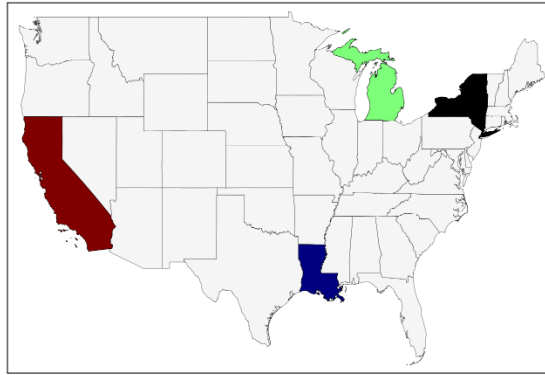


Figure 43: Top panel: Map of geographically distant states New York, Louisiana, Michigan and California. Middle panel: weekly P-scores for the states shown in the top panel. Lower panel: same as middle panel, with each curve scaled by its maximum. Vertical grey lines in the lower two panels indicate the week of the WHO’s pandemic declaration of March 11, 2020.

As can be seen in Figure 43 (middle panel), Michigan and Louisiana had large excess mortality peaks that were nonetheless dwarfed by that of New York, while California had discernible but relatively small first-peak period excess mortality. The rise-side half-maximum date for all four states is the same (slightly more than two weeks after the week of the pandemic declaration). The FWHM for New York and Louisiana is the same, about 4 weeks, while the FWHM for Michigan was about 5 weeks long.

The difference in excess mortality outcomes between New York and California is striking. Both states have large populations and urban areas, and both received significant air traffic volumes from China and East Asia in 2019 and early 2020, which is examined further in section 3.4.2.

Appendix A.2 contains additional figures showing the time-evolution of weekly P-scores for all USA states, organized in geographic subsets corresponding to USA census divisions. The figures in Appendix A.2 further demonstrate the high degree of heterogeneity in excess mortality patterns during the first-peak period. While several states had well-defined F-peaks, others either had essentially no first-peak period excess mortality, or significant excess mortality that did not exhibit a clearly defined peak, but rather extended beyond the first-peak period, similar to the case of California in Figure 43. Several states had relatively low excess mortality during the first-peak period, followed by higher excess mortality in the summer of 2020 (e.g. Texas, Alabama, Arkansas, Arizona, California, Florida, Georgia, Mississippi, Nevada, and South Carolina). The latter instances of high excess mortality in the summer of 2020 are shown in Appendix A.3, which contains graphs of weekly P-scores for each USA state for January to December of 2020.

3.3.6 USA counties

In this section we examine F-peaks at the level of USA counties. We focus on the counties within certain particular states that exhibited large F-peaks at the state level.

We find that, for the counties within a particular state, the county-level F-peaks, when they are present, are essentially synchronous.

Figure 44 shows results for the counties of New York State. As can be seen from the top-left and middle-left panels of Figure 44, large F-peaks were confined to the New York City urban area. The said peaks occurred in synchrony, as can be seen from the top-right (scaled) panel of the figure. Among the counties with large F-peaks, integrated first-peak period (March-May 2020) P-scores generally increased with population density (estimates from the 5-Year American Community Survey for 2017-2021) (lower-left panel of Figure 44) and with percent of the county's population living in poverty (estimates from the 5-Year American Community Survey for 2014-2018) (lower-right panel of Figure 44). These correlations are examined in more detail in section 3.6.1.

New York (counties)

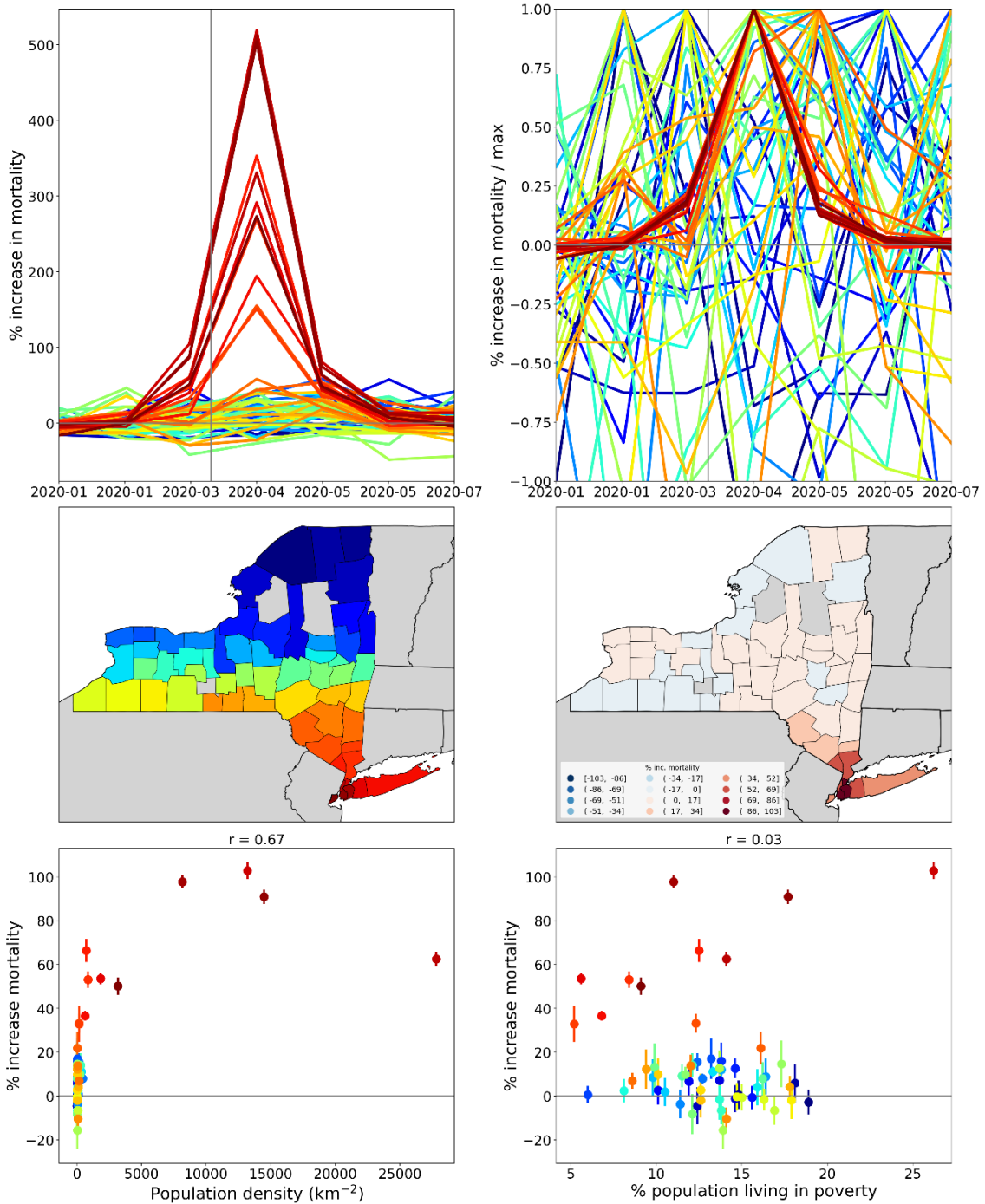


Figure 44: Top left: weekly P-scores for the counties of New York State. Top right: same as top left, with each curve scaled by its maximum. Middle left: map with counties colored as per the curves in top row and points in bottom row of panels. Middle right: heatmap showing integrated first-peak period (March-May 2020) P-score for each county. Bottom left: scatter plot of county integrated first-peak period P-score vs county population density. Bottom right: scatter plot of county integrated first-peak period P-score vs. county percent of population living in poverty. In the maps, dark grey (within NY State) indicates counties for which data was unavailable.

Figure 45 shows results for the counties of New Jersey. As can be seen, counties in the northern part of New Jersey had large F-peaks, especially the counties in the northeast of the state, which are within the New York City urban area. The peaks for the said northern counties rise and fall in synchrony, as can be seen from the top-right panel of the figure. The counties in the southern part of New Jersey had significantly smaller F-peaks, several of which occurred later in time than the peaks of the northern counties.

Similar to the case for New York State, among the New Jersey counties with large excess mortality peaks, integrated first-peak period P-scores generally increased with population density (lower-left panel) and with percent of the county's population living in poverty (lower-right panel).

New Jersey (counties)

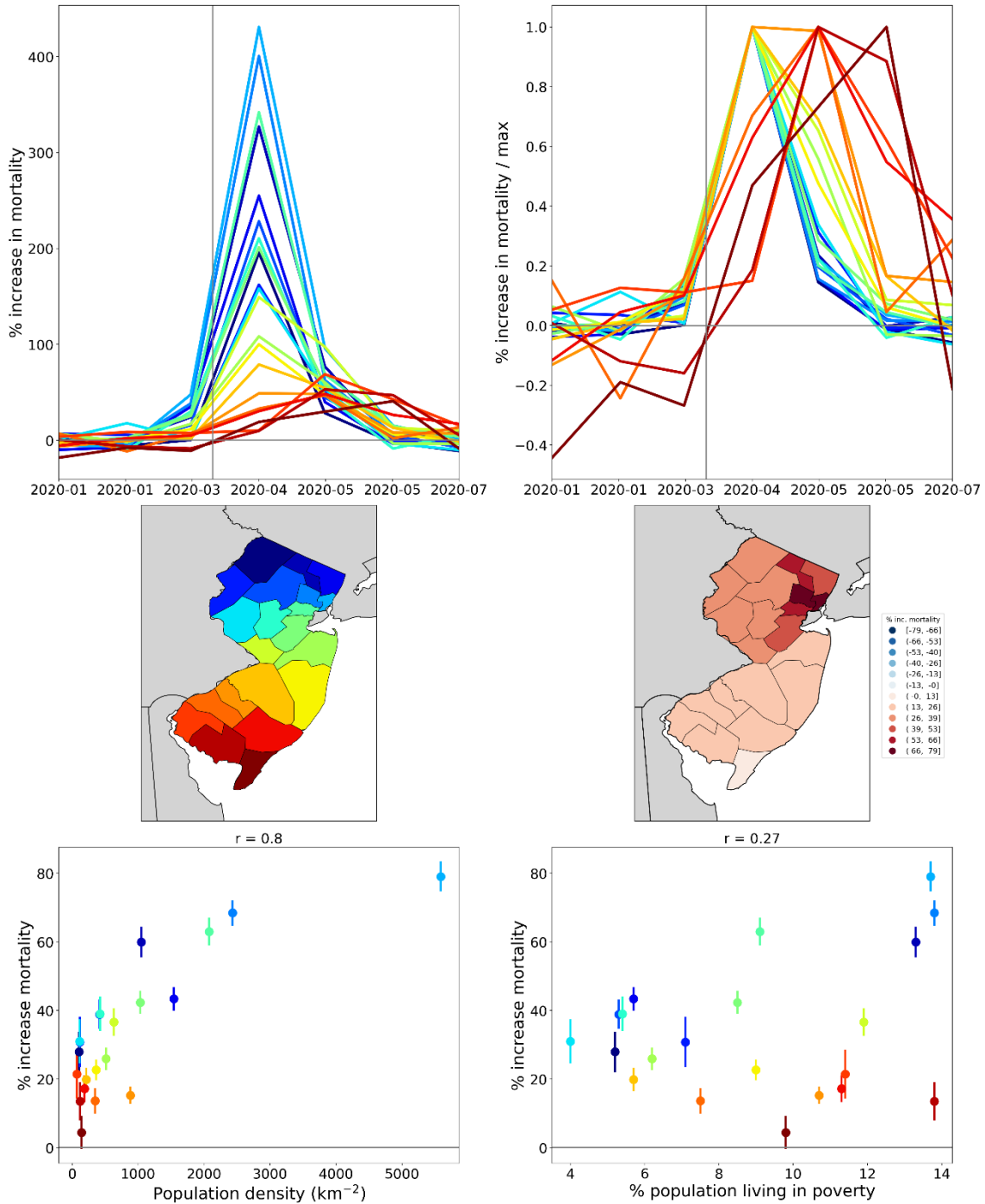


Figure 45: Top left: weekly P-scores for the counties of New Jersey. Top right: same as top left, with each curve scaled by its maximum. Middle left: map with counties colored as per the curves in top row and points in bottom row of panels. Middle right: heatmap showing integrated first-peak period (March-May 2020) P-score for each county. Bottom left: scatter plot of county integrated first-peak period P-score vs county population density. Bottom right: scatter plot of county integrated first-peak period P-score vs. county percent of population living in poverty.

Figure 46 shows results for the counties of Connecticut. Similar to the case for New Jersey, the largest peaks occurred in the counties within the New York City urban area, here in the western part of the state. The said western-county peaks rose and fell essentially in synchrony. Two low-population density counties in the eastern part of the state had smaller F-peaks that occurred later than the large peaks in the west.

For Connecticut, integrated first-peak period P-score increased with population density (lower-left panel), and there is a weak association between P-score and poverty (lower-right panel).

Connecticut (counties)

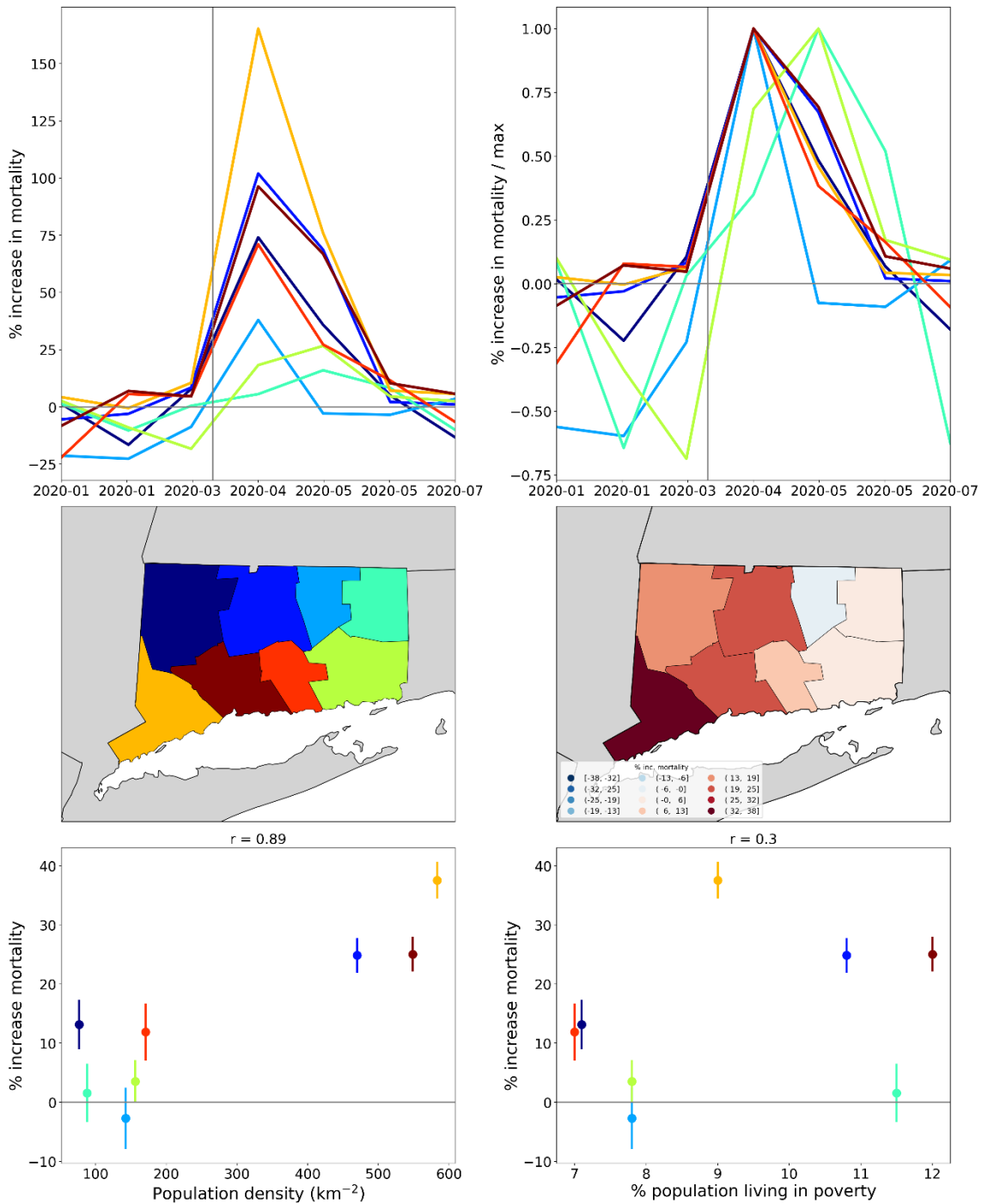


Figure 46: Top left: weekly P-scores for the counties of Connecticut. Top right: same as top left, with each curve scaled by its maximum. Middle left: map with counties colored as per the curves in top row and points in bottom row of panels. Middle right: heatmap showing integrated first-peak period (March-May 2020) P-score for each county. Bottom left: scatter plot of county integrated first-peak period P-score vs county population density. Bottom right: scatter plot of county integrated first-peak period P-score vs. county percent of population living in poverty.

Figure 47 shows results for the counties of Massachusetts.

The picture here is similar to the case of New Jersey and Connecticut, in that the largest F-peaks occurred in the higher-population density counties, which in this case are around the urban area of Boston. The said Boston-area peaks rose and fell essentially in synchrony. Three lower-population density counties outside of the Boston area (in the centre of the state and on the Cape Code peninsula in the south-east) had smaller F-peaks that occurred later in time; however, several other low population density counties that were far from Boston (e.g. Hampden County, in bright yellow) had F-peaks that occurred in synchrony with the peaks of the Boston area.

The relationship between county-level P-scores and various socioeconomic variables, including population density and poverty, are explored further in section 3.6.1, along with maps showing the geographic variation of the socioeconomic variables. The figures in section 3.6.1 include scatter plots for the counties of New York, New Jersey, Connecticut and Massachusetts, allowing a closer comparison of the relationship between integrated first-peak period P-score and socioeconomic variables in these four states, three of which contain parts of the New York City urban area. For example, from the figures and maps in section 3.6.1, it can be seen that integrated first-peak period P-score has a non-linear relationship with poverty for these four states, because poverty is highest at the centres of the New York City and Boston urban areas (where first-peak P-scores were high), decreases moving away from the inner-city and into the suburbs (where first-peak P-scores were moderate), and then increases again moving beyond the suburbs and into the rural areas (where first-peak P-scores are low).

Massachusetts (counties)

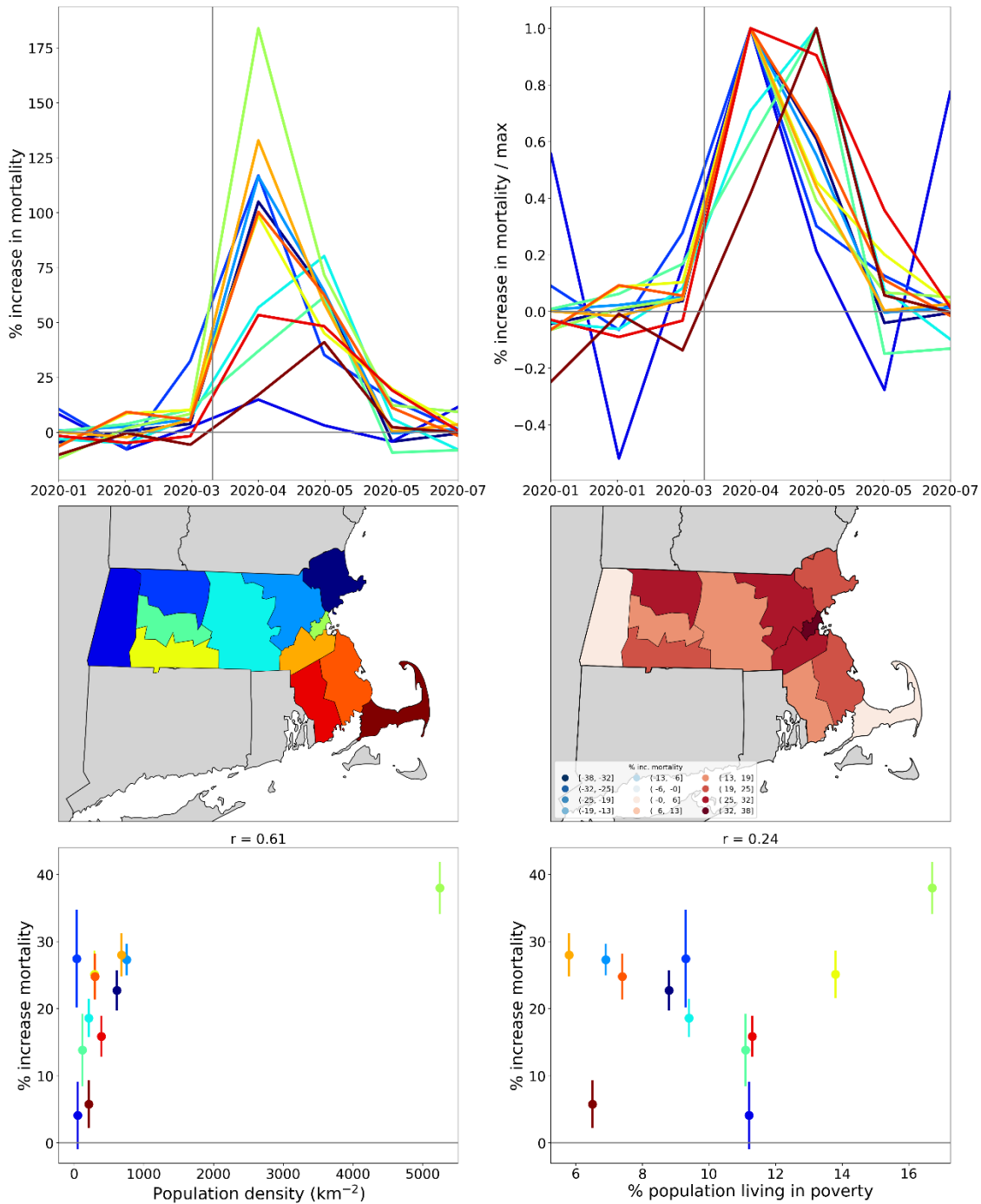


Figure 47: Top left: weekly P-scores for the counties of Massachusetts. Top right: same as top left, with each curve scaled by its maximum. Middle left: map with counties colored as per the curves in top row and points in bottom row of panels. Middle right: heatmap showing integrated first-peak period (March-May 2020) P-score for each county. Bottom left: scatter plot of county integrated first-peak period P-score vs county population density. Bottom right: scatter plot of county integrated first-peak period P-score vs. county percent of population living in poverty. In the maps, dark grey (within Massachusetts) indicates counties for which data was unavailable.

Figure 48 to Figure 53 show results for the counties of Pennsylvania, Michigan, and Louisiana. For each state, there is one figure showing results for all counties of the state, and a second figure showing the same results for only the 10 most populous counties in the state, to aid with visualization.

The F-peaks for counties with large excess mortality in these states rose and fell essentially in synchrony.

Integrated first-peak period P-scores generally increased with population density in these states (lower-left panels), although Louisiana had high integrated first-peak period P-scores in some lower population density counties.

The scatter plots for these states do not reveal a simple relationship between excess mortality and poverty, although we do note that the Pennsylvania's county with the highest integrated first-peak period P-score (Philadelphia County, PA) also has the highest population density and percent living in poverty in the state, which is similar to the results for the New York City urban area, as explored further below in section 3.6.1.

Pennsylvania (counties)

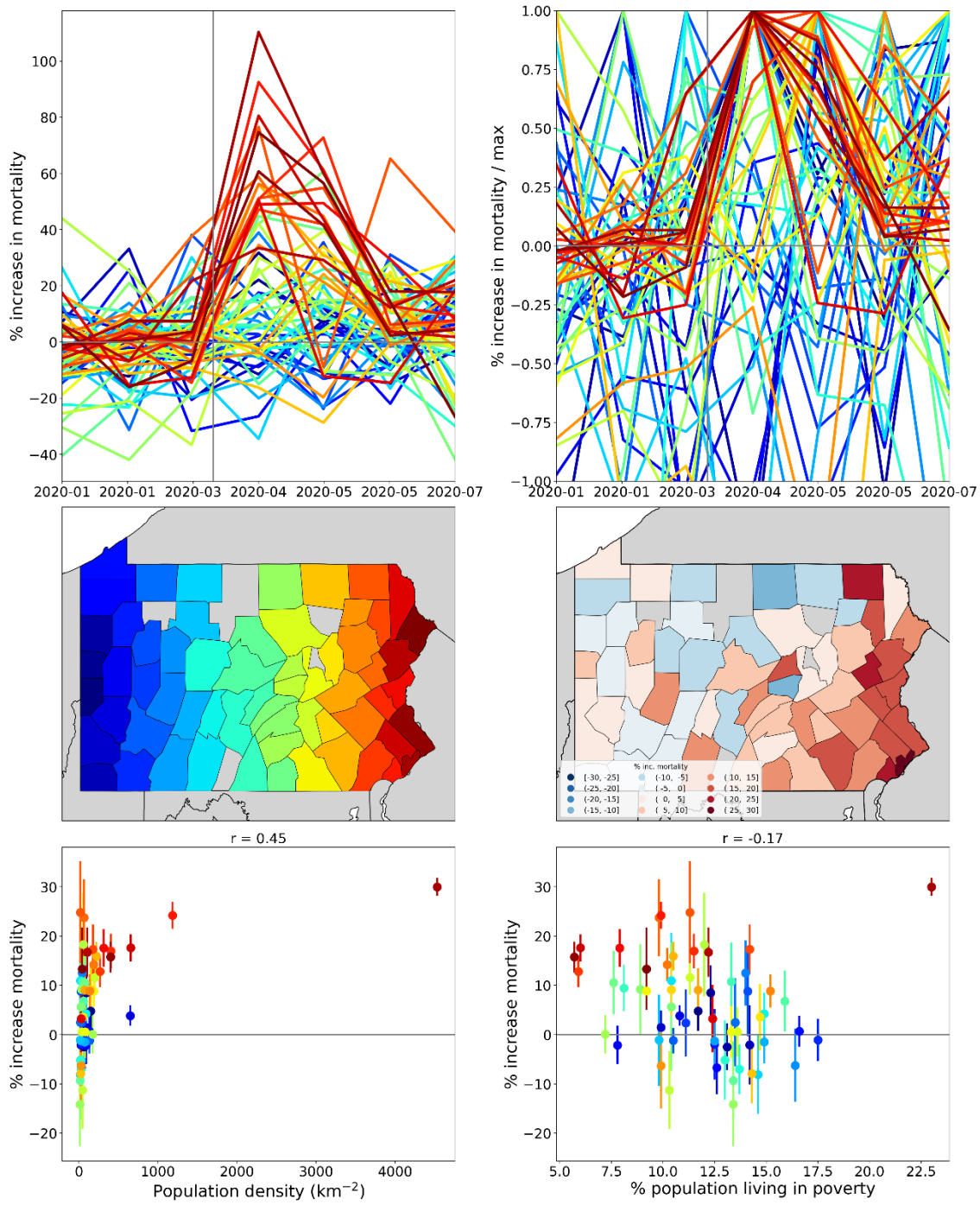


Figure 48: Top left: weekly P-scores for the counties of Pennsylvania. Top right: same as top left, with each curve scaled by its maximum. Middle left: map with counties colored as per the curves in top row and points in bottom row of panels. Middle right: heatmap showing integrated first-peak period (March-May 2020) P-score for each county. Bottom left: scatter plot of county integrated first-peak period P-score vs county population density. Bottom right: scatter plot of county integrated first-peak period P-score vs. county percent of population living in poverty. In the maps, dark grey (within Pennsylvania) indicates counties for which data was unavailable.

Pennsylvania (10 most populous counties)

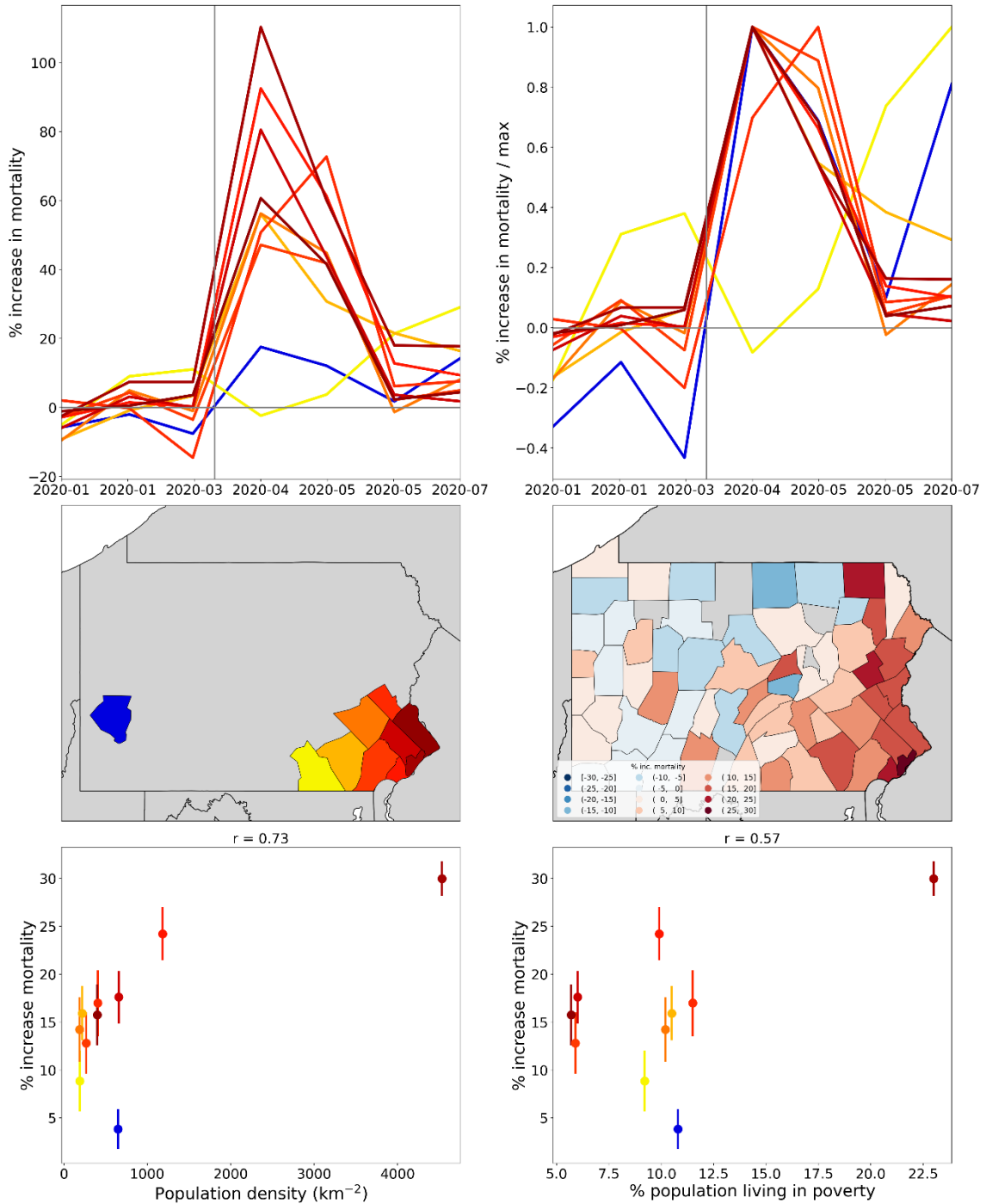


Figure 49: Same as Figure 48, showing only the 10 most populous counties in Pennsylvania.

Michigan (counties)

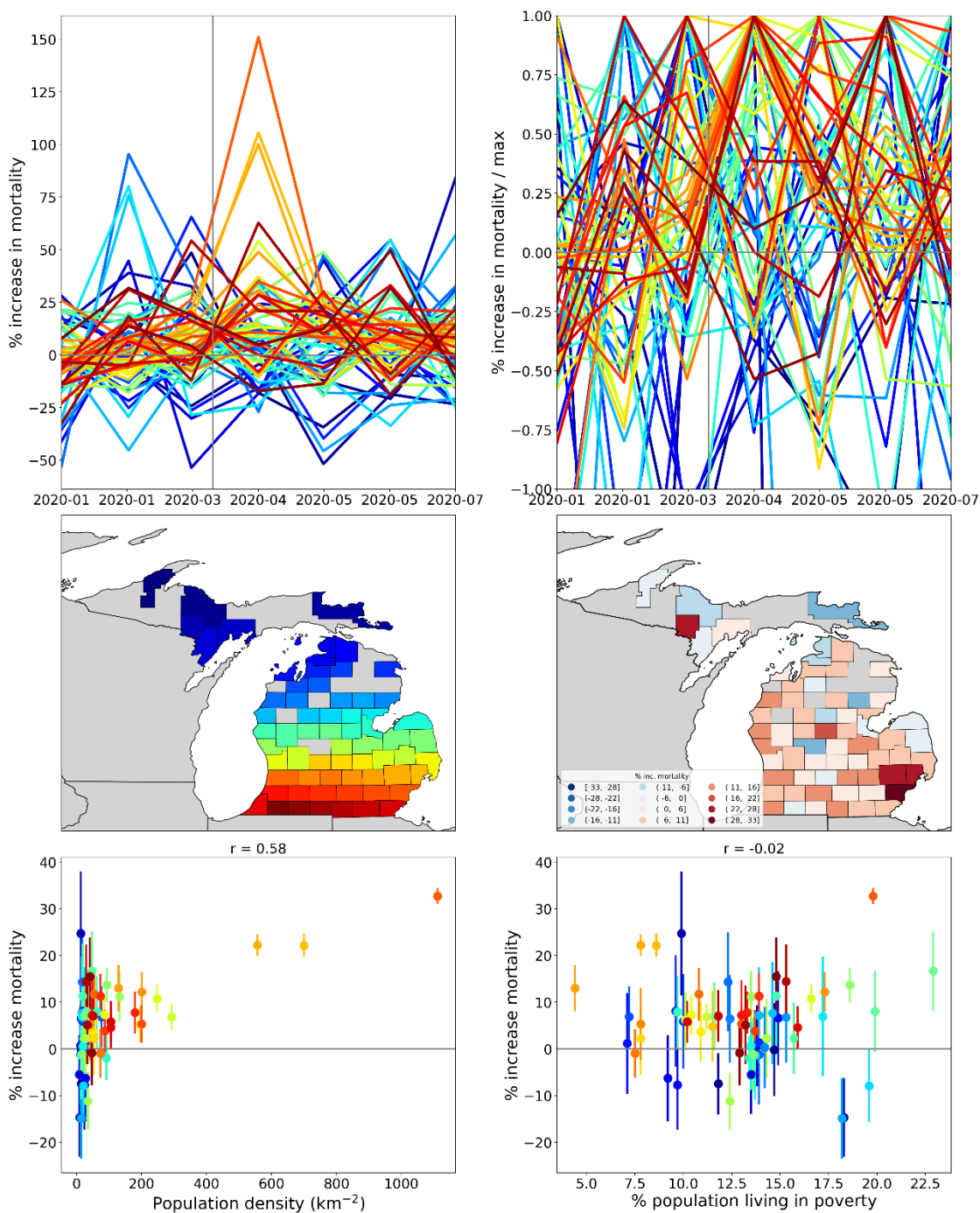


Figure 50: Top left: weekly P-scores for the counties of Michigan. Top right: same as top left, with each curve scaled by its maximum. Middle left: map with counties colored as per the curves in top row and points in bottom row of panels. Middle right: heatmap showing integrated first-peak period (March-May 2020) P-score for each county. Bottom left: scatter plot of county integrated first-peak period P-score vs county population density. Bottom right: scatter plot of county integrated first-peak period P-score vs. county percent of population living in poverty. In the maps, dark grey (within Michigan) indicates counties for which data was unavailable.

Michigan (10 most populous counties)

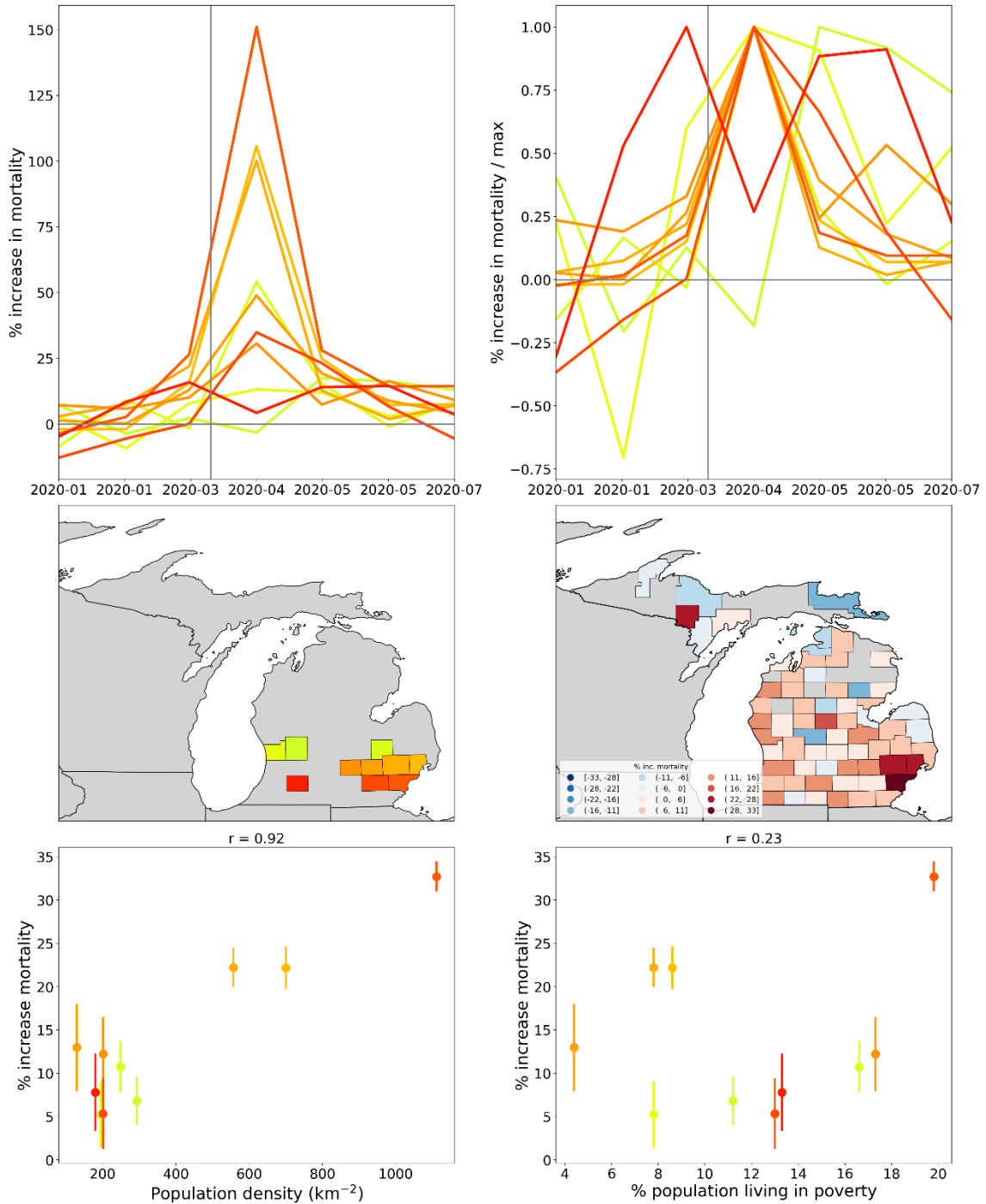


Figure 51: Same as Figure 50, showing only the 10 most populous counties in Michigan.

Louisiana (counties)

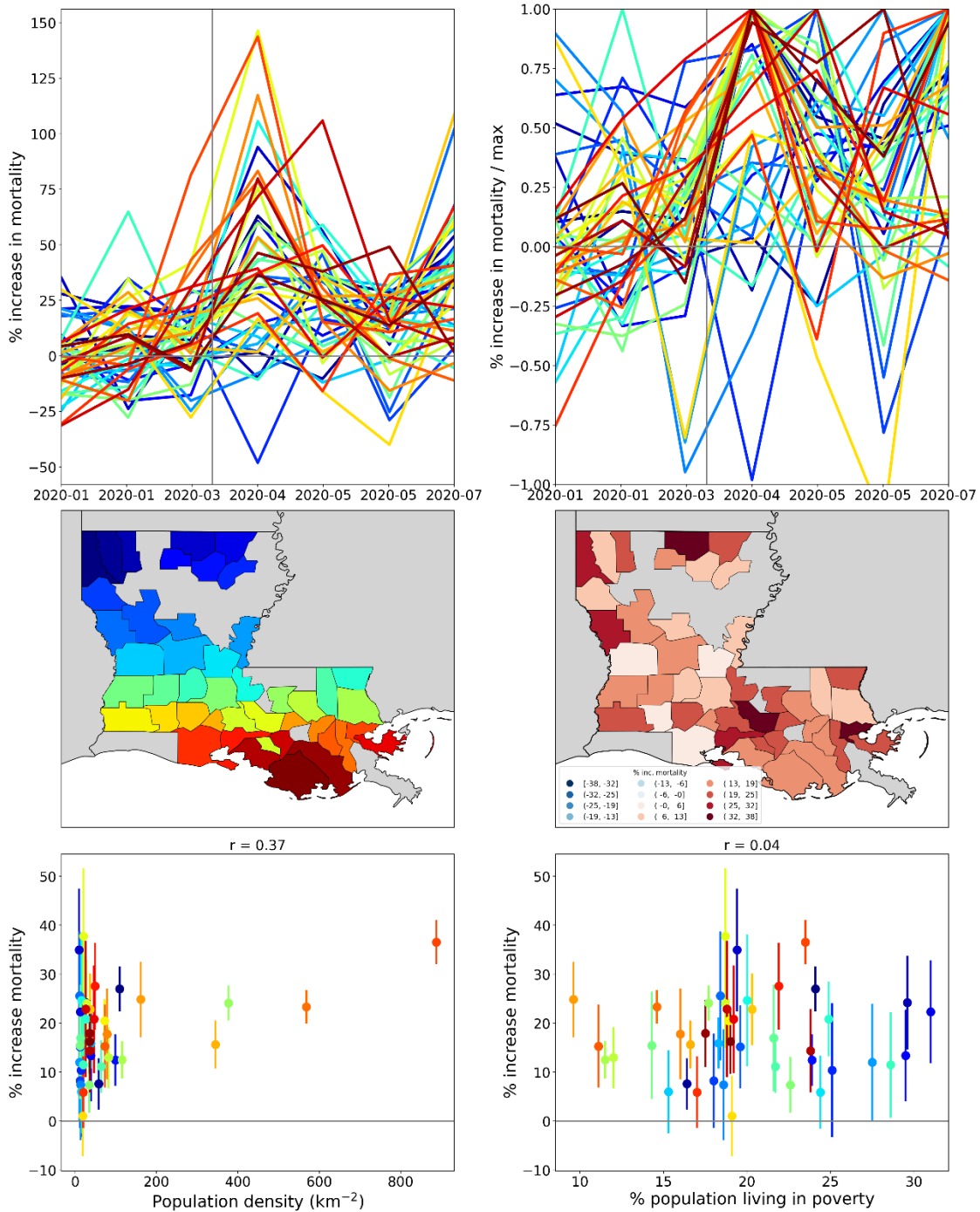


Figure 52: Top left: weekly P-scores for the counties of Louisiana. Top right: same as top left, with each curve scaled by its maximum. Middle left: map with counties colored as per the curves in top row and points in bottom row of panels. Middle right: heatmap showing integrated first-peak period (March-May 2020) P-score for each county. Bottom left: scatter plot of county integrated first-peak period P-score vs county population density. Bottom right: scatter plot of county integrated first-peak period P-score vs. county percent of population living in poverty. In the maps, dark grey (within Louisiana) indicates counties for which data was unavailable.

Louisiana (10 most populous counties)

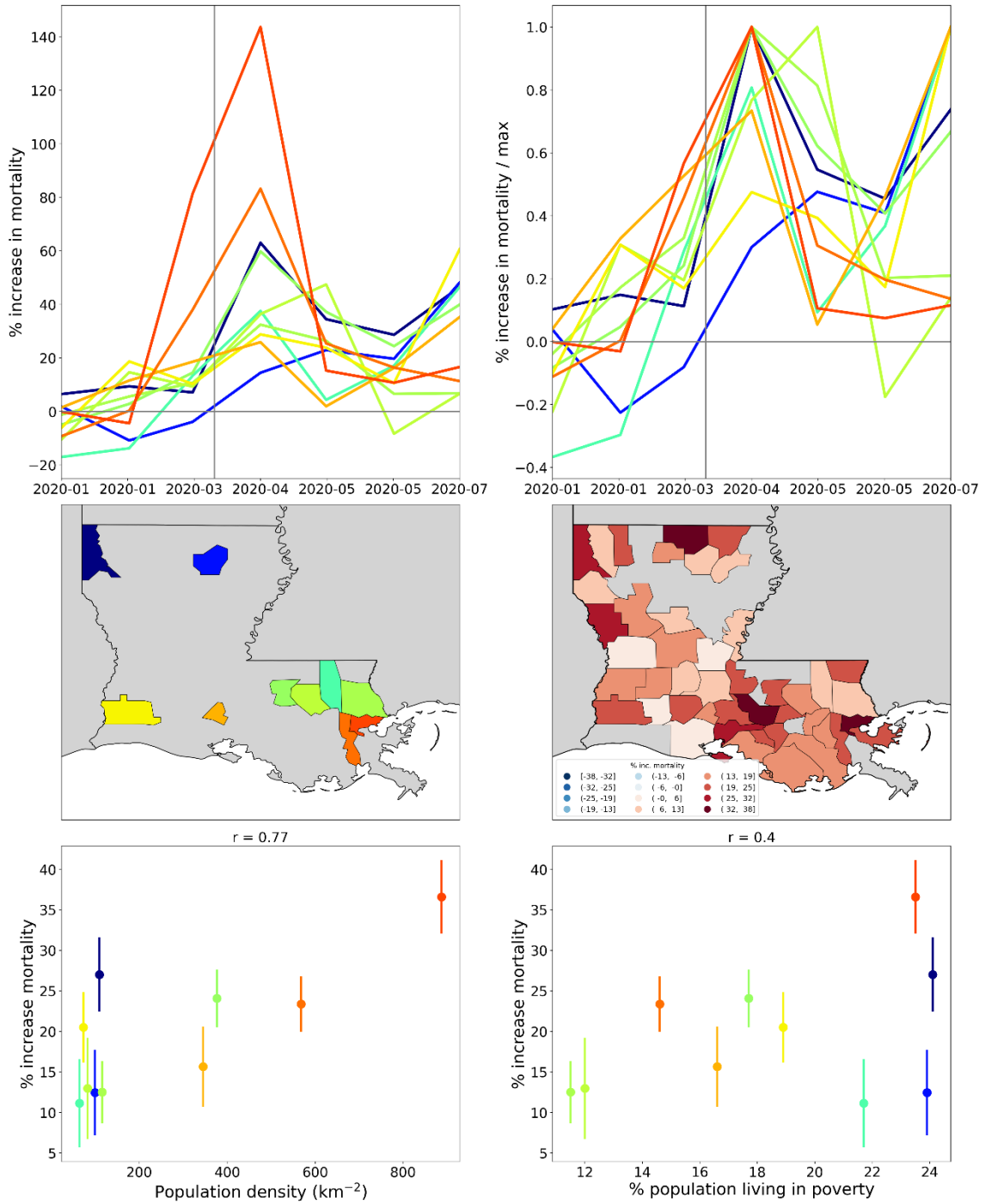


Figure 53: Same as Figure 52, showing only the 10 most populous counties in Louisiana.

3.4 Differing excess mortalities between regions with large international airports

In this section we compare the first-peak period excess mortalities of urban areas with large international airports in Italy (Rome vs Milan) and the United States (New York City vs Los Angeles and San Francisco). We compare the demographic and health system characteristics for these urban areas, as well as statistics on air passenger travel to and from China and East Asia prior to Covid.

3.4.1 *The case of Rome vs Milan in Italy*

Italy was the first European country to experience a rise in excess mortality in March 2020, and its F-peak is positioned earliest in time among European countries, with a rise-side half-maximum date equal to the week of the WHO's March 11, 2020 pandemic declaration (week of March 9-15, 2020), as shown in section 3.3.1.

Figure 54 shows results for five Italian NUTS2 regions: Piedmont, Lombardy, Veneto, Lazio and Campania.

The top panel of Figure 54 contains a map indicating the said five regions, and showing the locations (star markers) of the five largest airports in Italy by passenger volume:

1. Rome Fiumicino (FCO), in the Lazio NUTS2 region
2. Milan Malpensa (MXP) in the Lombardy NUTS2 region, which also serves the Piedmont NUTS2 region
3. Milan Bergamo (BGY) in the Lombardy NUTS2 region
4. Venice Marco Polo (VCE) in the Veneto NUTS2 region
5. Naples International Airport (NAP) in the Campania NUTS2 region

The middle panel of Figure 54 shows the weekly P-score values for each of the five regions. As can be seen, Lombardy region (which contains Milan) had an enormous F-peak, reaching a maximum of more than 300% in the week of March 30, 2020, and neighbouring Piedmont also had a large F-peak. In contrast, Lazio (the region containing Rome) and Campania (containing Naples) had comparatively negligible excess mortality during the first-peak period.

Italy, NUTS2 regions with 5 busiest airports

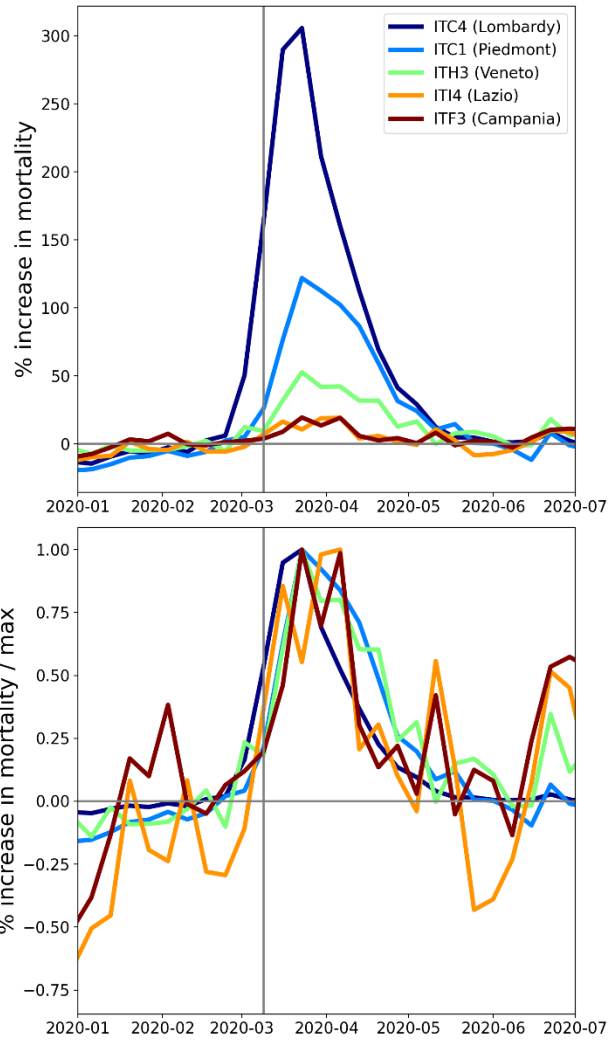
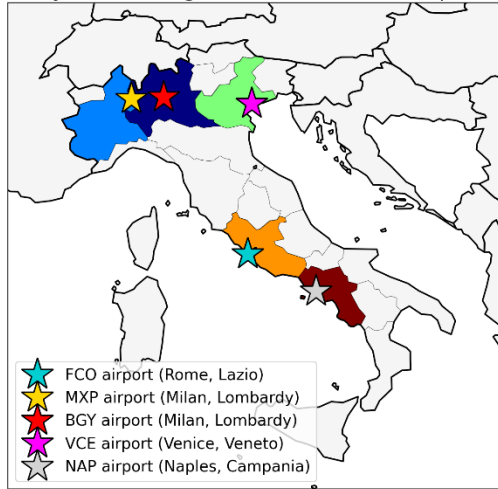


Figure 54: Top panel: Map of locations of the five busiest airports in Italy (stars) within their respective NUTS2 regions. Middle panel: Weekly P-scores for the five indicated NUTS2 regions. Bottom panel: Same as middle panel, with each curve scaled by its maximum.

Table 1 shows statistics about passenger volumes at the five largest Italian airports.

As can be seen from Table 1, Rome’s FCO airport had roughly the same number of total passengers in 2019 as the sum of the two large airports in the Lombardy region (MXP and BGY), and FCO had a significantly higher volume of passenger traffic to and from Chinese airports in each of 2017, 2018 and 2019, and more passenger traffic to and from airports in the Asia Pacific region in 2019, than the two Milan-area airports together.

Airport Name	Code	NUTS2 region	Total Passengers (2019)*	Num. passengers arriving directly from or traveling directly to a Chinese airport‡			Num. passengers directly to or from an Asia Pacific airport*** (2019)
				2017*	2018**	2019***	
Rome Leonardo da Vinci-Fiumicino	FCO	IT14 (Lazio)	43,354,887	443,762	413,882	506,898	2,019,300
Milan Malpensa	MXP	ITC4 (Lombardy) ITC1 (Piedmont)	28,705,638	246,437	272,783	346,887	1,269,474
Milan Bergamo	BGY	ITC4 (Lombardy)	13,792,266	none reported	none reported	none reported	0
Venice Marco Polo	VCE	ITH3 (Veneto)	11,507,301	none reported	none reported	none reported	73,247
Naples International Airport	NAP	ITF3 (Campania)	10,796,590	none reported	none reported	none reported	208

Table 1: Statistics on passenger volumes at Italy’s five busiest airports. Notes:

***Source: ENAC (2017); **Source: ENAC (2018); ***Source: ENAC (2019); ‡Only routes with more than 50,000 passengers per year were reported.**

Table 2 has demographic and health care characteristics of the NUTS2 regions in which the airports are located.

As can be seen from Table 2, Rome’s NUTS2 region (Lazio) and Milan’s NUTS2 region (Lombardy) had very similar demographic and health care characteristics in 2020, including similar values for the share of the population aged 65+ (22.2% in Lazio, 22.9% in Lombardy), share of the region’s population aged 80+ (7.0% in Lazio, 7.4% in Lombardy), number of hospital beds in the region per person aged 65+ (1.59% in Lazio, 1.58% in Lombardy) and the number of ICU beds in the region per person aged 65+ (0.038% in Lazio, 0.032% in Lombardy). The two regions also had virtually identical all-ages mortality rates (total number of deaths divided by

total population) for 2019. Despite these similarities, Lombardy had an integrated first-peak period P-score of 106%, roughly 18 times greater than that of Lazio (5.8%).

NUTS2 region	ITI4 (Lazio)	ITC4 (Lombardy)	ITC1 (Piedmont)	ITH3 (Veneto)	ITF3 (Campania)
Population in 2020 (millions) *	5.76	10.03	4.31	4.88	5.71
All-ages mortality rate in 2019 (per 1000 persons) *	10.1	10.1	12.4	10.1	9.5
Share pop. aged 65+ in 2020 (%) *	22.2	22.9	25.9	23.3	19.3
Share pop. aged 80+ in 2020 (%) *	7	7.4	8.6	7.3	5.3
Num. beds in hospitals in region in 2020 **	20,268	36,383	15,332	15,799	14,582
Num. beds in hospitals in region in 2020 / Population of region in 2020	1.59	1.58	1.34	1.35	1.33
Num. ICU beds in region in 2017 †	486	738	299	468	427
Num. ICU beds in region in 2017 / Num. people in region aged 65+ in 2020 (%)	0.038	0.032	0.027	0.041	0.039
Integrated first-peak period P-score and 1σ error (%)	5.8 ± 1.7	106.2 ± 2.5	47.9 ± 2.1	21.0 ± 1.7	6.6 ± 1.8

Table 2: Demographic characteristics of the NUTS2 regions in which Italy's five busiest airports are located. Notes: *Source: Eurostat (2024b); **Source: Eurostat (2024g); †Source: Pecoraro et al. (2020).

3.4.2 The case of New York City vs Los Angeles and San Francisco in the USA

Similar results to those for Rome and Milan in Italy are observed for USA urban areas served by major airports.

Figure 55 shows a heatmap of integrated first-peak period P-scores for the counties of the contiguous USA with sufficient data (same as the top panel of Figure 11), overlaid with circles centred on the eight urban areas with the largest airports by passenger traffic. The eight urban

areas, by decreasing order of total international air passengers served in 2019 are: New York City (NY), Miami (FL), Los Angeles (CA), San Francisco (CA), Chicago (IL), Atlanta (GA), Houston (TX) and Dallas (TX).

The diameters of the circles are proportional to urban area population (green), total number of international air passengers served in 2019 (blue) and the number of flights arriving from China in January 2020 (red).

The west coast cities of San Francisco and Los Angeles received large shares of their air traffic from China prior to the pandemic declaration of March 11, 2020, yet both cities had low first-peak period excess mortality. In contrast, New York City received fewer direct flights from China but had very high first-peak period excess mortality.

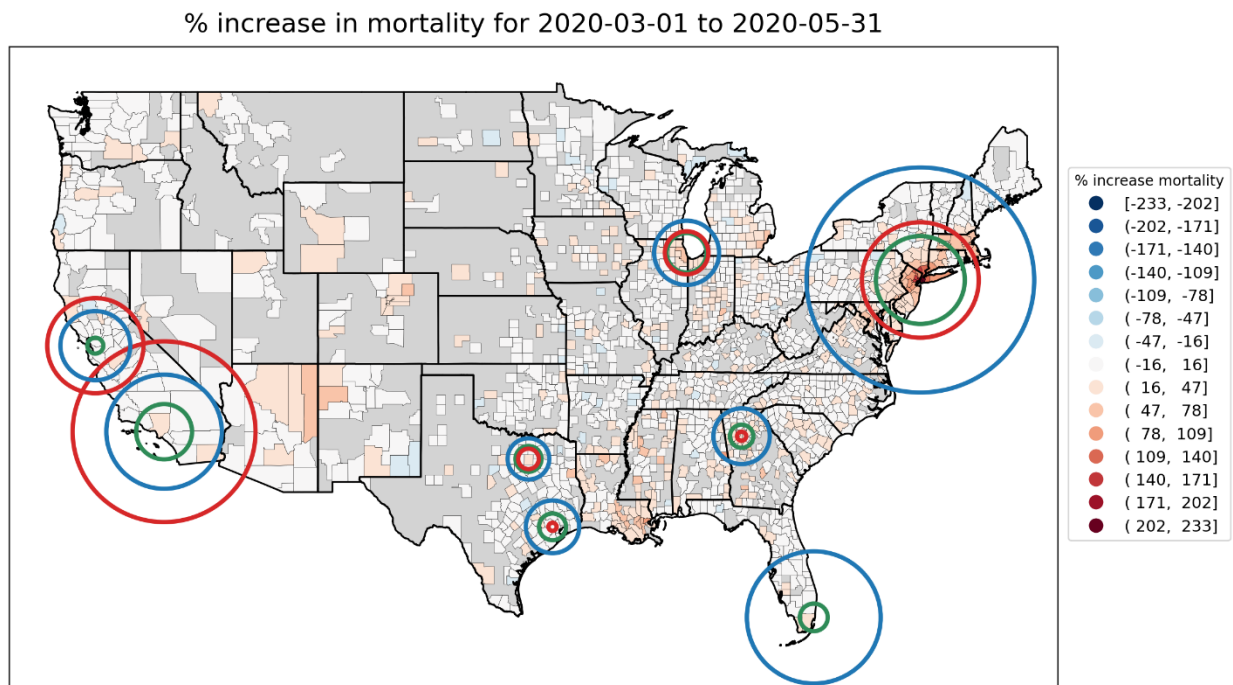


Figure 55: Integrated first-peak period P-scores for USA counties (heatmap) with circles centred on urban areas with major airports: New York City (NY), Miami (FL), Los Angeles (CA), San Francisco (CA), Chicago (IL), Atlanta (GA), Houston (TX) and Dallas (TX). Circle diameters are proportional to: green: urban-area population in 2020 (US Census Bureau, 2024c); blue: total number of international air passengers served in 2019 (Department of Transportation, 2020); red: number of flights arriving from China in January 2020 (Eder et al., 2020). Dark grey indicates counties for which data was unavailable.

The comparison between New York City and Los Angeles or San Francisco, is similar to the comparison between Milan and Rome. Table 3 shows several demographic, socioeconomic and health care system statistics for the three USA cities.

	New York City	Los Angeles	San Francisco
Total population (millions)	8.44	10.1	7.68
Total area (km ²)	778	10500	17900
Population density (km ⁻²)	10800	962	429
% population aged 65+	14.1	12.9	14.6
% living in poverty	18.6	15.7	9.1
% minority	67.9	73.7	60.3
% pop. that speaks English "less than well"	11.7	12.8	7.6
% pop. aged 25+ with no high school diploma	12.9	14.5	8.1
% households with more people than rooms	9.0	11.4	6.7
% single-parent households	9.6	9.4	6.6
Num. ICU beds per total pop. (%)	0.019	0.021	0.020
Num. ICU beds per pop. aged 65+ (%)	0.13	0.16	0.13
Integrated first-peak period P-score and 1 σ error (%)	200.2 \pm 2.5	23.9 \pm 1.8	7.3 \pm 1.3

Table 3: Demographic, socioeconomic, and health care system statistics for New York City (5 counties constituting the 5 boroughs of NYC), Los Angeles (Los Angeles County), and San Francisco (9 counties of the SF urban area: San Francisco, Marin, Sonoma, Napa, Solana, Contra Costa, Alameda, Santa Clara and San Mateo Counties). Data sources specified in section 2.

3.5 Deaths by institutional location for USA states and counties

In this section, we examine data regarding place of death during the first-peak period (March-May 2020), for USA states and counties.

In the following analyses, we focus on shares of deaths per institutional location. Graphs showing the number of deaths per month per institutional location, for each USA state, are included in Appendix B.

Figure 56 shows the shares (as fractions) of all of a given USA state’s first-peak period deaths that occurred in each of nine different locations (indicated in the legend below the figure), versus the integrated first-peak period P-score for the state, whereas in the bottom panel, the x-axis lists the state codes in order of increasing integrated first-peak period P-score.

As can be seen, there are three predominant death locations: “Medical Facility – Inpatient”, “Decedent’s home”, and “Nursing home or long-term care”.

The top panel of Figure 56 shows that the states of the USA can be grouped into five groups based on first-peak period P-score: one group with P-scores less than 22% (40 states), another group with P-scores of approximately 30% (six states: RI, MD, LA, IL, MI, DE), a third group with P-scores of approximately 50% (three states: CT, MA, DC), a fourth group comprising solely the

state of New Jersey with P-score = 85%, and a fifth group comprising solely the state of New York with P-score = 96%.

As can be seen from both the top and bottom panels of Figure 56, the third, fourth, and fifth groups (i.e., the five states with the highest integrated first-peak period P-scores: NY, NJ, CT, MA, DC) are not only distinguished from all other states by their large P-scores, but also by the fact that the largest share of deaths in these states during the first-peak period occurred in hospitals (“Medical Facility – Inpatient”), rather than at home (as for most other states) or in long-term care (in Rhode Island (RI), Minnesota (MN), Iowa (IA), North Dakota (ND) and South Dakota (SD)).

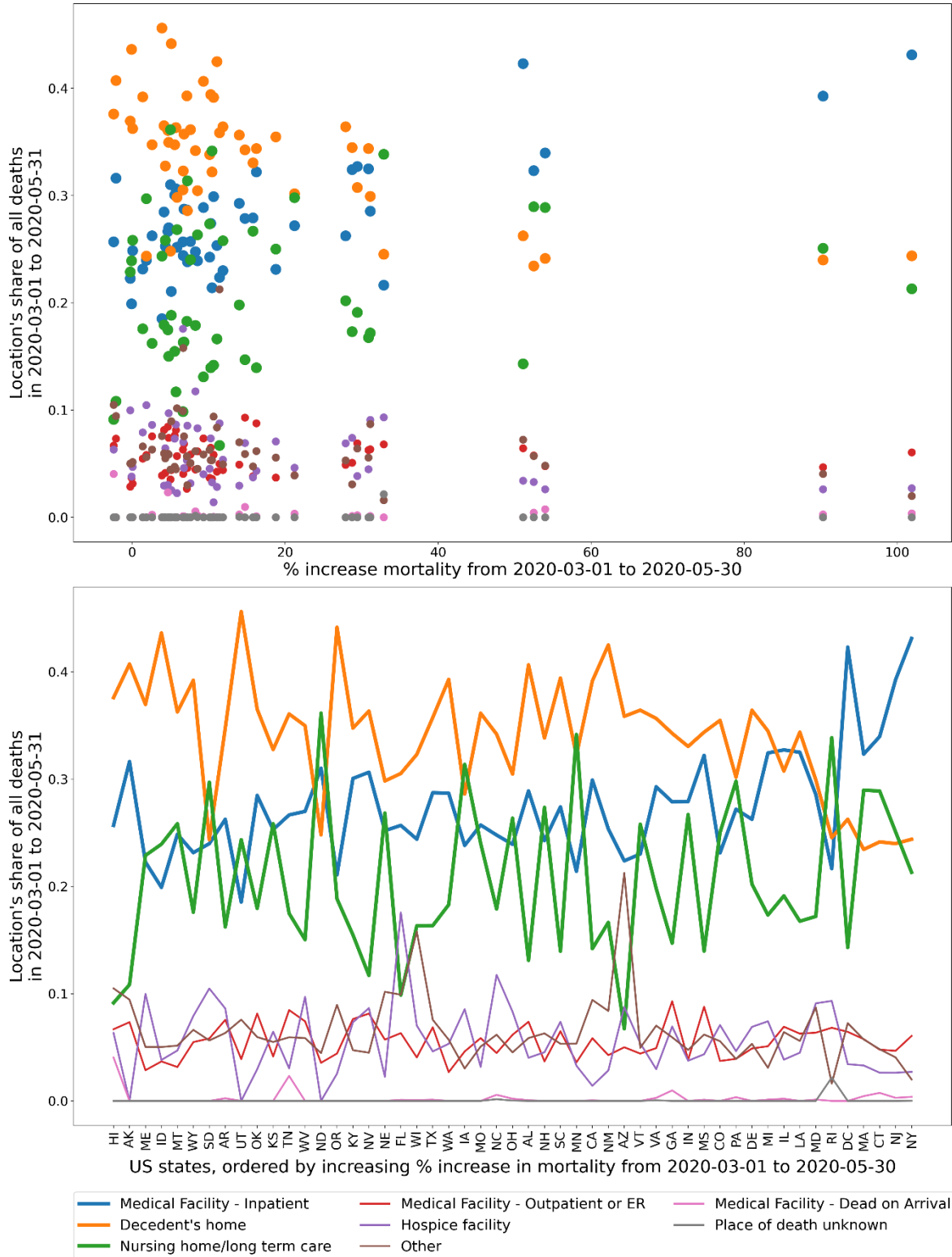


Figure 56: Top panel: Share (as a fraction) of all of a USA state's first-peak period deaths that occurred in a given location (location types indicated in the legend below the figure) vs the first-peak period P-score for the state. Bottom panel: Same y-axis as the top panel, but x-axis lists the USA states in order of increasing first-peak period P-score.

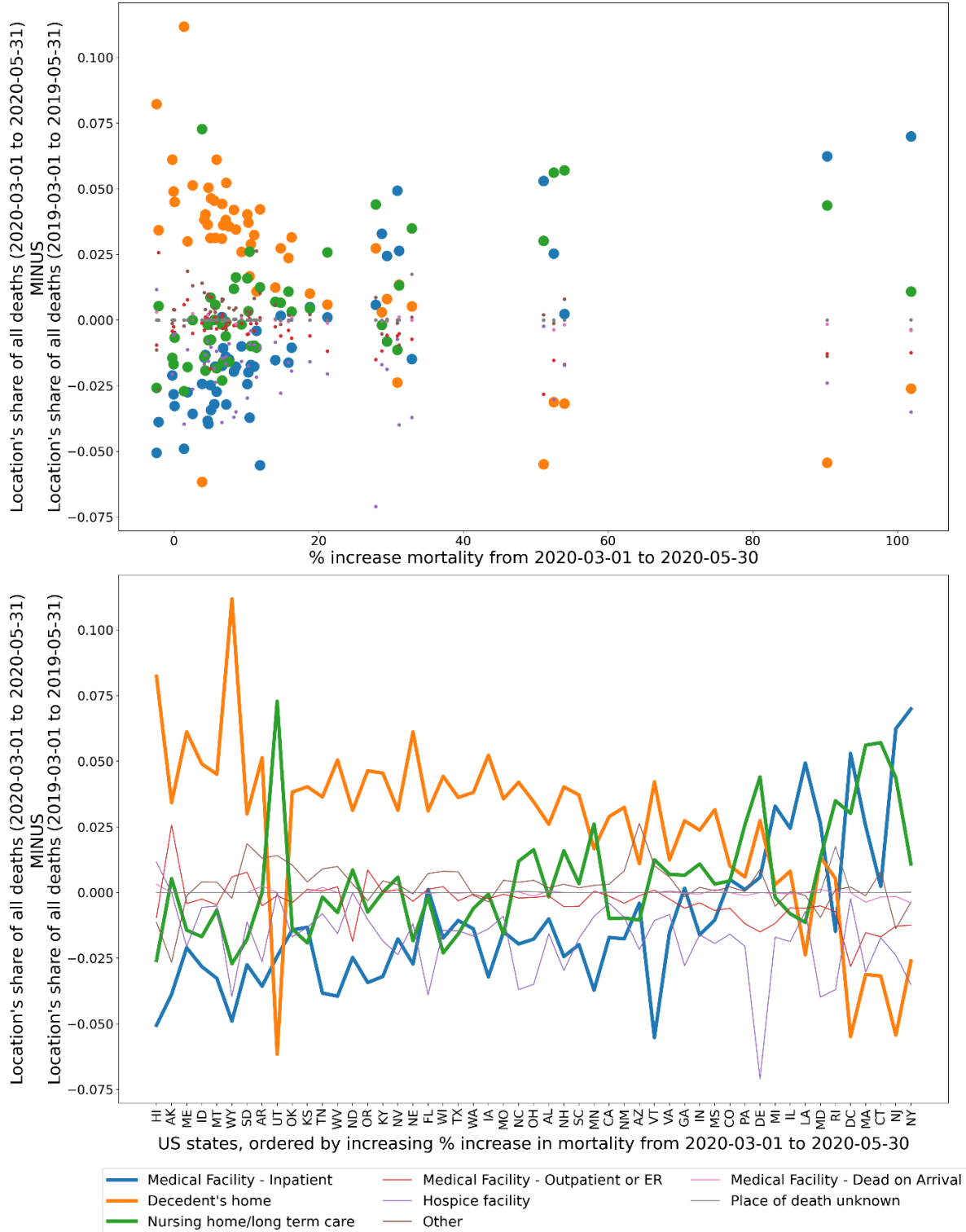


Figure 57: Top panel: Difference in the March-May 2020 share of all of a USA state’s deaths that occurred in a given location and the March-May 2019 share of all of the state’s deaths that occurred in the same location (as a difference of fractions), vs the first-peak period P-score for the state. Bottom panel: Same y-axis as the top panel, but x-axis lists the USA states in order of increasing first-peak period P-score.

Figure 57 has the same x-axes as Figure 56, but for Figure 57 the y-axes show the change in the share of deaths for each location from March-May 2019 to March-May 2020, expressed as a difference of fractions (not percentages). Here it can be seen that the first group of states (the states with the lowest integrated first-peak period P-scores) had an increased share of deaths occurring at home compared to the same time period in 2019 and a decreased share of deaths occurring in hospital. In contrast, the states with the highest integrated first-peak period P-scores had an increased share of deaths occurring in hospital or in nursing homes, and a decreased share of deaths occurring at home.

In the top panel of Figure 57, moving from left to right along the x-axis, there is a crossover from states with increased share of at-home deaths to states with increased share of hospital or nursing home deaths. This crossover occurs approximately at an integrated first-peak period P-score of 22%, which is the value separating the group of states with the lowest first-peak period P-scores (group of points at the left of the x-axis in Figure 57, top panel) from the second group of states, with first-peak period P-scores of approximately 30%. For the third, fourth and fifth groups of states, there was a decrease in the share of at-home deaths. An increase in the share of deaths occurring in hospital or nursing homes is thus a key characteristic of states with high integrated first-peak period P-scores, and for the states with highest P-scores, there was an accompanying decrease in the share of deaths occurring at home. Conversely, an increase in the share of at-home deaths and a decrease in the share of deaths in hospital are features of states with low integrated first-peak period P-scores.

Hospitals were the death-location with the largest change in share of deaths from March-May 2019 to March-May 2020 in New York (NY), New Jersey (NJ), District of Columbia (DC), Maryland (MD), Louisiana (LA), Illinois (IL) and Michigan (MI).

Nursing homes were the death-location with the largest change in share of deaths from March-May 2019 to March-May 2020 in Utah (UT), Connecticut (CT), Massachusetts (MA), Delaware (DE), Rhode Island (RI), Minnesota (MN) and Colorado (CO) (tied with home deaths).

To further probe how states with large integrated first-peak period P-scores may have had disproportionate deaths in hospitals, as opposed to at home or in nursing homes, we make graphs comparing how the share of first-peak period deaths occurring in a specific institutional location (e.g. in hospital) changed compared to the share of deaths occurring in the same location during the same time period (March-May) in 2019.

To do this, we use the ratio of a specific death location's share in the first-peak period (March-May of 2020) divided by the same death location's share in March-May of 2019. We make graphs of the said ratio for a particular death location on the y-axis, and a different death-location on the x-axis, using the three predominant death locations (hospital, home, and nursing home).

Figure 58 shows such a graph for deaths at home vs. deaths in hospital. In the top panel, the scatter plot point sizes are proportional to the integrated first-peak period P-score for the state.

The lower panel shows the same scatter plot with two-letter state codes in place of points. In either panel, the vertical grey line indicates the x-axis value of 1, and the horizontal grey line indicates the y-axis value of 1. The two grey lines thus divide the plot into four quadrants: in the top-right quadrant, both death locations increased their share during the first-peak period of 2020 compared to the same time period in 2019, whereas in the lower-left quadrant, both death locations decreased their share of all deaths during the first-peak period of 2020 compared to the same time period in 2019, and so on, for the other two quadrants.

As can be seen in Figure 58, the states with the largest integrated first-peak period P-scores (the largest circles in the top panel) are positioned in the lower-right quadrant of the scatter plot. This means that, for the states with the largest integrated first-peak period P-scores, deaths in March-May of 2020 were more likely to occur in hospitals and less likely to occur at home than in the same months in 2019.

Figure 59 shows the same type of plot as in Figure 58, with the same x and y axes, for county-level data. Here, the lower panel shows the two-letter state code of the state to which each county belongs.

Similar to the result in Figure 58, the counties with the largest integrated first-peak period P-scores (the largest circles in the top panel) are positioned in the lower-right quadrant of the scatter plot in Figure 59. This means that, for the counties with the largest integrated first-peak period P-scores, deaths in March-May of 2020 were more likely to occur in hospitals and less likely to occur at home than in the same months in 2019. The said lower-right quadrant counties mainly belonged to states with large integrated first-peak period P-scores, such as New York, New Jersey, Connecticut and Massachusetts, and they are urban counties with large population densities as shown in Figure 44 to Figure 47.

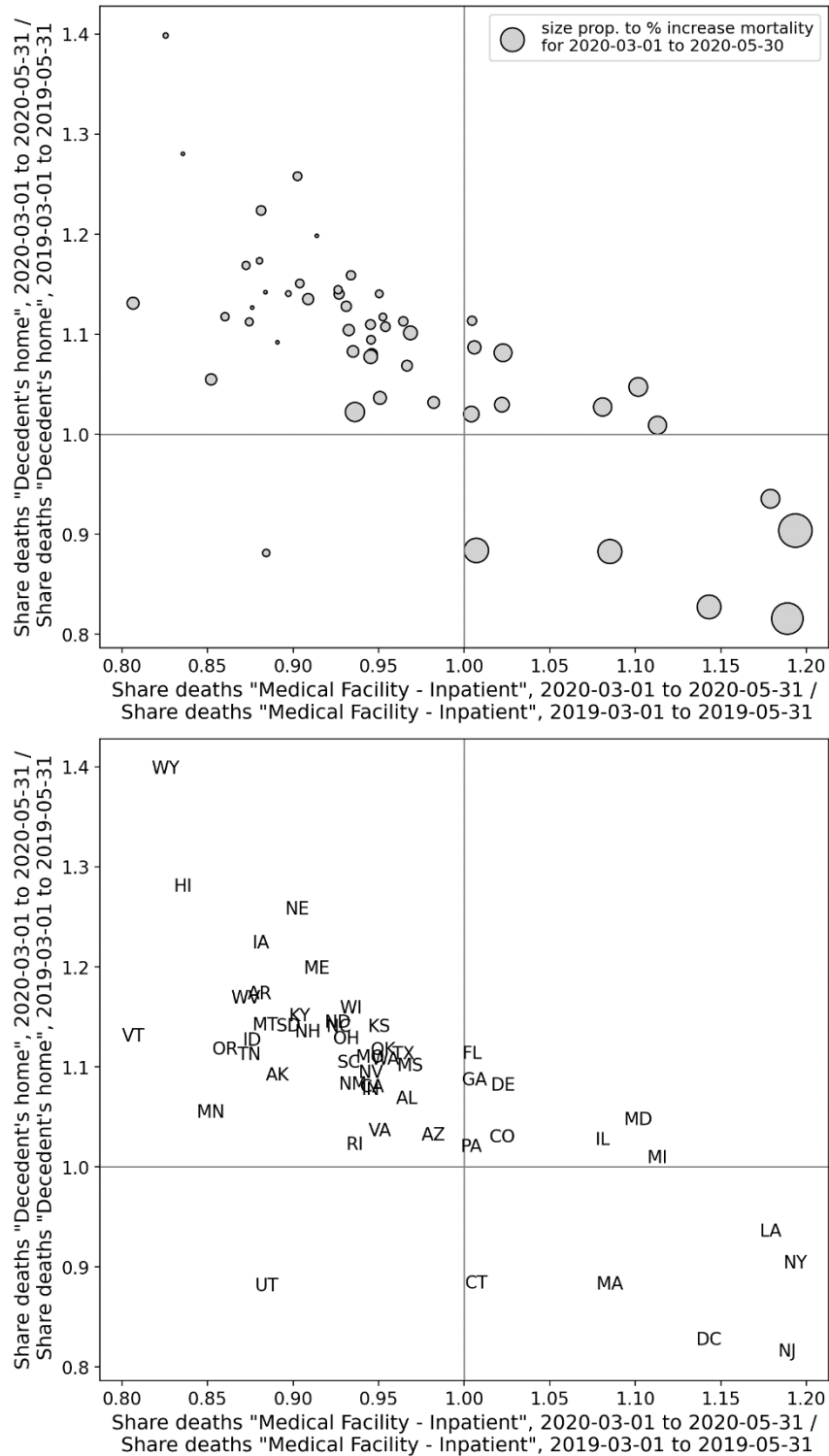


Figure 58: Top panel: y-axis: Share of all of a state’s deaths that took place at home in March-May of 2020 divided by the share of the same state’s deaths that took place at home in March-May of 2019; x-axis: same as y-axis, for deaths occurring in hospital. The size of each point is proportional to the integrated first-peak period P-score for the state. Bottom panel: Same as the top panel, showing the state codes.

Figure 58 and Figure 59 also show that the states and counties with the lowest integrated first-peak period P-scores are located in the top-left quadrant of the scatter plots. This means that the states and counties with the lowest P-scores for March-May of 2020 had smaller than normal (based on the same months in 2019) shares of deaths in hospital, and larger than normal shares of deaths at home.

Figure 60 shows the same type of scatter plot as in Figure 58, except that the y-axis now shows the ratio of the share of deaths occurring in long-term care facilities (LTC) in March-May of 2020 divided by the share of deaths occurring in LTC in March-May of 2019. In Figure 60, the states with the largest integrated first-peak period P-scores are positioned in the top-right quadrant of the plot, showing that both the share of deaths in hospital and the share of deaths in LTC increased during the first-peak period of 2020 as compared to 2019, for the states with the highest integrated first-peak period P-scores.

Figure 61 has the same x and y axes as Figure 60, for county-level data. Similar to the result in Figure 60, the counties with the largest integrated first-peak period P-scores are located in the top-right quadrant of the figure, such that both the share of deaths in hospital and deaths in LTC increased during the first-peak period of 2020 compared to 2019, for large-integrated-P-score counties.

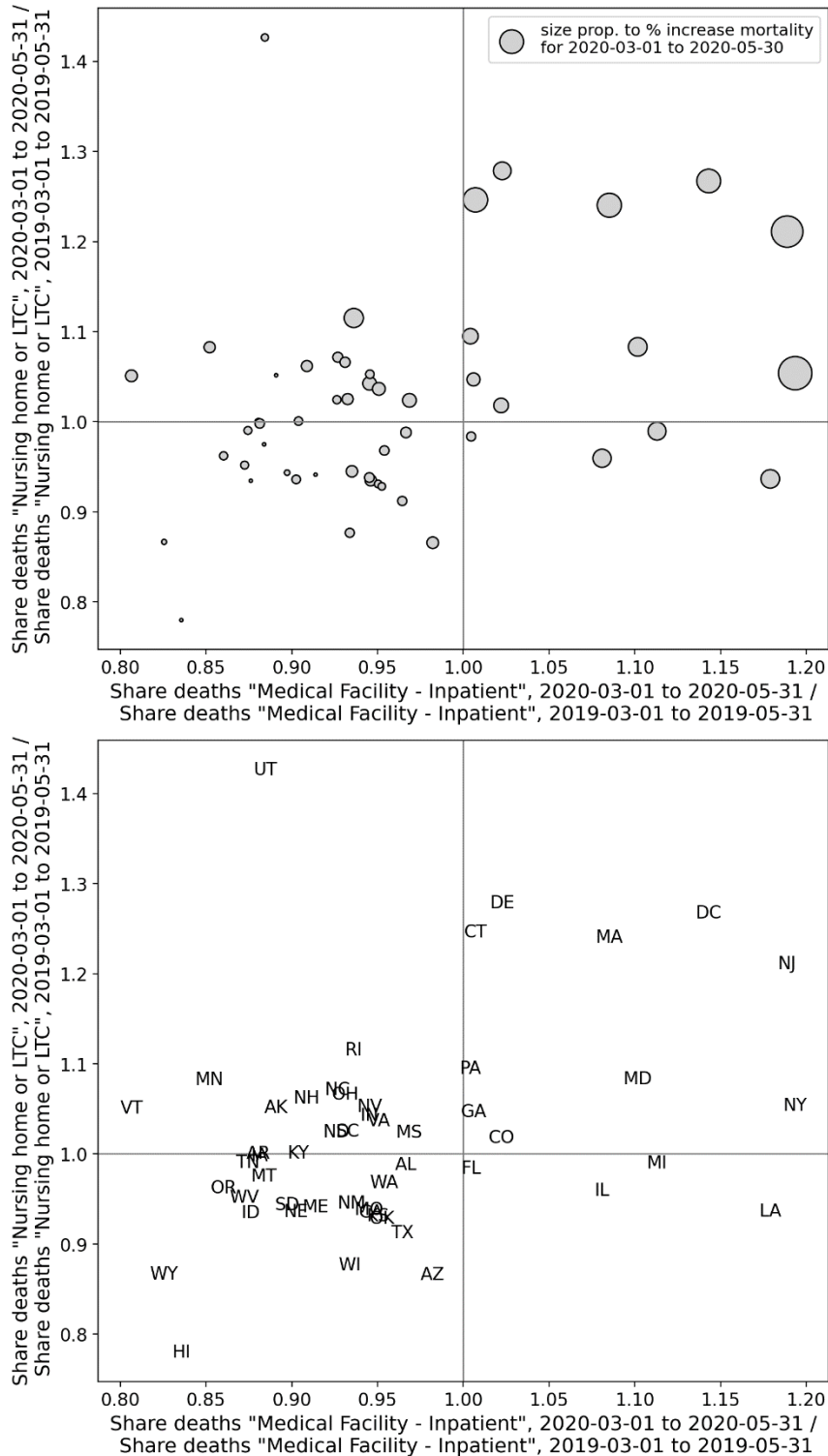


Figure 60: Top panel: y-axis: Share of all of a state’s deaths that took place in a nursing home or long-term care (LTC) in March-May of 2020 divided by the share of the same state’s deaths that took place in a nursing home or LTC in March-May of 2019; x-axis: same as y-axis, for deaths occurring in hospital. The size of each point is proportional to the integrated first-peak period P-score for the state. Bottom panel: Same as the top panel, showing the state codes.

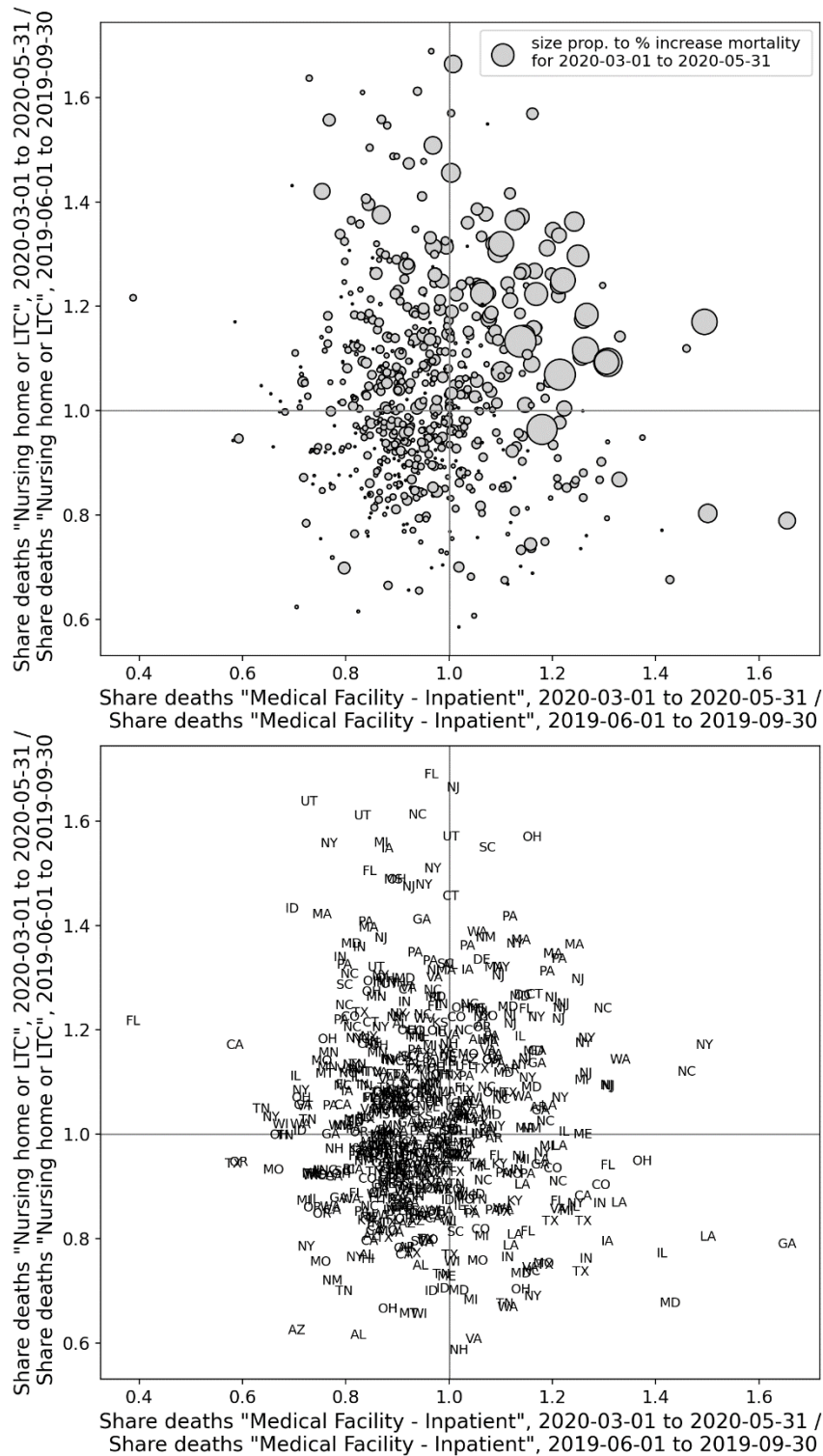
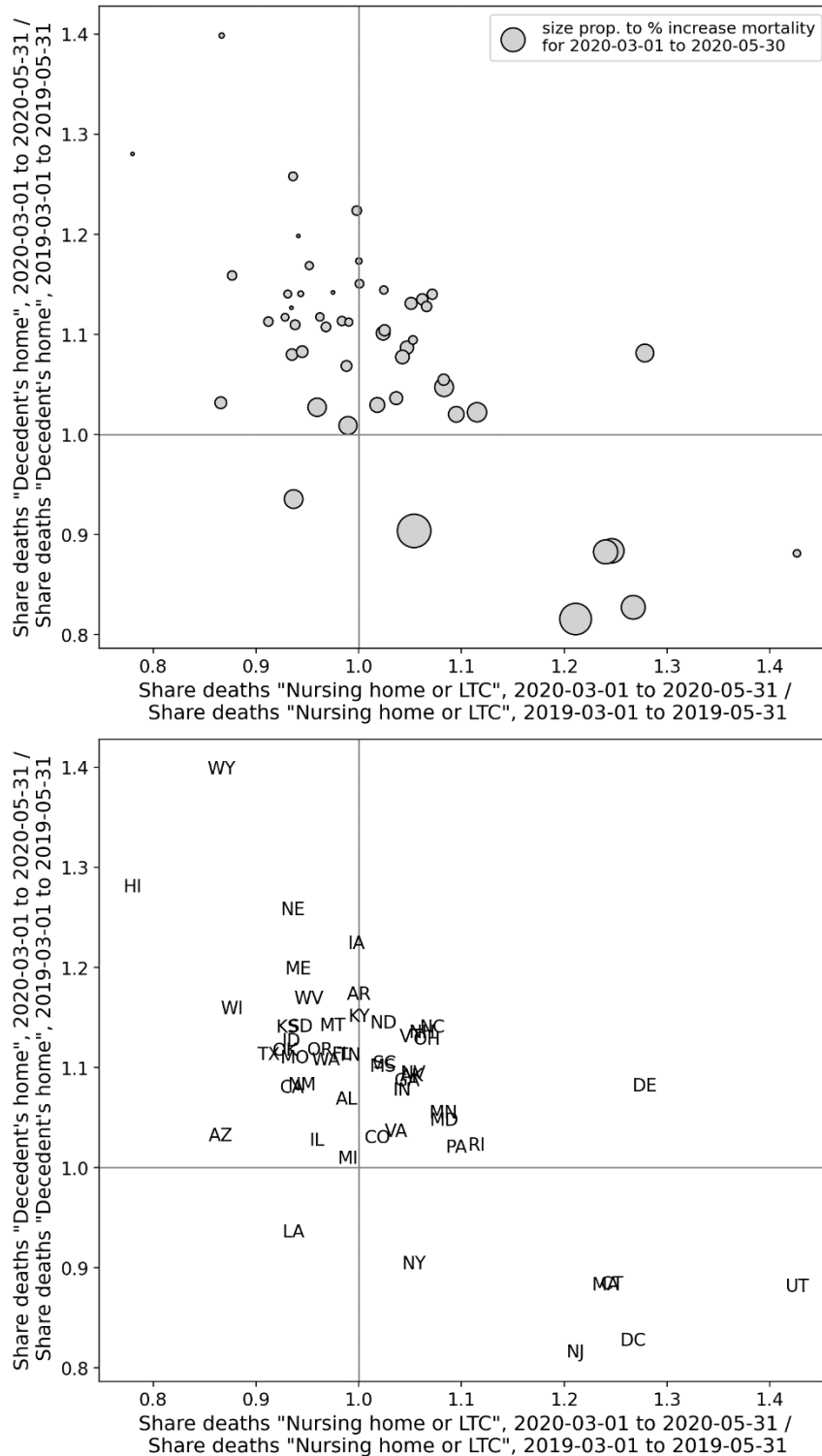


Figure 61: Top panel: y-axis: Share of all of a county’s deaths that took place in nursing homes or long-term care (LTC) in the first-peak period (2020) divided by the share of the same county’s deaths that took in nursing homes or LTC in March-May of 2019; x-axis: same as y-axis, for deaths occurring in hospital. The size of each point is proportional to the integrated first-peak period P-score for the county. Bottom panel: Same as the top panel, showing the state codes of the counties.

Figure 62 shows the same type of scatter plot as in Figure 58 and Figure 60, with home deaths on the y-axis and LTC deaths on the x-axis, for state-level data.

Figure 63 has the same x and y axes as Figure 62, for county-level data.

In Figure 62 and Figure 63, the largest circles are positioned in the lower-right quadrant, indicating an increase in the share of LTC deaths and a decrease in the share of home deaths compared to 2019, for the states and counties with the largest integrated first-peak period P-scores.



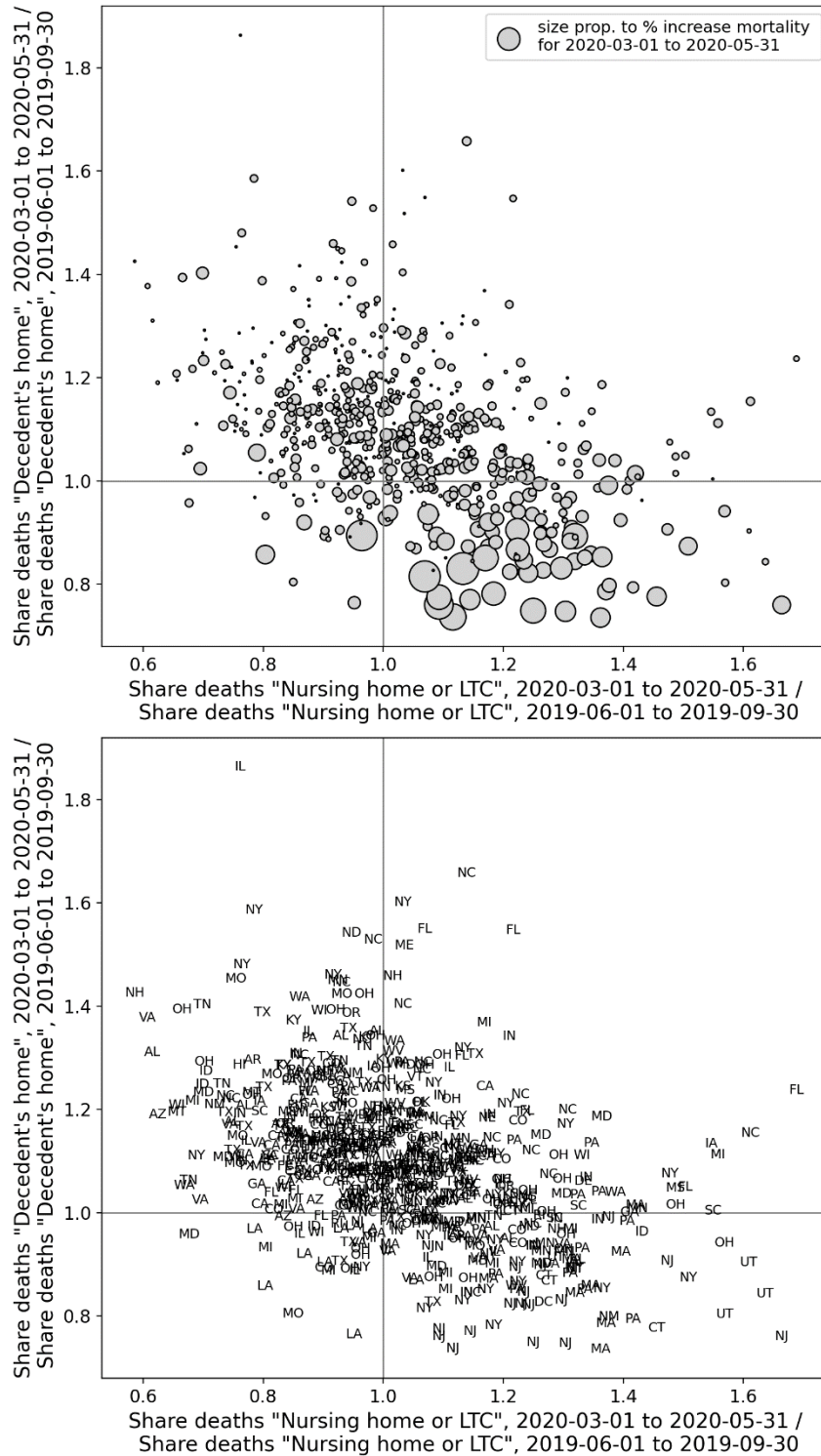


Figure 63: Top panel: y-axis: Share of all of a county’s deaths that took place at home in the first-peak period (2020) divided by the share of the same county’s deaths that took place at home in March-May of 2019; x-axis: same as y-axis, for deaths occurring in nursing homes or long-term care (LTC). The size of each point is proportional to the integrated first-peak period P-score for the county. Bottom panel: Same as the top panel, showing the state codes of the counties.

3.6 Excess mortality P-scores vs socioeconomic variables

3.6.1 USA counties

This section contains a series of scatter plots (Figure 64 to Figure 98) showing integrated P-scores for the first-peak period (March-May 2020) and summer-peak period (June-September 2020) vs socioeconomic variables, for the counties of the USA with available data.

Also included are heatmaps (Figure 99 to Figure 133) showing how each socioeconomic variable varies across the USA counties. Here, each figure includes a map of the entire contiguous USA (top panel) and a blow-up around the New York City urban area (bottom panel).

The heatmaps of values of the socioeconomic variables (Figure 99 to Figure 133) are needed to help interpret or understand the many complex relations or structures observed in the scatter plots (Figure 64 to Figure 98) of integrated P-score versus socioeconomic variable, which are not simple scatter plots showing only variable degrees of correlation. Rather, the said scatter plots have intricate structures, suggesting subgroups of counties, which have geographical relations.

Table 4 lists the socioeconomic variables for the scatter plots and heatmaps in this section:

Figure (scatter)	Figure (heatmap)	USA county-level socioeconomic variable	Year(s)
Figure 64	Figure 99	Population	2019
Figure 65	Figure 100	Log(Population)	2019
Figure 66	Figure 101	Population density	2017-2021 ACS *
Figure 67	Figure 102	Log(Population density)	2017-2021 ACS
Figure 68	Figure 103	Per capita income	2014-2018 ACS **
Figure 69	Figure 104	% living in poverty	2014-2018 ACS
Figure 70	Figure 105	% unemployed	2014-2018 ACS
Figure 71	Figure 106	Gini coefficient	2014-2018 ACS
Figure 72	Figure 107	Inter-county disparity	2014-2018 ACS
Figure 73	Figure 108	% households with no vehicle available	2014-2018 ACS
Figure 74	Figure 109	% households with more people than rooms	2014-2018 ACS
Figure 75	Figure 110	% living in housing structures with 10+ units	2014-2018 ACS
Figure 76	Figure 111	% of population that speaks English “less than well”	2014-2018 ACS
Figure 77	Figure 112	% minority	2014-2018 ACS
Figure 78	Figure 113	% aged 25+ with no high school diploma	2014-2018 ACS
Figure 79	Figure 114	% aged 65+	2014-2018 ACS
Figure 80	Figure 115	% aged 17 and under	2014-2018 ACS

Figure 81	Figure 116	% households that are single-parent households	2014-2018 ACS
Figure 82	Figure 117	% with a disability	2014-2018 ACS
Figure 83	Figure 118	% with diabetes	2018
Figure 84	Figure 119	% with obesity	2018
Figure 85	Figure 120	% of votes cast in the 2016 election that were for the Democratic presidential candidate	2016
Figure 86	Figure 121	% deaths occurring at home in March-May 2019	2019
Figure 87	Figure 122	% deaths occurring at home in June-September 2019	2019
Figure 88	Figure 123	% deaths occurring in hospital in March-May 2019	2019
Figure 89	Figure 124	% deaths occurring in hospital in June-September 2019	2019
Figure 90	Figure 125	% deaths in hospital in March-May 2020 minus % deaths occurring in hospital in March-May 2019	2019, 2020
Figure 91	Figure 126	% deaths in hospital in June-September 2020 minus % deaths occurring in hospital in June-September 2019	2019, 2020
Figure 92	Figure 127	Number of prescription drug claims per person	2017
Figure 93	Figure 128	Number of antibiotic prescription drug claims per person	2017
Figure 94	Figure 129	% aged 18+ with at least one dose of a COVID vaccine by 2021-12-31	2020, 2021
Figure 95	Figure 130	% aged 65+ with at least one dose of a COVID vaccine by 2021-12-31	2020, 2021
Figure 96	Figure 131	% aged 18+ with completed primary series of a COVID vaccine by 2021-12-31	2020, 2021
Figure 97	Figure 132	% aged 65+ with completed primary series of a COVID vaccine by 2021-12-31	2020, 2021
Figure 98	Figure 133	Number of ICU beds per county	2018, 2019

Table 4: Socioeconomic variables shown on x-axes in Figure 64 to Figure 98 and in maps in Figure 99 to Figure 133. Notes: *"2017-2021 ACS" indicates that the data corresponds to an estimate obtained from the 5-Year American Community Survey for 2017-2021; **"2014-2018 ACS" indicates that the data corresponds to an estimate obtained from the 5-Year American Community Survey for 2014-2018.

Each of the scatter-plot figures Figure 64 to Figure 97 is for one socioeconomic variable. Each figure has six panels, arranged in three rows and two columns, as follows. The top row of panels shows the integrated first-peak period P-score for the county vs the value of the socioeconomic

variable for the county, using data points with error bars (top row, left panel) and using the two-letter code for the state to which the county belongs in place of data points (top row, right panel). The middle row of panels shows the same thing as the top row, for the summer-peak period (June-September 2020). In the bottom row of panels, only counties from the four states with the highest state-level integrated first-peak period P-scores are shown. The four states are New York (NY), New Jersey (NJ), Connecticut (CT) and Massachusetts (MA). The left panel of the bottom row shows results for the NY-NJ-CT-MA states for the first-peak period, and the right panel is for the summer-peak period. For all six panels, the y-axis range is fixed at a value of 250% (slightly higher than the maximum integrated first-peak period P-score of 233% for Bronx County, NY). Pearson correlation coefficients (“r”) stated in the panels are for the data points shown in the panel.

Figure 98 is similar to Figure 64 to Figure 97, except that the y-axes show the number of excess deaths per day rather than P-score, and the x-axes show the number of intensive care unit (ICU) beds per county.

The scatter plots reveal many features about the populations that experienced high and low integrated first-peak period P-scores and allow comparison with the immediately-following summer-peak period, which contrasts with the first-peak period in some important ways.

Regarding the first-peak period, the scatter plots in Figure 64 to Figure 98 often exhibit a two-branch structure, in which many counties are arranged horizontally along the x-axis with low P-scores and a wide range of values of the socioeconomic variable (“lower branch”) whereas a separate branch of counties has positively correlated P-scores that rise up to high values with large values of the socioeconomic variable (“upper branch”). The upper branch is mostly made up of counties from the top-four (P-score) states (NY, NJ, CT and MA), especially the counties within the New York City urban area (in NY, NJ and CT).

Variables for which the said two-branch structure for the first-peak period can be seen include population, log(population), population density, log(population density), per capita income, % living in poverty, Gini coefficient, inter-county disparity, % households with no vehicle available, % households with more people than rooms, % living in structures with 10+ units, % who speak English “less than well”, % minority, % aged 25+ with no high school diploma, % single-parent households, % deaths occurring in hospital in March-May 2019, % deaths occurring in hospital in June-September 2019, and share of votes cast in the 2016 election that were for the Democratic presidential candidate.

For socioeconomic variables with clearly defined upper branches, the correlation coefficients are often large for the counties of the four states with highest integrated first-peak period P-scores (the “NY-NJ-CT-MA counties”), as shown in the lower-left panels of the figures. The variables with the highest correlation coefficients for NY-NJ-CT-MA counties are as follows:

- % who speak English “less than well” (Figure 76, $r = 0.89$);

- log[population density] (Figure 67, $r = 0.85$);
- % minority (Figure 77, $r = 0.85$);
- % households with more people than rooms (Figure 74, $r = 0.83$);
- population (Figure 64, $r = 0.77$);
- log[population] (Figure 65, $r = 0.72$);
- % living in housing structures with more than 10 units (Figure 75, $r = 0.72$); and
- share of votes cast in the 2016 election that were for the Democratic presidential candidate (Figure 85, $r = 0.68$).

For some variables with scatter plots exhibiting two-branch structures, the behaviour for the NY-NJ-CT-MA counties is not a simple linear correlation but rather a more complex relationship that depends on population geography. For example, the percentage of people living in poverty is relatively high in the rural areas of New York State far from the New York City urban area (see the map in bottom panel of Figure 104). In the said rural areas, integrated first-peak period P-scores were low (see the maps in Figure 12). Moving from the rural areas of New York State toward the New York City urban area, one first crosses suburban areas with low poverty and moderate first-peak period P-scores. Continuing toward the centre of the New York City urban area, poverty increases to its highest values and so do the county-level first-peak period P-scores. This results in a non-linear “<”-shaped pattern of the scatter plot in the lower-left panel of Figure 69, with a near-zero correlation coefficient ($r=0.05$). However, first-peak period P-score is strongly correlated with % living in poverty for the highest-P-score (e.g. P-score > 100%) counties in Figure 69, which are all close to the centre of the New York City urban area, and which have the highest P-scores in the entire USA.

Similar “<”-shaped rural-to-suburban-to-inner-city patterns for the NY-NJ-CT-MA counties are seen in the scatter plots for

- the percentage of the county’s population aged 25+ with no high school diploma (Figure 78, lower-left panel, and see the map for this variable in Figure 113, bottom panel); and
- the percentage of single-parent households (Figure 81, lower-left panel and map in Figure 116, bottom panel).

A “<”-shaped or C-shaped pattern is also seen for the NY-NJ-CT-MA counties for variables for which a two-branch structure is less distinct in the all-counties scatter plots, such as

- the percentage of the population with a disability (Figure 82, lower-left panel, and map in Figure 117, bottom panel);
- the percentage of the population with diabetes (Figure 83, lower-left panel, and map in Figure 118, bottom panel); and
- the percentage of the population with obesity (Figure 84, lower-left panel, and map in Figure 119, bottom panel).

For per capita income (Figure 68), the upper branch of the scatter plot exhibits a “gamma” (γ) shape, especially visible for the NY-NJ-CT-MA counties in the lower-left panel. The county with the highest per capita income in the USA is Manhattan (New York County, NY), whereas other counties in the inner New York City urban area, such as the Bronx (Bronx County, NY), Queens (Queens County, NY), Brooklyn (Kings County, NY) and Hudson County, NJ have high P-scores but low per capita incomes.

The scatter plot for the Gini coefficient (Figure 71, top row of panels) has a less-well-defined two-branch structure than for other variables, with a larger range of first-peak period P-score values (y-axis) at high values of the Gini coefficient (x-axis) than for high values of other socioeconomic variables with two-branch scatter plots.

The inter-county disparity (Figure 72) is a measure we define and calculate as the maximum per capita income among the neighbours of a county of interest (the “target county”) minus the target county’s per capita income. The scatter plot for the inter-county disparity is shown in Figure 72. The highest values of the inter-county disparity are for the low per capita income counties that neighbour Manhattan (New York County, NY), including the Bronx, Queens, Brooklyn and Hudson County, NJ, which also had the four highest first-peak period P-scores among USA counties. Manhattan is an outlier with a large negative value of the inter-county disparity in Figure 72, due to its much larger per capita income than its neighbours.

Regarding age structure, Figure 79 shows that the counties with large integrated first-peak period P-scores had relatively low shares of people aged 65+. For the NY-NJ-CT-MA counties, P-scores decreased with increasing share of people aged 65+, with a correlation coefficient of $r = -0.49$. Figure 80 shows that the highest P-score counties had average shares of people aged 17 and under (top panels), and for the NY-NJ-CT-MA counties, P-scores increased with increasing share of people aged 17 and under, with a correlation coefficient of $r = 0.38$.

The data on number of prescription drug claims pertains to claims made by beneficiaries of the USA federal government-funded Medicare Part D plan, which had approximately 63 million total beneficiaries in 2019 (Tarazi et al., 2022). The counties with the highest P-scores had relatively low values of both number of all kinds of prescriptions per person (Figure 92, map in Figure 127) and number of antibiotic prescriptions per person (Figure 93, map in Figure 128).

The number of excess deaths per day vs the number of ICU beds per county (Figure 98) has a positive correlation, as expected given that both the raw number of excess deaths and the number of ICU beds would generally scale with the county’s population. The three counties with the highest excess mortalities – the Bronx, Queens, and Brooklyn (Kings County, NY) – are outliers on this plot with mid-range numbers of ICU beds and very large excess mortality.

The scatter plots in Figure 64 to Figure 98 also show results for the summer-peak period for all counties with available data (middle row of panels) and for the NY-NJ-CT-MA counties (bottom-right panels).

Summer-peak period P-scores were large in states and counties in the southern USA, as shown in the heatmaps of integrated summer-peak period P-scores in Figure 134 and Figure 135. At the county level, the highest summer-peak period P-scores occurred in counties in Texas, Arizona, and California, along the border with Mexico, as well as in the state of Mississippi, along the Mississippi river.

In contrast to the first-peak period, the counties with the highest summer-peak P-scores had low populations and low population-densities (middle panels of Figure 64 to Figure 67), low per capita incomes (Figure 68), and low values for percent of households with no vehicle available (Figure 73) and percent living in housing structures with 10+ units (Figure 75).

The relationship between P-score and poverty is also different for the summer-peak period than the first-peak period. Whereas in the first-peak period, the scatter plot shows a distinct two-branch structure (top panels of Figure 69), in the summer-peak period the scatter plot shows an overall positive correlation between integrated P-score and poverty ($r = 0.39$), with four high-poverty Texas counties along the Mexican border rising above the pack with the highest P-scores of around 150%. Variables with similar scatter-plot patterns to poverty for the summer-peak period include Gini coefficient (Figure 71) with $r = 0.24$, percent single-parent households (Figure 81) with $r = 0.36$, and percent aged 25+ with no high school diploma (Figure 78) with $r = 0.44$. Percent with diabetes (Figure 83) with $r = 0.18$, and percent with a disability (Figure 82) with $r = 0.11$ arguably follow this pattern as well but with weaker correlation coefficients, and for these two variables, the four Texan counties with large summer-peak period P-scores have mid-to-low values, unlike for poverty, Gini coefficient, percent single-parent households, and percent aged 25+ with no high school diploma.

There is no clear evidence for a correlation between integrated summer-peak period P-score and the rate of obesity when considering all USA counties, as can be seen from the middle panels of Figure 84. In this case, the four Texan counties with the highest summer-peak period P-scores are spread out along the x-axis from low to high values of the obesity rate. However, obesity is a variable with one of the largest correlation coefficients for the NY-NJ-CT-MA counties in the summer-peak period (Figure 84, lower-right panel), with $r = 0.41$.

Regarding the NY-NJ-CT-MA counties during the summer-peak period, the variables with the largest correlation coefficients were:

- percent with a disability (Figure 82, $r = 0.43$);
- percent with obesity (Figure 84, $r = 0.41$);
- percent single parent households (Figure 81, $r = 0.37$); and
- percent with diabetes (Figure 83, $r = 0.34$).

A two-branch pattern that is somewhat similar to that seen in the first-peak period is observed for the summer-peak period for the share of votes cast that were for the Democratic

presidential candidate in 2016 (Figure 85) and for the percent of households with more people than rooms (Figure 74).

The counties with the highest summer-peak period P-scores were also among the counties with the highest shares of minorities (Figure 77) and people who spoke English “less than well” (Figure 76). The butterfly shape of the scatter plot for the summer-peak period in Figure 76 (% who speak English “less than well”) is due to high P-scores in counties in the Mississippi river area (high rate of speaking English) and high P-scores in counties along the Mexican border (low rate of speaking English), as per the map in the top panel of Figure 111. Both geographic areas have large shares of minorities, as per the map in the top panel of Figure 112.

The scatter plots for P-score vs percent of the population aged 65+ are similar for the first-peak and summer-peak periods (Figure 79). In both cases, the counties with the highest P-scores have low shares of people aged 65+. The scatter plots for the number of prescriptions per person (Figure 92) and number of antibiotic prescriptions per person (Figure 93) are also similar for the first-peak and summer-peak periods.

The share of the population aged 17 and under has a two-branch structure for the summer-peak period (Figure 80, middle panels), whereas this was not clearly the case for the first-peak period when considering all counties (Figure 80, top panels).

Several scatter plots in this section use the data on location of death presented in section 3.5, on the x-axis. Figure 88 shows the share of deaths occurring in hospital in March-May 2019, and Figure 89 shows the share of deaths occurring in hospital for June-September 2019. As mentioned above, Figure 88 and Figure 89 are scatter plots in which a two-branch structure for the first-peak period can be seen. Counties in the New York City urban area had high pre-COVID-period shares of deaths occurring in hospital, as can be seen from the lower left panels of Figure 88 and Figure 89.

Figure 90 shows the difference in the share of deaths occurring in hospital in March-May 2020 and the share of deaths occurring in hospital in March-May 2019. From this graph, it can be seen that the counties in the New York City urban area had among the largest increases in share of deaths occurring in hospital during the first-peak period compared to one year earlier (top row of panels), and that first-peak period integrated P-score increased with the increase in share of deaths occurring in hospital with a Pearson correlation coefficient of 0.71.

Figure 91 shows the difference in the share of deaths occurring in hospital in June-September 2020 and the share of deaths occurring in hospital in June-September 2019. The counties with the highest summer peak integrated P-scores, which were in the southwest USA including in Texas, also had the largest increases in share of deaths occurring in hospital during the summer peak compared to one year earlier.

Figure 86 has the percent of deaths occurring at home in March-May 2019, and shows that the high integrated first-peak period P-score counties in the New York City urban area had low

shares of deaths occurring at home, relative to the other counties with available data. Figure 87 shows the percent of deaths occurring at home in June-September 2019, for completeness.

Figure 94 to Figure 97 use COVID vaccination uptake data as of December 31, 2021 on the x-axes. Although the COVID vaccination campaign began in December 2020, after the first-peak period (March-May 2020) and the summer-peak period (June-September 2020), we include COVID vaccination uptake data as a potential indicator of the degree to which a county's population interacts with or seeks or receives treatment from the medical system. A caveat: the COVID vaccination uptake data appears to be unreliable for the State of Georgia, which has markedly lower (but non-zero) values of vaccination uptake than neighbouring states, as can be seen from the maps in Figure 129 to Figure 132.

Figure 94 shows the percentage of the population aged 18+ that had received at least one dose of a COVID vaccine by December 31, 2021, and Figure 95 shows the same thing for the population aged 65+. In both Figure 94 and Figure 95, it can be seen that, for the counties with the highest integrated first-peak period P-scores and the counties with the highest integrated summer-peak P-scores, nearly 100% of the population received at least one dose of a COVID vaccine up to the end of 2021.

Similarly, Figure 95 (Figure 96) shows the percentage of the population aged 18+ (aged 65+) with a completed series of a COVID vaccine by December 31, 2021. The counties with the highest integrated first-peak period and summer-peak period P-scores were among the counties with the highest vaccine uptake up to the end of 2021.

Integrated P-score vs Population

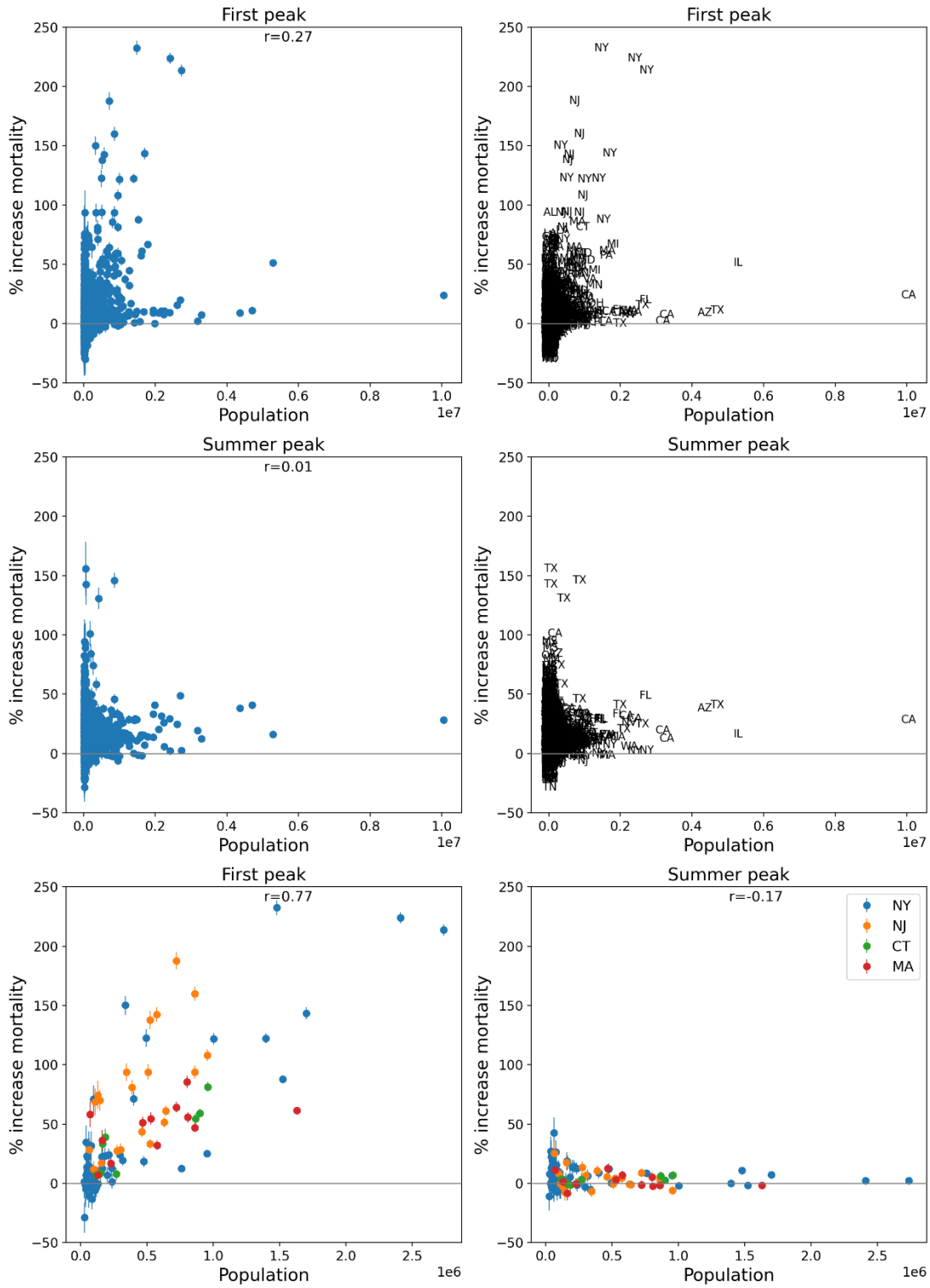


Figure 64: Integrated P-scores for first-peak and summer-peak periods for USA counties vs population in 2019. Bottom two panels: four states with largest integrated first-peak period P-scores.

Integrated P-score vs \log_{10} [Population]

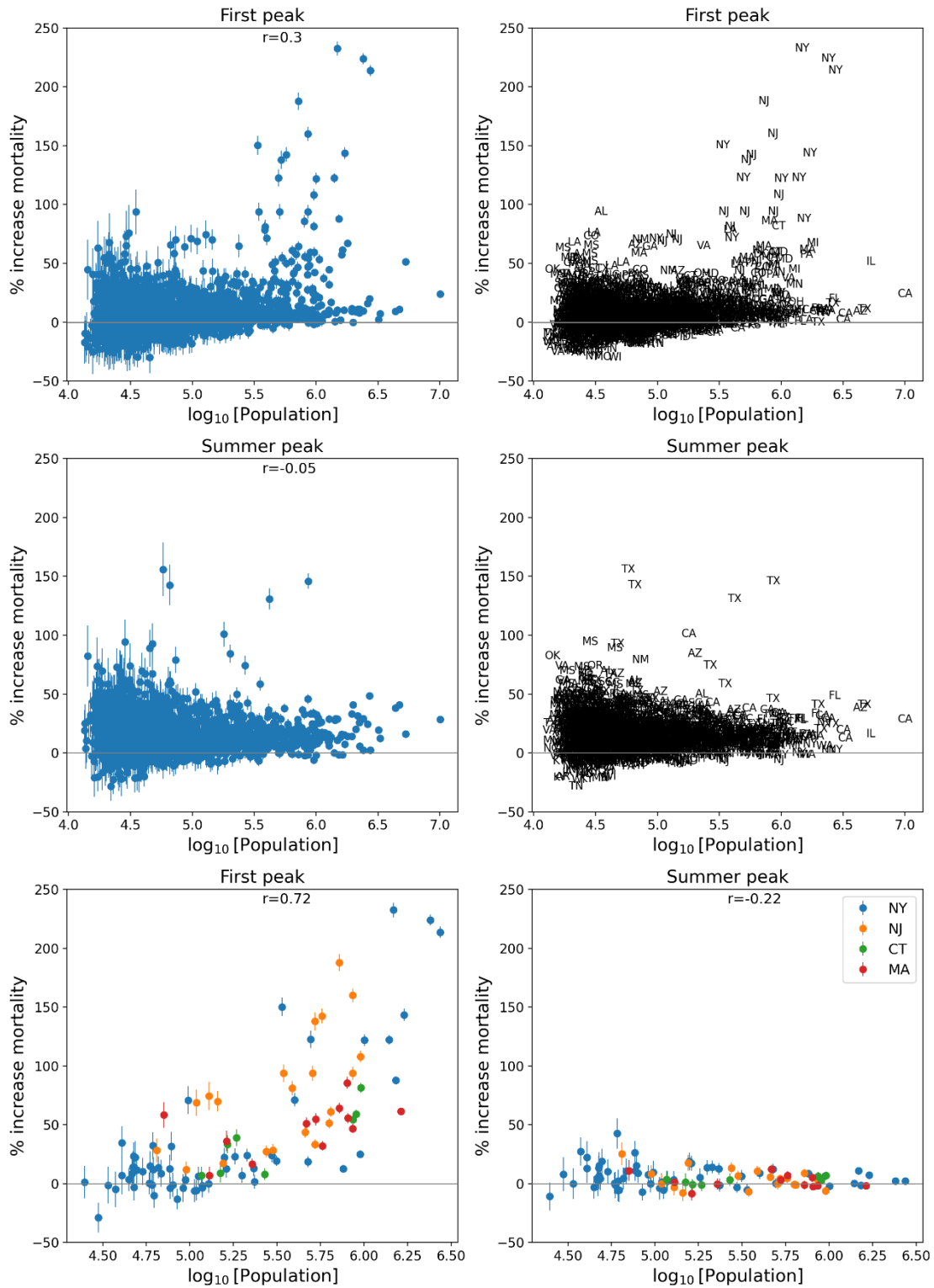


Figure 65: Same as Figure 64, with x-axis showing the logarithm of 2019 population.

Integrated P-score vs Population density (km^{-2})

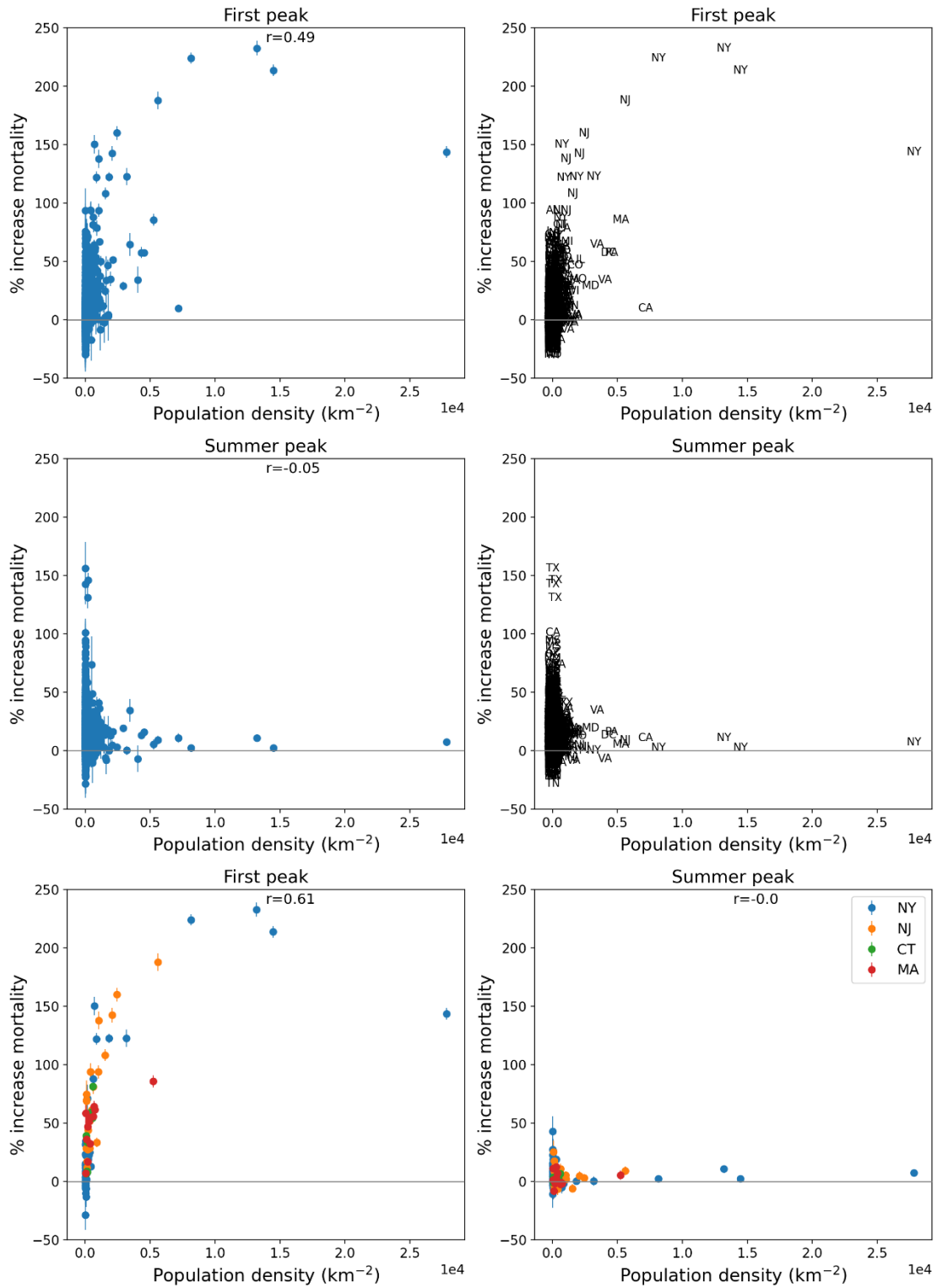


Figure 66: Same as Figure 64, with x-axis showing the population density (estimates from the 5-Year American Community Survey for the years 2017-2021).

Integrated P-score vs \log_{10} [Pop. density (km^{-2})]

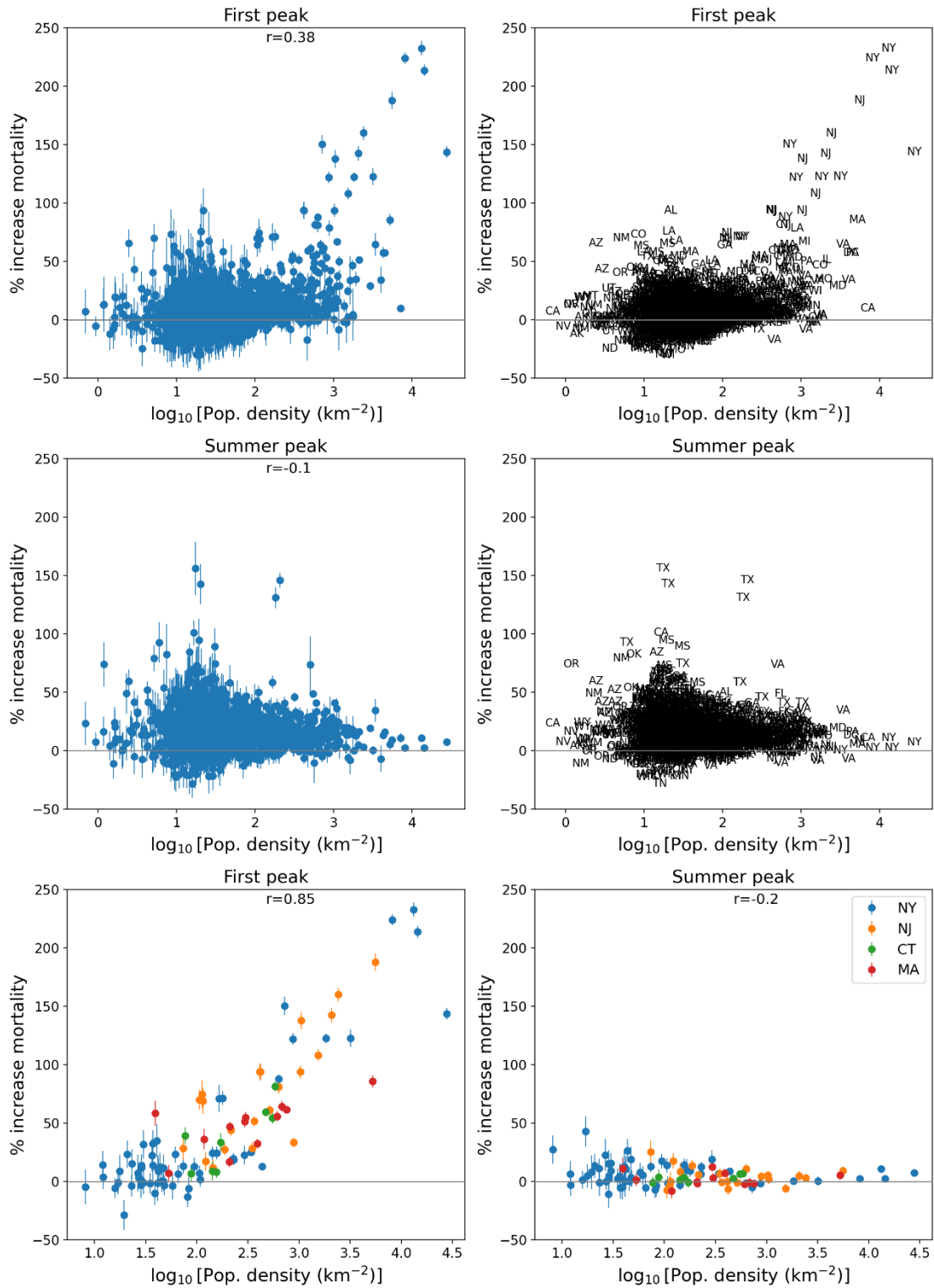


Figure 67: Same as Figure 64, with x-axis showing the logarithm of population density (estimates from the 5-Year American Community Survey for the years 2017-2021).

Integrated P-score vs Per capita income

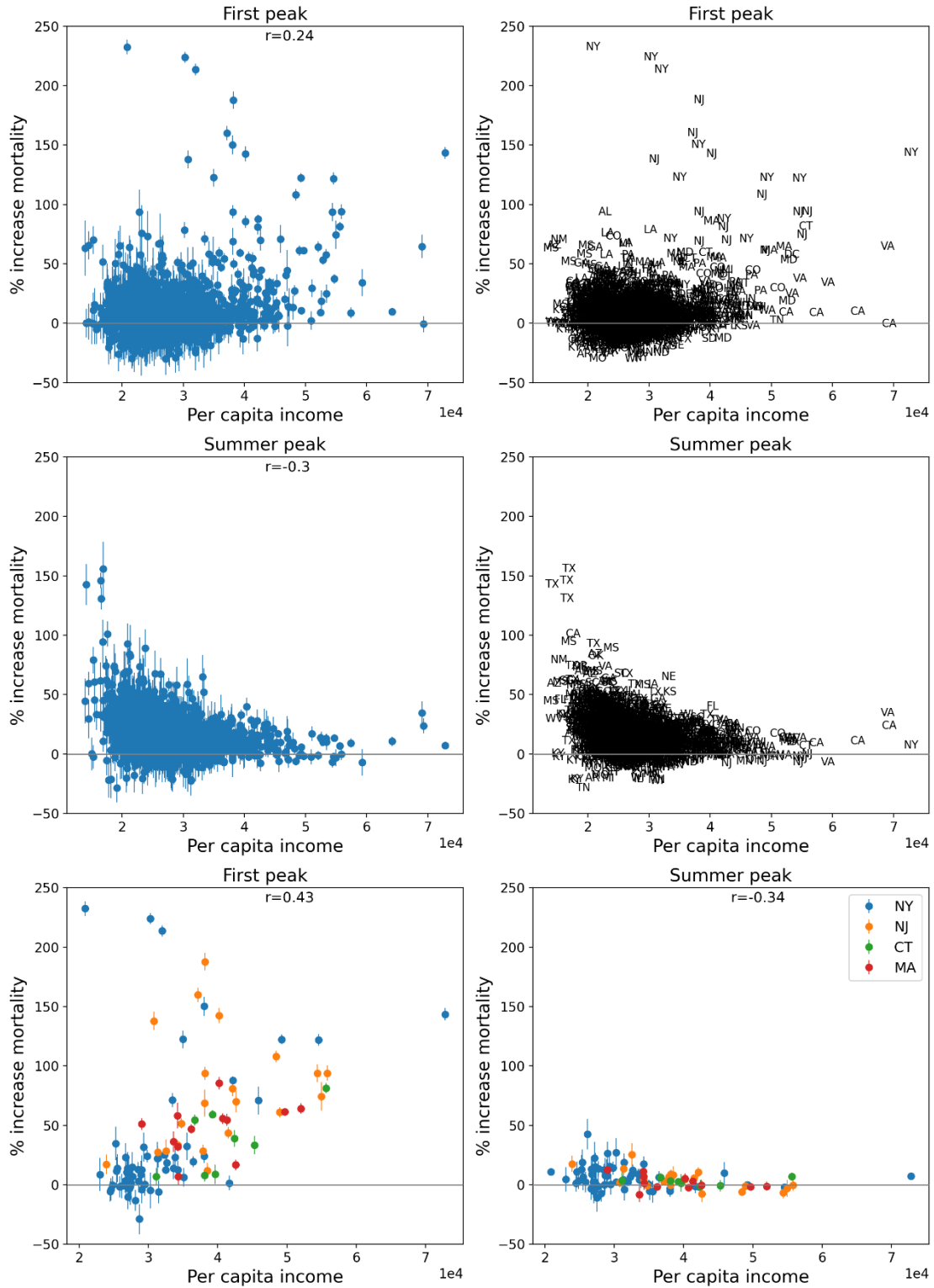


Figure 68: Same as Figure 64, with x-axis showing per capita income (estimates from the 5-Year American Community Survey for the years 2014-2018).

Integrated P-score vs Gini coefficient

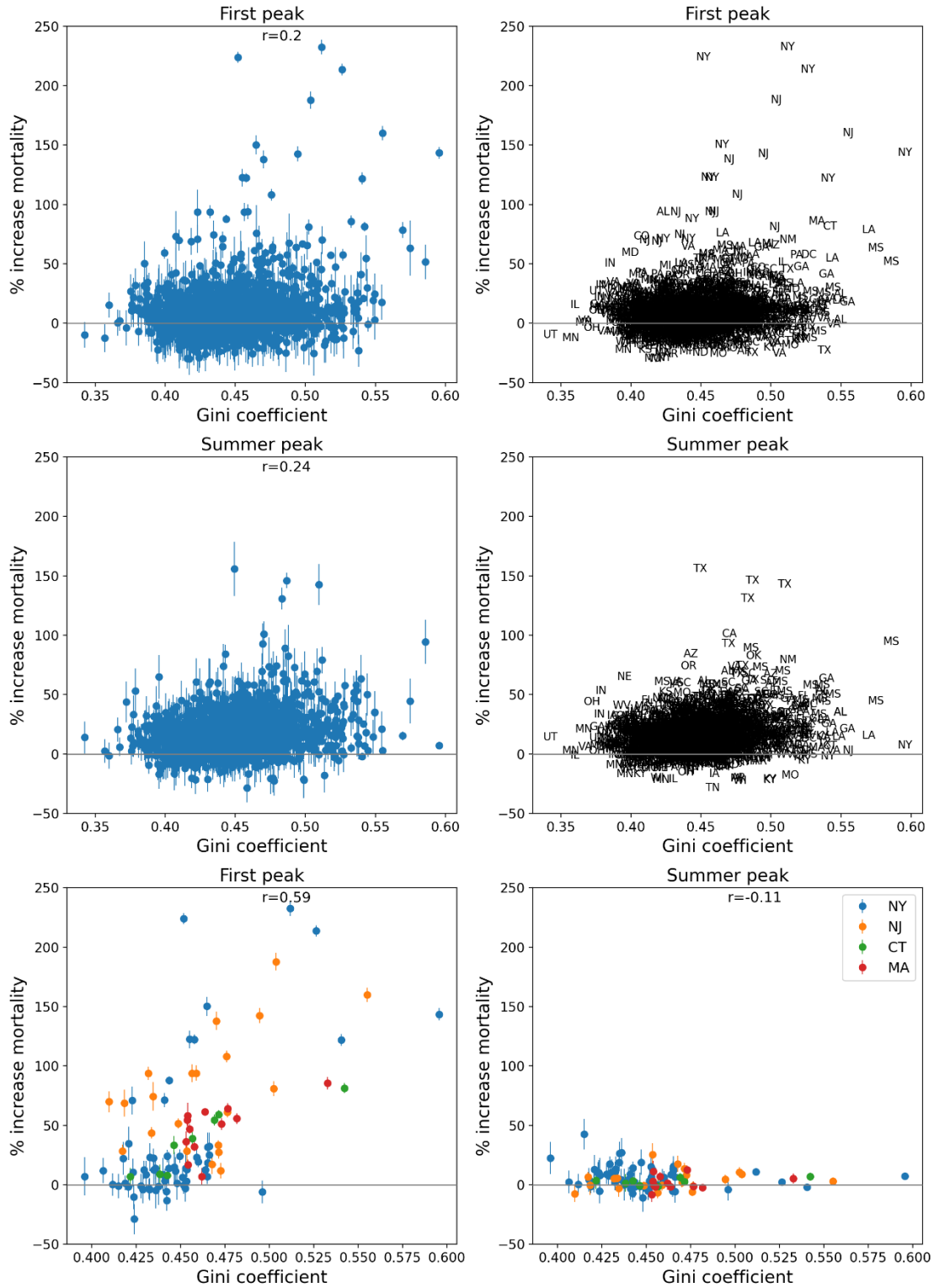


Figure 71: Same as Figure 64, with x-axis showing the Gini coefficient for the county (estimates from the 5-Year American Community Survey for the years 2014-2018).

Integrated P-score vs Inter-county disparity
(Max neighbour PCI - Target PCI)

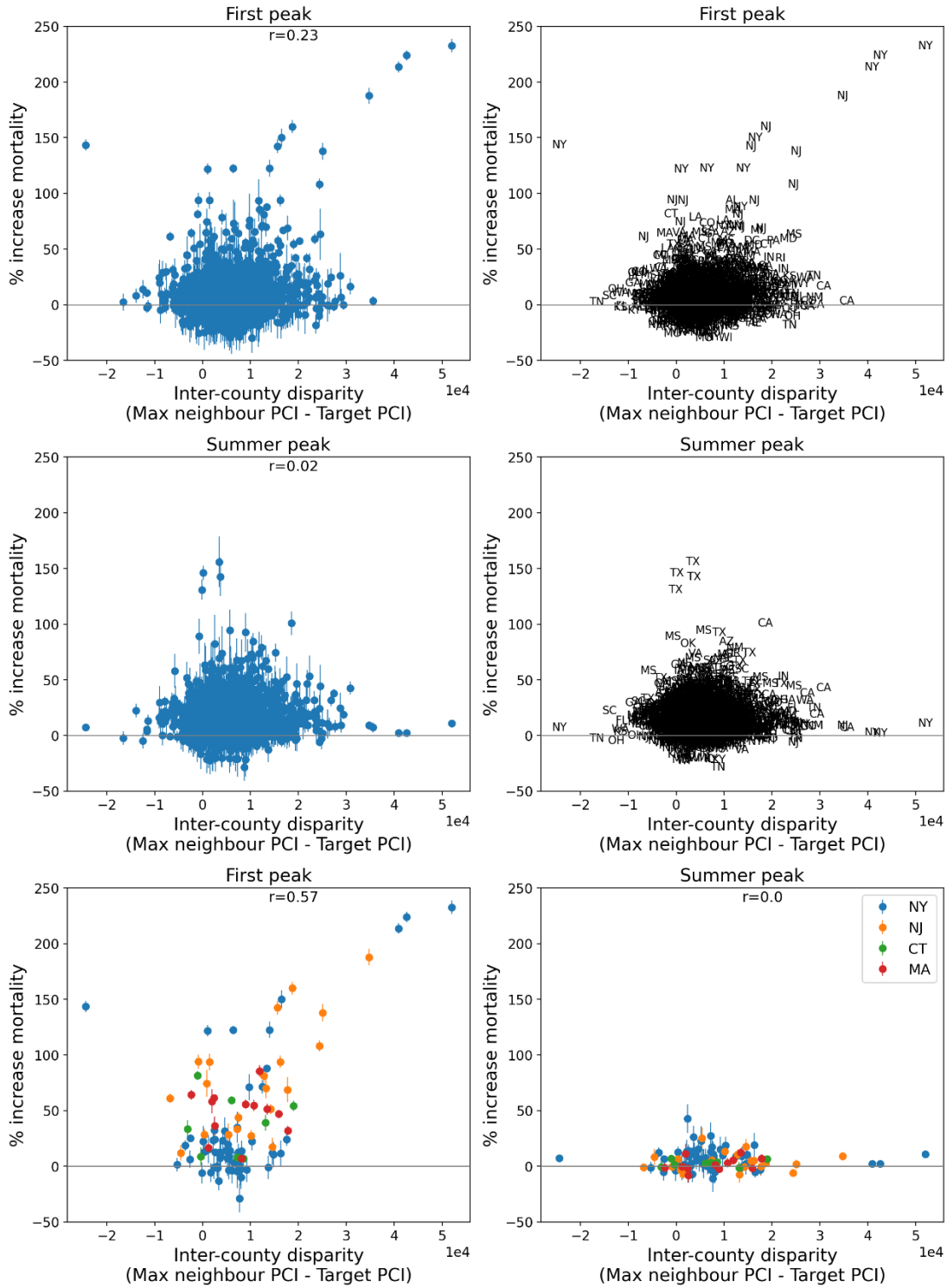


Figure 72: Same as Figure 64, with x-axis showing inter-county disparity, equal to the maximum of the county of interest's (target county) neighbors' per capita incomes (PCI), minus the target county's PCI (estimates from the 5-Year American Community Survey for the years 2014-2018).

Integrated P-score vs % households with more people than rooms

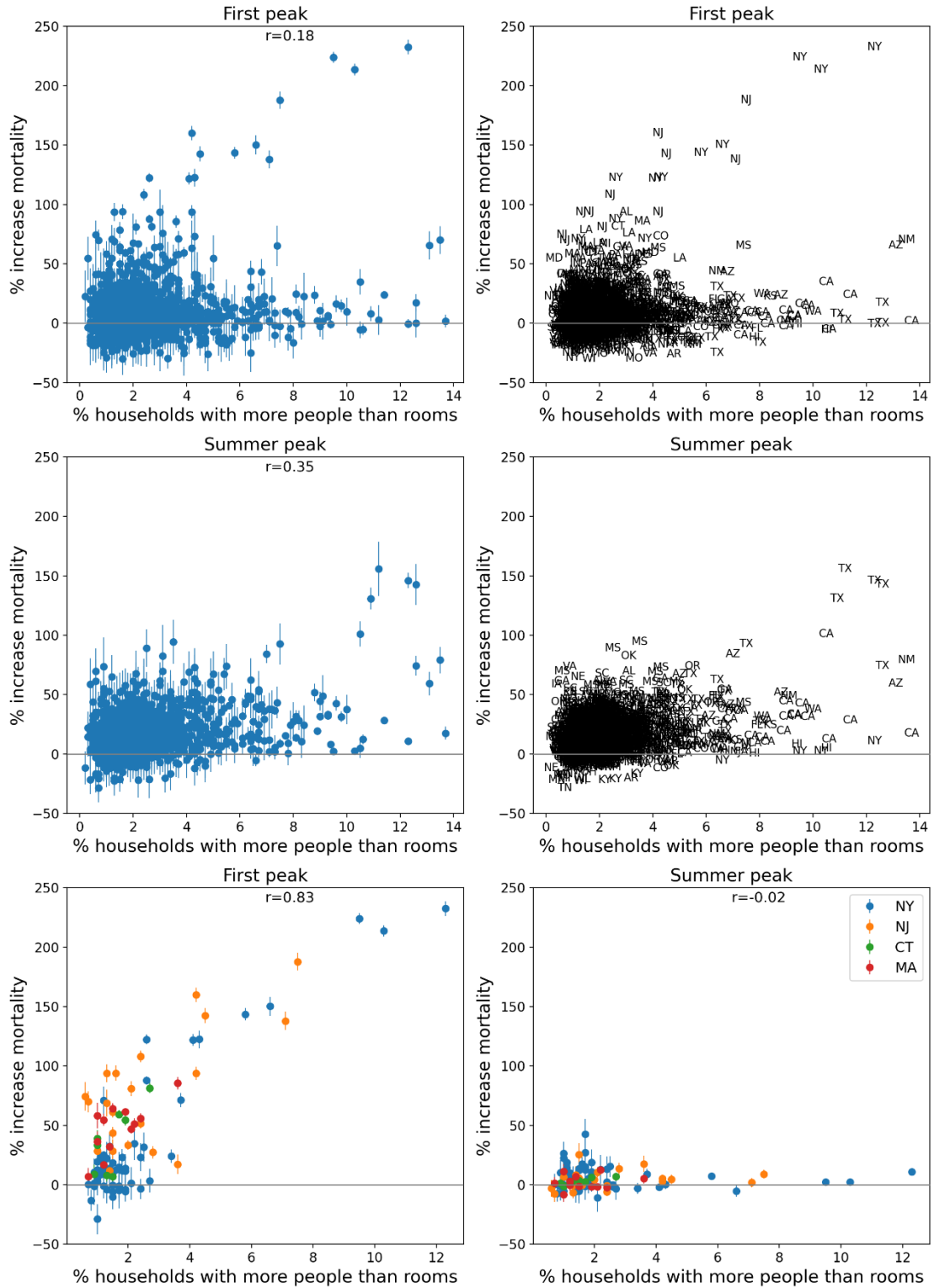


Figure 74: Same as Figure 64, with x-axis showing the % of households in the county with more people than rooms (estimates from the 5-Year American Community Survey for the years 2014-2018).

Integrated P-score vs % living in housing structures with 10+ units

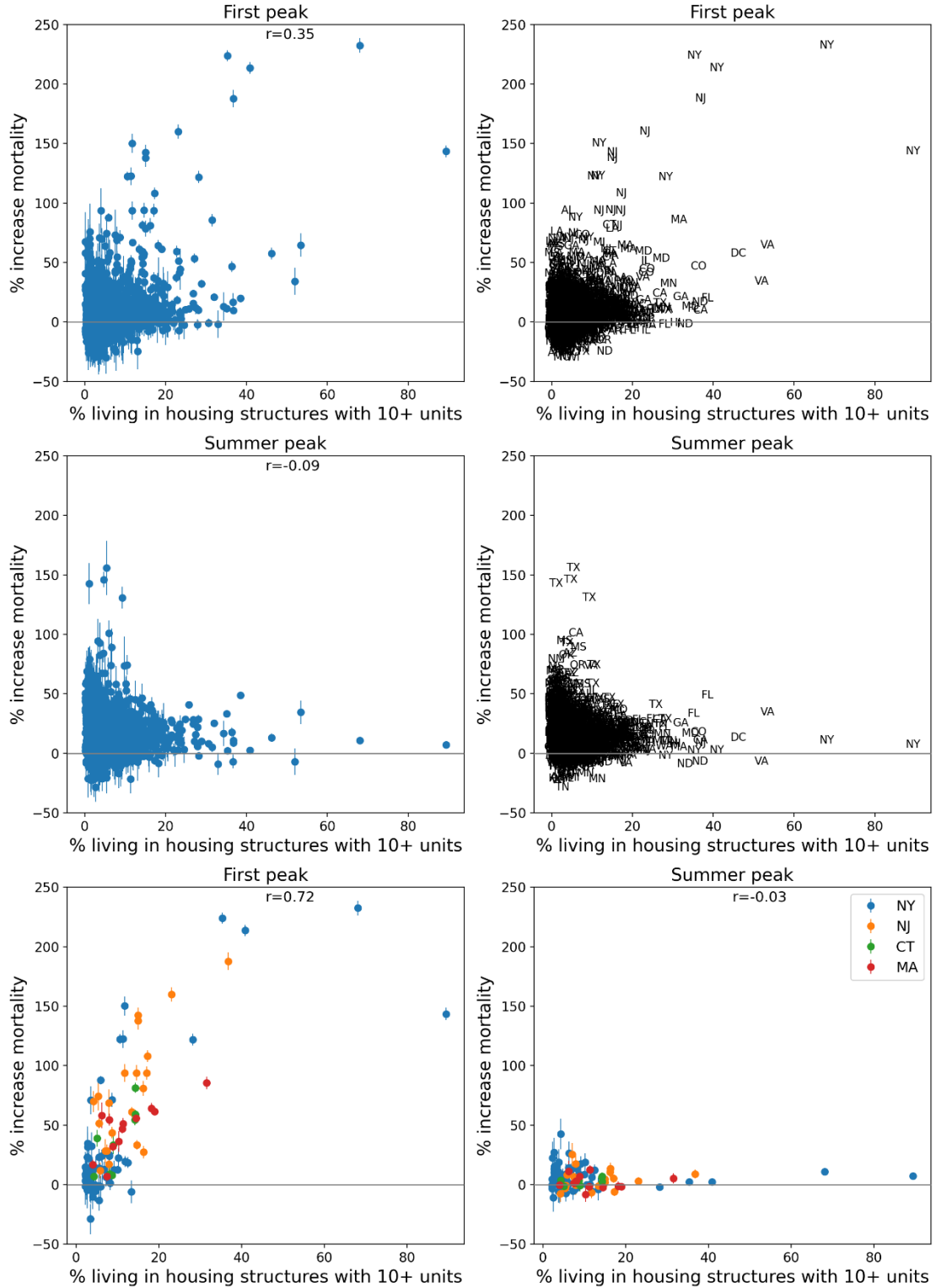


Figure 75: Same as Figure 64, with x-axis showing the % of the county's population living in housing structures with more than 10 units (estim. from 5-Year American Community Survey for 2014-2018).

Integrated P-score vs % who speak English "less than well"

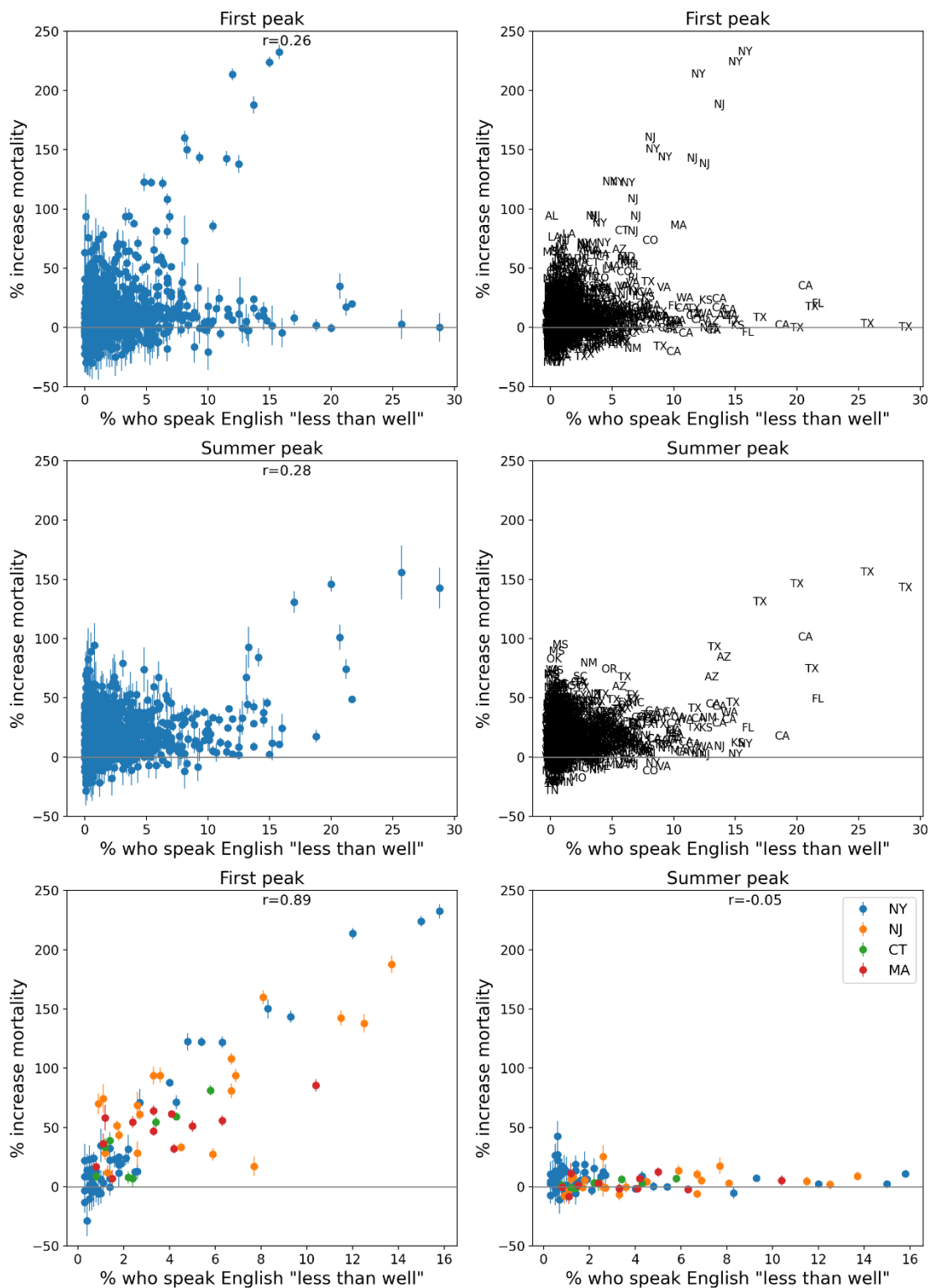


Figure 76: Same as Figure 64, with x-axis showing the % of the county's population that speaks English "less than well" (estimates from the 5-Year American Community Survey for the years 2014-2018).

Integrated P-score vs % minority

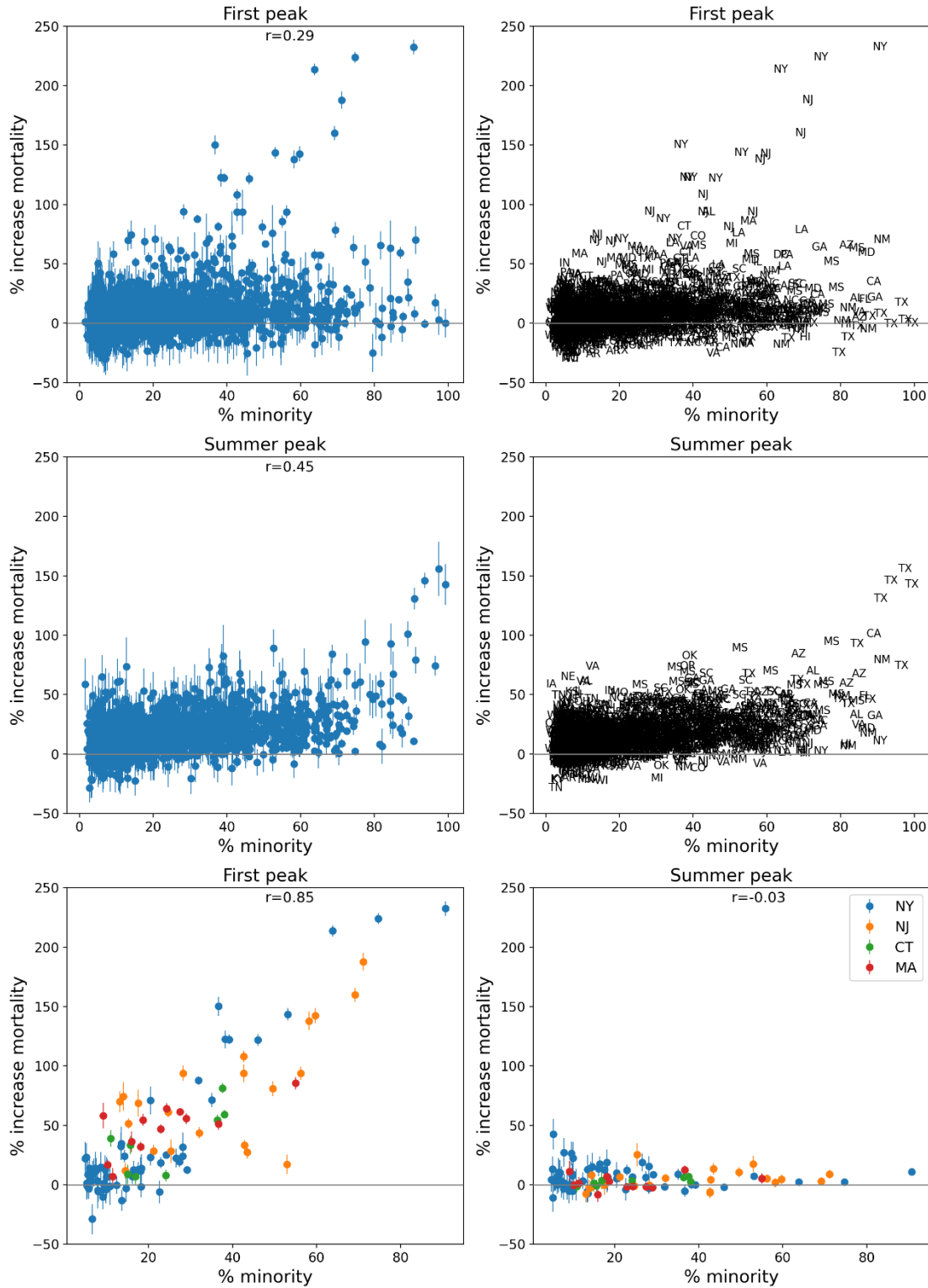


Figure 77: Same as Figure 64, with x-axis showing the % of the county's population that is a minority (non-white) (estimates from the 5-Year American Community Survey for the years 2014-2018).

Integrated P-score vs % aged 25+ with no high school diploma

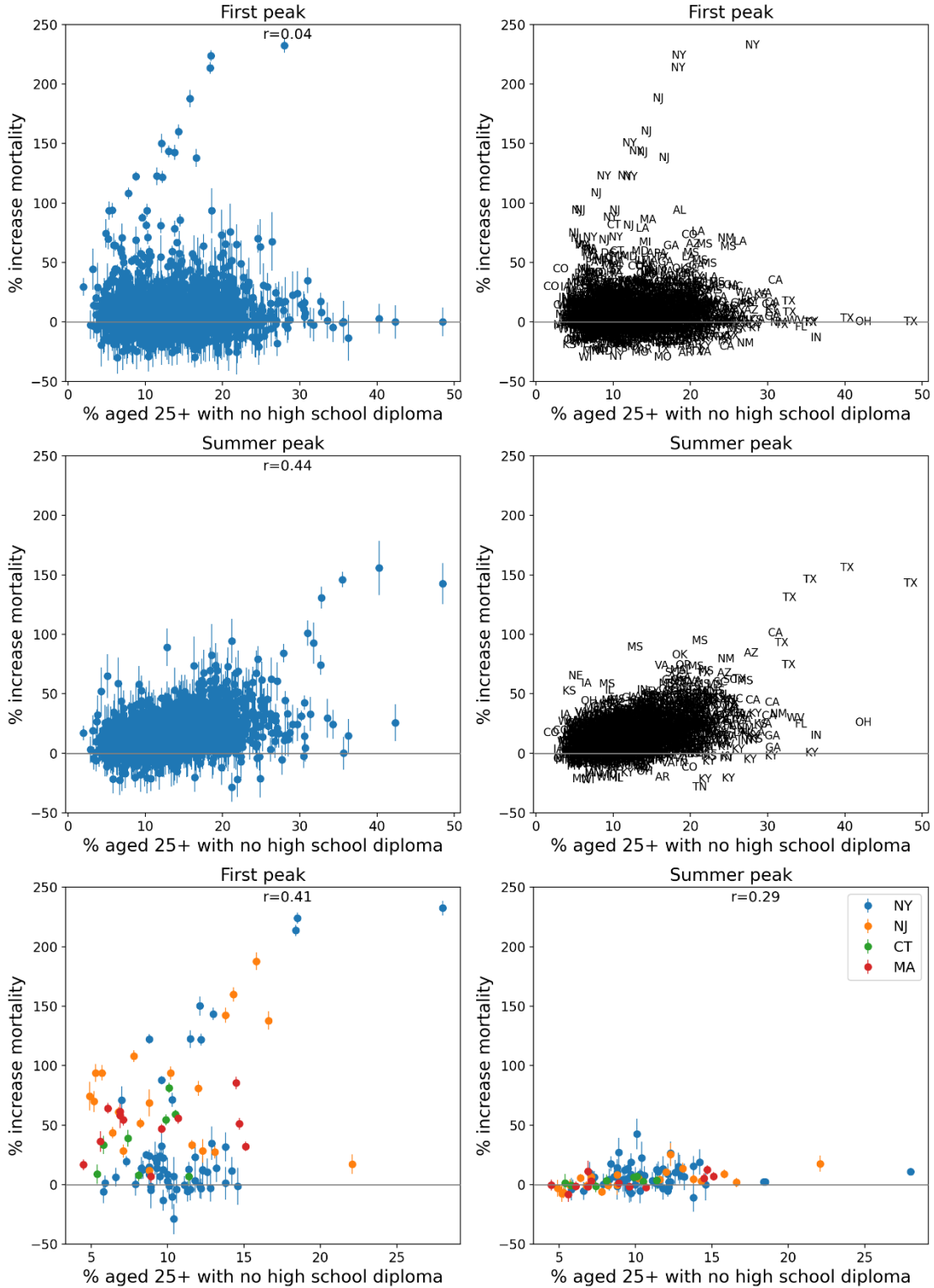


Figure 78: Same as Figure 64, with x-axis showing the % of the county's population aged 25+ with no high school diploma (estimates from the 5-Year American Community Survey for 2014-2018).

Integrated P-score vs % population aged 65+

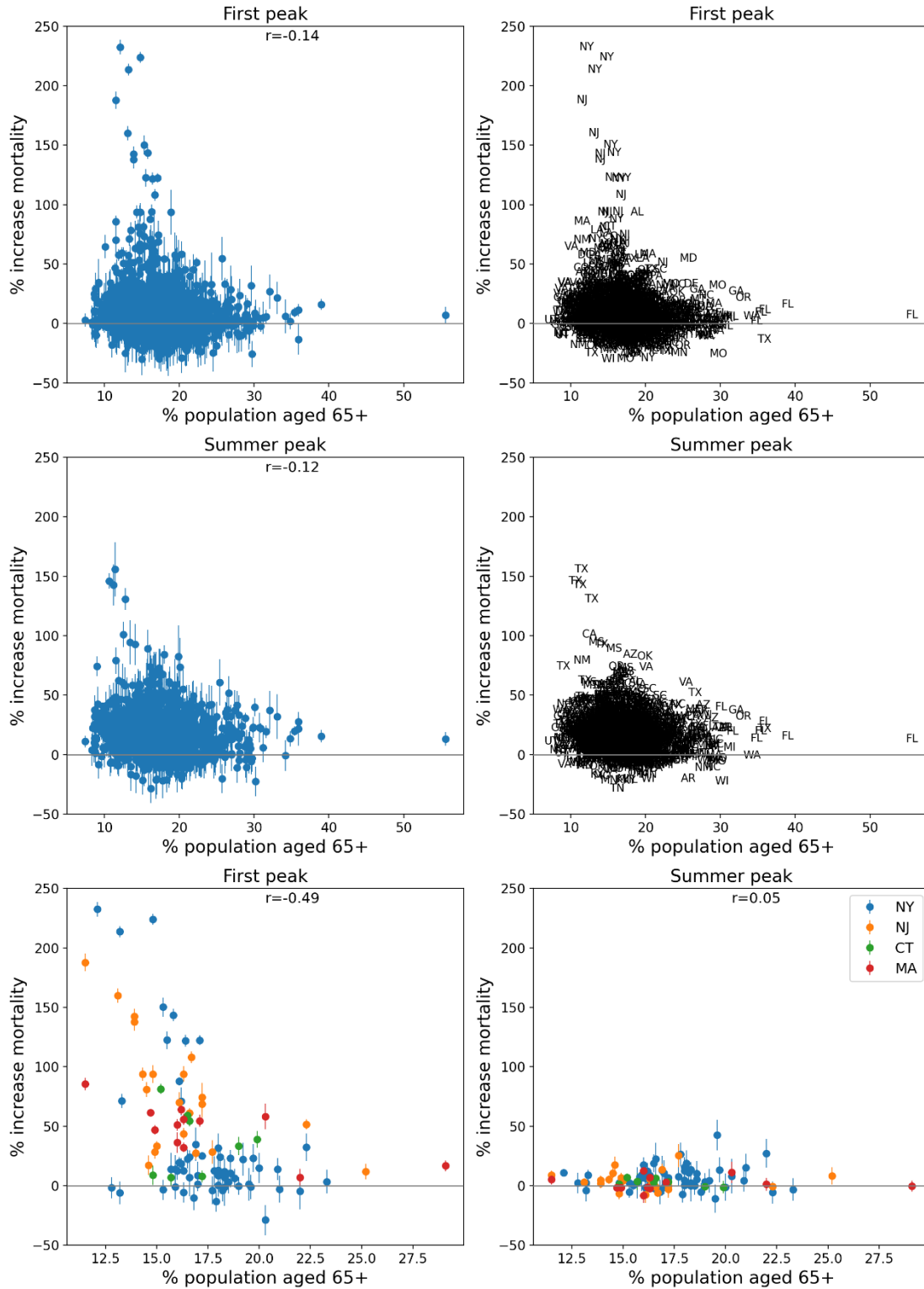


Figure 79: Same as Figure 64, with x-axis showing the % of the county's population that is aged 65+ (estimates from the 5-Year American Community Survey for the years 2014-2018).

Integrated P-score vs % population aged 17 and under

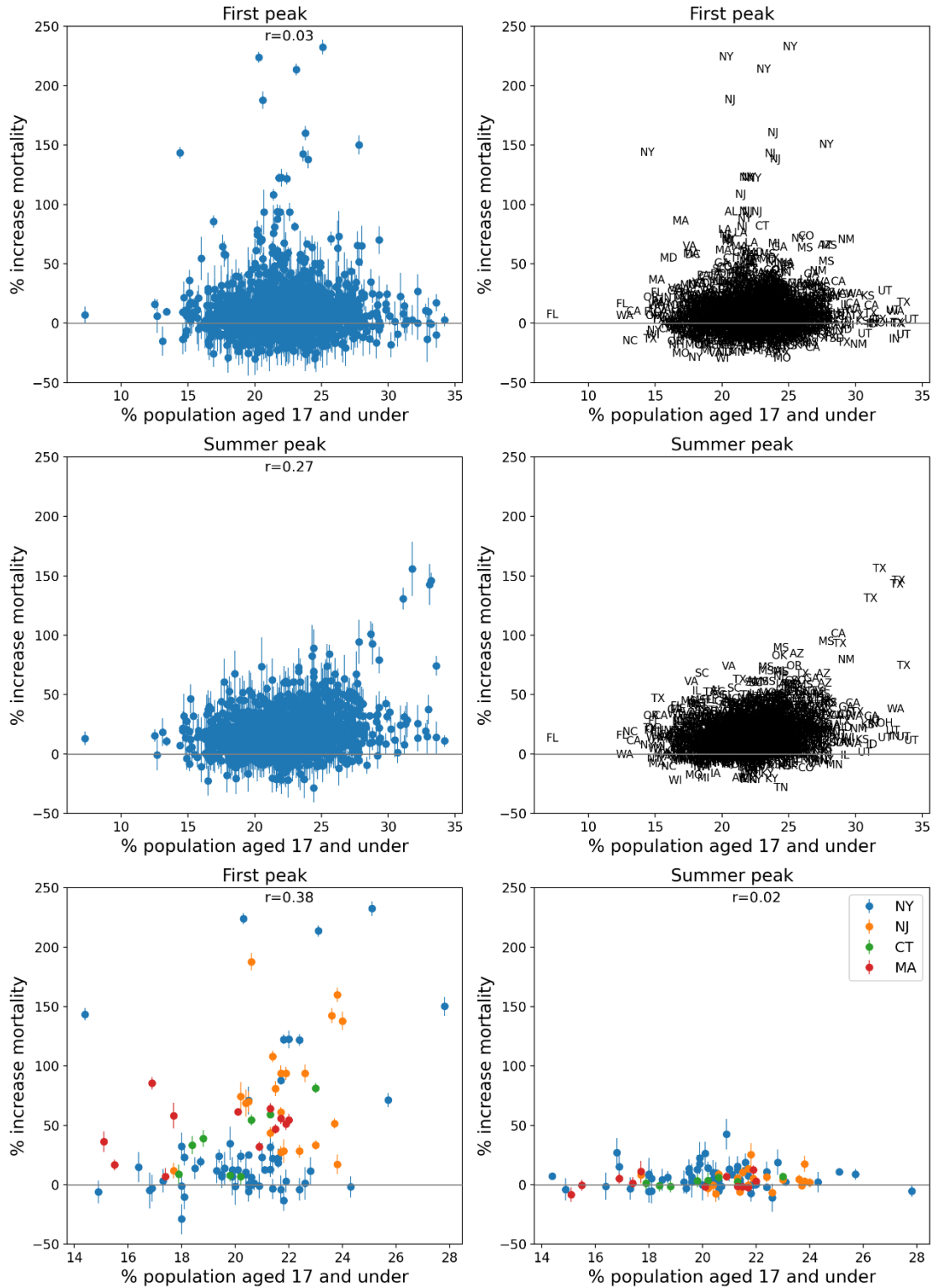


Figure 80: Same as Figure 64, with x-axis showing the % of the county's population that is aged 17 and under (estimates from the 5-Year American Community Survey for the years 2014-2018).

Integrated P-score vs % single-parent households

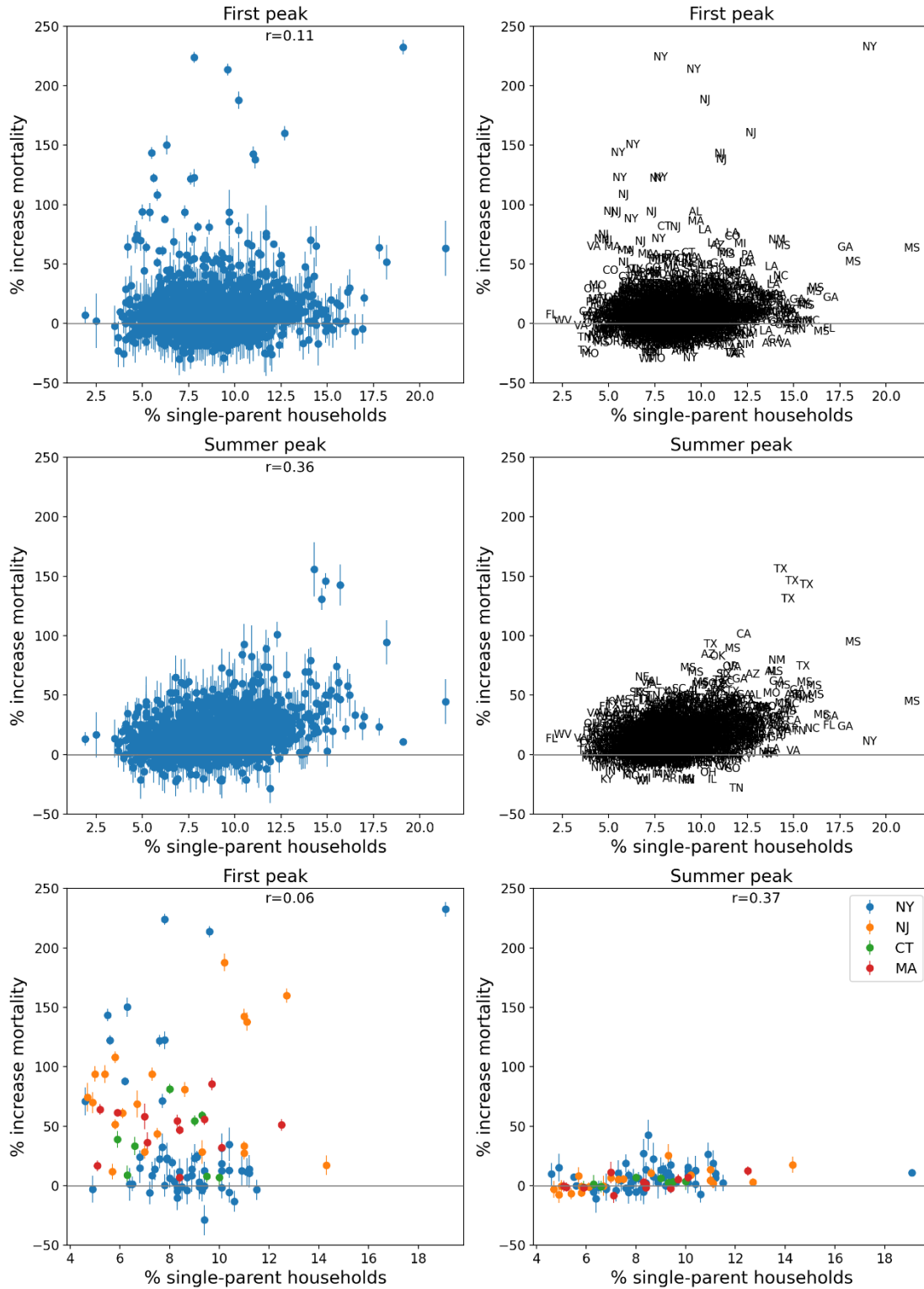


Figure 81: Same as Figure 64, with x-axis showing the % of the county's households that are single-parent households (estimates from the 5-Year American Community Survey for the years 2014-2018).

Integrated P-score vs % with disability

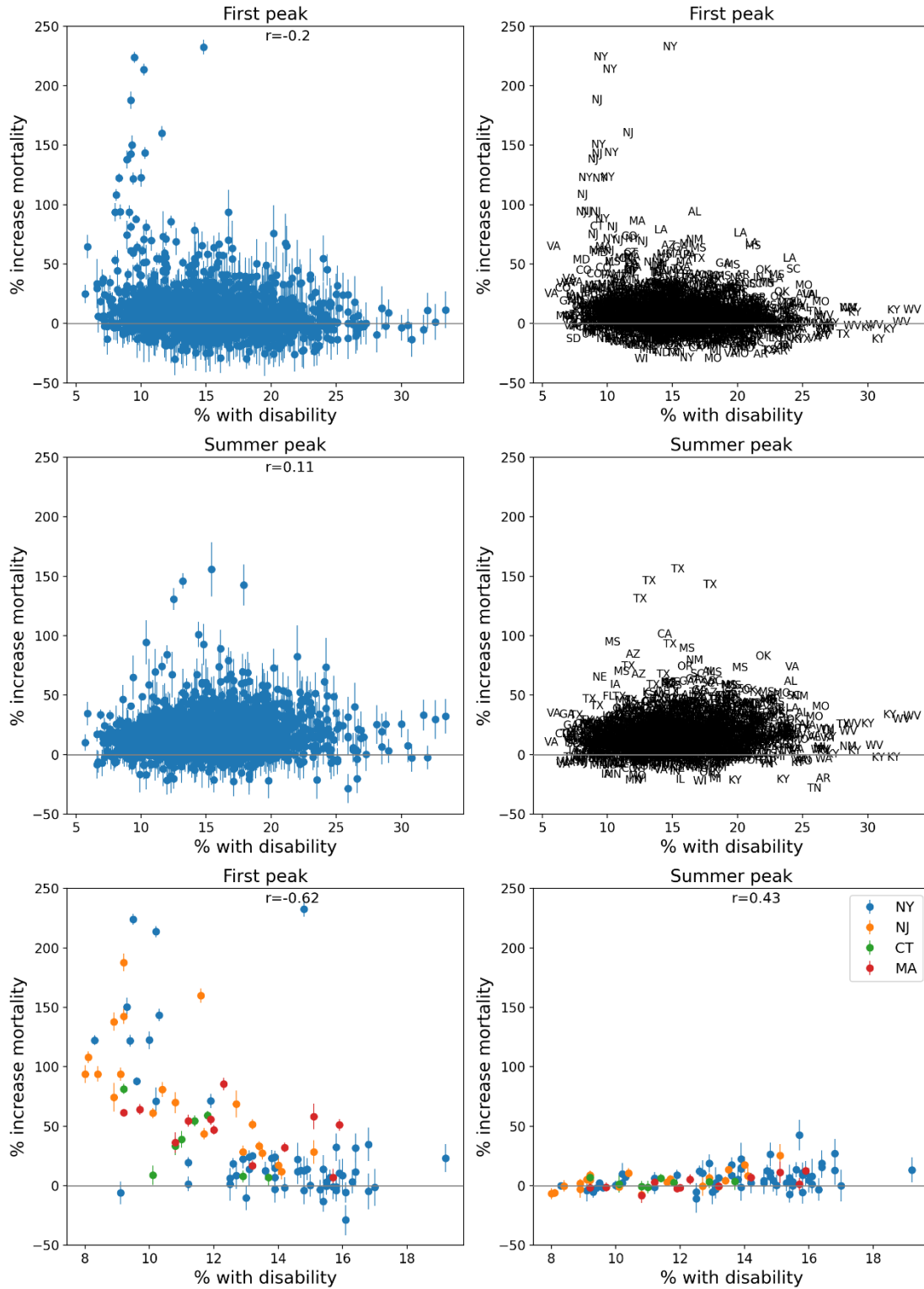


Figure 82: Same as Figure 64, with x-axis showing the % of the county's population with a disability (estimates from the 5-Year American Community Survey for the years 2014-2018).

Integrated P-score vs % diabetes

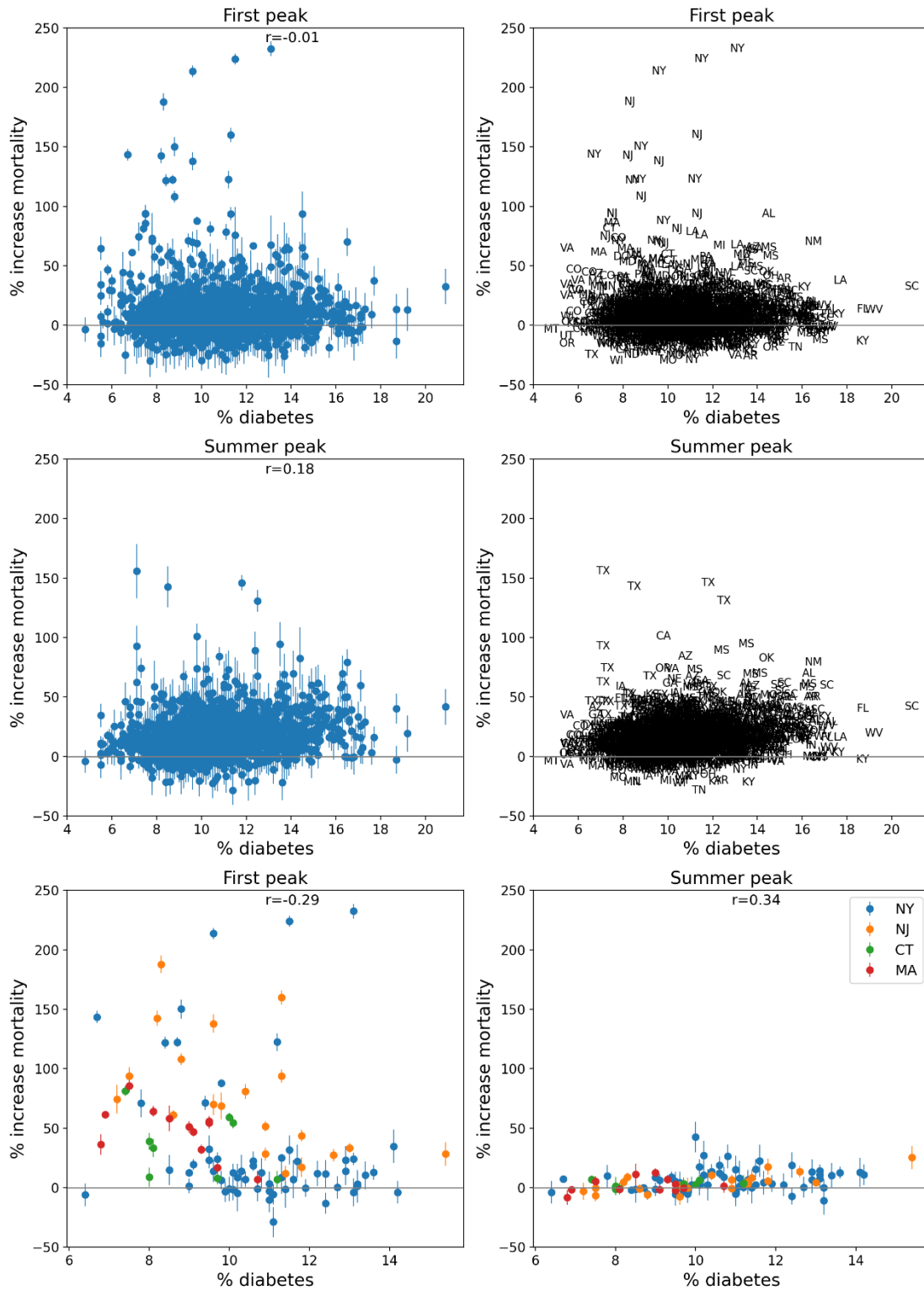


Figure 83: Same as Figure 64, with x-axis showing the % of the county's population with diabetes in 2018.

Integrated P-score vs % obesity

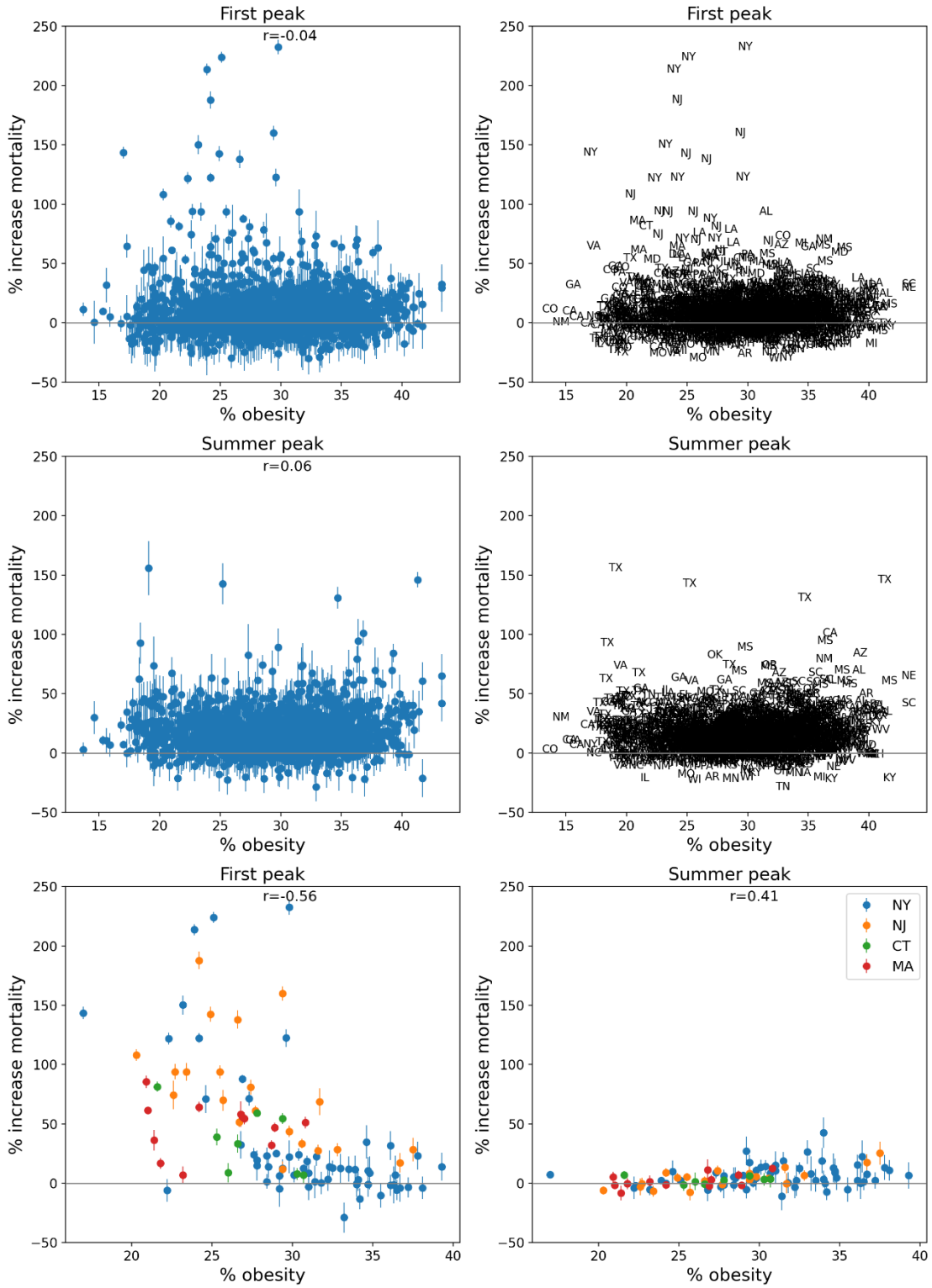


Figure 84: Same as Figure 64, with x-axis showing the % of the county's population with obesity in 2018.

Integrated P-score vs Share of votes cast that were for the Democratic presidential candidate in 2016

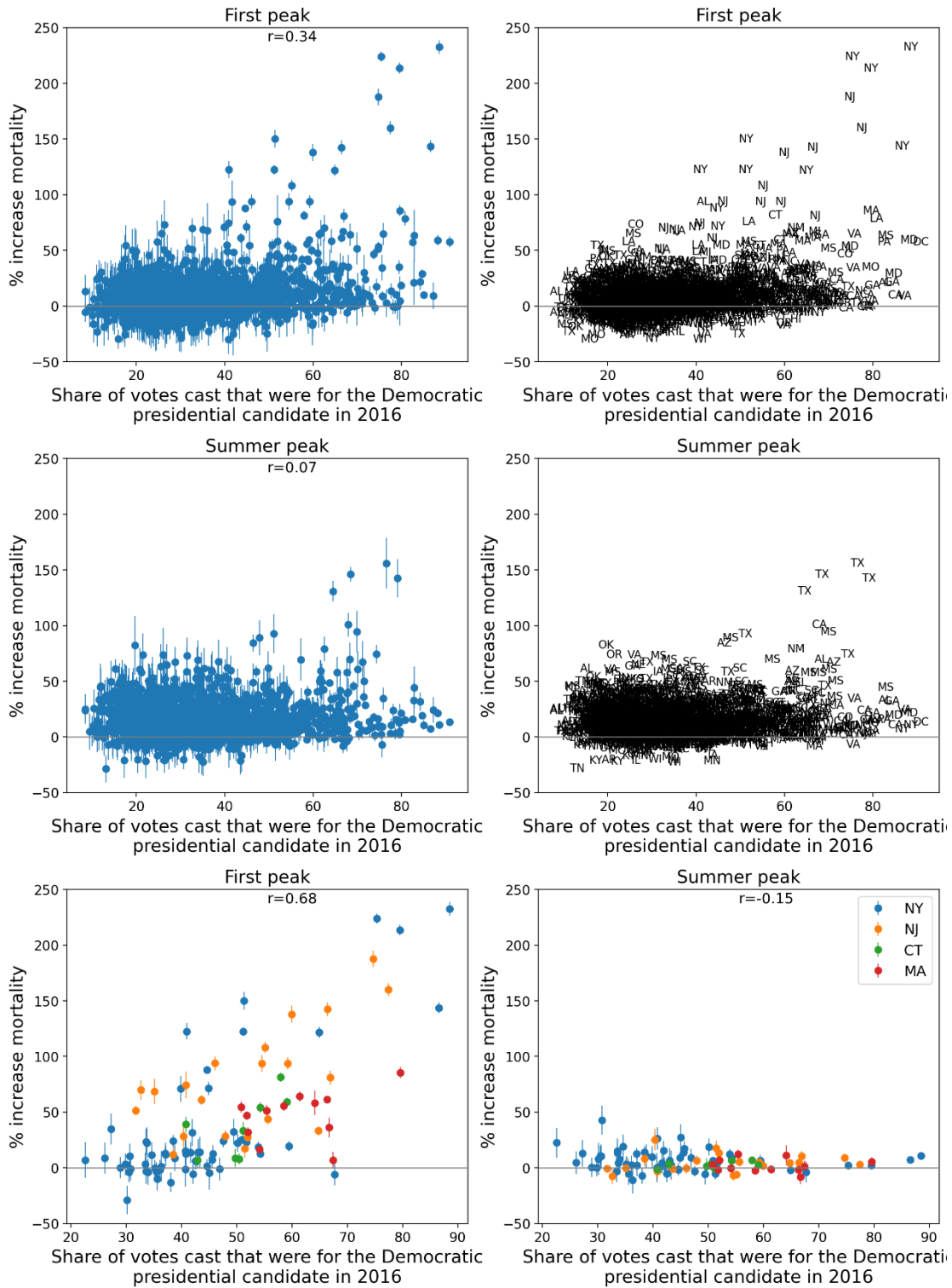


Figure 85: Same as Figure 64, with x-axis showing the % of the votes cast in the 2016 USA election that were for the Democratic Party's presidential candidate.

Integrated P-score vs % deaths occurring at home in Mar-May 2019

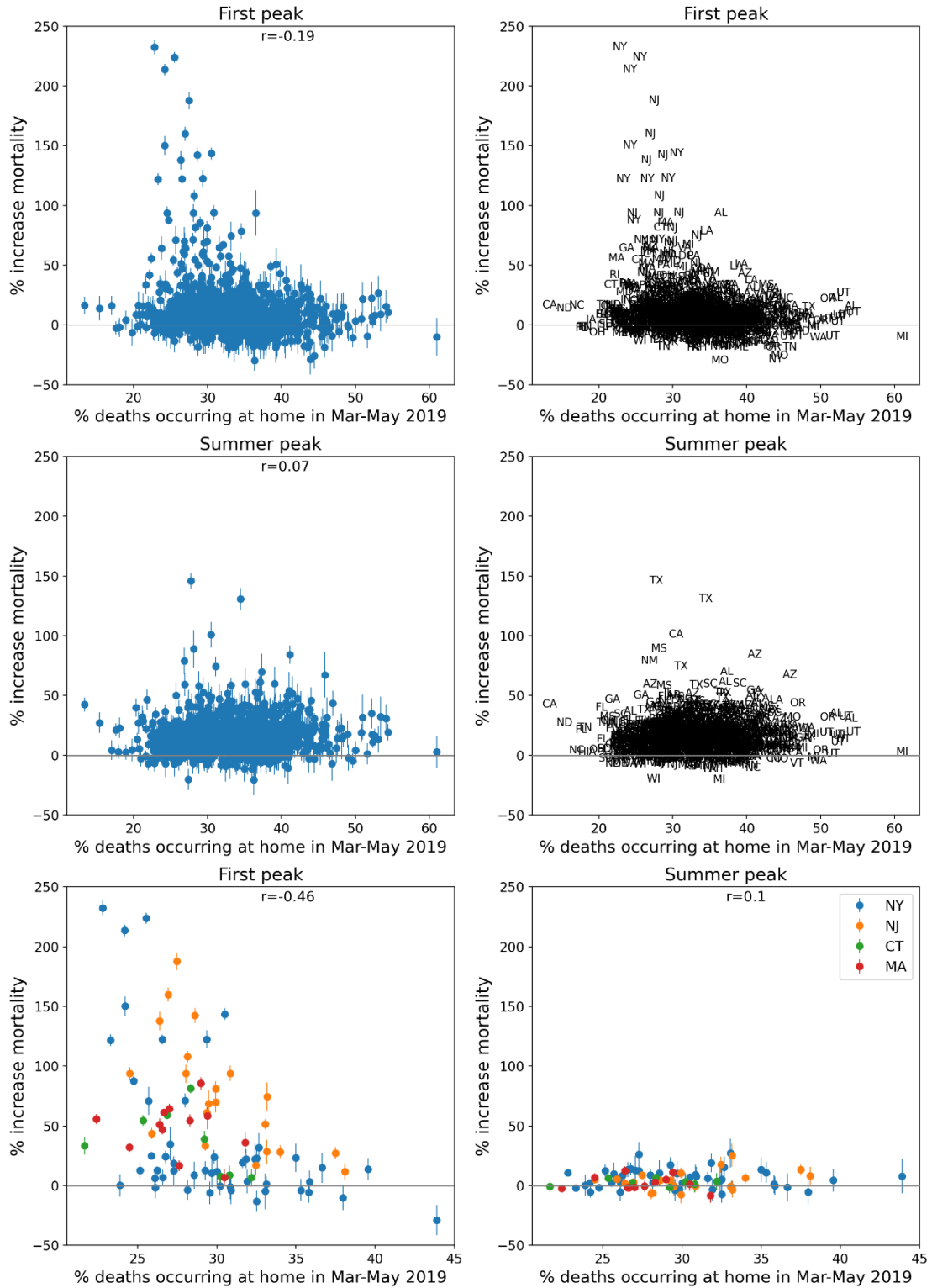


Figure 86: Same as Figure 64, with x-axis showing the % of all deaths in the county in March-May 2019 that occurred at home.

Integrated P-score vs % deaths occurring at home in Jun-Sep 2019

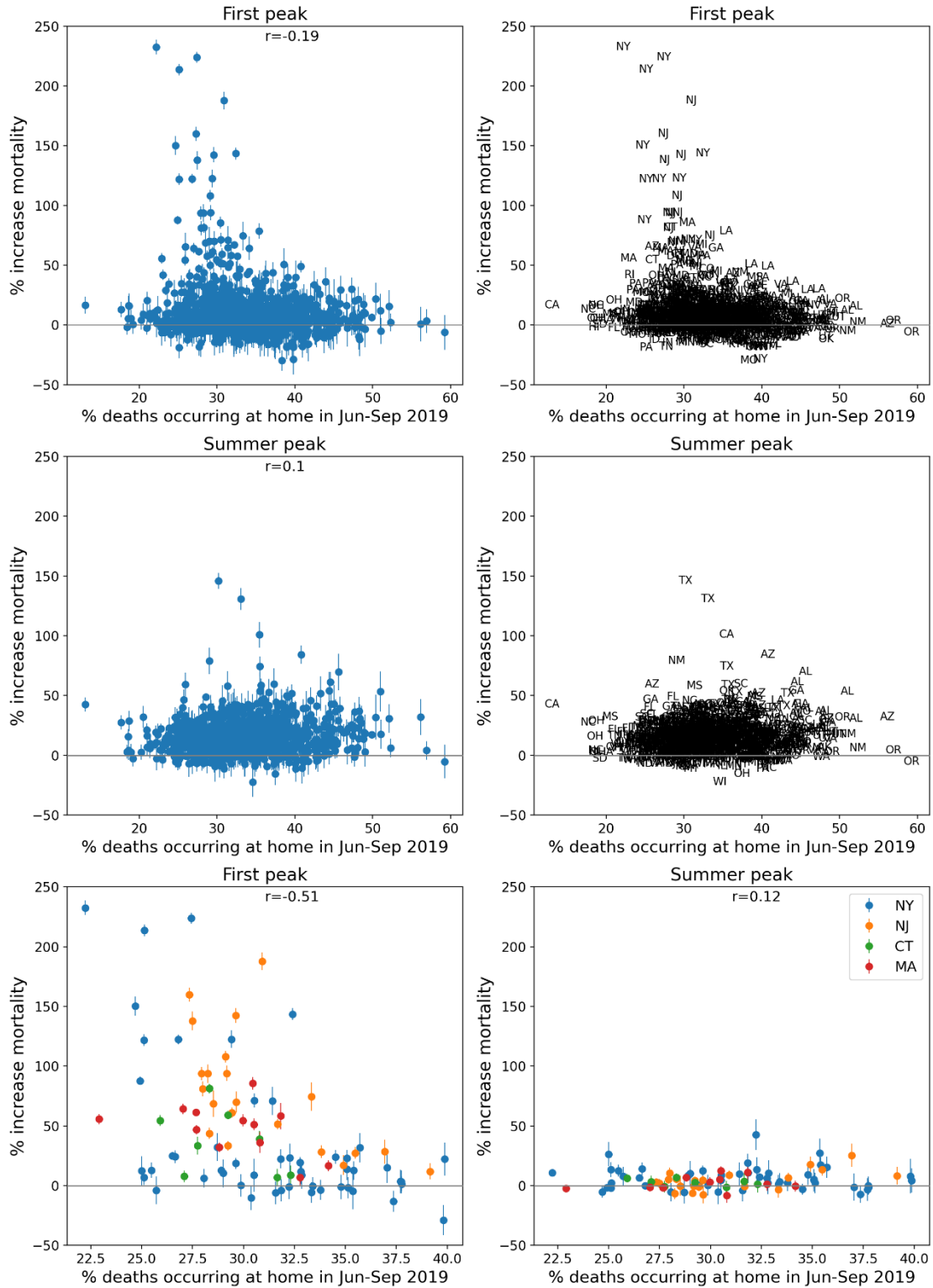


Figure 87: Same as Figure 64, with x-axis showing the % of all deaths in the county in June-September 2019 that occurred at home.

Integrated P-score vs % deaths occurring in hospital in Mar-May 2019

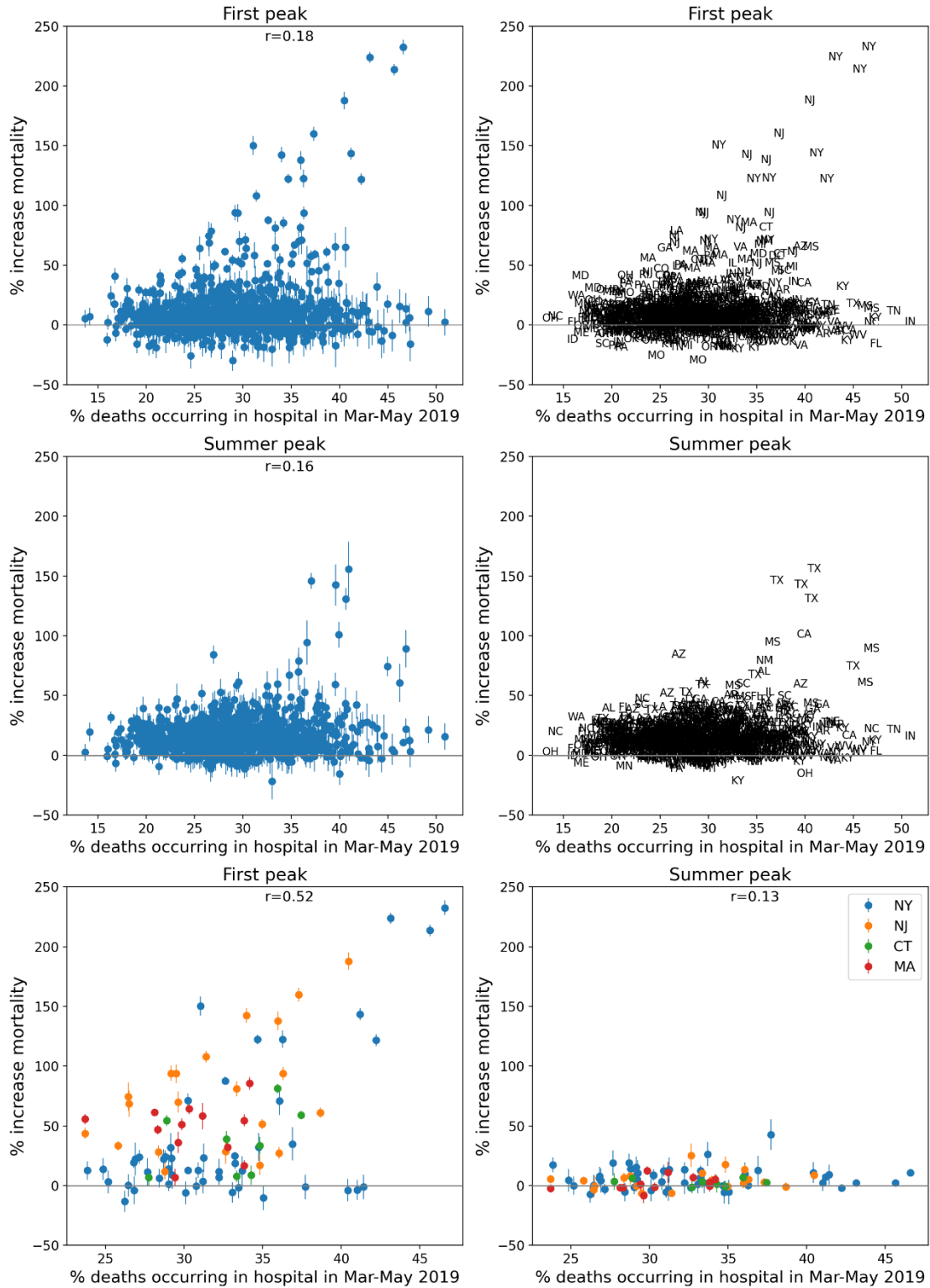


Figure 88: Same as Figure 64, with x-axis showing the % of all deaths in the county in March-May 2019 that occurred in hospital (“Medical Facility – Inpatient”).

Integrated P-score vs % deaths occurring in hospital in Jun-Sep 2019

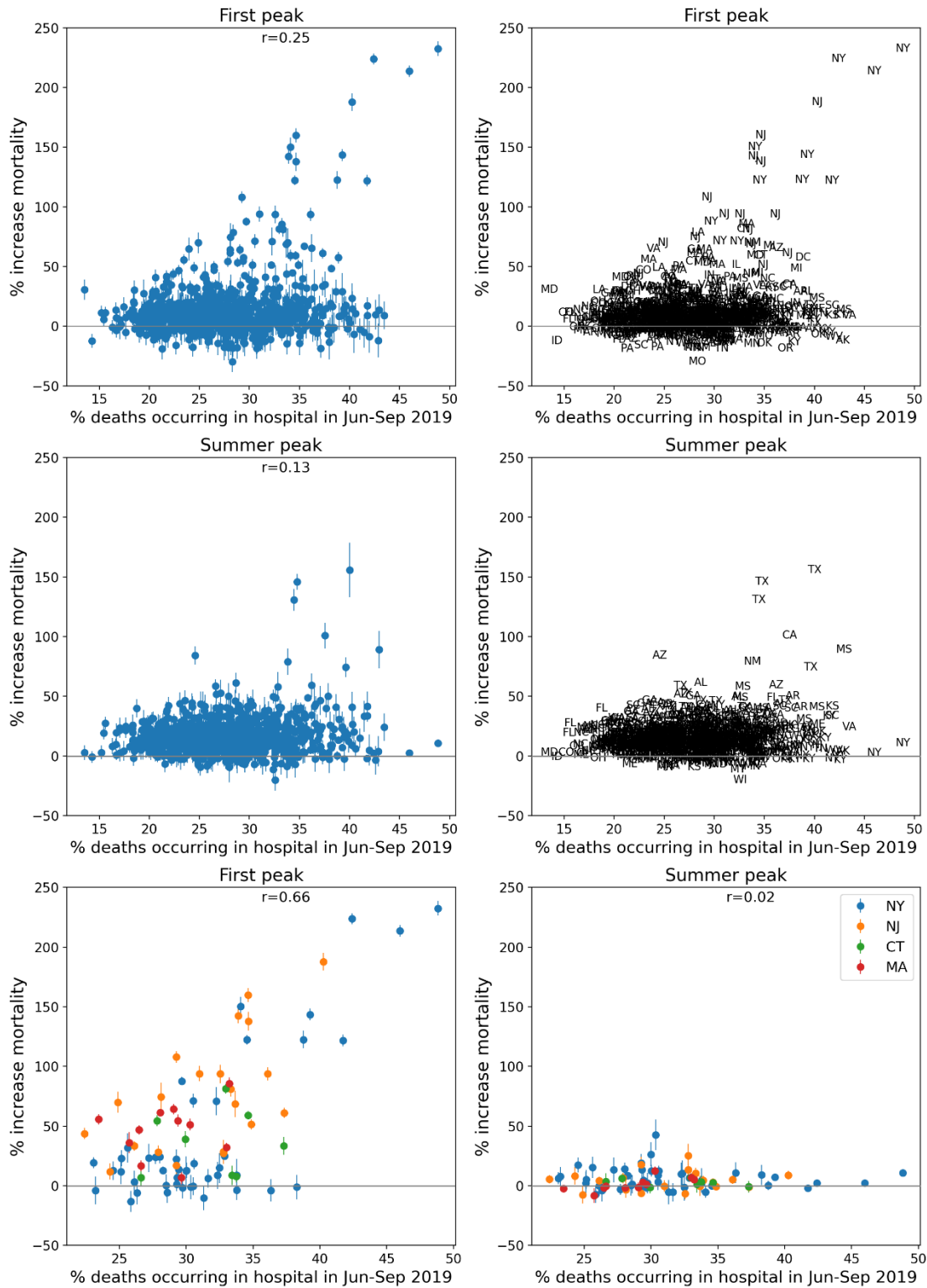


Figure 89: Same as Figure 64, with x-axis showing the % of all deaths in the county in June-September 2019 that occurred in hospital (“Medical Facility – Inpatient”).

Integrated P-score vs % deaths occurring in hospital in Mar-May 2020
 MINUS
 % deaths occurring in hospital in Mar-May 2019

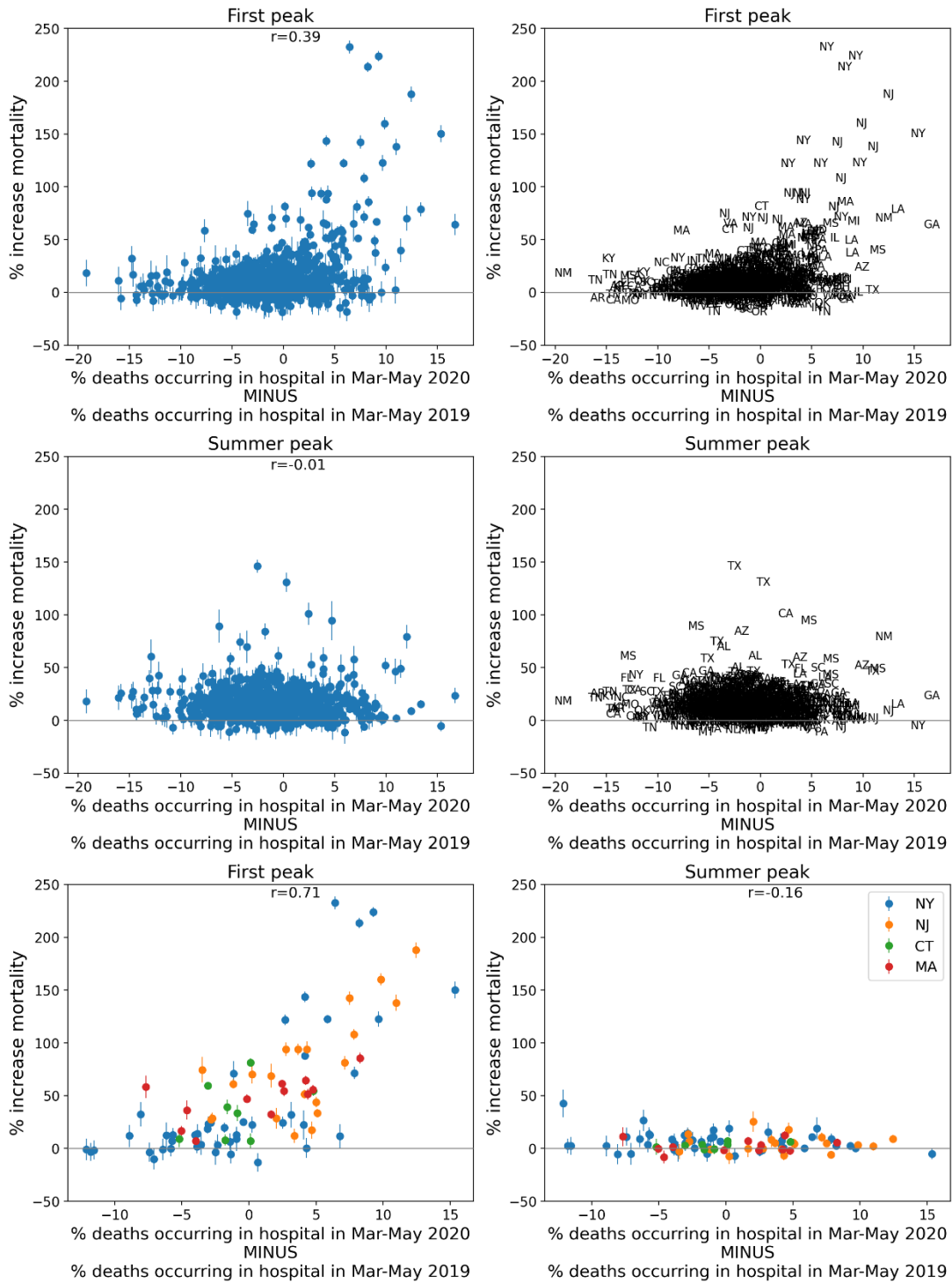


Figure 90: Same as Figure 64, with x-axis showing the difference in the % of all deaths in the county in March-May 2020 that occurred in hospital (“Medical Facility – Inpatient”) and the % of all deaths in the county in March-May 2019 that occurred in hospital.

Integrated P-score vs % deaths occurring in hospital in Jun-Sep 2020
MINUS
% deaths occurring in hospital in Jun-Sep 2019

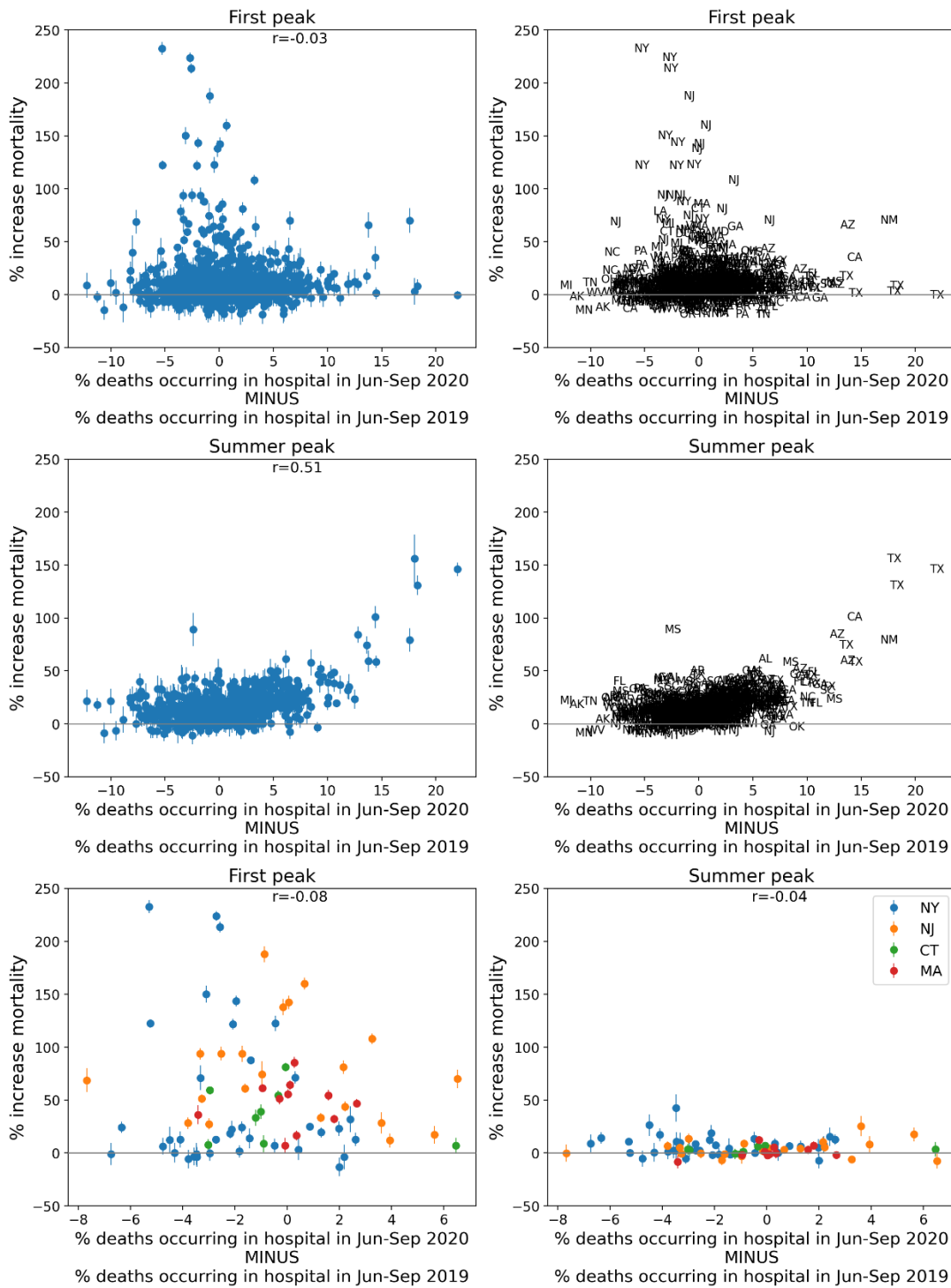


Figure 91: Same as Figure 64, with x-axis showing the difference in the % of all deaths in the county in June-September 2020 that occurred in hospital (“Medical Facility – Inpatient”) and the % of all deaths in the county in June-September 2019 that occurred in hospital.

Integrated P-score vs Num. prescription drug claims / pop

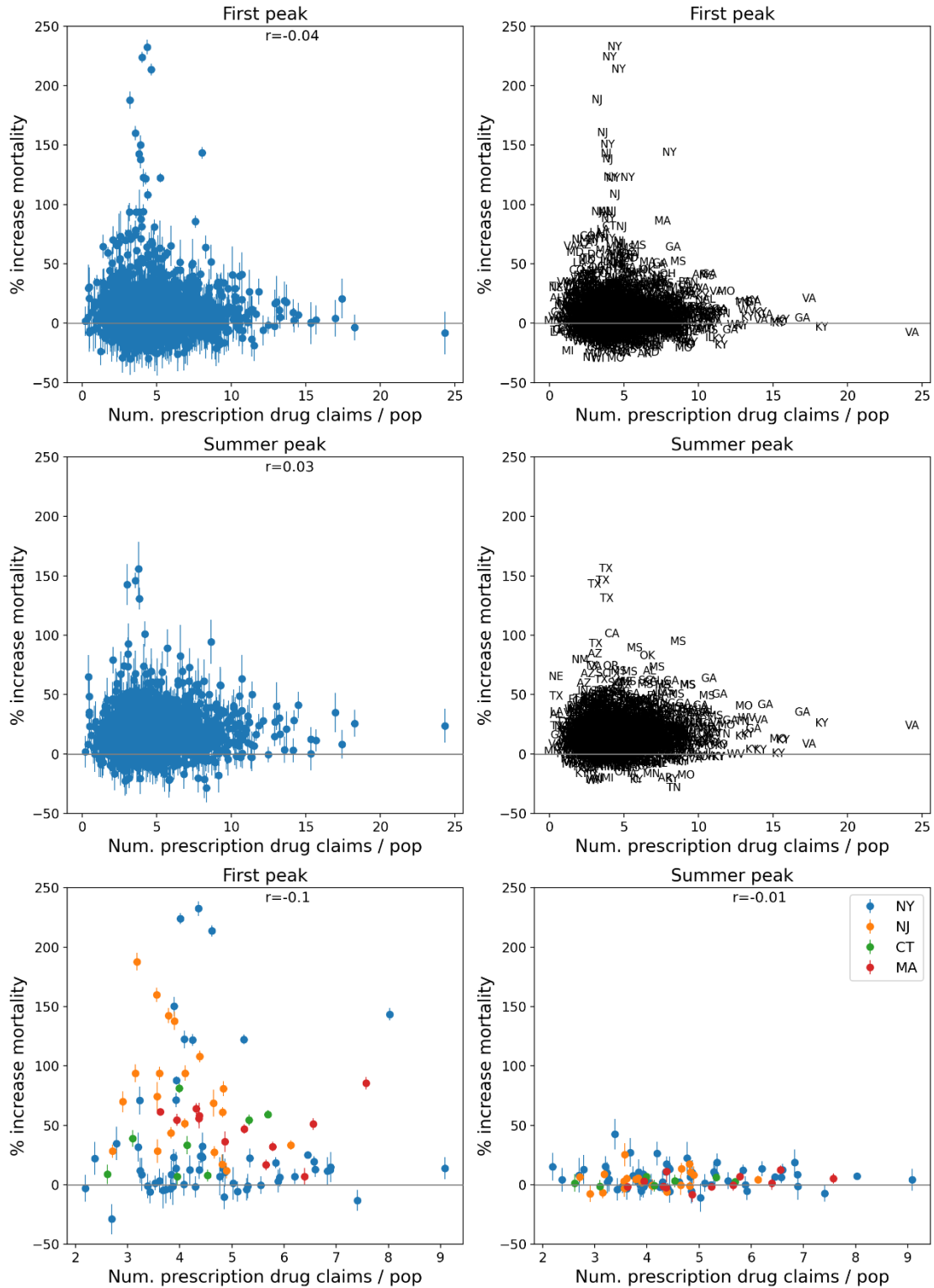


Figure 92: Same as Figure 64, with x-axis showing the number of prescription drug claims per population in the county in 2017.

Integrated P-score vs Num. antibiotic claims / pop

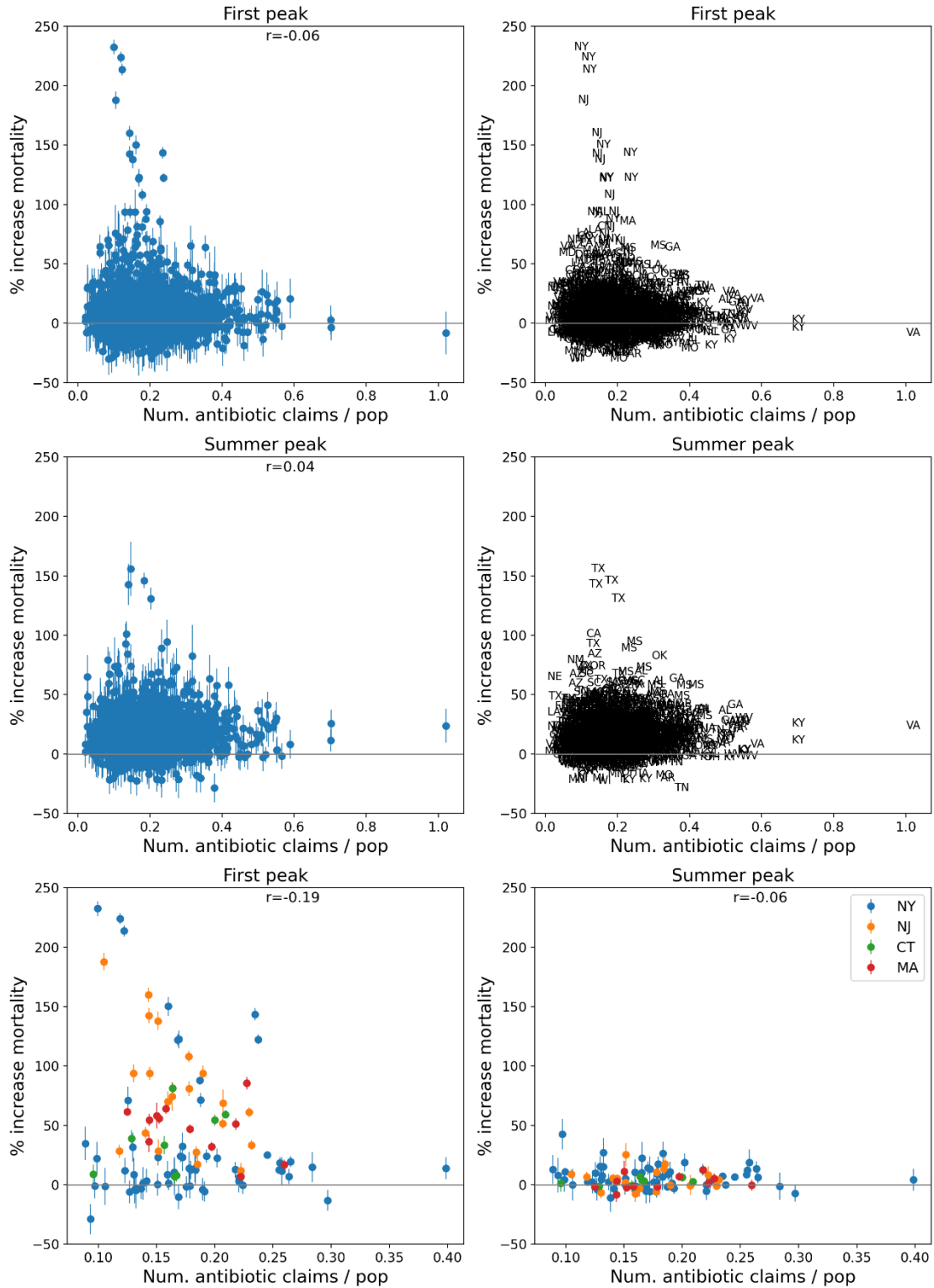


Figure 93: Same as Figure 64, with x-axis showing the % of the number of antibiotic prescription drug claims per population in the county in 2017.

Integrated P-score vs % pop 18+ with at least one dose
as of 2021-12-31

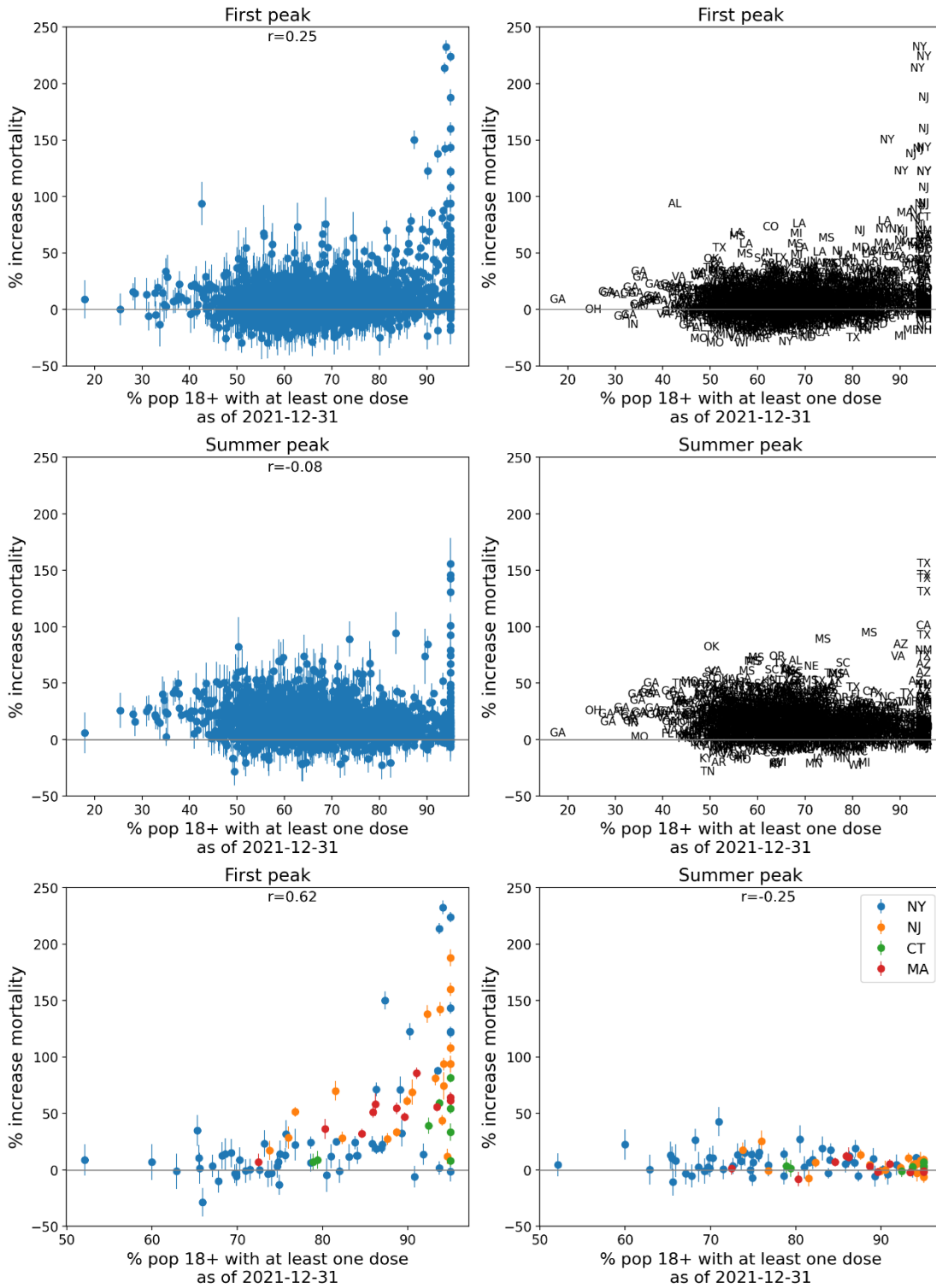


Figure 94: % of the population aged 18+ having received at least one dose of a COVID vaccine by December 31, 2021.

Integrated P-score vs % pop 65+ with at least one dose
as of 2021-12-31

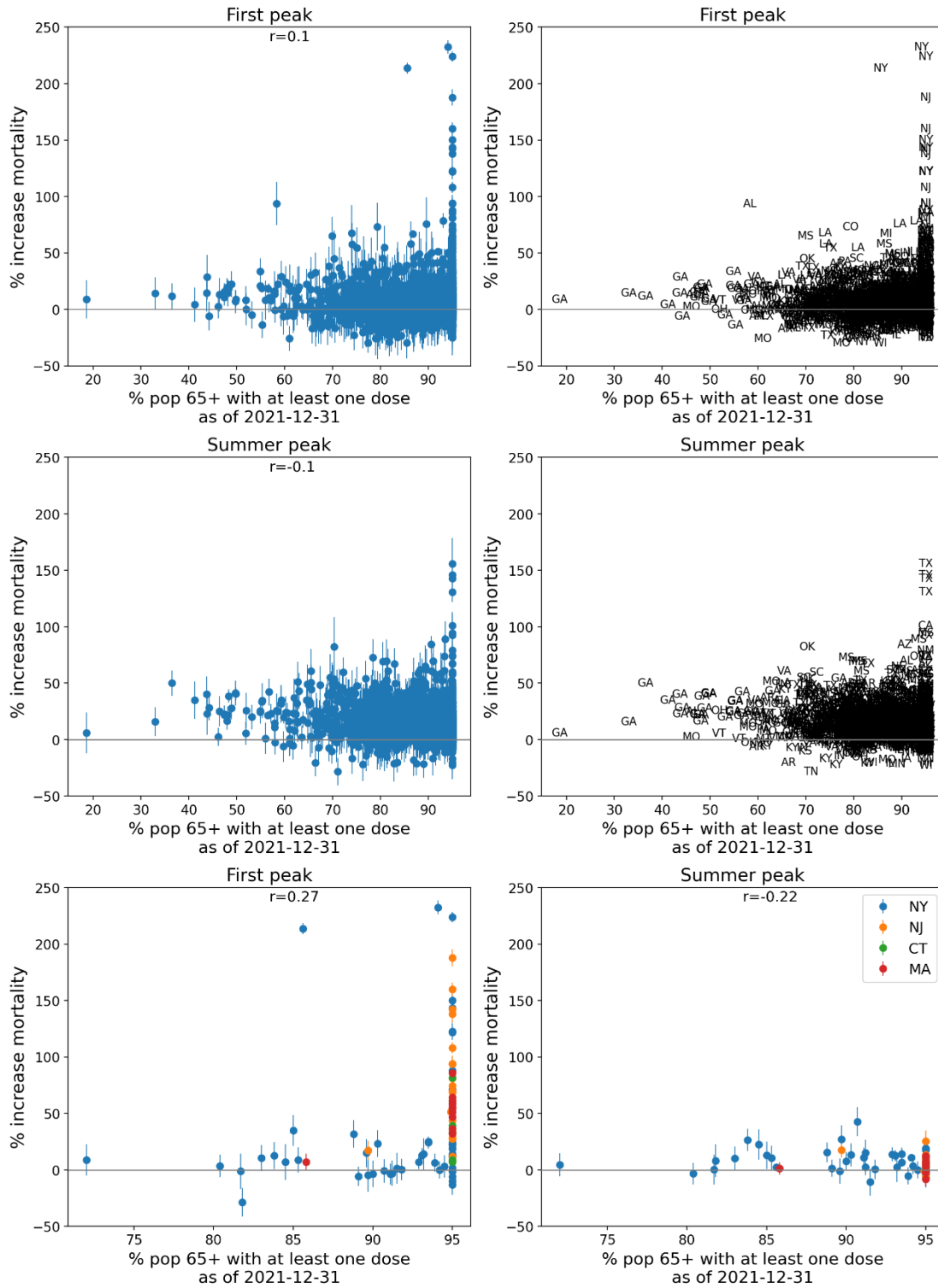


Figure 95: % of the population aged 65+ having received at least one dose of a COVID vaccine by December 31, 2021.

Integrated P-score vs % pop 18+ with primary series completed as of 2021-12-31

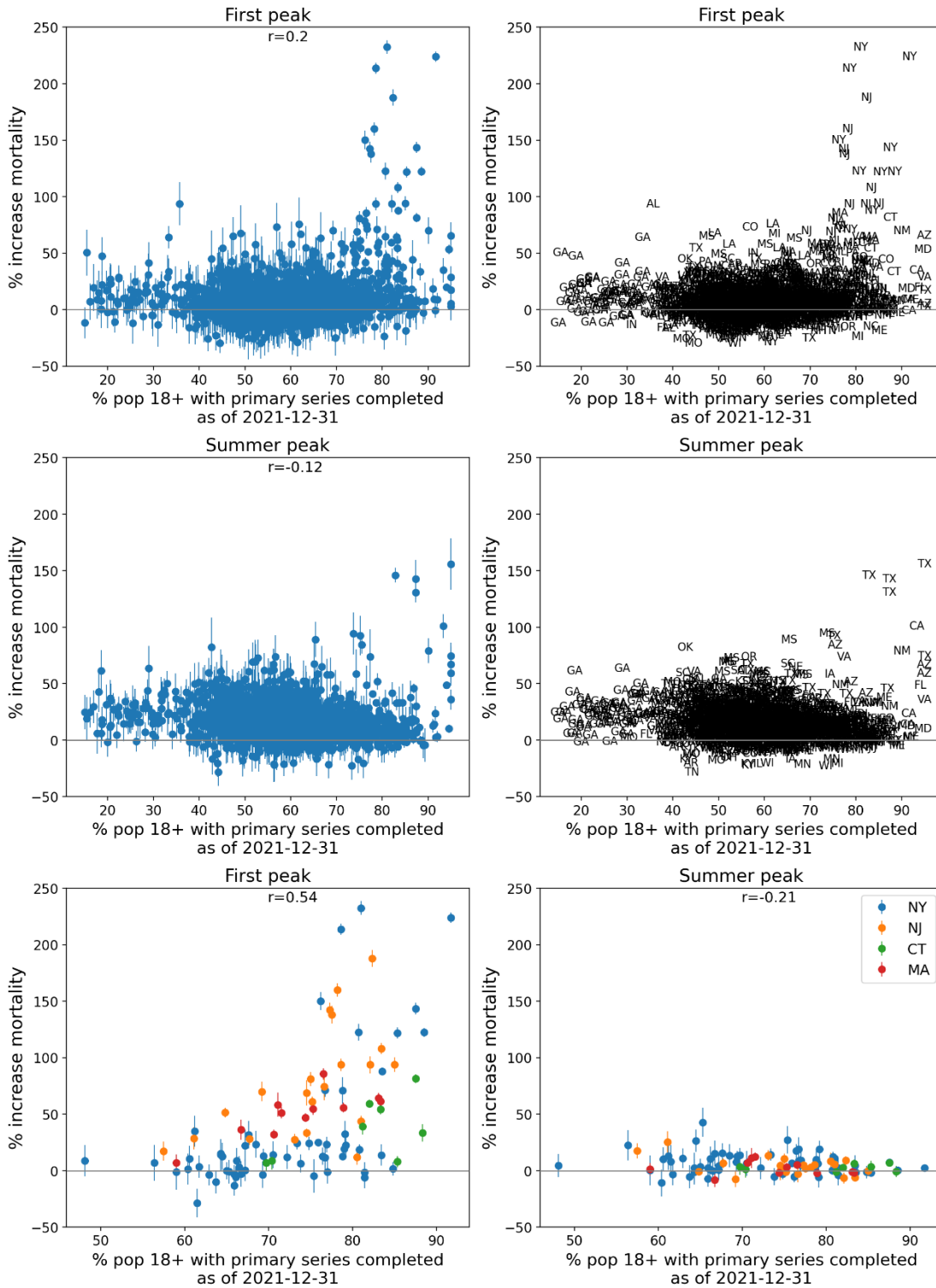


Figure 96: % of the population aged 18+ with primary series of a COVID vaccine completed by December 31, 2021.

Integrated P-score vs % pop 65+ with primary series completed as of 2021-12-31

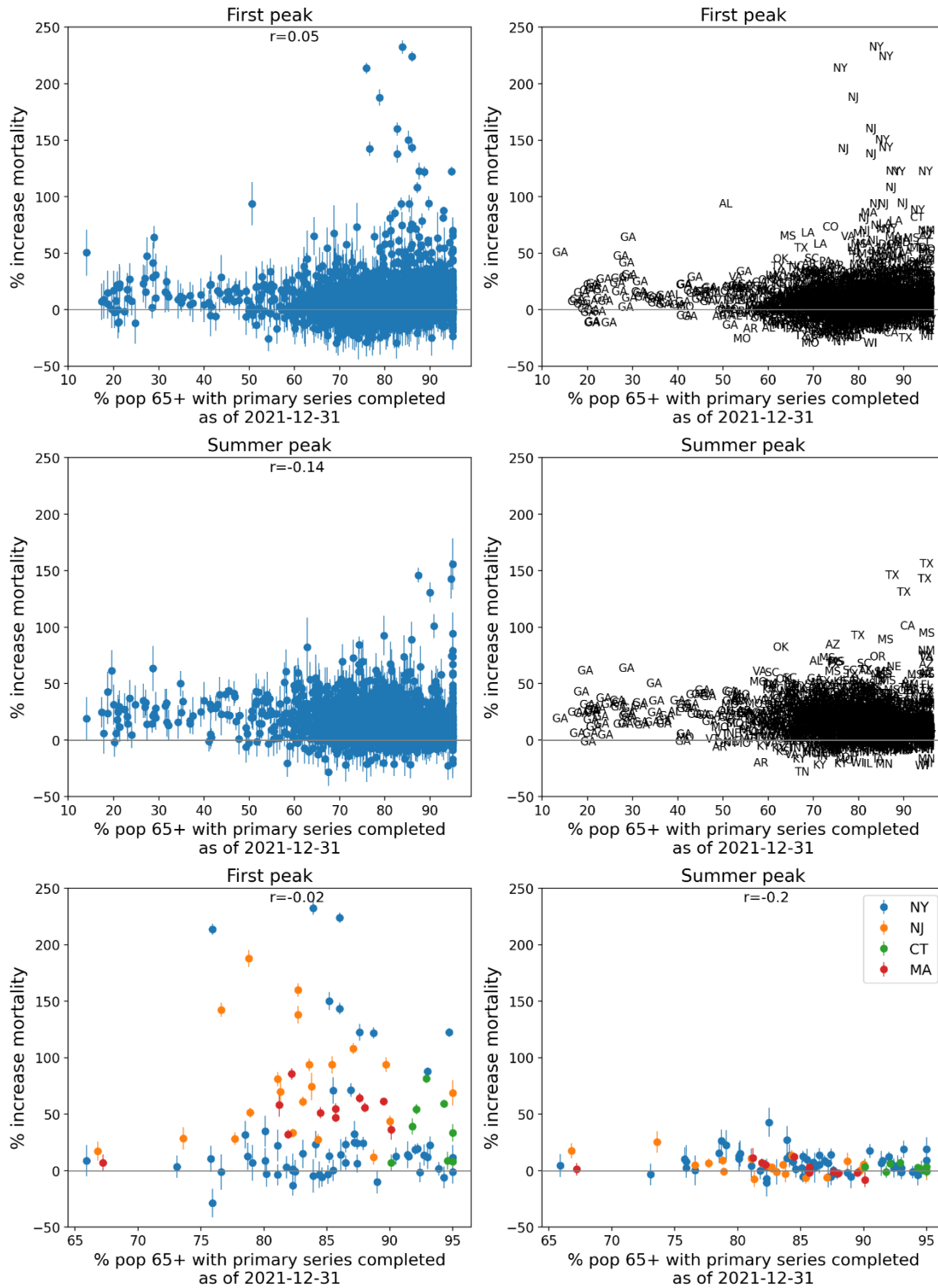


Figure 97: % of the population aged 65+ with primary series of a COVID vaccine completed by December 31, 2021.

Excess deaths per day vs Number of ICU beds

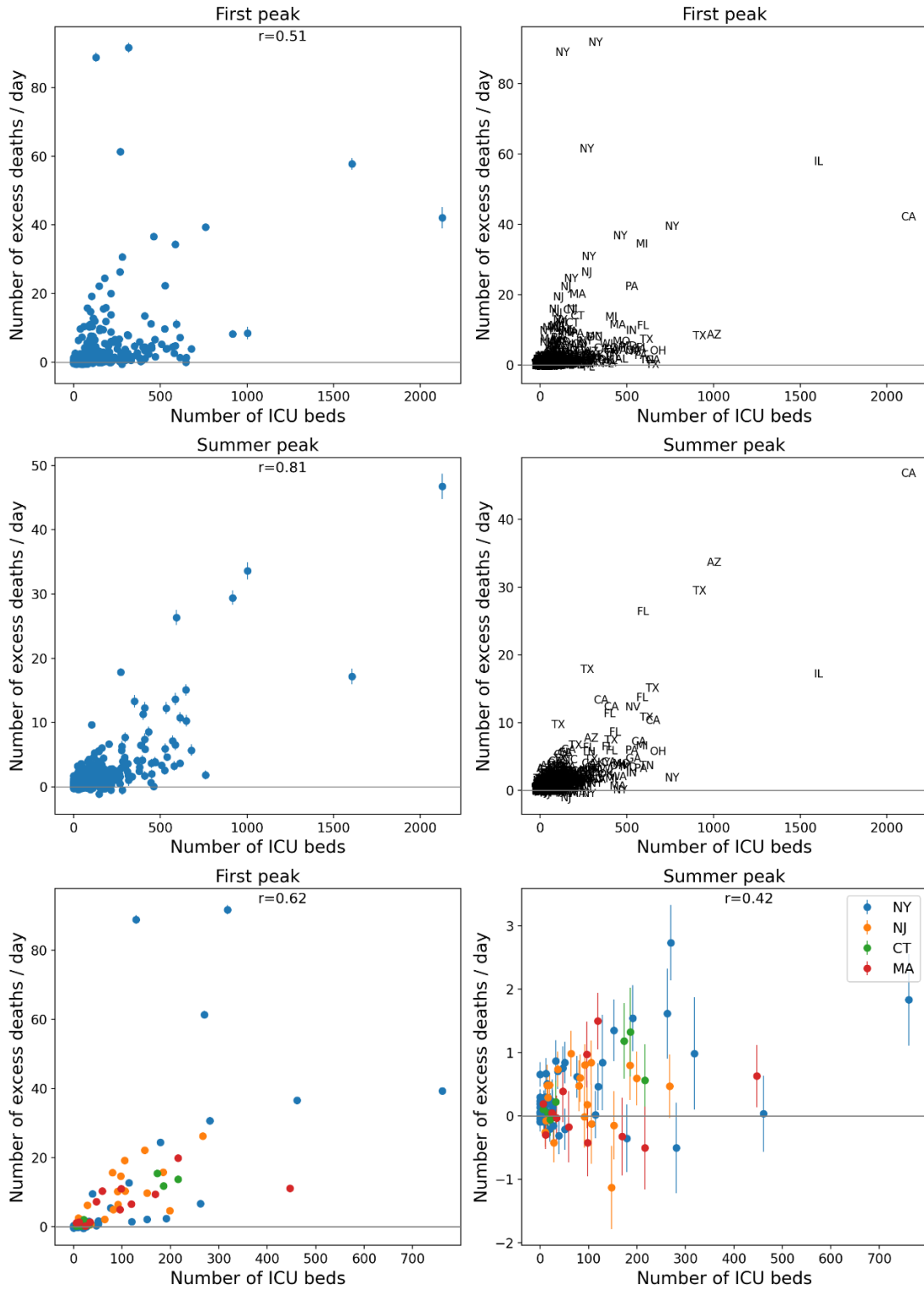


Figure 98: Number of excess deaths per day for first-peak (top row) and summer-peak (middle row) periods vs number of ICU beds, for USA counties. Bottom two panels: four states with largest integrated first-peak period P-scores. ICU data is for 2018-2019.

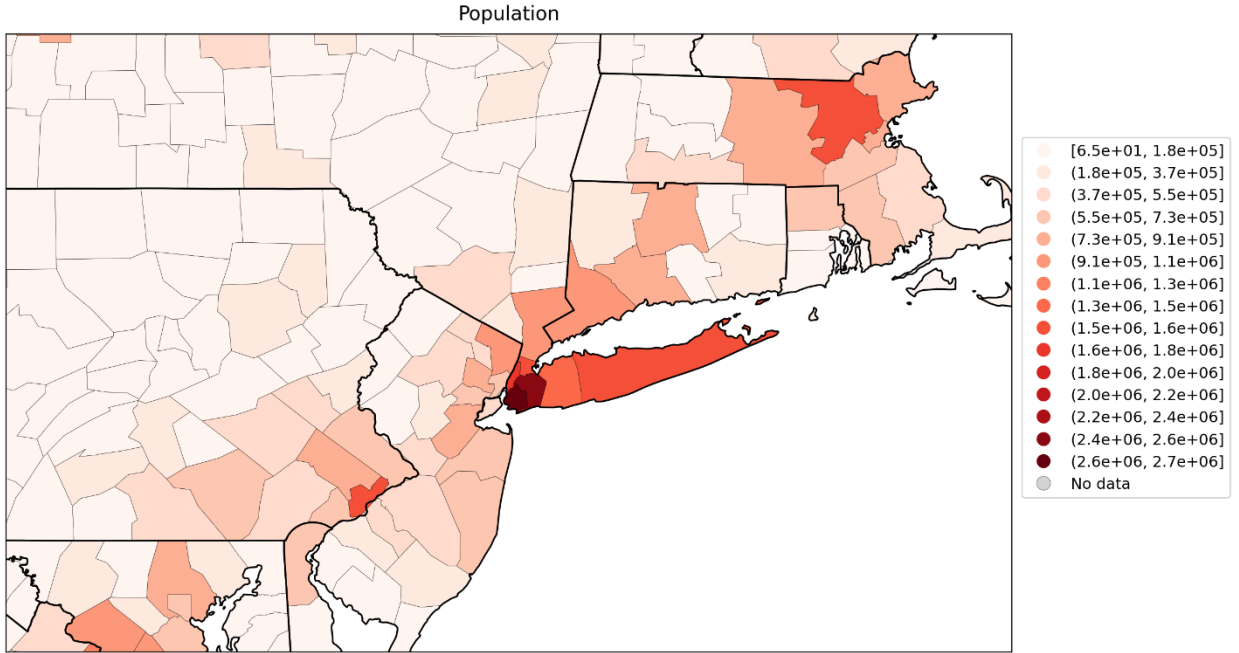
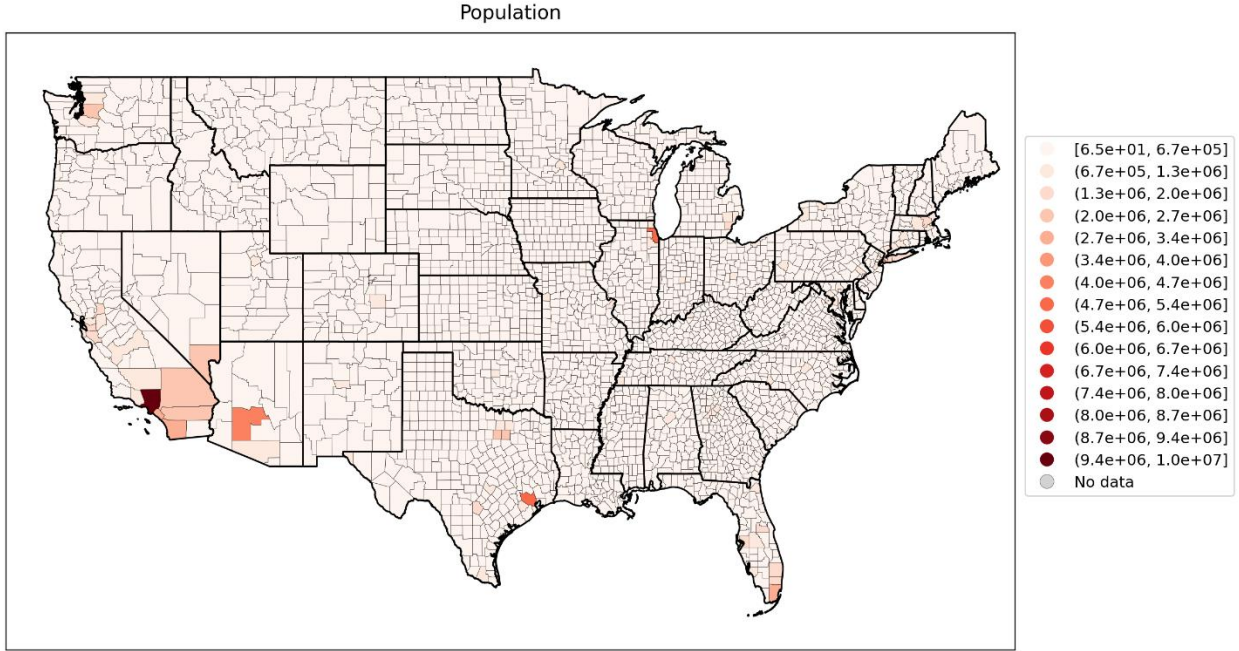


Figure 99: Map of 2019 population of USA counties for the contiguous USA (top panel) and a blow-up centred on the New York City urban area (bottom panel).

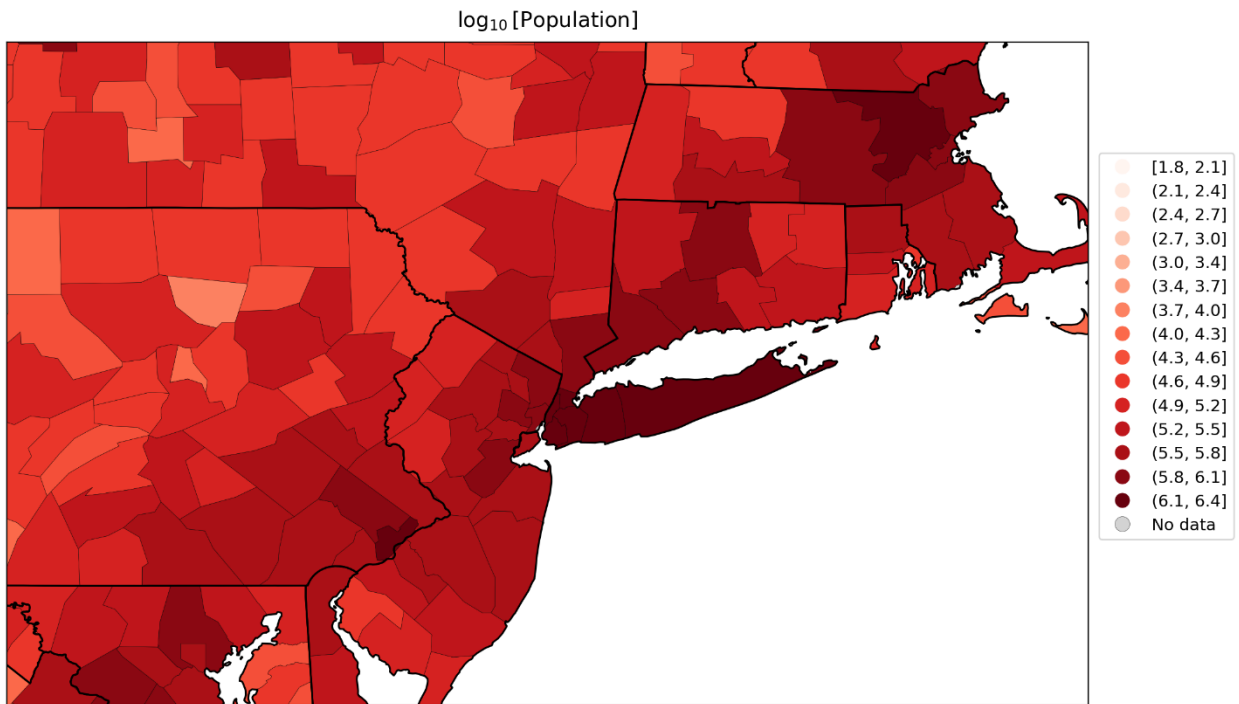
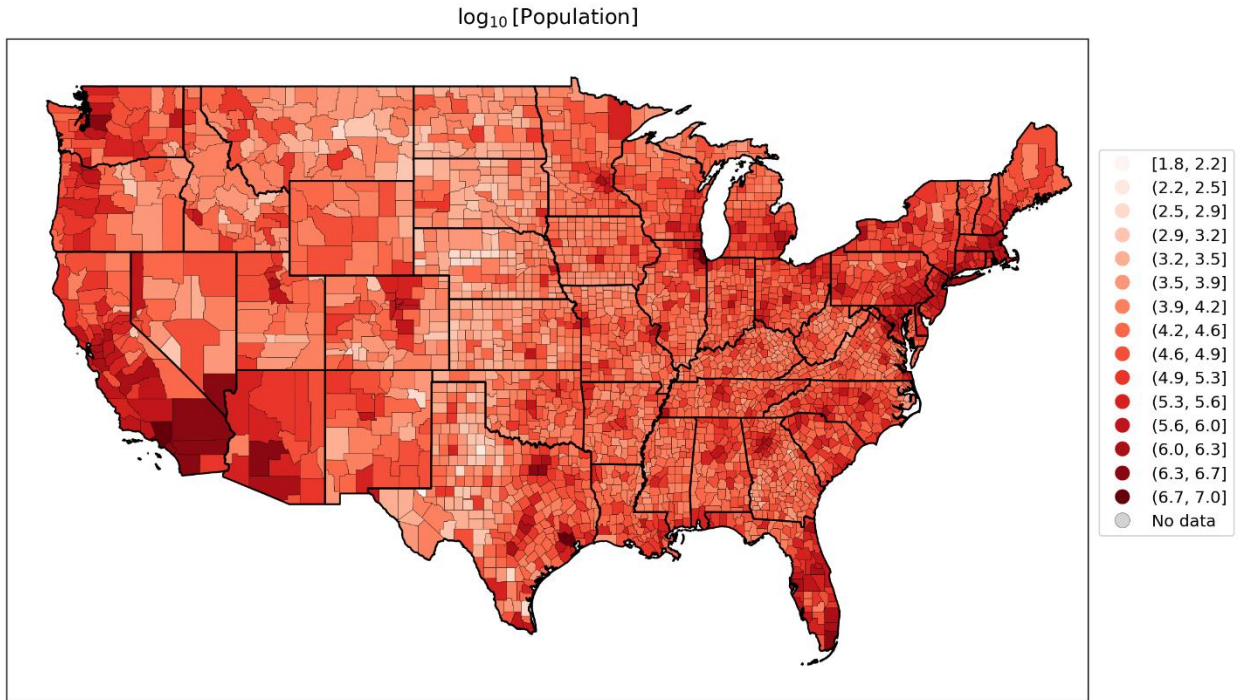


Figure 100: Map of logarithm of 2019 population per county for the contiguous USA (top panel) and a blow-up centred on the New York City urban area (bottom panel).

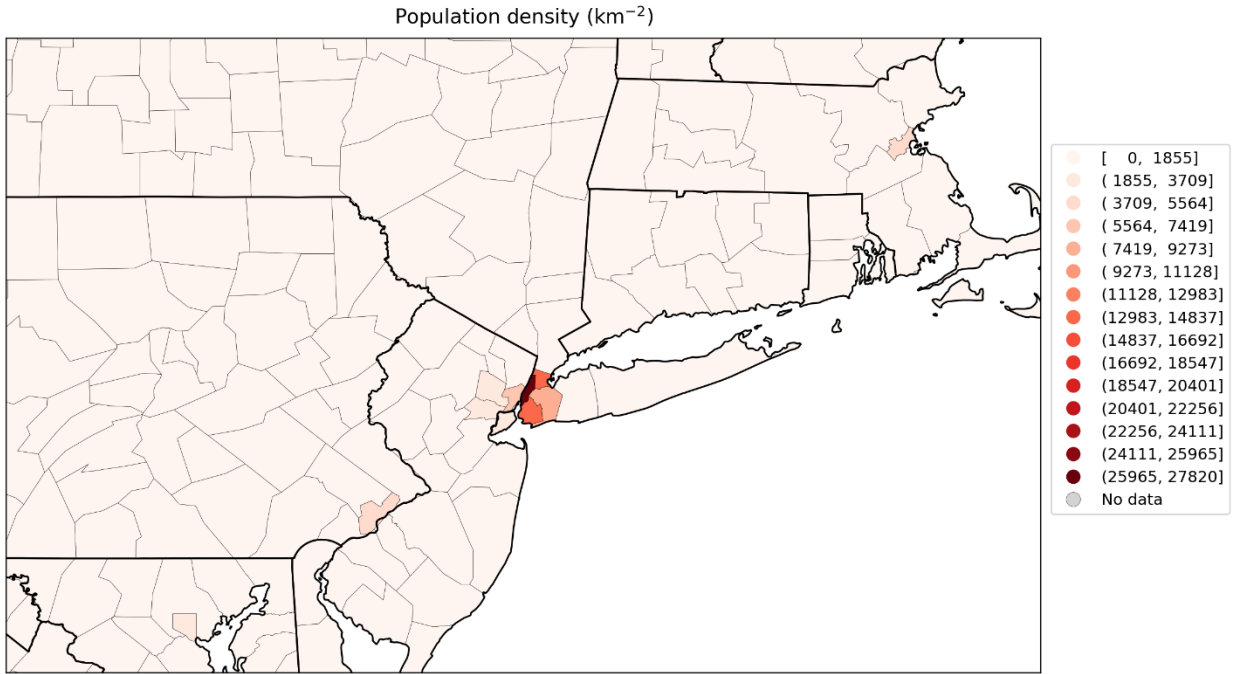
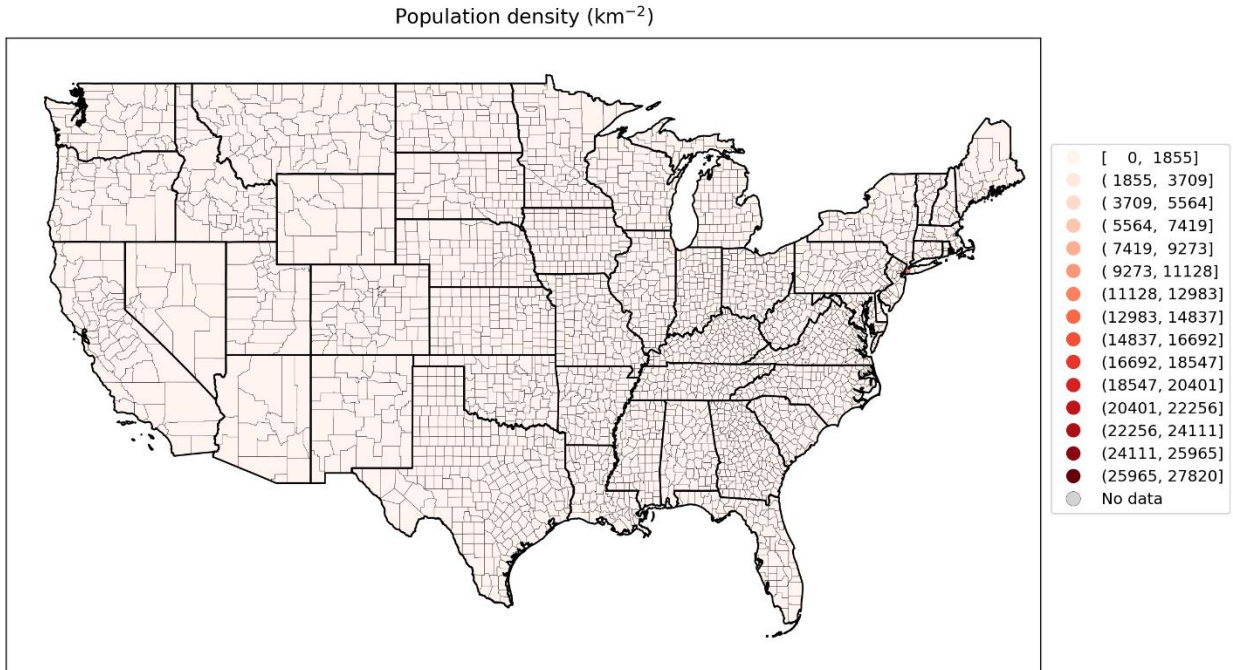


Figure 101: Map of population density per county for the contiguous USA (top panel) and a blow-up centred on the New York City urban area (bottom panel) (estimates from the 5-Year American Community Survey for the years 2017-2021).

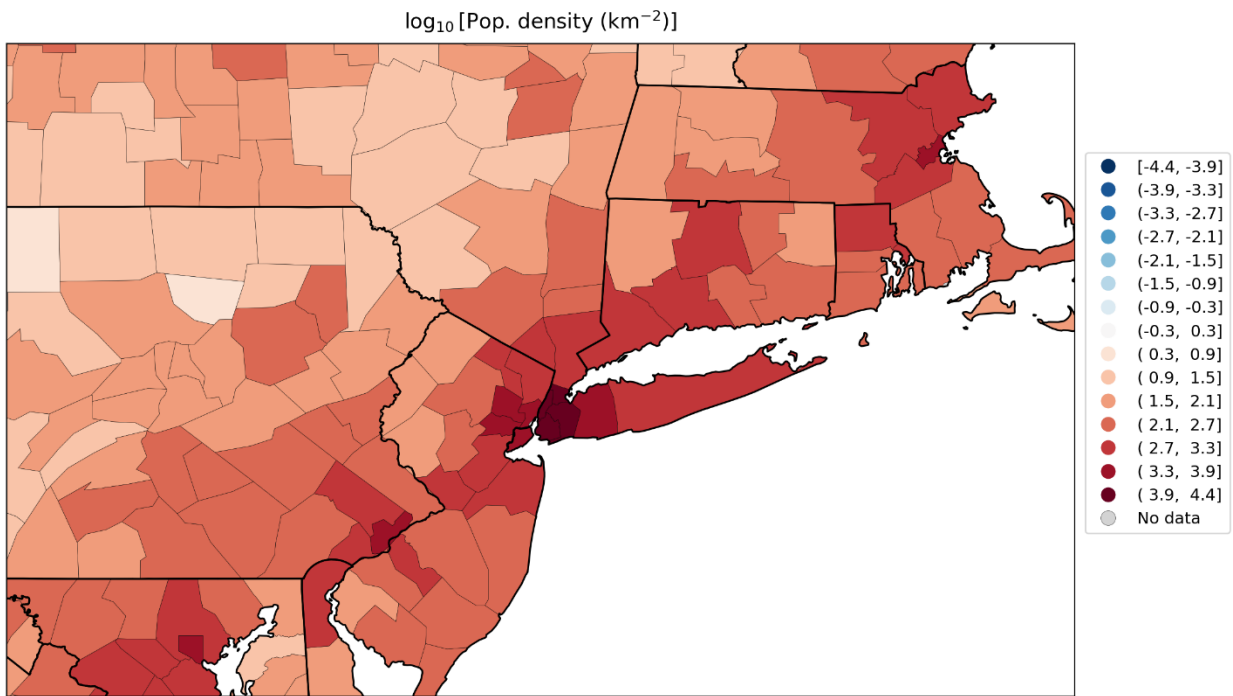
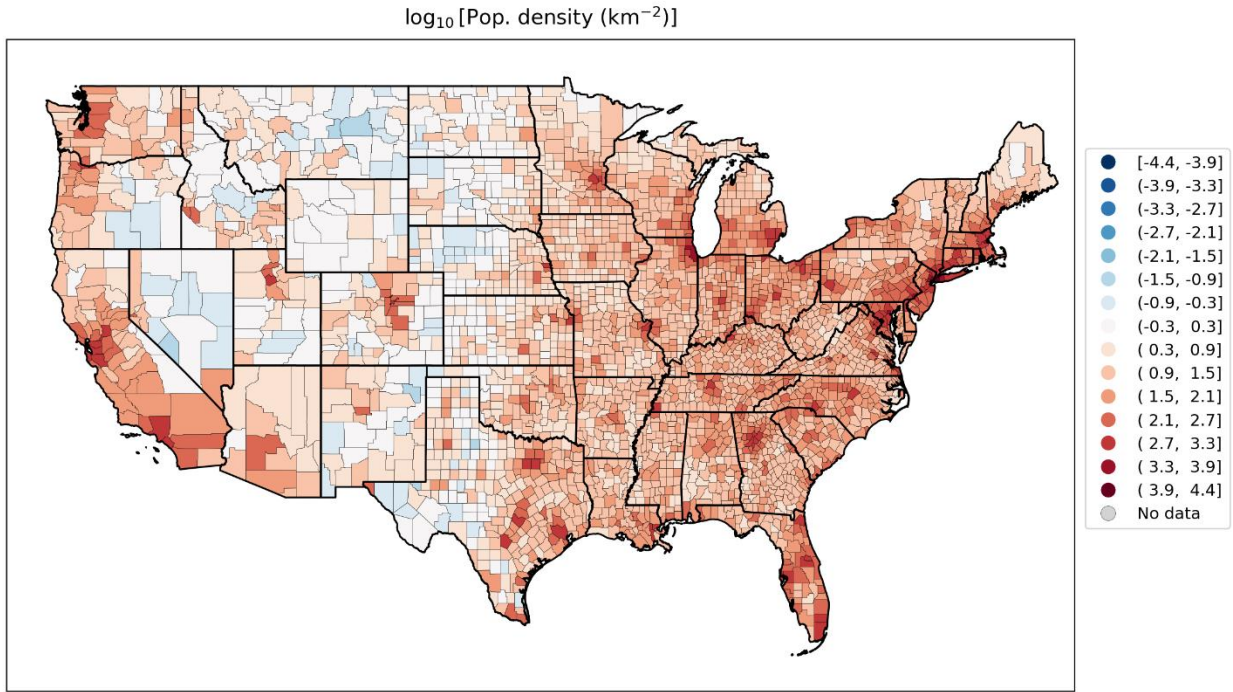


Figure 102: Map of logarithm of population density per county for the contiguous USA (top panel) and a blow-up centred on the New York City urban area (bottom panel) (estimates from the 5-Year American Community Survey for the years 2017-2021).

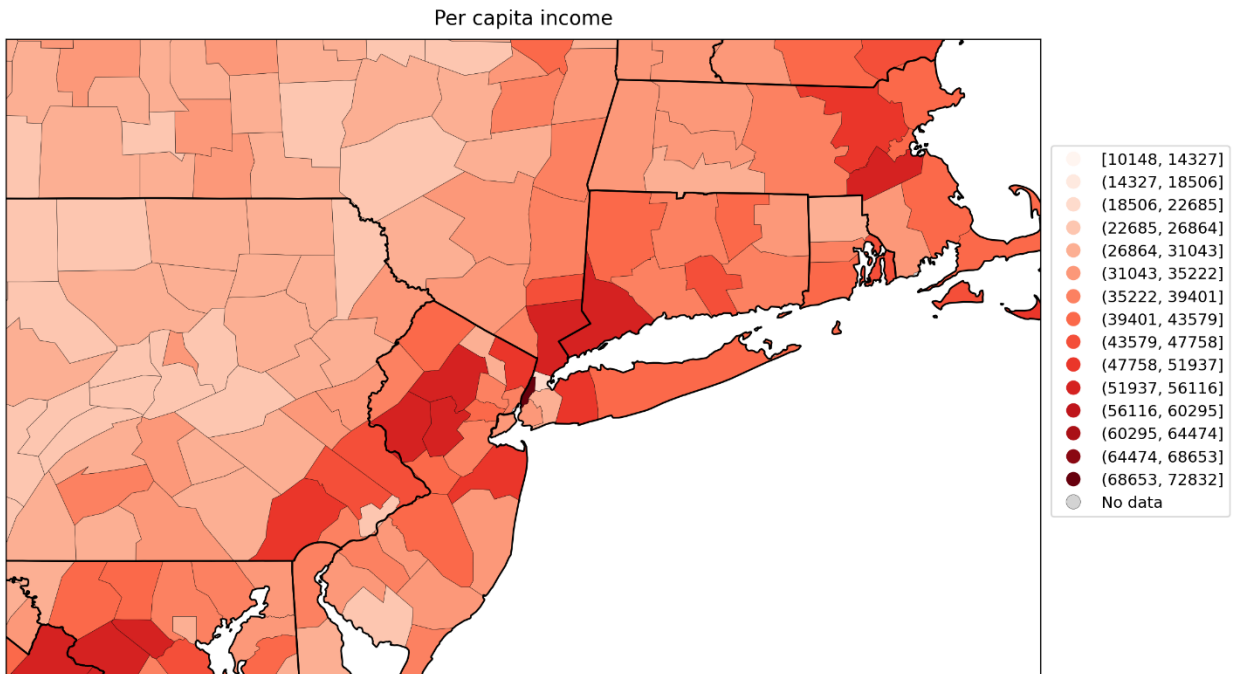
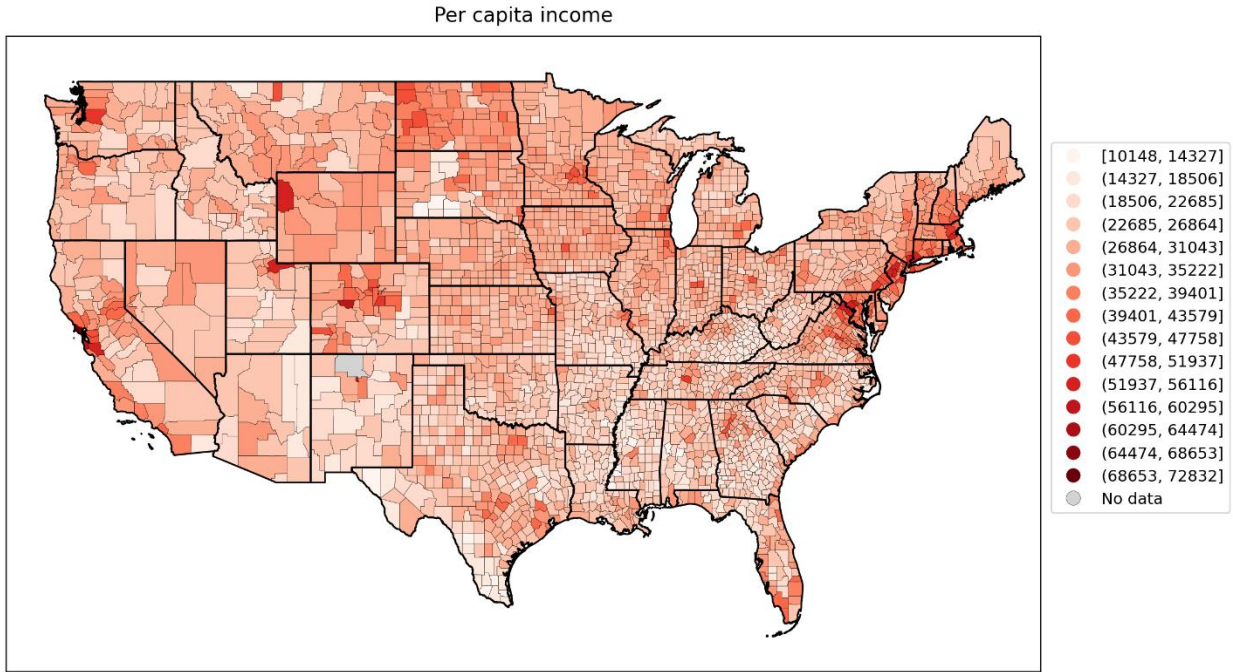


Figure 103: Map of per capita income per county for the contiguous USA (top panel) and a blow-up centred on the New York City urban area (bottom panel) (estimates from the 5-Year American Community Survey for the years 2014-2018).

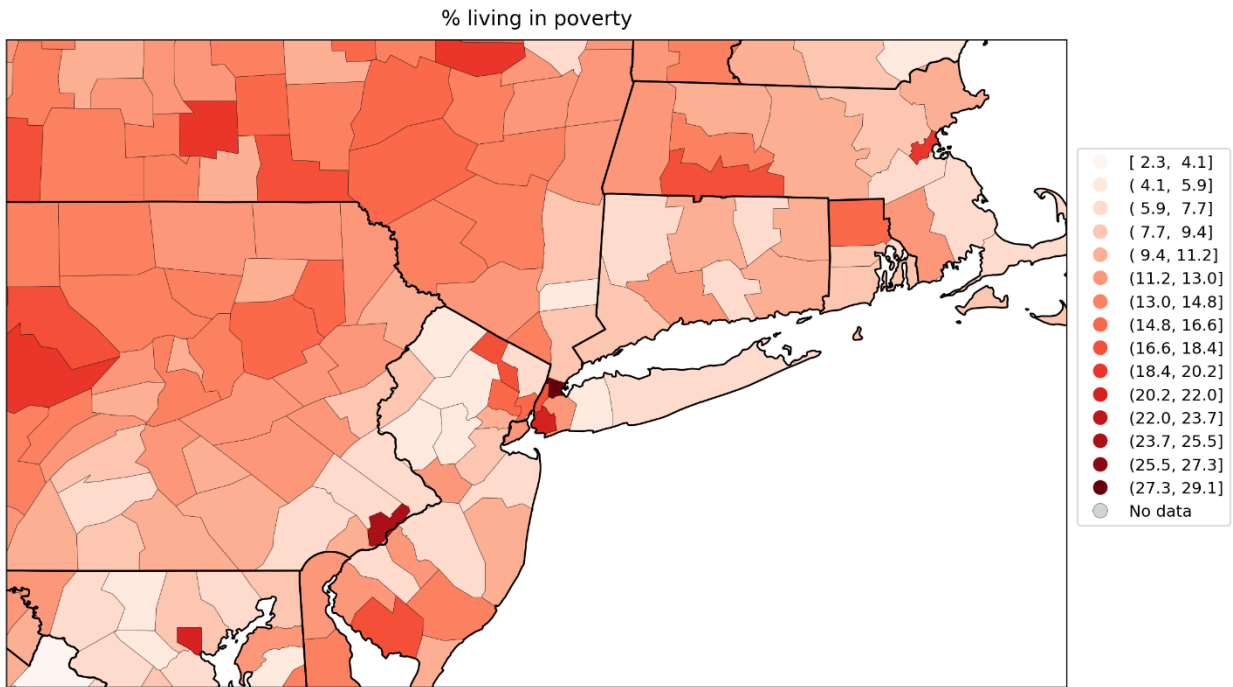
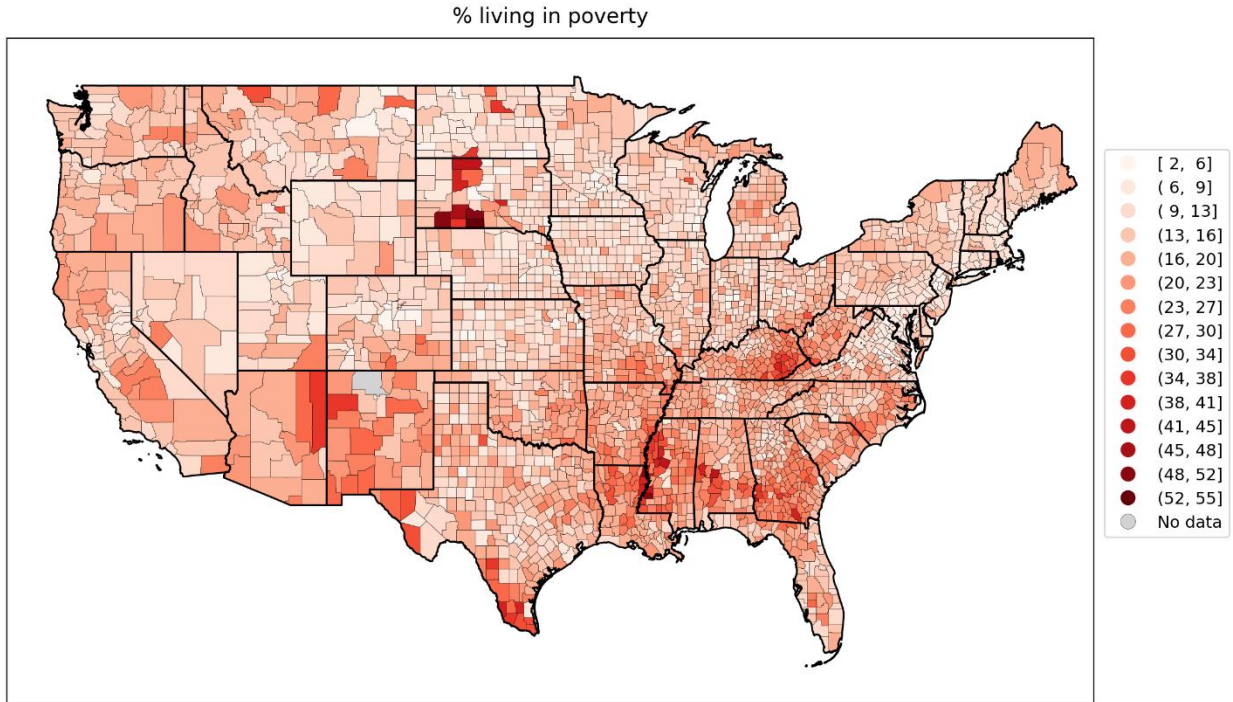


Figure 104: Map of % living in poverty per county for the contiguous USA (top panel) and a blow-up centred on the New York City urban area (bottom panel) (estimates from the 5-Year American Community Survey for the years 2014-2018).

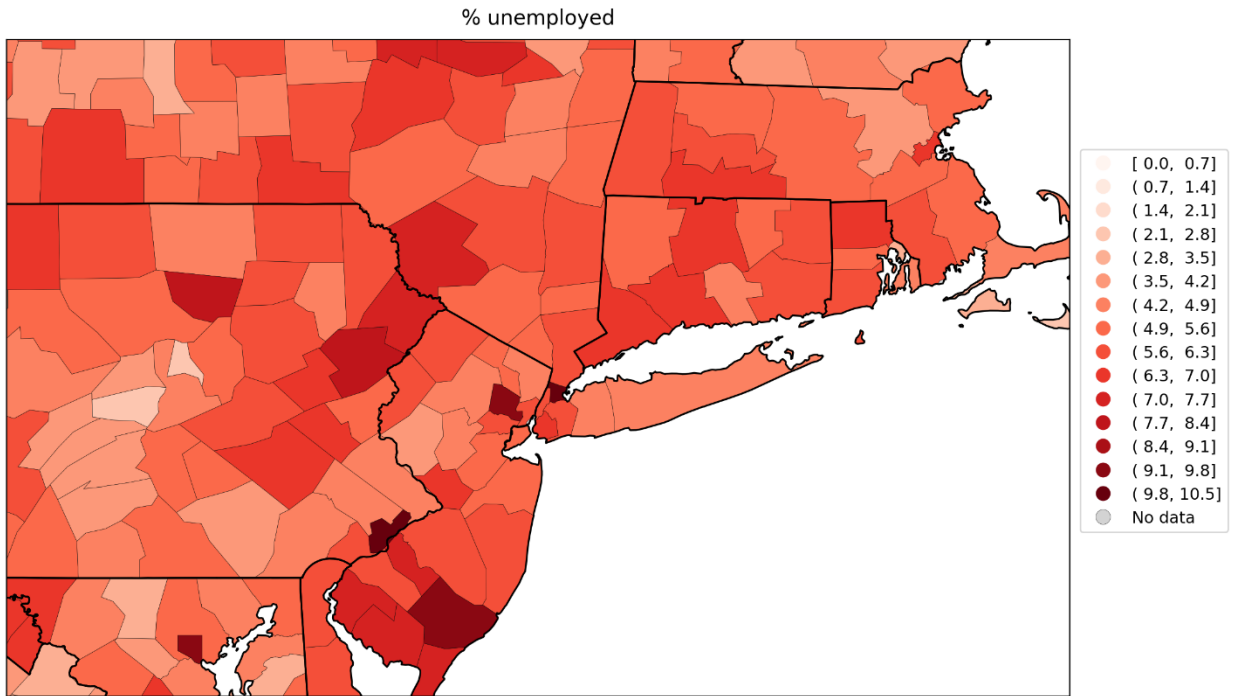
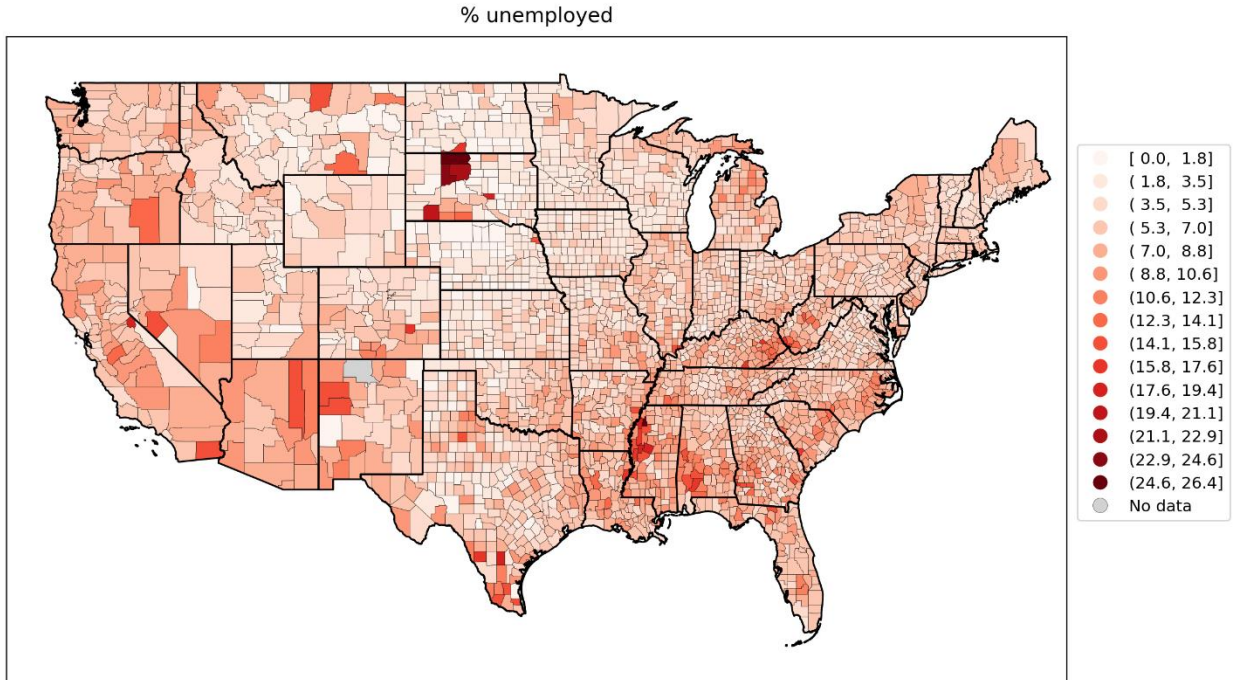


Figure 105: Map of % unemployed per county for the contiguous USA (top panel) and a blow-up centred on the New York City urban area (bottom panel) (estimates from the 5-Year American Community Survey for the years 2014-2018).

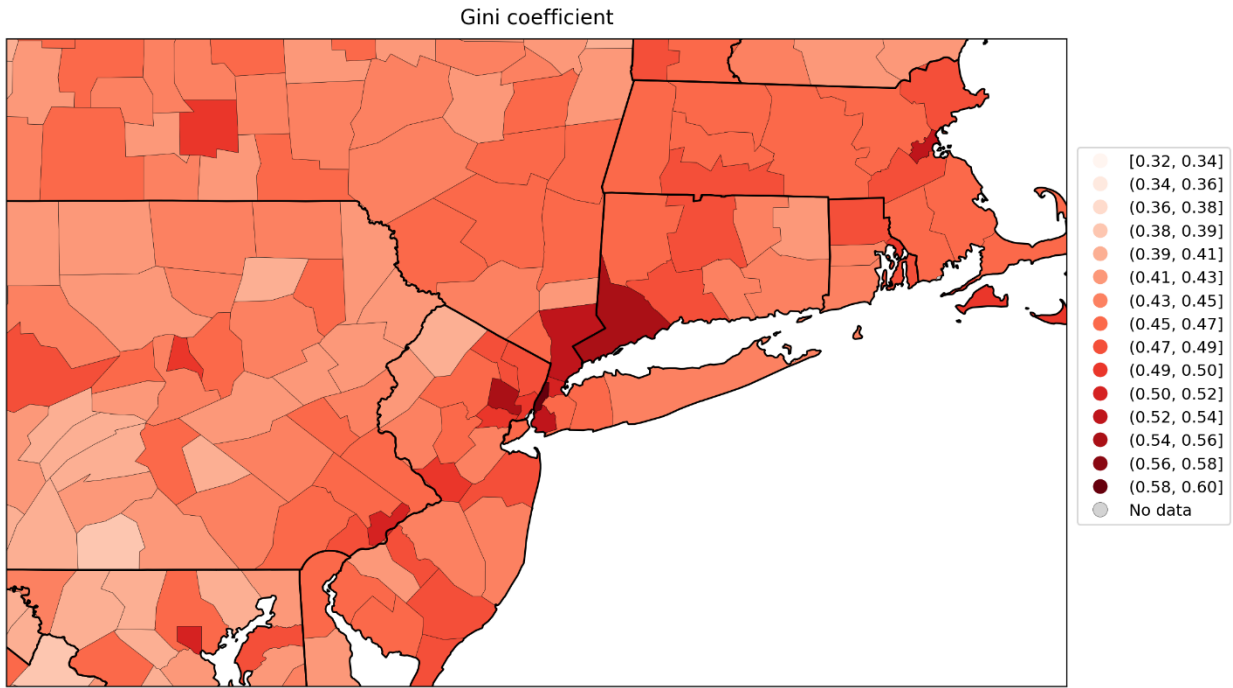
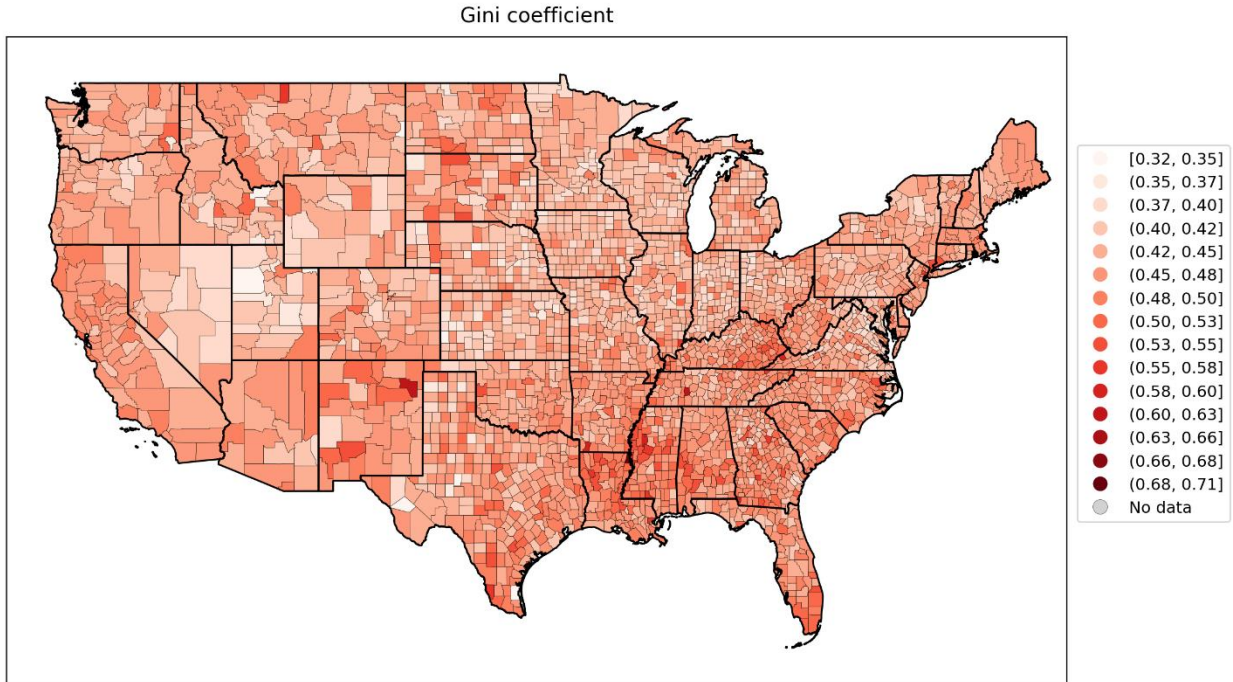
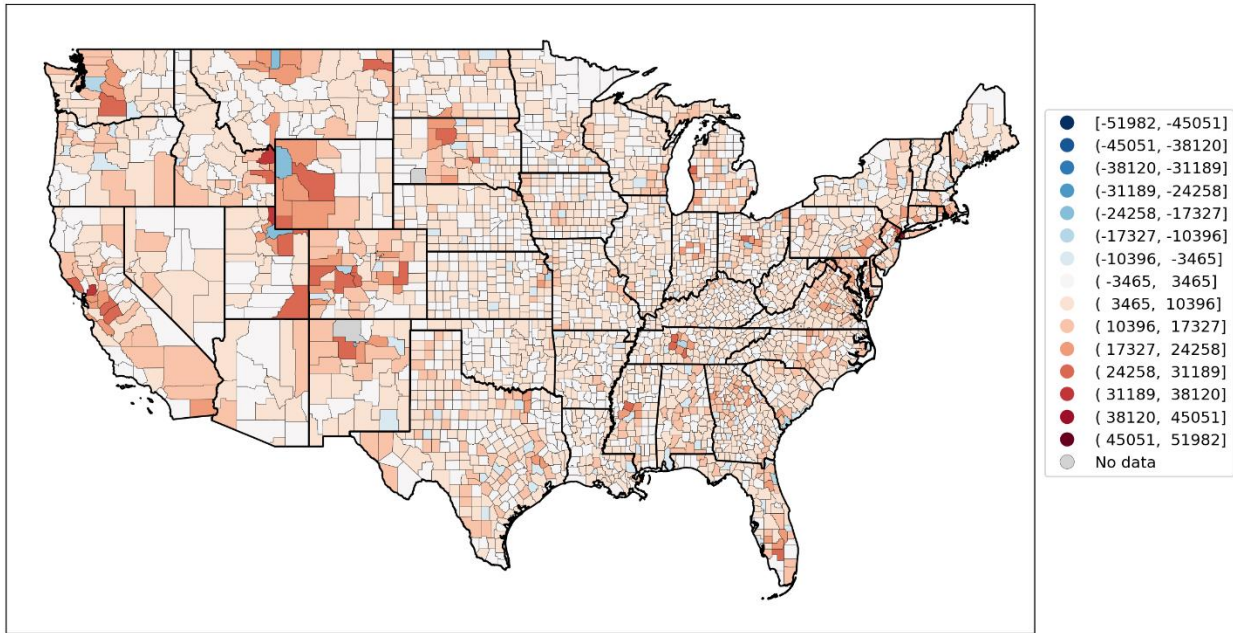


Figure 106: Map of Gini coefficient of inequality for the counties of the contiguous USA (top panel) and a blow-up centred on the New York City urban area (bottom panel) (estimates from the 5-Year American Community Survey for the years 2014-2018).

Inter-county disparity
(Max neighbour PCI - Target PCI)



Inter-county disparity
(Max neighbour PCI - Target PCI)

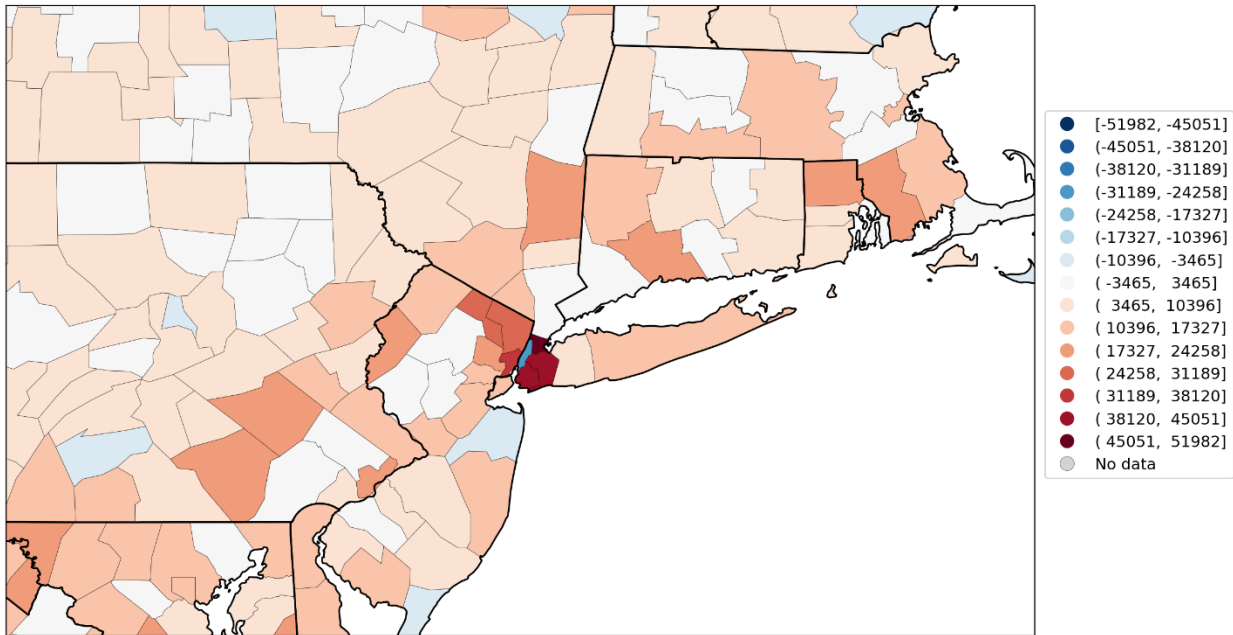
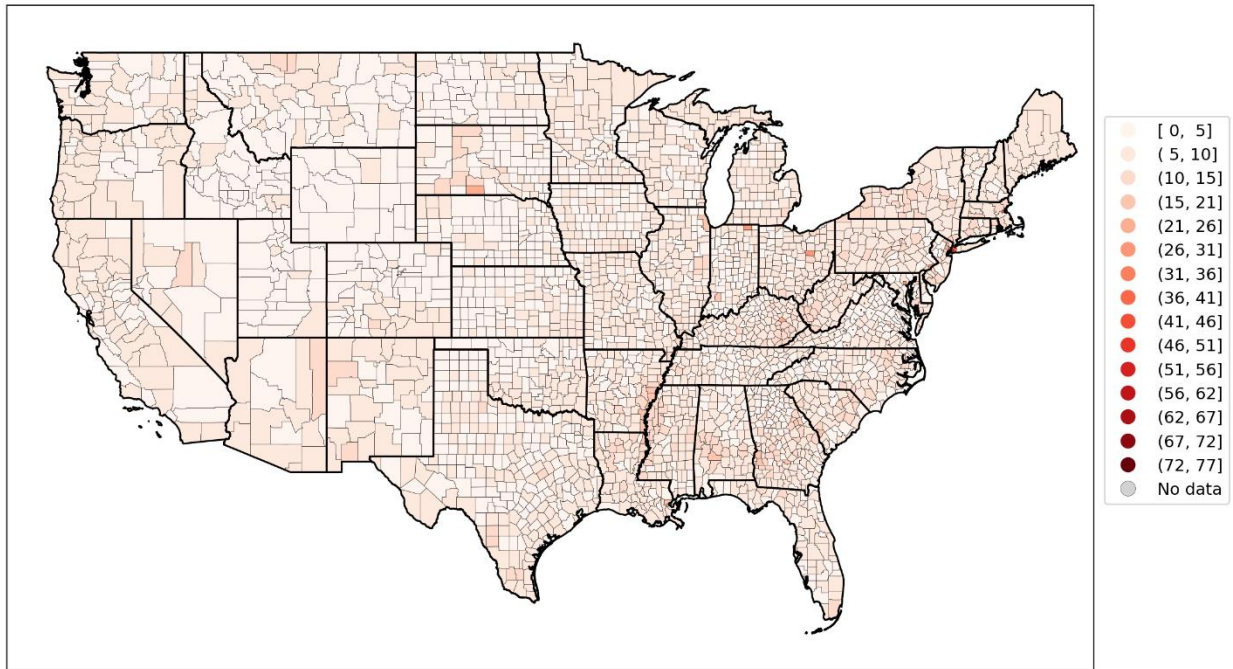


Figure 107: Map of inter-county disparity for the counties of the contiguous USA (top panel) and a blow-up centred on the New York City urban area (bottom panel) (estimates from the 5-Year American Community Survey for the years 2014-2018).

% households with no vehicle available



% households with no vehicle available

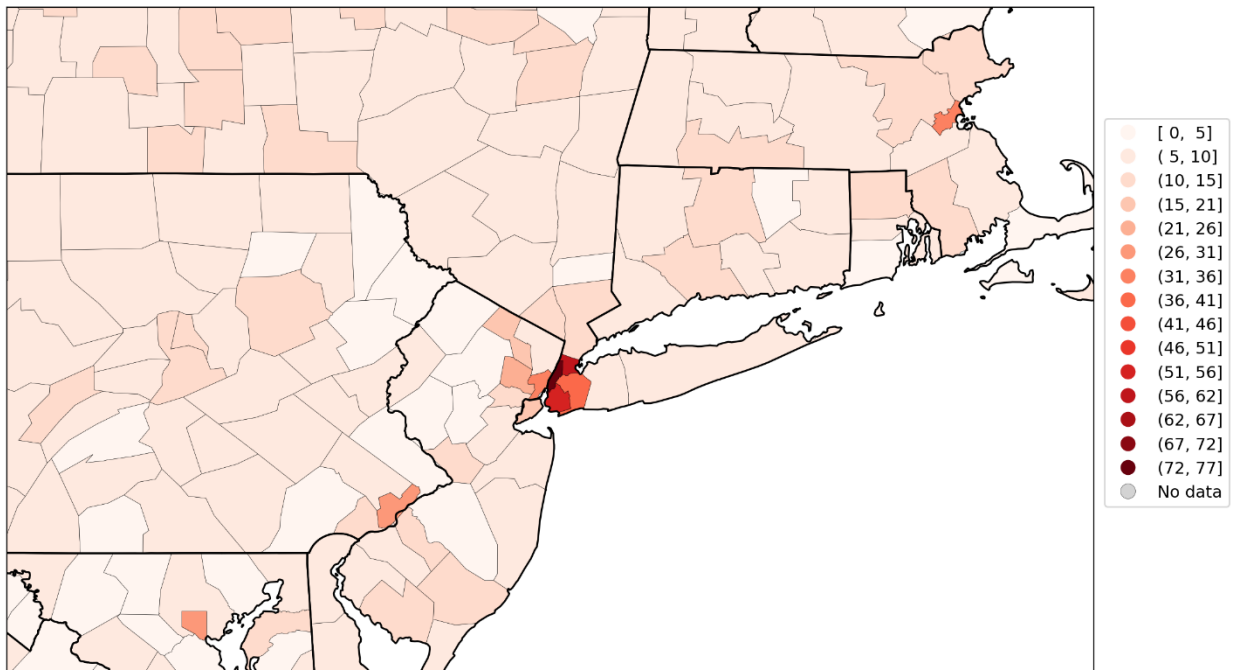
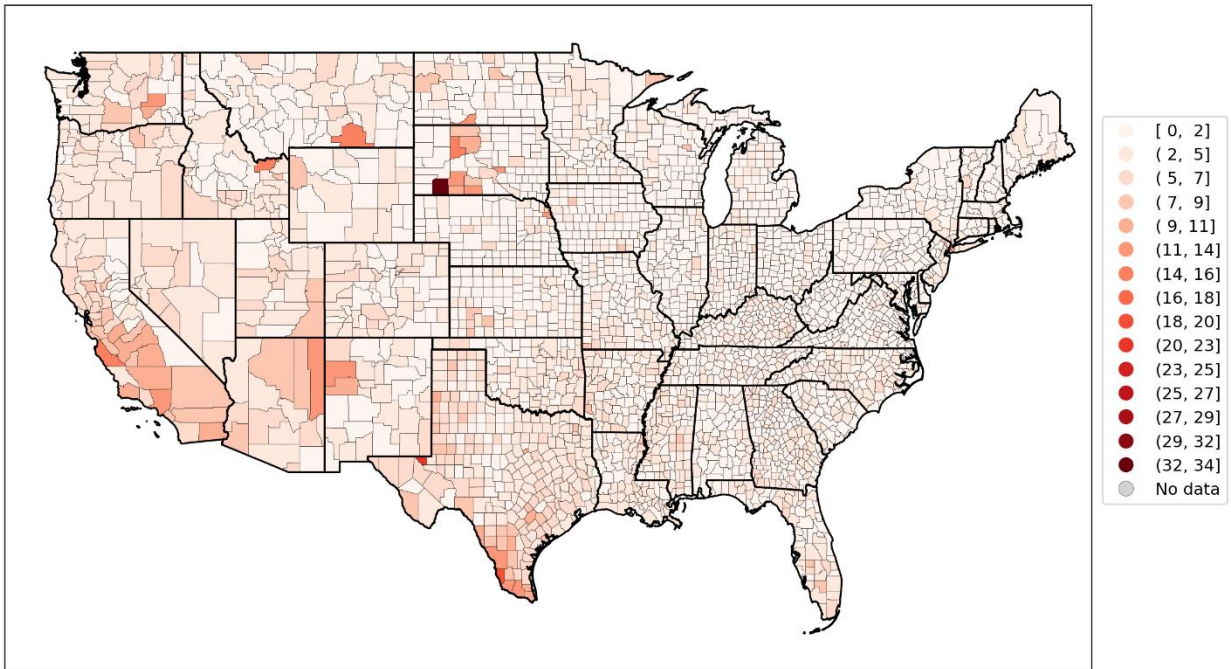


Figure 108: Map of % households with no vehicle available for the counties of the contiguous USA (top panel) and a blow-up centred on the New York City urban area (bottom panel) (estimates from the 5-Year American Community Survey for the years 2014-2018).

% households with more people than rooms



% households with more people than rooms

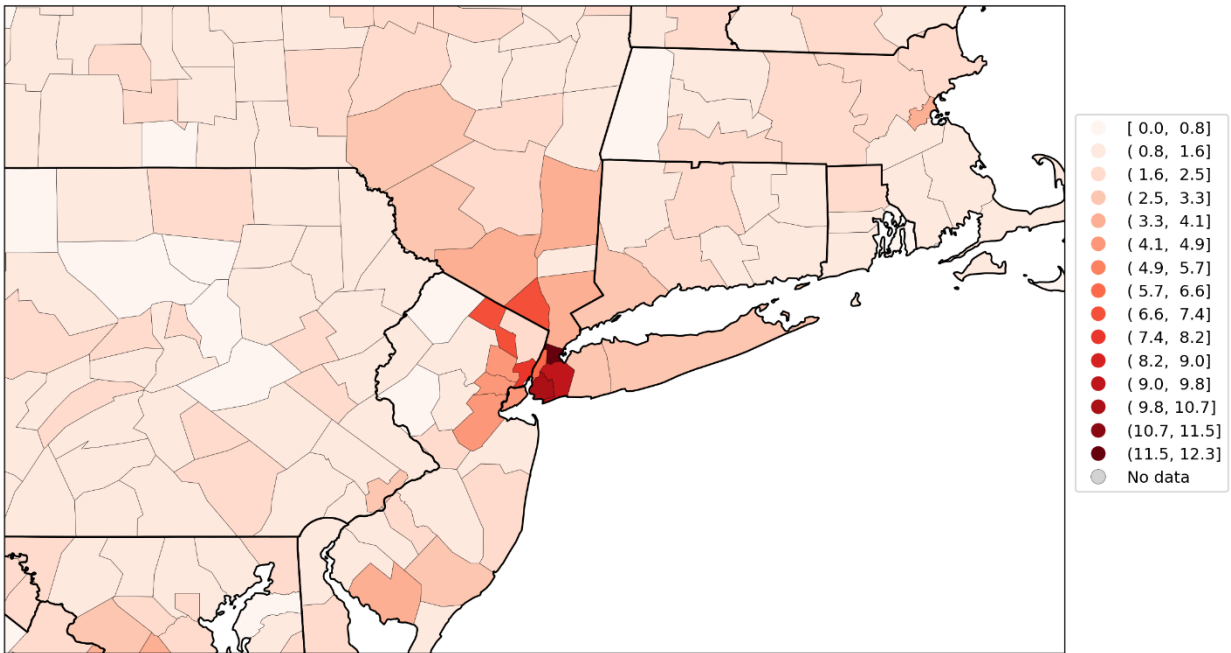


Figure 109: Map of percent households with more people than rooms per county for the contiguous USA (top panel) and a blow-up centred on the New York City urban area (bottom panel) (estimates from the 5-Year American Community Survey for the years 2014-2018).

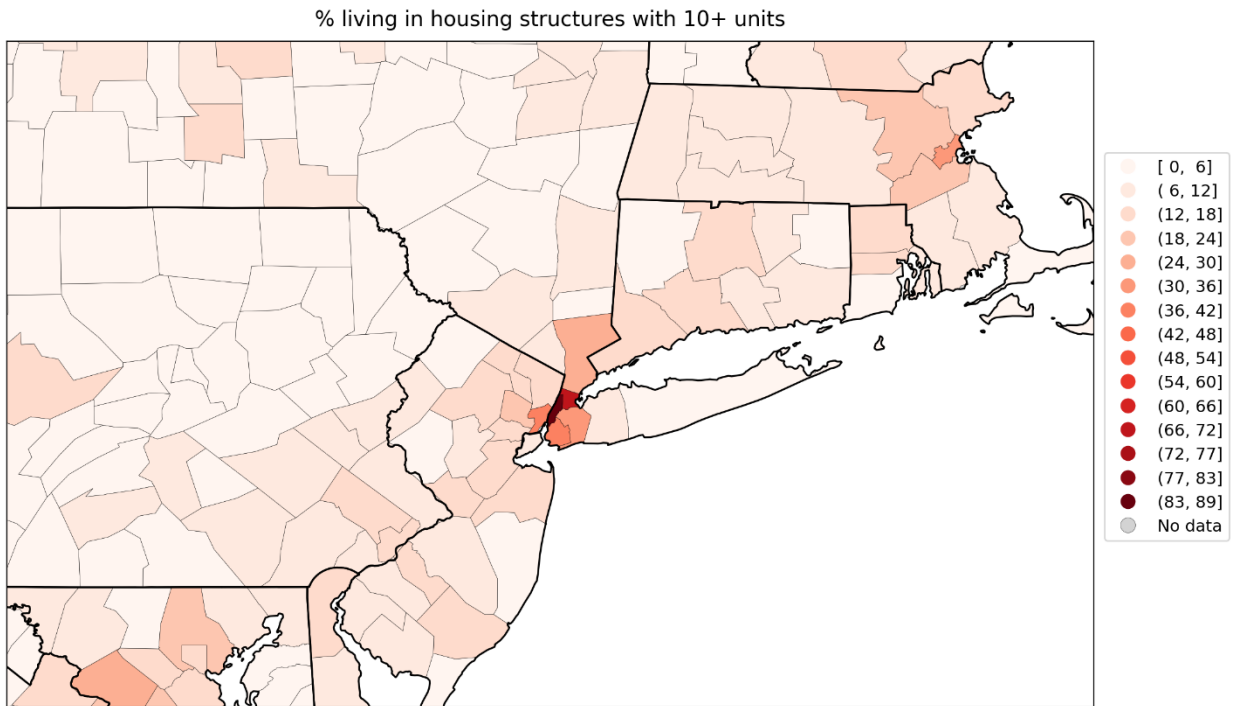
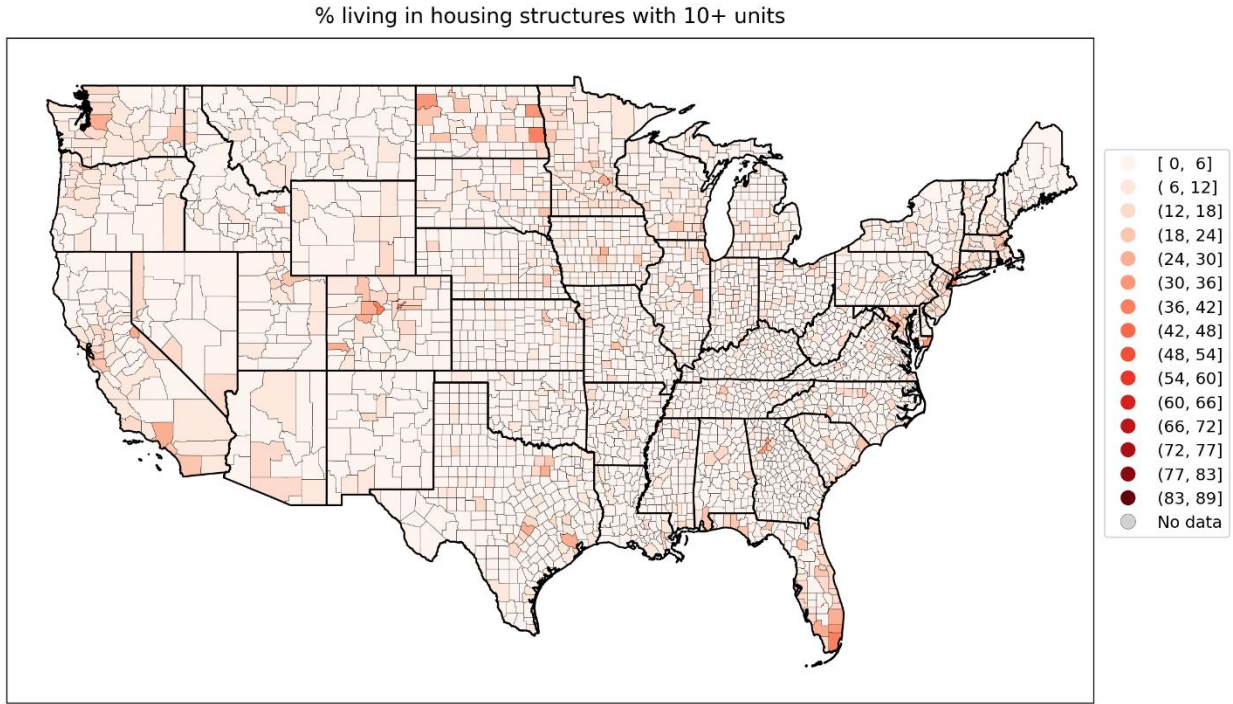
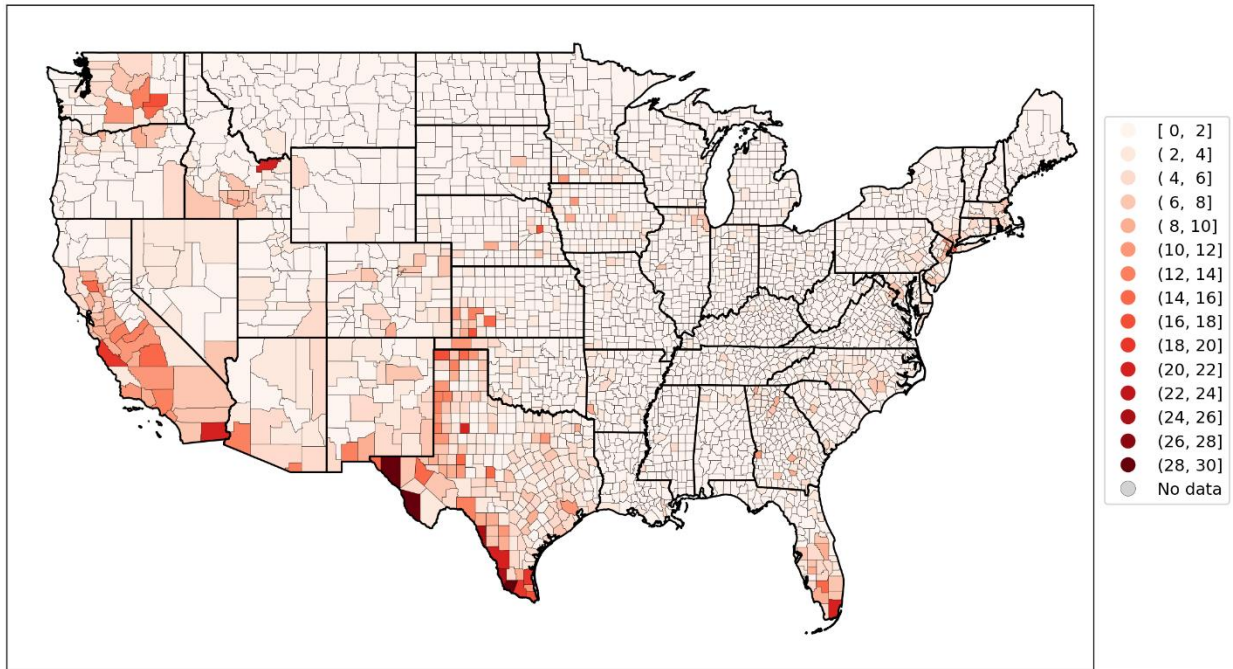


Figure 110: Map of percent living in housing structures with more than 10 units per county for the contiguous USA (top panel) and a blow-up centred on the New York City urban area (bottom panel) (estimates from the 5-Year American Community Survey for the years 2014-2018).

% who speak English "less than well"



% who speak English "less than well"

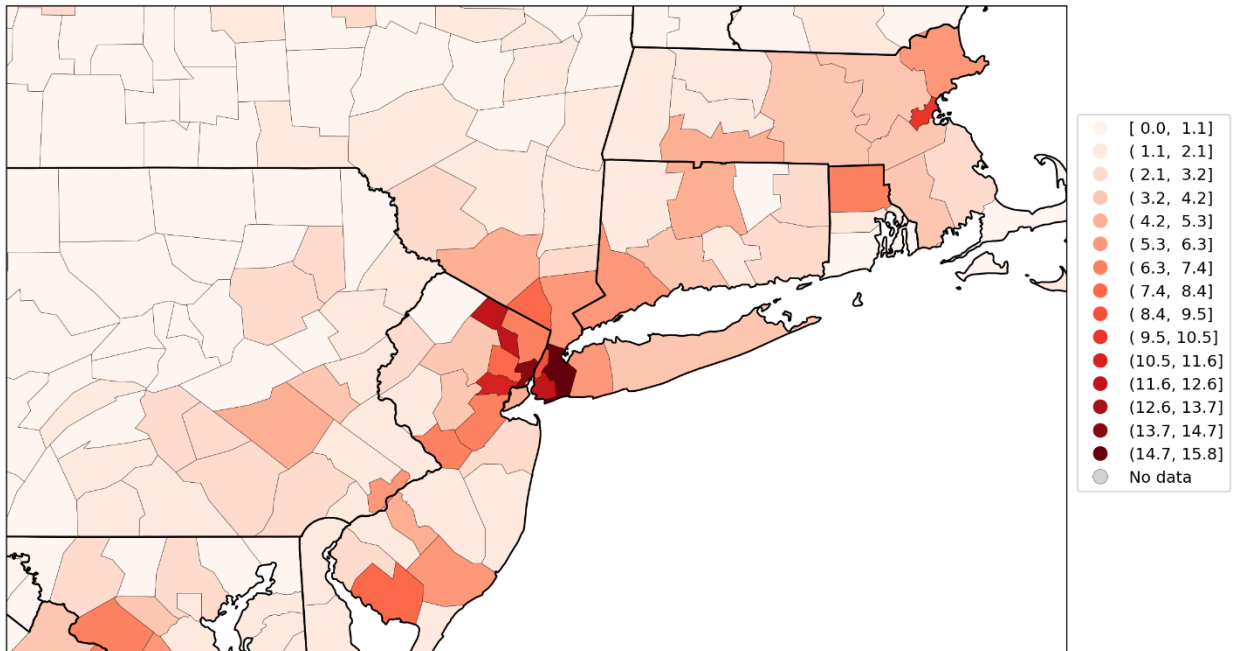


Figure 111: Map of % who speak English “less than well” for the contiguous USA (top panel) and a blow-up centred on the New York City urban area (bottom panel) (estimates from the 5-Year American Community Survey for the years 2014-2018).

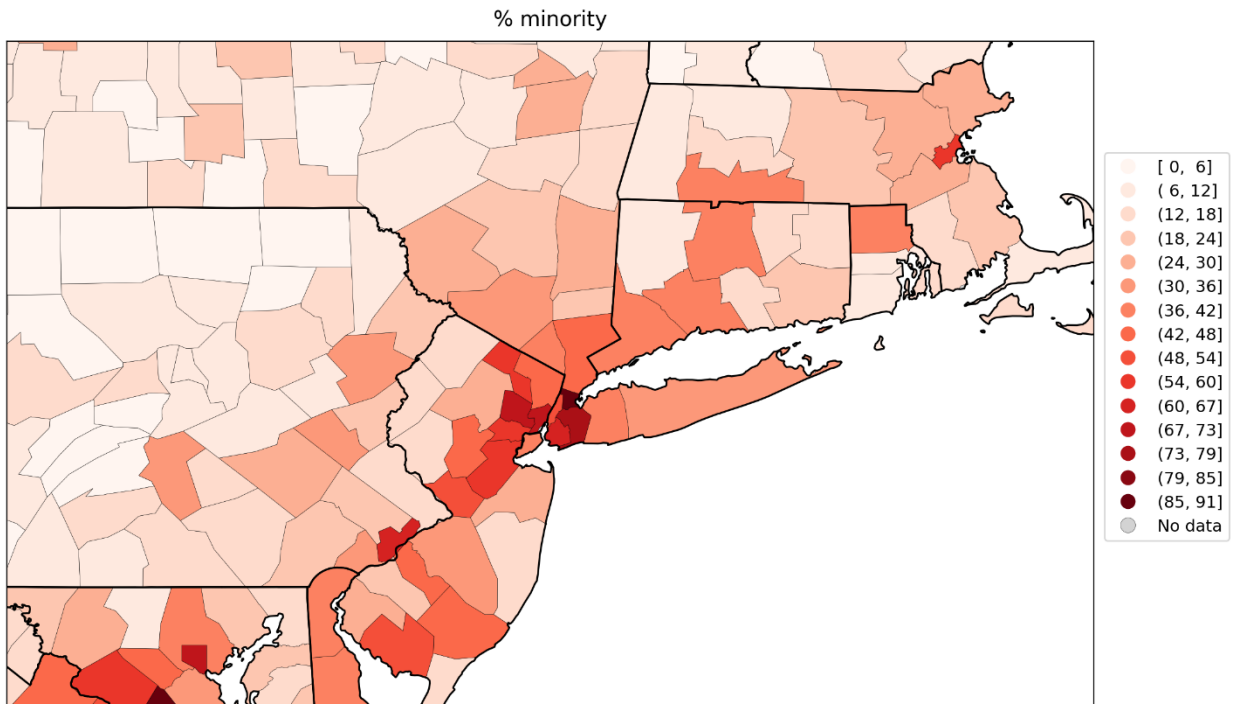
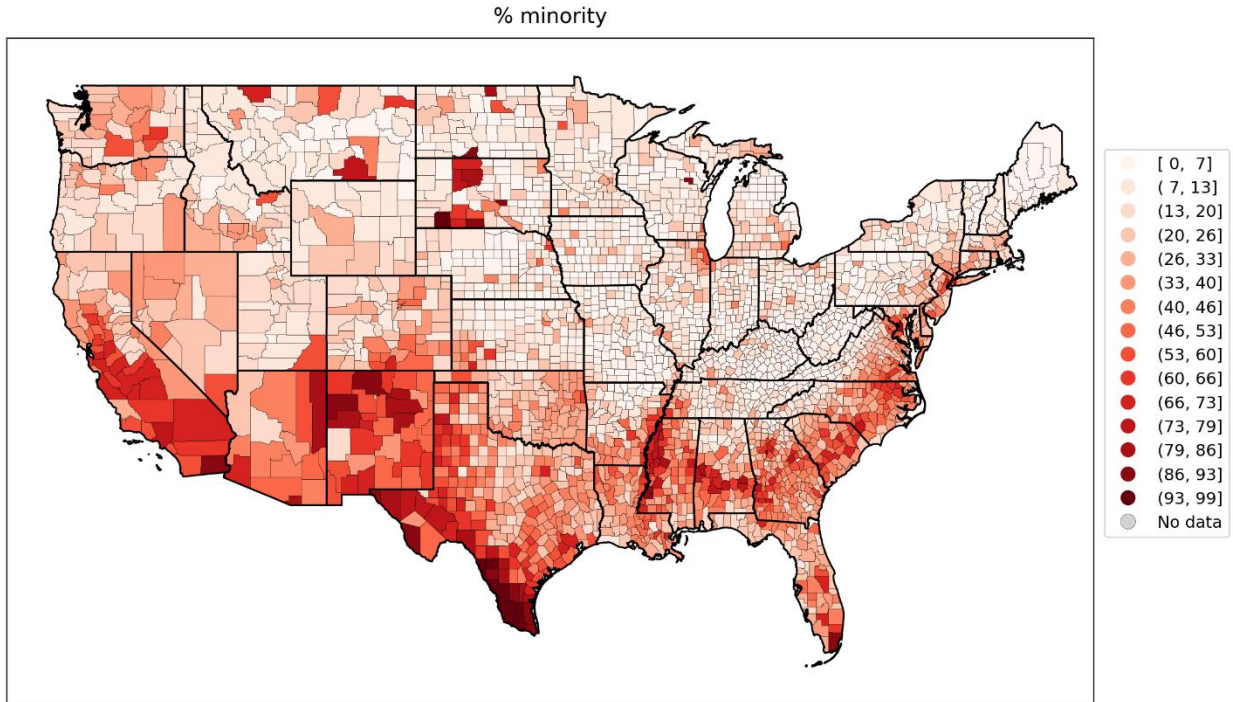
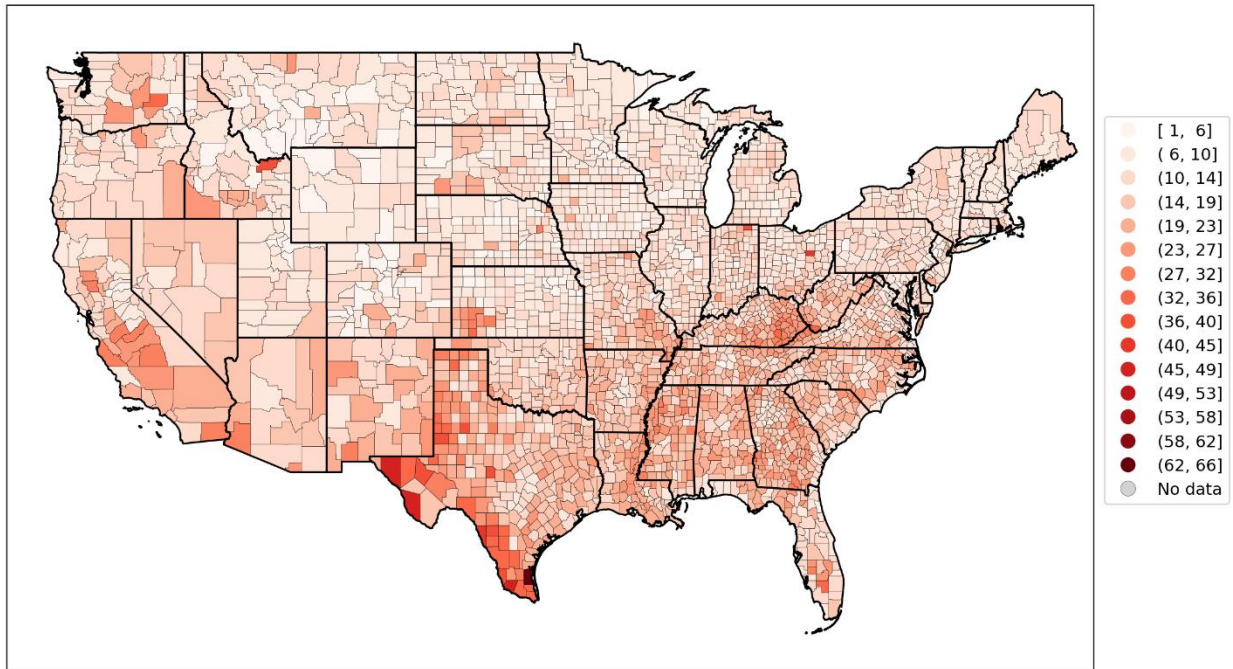


Figure 112: Map of % minority for the contiguous USA (top panel) and a blow-up centred on the New York City urban area (bottom panel) (estimates from the 5-Year American Community Survey for the years 2014-2018).

% aged 25+ with no high school diploma



% aged 25+ with no high school diploma

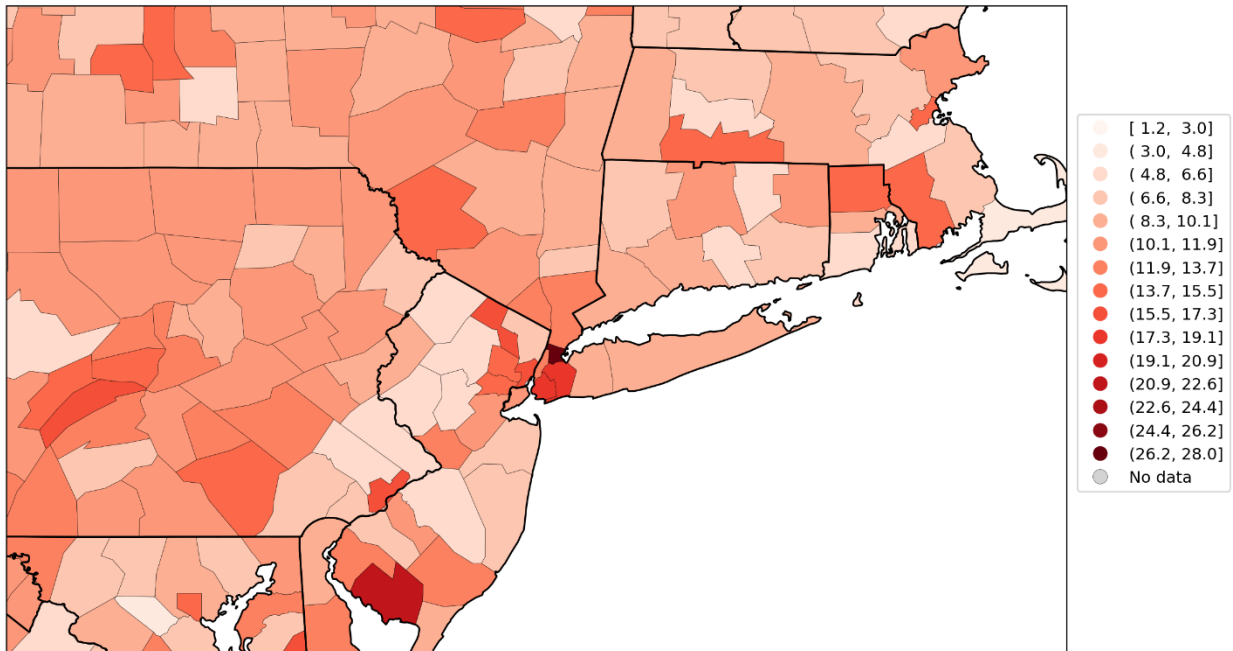


Figure 113: Map of % aged 25+ with no high school diploma for the contiguous USA (top panel) and a blow-up centred on the New York City urban area (bottom panel) (estimates from the 5-Year American Community Survey for the years 2014-2018).

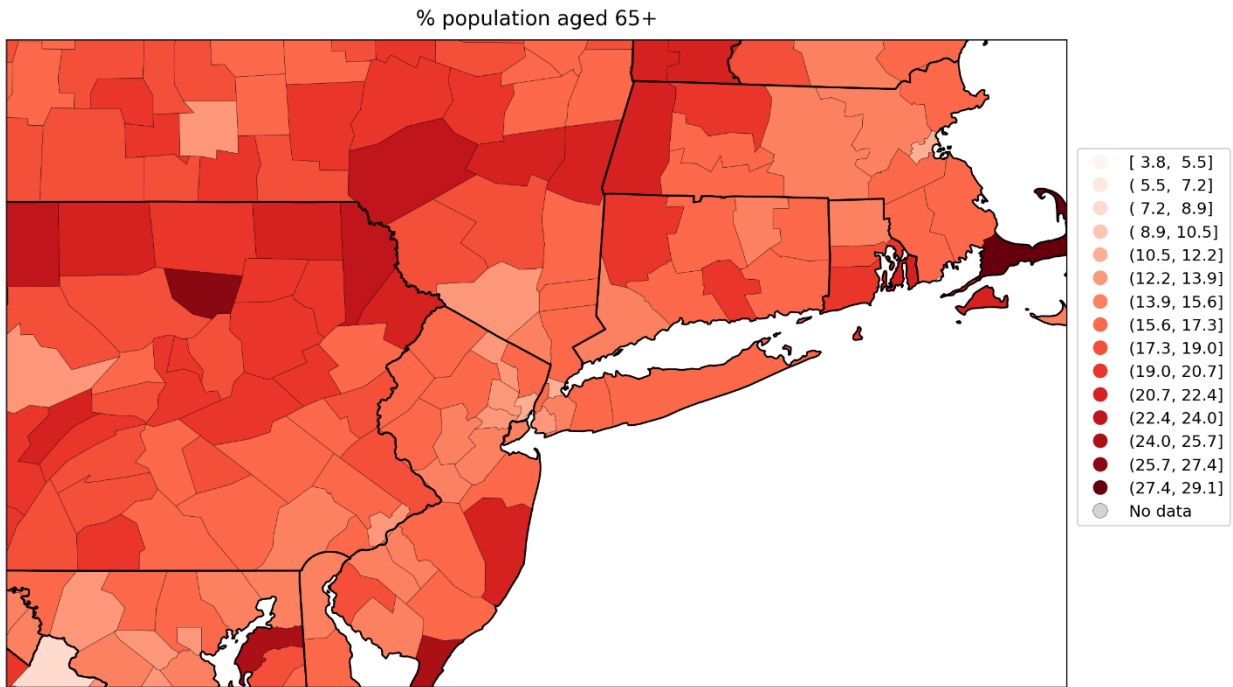
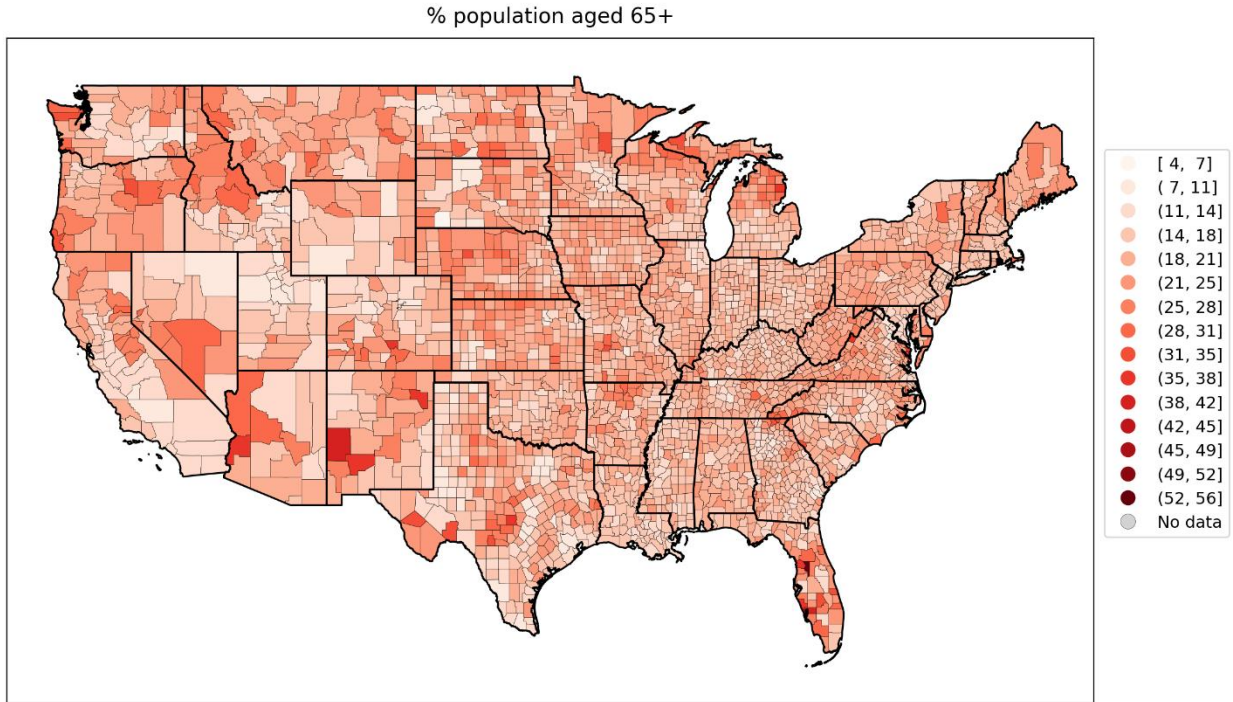
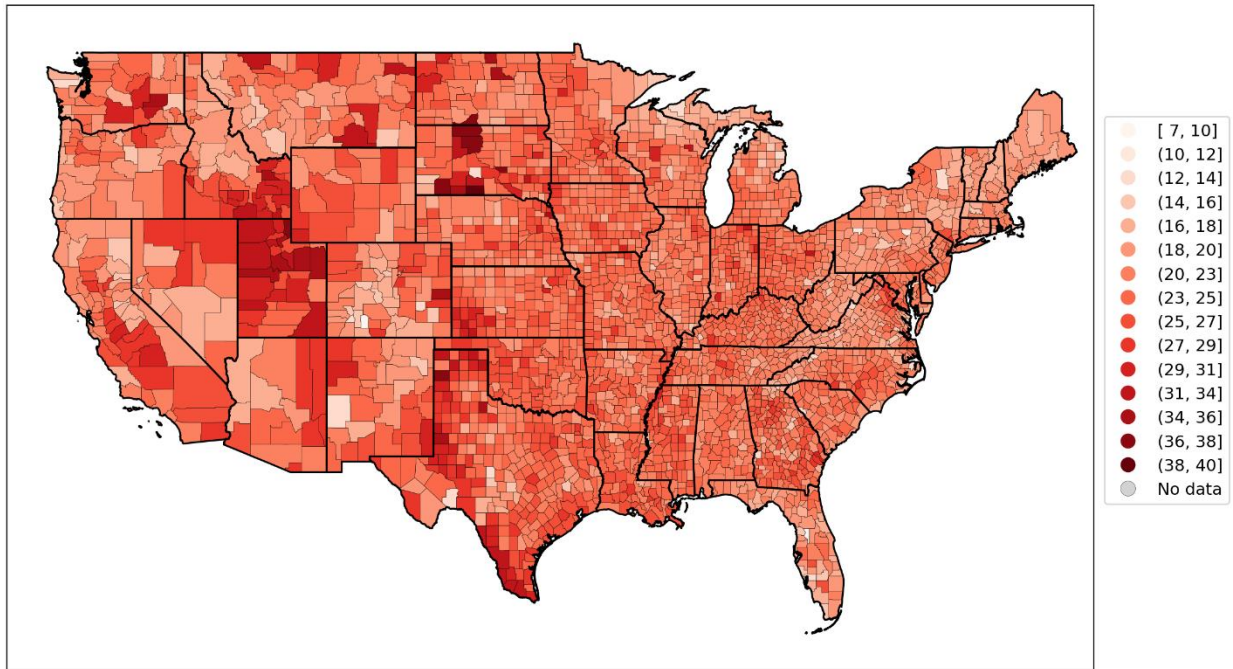


Figure 114: Map of percent of the population aged 65+ per county for the contiguous USA (top panel) and a blow-up centred on the New York City urban area (bottom panel) (estimates from the 5-Year American Community Survey for the years 2014-2018).

% population aged 17 and under



% population aged 17 and under

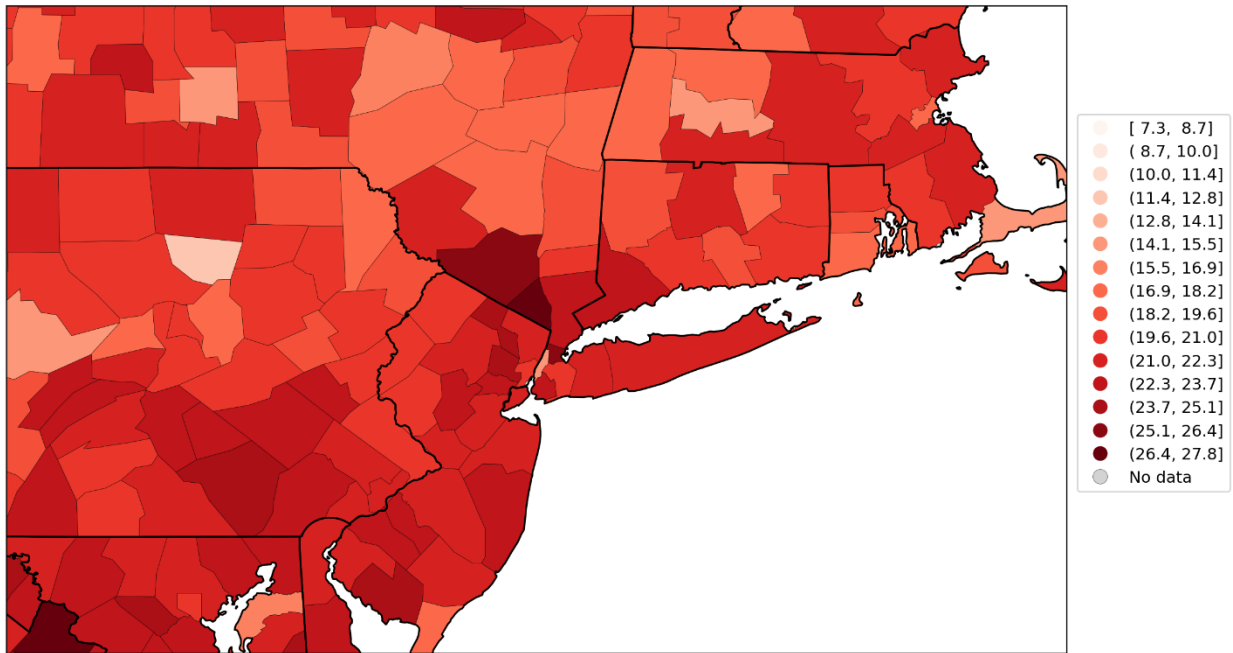


Figure 115: Map of percent of the population aged 17 and under per county for the contiguous USA (top panel) and a blow-up centred on the New York City urban area (bottom panel) (estimates from the 5-Year American Community Survey for the years 2014-2018).

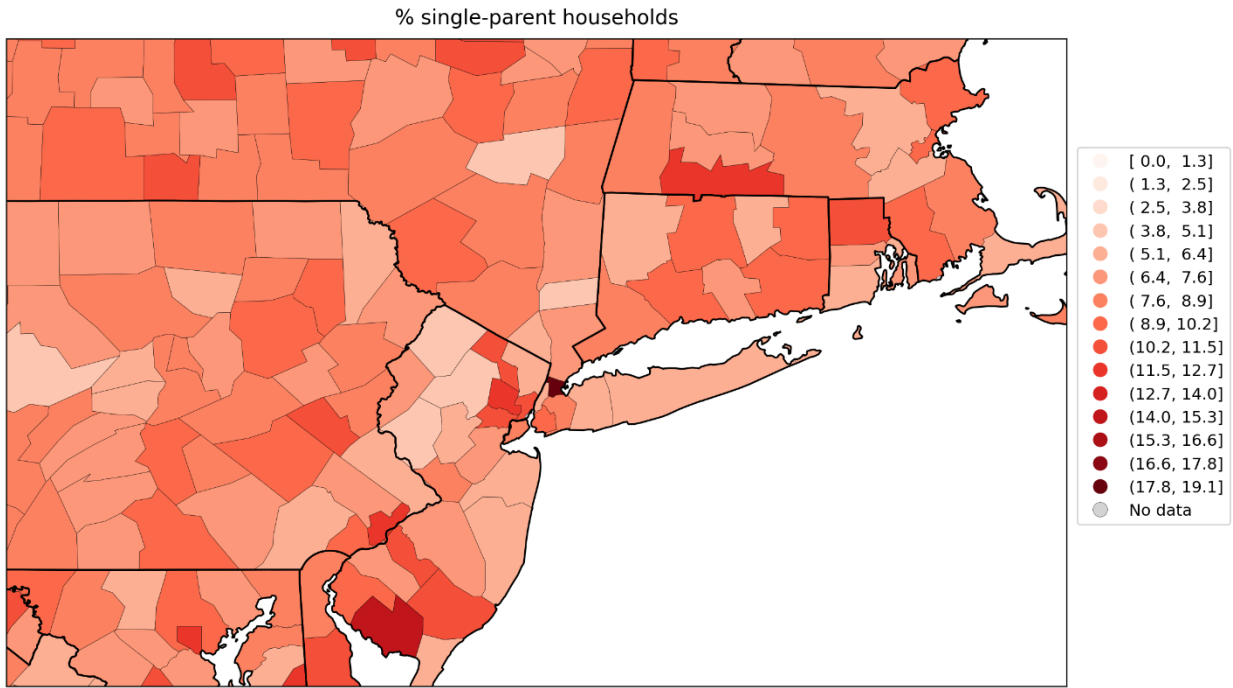
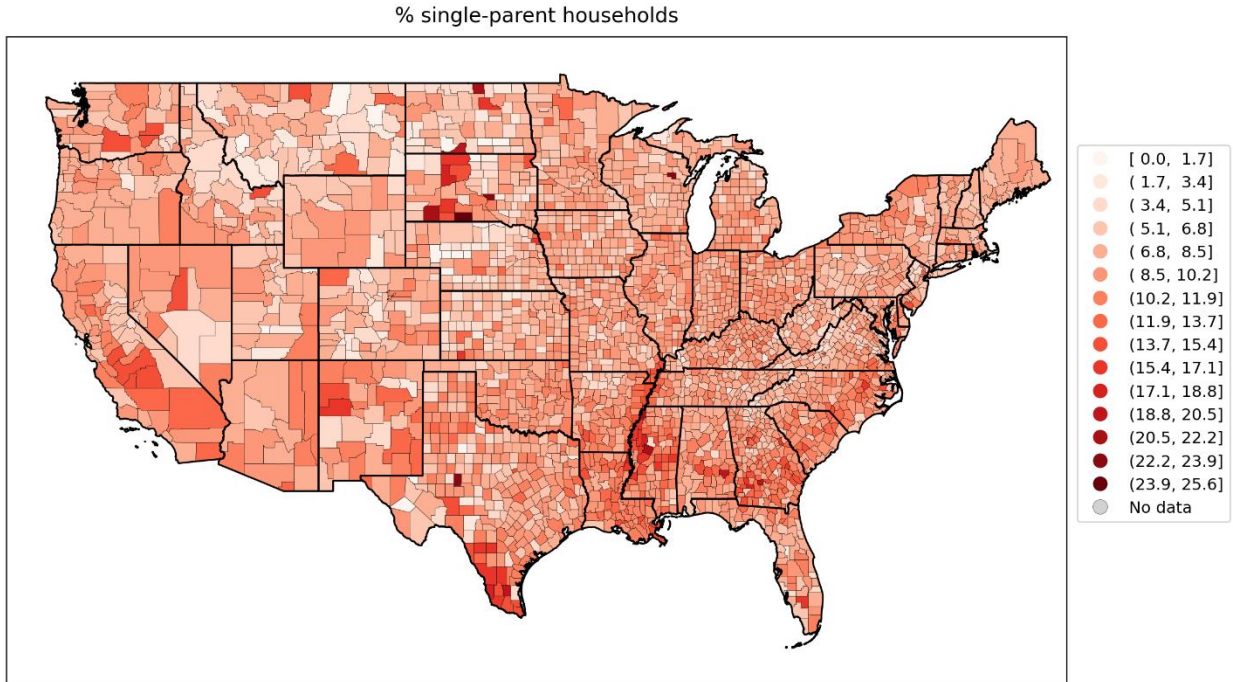


Figure 116: Map of % of the county's households that are single-parent households for the counties of the contiguous USA (top panel) and a blow-up centred on the New York City urban area (bottom panel) (estimates from the 5-Year American Community Survey for the years 2014-2018).

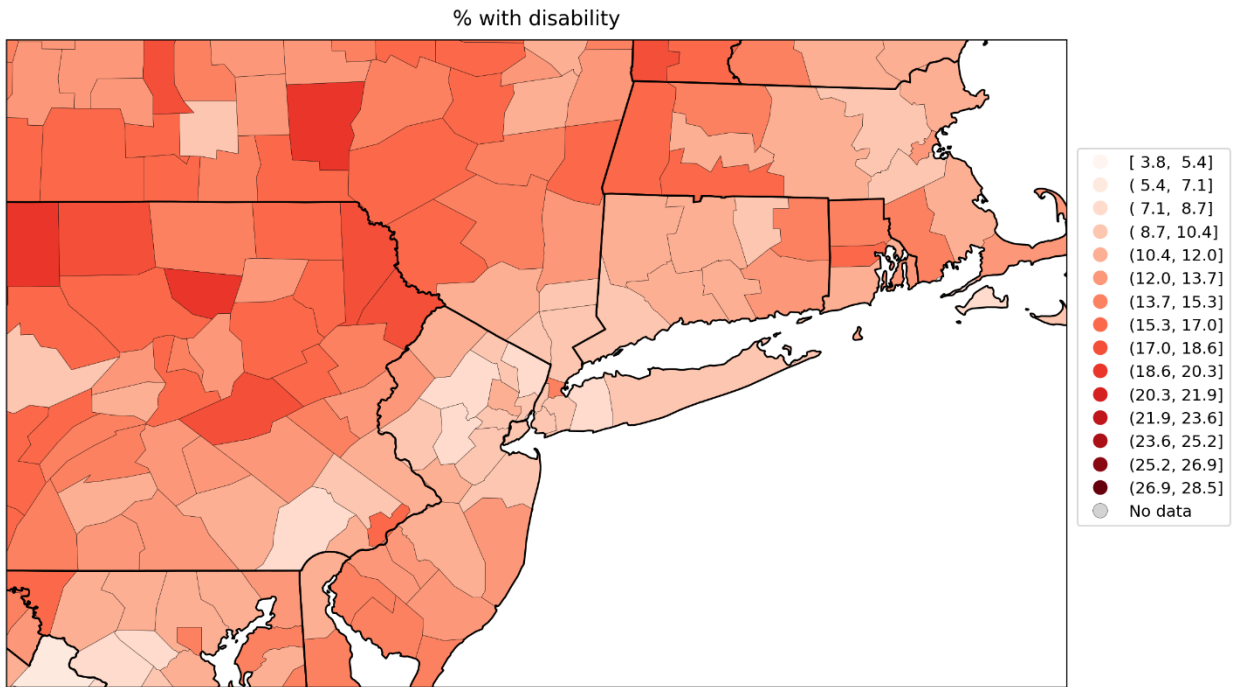
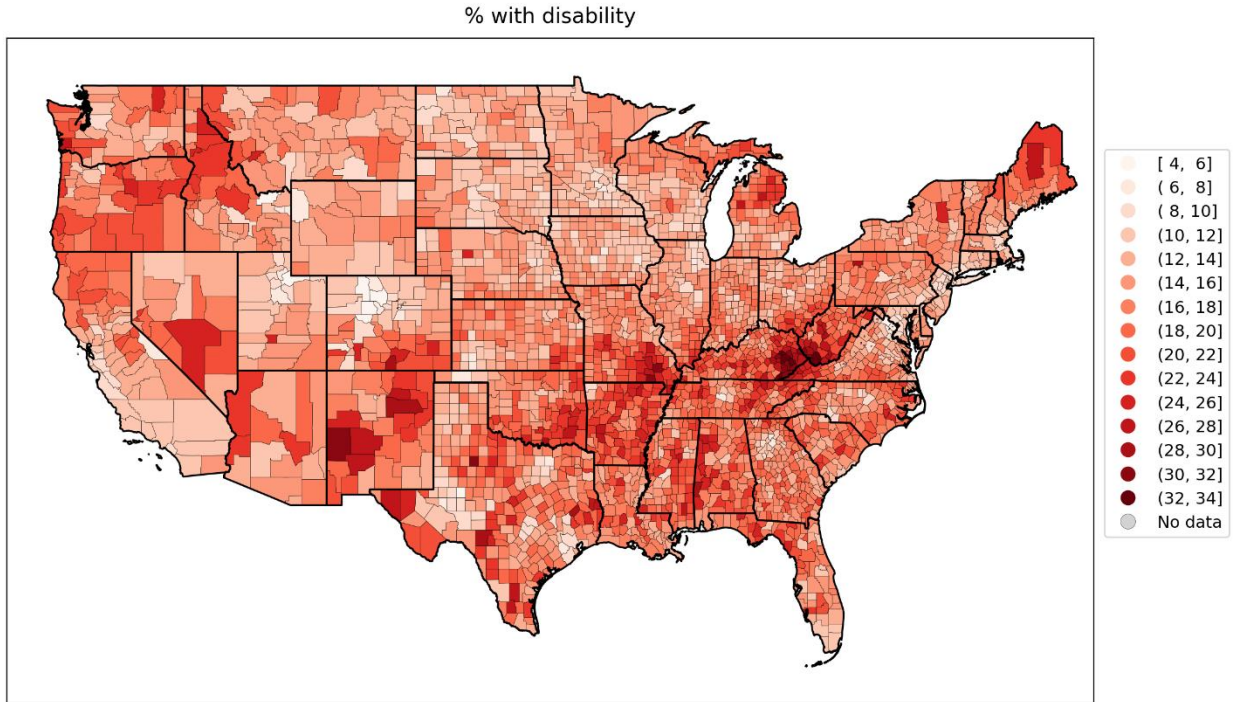


Figure 117: Map of % of the population with a disability, for the counties of the contiguous USA (top panel) and a blow-up centred on the New York City urban area (bottom panel) (estimates from the 5-Year American Community Survey for the years 2014-2018).

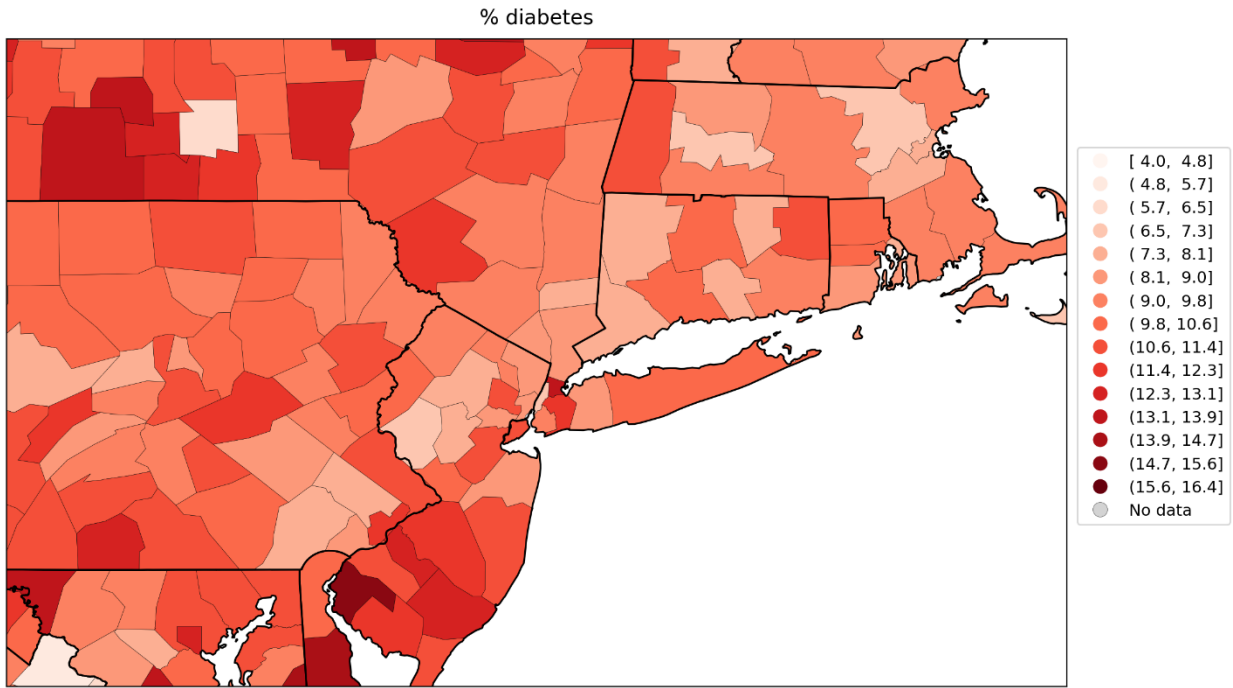
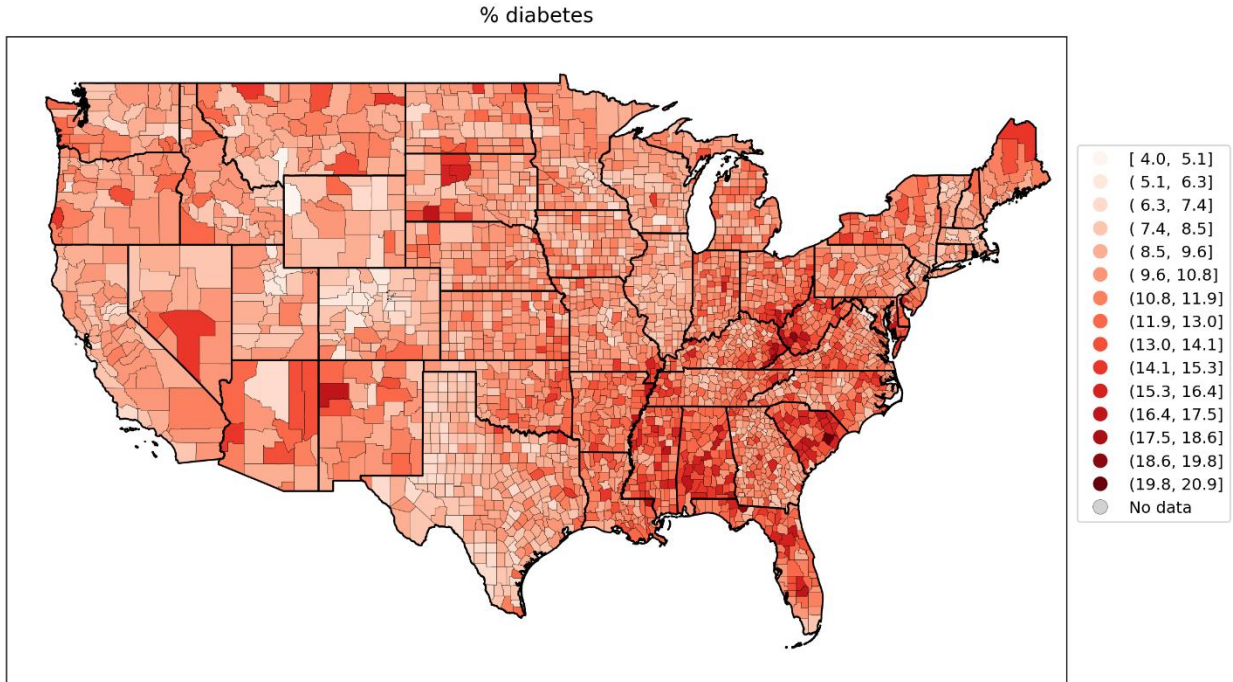


Figure 118: Map of % of the population with diabetes in 2018, for the counties of the contiguous USA (top panel) and a blow-up centred on the New York City urban area (bottom panel).

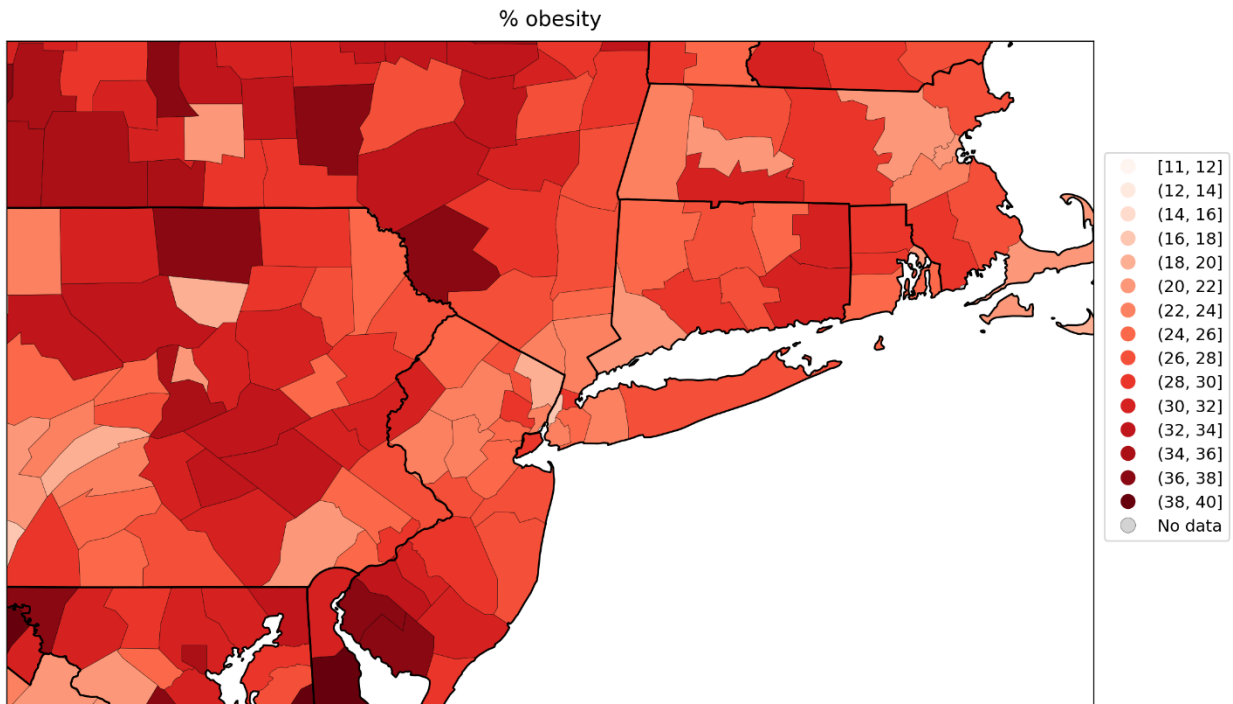
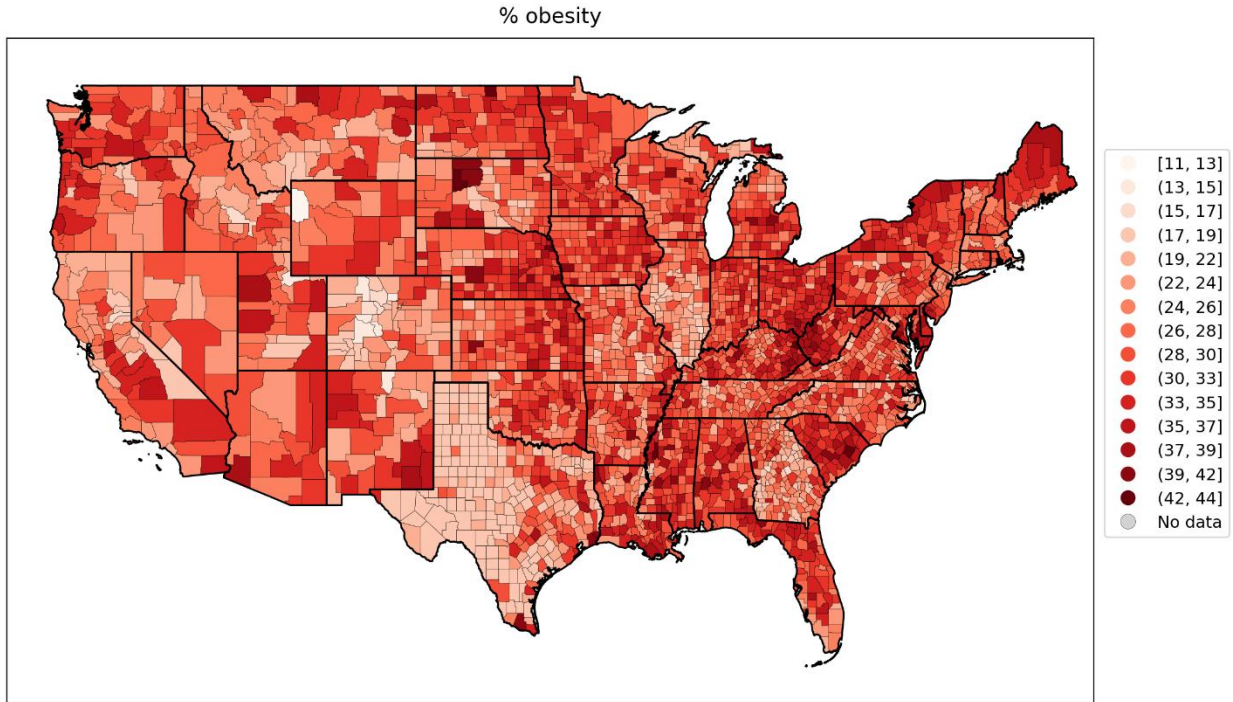
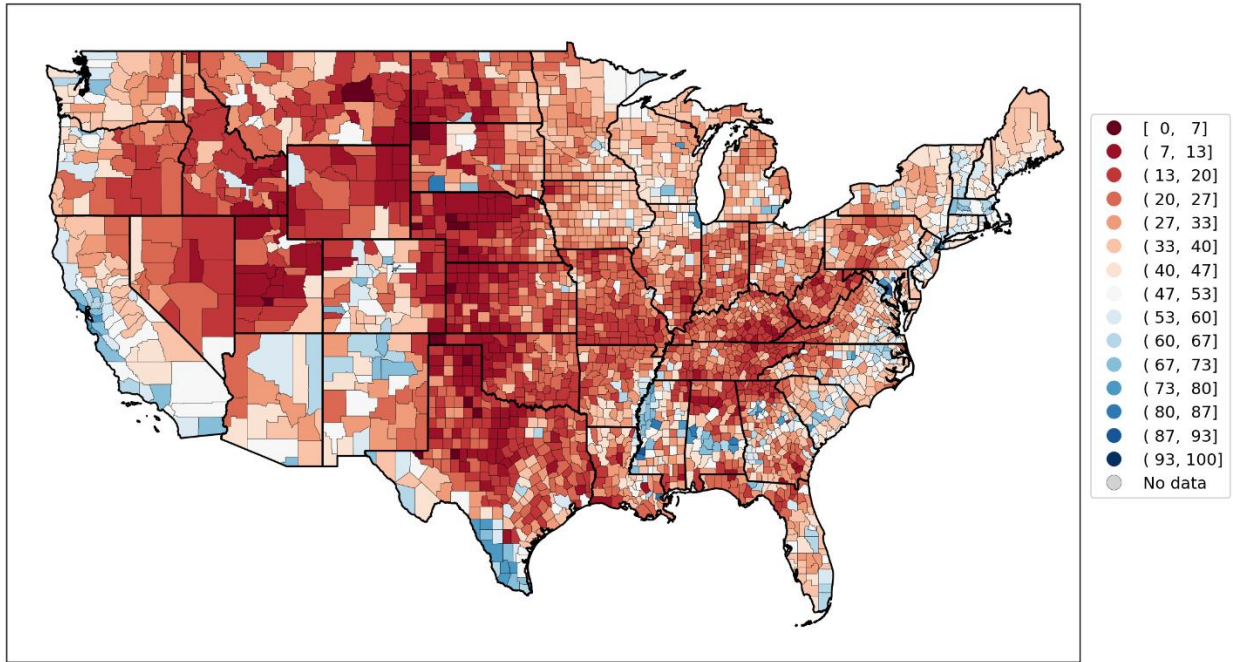


Figure 119: Map of % of the population with obesity in 2018, for the counties of the contiguous USA (top panel) and a blow-up centred on the New York City urban area (bottom panel).

Share of votes cast that were for the Democratic presidential candidate in 2016



Share of votes cast that were for the Democratic presidential candidate in 2016

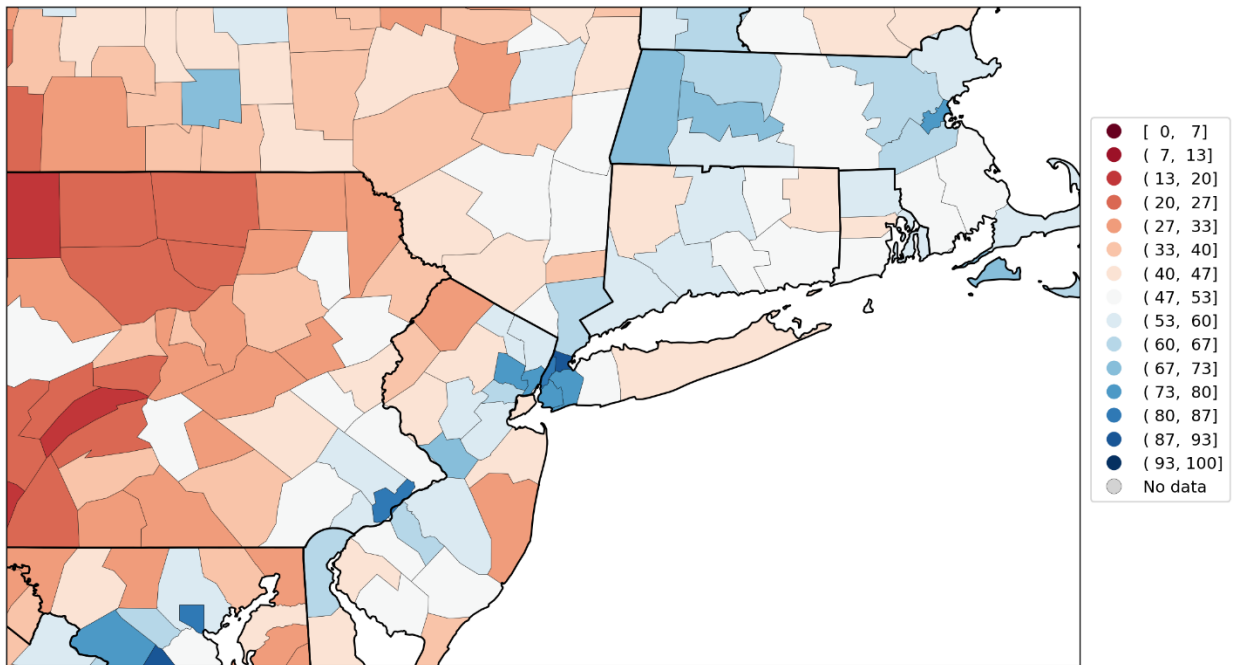
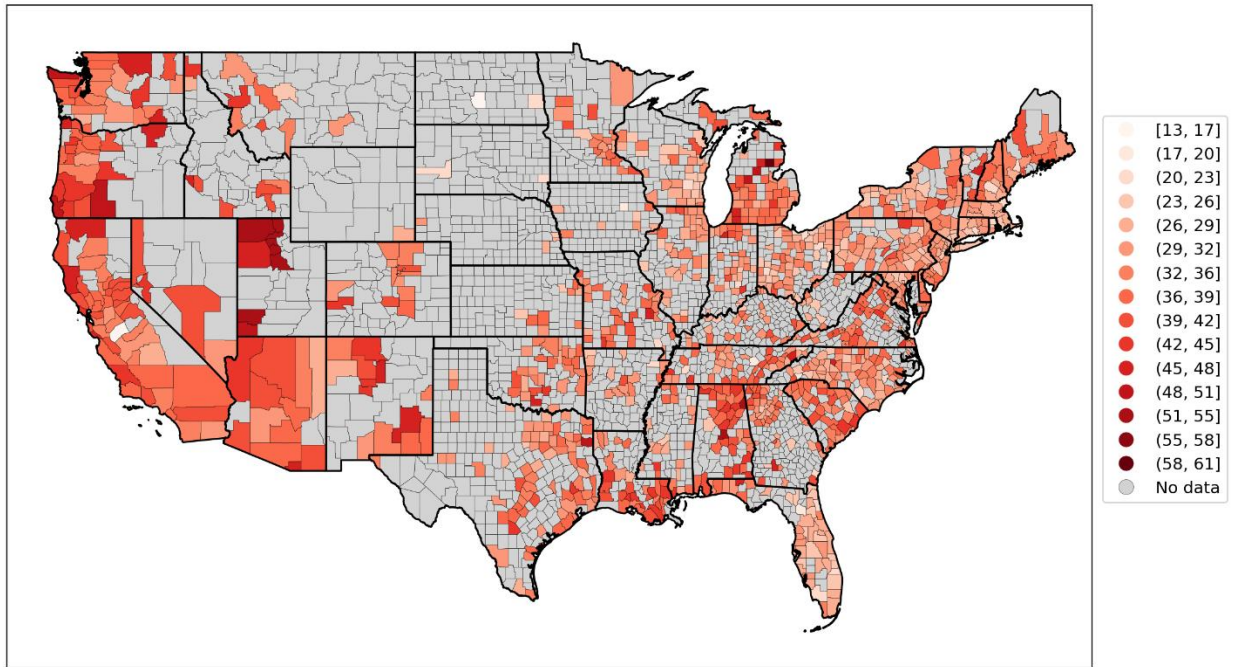


Figure 120: Map of share of all votes cast that were for the Democratic Party's presidential candidate in the 2016 election, for the counties of the contiguous USA (top panel) and a blow-up centred on the New York City urban area (bottom panel).

% deaths occurring at home in Mar-May 2019



% deaths occurring at home in Mar-May 2019

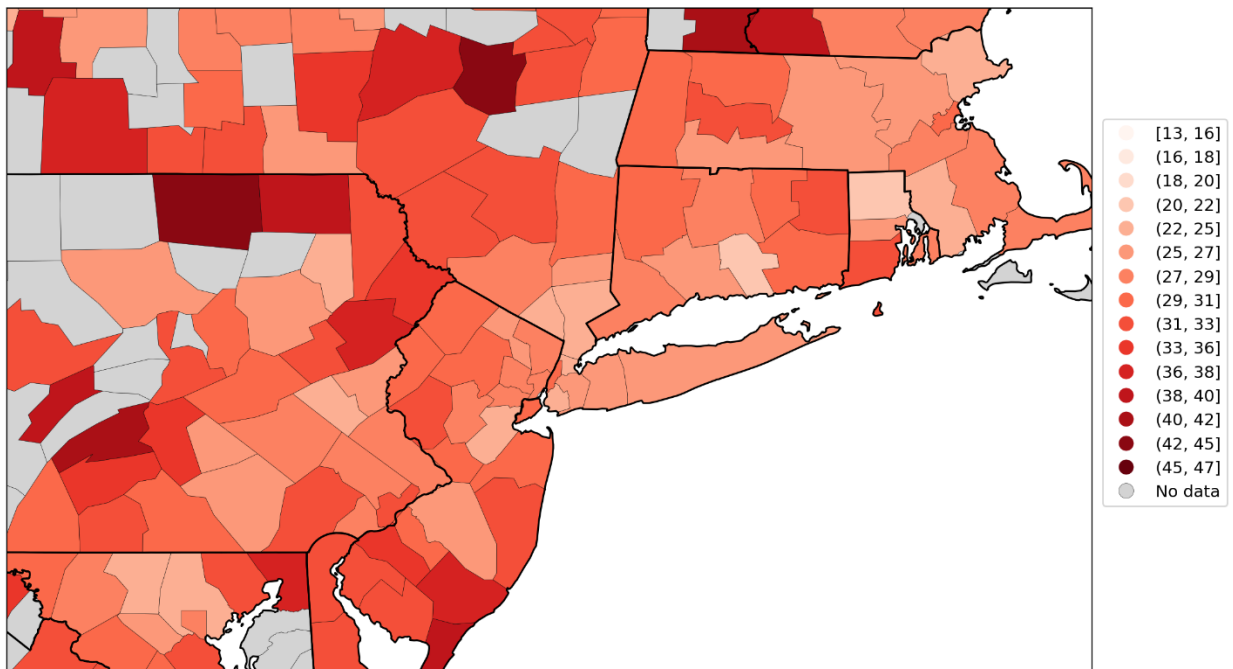
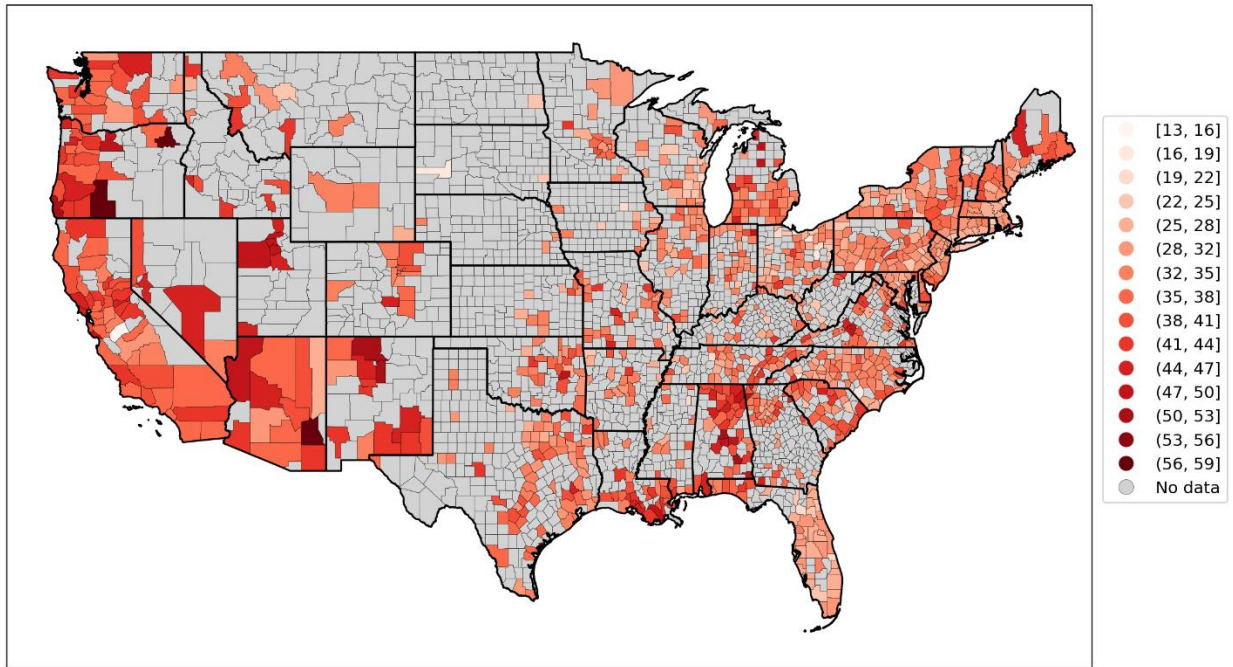


Figure 121: % of all deaths in the county that occurred at the decedent's home during March-May 2019, for the counties of the contiguous USA (top panel) and a blow-up centred on the New York City urban area (bottom panel).

% deaths occurring at home in Jun-Sep 2019



% deaths occurring at home in Jun-Sep 2019

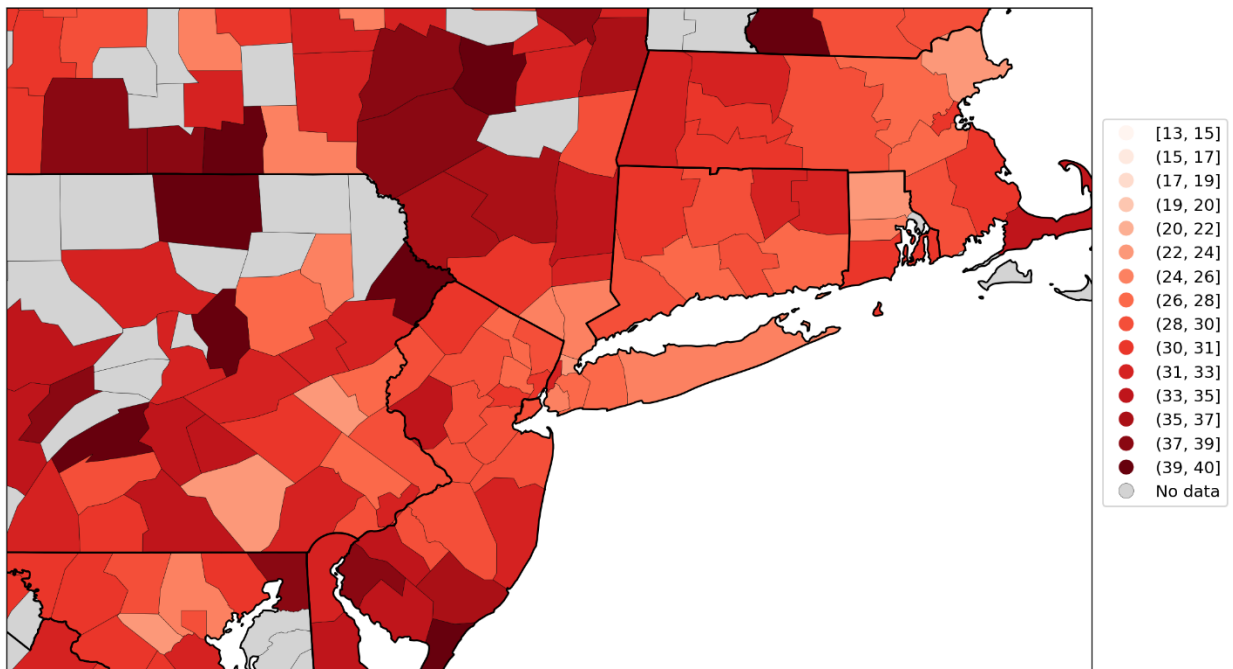
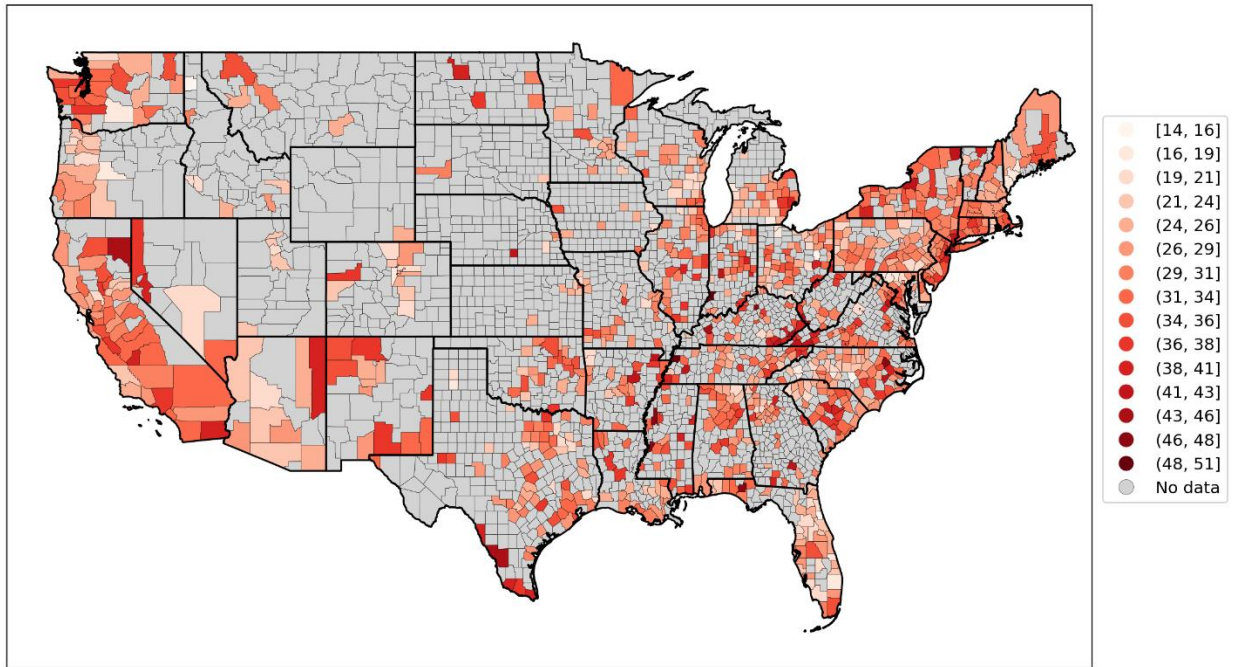


Figure 122: Map of % of all deaths in the county that occurred at the decedent's home during June-September 2019, for the counties of the contiguous USA (top panel) and a blow-up centred on the New York City urban area (bottom panel).

% deaths occurring in hospital in Mar-May 2019



% deaths occurring in hospital in Mar-May 2019

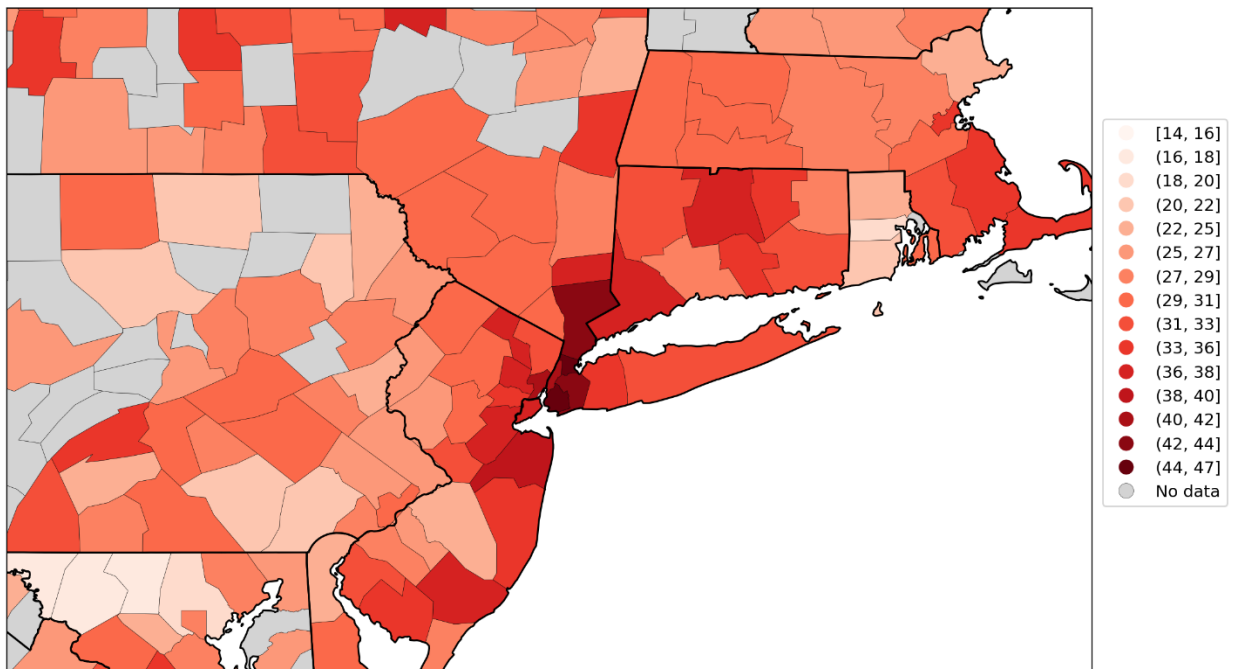
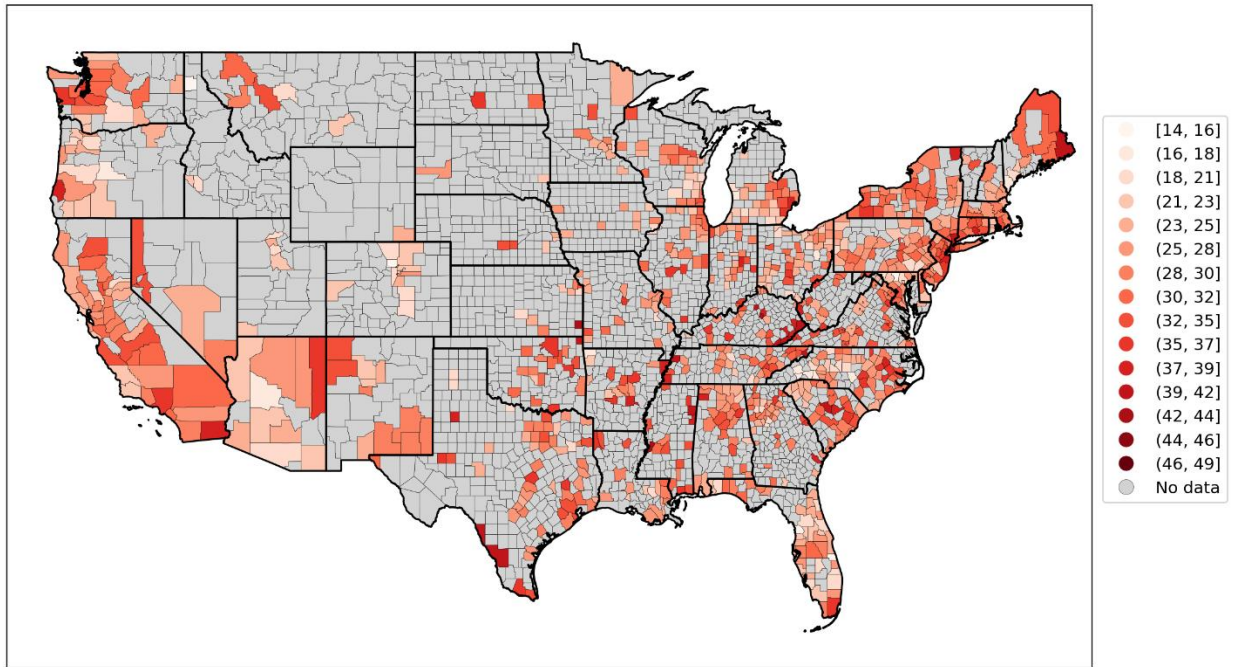


Figure 123: Map of % of all deaths in the county that occurred in hospital during March-May 2019, for the counties of the contiguous USA (top panel) and a blow-up centred on the New York City urban area (bottom panel).

% deaths occurring in hospital in Jun-Sep 2019



% deaths occurring in hospital in Jun-Sep 2019

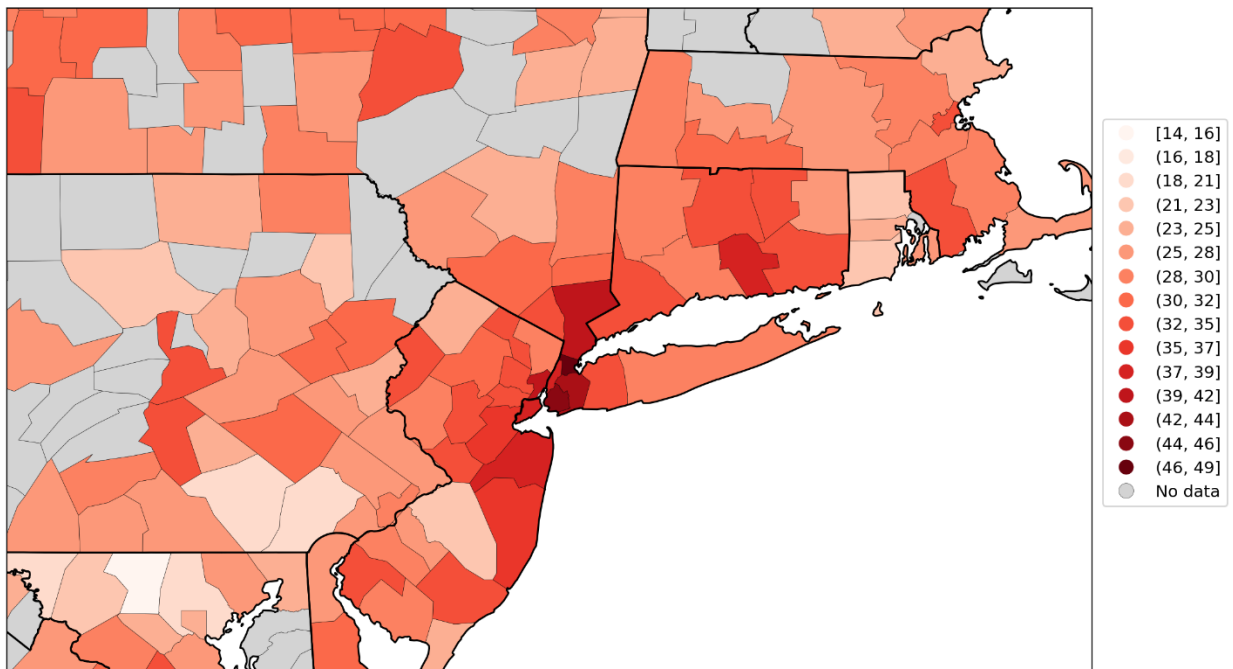
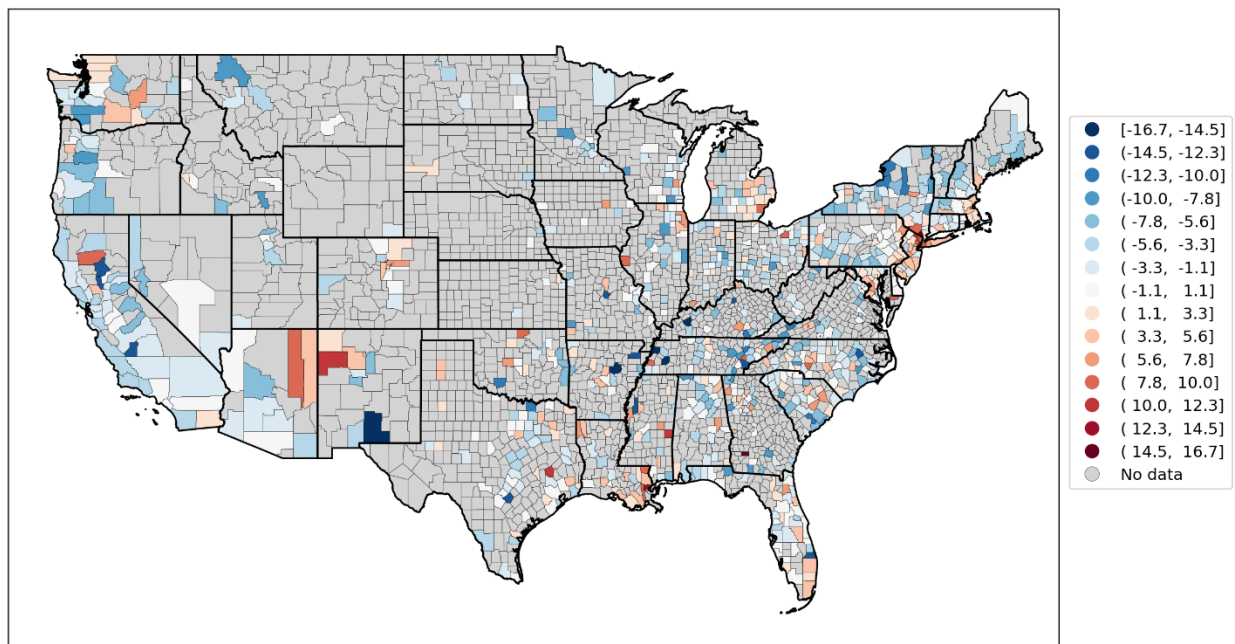


Figure 124: Map of % of all deaths in the county that occurred in hospital during June-September 2019, for the counties of the contiguous USA (top panel) and a blow-up centred on the New York City urban area (bottom panel).

% deaths occurring in hospital in Mar-May 2020
 MINUS
 % deaths occurring in hospital in Mar-May 2019



% deaths occurring in hospital in Mar-May 2020
 MINUS
 % deaths occurring in hospital in Mar-May 2019

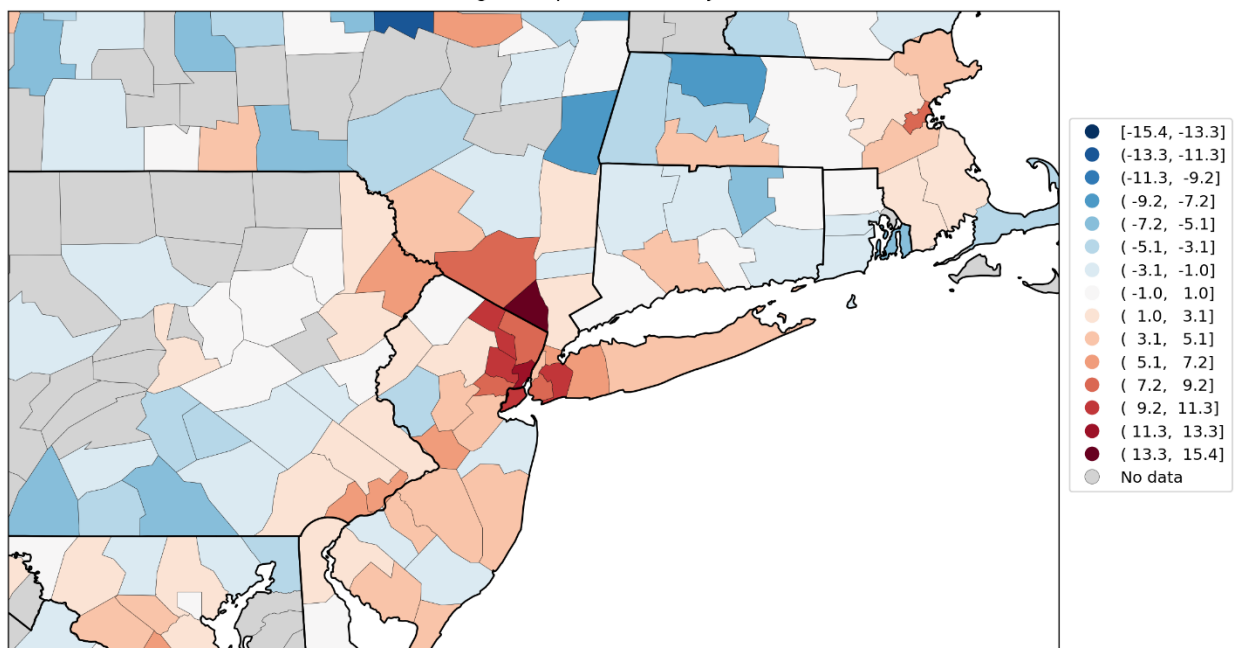
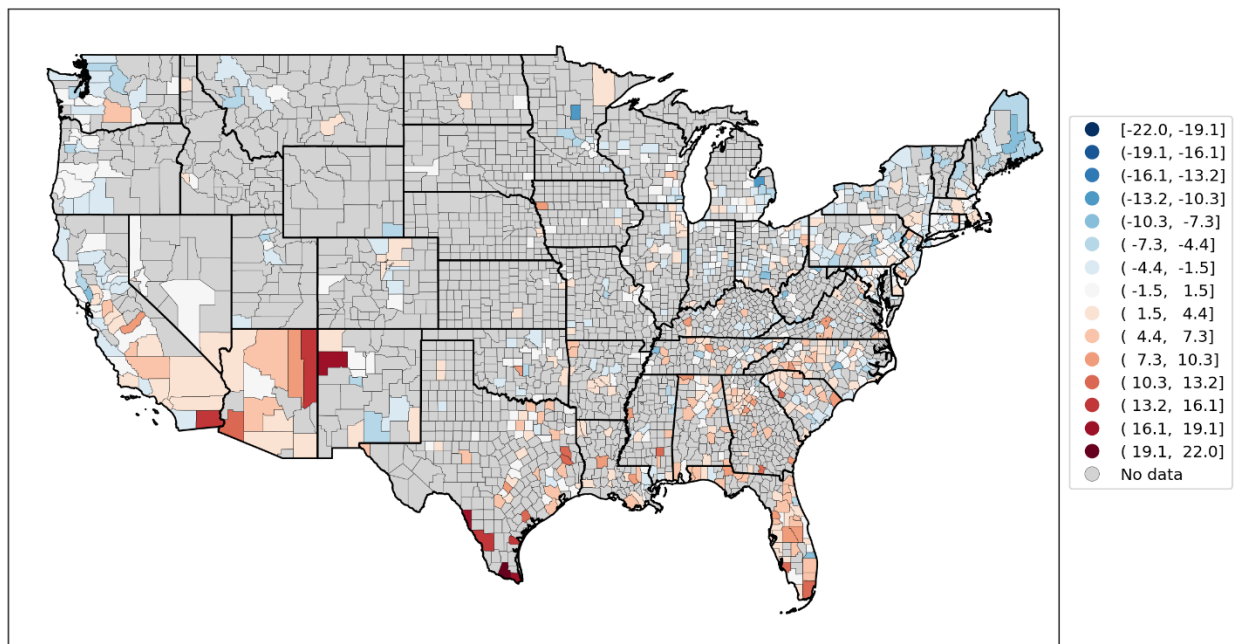


Figure 125: Map of difference in the % of all deaths in the county that occurred at home during the first-peak period (March-May 2020) and the % of deaths in the county that occurred at home during March-May 2019, for the counties of the contiguous USA (top panel) and a blow-up centred on the New York City urban area (bottom panel).

% deaths occurring in hospital in Jun-Sep 2020
MINUS
% deaths occurring in hospital in Jun-Sep 2019



% deaths occurring in hospital in Jun-Sep 2020
MINUS
% deaths occurring in hospital in Jun-Sep 2019

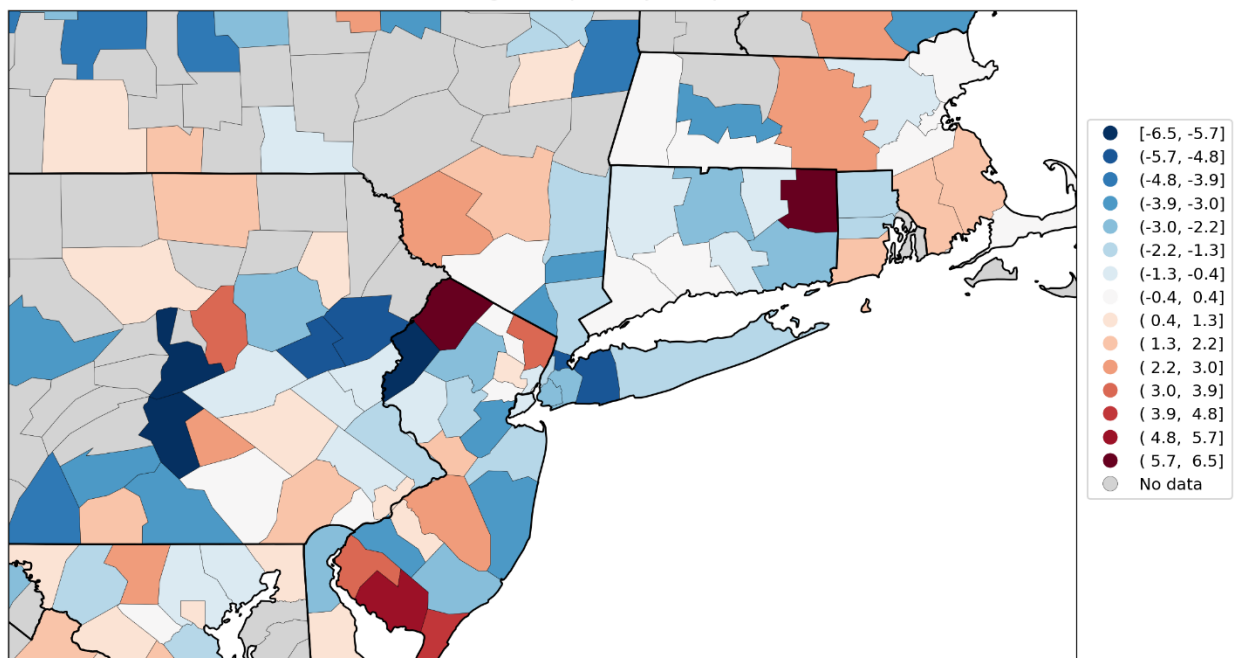
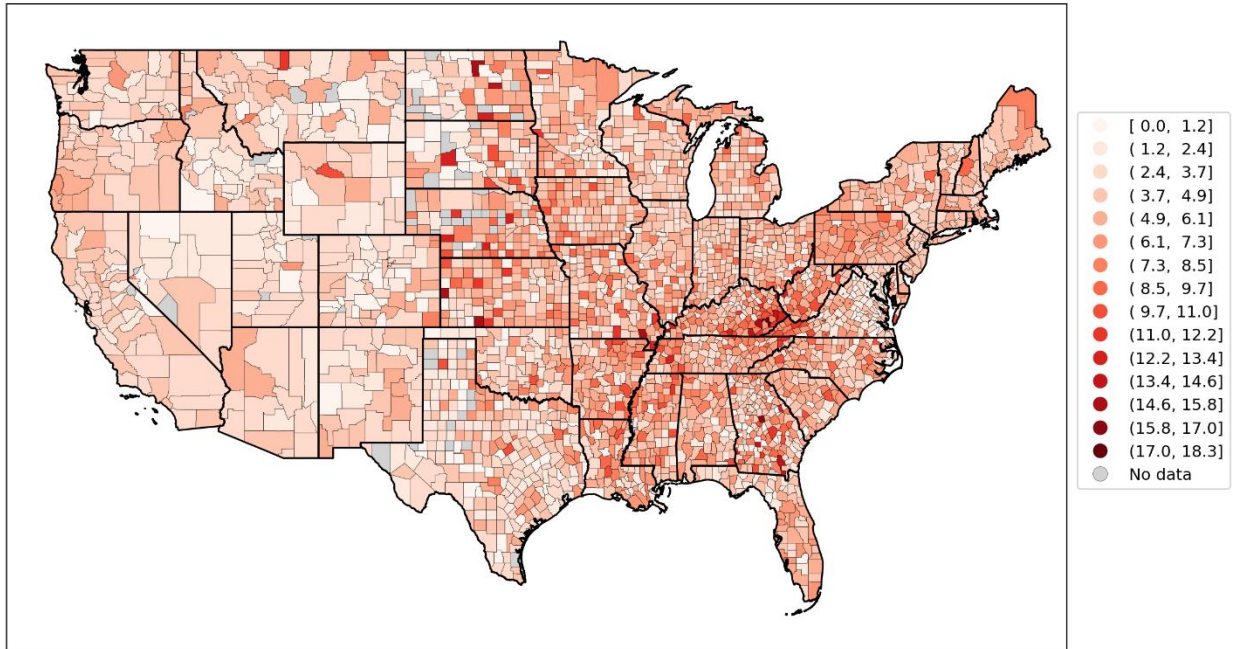


Figure 126: Map of difference in the % of all deaths in the county that occurred at home during the summer-peak period (June-September 2020) and the % of deaths in the county that occurred at home during June-September 2019, for the counties of the contiguous USA (top panel) and a blow-up centred on the New York City urban area (bottom panel).

Num. prescription drug claims / pop



Num. prescription drug claims / pop

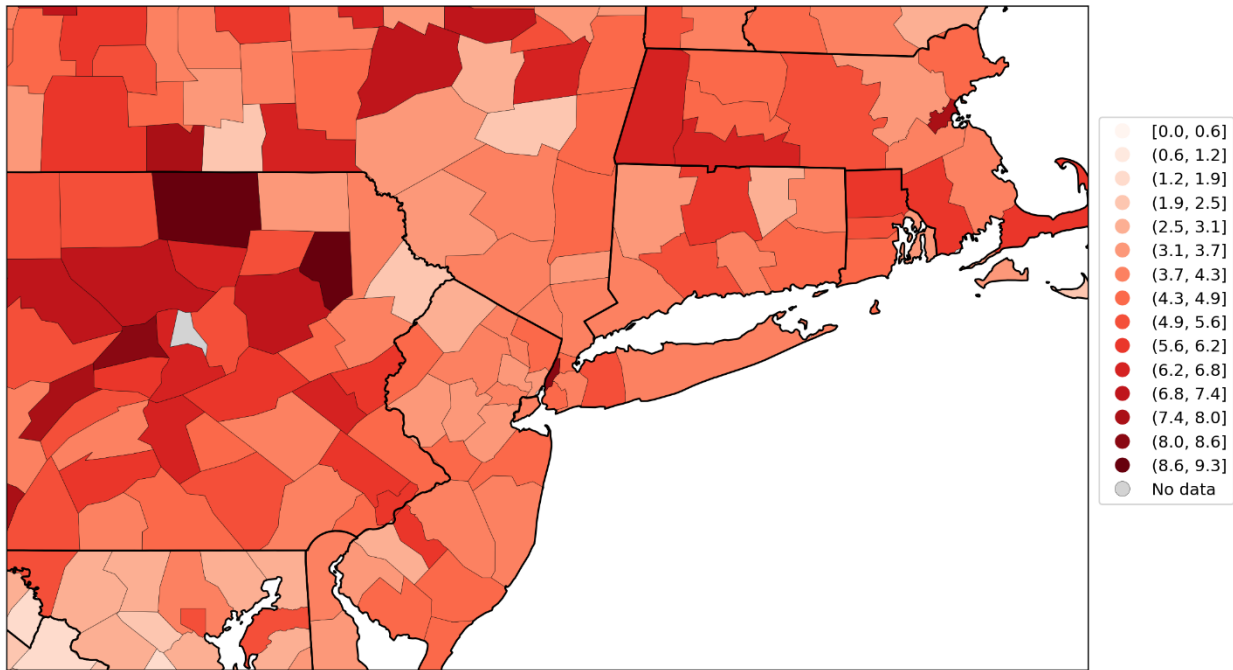


Figure 127: Map of number of prescription drug claims per person in 2017, for the counties of the contiguous USA (top panel) and a blow-up centred on the New York City urban area (bottom panel).

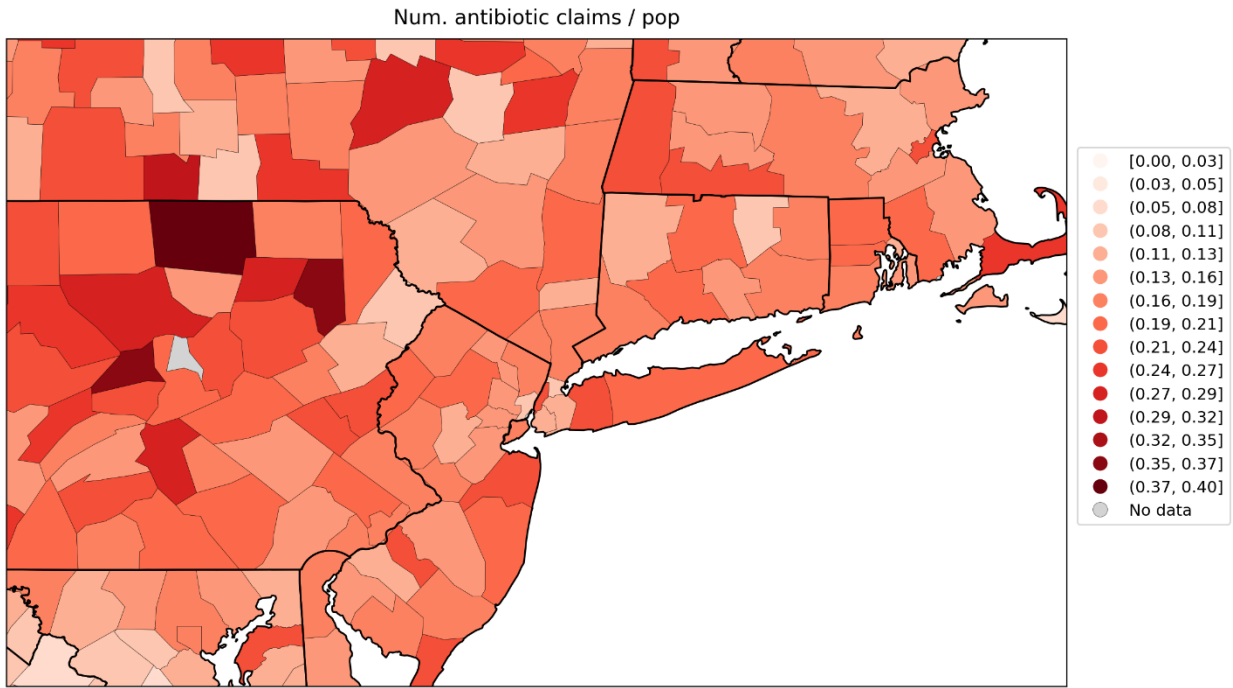
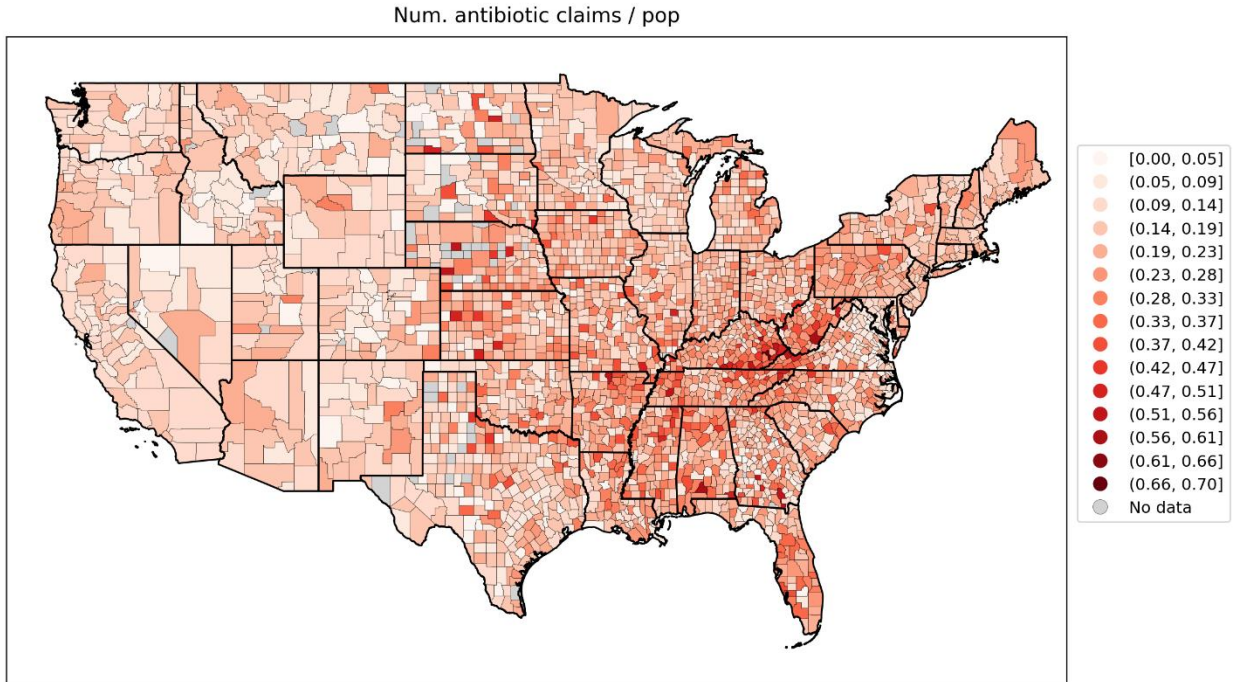
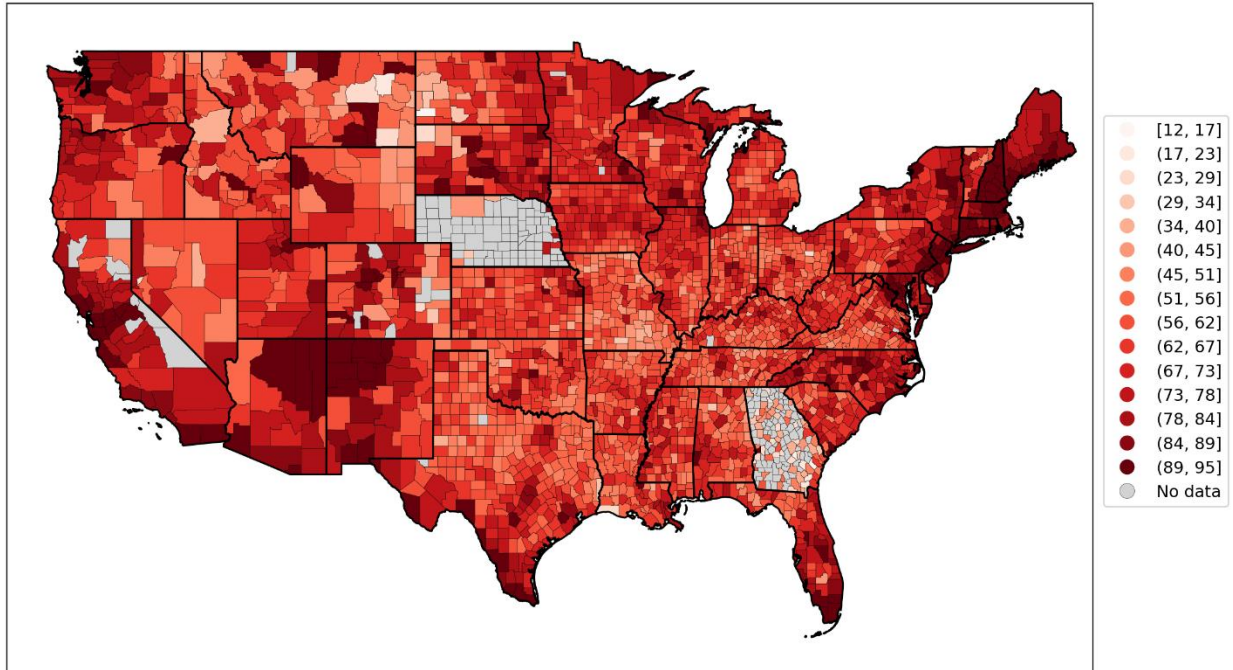


Figure 128: Map of number of antibiotic prescription drug claims per person in 2017, for the counties of the contiguous USA (top panel) and a blow-up centred on the New York City urban area (bottom panel).

% pop 18+ with at least one dose
as of 2021-12-31



% pop 18+ with at least one dose
as of 2021-12-31

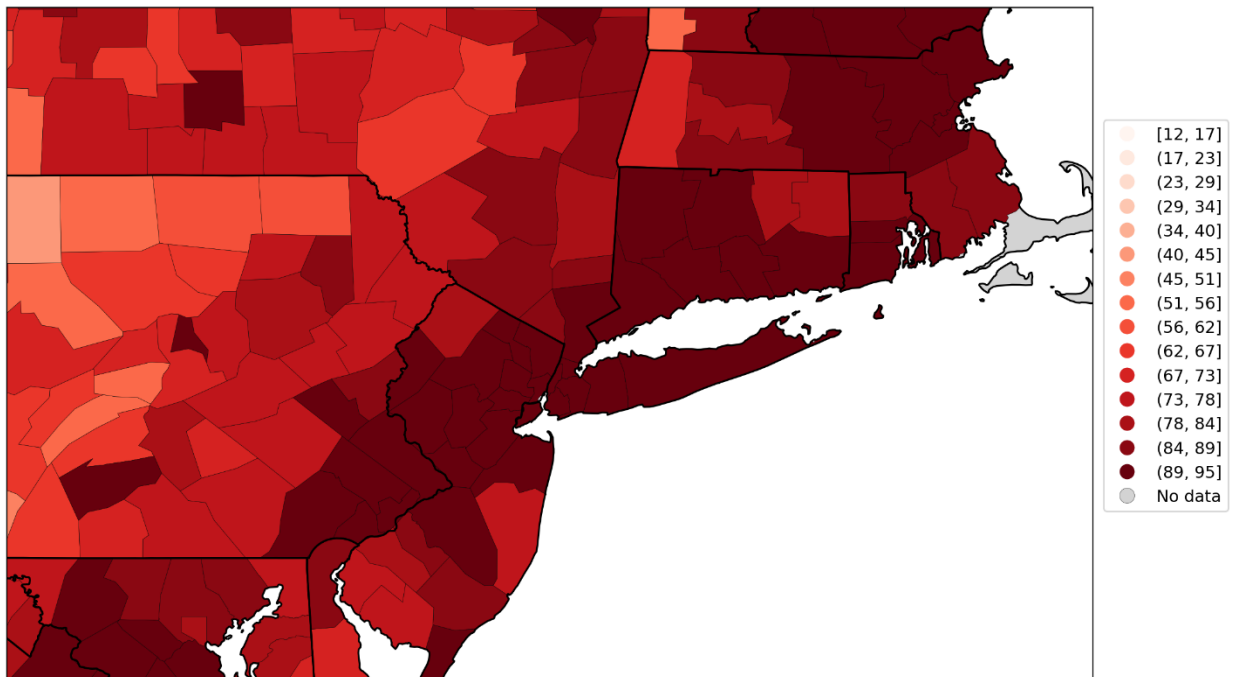
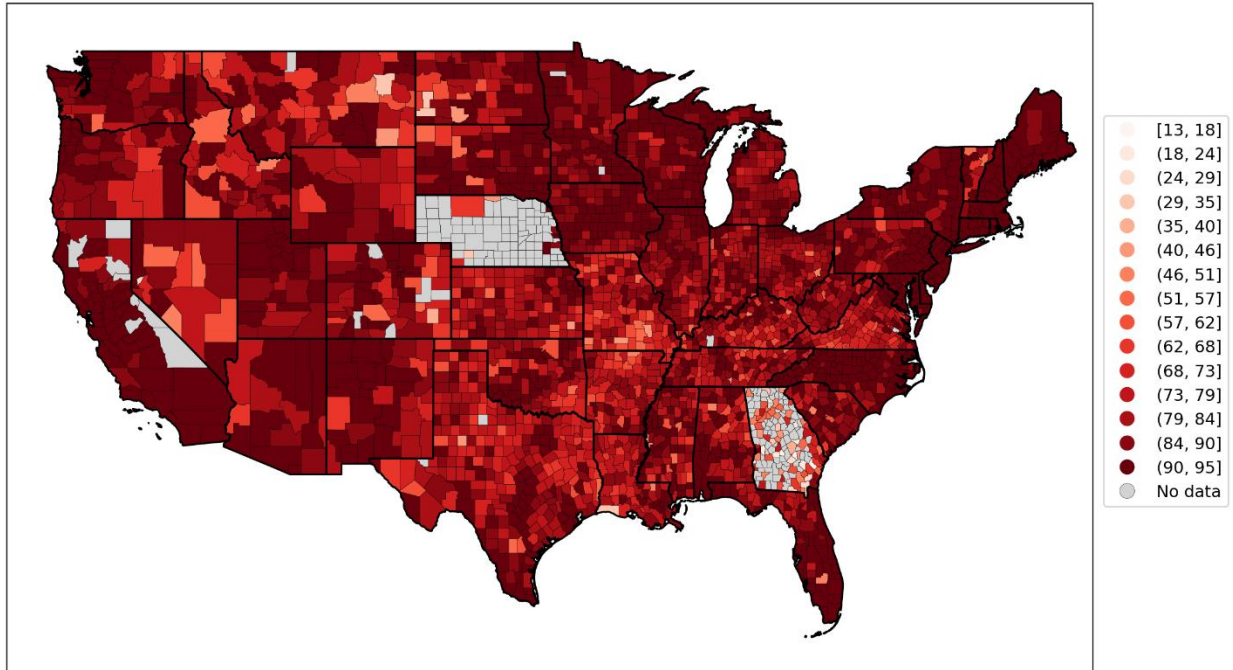


Figure 129: Map of % of the population aged 18+ having received at least one dose of a COVID vaccine by December 31, 2021, for the contiguous USA (top panel) and a blow-up centred on the New York City urban area (bottom panel).

% pop 65+ with at least one dose
as of 2021-12-31



% pop 65+ with at least one dose
as of 2021-12-31

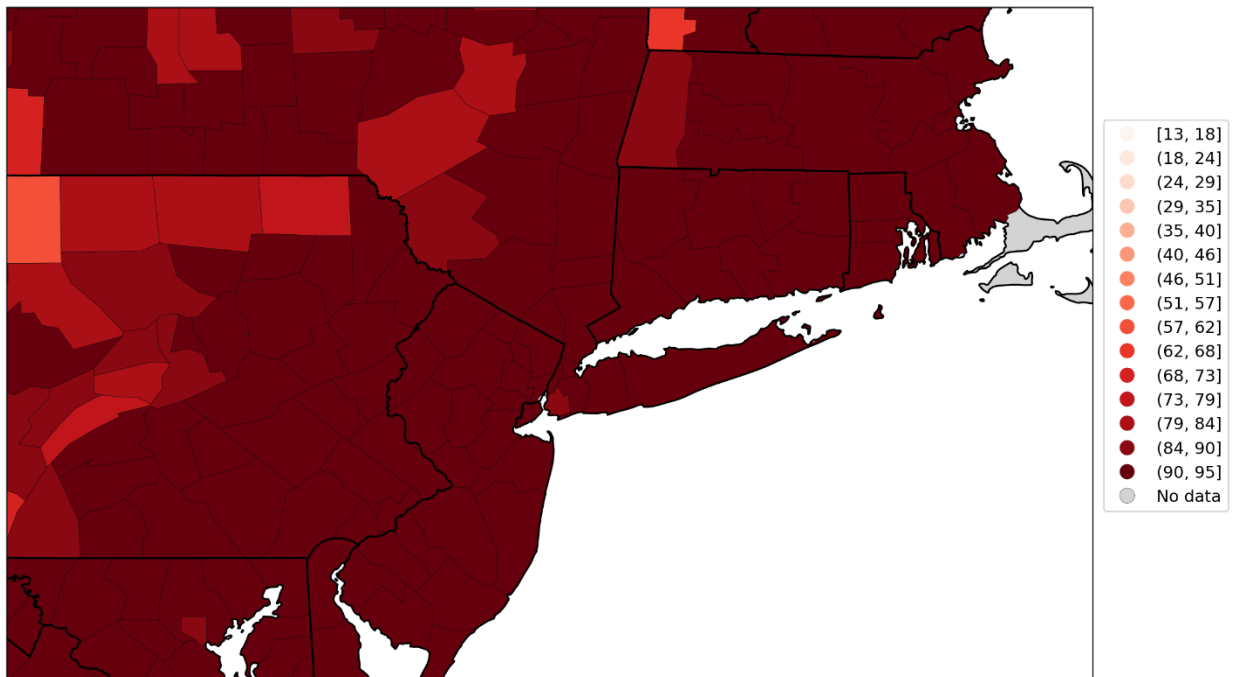
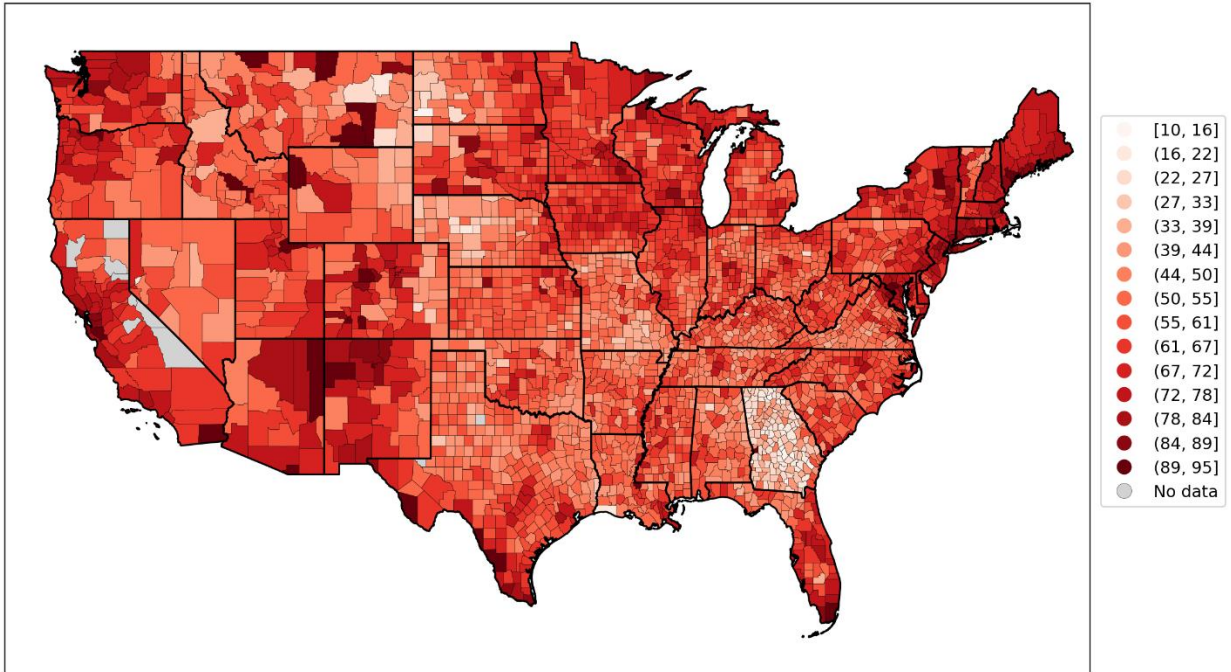


Figure 130: Map of % of the population aged 65+ having received at least one dose of a COVID vaccine by December 31, 2021, for the contiguous USA (top panel) and a blow-up centred on the New York City urban area (bottom panel).

% pop 18+ with primary series completed
as of 2021-12-31



% pop 18+ with primary series completed
as of 2021-12-31

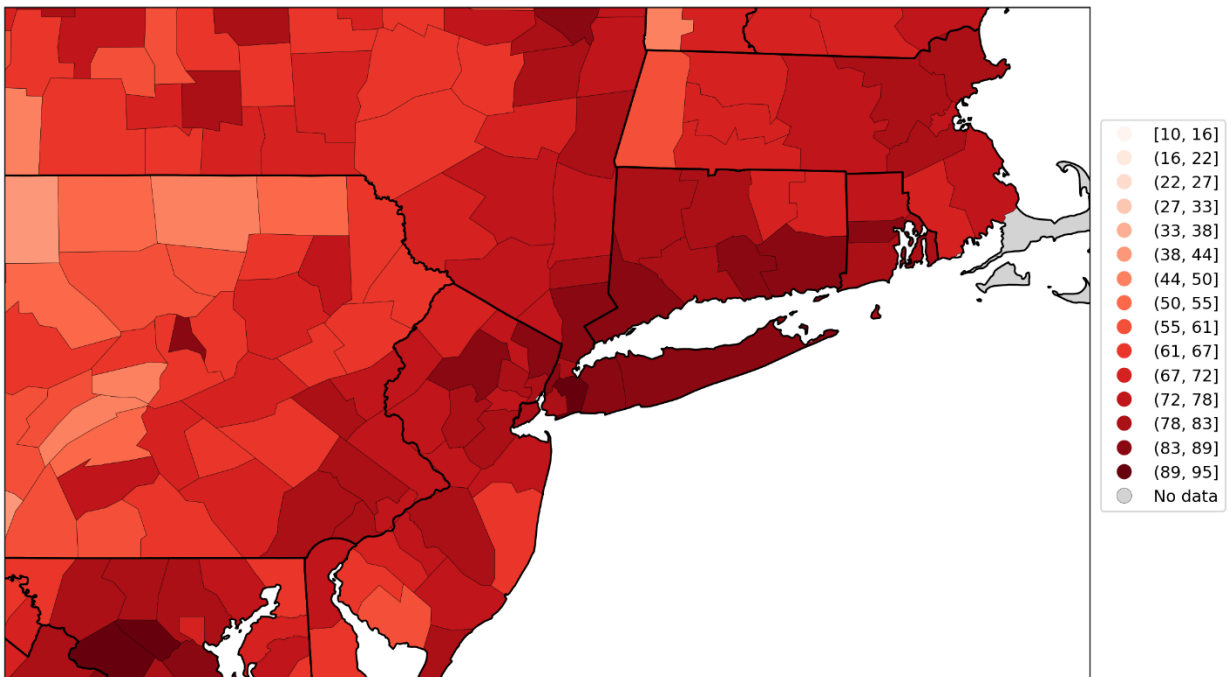
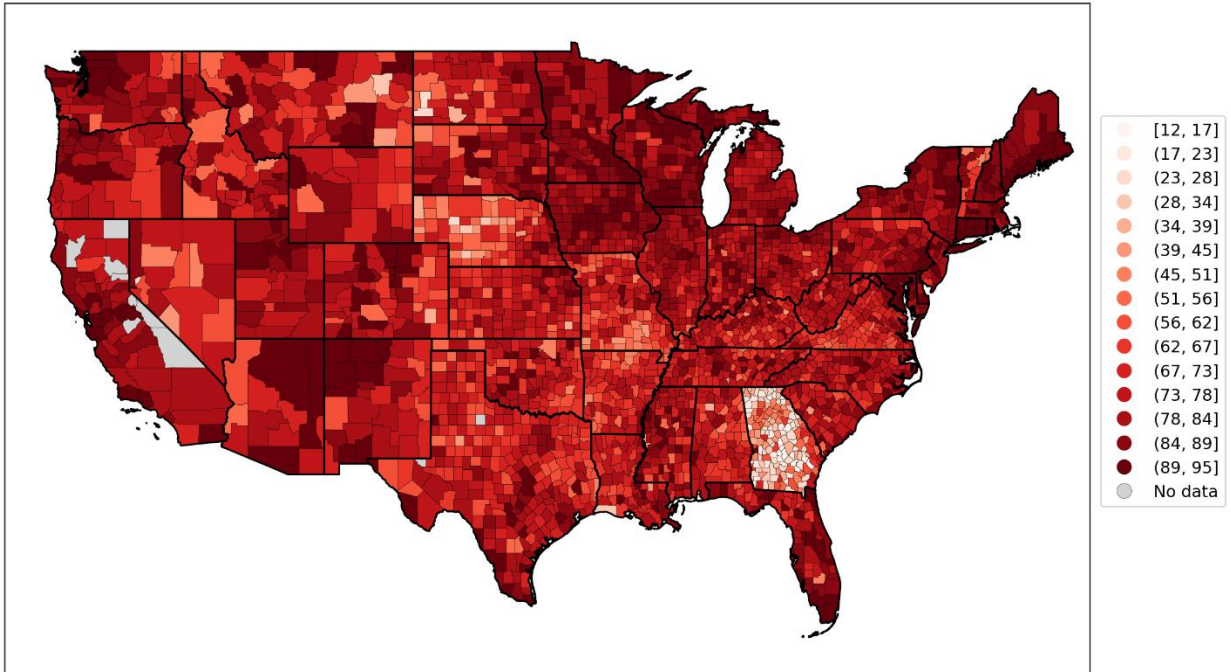


Figure 131: Map of % of the population aged 18+ with primary series of a COVID vaccine completed by December 31, 2021, for the contiguous USA (top panel) and a blow-up centred on the New York City urban area (bottom panel).

% pop 65+ with primary series completed
as of 2021-12-31



% pop 65+ with primary series completed
as of 2021-12-31

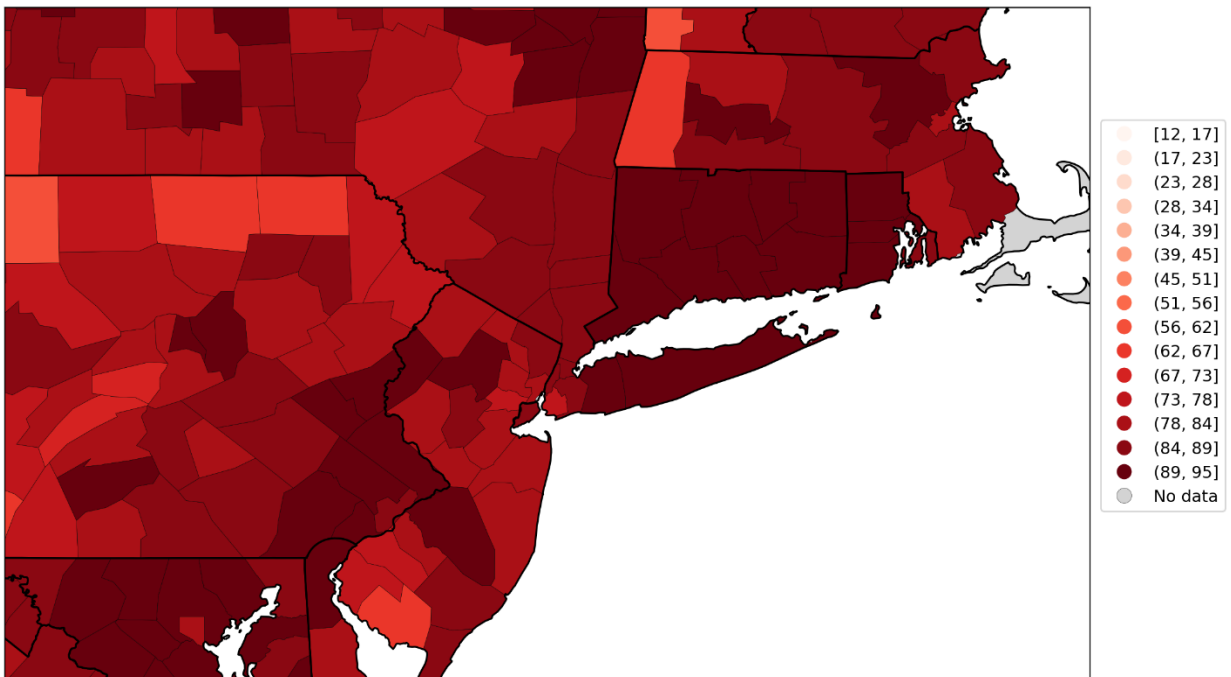


Figure 132: Map of % of the population aged 65+ with primary series of a COVID vaccine completed by December 31, 2021, for the contiguous USA (top panel) and a blow-up centred on the New York City urban area (bottom panel).

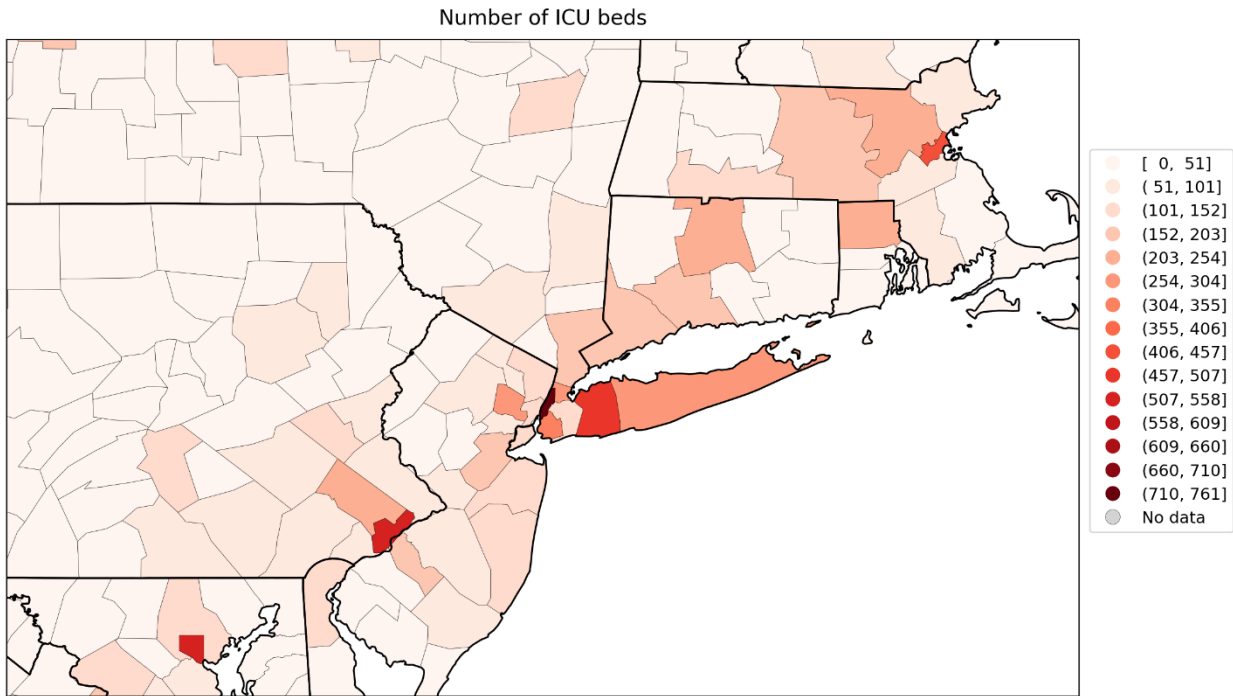
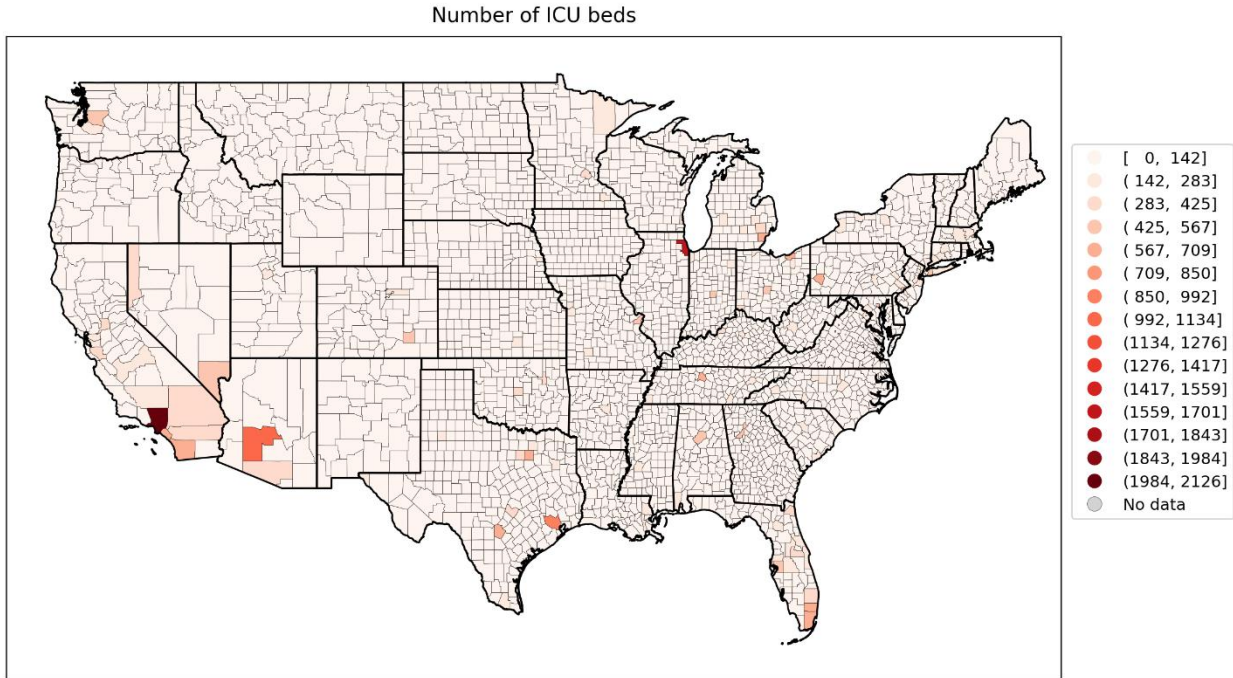


Figure 133: Map of number of ICU beds per county for the contiguous USA (top panel) and a blow-up centred on the New York City urban area (bottom panel). Data is for 2018-2019.

% increase mortality (2020-05-31 to 2020-09-26)

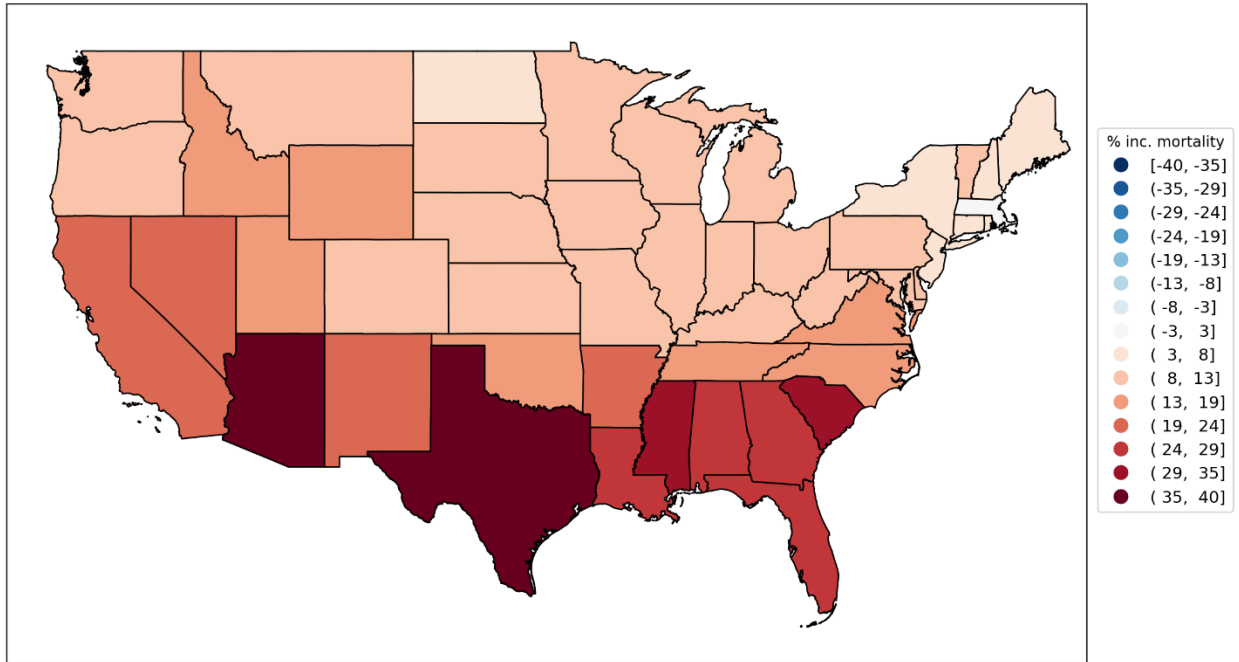
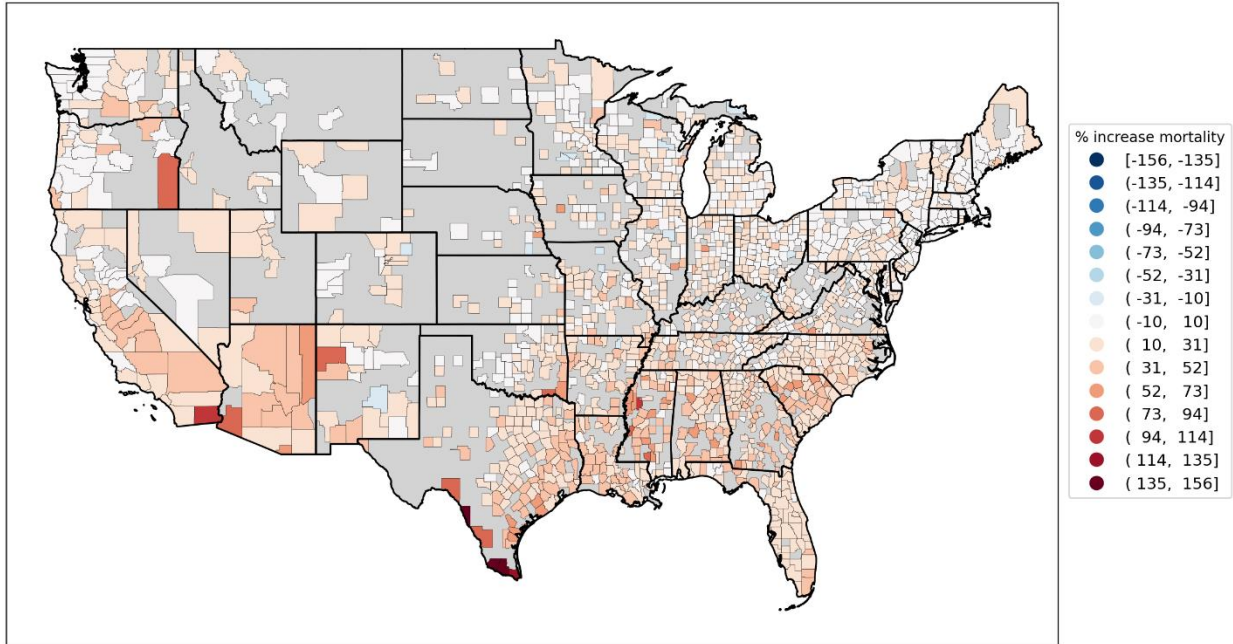


Figure 134: Map of integrated summer-peak period (June-September 2020) P-scores for USA states.

% increase in mortality for 2020-06-01 to 2020-09-30



% increase in mortality for 2020-06-01 to 2020-09-30

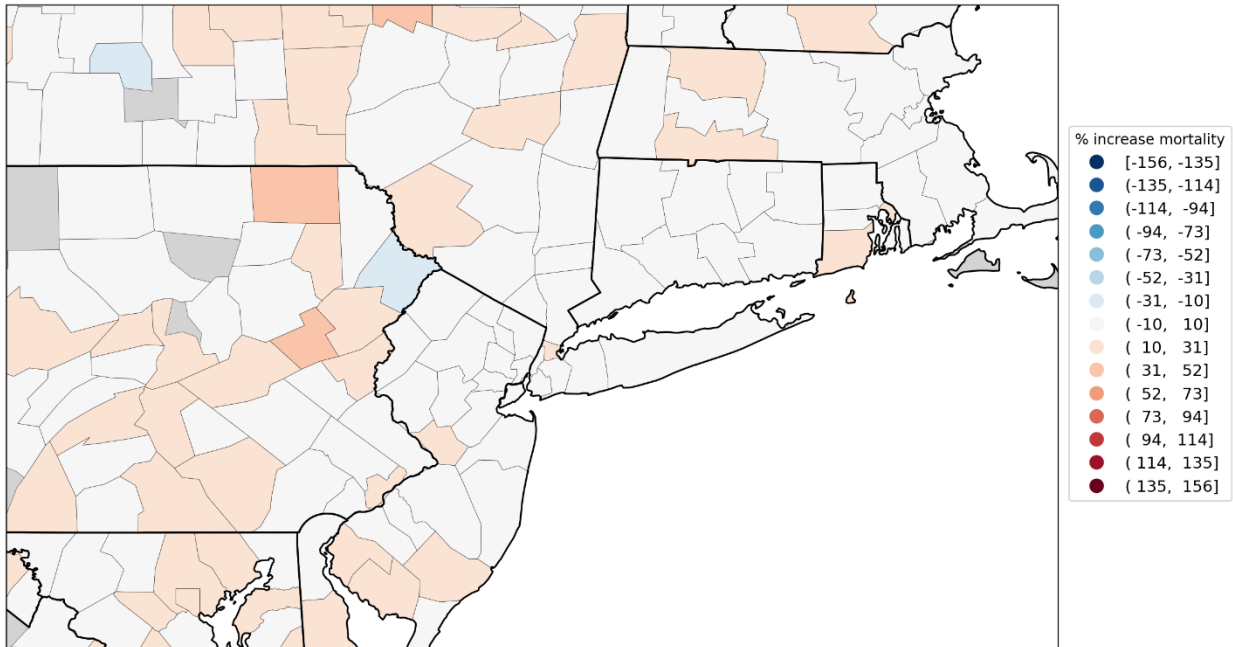


Figure 135: Map of integrated summer-peak period (June-September 2020) P-scores for the counties of the contiguous USA (top panel) and a blow-up centred on the New York City urban area (bottom panel). The color range for both panels extends to the maximum integrated summer-peak period P-score value in the USA (Maverick County, TX; P-score = 156%). Dark grey indicates counties for which data was unavailable.

3.6.2 European subnational regions

The figures in this section show scatter plots of integrated P-scores for the first-peak and summer-peak periods vs socioeconomic variables, for European subnational regions. For each socioeconomic variable, we also include a heatmap showing how it varies across the geographic regions with available data, as was done above for USA counties.

We first examine scatter plots of integrated first-peak period and summer-peak period P-scores for the NUTS2 regions of Europe vs population in 2019, $\log(\text{population})$, population density in 2018, $\log(\text{population density})$, and at-risk-of-poverty rate in 2019. This is shown in Figure 136 to Figure 140, with maps in Figure 142 to Figure 146.

Following the figures for the NUTS2 regions of Europe, we also include additional figures with scatter plots and maps examining the gross disposable household income per capita for the NUTS3 regions of the UK (Figure 147 to Figure 149), and for a set of socioeconomic variables for the NUTS3 regions of London, UK (Figure 150 to Figure 157).

European NUTS2 regions

Each of Figure 136 to Figure 140 has six panels, similar to the scatter plots for the USA counties in section 3.6.1: the top row of panels is for the first-peak period, the middle row of panels is for the summer-peak period, and the bottom row shows the first-peak period (lower-left panel) and summer-peak period (lower-right panel) data points for the four European countries with the highest integrated first-peak period P-scores at the national level: Spain (ES), United Kingdom (UK), Italy (IT) and Belgium (BE). The y-axis ranges are the same for all panels, to facilitate comparison.

Figure 141 contains maps of integrated first-peak period P-scores for the NUTS2 regions of Europe (left panel) and for a blow-up of the NUTS2 regions of England and Wales, UK (right panel). Mortality data was unavailable at the NUTS2 level for the dark grey-colored countries in the left panel of Figure 141, including Germany, such that these countries do not contribute to the scatter plots in Figure 136 to Figure 140.

Figure 142 to Figure 146 contain heatmaps showing how the population, $\log(\text{population})$, population density, $\log(\text{population density})$, and at-risk-of-poverty rate vary across the NUTS2 regions of Europe (left panel) and England and Wales, UK (right panel).

In Figure 136 (integrated P-scores vs population), in the first-peak period, there is an upper branch of the scatter plot for which P-scores increase with increasing population, and a lower branch in which P-scores remain low with increasing population. This is similar to the case for first-peak period P-scores in the USA counties (Figure 64, top row of panels). Unlike in the USA (Figure 64, middle row of panels), there were no European regions with large summer-peak period P-scores. Figure 137 has P-scores vs the logarithm of population, for comparison.

Figure 138 shows integrated P-scores vs population density. The NUTS2 regions with the highest first-peak period P-scores, in Spain and Italy, were not among the highest-density NUTS2 regions due to their relatively large geographic areas. However, the said regions nonetheless contain major cities and densely populated urban areas, specifically: ITC4 (Lombardy, Italy) contains the urban area of Milan; ES30 (Madrid, Spain) is the Spanish capital region; and ES42 (Castile-La Mancha, Spain) contains part of the Madrid metropolitan area as well as densely-populated industrialized zones. Several UK regions stand out for their high population densities and high first-peak period P-scores. These are within the urban areas of London (UKI4, UKI3, UKI7, UKI5, UKI6), Birmingham (UKG3), Liverpool (UKD7) and Greater Manchester (UKD3). The capital region of Belgium (BE10, Brussels) also stands out for having high population density and a high integrated first-peak period P-score. Separately, there is a lower branch of the scatter plot, extending horizontally along the x-axis in the panels in the top row of Figure 138, showing that several high-density regions in central and eastern Europe had low integrated first-peak period P-scores. This is similar to the scatter plot of integrated P-score vs population density for the USA counties, in Figure 66. The Spanish region of Ceuta (ES63), which is an autonomous city on the northern coast of Africa, also has high population density and low first-peak period P-score.

Figure 139 shows P-score vs the logarithm of population density. The lower-left panel shows a strong correlation between integrated first-peak period P-score and $\log(\text{population density})$ for the NUTS2 regions of the UK. This can also be seen on the linear scale, in the lower-left panel of Figure 138. This correlation with population density is reminiscent of the result for the counties of the New York City urban area as seen in Figure 67 (section 3.6.1), and motivates further examination of scatter plots for the higher-resolution NUTS3 regions of the UK, further below.

Figure 140 shows integrated P-scores vs the at-risk-of-poverty rate. The at-risk-of-poverty rate is the percentage of the region's population that live in households with equivalised disposable income of less than 60% of that of the national median (Eurostat, 2024d; ONS, 2021). Poverty data was unavailable for the countries and regions shown in dark grey in Figure 146, including Belgium, France, and Germany.

As can be seen in Figure 140, the largest first-peak period P-scores are generally at mid-range values of the at-risk-of-poverty rate. This is similar to the case for the USA counties (Figure 69, top row of panels), in that, when considering all of Europe or all of the USA, it is not the highest-poverty regions that had the highest integrated first-peak period P-scores.

In the USA, there was a strong positive correlation between P-score and poverty when considering only the counties with the highest P-scores (e.g. the counties with P-scores > 100%), which are mostly located in the high-density inner-city area of the New York City urban area (Figure 69, lower-left panel). While first-peak period P-scores increased with population density in the UK (Figure 138 and Figure 139, lower-left panels), like in the New York City urban area (Figure 66 and Figure 67, lower-left panels), there is no apparent correlation with poverty for the UK NUTS2 regions, in Figure 140 (lower-left panel). However, a positive correlation

between first-peak period integrated P-score and poverty and other socioeconomic vulnerability indicators is observed using data for higher geographic-resolution (NUTS3) regions and focusing on the London area, which had the highest P-scores in the UK. This is shown below.

Integrated P-score vs Population

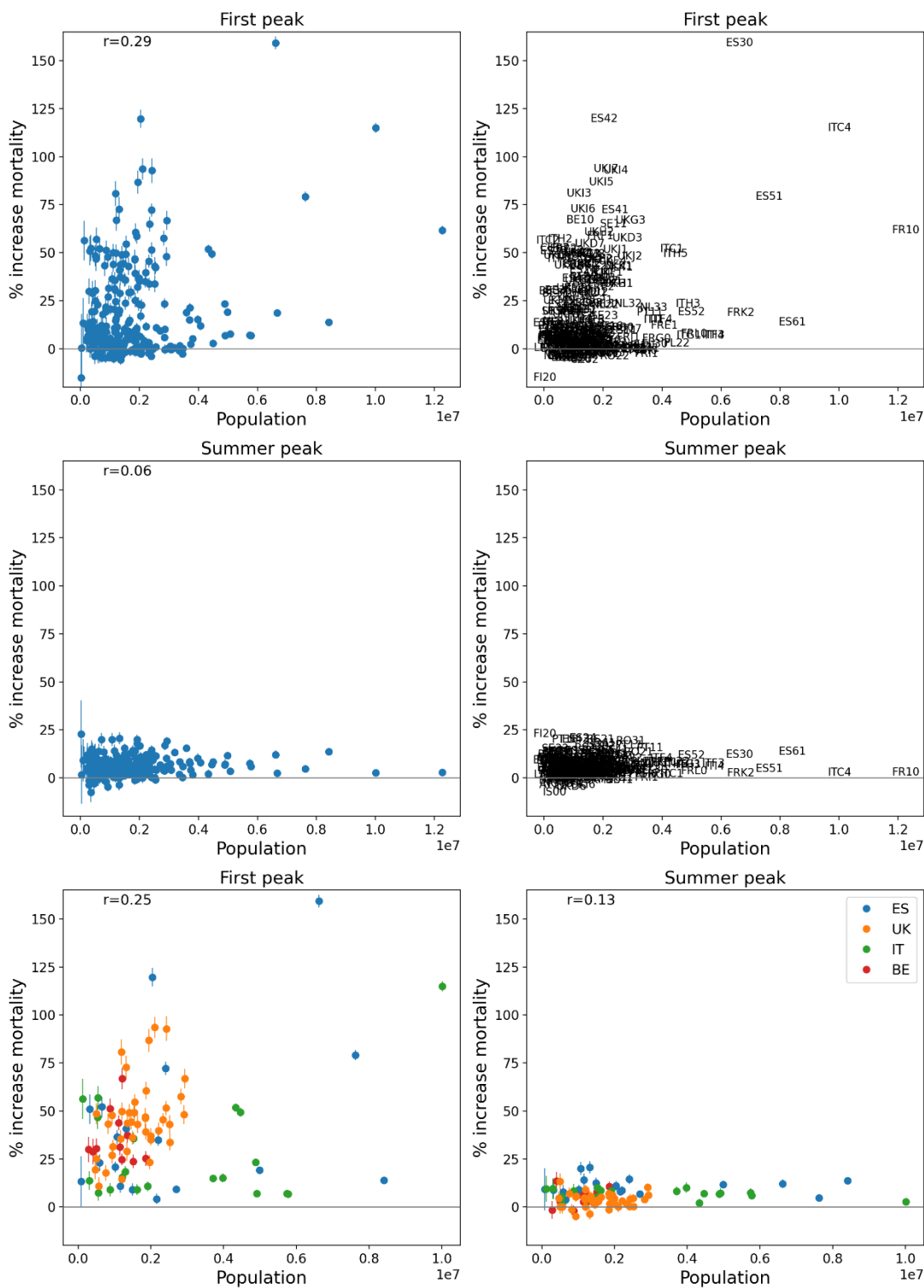


Figure 136: Integrated excess mortality P-scores for first-peak and summer-peak periods for European NUTS2 regions vs population for 2019. Bottom row: four countries with highest integrated first-peak P-scores.

Integrated P-score vs \log_{10} [Population]

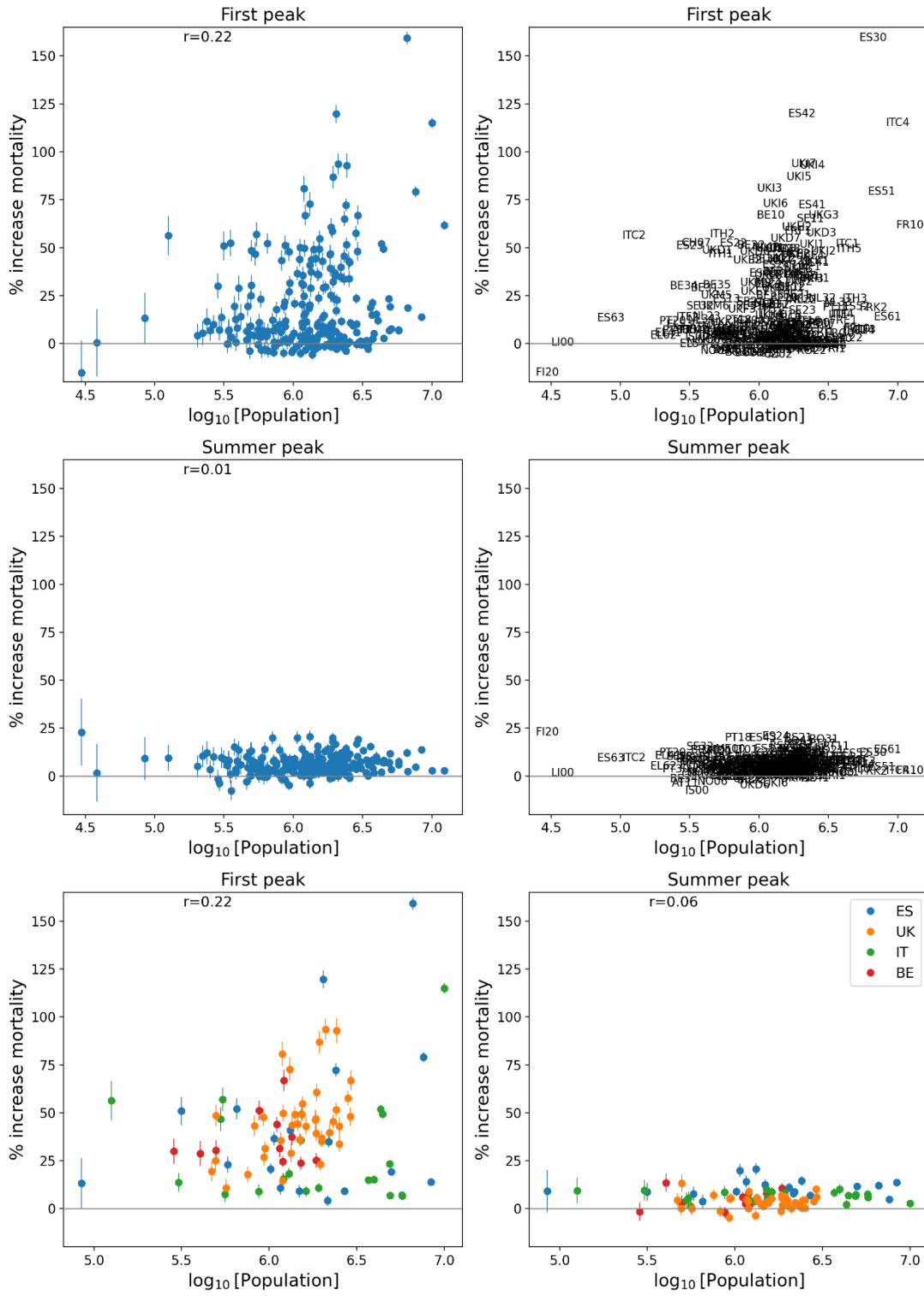


Figure 137: Same as Figure 136, except that the x-axis shows the logarithm of population for 2019.

Integrated P-score vs Population density (km⁻²)

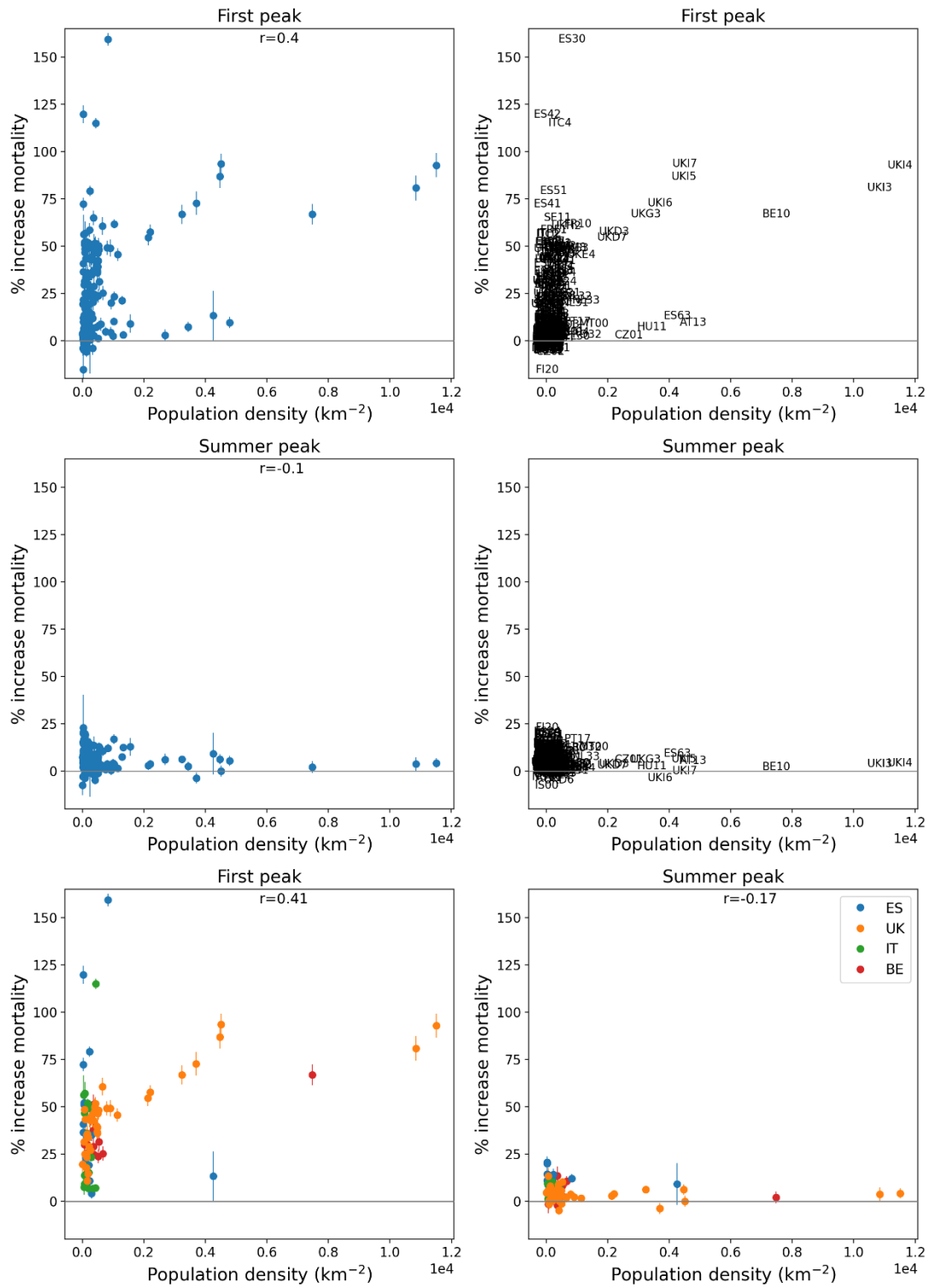


Figure 138: Same as Figure 136, except that the x-axis shows population density for 2018.

Integrated P-score vs \log_{10} [Pop. density (km^{-2})]

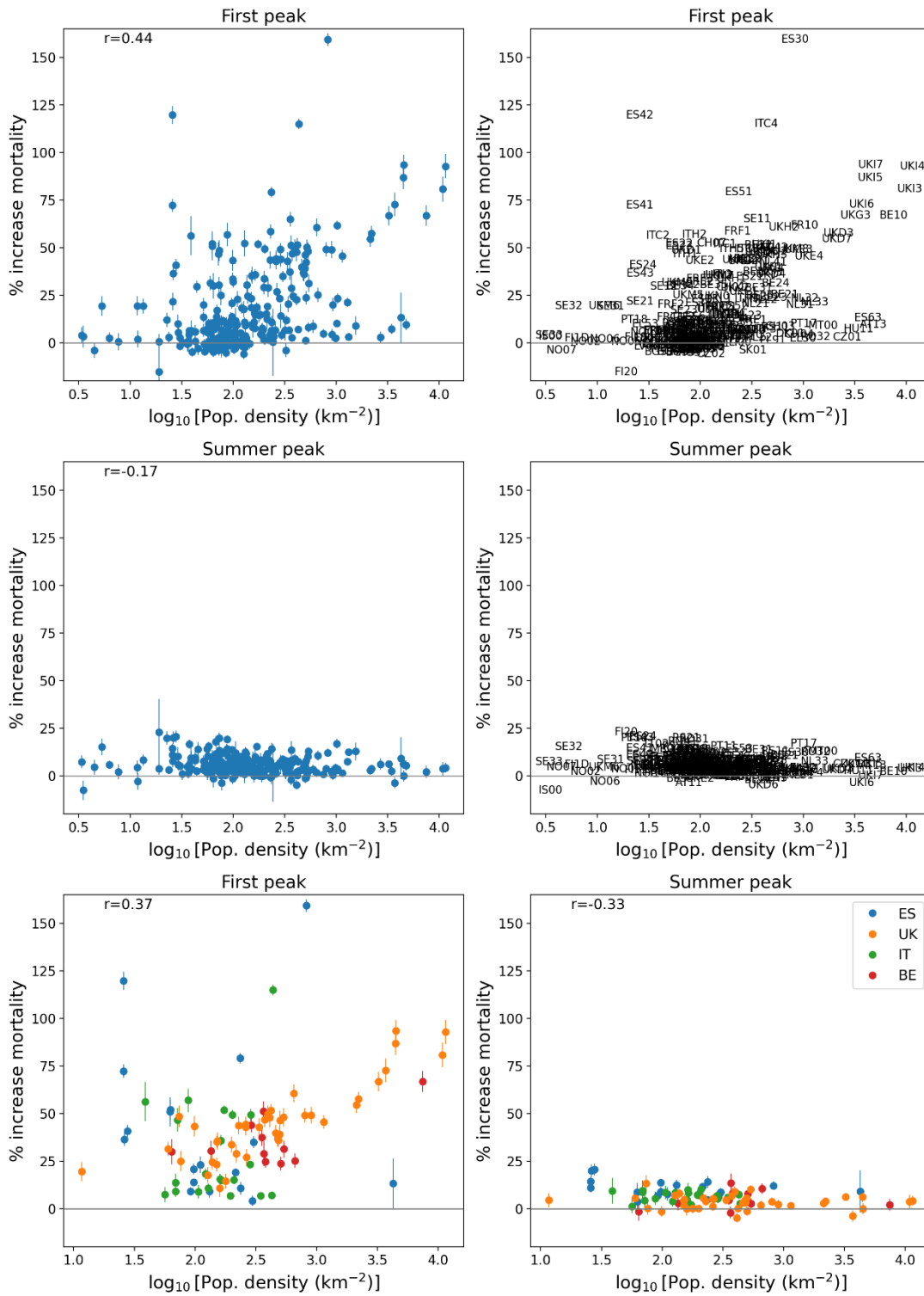


Figure 139: Same as Figure 136, except that the x-axis shows the logarithm of population density for 2018.

Integrated P-score vs At-risk-of-poverty rate (%)

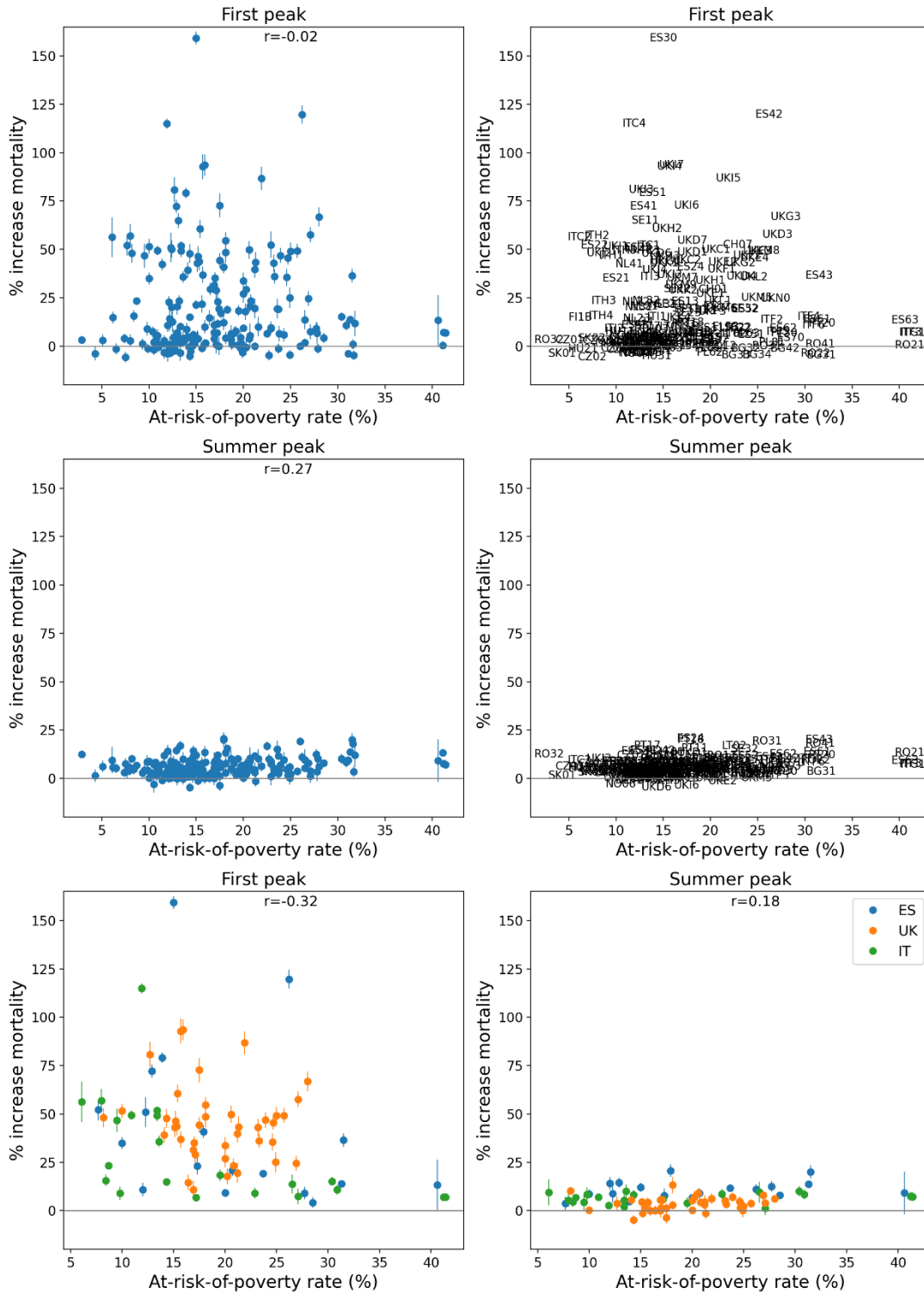


Figure 140: Same as Figure 136, except that the x-axis shows the percentage of the population at risk of poverty in 2019. Poverty data was unavailable for the dark grey countries in Figure 146.

% increase in mortality (2020-02-24 to 2020-05-31)

% increase in mortality (2020-02-24 to 2020-05-31)

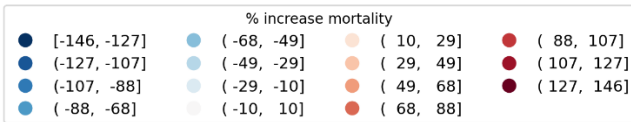
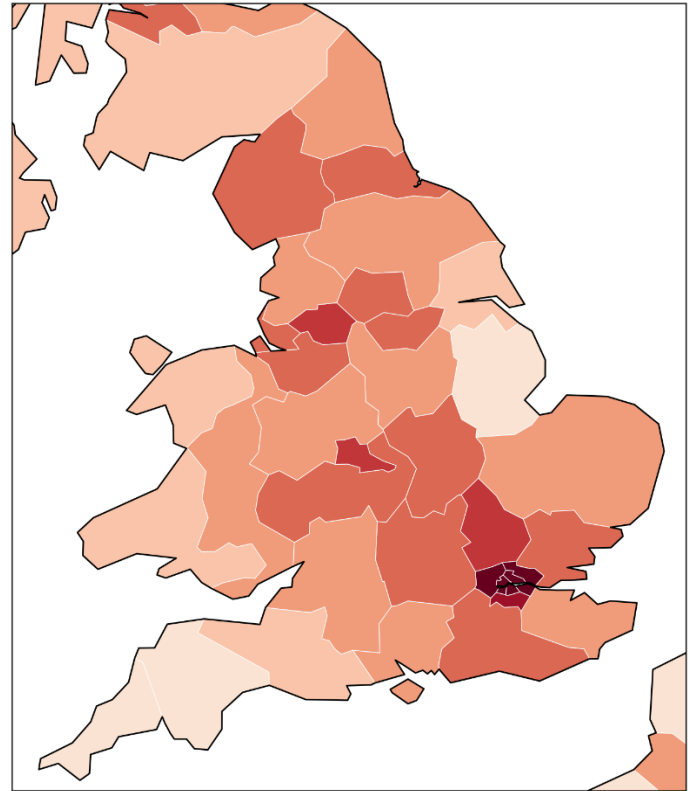
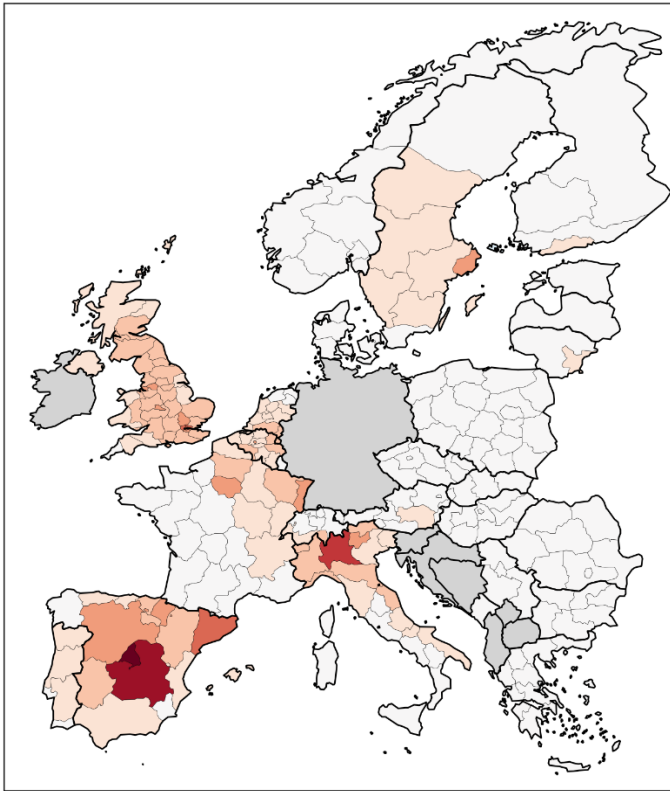
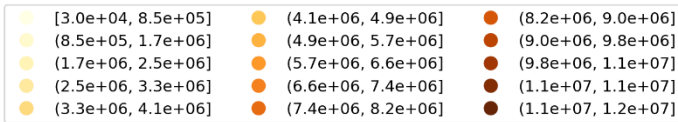
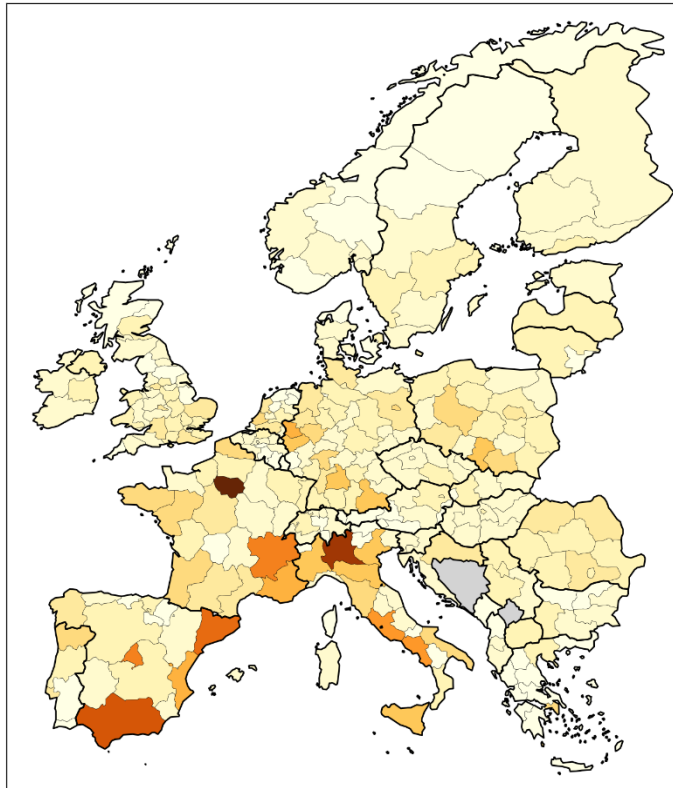


Figure 141: Integrated first-peak period P-scores for NUTS2 regions of Europe (left panel) and England and Wales, UK (right panel). Color range extends to the maximum value in the regions shown in each panel. Dark grey indicates countries for which data was unavailable.

Population (NUTS2 regions)



Population (NUTS2 regions)

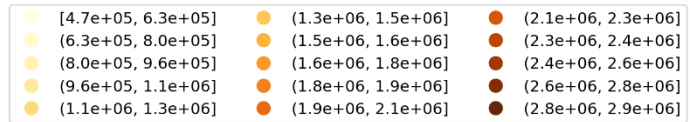
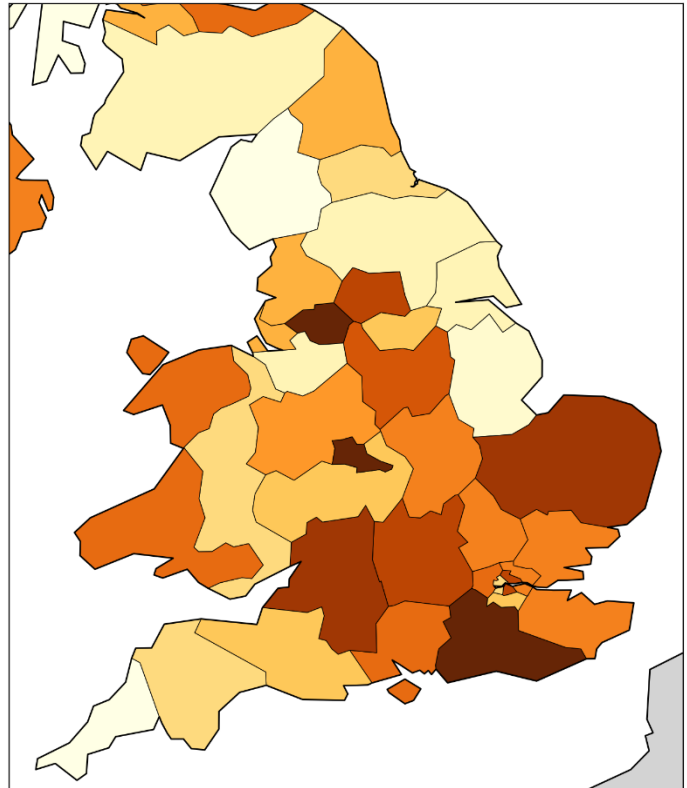


Figure 142: Population in 2019 for NUTS2 regions of Europe (left panel) and England and Wales, UK (right panel). Dark grey indicates countries for which data was unavailable.

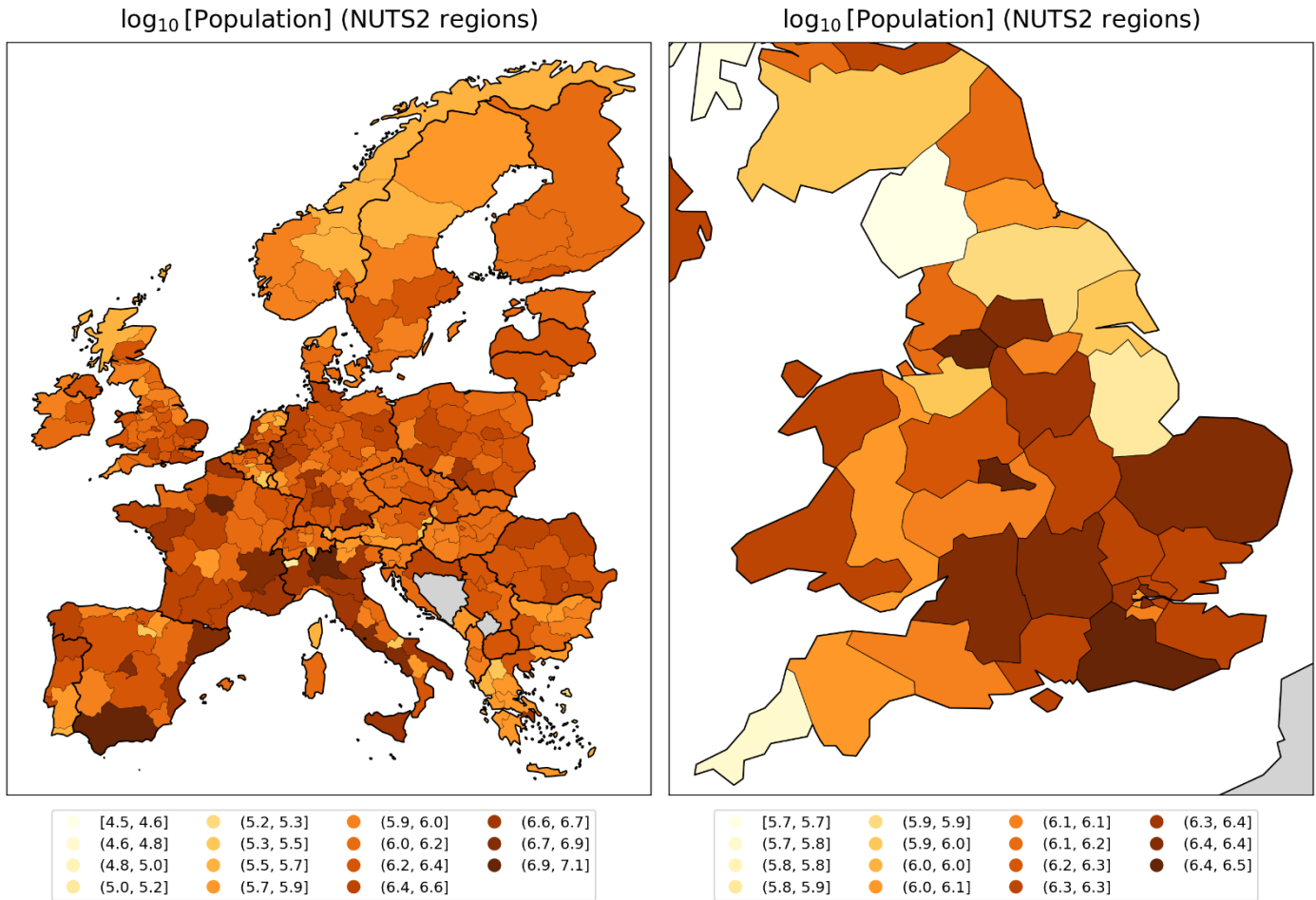


Figure 143: Logarithm of 2019 population for NUTS2 regions of Europe (left panel) and England and Wales, UK (right panel). Dark grey indicates countries for which data was unavailable.

Population density (km⁻²) (NUTS2 regions)



Population density (km⁻²) (NUTS2 regions)

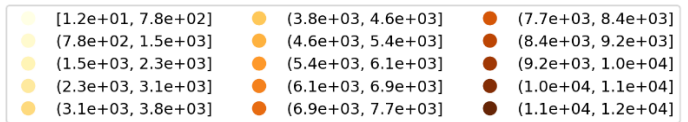
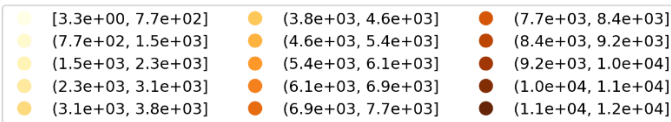
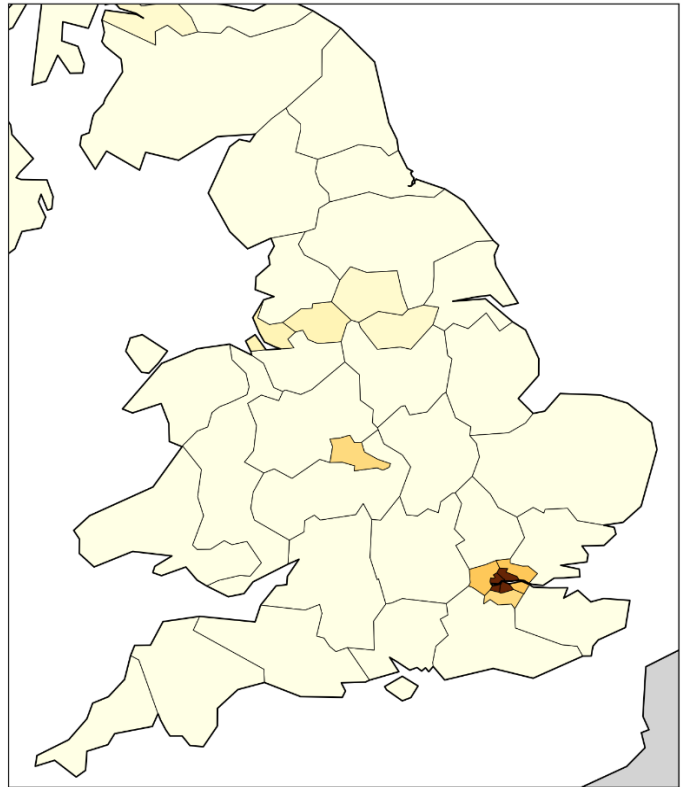
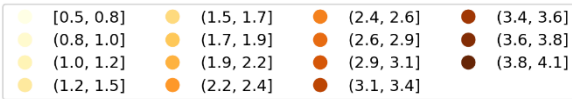
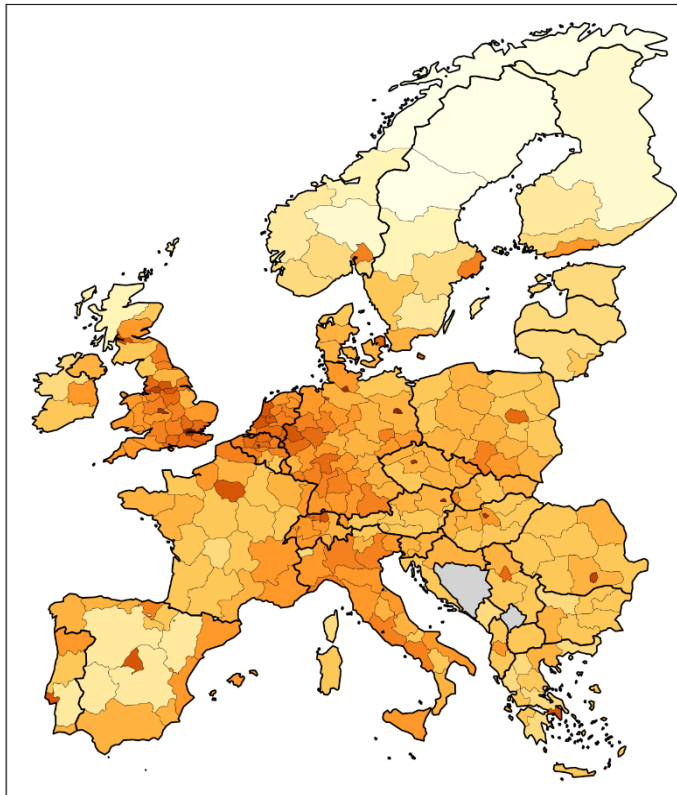


Figure 144: Population density (persons per km²) in 2018 for NUTS2 regions of Europe (left panel) and England and Wales, UK (right panel). Dark grey indicates countries for which data was unavailable.

log₁₀[Pop. density (km⁻²)] (NUTS2 regions)



log₁₀[Pop. density (km⁻²)] (NUTS2 regions)

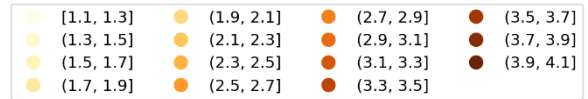
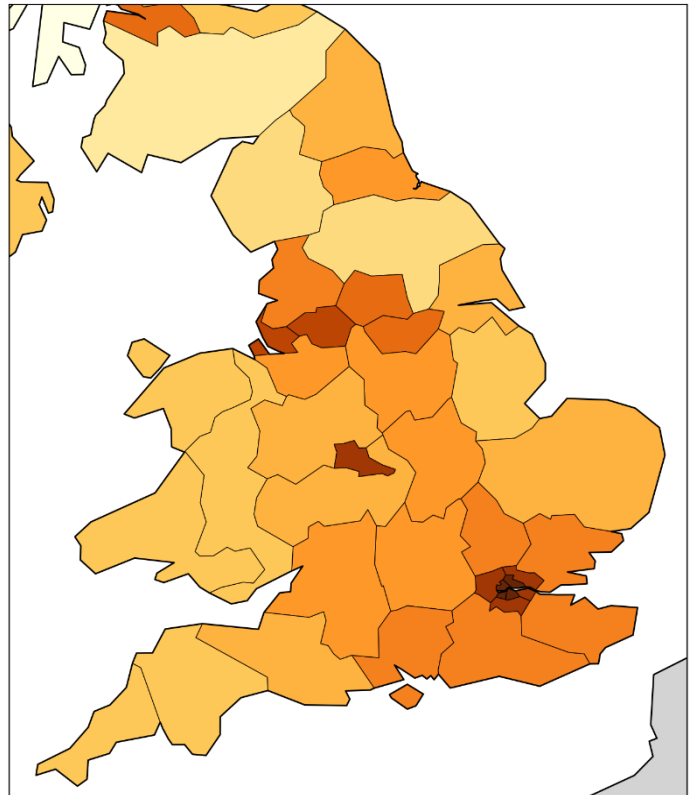
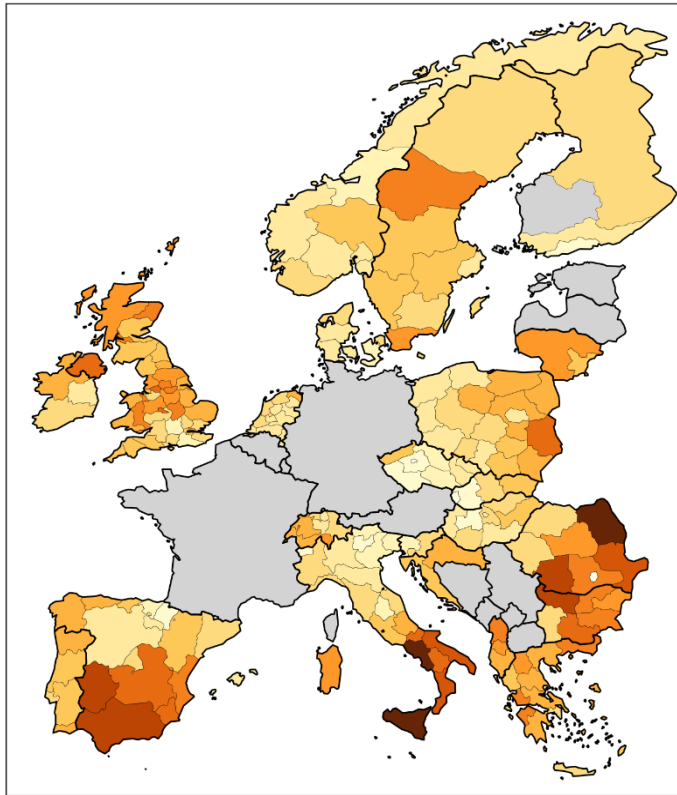


Figure 145: Logarithm of population density (persons per km²) in 2018 for NUTS2 regions of Europe (left panel) and England and Wales, UK (right panel). Dark grey indicates countries for which data was unavailable.

At-risk-of-poverty rate (%) (NUTS2 regions)



At-risk-of-poverty rate (%) (NUTS2 regions)

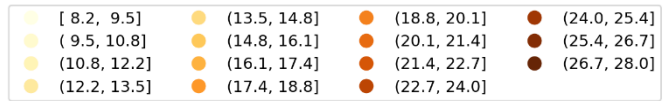
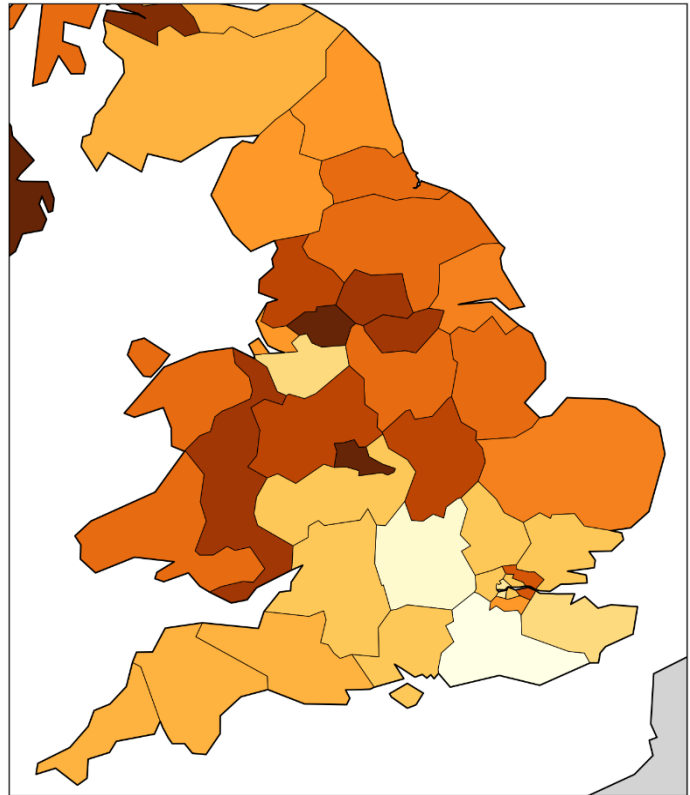


Figure 146: At-risk-of-poverty rate in 2019 for NUTS2 regions of Europe (left panel) and England and Wales, UK (right panel). The at-risk-of-poverty rate is the percentage of the region’s population that live in households with equivalised disposable income of less than 60% of that of the national median Eurostat, 2024d; ONS, 2021). Dark grey indicates countries for which data was unavailable.

NUTS3 regions of the UK and London

Before focusing on the London area in more detail, we first show graphs of one socioeconomic variable for the NUTS3 regions of the entire UK. This variable is the gross disposable household income (GDHI) per capita, for the year 2019. An individual's GDHI is their income after distribution measures such as taxation and government benefits have been applied (ONS, 2024).

Figure 147 shows the integrated first-peak period P-score for the NUTS3 regions of the UK vs GDHI per capita (left panel) and the logarithm of GDHI per capita (right panel).

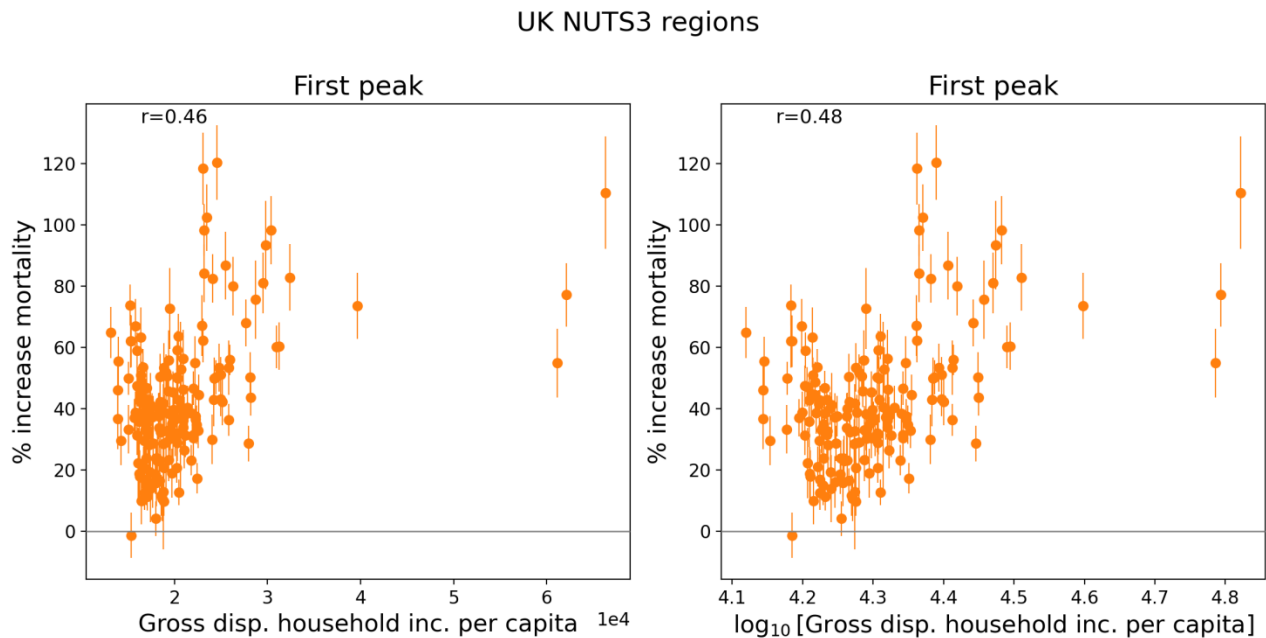


Figure 147: Integrated first-peak period P-score vs Gross disposable household income per capita in 2019 for NUTS3 regions of the UK.

Figure 148 contains maps showing GDHI per capita and log(GDHI per capita) for the UK. Some NUTS3 regions in Northern Ireland and Scotland are omitted from the maps to allow better visualization of the NUTS3 regions in and around London, which have the highest GDHI per capita values in the UK. (For comparison, GDHI per capita for the Northern Ireland NUTS3 regions ranges from 15,317 to 18,875 pounds and for the Scottish NUTS3 regions with available data it ranges from 16,966 to 24,418 pounds.)

A copy of Figure 8, showing the integrated first-peak period P-scores for England and Wales, UK, is included below as Figure 149 to facilitate comparison with the maps in Figure 148.

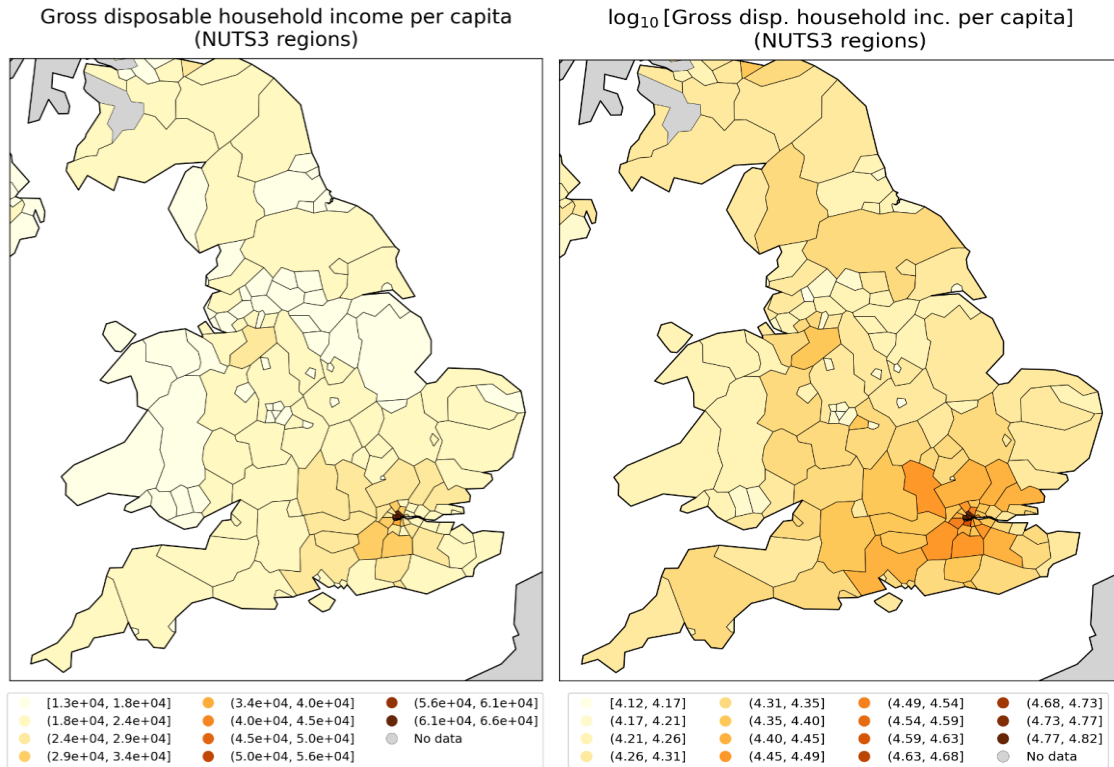


Figure 148: Map of gross disposable household income per capita in 2019 for the NUTS3 regions of England and Wales, UK. Left panel: linear scale; right panel: logarithmic scale. Dark grey indicates regions for which data was unavailable.

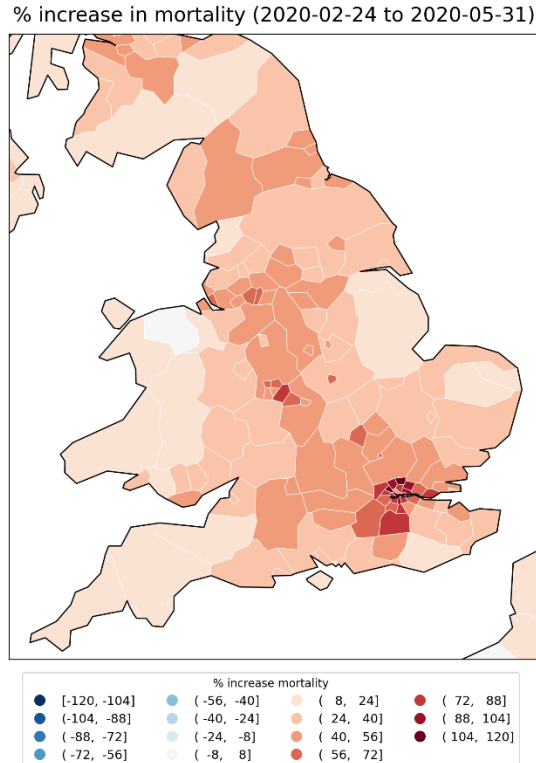


Figure 149: Map of integrated first-peak period P-scores for the NUTS3 regions in England and Wales (UK). (Copy of Figure 8.)

As can be seen from the scatter plots in Figure 147, the UK NUTS3 regions with the highest integrated first-peak P-scores were generally regions with mid to high GDHI per capita values. These higher-GDHI per capita NUTS3 regions are located in the area around London (Figure 148) and had the highest integrated first-peak period P-scores in the UK (Figure 149).

Focusing now on London, Figure 150 shows scatter plots of integrated first-peak period P-scores for the 21 NUTS3 regions of London vs the following socioeconomic variables: population, population density, GDHI per capita, percent living in poverty, percent minority (non-white), and percent born outside of the UK.

Here, population, population density and GDHI per capita are for the year 2019 (Greater London Authority, 2023; ONS, 2024), the values for percent non-white and percent born outside of the UK are from the 2021 UK census (ONS, 2022a, 2022b), and the percent living in poverty is from pooled data for five years of survey data for the financial years 2017/18 to 2022/23, excluding 2020/21 due to data quality concerns (Trust for London, 2024).

Maps of these variables for the London NUTS3 regions are in Figure 152 to Figure 157, and a blow-up map of integrated first-peak period P-scores for the London and immediately surrounding regions is in Figure 151.

Figure 150 (top row of panels) shows that within London, there is no correlation between integrated first-peak period P-score and population or population density, unlike for the NUTS2 regions of the entire UK (Figure 136 to Figure 139). Similarly, and as expected from Figure 147, there is no correlation between integrated first-peak period P-score and GDHI per capita within London, as shown in the left panel of the middle row of panels in Figure 150.

In contrast, Figure 150 (for the NUTS3 regions of London) shows a positive correlation between first-peak period P-score and

- the rate of poverty (Figure 150, middle row, right panel) with $r = 0.58$;
- the percent of the population that is non-white (Figure 150, bottom row, left panel) with $r = 0.64$; and
- the percent of the population born outside of the UK (Figure 150, bottom row, right panel) with $r = 0.62$.

London NUTS3 regions

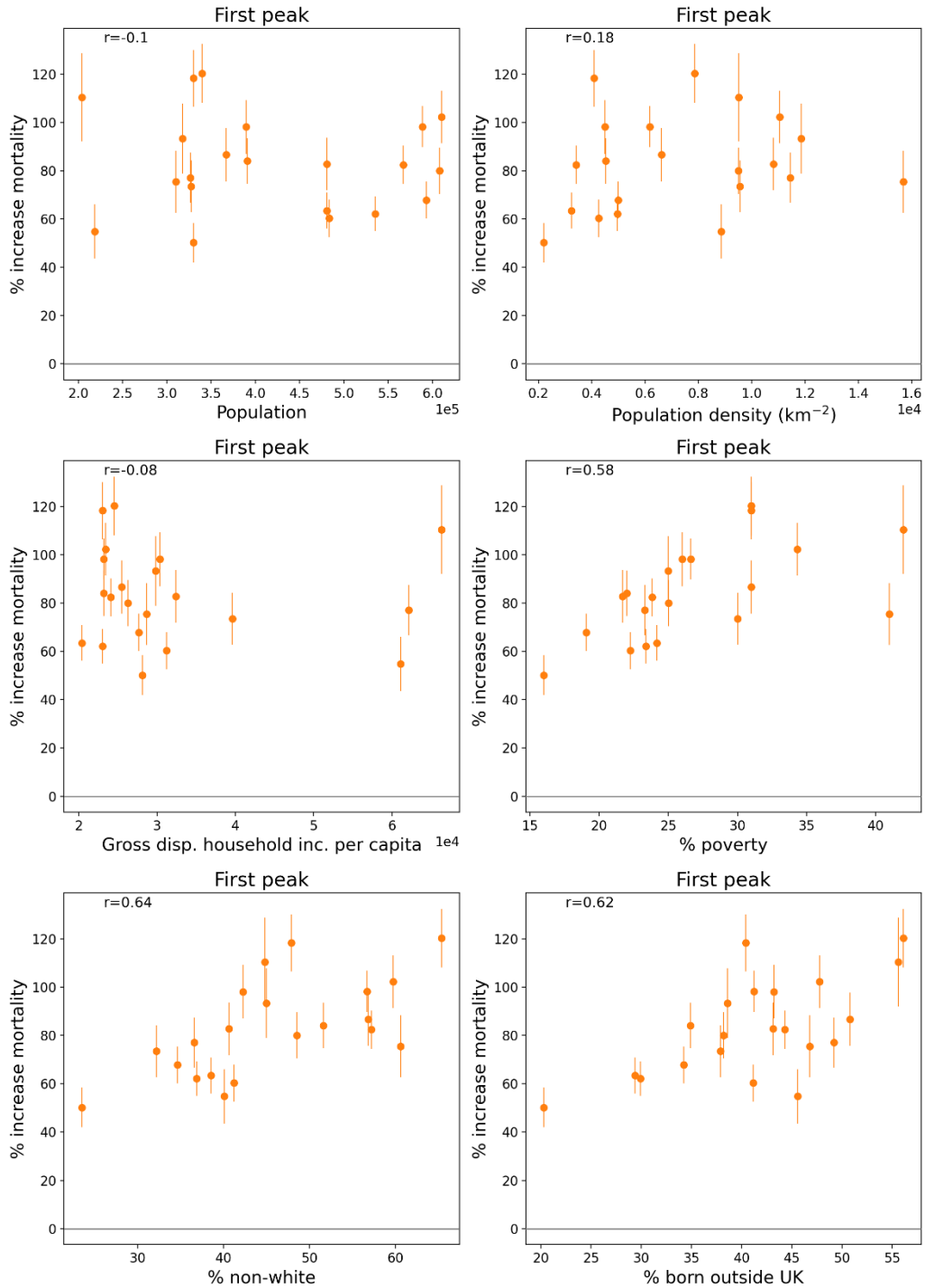


Figure 150: Integrated first-peak period P-scores for the NUTS3 regions of London, UK, vs population (2019), population density (2019), GDHI per capita (2019), percentage of the population living in poverty (pooled data for 2017/18 to 2022/23 financial years, excluding 2020/21), percentage of the population that is non-white (2021), and percentage of the population born outside of the UK (2021).

% increase in mortality (2020-02-24 to 2020-05-31)
 (NUTS3 regions of London, UK)

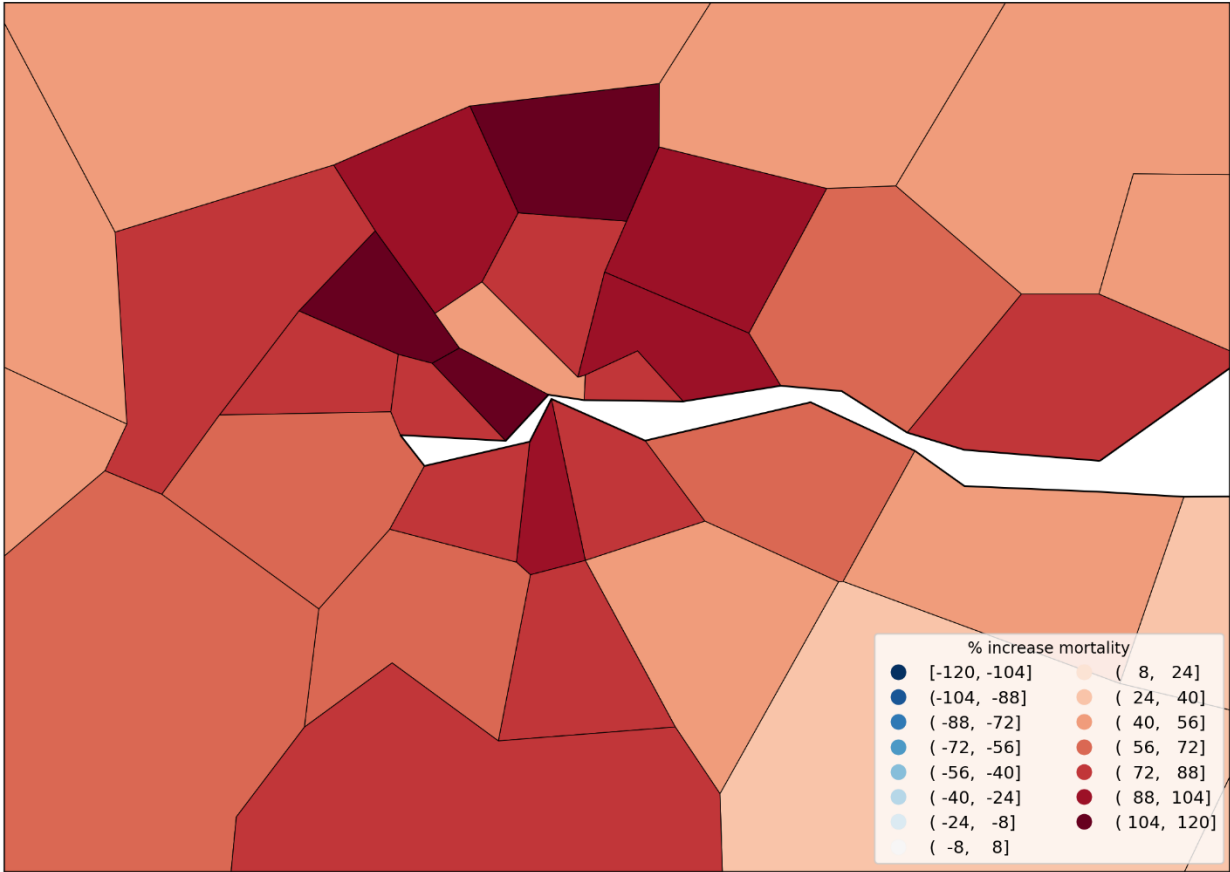


Figure 151: Map of integrated first-peak period P-scores for the NUTS3 regions of London, UK, plus the immediately surrounding regions.

Population
(NUTS3 regions of London, UK)

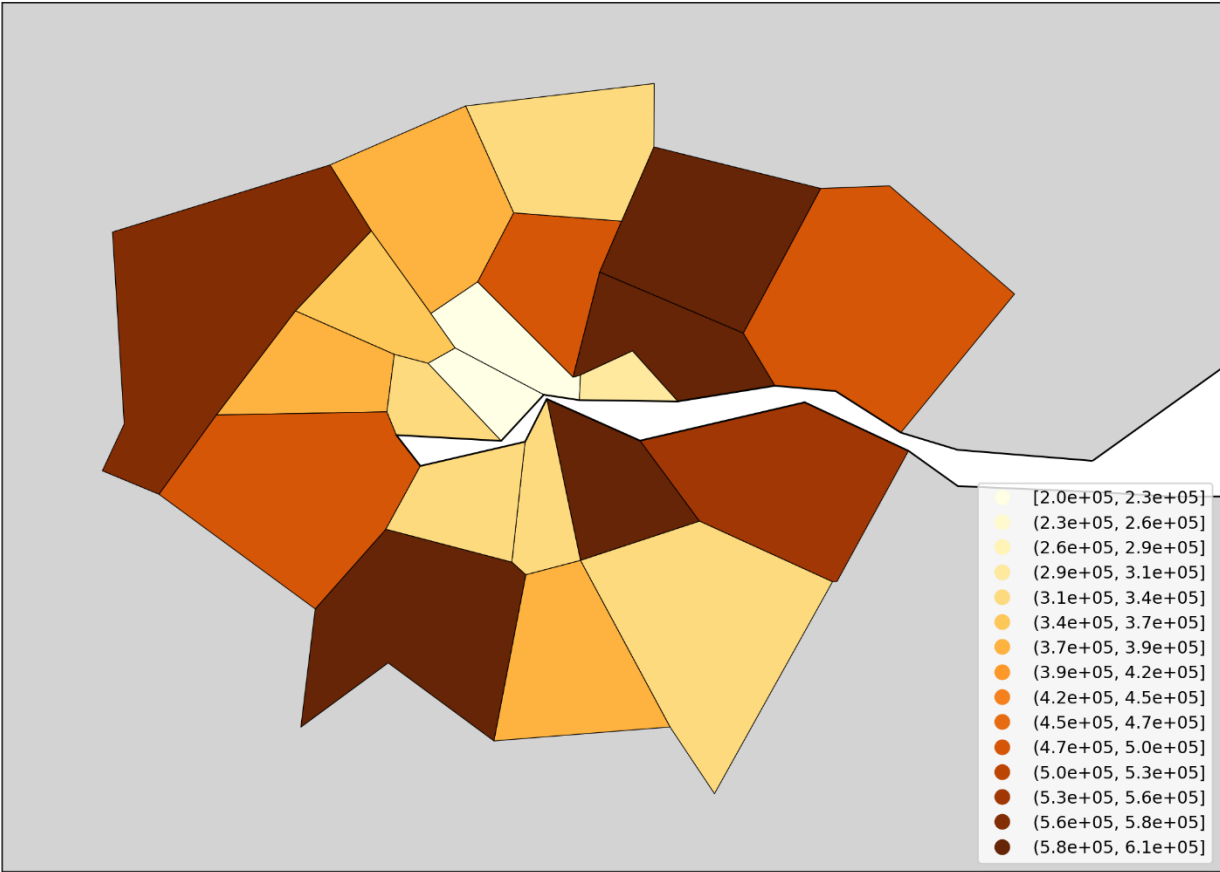


Figure 152: Map of population in 2019 for the NUTS3 regions of London, UK.

Population density (km⁻²)
(NUTS3 regions of London, UK)

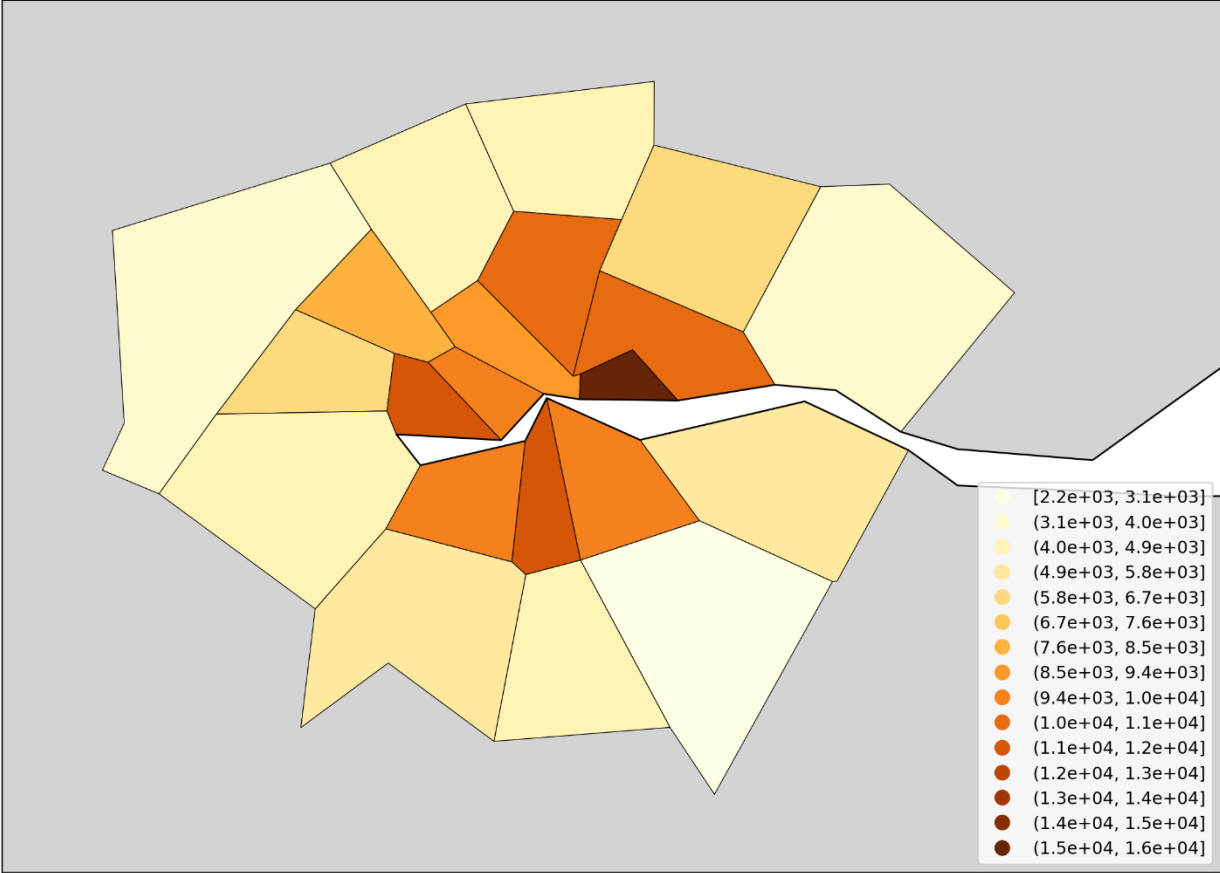


Figure 153: Map of population density in 2019 for the NUTS3 regions of London, UK.

Gross disposable household income per capita
(NUTS3 regions of London, UK)

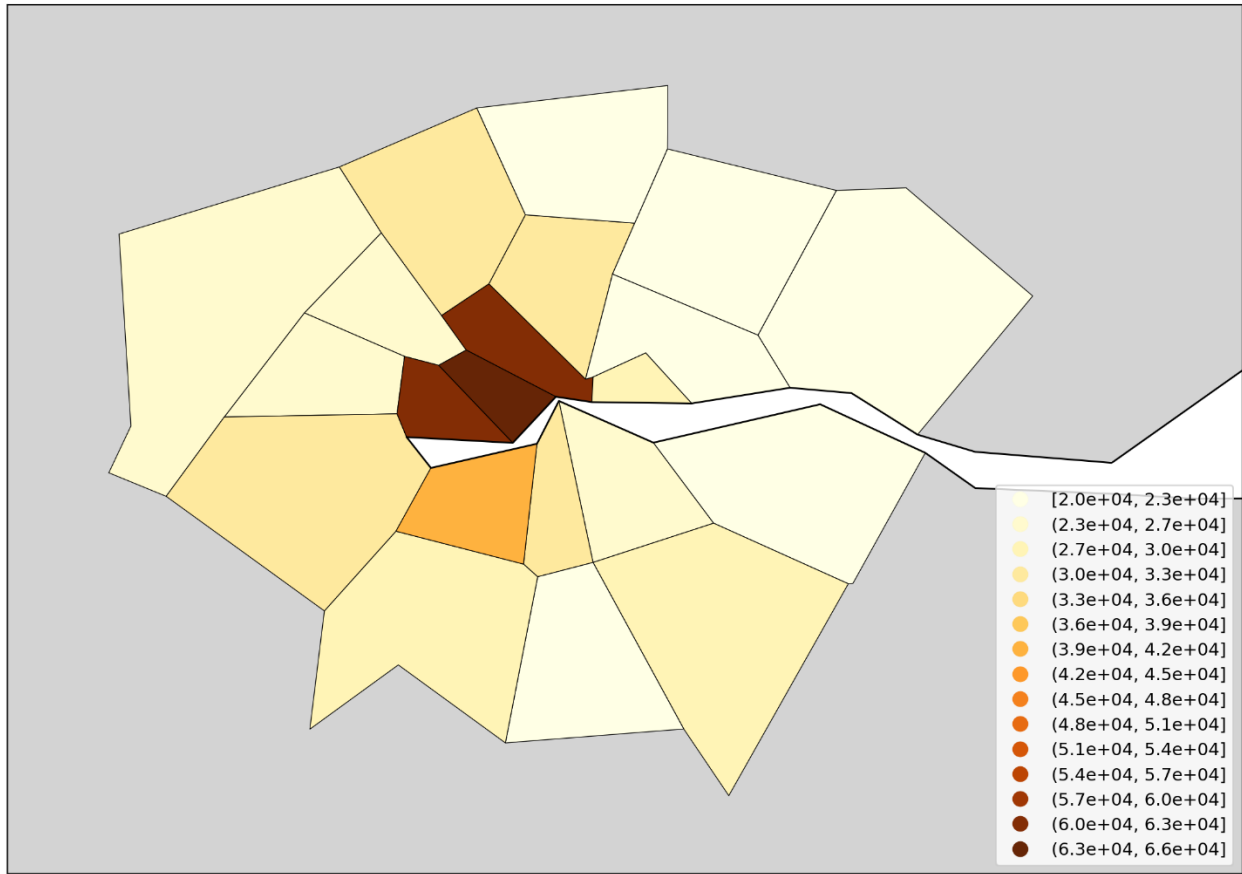


Figure 154: Map of gross disposable household income per capita in 2019 for the NUTS3 regions of London, UK.

% poverty
(NUTS3 regions of London, UK)

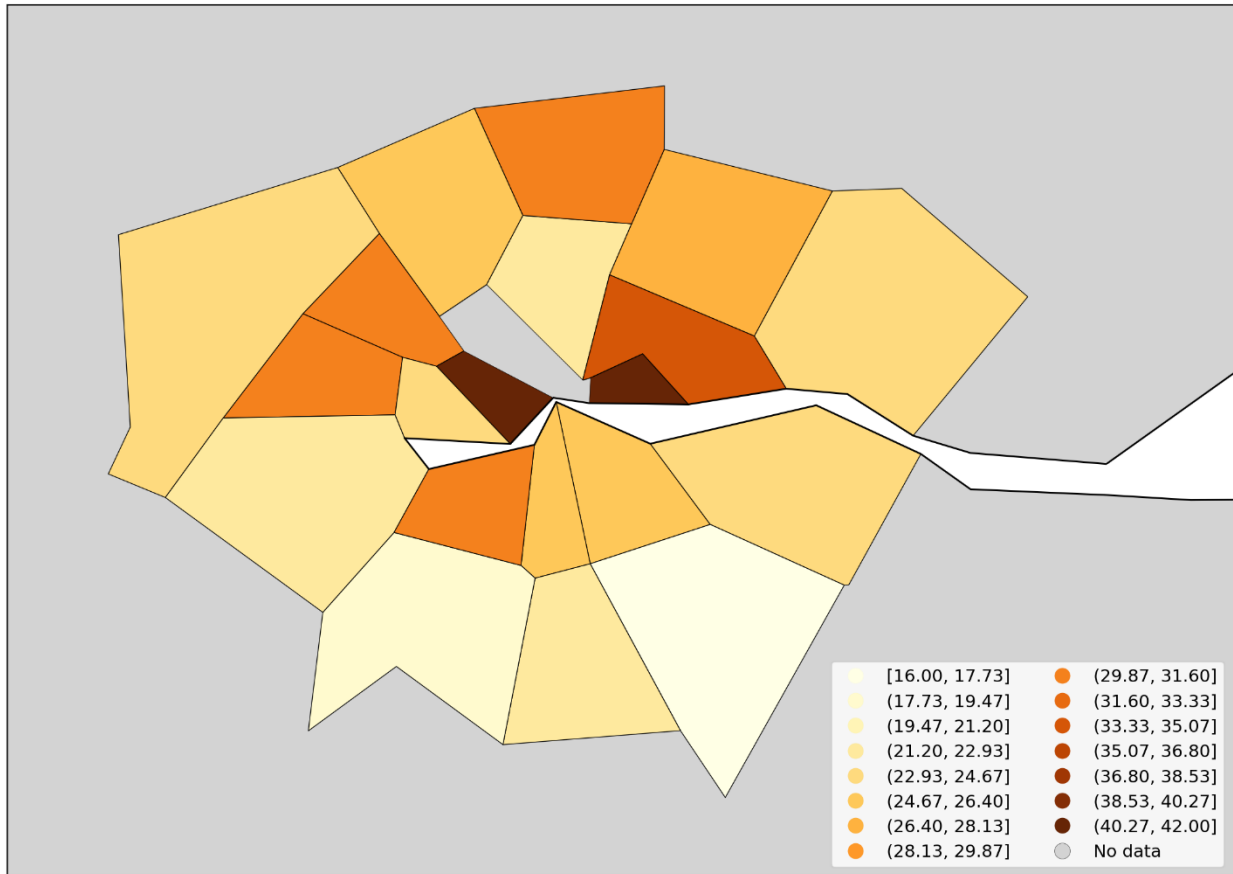


Figure 155: Map of percentage of the population living in poverty (pooled data for 2017-2022, excluding 2021) for the NUTS3 regions of London, UK. Dark grey (within London) indicates regions for which data was unavailable.

% non-white
(NUTS3 regions of London, UK)

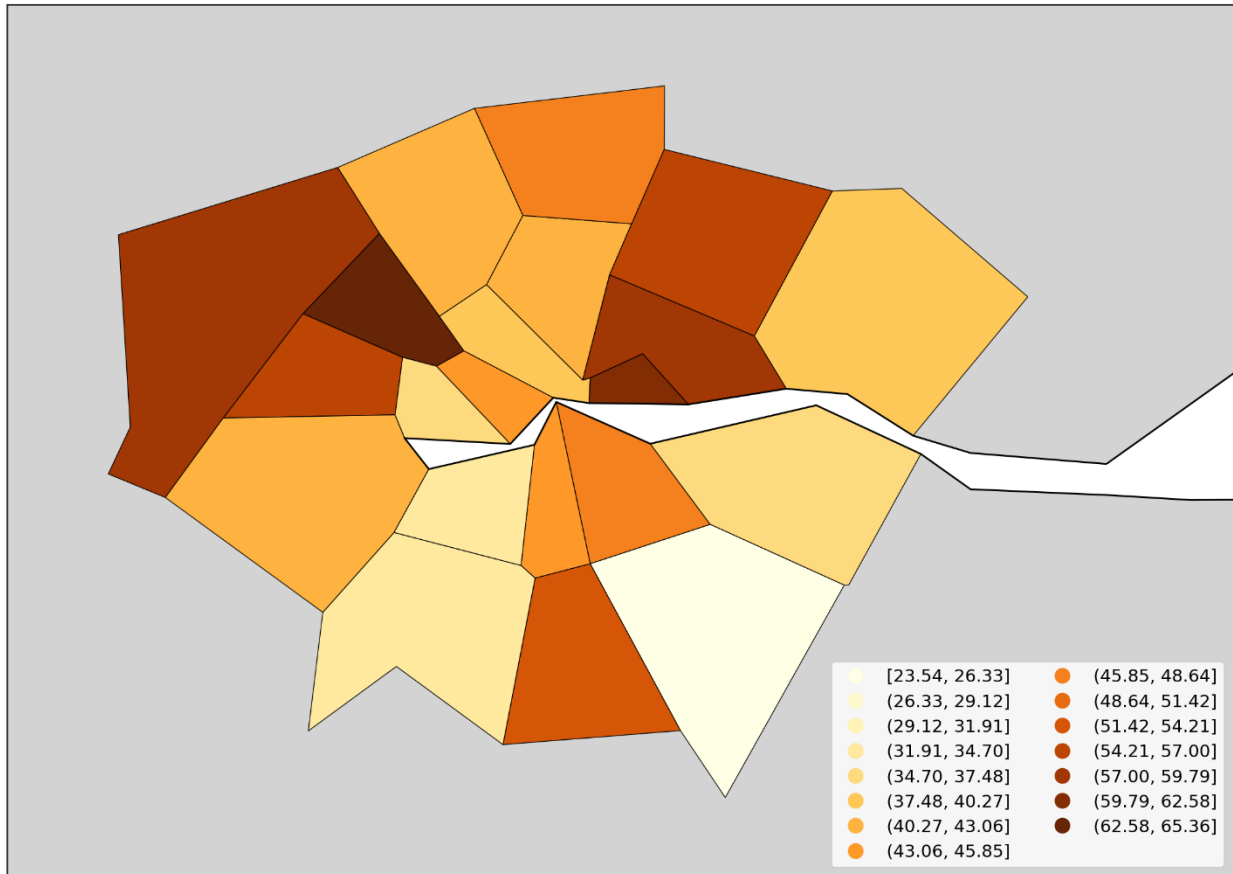


Figure 156: Map of percentage of the population that is non-white in 2021 for the NUTS3 regions of London, UK.

% born outside UK
(NUTS3 regions of London, UK)

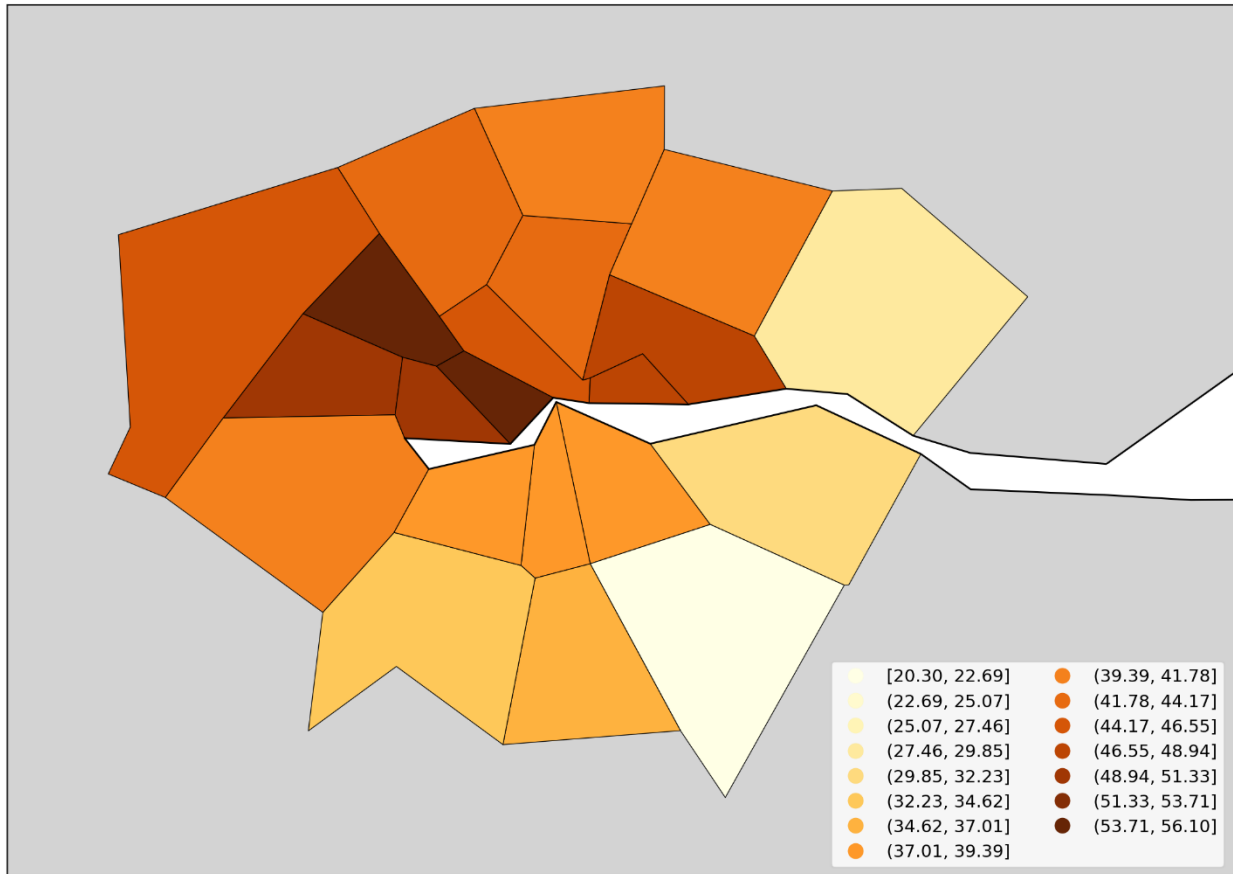


Figure 157: Map of percentage of the population born outside of the UK (2021 census), for the NUTS3 regions of London, UK.

4. Discussion

4.1 Overview of the Discussion

In this paper we have examined excess all-cause mortality in Europe and the USA during the first weeks and months following the World Health Organization's March 11, 2020 declaration of a COVID-19 pandemic, using data with high geographic and temporal resolution.

The said excess all-cause mortality (by week, month, or longer integration period) is calculated as a P-score. P-score measures the relative excess mortality for a population, compared to the predicted historic, normal or unperturbed mortality for the population (for the given time period), and is thus inherently adjusted for the age structure and health frailty of the specific population in the jurisdiction of consideration at the same time (section 2.3).

We focused on the period March-May 2020, which we call the "first-peak period", and also examined the "summer peak period" (June-September 2020).

Our study may be the highest resolution hemispheric-scale geotemporal study to date of excess all-cause mortality and thus offers a robust test of the pandemic viral spread paradigm for so-called COVID-19 during 2020.

4.1.1 Summary of main features of the Results

The Results section (section 3) brings to light several main observations:

- **Geographic heterogeneity of first-peak period excess mortality:** Sections 3.1 and 3.2 demonstrate that there was a high degree of geographic heterogeneity in excess mortality in the USA and Europe, with a handful of geographic regions having essentially synchronous (within weeks of each other) large peaks of first-peak period excess mortality ("F-peaks") and all other regions having low or negligible excess mortality in the said first-peak period.
- **Temporal synchrony of first-peak period excess mortality:** Section 3.3 shows that F-peaks for USA states and European countries were almost all positioned within three or four weeks of one another and no earlier than the week of the WHO's pandemic declaration. For a given large-F-peak European country, the F-peaks for all subnational regions rose and fell in lockstep synchrony but showed large variation in peak height and total integrated excess mortality. A similar result was seen for the counties of large-F-peak USA states.
- **Dramatic differences in first-peak period excess mortality for comparable cities with large airports in the same countries:** Section 3.4 compares cities with large airports in

the same country (Rome vs Milan in Italy, and Los Angeles and San Francisco vs New York City in the USA) and shows that there was a dramatic difference in first-peak period excess mortality between the compared cities, despite their having similar demographics, health care systems, and international air travel traffic, including from China and East Asia.

- **Increased share of deaths occurring in hospitals for jurisdictions with large F-peaks:** Section 3.5 shows that the share of deaths occurring in hospitals and in nursing homes increased during the first-peak period (March-May 2020) compared to March-May 2019, for the USA states or counties with the largest F-peaks, and the share of home deaths increased compared to 2019 in the large majority of studied USA states or counties having small, negligible or undetected F-peaks.
- **Correlations with socioeconomic vulnerability in regions with large F-peaks:** Section 3.6 shows that integrated first-peak period P-scores were correlated with increasing socioeconomic vulnerability for the counties of the USA states with the largest F-peaks, and for the boroughs of London, UK, while much structure and complexity in the all-jurisdiction scatter plots occurs due to geo-socioeconomic gradients and heterogeneity. Furthermore, there are large qualitative differences between first-peak and summer-peak period scatter plots.

In short, there is essential synchrony (within weeks following the WHO's announcement of a pandemic) in mortality hotspots (large "F-peaks") across countries and states on two continents in the Northern Hemisphere, extreme geographical heterogeneity of the magnitude of any excess all-cause mortality in the time period ("first-peak period", March-May 2020), dramatic differences in the occurrences of hotspots (presence or absence) in entirely comparable large cities in the same countries, systematic increases in shares of institutional (versus home) deaths in mortality hotspot jurisdictions, and strong correlations between hotspot intensity (P-scores) and socioeconomic vulnerability in high-geographical-resolution sectors within hotspot urban regions.

4.1.2 Large-scale spatial epidemic models and their caveats

In sections 4.2 to 4.4 below, we compare our results regarding geographic heterogeneity and temporal synchrony of first-peak period excess mortality with predictions from large-scale spatial epidemic models that have been applied to declared viral respiratory pandemics (including SARS (2002-2004), H1N1 (2009-2010), and COVID-19 (2020-2023)).

In this section, we briefly outline the two main strains of large-scale spatial epidemic models — meta-population models and agent-based models — and explain important caveats (structural features) for each of them that cause their results to be biased toward exaggerated synchrony in epidemic peak timing for different jurisdictions.

The said caveats are not addressed by the authors of the global-spread modeling studies themselves. The authors of the global-spread modeling studies do not explore or quantify the consequences of their problematic simplifications that we have identified. However, extensive fundamental studies of epidemic dynamics on generic connected networks (Pastor-Satorras et al., 2015) suggest that the said simplifications may have large consequences, as do higher resolution studies of urban regions.

Stated (maybe too) succinctly: if person-to-person spread is what explains the large geographical heterogeneity of attack rates, then the same spread will not also produce synchronous attack-rate peaks, which we observe both across the hemisphere and within countries and states (assuming that attack rates must be related to excess all-cause mortality, in sufficiently comparable health contexts).

Meta-population models

One important strain of large-scale spatial model are the so-called meta-population models (Colizza et al., 2007; Balcan et al., 2009, 2010; Pastor-Satorras et al., 2015; Davis et al., 2021). These models consist of a set of populations corresponding to airport catchment areas that are linked to one another by human mobility (travel) on the international air traffic network and via shorter-scale commuting networks. Within each catchment area, an epidemic can be initiated when an infected individual travels to the area. The spread of the epidemic within a particular population is taken to be non-spatial and is modeled as a system of stochastic dynamical equations, where the state variables are the numbers of individuals in the population that belong to each of a set of health compartments (e.g. susceptible, exposed, infected or recovered).

While the health compartments in meta-population models can be divided up to admit a greater degree of (non-spatial) heterogeneity in the transmission dynamics, for example, with respect to age (e.g. using separate compartments for infectious old and infectious young people), social setting (e.g. at work, school, or in the general community) or health status (symptomatic people may interact less than non-symptomatic people), the models use a form of homogeneous mixing in that all individuals within a sub-population corresponding to a health compartment have equal probability of having contacts with individuals belonging to any other sub-population, within a given population.

Therefore, an important caveat of meta-population models is that they do not consider spatial heterogeneity within the individual airport catchment areas where local epidemics take place. Such spatial heterogeneity could be included, for example, by modeling each catchment area as a set of individuals whose contact patterns are determined by their position in a social network structured to mimic the real social network of the area's population, which live in neighbourhoods with different population densities and demographic characteristics, such as household size and age structure, social class structure, and so on.

Models that consider local spatial heterogeneity of contact patterns at the scale of a large city find large variation in epidemic peak shape, timing and severity across neighbourhoods within a city, and large variation in shape, timing and severity when comparing the aggregate city-wide epidemic peak for a given city with that of another city (Thomas et al., 2020).

By eschewing such local spatial heterogeneity in contact patterns within airport catchment areas and instead using homogeneous mixing for the entire spatial extent of the catchment area, meta-population models produce an exaggerated degree of synchrony in epidemic peak timing for regions around the world.

Basically, in a global transmission chain for a novel pathogen emerging in Asia, one should expect that allowing spatial heterogeneity with its associated increased stochasticity at each of the transport hubs (in each of the airport catchment populations) would produce much greater variation in local epidemic occurrence and timing across Europe and North America and around the world. Using spatially homogeneous airport catchment populations corresponds to a large damping of the said stochasticity at each of the transport hubs in a complex network. This is not addressed by the authors of the meta-population model studies.

Agent-based models

Another strain of large-scale spatial epidemic models are the so-called individual-based or agent-based models. In these models, all individuals in the population of a country or territory of interest are explicitly represented, such that each can have his or her own individual-specific characteristics such as age, place of residence, type of work or school environment, propensity to travel or commute, and so on, which determine contact patterns and therefore transmission dynamics (Ferguson et al., 2006; Merler & Ajelli, 2010, Ajelli et al., 2010, Ferguson et al., 2020).

Agent-based models consider a higher degree of spatial heterogeneity of contact patterns than meta-population models. However, they focus on a particular country or territory, such as the USA (Ferguson et al., 2006, 2020), the UK (Ferguson et al., 2006, 2020), Italy (Ajelli et al., 2010) or all of Europe (Merler & Ajelli, 2010). To model the impact of a global pandemic on the territory of interest, a means of exchanging individuals with the world outside of the territory of interest is required, and this is crucial because the initial (and subsequent) “seed” infected individuals in the model typically arrive from the outside world.

To do this seeding into the territory of interest, the agent-based models use simplifying assumptions, such as representing the rest of the world as a single homogeneously-mixed population in which an epidemic has already been seeded and is evolving. Infected individuals from the outside world are then dropped into the territory of interest at certain locations. For example, in the models of Ferguson et al. (2006), Merler & Ajelli (2010) and Ferguson (2020), infected seed individuals are dropped into geographic cells within the territory of interest with a probability proportional to the population of the cell.

The overly simplistic seeding procedures used in the agent-based models cause these models to have a bias toward exaggerated synchronicity of epidemic peak timing for different locations in the territory of interest, since different locations receive seed infectious individuals in proportion to their populations at the same, externally-determined rate. The agent-based model in Ajelli et al. (2010) uses a meta-population model to seed infectious individuals in the country of interest (Italy), who are imported at international airports, again imposing artificially induced synchrony, from an external meta-population model that itself has artificial synchrony (damped stochasticity).

Both large-scale spatial model strains

One should conclude that it is likely that addressing the said caveats for large-scale spatial meta-population and agent-based epidemic models (along the lines of: Pastor-Satorras et al., 2015) would necessarily produce greater stochastic variation of epidemic curves from one realization of the simulation to the next, as well as a large spread in timing of the epidemic peak from one jurisdiction to another.

As a final although secondary note, none of the models consider heterogeneity of social status or poverty, which have consistently been shown to be factors highly correlated to excess mortality (e.g., Rancourt et al., 2024) and will also correlate to travel mobility. This omission may additionally bias the models towards artificial local-population homogeneity and inter-population synchrony.

4.1.3 Incompatibility of first-peak period excess mortality outcomes with the paradigm of infectious disease spread, and alternative hypothesis of iatrogenic cause of excess mortality

In section 4.2, we discuss the geographic heterogeneity of excess all-cause mortality during the first-peak period, in comparison with the predictions of large-scale spatial epidemic models.

In section 4.3, we make the same comparison regarding the temporal synchrony of all-cause mortality peaks.

In section 4.4, we discuss our results regarding the dramatic difference in first-peak period excess mortality for pairs of cities in Italy and the USA with comparable demographics, health care systems, and volumes of international air traffic from China and East Asia.

We find that our results regarding first-peak period excess mortality are incompatible with the predictions of the leading spatial epidemic models.

This leads us to consider that first-peak period excess mortality could not have been caused by a spreading respiratory virus and may instead have been caused by mistreatment of patients in hospitals and care homes, coupled with increased susceptibility to pneumonia induced by a high level of biological stress due to lockdown measures. We discuss this possible explanation

for first-peak period excess mortality in sections 4.4 and 4.5, drawing on our results regarding institutional location of death in the USA and the relationship between first-peak period P-scores and socioeconomic variables at the state and county level in the USA and at subnational geographic resolutions in Europe.

4.2 Geographic heterogeneity of first-peak period excess mortality is incompatible with the paradigm of infectious respiratory disease spread

4.2.1 National-level (Europe) and state-level (USA) heterogeneity of excess mortality

At the geographic resolution of countries in Europe (Figure 2) and states in the USA (Figure 9), it is evident that first-peak period excess mortality was confined to a few countries or states with high or very high excess mortality, while most other countries or states had low first-peak period excess mortality.

Figure 158 is a copy of Figure 2 with a yellow line added which runs from north to south along international borders, dividing mainland Europe into western and eastern parts. As can be seen, first-peak period excess mortality (integrated first-peak period P-score > 5 %) was confined to the countries in the western part of Europe (plus Sweden, in the north). While the western European countries had large first-peak period excess mortality, the countries in the eastern part of Europe had negligible excess mortality in March-May 2020 (integrated first-peak period P-score \leq 5 %).

% increase in mortality (2020-02-24 to 2020-05-31)

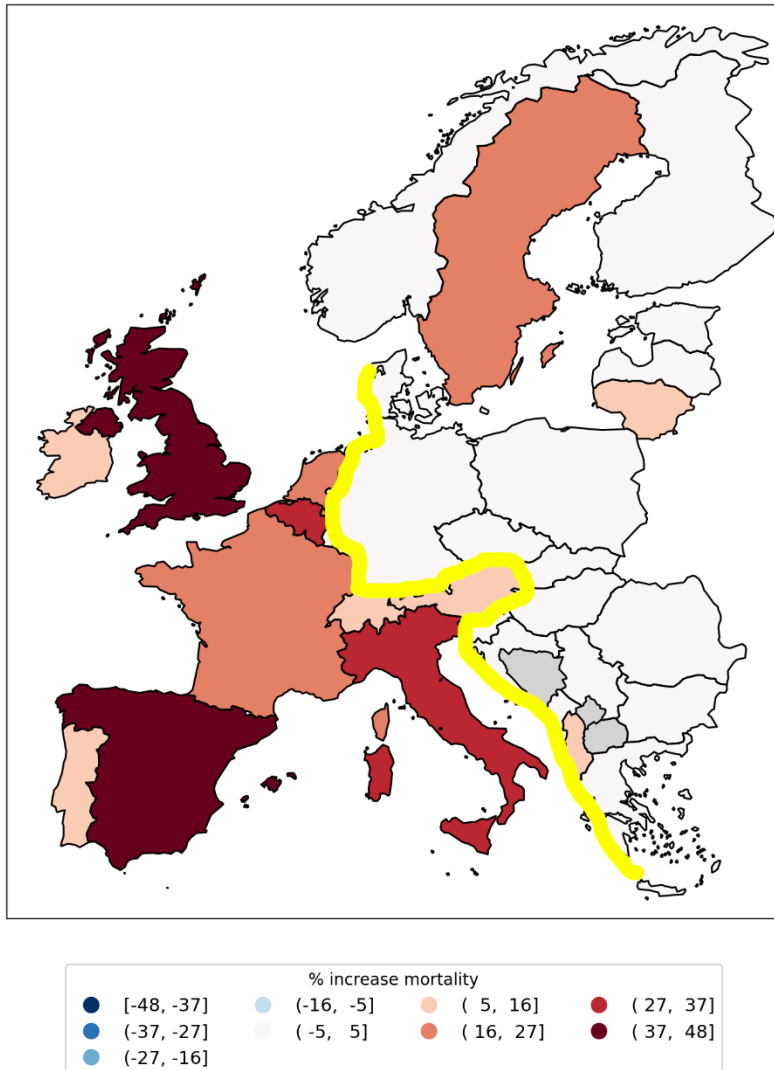


Figure 158: Copy of Figure 2, with added yellow line dividing Europe into countries with high (P-score > 5 %, western part) and low (P-score ≤ 5 %, eastern part) integrated first-peak period P-scores.

Albania (immediately to the east of the yellow line in Figure 158, in southern Europe) is colored light red in Figure 158 because it has an integrated first-peak period P-score of $7.1\% \pm 2.6\%$. However, a large contribution to Albania's first-peak period excess mortality is due to an unrelated sharp mortality peak caused by a heatwave affecting the eastern Mediterranean region in mid-May 2020 (Financial Mirror, 2020; Korosec, 2020; Mitropoulos et al., 2023), which can be seen in the figures showing weekly P-scores for European countries in Appendix A.1. Therefore we have placed Albania to the east of the yellow line in Figure 158. The mid-May 2020 heatwave also caused elevated weekly P-scores in Cyprus, Greece, and Bulgaria, as can be seen in the figures in Appendix A.1.

The result shown in Figure 158 is incompatible with the paradigm of a respiratory disease pandemic caused by a novel pathogen that spreads by person-to-person contact. Meta-population models of respiratory disease pandemics predict air travel to be the main driver of international infection spread (Colizza et al. 2007; Balcan et al., 2010; Brockmann & Helbing, 2013; Davis et al., 2021), with no countries with major airports being spared. In this regard, we note that flight restriction measures are predicted not to have any significant impact on global pandemic disease spread unless disruptions to air travel are near total (Cooper et al., 2006; Epstein et al., 2007; Bajardi et al., 2011; Chinazzi et al., 2020). There are large airports in Germany, Greece, Denmark, and other countries to the east of the yellow line in Figure 158, yet these countries would have avoided receiving the virus before or during the spring of 2020 whereas the countries to the west of the yellow line in Figure 158 would have received the virus by air travel and experienced large infection rates. Similarly, Merler & Ajelli (2010) found that an agent-based model of viral respiratory pandemic spread in Europe predicts similar cumulative attack rates for all European countries, in the range 31-38% (their Figure 5).

As in Europe, first-peak period excess mortality in the USA (Figure 9) was confined to a few states with high or very high integrated first-peak period P-scores, especially the northeastern states of New York, New Jersey, Connecticut, and Massachusetts, whereas the majority of states had low or negligible first-peak period excess mortality, including large and populous states like California, Texas, and Florida. This has been known and documented since early 2020 (Rancourt, 2020; Rancourt et al., 2021a, 2022b).

Davis et al. (2021) applied the global epidemic and mobility (GLEAM) meta-population model to the initial stage of a pandemic originating in Wuhan, China in November 2019 and which spreads to Europe and the USA during January-March 2020. In the Davis et al. (2021) model, contact frequencies depend on age structure and social setting of interaction (whether at school, work, home or in the general community), and probability of travel depends on age and location-specific travel reductions, using data on actual traffic changes that occurred in the time period being modeled. They predict a high probability of generating 100 infections by February 21, 2020 for essentially all regions with large airports in Europe and the USA, as can be seen in their Figure 1c (copied below as our Figure 159), including many regions in which, on the contrary, we observe low or negligible first-peak period P-scores, such as the countries to the east of the yellow line in the map shown in Figure 158, and California, Texas, and Florida in the USA (Figure 9).

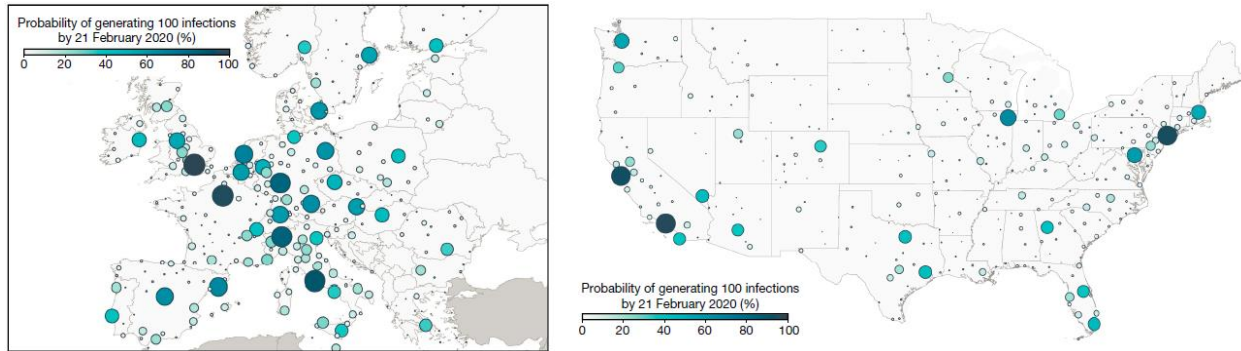


Figure 159: Copy of Figure 1c from Davis et al. (2021). Their caption reads: “[...] c, The probability that a city in Europe (left) and the USA (right) had generated at least 100 cumulative infections by 21 February 2020. Color and circle size are proportional to the probability.”

4.2.2 Subnational (Europe) and county-level (USA) excess mortality

At higher geographic resolutions, a similar result is found. We examined the NUTS1, NUTS2, and NUTS3 subnational statistical regions in Europe (sections 3.2.2 to 3.2.4) and counties in the USA (section 3.2.6). For each geographic resolution, there are a small number of regions with very large first-peak period excess mortalities, while the large majority of regions have small or negligible excess mortality.

This includes high population-density regions in Europe with small first-peak period excess mortality, especially in Germany, southern Italy, and across eastern Europe (Figure 3 to Figure 7, including the population density map in Figure 4). The same is true for the USA, with high population-density counties in Ohio, western Pennsylvania, Florida, Georgia, Texas, California, and other states having small first-peak period excess mortality (Figure 10 to Figure 15).

The maximum P-score among all regions at a given resolution increases with increasing resolution (e.g. compare Figure 2, Figure 3, Figure 5, and Figure 7 for the NUTS0 to NUTS3 regions of Europe, respectively), which is a consequence of the fact that excess deaths were concentrated in a small number of highly-localized geographic regions, in densely populated urban areas with large hospitals.

The geographic confinement of first-peak period excess mortality to specific localized regions is particularly striking for subnational regions located along international borders in Europe.

At the national geographic resolution (Figure 2), Germany had a near zero integrated first-peak period P-score, yet it is bordered to its west by countries (France, Belgium, and the Netherlands) with large integrated first-peak period P-scores. Our results for the NUTS1 geographic resolution (Figure 3, partially reproduced as Figure 160 below, for convenience) show that the regions of France, Belgium, and the Netherlands that are situated along the international border with Germany are among the subnational regions with the largest

integrated first-peak period P-scores in those countries, whereas the western border regions within Germany had small or negligible integrated first-peak period P-scores.

% increase in mortality (2020-02-24 to 2020-05-31)

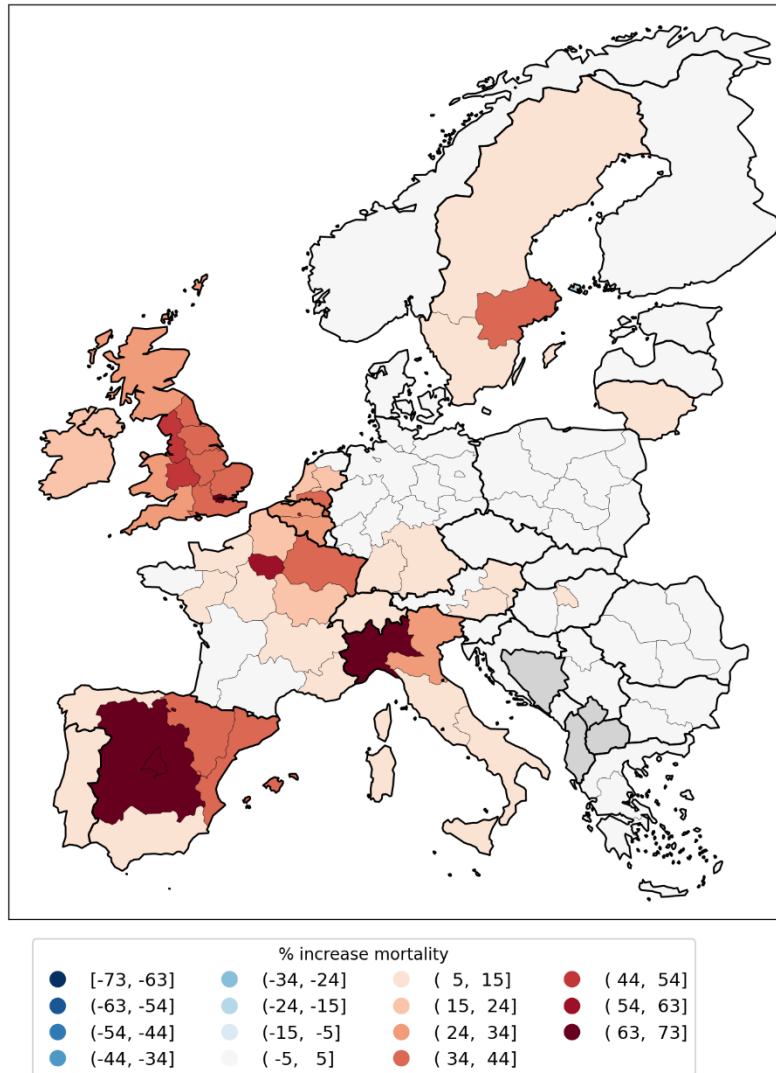


Figure 160: Copy of the right panel of Figure 3, showing a map of integrated first-peak period P-scores for European NUTS1 regions, with color range capped at a value of 73%. Dark grey indicates countries for which data was not available.

We examined the excess mortality data for the said regions along both sides of Germany’s western border in more detail in section 3.3.4, using graphs of weekly P-scores for each region (Figure 33). The results show that the western German border regions had either small or non-existent peaks of first-peak period excess mortality (“F-peaks”), whereas regions that they share a border with in France, Belgium, and the Netherlands had F-peaks with much larger peak heights. For example, the height of the F-peak for the western German border region with the largest integrated first-peak period P-score, DE1 (Baden-Württemberg), was about five times

smaller than the height of the F-peak for the French eastern border region FRF (Grand Est), which borders DE1. All such F-peaks, both in the western German NUTS1 regions or their bordering French, Dutch, or Belgian NUTS1 regions, rose and fell in synchrony.

We also showed that a significant volume of passenger and commercial traffic continued to cross the international borders between Germany and France, Belgium, Luxembourg, and the Netherlands, despite border control measures during the first-peak period (see section 3.3.4, including Figure 34).

The four countries France, Belgium, the Netherlands, and Luxembourg have similar demographics and health care systems to Germany, and the geographic area containing the NUTS1 regions on either side of the German border with the said four countries is the most densely-populated multi-national region on the European mainland (see the map of population density in Figure 4).

Not only would the virus have had to fail to arrive at one of the large German airports (such as Frankfurt Airport, one of the largest airports in Europe, located in the German NUTS1 region of Hesse, which touches four of the five western German NUTS1 border regions), but the virus would have had to arrive in the Netherlands, Belgium, and France and fail to be carried eastward across the border into Germany from one of those countries, despite significant cross-border traffic flow. Either that, or the virus would have had to infect people in western Germany at a similar large rate as in eastern France, Belgium, and the Netherlands, while having a much smaller infection fatality ratio in Germany than in its neighbouring countries. Neither scenario is consistent with the paradigm of pandemic respiratory disease spread, which predicts homogenous infection and mortality outcomes for interconnected and neighbouring populations with similar population densities, demographics, and health care systems.

Similar results were found for the NUTS1 subnational regions along Spain's border with Portugal (Figure 35 and Figure 37), Spain's border with France (Figure 36 and Figure 37), and Italy's international borders with France, Switzerland, Austria, and Slovenia (Figure 38 and Figure 39).

The large difference in peak magnitudes (F-peak weekly P-scores) between subnational European regions sharing an international border, where cross-border passenger and commercial traffic was not extinguished but rather continued at a significant volume, constitutes an apparently insurmountable constraint on the hypothesis that first-peak period excess mortality was caused by a novel and highly virulent spreading pathogen.

The same can be said regarding large differences in excess mortality outcomes for different subnational regions within the same country, many examples of which can be seen in the high-resolution maps of integrated first-peak period P-scores in section 3.2. Of particular interest are subnational regions that are within the same country and that each have similar demographics and health care systems as well as large airports, but which have dramatically different first-peak period excess mortality. We made this comparison for pairs of cities in Italy (Milan vs

Rome) and the United States (New York vs Los Angeles and San Francisco) in section 3.4, and the latter results are discussed below in section 4.4.

4.3 Temporal synchronicity of F-peaks across jurisdictions is incompatible with the paradigm of infectious respiratory disease spread

4.3.1 Near synchronous timing of F-peaks across Europe and the USA

As shown in Figure 1, at the continental scale, both Europe and the USA had large whole-region F-peaks, which rose at nearly the same time, almost immediately following the March 11, 2020 pandemic declaration. For Europe, the rise-side half-maximum is positioned one week after the week of the declaration, and for the USA the rise-side half-maximum is positioned two weeks after the week of the declaration. The F-peaks for the two continental-scale regions on opposite sides of the Atlantic Ocean rose within one week of one another.

The European countries with discernible F-peaks all had rise-side half-maximum dates within three weeks after or equal to the week of the March 11, 2020 pandemic declaration (week of March 9-15, 2020). The country with the earliest rise-side half-maximum date was Italy (rise-side half-maximum date equal to the week of the pandemic declaration) and the country with the latest rise-side half-maximum date was the UK (rise-side half-maximum date equal to three weeks after the week of the pandemic declaration). This is shown in section 3.3.1, in additional figures in Appendix A.1, and in a table listing P-scores, P-score error values, and rise-side half-maximum dates in Appendix C.1. A country's F-peak was considered to be discernible for the purpose of determining a rise-side half-maximum date if the ratio of its P-score value divided by the 1σ error on its P-score value was at least 3.

Results regarding the timing of F-peaks for USA states are shown in section 3.3.5. The USA states with discernible F-peaks had rise-side half-maximum dates ranging as follows, expressed as the number of weeks after the week of the pandemic declaration:

- one week (Washington State and Oregon)
- two weeks (14 states, including New York State and New Jersey, which had the largest first-peak period integrated P-scores among USA states)
- three weeks (12 states, including Connecticut, Massachusetts, and District of Columbia, which had the third, fourth, and fifth highest integrated first-peak period P-scores among USA states, respectively)
- four weeks (North Carolina)
- five weeks (Rhode Island, Delaware, Minnesota, Ohio, and New Hampshire)
- six weeks (Iowa)
- seven weeks (New Mexico)

The remaining 15 USA states did not have discernible F-peaks. The rise-side half-maximum dates for USA states are shown on a map in Figure 42 (top panel).

Many states with identical rise-side half-maximum dates to New York State (two weeks after the week of the March 11, 2020 pandemic declaration) are located far from New York, whether on the Pacific coast (California), in the Rocky Mountains (Colorado), on the Gulf coast (Louisiana), in the Southeast (Georgia), or in the Great Lakes region (Michigan). The synchrony of F-peak emergence for New York State, California, Louisiana, and Michigan is illustrated in Figure 43. The synchrony of F-peak emergence of other states with New York State is shown in the graphs in Appendix A.2.

A table listing P-scores, P-score error values, and rise-side half-maximum dates for USA states is in Appendix D.1.

The largest F-peaks among USA states and European countries thus all had rise-side half-maximum dates that were no earlier than the week of the pandemic declaration and that were within three weeks of one another. Large-scale spatial epidemic models predict a spread of approximately one month in epidemic peak timing across countries in Europe and states in the USA (Merler & Ajelli, 2010; Brockman & Helbing, 2013; Davis et al., 2021). However, these models are subject to important caveats that bias their results toward exaggerated synchronicity of the epidemic peaks for different jurisdictions, as we have discussed in section 4.1. Introducing spatial heterogeneity of contact patterns within the airport catchment areas in meta-population models, or removing the oversimplification of using a homogeneously mixed single-population global pandemic model for the importation of seed infectious individuals in agent-based models, would most likely produce larger spread in peak timing between jurisdictions in these models.

Therefore, the high degree of synchrony (within 3 weeks) of the large F-peaks in the hemisphere, on two distant continents, and the fact that not a single F-peak-like excess mortality event (i.e., rise—peak—fall or rise—plateau) occurs prior to the WHO's March 11, 2020 declaration of a pandemic, are both incompatible with the paradigm of infectious respiratory disease spread (and see: Rancourt, 2020). A virus would not wait for a political announcement before immediately causing surges in mortality in hotspots dispersed on two continents.

4.3.2 Simultaneous rise and fall of F-peaks for subnational regions within a given European country and for counties of a given USA state

Europe

Section 3.3.2 shows graphs of weekly P-scores during the first-peak period for all the NUTS1 subnational regions for particular European countries (Italy, Spain, France, Belgium, Netherlands, UK, Sweden, and Germany).

A remarkable result is observed. Within any given country, all of the country's subnational regions' weekly P-scores rose and fell essentially in synchrony with one another. The graph for the NUTS1 regions in Spain (Figure 18, reproduced below as Figure 161, for convenience) is a particularly striking example, with regional peaks that differ in height by up to a factor of 13 rising and falling in lock step with one another.

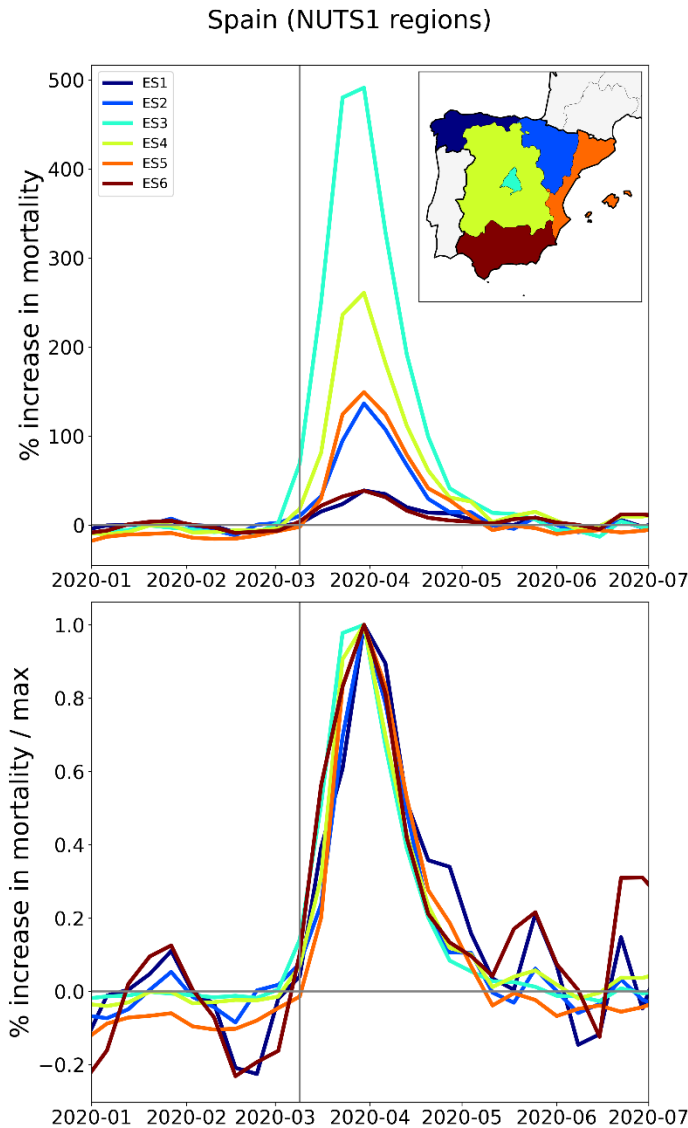


Figure 161: Copy of Figure 18. Top panel: weekly P-scores during the first-peak period for the NUTS1 regions of Spain. Bottom panel: same as top panel, with each curve scaled by its maximum.

Similar results are shown for the NUTS2 regions within a given large-F-peak European country, in section 3.3.3, and for the counties within a given large-F-peak USA state, in section 3.3.6.

The same timing of F-peaks across all of a European country's subnational regions (regardless of peak height) is inconsistent with the paradigm of a novel and virulent pathogen that would have spread through the society via person-to-person contact. Models of spatial spread of

epidemics that account for heterogeneous population densities and connection patterns across a geographic territory predict large variation in the timing, shape, and severity of epidemic peaks across regions within the territory (Ferguson et al., 2006; Merler & Ajelli, 2010; Thomas et al., 2020).

Thomas et al. (2020) modeled COVID-19 spread at the level of census tracts within USA cities, and found that “[i]nstead of one common curve, we see that tracts vary wildly in onset time and curve width, with some tracts showing peaks weeks or months after the initial aggregate spike has passed”.

Figure 1 of Thomas et al. (2020) is copied below, as Figure 162. For Seattle (left panel) and Washington D.C. (right panel), the figure shows curves of the number of infections per day for each census tract in the city (grey curves, left y-axes) and the number of infections per day for the entire city (aggregate of all census tracts) (red curves, right y-axes).

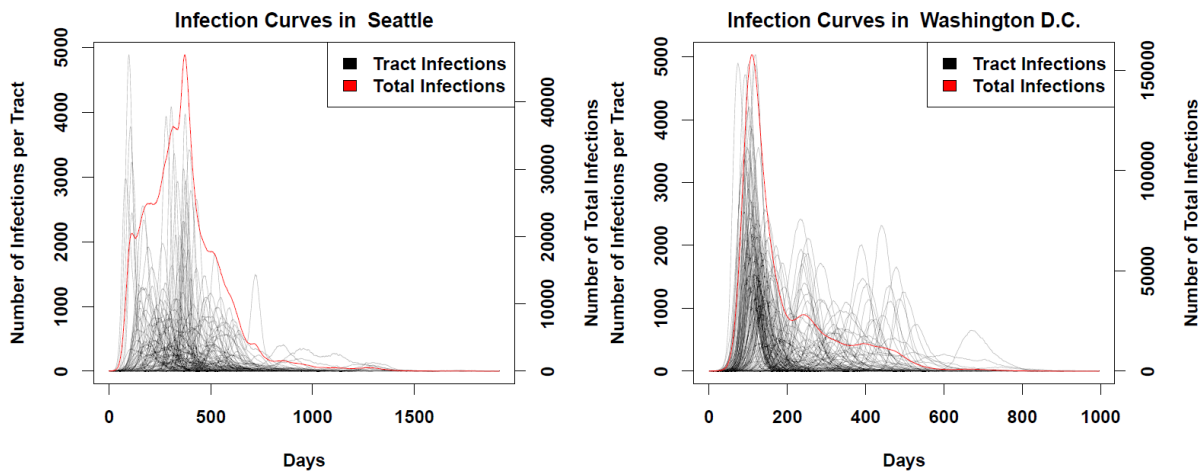


Figure 162: Copy of the upper two panels of Figure 1 from Thomas et al. (2020). Their figure caption has: “[Left] Infection curves for Seattle, WA. The red line is the curve for the whole city, while the black lines are the infection curves for each tract in the city. While the red curve is relatively smooth, this smoothness hides a significant amount of heterogeneity in the timing of the infection curves for each census tract. [Right] Infection curves for Washington, DC. As with Seattle, the city-level curve conceals considerable spatial variability in the infection’s progress.”

As can be seen from Figure 162, not only do different census tracts within a single city have large variation in epidemic peak timing, height, and width, but the aggregate (red) curves for Seattle and Washington D.C. also have very different peak timing, height, and width. Whereas the aggregate curve for Washington D.C. peaks after about 100 days after seeding, the aggregate curve for Seattle peaks after about 400 days after seeding. The Seattle aggregate curve also has a much larger full-width at half-maximum (FWHM) than that of Washington D.C.

Ferguson et al. (2006) used an agent-based model to simulate an influenza pandemic in the USA and Great Britain in which contact frequencies were determined by population density, household size and age structure, workplace or school size, and travel patterns. The simulations

for the USA were independent of the simulations for Great Britain. In each case, the epidemic was seeded by infected people arriving in the country of interest from the rest of the world, which is modeled as a single, homogeneously mixed population. They predicted that epidemic curves (i.e., infection prevalence or incidence, prior to recovery and thus acquired immunity) in rural areas would occur weeks later than in urban centres, which contrasts with the synchrony of F-peaks across all subnational regions (whether urban or rural) of a given large-F-peak European country shown in section 3.3.

Merler & Ajelli (2010) used an agent-based model to simulate an influenza pandemic in Europe. Similar to Ferguson et al. (2006), contact frequencies were determined by population density, household size and age structure, workplace or school size, and travel patterns, and seed infections arrived by international air travel from the outside world, modeled as a single, homogeneously mixed population. Merler & Ajelli considered spatial heterogeneity of the sociodemographic structure and travel patterns within the geographic territory of interest, which was not considered in Ferguson et al. (2006). Like in Ferguson et al. (2006), the Merler & Ajelli (2010) model predicts that epidemic curves in rural areas would occur weeks later than in urban centres.

Therefore, the observed synchrony of F-peaks across all subnational regions (whether urban or rural) of a given large-F-peak European country shown in section 3.3 is incompatible with models of the spread of the presumed pathogen, and the model simplifications (of suppressed spatial heterogeneity, and of damped seeding stochasticity, see section 4.1.2) would only make the said incompatibility more so.

Additionally, while larger values of the basic reproduction number (usually denoted " R_0 ") tend to reduce the variation in peak timing between different regions in the models, larger values of the basic reproduction number also have the predicted consequence that essentially all regions become infected to comparable high degrees, which is contrary to our many observations of geographical heterogeneity of integrated first-peak period P-score magnitudes.

Our repeatedly observed combination of a high degree of heterogeneity in peak size and peak presence versus absence, together with a high degree of synchronicity of peak timing across many distant regions, is inconsistent with the predictions of the pandemic models of a spreading viral respiratory pathogen. Stated simply, person-to-person respiratory contact spread models cannot simultaneously produce both geographical heterogeneity of attack rate and synchronous peaks of attack rate, which are uncontroversially presumed to translate to mortality expressed as P-score.

USA

A similar result to that seen for subnational regions in Europe is found for the counties within a given state in the USA, as shown in the figures in section 3.3.6. For example, for the counties in New York State (Figure 44) that had large integrated first-peak period P-scores, the F-peaks rose and fell in a strikingly synchronous fashion.

Figure 163 shows monthly P-scores for the counties of the New York City Metropolitan Area (“NYC Metro Area”), which has a population of 19.5 million people (US Census Bureau, 2023). As can be seen, all counties within the NYC Metro Area had F-peaks that emerged in synchrony and had peak P-scores in the same month (April 2020). Most F-peaks also fell in synchrony, although some counties on the periphery of the metro area with relatively low population densities and relatively low peak P-scores had fall-side half-maximum dates up to about one month later than for the majority of the metro counties.

Such synchronicity of peak timing is opposite to the predictions of spatial epidemic models in which contact patterns depend on connections in a social network structured to represent a real-world city, such as that of Thomas et al. (2020), which predicts a wide range of peak timing, width, and severity for different neighbourhoods within the urban areas of USA cities (see their Figures 1 and 2; their Figure 1 is partially copied above as our Figure 162).

A similar result can be seen for the counties in the urban areas of Boston (Figure 47), Philadelphia (Figure 49), and Detroit (Figure 51).

Counties in the New York City metropolitan area
(New York-Newark, NY-NJ-CT-PA Combined Statistical Area)

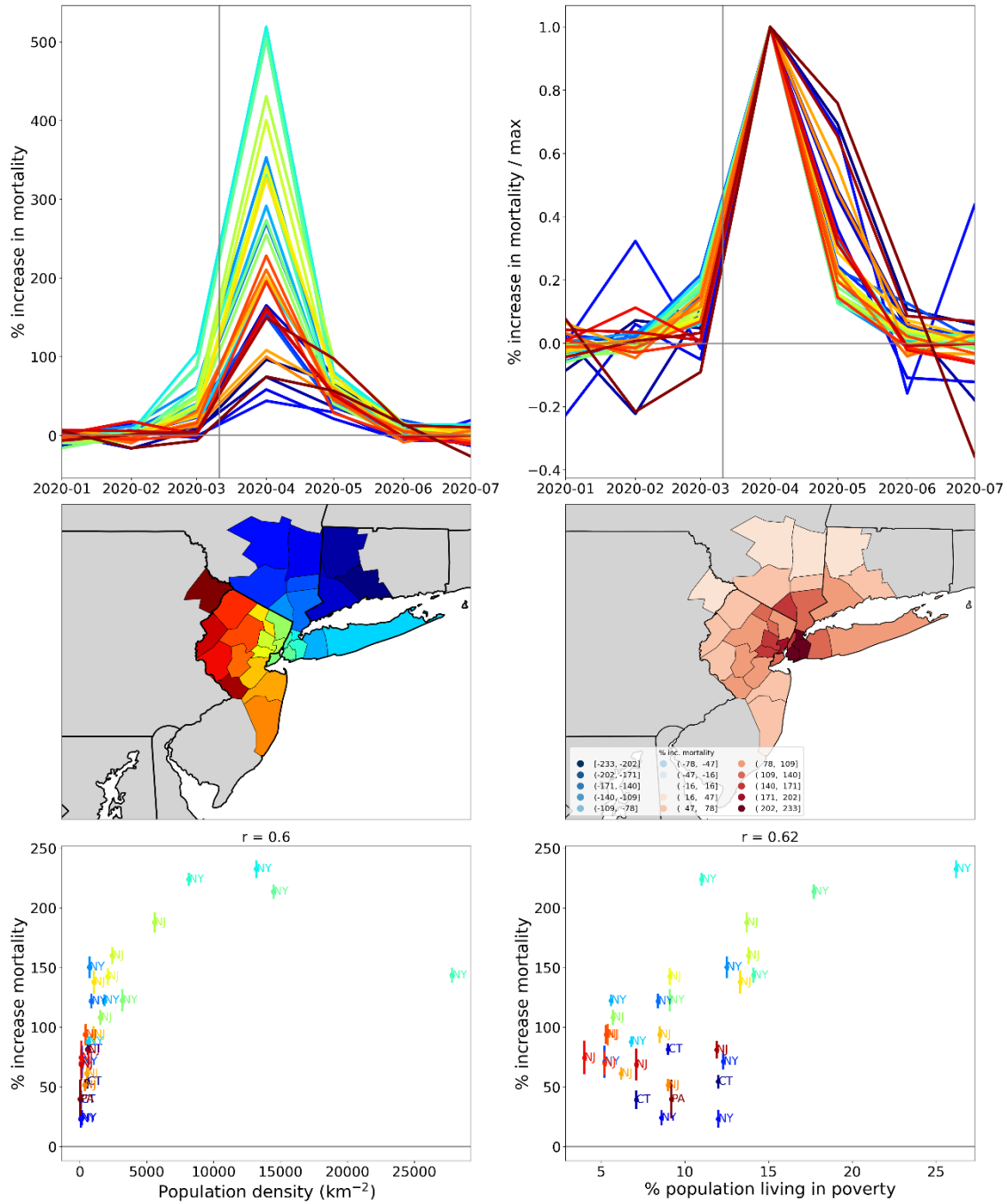


Figure 163: Top left: monthly P-scores for the counties of the New York City Metropolitan Area. Top right: same as top left, with each curve scaled by its maximum. Here, the vertical grey solid lines indicate the date at which the WHO declared a pandemic. Middle left: map with counties colored as per the curves in top row and points in bottom row of panels. Middle right: heatmap showing integrated first-peak period (March-May 2020) P-score for each county. Bottom left: scatter plot of county integrated first-peak period P-score vs county population density. Bottom right: scatter plot of county integrated first-peak period P-score vs. county percent of population living in poverty.

When one considers only the counties of New Jersey (even though many of the northern counties of New Jersey belong to the NYC Metro Area) as in Figure 45, it can be seen that the largest F-peaks (blue curves in Figure 45) have synchronous rises and falls, whereas the intermediate F-peaks (yellow curves in Figure 45) have essentially the same rise-side half-maximum dates as the large F-peaks (blue curves) but do not fall as quickly, such that their fall-side half-maximum dates occur later in time than for the large F-peaks (blue curves). Additionally, the counties in the south of the state with the smallest F-peaks (red curves in Figure 45), which are also far from the New York City urban area and have the lowest population densities in the state, have delayed rise-side and fall-side half-maximum dates compared to the large and intermediate F-peaks. A somewhat similar pattern is seen for Connecticut, with the two eastern-most counties of that state having lower peak height, later rise-side half-maximum dates, and low population densities.

The said pattern of staggering or delay in the timing of peaks for different counties within the same state, with lower population-density counties having systematically lower peak heights, larger peak widths, and later rise-side half-maximum dates, which is most clearly seen in New Jersey, is reminiscent of the behaviour of simple deterministic one-population susceptible-infectious-recovered (SIR) epidemic models with homogeneous population mixing, when contact frequency is varied. For example, if one generates an array of independent curves of new cases per time from such an SIR model, where the contact frequency input parameter is varied but the recovery rate input parameter is held constant, one will obtain curves with lower peaks, larger widths, and later rise-side half-maximum dates for lower values of the contact frequency (e.g. see the graphs in the supporting information of Hickey & Rancourt (2023a) or Hickey & Rancourt (2023b)). Here, the lower contact frequency in the model could be considered analogous to lower population density.

However, the said pattern of behaviour of the monthly (weekly for Europe) P-score time-series for the counties of New Jersey and to some extent in Connecticut is not seen in most other jurisdictions studied in this paper (see the figures in section 3.3, in particular), which necessarily raises the question of whether other explanations, beyond such modeling interpretations, apply to New Jersey and Connecticut.

In this regard, it is possible that large urban hospitals close to the centre of the New York City urban area (in both New Jersey and Connecticut) were more aggressive in applying treatments such as mechanical ventilation in March-May 2020 (further discussed in section 4.4) than smaller and institutionally different rural and semi-rural hospitals and care facilities in those states. Less aggressive treatments would kill fewer patients overall, and would take longer to kill on average (i.e., affected patients would spend more days in hospital, on average, before succumbing to the negative effects of the treatment). In this way, institutional resistance to or slowness in applying aggressive measures, which would be stronger in rural areas far from the urban centre, would produce F-peaks with later onset, lower peak height and wider peak width.

Europe and USA

Overall, the high degree of synchronicity in F-peaks (if presumed to correspond to epidemic curves) in the subnational regions on several spatial resolutions in Europe and the USA, together with the large concomitant geographical heterogeneity of first-peak period P-scores (if presumed to correspond to attack rates or infection fatality ratios), is contrary to applications of the paradigm of pandemic spread of a contagious disease of the type presumed. All such applications are expected to give large spreads in infection arrival times and epidemic-curve peak or rise times, more so than current large-scale spatial models predict given their simplified structural designs (see above, and “caveats” section 4.1.2). Within realistically structured models, geotemporal synchrony would only be achieved by significantly increasing contagion and transmission rates, which in turn would produce attack-rate geographical homogeneity, contrary to the observed large geographical heterogeneity, including outright infection deserts (eastern Europe) and inter-city inconsistencies (Milan vs Rome, and New York City vs Los Angeles and San Francisco). Instead, a simpler and more direct model of institutional iatrogenic deaths imposes itself (sections 4.4 and 4.5), within the context of socioeconomic disparity (section 4.5), combined with large-scale pandemic response measures (section 4.3.3).

4.3.3 Staggering in time of F-peaks of different countries in Europe linked to date of first national lockdown

At the NUTS0 (national-level) geographic resolution, the F-peaks for European countries, while occurring within a few weeks of one another, did not all rise and fall in synchrony, as can be seen from Figure 16. Rather, Italy experienced the earliest F-peak, with a rise-side half-maximum date during the week of the WHO’s March 11, 2020 pandemic declaration, whereas the UK had the latest rise-side half-maximum date approximately three weeks later.

Figure 164 shows the weekly P-scores (top panel) and maximum-scaled weekly P-scores (bottom panel) for Italy, Spain, and the UK, with dashed lines indicating the date that each country implemented its first national “lockdown” containment measure (Silverio et al., 2020; Redondo-Bravo et al., 2020; Institute for Government Analysis, 2022). These three countries had the highest integrated first-peak period P-scores among European countries (Appendix C.1).

Figure 165 shows the weekly P-scores (top panel) and maximum-scaled weekly P-scores (bottom panel) for the NUTS1 regions of the UK, with the black dashed line indicating the date that the UK implemented its first national lockdown.

European countries IT, ES and UK, with dates of first national lockdown

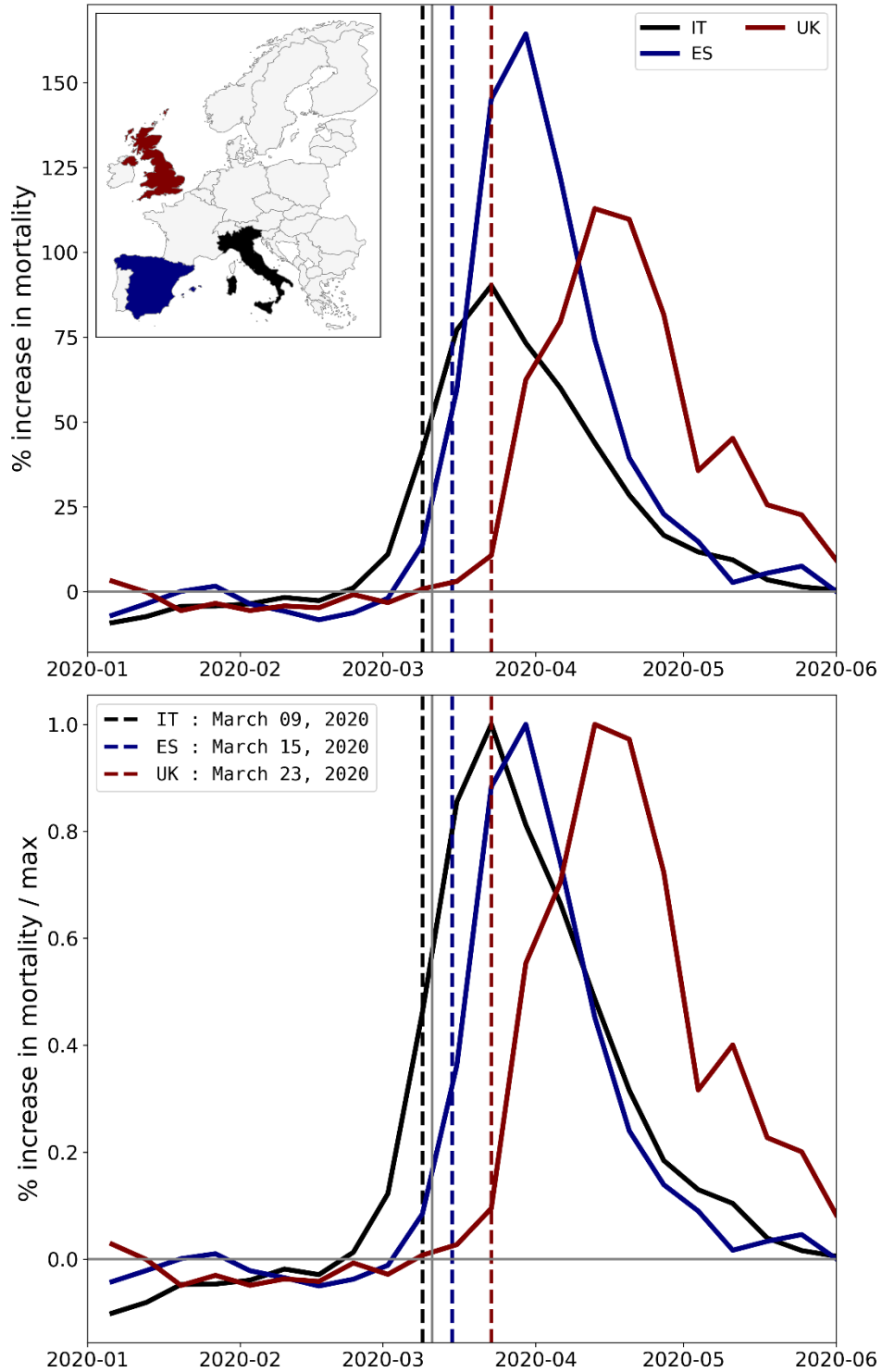


Figure 164: Top panel: weekly P-scores during the first-peak period for European countries Italy, Spain, and the UK. Bottom panel: same as top panel, with each curve scaled by its maximum. Dashed colored vertical lines indicate the date that each country implemented its first national lockdown. Solid grey vertical line indicates the date of the pandemic declaration (March 11, 2020).

NUTS1 regions of UK, with date of first national lockdown

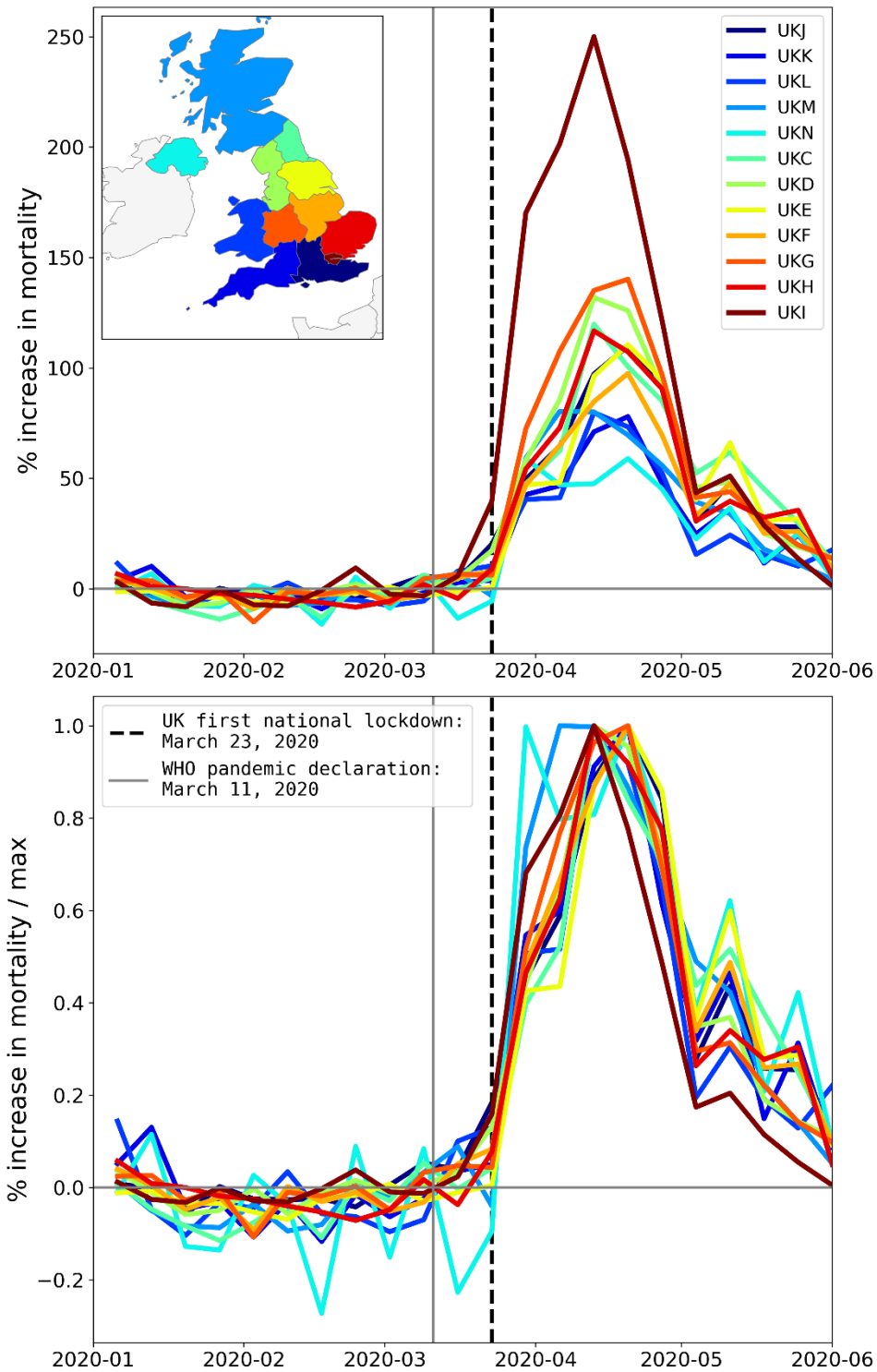


Figure 165: Top panel: weekly P-scores during the first-peak period for the NUTS1 regions of the UK, color coded as per the map inset. Bottom panel: same as top panel, with each curve scaled by its maximum. Dashed black vertical line indicates the date the UK implemented its first national lockdown. Solid grey vertical line indicates the date of the pandemic declaration (March 11, 2020).

As can be seen from Figure 164, for Italy, Spain, and the UK, each first national lockdown was implemented at a time when the nation's P-score was relatively low.

In Figure 164 (and in all graphs in this article showing weekly P-scores for European countries), the data point for each weekly P-score is placed at the date of the Monday of the week consisting of the seven days beginning on Monday and ending on Sunday. For Italy, in the week preceding the first national lockdown (week of March 2-8, 2020), the national-level P-score was $11\% \pm 6\%$, whereas in the following week (week of March 9-15, 2020), which began with the implementation of the first national lockdown on Monday, March 9, 2015, the national-level P-score was $42\% \pm 4\%$.

In Spain, the first national lockdown was implemented on Sunday, March 15, 2020, at the end of the week of March 9-15, 2020, which had a weekly P-score of $14\% \pm 4\%$, whereas the P-score for the week of March 16-22, 2020 for Spain was $60\% \pm 4\%$.

For the UK, the P-score for the week immediately preceding the implementation of the first national lockdown (the week of March 16-22, 2020) the P-score was $3\% \pm 6\%$, which is indistinguishable from 0%, whereas the first significantly positive P-score ($11\% \pm 2\%$) occurred during the week of March 23-29. Therefore, at the national geographic resolution, the F-peak in the UK began to rise in the week that began with the national lockdown implementation on Monday, March 23, 2020.

At the NUTS1 geographic resolution (Figure 165), it can be seen that the F-peaks for subnational regions in the UK rose rapidly and essentially simultaneously beginning in the week of March 23-29, 2020, the week that began with the national lockdown implementation on Monday, March 23, 2020, with no subnational F-peak beginning to rise prior to the week of March 23-29, 2020.

The onset sequence "Italy then Spain then UK" of the three most impacted countries in Europe is not supported by pandemic-model arrival times of significant infections (Figure 159). Within pandemic modelling efforts, it seems one would need to assume concocted particular conditions to produce the observed said onset (and continuance) sequence, in particular given Heathrow Airport in London.

It appears that a natural explanation is to associate the observed said onset sequence with immediate deleterious consequences accompanying the national lockdowns. It is not unreasonable to postulate that the same socio-political and media context leading to a national lockdown and the lockdown itself would influence institutional behaviour in establishments that house the most vulnerable members of society, and cause significant disruptions in the life-supporting operations of those establishments (Rancourt, 2024).

Basically, the time sequence and proximity in time of F-peaks in the largest F-peak countries in Europe is difficult to reconcile with the paradigm of a spreading pandemic-causing respiratory

virus, but is associated with the presumed onsets of institutional response measures and with the dates of first national lockdowns in particular.

4.4 Deadly medical treatments were prevalent in first-peak period mortality hotspots

Section 3.4 contains results comparing first-peak period excess mortality (as P-scores) for pairs of regions containing cities with large international airports that had very different first-peak period excess mortality outcomes (P-scores). Recall that P-score measures the relative excess mortality for a population, compared to the predicted historic, normal or unperturbed mortality for the population, and is thus inherently adjusted for the age structure and health frailty of the specific population in the jurisdiction of consideration (section 2.3).

We studied the region of Milan (Lombardy) vs the region of Rome (Lazio) in Italy in section 3.4.1, and New York City vs Los Angeles and San Francisco in the USA in section 3.4.2.

4.4.1 Italy

The dominant explanation for Italy's F-peak is that it was due to an outbreak of COVID-19 in Northern Italy, a region with an elderly and therefore vulnerable population, wherein the novel pathogen (namely SARS-CoV-2) would have arrived in Europe via air travel from China (Cereda et al., 2021; Riccardo et al., 2020; Spiteri et al., 2020; Boccia et al., 2020).

If the said dominant view were correct, then similar excess mortality outcomes would have occurred in different Italian regions with similar volumes of air passenger traffic and demographic and health care characteristics. We tested this in some detail.

In section 3.4.1, we showed that air travel into Italy in 2019, including via direct flights from China and from the Asia Pacific region, is not associated with large first-peak period excess mortality (P-scores) in the regions served by Italy's largest airports. In fact, the opposite occurred: the region containing Rome (Lazio) had significantly higher volumes of passengers traveling to and from Chinese airports in each of 2017, 2018 and 2019 than the region of Milan (Lombardy), yet Lombardy had much greater first-peak period excess mortality than Lazio: Lombardy's integrated first-peak period P-score was $106.2\% \pm 2.5\%$, approximately 18 times greater than Lazio's integrated first-peak period P-score value of $5.8\% \pm 1.7\%$.

This large difference in outcomes is striking given that the two regions have very similar age structures and health care system resources, including similar values for the share of the population aged 65+ (22.2% in Lazio, 22.9% in Lombardy), the share of the population aged 80+ (7.0% in Lazio, 7.4% in Lombardy), number of hospital beds in the region per person aged 65+ (1.59% in Lazio, 1.58% in Lombardy) and number of ICU beds in the region per person aged 65+

(0.038% in Lazio, 0.032% in Lombardy). The two regions also had virtually identical pre-COVID all-ages mortality rates for 2019 (10.1 deaths per 1000 people in both Lazio and Lombardy). We could not find any socioeconomic characteristic that might explain the measured P-score difference.

The said large difference in P-score between Lazio and Lombardy regions is inconsistent with the predictions of spatial epidemic models. Davis et al. (2021), applying the GLEAM meta-population model to the spread of a global pandemic originating in Wuhan, China in November 2019, predict that Rome and Milan would have had an equally high probability of generating 100 infections by February 21, 2020 (their Figure 1c, copied as our Figure 159). Ajelli et al. (2010) compared results of a meta-population model versus an agent-based model for a viral respiratory epidemic affecting Italy, and found that for both types of models, both Rome and Milan have large attack rates (their Figure 6).

Possible explanations that have been advanced by various authors to account for the dramatically different mortality outcomes in different Italian regions during March-May 2020 include:

- that the onset of outbreaks in Northern Italy occurred before national containment measures were implemented, whereas the onset of outbreaks in other regions of Italy occurred after measures were implemented (La Maestra et al., 2020)
 - this is contradicted by the synchrony of the F-peaks in the different Italian regions, as shown in Figure 17, Figure 25 and Figure 54
 - this would also be contradicted by the dominant view that the SARS-CoV-2 pathogen was circulating in Italy weeks before the first reported case of locally acquired infection dated February 20, 2020 (La Maestra et al., 2020; Zehender et al., 2020; Cereda et al., 2021; Apolone et al., 2021; Alteri et al., 2021; Davis et al., 2021).
- that poor air quality in Northern Italy, including Lombardy, could have increased infectiousness and severity of infection with COVID-19, causing higher mortality in the northern regions (Coker et al., 2020; Ottaiano et al., 2021)
 - this is contradicted by a recent systematic review and meta-analysis of the relationship between particulate matter air pollution and COVID-19 infection severity and mortality, which found no reliable evidence of an increase in mortality risk due to air pollution (Sheppard et al., 2023)
 - regardless, the magnitude of the effect would be much smaller than necessary to account for the observed large difference in first-peak period excess mortality between Lombardy and Lazio, Campania and other Italian regions

→ also, there are a number of areas in Eastern Europe with comparable annual mean air pollution levels to Northern Italy, including in Central and Southern Poland, Central Serbia, and the area around the Bulgarian capital (see the map in Figure 166, reproduced from European Environment Agency (2018)), but these areas had essentially zero excess mortality during the first-peak period, as shown in the maps in section 3.2.

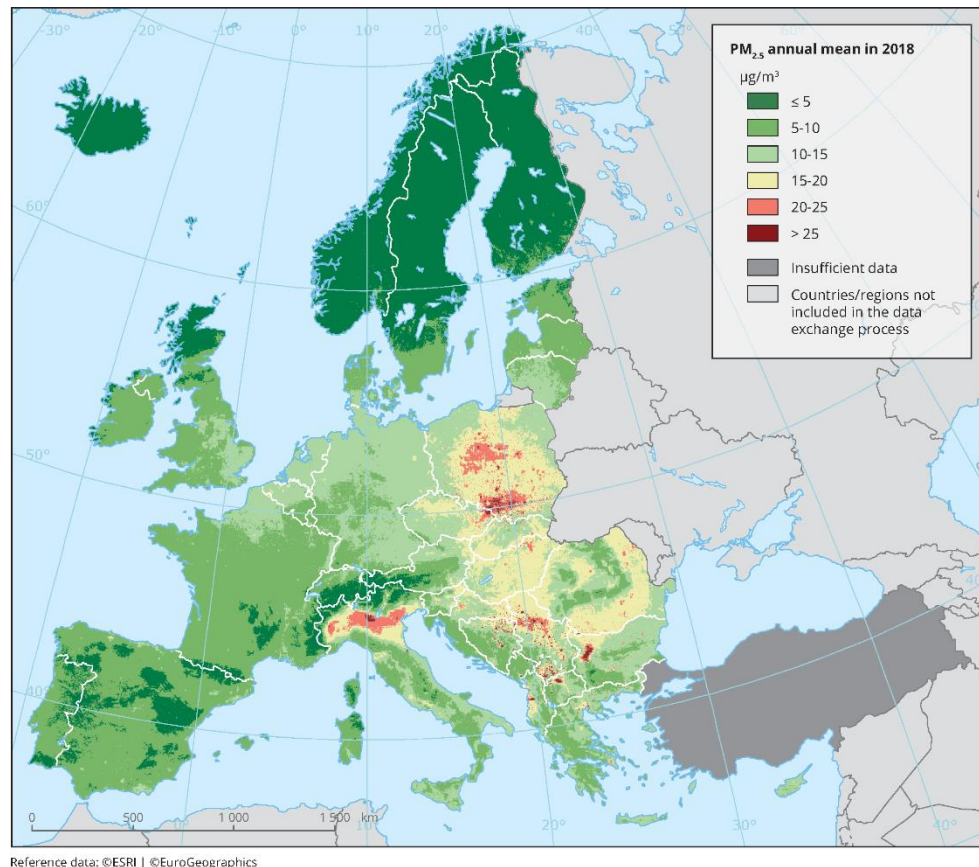


Figure 166: Calculated concentrations of airborne fine particulate matter (PM_{2.5}) (annual mean) [Copy of the figure in European Environment Agency (2018)].

- that, within Italy's decentralized health system, different regions adopted different strategies in response to the perceived threat of COVID-19 (Capano & Lippi, 2021; Bosa et al., 2021), which is addressed as follows.

Regarding the latter explanation (different health care system responses in different regions), the northern regions of Italy, especially Lombardy, stand out from other Italian regions due to their decisions to greatly increase the intensive care unit (ICU) capacity in hospitals and to systematically treat patients diagnosed with COVID-19 using invasive mechanical ventilators.

Lombardy created an emergency task force on February 21, 2020 to increase the surge capacity of ICUs in the region. Whereas Lombardy had 738 ICU beds prior to the crisis, 130 additional ICU beds were created by February 23, 2020, and on April 2, 2020, the region had 1750 ICU

beds (Rezoagli et al., 2021). An additional 250 ICU beds were created in Milan, in a temporary hospital constructed in 20 days on a site spanning 25,000 square meters, opened on March 31, 2020 (Rezoagli et al., 2021). Within the first fourteen days after the creation of the task force, 16% of all patients in Lombardy who tested positive for COVID-19 were admitted to an ICU (Grasselli et al., 2020a). In the three Northern Italian regions of Lombardy, Emilia-Romagna, and Veneto, 12.6% of people admitted to a hospital with COVID-19 were admitted to an ICU (Rezoagli et al., 2021).

Mechanical ventilation was intensively used to treat ICU patients diagnosed with COVID-19 in Lombardy. A retrospective case series study of critically ill patients admitted to ICUs in Lombardy from February 20 to March 18, 2020 found that, among 1300 patients with available data, mechanical ventilation was applied to 88% of the patients and non-invasive ventilation was applied to 11% of the patients (Grasselli et al., 2020b). As of March 25, 2020, 26% of all 1581 patients with available ICU disposition data had died in the ICU, 58% were still in the ICU, and 16% had been discharged from the ICU (Grasselli et al., 2020b). A later study covering 3988 patients admitted to ICUs in Lombardy up to April 22, 2020 found similar rates of mechanical ventilation and higher mortality rates; for example, for the first 1715 patients, as of May 30, 2020, 48.7% had died in the ICU and 0.8% were still in the ICU (Grasselli et al., 2020c). In Bergamo province, in Lombardy region, all patients hospitalized in the ICU with COVID-19 were placed on mechanical ventilators, and out of the first 510 patients with COVID-19 who were admitted, 30% died (Fagioli et al., 2020). At the national level, the Italian government attributed 845 million Euros to increase the number of ICU beds to be used for invasive mechanical ventilation “up to 14% of the total hospital beds” (Rezoagli et al., 2021).

Treatment with mechanical ventilators has serious and often fatal risks including ventilator-associated pneumonia (VAP) and ventilator-induced lung injury (VILI), not unrelated to the dominant geriatric risk of aspiration pneumonia (Rancourt, 2024).

VAP is the most frequent intensive-care-unit-acquired infection, and a significant cause of morbidity and mortality (American Thoracic Society, 2005; Joseph et al., 2010; Bouadma et al., 2015). The mortality rate of VAP has been found to range from 20% to 76% depending on the circumstances of the study (Chastre & Fagon, 2002; Davis, 2006; Joseph et al., 2010), with an overall estimated attributable mortality of 9-13% (Melsen et al., 2011; Melsen et al., 2013) and subgroup estimated attributable mortalities of 69% for surgical patients and 36% for patients with an intermediate severity of illness score (Melsen et al., 2013). Incidence rates of VAP range from 6 to 52% (Joseph et al., 2010).

VILI refers to a constellation of pulmonary consequences and structural damage caused by exposing the lungs to abnormal transpulmonary pressure from ventilation (Slutsky & Ranieri, 2013; Gattinoni et al., 2017).

Beyond the known high mortality rates associated with adverse effects of standard mechanical ventilator treatment, in the panic of the first-peak period of 2020 in Lombardy, untested

ventilation methods were used due to the shortage of standard ventilators. For example, anesthesia machines, which are not designed to support critically ill patients for long times, were used as ventilators in Niguarda Hospital in Milan, Lombardy. Patients who were mechanically ventilated with anesthesia machines had a “remarkably high” mortality rate of 70.6% and a “remarkably reduced” 60-day survival probability compared to those treated with standard mechanical ventilators, who had a mortality rate of 37.5% (Bottiroli et al., 2021).

A recent study of first-peak period excess mortality across the 91 health care districts of Lombardy region found a strong positive relationship between COVID-19 hospitalizations and excess mortality, estimating that each additional hospitalized COVID-19 patient per 1000 inhabitants resulted in a 15.5% increase in excess all-cause mortality for the district (Paganuzzi et al., 2024). In the neighbouring region of Veneto, which had a much smaller excess-mortality peak than Lombardy (see Figure 54) hospital admissions were limited to the most severe cases and the health care response focused more on home care assistance (Gilbertoni et al., 2021).

From a whole-country perspective, a study of regional differences in first-peak period mortality among Italian NUTS2 regions found that the factor with the strongest effect on COVID-19-assigned mortality rate (not all-cause excess mortality P-score) was the prevalence of older individuals living in multigenerational households, which decreased mortality (Basellini & Camarda, 2022).

The picture that emerges for Italy is one of distinct hotspots of first-peak period excess mortality (P-scores) associated with a surge in intensive care unit admissions, where aggressive and dangerous treatments were applied. Regions that did not surge their intensive care unit admissions did not experience large P-scores, while having similar pre-COVID demographic and health care system characteristics and similar volumes of air traffic with China and East Asia, and despite the presumption that the novel pathogen was circulating in Italy for several weeks before the northern Italian regions implemented their emergency responses beginning on February 21, 2020. Scathing reports of “killing fields” in Italian hospitals due to the intensive use of mechanical ventilators do not appear to be an exaggeration (McCrae & Watson, 2023).

Therefore, the large difference in Milan-vs-Rome first-peak period P-score mortality is incompatible with the paradigm of a spreading pandemic-causing respiratory virus, and the large P-scores for the Milan region (Lombardy) appear to have been caused in large part by increased deadly ICU measures, especially widespread and often experimental mechanical ventilation.

4.4.2 USA

In section 3.4.2, we compared New York City vs Los Angeles and San Francisco, in the USA.

Figure 55 shows that New York City had a much higher integrated first-peak period P-score than Los Angeles or San Francisco, but received less international air traffic in 2019 and fewer flights

from China in January 2020 than Los Angeles and San Francisco. New York City had similar demographic and health care system characteristics to Los Angeles and San Francisco (Table 3). The population density of the five New York City counties considered in Table 3 is much higher than the density for the total of the nine San Francisco-area counties used in Table 3 or for Los Angeles County; however, the land area of the counties in Los Angeles and San Francisco are generally much larger than in New York City, and there are sub-county areas with high density in the two west-coast cities. For example, San Francisco County (one of the nine counties used to obtain the statistics for the San Francisco urban area in Table 3) has a population density of 7200 persons per km².

Similar to the case of Lazio and Lombardy in Italy, the large difference in outcomes between Los Angeles and San Francisco versus New York City is inconsistent with the predictions of spatially heterogeneous stochastic epidemic models. Davis et al. (2021), applying the stochastic, spatially heterogeneous GLEAM model to the spread of a global pandemic originating in Wuhan, China in November 2019, predict that Los Angeles, San Francisco, and New York City would all have had an equally high probability of generating 100 infections by February 21, 2020 (their Figure 1c, copied as our Figure 159).

To further investigate the different first-peak period P-score outcomes for different regions in the USA, we examined data regarding the location in which death occurred, including as an in-patient of a hospital, in a nursing home, or at the decedent's home. These results are presented in section 3.5.

The figures in section 3.5 show that, for the USA states with the highest integrated first-peak period P-scores, the location with the highest share of deaths was the hospital, whereas for the states with lowest integrated first-peak period P-scores, the location with the highest share of deaths was the decedent's home (Figure 56).

Similarly, states and counties with high integrated first-peak period P-scores had large increases in the share of deaths occurring in hospitals in March-May 2020 as compared to the same time period in 2019. The same states and counties had large decreases in the share of deaths occurring at home in March-May 2020 compared to the same time period in 2019 (Figure 57 to Figure 59). Conversely, states and counties with low integrated first-peak period P-scores had increased shares of deaths occurring at home in March-May 2020 compared to the same time period in 2019, and decreased shares of deaths occurring in hospital in March-May 2020 compared to the same time period in 2019 (Figure 57 to Figure 59).

Most states and counties with high integrated first-peak period P-scores also had an increase in the share of deaths occurring in nursing homes (Figure 57, Figure 60 to Figure 63).

There was thus a disproportionate number of deaths that occurred in hospitals (or in nursing homes in some states or counties, such as Rhode Island) in the hotspots of excess mortality in March-May 2020 in the United States. This echoes the situation for the Italian hotspot regions discussed in section 4.4.1.

Like in Lombardy, New York City surged its intensive care beds and admissions, and systematically applied mechanical ventilation, with high mortality rates (Nishikimi et al., 2022). An April 2020 study of COVID-19 patients treated by New York City area hospitals found that among the 2634 patients in the study who were discharged or died, 14.2% (373 patients) were treated in an ICU and 12.2% (320 patients) were placed on mechanical ventilation. Of those placed on mechanical ventilation, 88.1% (282 patients) died. Among patients who were put on mechanical ventilators, patients aged 18–65 had a mortality rate of 76.4% and patients aged 65+ had a mortality rate of 97.2% (Richardson et al., 2020). A separate study of 1966 mechanically ventilated COVID-19 patients in New York City hospitals during March and April 2020 found that 61% died within 28 days of intubation (Nishikimi et al., 2022).

Like in Lombardy, untested ventilation methods were used in New York City, including the use of anesthesia machines for ventilation, or treating two patients with a single ventilator ("ventilator sharing") (Beitler et al., 2020). Ventilator sharing for patients with acute respiratory distress syndrome had no precursor in the scientific literature prior to Covid (Hess et al., 2020), and several medical professional societies in the USA issued a joint statement warning against this practice due to its potential hazards in March 2020 (ASA et al., 2020; Cook, 2020).

Also, similar to the case of Italy, USA states that did not make expanding ICU capacity a significant part of their health care system response experienced much lower first-peak period excess mortality (Mathews et al., 2021).

The remarkable difference in first-peak period P-scores in different regions of the USA with similar demographics and health care systems, and which received similar volumes of flights from China and East Asia (here New York City compared to Los Angeles and San Francisco) is most plausibly explained by a significant difference in treatment, rather than a novel and virulent pathogen that spreads from human-to-human contact but which would have arrived by air only in New York City and not in other large cities with similar populations and air traffic.

The large difference in New York City vs Los Angeles and San Francisco first-peak period P-scores is incompatible with the paradigm of a spreading pandemic-causing respiratory virus (section 3.4), and the large P-scores for New York City appear to have been caused in large part by increased deadly ICU measures, especially widespread and often experimental mechanical ventilation, which is the same circumstances as in the Milan, Italy hotspot.

4.4.3 Other European countries

Like Lombardy and New York City, the UK made extensive use of mechanical ventilators, with high mortality rates (Mahase, 2020; Wunsch, 2020; Torjesen, 2021; Mcrae & Watson, 2023). The same is true for Belgium (Taccone et al., 2021; de Terwangne et al., 2021), whose capital region (BE10, Brussels) also stands out for having high population density and a high integrated

first-peak period P-score in Figure 138. In Spain, mechanical ventilators were also frequently used for COVID-19 patients in ICUs (Redondo-Bravo et al., 2020).

Another significant contributor to first-peak period excess mortality in Spain may have been from treating patients with a combination of the anti-malarial drug hydroxychloroquine (HCQ) and the antibiotic azithromycin (AZM).

The combination of HCQ with AZM was proposed as a treatment for COVID-19 in a paper by Professor Didier Raoult and co-authors published in the *International Journal of Microbial Agents* on March 20, 2020 (the “Raoult paper”) (Gautret et al., 2020). The Raoult paper was highly publicized and the treatment was used in many countries around the world (Accinelli et al., 2021; Hentschke-Lopes et al., 2022; Rich, 2020). However, the combination of HCQ and AZM was subsequently found to have significant health risks.

For example, the combination of HCQ with AZM was associated with a significant increase in the risk of 30-day cardiovascular mortality or heart failure in a study of almost one million rheumatoid arthritis patients (Lane et al., 2020), and HCQ with AZM was associated with increased mortality in a systematic review and meta-analysis of patients diagnosed with COVID-19 (Fiolet et al., 2021).

The Raoult paper was retracted by the journal on December 26, 2024 (Gautret et al., 2025).

HCQ was widely used as a COVID-19 treatment in Spain during March-May 2020, with clinical studies reporting HCQ exposure ranging from 65% to 92% (Pradelle et al., 2024a; Gutiérrez-Abejón et al., 2020; Martínez-Sanz et al., 2021; Pérez-Belmonte et al., 2020; Gil-Rodrigo et al., 2020; Casas-Rojo et al., 2020; Núñez-Gil et al., 2020; Prats-Urbe et al., 2021).

AZM use also skyrocketed in Spain during March 2020, as the number of AZM tablets consumed in Spanish hospitals in March 2020 was more than four times its level for the month of March in 2017, 2018, or 2019, and more than three times its maximum for any month in the years 2017-2019, as can be seen in Figure 167 (right panel), which is a copy of Figure 1 from Gonzalez-Zorn (2021).

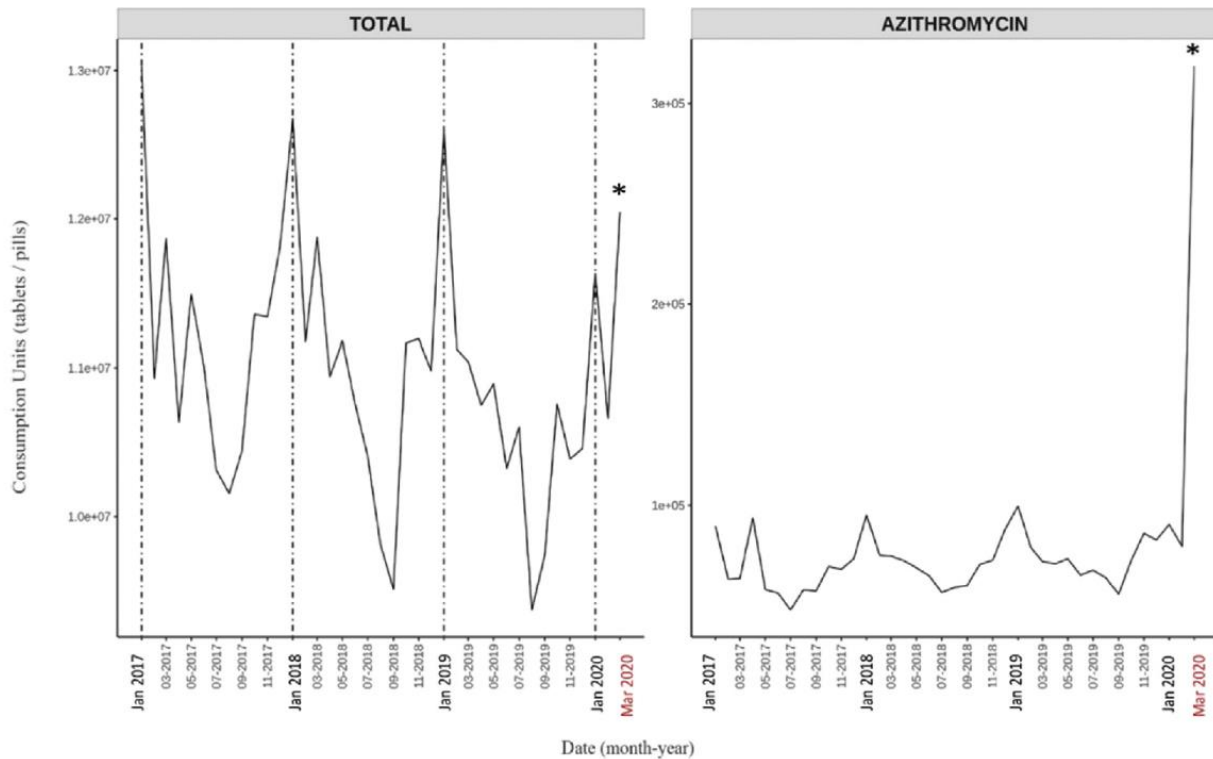


Figure 167: Copy of Figure 1 from Gonzalez-Zorn (2021). The original caption has: “Fig. 1. Use of antibiotics in Spanish hospitals from January 2017 to 31 March 2020. Total intrahospital antibiotic (left) and azithromycin (right) use show consumption peaks in March 2020 during the coronavirus disease 2019 (COVID-19) pandemic. [...]”.

HCQ itself has a narrow therapeutic index (Mackenzie 1983; Doyno et al., 2020; Bailey & Köhnlein, 2020), meaning that a toxic dosage of HCQ is not much larger than the normally recommended therapeutic dosage. HCQ is “extremely toxic in overdose” (Juurlink, 2020), which can cause central nervous system toxicity and lethal heart arrhythmias (Bailey & Köhnlein, 2020; Marquardt & Albertson, 2001; Juurlink, 2020).

Clinical studies conducted in 2020 on the effect of HCQ in patients diagnosed with COVID-19 used doses of HCQ that were considered to be surprisingly high by clinicians (Lacout et al., 2021) and potentially in the fatal range (Bailey & Köhnlein, 2020; Puliye, 2020). For example, the large Randomised Evaluation of Covid-19 Therapy (RECOVERY) trial in the UK used a dosage of 2400 mg on the first day, followed by 800 mg per day for the next 9 days or until discharge (RECOVERY Collaborative Group, 2020) whereas the normal dose is 200-400 mg per day (NHS, 2022). RECOVERY involved all major UK hospitals, 3500 medical professionals, and at least 11,000 patients assigned to different study arms (Wise & Coombes, 2020). Watson et al. (2020) evaluated dosage toxicity in clinical trials in which either chloroquine (CQ) or HCQ was used as a treatment for COVID-19. One clinical trial using CQ (Borba et al., 2020) and another trial using HCQ (the “PATCH” trial) were found to have a significant risk of dangerous toxicity (Watson et al., 2020). The Borba et al. (2020) trial was stopped early due to cardiac toxicity and higher

mortality in the high dose group (Watson et al., 2020). Watson et al. (2020) predicted the dosage used by the RECOVERY trial to be in the safe range.

One might infer that, in the frenzied context of the early stage of the declared COVID-19 pandemic, in which the medical establishment rushed to find treatments for the alleged novel disease, clinicians would have been less restrained than normal in prescribing exceptional high single and cumulative doses of the well-known, widely available, and inexpensive medications HCQ and CQ, which had received high-profile media and governmental attention, potentially causing many fatal overdoses.

A systematic review and meta-analysis by Pradelle et al. estimated approximately 2000 HCQ-related deaths in Spain (median estimate of 1895 with range of 1475-2094) (Pradelle et al., 2024a). The Pradelle et al. article was retracted by the journal *Biomedicine and Pharmacotherapy* in October 2024, on the journal's stated basis that there were issues with the reliability and choice of data, in particular the Belgian dataset used in the article, and that an assumption that all patients that entered the clinic were treated the same pharmacologically was incorrect (Pradelle et al., 2024b).

The overuse of sedatives was also, generally, a feature of Covid response.

Covid restrictions on patients and long-term care residents (including: disrupted general care such as hydration, disrupted treatments for pain and comorbidities, COVID-19 treatments, testing, restraints, social isolation and quarantine without family, immobilization, and sleep disruption) are significant risk factors for delirium. A large resulting increase in the incidence of delirium was predicted and was anticipated to potentially lead to a grave problem of over-sedation, especially given the challenges in applying the established clinical practice guidelines for delirium prevention due to pandemic measures (Kotfis et al., 2020; LaHue et al., 2020).

Sedatives such as midazolam or propofol, which are typically administered to mechanically ventilated patients in ICUs (Caballero et al., 2024; Marinella, 1997), have been suggested as possible contributors to excess mortality in France (Marliot et al., 2020; Chaillot, 2024) and the UK (Sy, 2024). Midazolam has been found to be associated with serious adverse effects in critically ill patients including "delayed awakening and extubation, longer mean ICU and hospital lengths of stay, a higher risk of delirium and cognitive dysfunction, and increased mortality." (Caballero et al., 2024). Prescription of sedatives including midazolam in ICUs increased to much higher levels than normal during the first-peak period (March-May 2020) in several countries (Marliot et al., 2020; Machado-Duque et al., 2022; Sy, 2024).

Prescribing of drugs such as antipsychotics, sedatives, antidepressants, anticonvulsants, and opioids was also significantly increased in long-term care homes in many countries during March-May 2020 (McDermid et al., 2023; Campitelli et al., 2021; Machado-Duque et al., 2022; Maxwell et al., 2024), including in the UK, where the increase in prescriptions was found to be disproportionately concentrated in one third of the sampled nursing homes, among which a

median value of 59% of residents per care home were prescribed antipsychotics in 2020-2022 (McDermid et al., 2023).

Overall, the hotspot countries of Spain and the UK, and other countries, had a high probability of overuse of dangerous and experimental pharmaceutical treatments during the first-peak period. This appears not to have been practiced in Germany (Bailey & Köhnlein, 2020), which had small or negligible first-peak period P-scores.

4.5 Socioeconomic characteristics of first-peak period mortality hotspots

Section 3.6.1 contains scatter plots for integrated first-peak period (March-May 2020) and integrated summer-peak period (June-September 2020) P-scores vs many different socioeconomic variables, for the counties of the USA having available data. These scatter plots are remarkable because they contain many hundreds of points and show much structure beyond simple unimodal trends.

4.5.1 *Integrated first-peak period P-scores vs socioeconomic variables for USA counties*

Regarding the first-peak period, the main result that emerges from the scatter plots is a strong correlation between increased integrated first-peak period P-score and increasing socioeconomic vulnerability for the counties in the New York City urban area.

The Pearson correlation coefficient, r , was greater than 0.7 for the counties in the four USA states with the highest state-level integrated first-peak period P-scores (NY, NJ, CT, and MA) for the following socioeconomic variables:

- % who speak English “less than well” (Figure 76, $r = 0.89$),
- $\log[\text{population density}]$ (Figure 67, $r = 0.85$),
- % minority (Figure 77, $r = 0.85$),
- % households with more people than rooms (Figure 74, $r = 0.83$),
- population (Figure 64, $r = 0.77$),
- $\log[\text{population}]$ (Figure 65, $r = 0.72$), and
- % living in housing structures with more than 10 units (Figure 75, $r = 0.72$).

For the counties with the highest integrated first-peak period P-scores (P-score > 100%), which are in the centre of the New York City urban area, including the five boroughs of New York City, there are also strong evident correlations with:

- % population living in poverty (Figure 69),
- % population aged 25+ with no high school diploma (Figure 78), and

- % households that are single-parent households (Figure 81).

Whereas integrated first-peak period P-score increased with increasing socioeconomic vulnerability for the counties in the New York City urban area, there were also many counties in other areas of the USA with similar or higher levels of socioeconomic vulnerability that had low or negligible integrated first-peak period P-scores. This creates a “two-branch” structure in many of the scatter plots, as described in section 3.6.1. For example, the percentage of people who speak English “less than well” (Figure 76) and the percentage minority (Figure 77) prominently show the said two-branch structure.

The presence of such a two-branch behaviour regarding integrated first-peak period P-score vs increasing socioeconomic vulnerability is a constraint on the hypothesis that a novel and virulent pathogen is responsible for excess mortality during the first-peak period (March-May 2020). That is, the presumed pathogen would be one that kills more with increasing poverty, crowded living conditions and other indicators of socioeconomic frailty of the population, but only in a few specific geographic locations within the same country, and not elsewhere.

4.5.2 Integrated summer-peak period P-score vs socioeconomic variables for USA counties

For the summer-peak period, the states with the highest P-scores were in the south of the country (Figure 134), particularly in counties on the border with Mexico in Texas (TX), Arizona (AZ), and California (CA), and counties along the southern Mississippi river (Figure 135).

The scatter plots for the summer-peak period (middle row of panels in Figure 64 to Figure 98) show that the counties with the highest integrated summer-peak period P-scores had high measures of socioeconomic vulnerability, including:

- low per capita income (Figure 68),
- high poverty (Figure 69),
- high prevalence of crowded living conditions (Figure 74),
- low rates of speaking English, especially for the counties near the Mexican border (Figure 76, map in Figure 111),
- high percentage minority (Figure 77),
- high percentage of the population aged 25+ with no high school diploma (Figure 78), and
- high rate of single-parent households (Figure 81).

Remarkably, the slopes of P-score vs socioeconomic parameter are very different, and much smaller, for the summer-peak period, compared to the first-peak period for counties in large-F-peak states. The presumed virus would need to give rise to qualitatively different sensitivities to

socioeconomic vulnerability in different states in late winter and nowhere give rise to the higher sensitivities in summer and fall.

4.5.3 Correlation between P-scores and degree of interaction with the medical system

Another striking result that emerges from the scatter plots in section 3.6.1 relates to the degree of interaction of the county's population with hospitals and the medical system.

For the counties in the NY-NJ-CT-MA states, especially the counties in the New York City urban area, there is a strong correlation between integrated first-peak period P-score and the share of deaths that occurred in hospital in March-May 2019 (Figure 88, $r = 0.52$ for all the NY-NJ-CT-MA counties with available data) or June-September 2019 (Figure 89, $r = 0.66$ for all the NY-NJ-CT-MA counties with available data).

There is an even stronger correlation ($r = 0.71$) for the NY-NJ-CT-MA counties when the change in share of deaths occurring in hospital from March-May 2019 to March-May 2020 is plotted on the x-axis (Figure 90).

Interestingly, the counties with high integrated summer-peak period P-scores in the southwestern USA in Texas (TX), New Mexico (NM), Arizona (AZ), and California (CA) had high shares of deaths occurring in hospital in June-September 2019 (Figure 89), and there is a striking correlation for the same said counties with the change in share of deaths occurring in hospital from June-September 2019 to June-September 2020 (Figure 91). In the middle row of panels in Figure 91, the scatter plot of integrated summer-peak period P-score vs the change in share of hospital deaths from 2019 to 2020 has a relatively small positive slope for values of the x-axis less than about 10%, and the slope increases dramatically above a value of around 10% on the x-axis.

As another indicator of the degree of interaction of a county's population with the medical system, or of the tendency for the county's population to seek or receive medical treatment, we examined vaccination uptake up to the end of 2021. This is shown in Figure 94 to Figure 97, where it can be seen that all counties with high integrated first-peak period or summer-peak period P-scores had high vaccination uptake in 2021.

Counties with the highest integrated first-peak period or summer-peak period P-scores thus had both high socioeconomic vulnerability and a high degree of interaction with the medical system. The role of hospitals in the first-peak period mortality catastrophe, and in subsequent COVID-era excess mortality events, should be examined further. We briefly consider this in relation to the urban New York City county of the Bronx, as follows.

4.5.4 The Bronx

The Bronx was the county with the highest integrated first-peak period P-score in the entire USA, with a value of $232.5\% \pm 7.4\%$. The Bronx is the poorest of the five boroughs of New York City, and it is also the poorest county in the New York City urban area and the NY-NJ-CT-MA states (see Figure 69, lower left panel: the Bronx can be easily identified as it is the county with the highest y-axis value (P-score) in the figure).

The Bronx has a high value of most socioeconomic vulnerability variables, including percentage of minority (non-white) residents (Figure 77), percentage of residents who speak English “less than well” (Figure 76) and percentage of people living in crowded living conditions (Figure 74).

The population of the Bronx has a high rate of underlying health conditions, including much higher rates of asthma than the rest of New York City (Simon & Ebbs, 2020; Maantay, 2007). The Bronx had the highest per capita rate of COVID testing of the five New York City boroughs in the spring of 2020 (Freytas-Tamura et al., 2020). A high per capita rate of COVID testing indicates both a higher resulting rate of dangerous medical interventions and a higher degree of contact with the medical establishment (testing occurs prior to death).

SBH Health System (formerly St. Barnabas Hospital) is a large low-budget safety-net hospital in the Bronx serving indigent residents, including those without medical insurance (Shabsigh, 2022; Clark & Shabsigh, 2022). SBH Health System increased its in-patient capacity by 50% and its critical-care capacity by more than 500% within three weeks in March and April of 2020, receiving many patients diagnosed with COVID-19 (Shabsigh, 2022).

Ventilators were applied to many patients at SBH Health System, as shown in Figure 168, which is a copy of Figure 10.1 from Babaev et al. (2022).

SBH Health System also made a large purchase of Hydroxychloroquine in the first quarter of 2020, and an increased purchase of Azithromycin, as shown in Figure 169, which is a copy of Figure 11.4 from Cassidy (2022).

Treatment with ventilators or with hydroxychloroquine plus azithromycin may have been responsible for a large portion of excess mortality in first-peak period hotspots, as discussed in section 4.4.3.

SBH also increased its purchases of Midazolam and Propofol in the first quarter of 2020 (Figure 169). As discussed above in section 4.4.3, both drugs are used for sedation of mechanically ventilated patients, and Midazolam in particular has been suggested as a possible contributor to excess mortality in several countries.

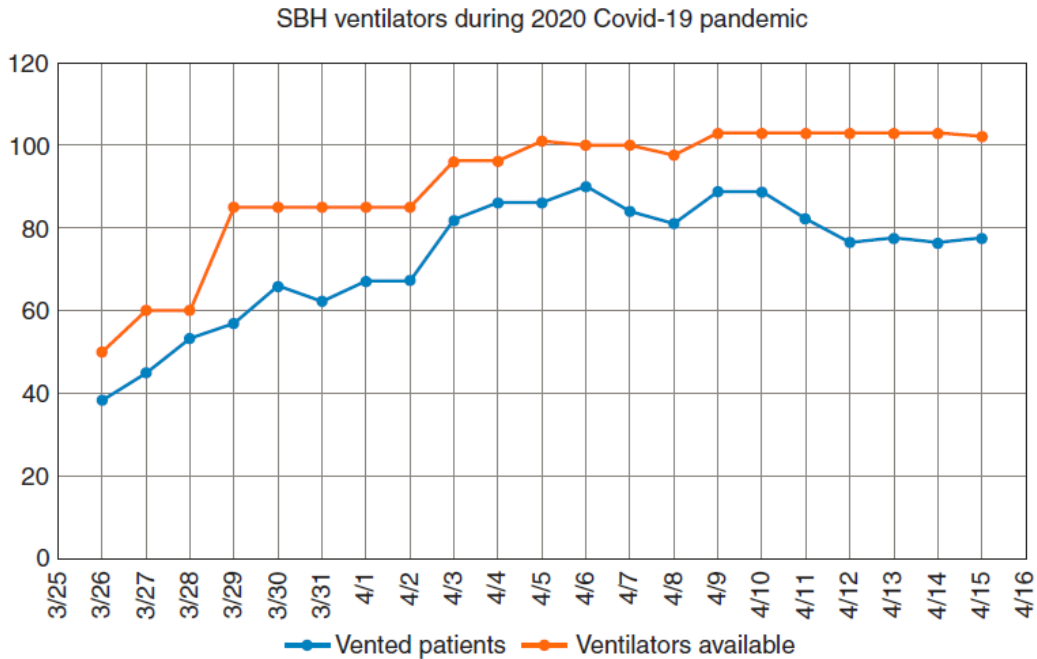


Figure 168: The number of available ventilators (orange) and patients on ventilators (blue) at SBH Health system in March and April 2020 [Copy of Figure 10.1 from Babaev et al. (2022)].

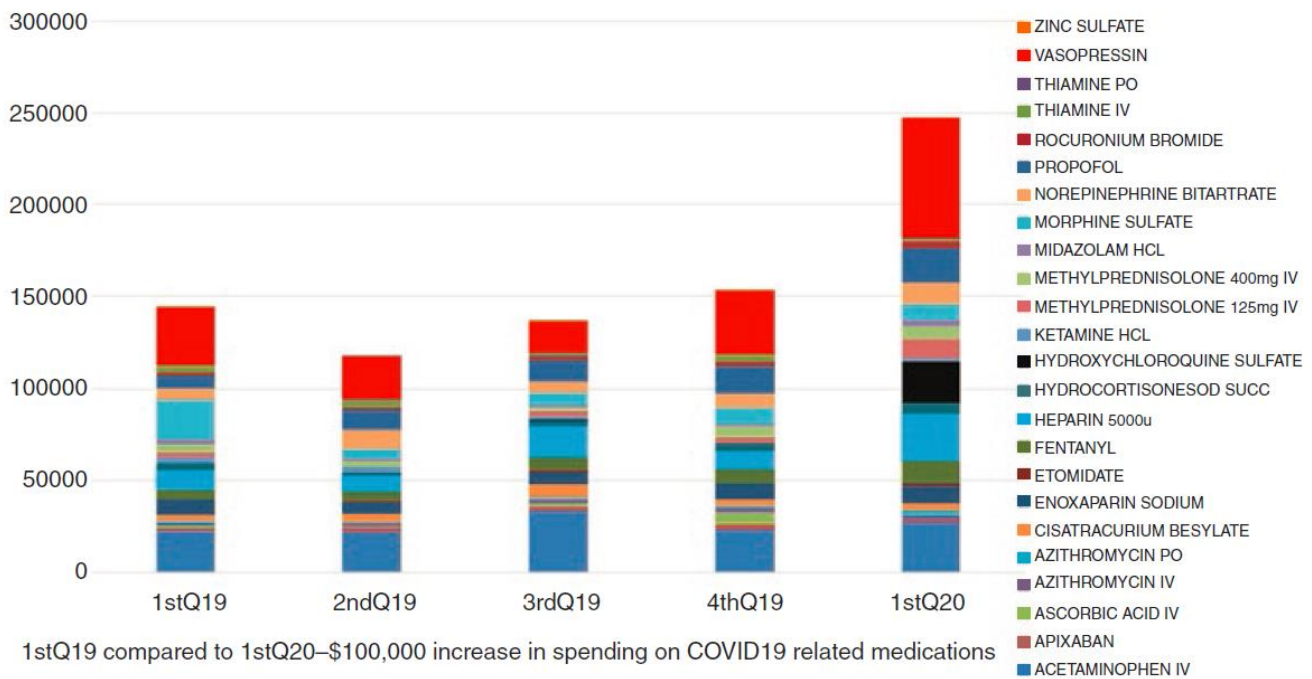


Figure 169: Increase in pharmacy expense during the pandemic in Q1 of 2020 at SBH Health System [Copy of Figure 11.4 from Cassidy (2022)].

Therefore, there is every indication that the exceptionally large age and frailty adjusted first-peak period mortality (P-score) for the Bronx, like for Milan, Italy, was from hospital procedures performed on disadvantaged populations in the catchment areas of large hospitals implementing open-access and patient-recruitment policies.

4.5.5 The role of large “safety net” hospital complexes in regions with high inequality

In addition to the high values of the socioeconomic vulnerability variables noted in the preceding section, The Bronx is also the county with the highest value of the inter-county disparity in the entire USA (Figure 72), due to its low per capita income and its adjacency to the high-per capita income borough of Manhattan (New York County, NY).

Large hospitals can exist in poor neighbourhoods that are in close proximity to rich neighbourhoods due, in part, to philanthropic organization and funding. It is possible that the combination of a large medical-system presence within a socioeconomically vulnerable population with a high rate of underlying health conditions, including respiratory conditions, resulted in many frail people being tested, attending hospital with a positive test, and subsequently perishing due to an arguably reckless application of dangerous treatments including invasive mechanical ventilation.

A potentially similar effect of excess mortality caused by large hospitals located in urban areas with high socioeconomic vulnerability and in proximity to wealthy populations may have occurred in London, UK.

The UK NUTS3 region with the highest integrated first-peak period P-score was the London borough of Brent (UKI72, in northwest London) (Figure 151; Figure 8). Similar to the Bronx, Brent has a high percentage of non-white residents (Brent is the darkest colored region on the map in Figure 156), and a high percentage of Brent’s population was born outside the UK (Figure 157).

Bordering Brent to the southeast is the borough of Westminster which had the third-highest integrated first-peak period P-score among UK NUTS3 regions (Figure 151). Despite its high gross disposable household income per capita (Figure 154), Westminster had the highest rate of poverty among London NUTS3 regions with available data (Figure 155). Westminster also has a high percentage of residents born outside the UK. Westminster and Brent are the two darkest colored regions on the map in Figure 157, Westminster being the one with a waterfront on the River Thames, which runs through London.

Northwick Park Hospital (NPH) is a major hospital located in Brent, serving “an ethnically and socioeconomically diverse population in Northwest London” (Goodall et al., 2020). NPH reportedly has the busiest emergency department among London hospitals (Keane, 2023; Williams, 2024).

The New York City borough of the Bronx and the London boroughs of Brent and Westminster are therefore examples of areas in which it may have been exceptionally dangerous to be poor or have low socioeconomic status while living near well-meaning wealthy people who donate to and support the establishment of large hospital complexes to serve their impoverished neighbours, possibly out of guilt or to avoid accountability given the palpable contrast in neighbouring and overlapping neighbourhoods. We might add medical professional zeal, and a lower barrier to provide experimental treatments, in institutions intended to serve the disadvantaged.

4.6 Pneumonia induced by biological stress of lockdown measures

In this subsection, following Rancourt (2024), we propose transmissionless self-infection bacterial pneumonias as a plausible proximal medical cause-of-death mechanism for the excess mortality in the F-peaks (“first peaks”, occurring March-May 2020), which consolidates and is consistent with three overarching observations:

- Many studies find that the excess all-ages all-cause mortality in the first-peak period is closely equal to assigned COVID-19 deaths in this period (e.g., Rancourt et al., 2021a, for the USA). That is, that the first-peak period excess deaths are associated with respiratory conditions.
- The geotemporal evolution of the F-peak excess mortality is inconsistent with the paradigm of a spreading viral respiratory disease, as discussed above in sections 4.2 and 4.3.
- A significant portion of first-peak period excess mortality may have been caused by the application of dangerous medical treatments in excess mortality hotspots such as New York City, Lombardy, Madrid, and London, as discussed above in sections 4.4 and 4.5.

Rancourt (2024) proposed that virtually all excess mortality during the Covid period (2020-2023) was caused by transmissionless self-infection bacterial pneumonias induced by biological stress (in the sense of medical researcher Hans Selye, which includes psychological stress) arising from the coordinated and largescale mandates, measures, so-called responses, and medical assaults including testing, diagnostic bias, isolation, denial of treatment (especially antibiotics for pneumonia), mechanical ventilation, sedation, experimental and improper treatments, and vaccination. This would include iatrogenic deaths of individuals treated for the said pneumonias. Exceptions would include younger individuals that died from accidental drug overdoses (e.g., fentanyl) and alcoholic liver disease.

Public health measures, including lockdowns and “shelter-in-place” policies, were severe during the first-peak period (March-May 2020) in excess mortality hotspots. Such measures — applied in a context of fear and panic stimulated by mass media and government pronouncements — subject many individuals to a high level of biological stress. In this state of elevated stress,

which results in immune response suppression, many individuals may have developed self-infection pneumonia, either via introduction of microbes into the respiratory system due to aspiration or via changes to the respiratory system microbiome itself without aspiration (Rancourt, 2024).

Socioeconomic vulnerability, including racial minority status and poverty, are important risk factors for bacterial pneumonia in the USA (Burton et al., 2010; Flory et al., 2009), which may explain the strong correlations between excess mortality P-scores and socioeconomic vulnerability in the USA counties with the largest integrated first-peak period P-scores. Poor or otherwise socioeconomically vulnerable individuals bore a disproportionate share of the negative stress burden of first-peak period lockdown measures. One need only compare remote-working middle and upper-middle class people living in spacious homes with private outdoor spaces with people confined to small apartments or isolated in care homes.

Therefore, our demonstration that the geotemporal evolution of first-peak period excess mortality P-scores is inconsistent with (i.e., disproves) the paradigm of a spreading pandemic-causing viral respiratory disease is nonetheless consistent with the majority of the excess deaths being associated with severe respiratory conditions, in a period when antibiotic treatment was often denied (Rancourt et al., 2021a).

5. Conclusion

Using high-resolution all-cause mortality data for Europe and the USA, we have shown that geotemporal mortality patterns during the early months of the declared SARS-CoV-2 pandemic are incompatible with the paradigm of a spreading viral respiratory disease.

It appears that the excess mortality could not have been caused by a viral pandemic. Instead,

- the essential synchrony (within weeks) in mortality hotspots (large “first peaks” or “F-peaks”) immediately following the WHO’s March 11, 2020 announcement of a pandemic, across countries and states on two continents in the Northern Hemisphere,
- the absence of a single F-peak-like excess mortality event (i.e., rise—peak—fall or rise—plateau) prior to the WHO’s March 11, 2020 declaration of a pandemic,
- the extreme geographical heterogeneity of the magnitude of any excess all-cause mortality as P-score in the time period (“first-peak period”) of the said hotspots,
- the striking differences in the occurrences of hotspots (presence or absence) in entirely comparable large cities in the same countries (Milan vs Rome in Italy; New York City vs Los Angeles and California in the USA),
- the systematic increases in shares of institutional (versus home) deaths in mortality hotspot jurisdictions, and

- the strong correlations to socioeconomic vulnerability of hotspot intensity in high-geographical-resolution sectors within hotspot urban regions,

suggest the alternative hypothesis that first-peak period excess mortality, where it occurs, was of institutional and iatrogenic origin, caused by mistreatment of frail and vulnerable people in hospitals and nursing homes.

In our extensive Discussion (section 4), we compared our results regarding all-cause mortality P-scores (excess number of deaths divided by expected number of deaths for a time-period, expressed as a percent) with the predictions of large-scale spatial epidemic models, and found that the leading models predicted geotemporal infection and mortality patterns that are of a qualitatively different character than the observed P-scores. The observed geotemporally resolved P-scores are incompatible with the predictions of large-scale spatial epidemic models. We argued (sections 4.1.2, 4.2, and 4.3) that the known insufficiencies of the said models can only bolster our conclusion. Basically, spread must produce spread and pandemic contagiousness must produce widespread penetration, whereas we observe synchrony and both largescale and small-scale patchiness.

The empirical results presented herein provide hard constraints on any and all other contagious spread models. Any model or explanation regarding the cause of excess all-cause mortality during March-May 2020 must comply with our empirical results.

Our analysis of correlations between excess mortality P-scores and socioeconomic variables at the resolution of boroughs in New York City and London, UK exposes the striking observation that the most extreme first-peak period excess mortality occurred in neighbourhoods in which very poor or socioeconomically vulnerable people live in close proximity to very wealthy people. This was examined in some detail for New York City borough of The Bronx, and the London boroughs of Brent and Westminster, in sections 4.5.4 and 4.5.5. We propose that this may be due to the existence of large “safety-net” hospital complexes in poor neighbourhoods that are funded in large part by philanthropy of wealthy residents who live in nearby areas of the same city, such as within the same borough (Brent and Westminster) or in a neighbouring borough (Manhattan, which is adjacent to The Bronx). The same kind of circumstances were present in the Milan area of Italy, in which large hospitals recruited into turbo-charged ICU facilities from large catchments of poor and vulnerable clients. If you were poor, it appears it was especially dangerous to live near well-meaning wealthy social classes offering large-hospital facilities.

This means that the paradigm that a spreading viral respiratory disease caused the excess mortality during Covid is false. The said paradigm is disproved by empirical observations of high-resolution (weekly-monthly, county-region) geotemporal variations of age and frailty adjusted excess mortality (P-score) on two continents in the Northern Hemisphere.

Instead, the excess mortality appears to be entirely iatrogenic and induced by the imposed so-called pandemic response.

Therefore, if this is correct, any comments about circulating viruses or variants (e.g., based on PCR or antibody tests of bodily fluids), whether true or false, are irrelevant to the excess mortality.

It is time to acknowledge that a paradigm shift may be necessary, and to adjust epidemiological thinking accordingly.

6. References

Aarstad & Kvitastein, 2023: Aarstad J, Kvitastein OA. Is there a Link between the 2021 COVID-19 Vaccination Uptake in Europe and 2022 Excess All-Cause Mortality? *Asian Pacific Journal of Health Science*. 2023;10:25-31. <https://doi.org/10.21276/apjhs.2023.10.1.6>.

Accinelli et al., 2021: Accinelli RA, Ynga-Meléndez GJ, León-Abarca JA, López LM, Madrid-Cisneros JC, Mendoza-Saldaña JD. *Travel Med Inf Dis*. 2021;44:102163. <https://doi.org/10.1016/j.tmaid.2021.102163>.

Achilleos, S. et al., 2021: Achilleos S, Quattrocchi A, Gabel J, Heraclides A, Kolokotroni O, Constantinou C, et al. Excess all-cause mortality and COVID-19-related mortality: a temporal analysis in 22 countries, from January until August 2020. *Int J Epidemiol*. 2022;51:35-53. <https://doi.org/10.1093/ije/dyab123>.

Ackley et al., 2021: Ackley CA, Lundberg DJ, Ma L, Ela IT, Preston SH, Stokes AC. County-level estimates of excess mortality associated with COVID-19 in the United States. *SSM - Population Health*. 2022;17:101021. <https://doi.org/10.1016/j.ssmph.2021.101021>.

Acosta et al., 2022: Acosta RJ, Patnaik B, Buckee C, Kiang MV, Irizarry RA, Balsari S, et al. All-cause excess mortality across 90 municipalities in Gujarat, India, during the COVID-19 pandemic (March 2020-April 2021). *PLOS Glob Public Health*. 2022;2:e0000824. <https://doi.org/10.1371/journal.pgph.0000824>.

Al Wahaibi et al., 2021: Al Wahaibi A, Al-Maani A, Alyaquobi F, Al Harthy K, Al-Jardani A, Al Rawahi B, et al. Effects of COVID-19 on mortality: A 5-year population-based study in Oman. *Int J Infect Dis*. 2021;104:102-107. <https://doi.org/10.1016/j.ijid.2020.12.054>.

Alessandria et al., 2025: Alessandria M, Malatesta G, Di Palmo G, Cosentino M, Donzelli A. All-cause mortality according to COVID-19 vaccination status: An analysis of the UK office for National statistics public data [version 2; peer review: 2 approved]. *F1000Research*. 2025;13:886. <https://doi.org/10.12688/f1000research.154058.2>.

Alteri et al., 2021: Alteri C, Cento V, Piralla A, Costabile V, Tallarita M, Colagrossi L, et al. Genomic epidemiology of SARS-CoV-2 reveals multiple lineages and early spread of SARS-CoV-2 infections in Lombardy, Italy. *Nat Commun.* 2021;12:434. <https://doi.org/10.1038/s41467-020-20688-x>.

Amaro, 2020: Amaro S. Germany seals off borders as European countries report record jump in coronavirus deaths. *CNBC*. 16 March 2020. Accessed on 2024-10-01 from: <https://www.cnbc.com/2020/03/16/coronavirus-update-germany-seven-other-eu-countries-close-borders.html> [Archived at: <https://archive.is/j9RX7>].

American Thoracic Society, 2005: American Thoracic Society. Guidelines for the Management of Adults with Hospital-acquired, Ventilator-associated, and Healthcare-associated Pneumonia. *Am J Respir Crit Care Med.* 2005;171:388–416. <https://doi.org/10.1164/rccm.200405-644ST>.

Anand et al., 2021: Anan A, Sandefur J, Subramanian A. Three New Estimates of India's All-Cause Excess Mortality during the COVID-19 Pandemic. *CGD Working Paper 589*. Washington, DC: Center for Global Development. Accessed on 2025-03-12 from: <https://cgdev.org/publication/three-new-estimates-indias-all-cause-excess-mortality-during-covid-19-pandemic>.

Apolone et al., 2021: Apolone G, Montomoli E, Manenti A, Boeri M, Sabia F, Hyseni I, et al. Unexpected detection of SARS-CoV-2 antibodies in the prepandemic period in Italy. *Tumori J.* 2021;107:446-451. <https://doi.org/10.1177/0300891620974755>.

ASA et al., 2020: Joint Statement on Multiple Patients Per Ventilator. *American Society of Anesthesiologists*. 25 March 2020. Accessed 2025-05-08 from: <https://www.asahq.org/about-asa/newsroom/news-releases/2020/03/joint-statement-on-multiple-patients-per-ventilator>.

ATSDR, 2024: Agency for Toxic Substances and Disease Registry. SVI Data & Documentation Download. Accessed on 2024-10-31 from: https://www.atsdr.cdc.gov/placeandhealth/svi/data_documentation_download.html.

Aune et al., 2023: Aune KT, Grantz KH, Menezes NP, Robsky KO, Gurley ES, Marx MA, et al. Demographic and Geographic Characterization of Excess Mortality During the COVID-19 Pandemic in Baltimore City, Maryland, March 2020 to March 2021. *American Journal of Epidemiology.* 2024 Feb 1;193(2):267–76.

Babaev et al., 2022: Babaev A, Martin-Johnson T, Klion M. Respiratory therapy and proning. In: Shabsigh R, editor. *Health crisis management in acute care hospitals: Lessons learned from COVID-19 and beyond*. Cham: Springer; 2022. pp. 165-182. <https://link.springer.com/book/10.1007/978-3-030-95806-0>.

- Bailey & Köhnlein, 2020: Bailey S, Köhnlein C. PCR Pandemic: Interview with Virus Mania's Dr Claus Köhnlein. 26 October 2020. Accessed 2025-05-07 from: <https://odysee.com/@drsambailey:c/pcr-pandemic-interview-with-virus-mania:9>.
- Bajardi et al., 2011: Bajardi P, Poletto C, Ramasco JJ, Tizzoni M, Colizza V, Vespignani A. Human Mobility Networks, Travel Restrictions, and the Global Spread of 2009 H1N1 Pandemic. PLOS One. 2011;6:e16591. <https://doi.org/10.1371/journal.pone.0016591>.
- Balcan et al., 2010: Balcan D, Gonçalves B, Hu H, Ramasco JJ, Colizza V, Vespignani A. Modeling the spatial spread of infectious diseases: The GLobal Epidemic and Mobility computational model. J Comput Sci. 2010;1:132-145. <https://doi.org/10.1016/j.jocs.2010.07.002>.
- Basellini & Camarda, 2022: Basellini U, Camarda CG. Explaining regional differences in mortality during the first wave of Covid-19 in Italy. Population Studies. 2022;76:99-118. <https://doi.org/10.1080/00324728.2021.1984551>.
- Beitler et al., 2020: Beitler JR, Mittel AM, Kallet R, Kacmarek R, Hess D, Branson R, et al. Ventilator Sharing during an Acute Shortage Caused by the COVID-19 Pandemic. Am J Resp Crit Care Med. 2020;202:600-604. <https://doi.org/10.1164/rccm.202005-1586LE>.
- Bilinski & Emanuel, 2020: Bilinski A, Emanuel EJ. COVID-19 and Excess All-Cause Mortality in the US and 18 Comparison Countries. JAMA. 2020;324(20):2100–2102. doi:10.1001/jama.2020.20717. <https://jamanetwork.com/journals/jama/fullarticle/2771841>.
- Bilinski et al., 2023: Bilinski A, Thompson K, Emanuel E. COVID-19 and Excess All-Cause Mortality in the US and 20 Comparison Countries, June 2021-March 2022. JAMA. 2023;329:92–94. <https://doi.org/10.1001/jama.2022.21795>.
- Boccia et al., 2020: Boccia S, Ricciardi W, Ioannidis JPA. What Other Countries Can Learn From Italy During the COVID-19 Pandemic. JAMA Intern Med. 2020;180(7):927-928. <https://doi.org/10.1001/jamainternmed.2020.1447>.
- Bonnet et al., 2024: Bonnet F, Grigoriev P, Sauerberg M, Alliger I, Mühlichen M, Camarda CG. Spatial Variation in Excess Mortality Across Europe: A Cross-Sectional Study of 561 Regions in 21 Countries. Journal of Epidemiology and Global Health. 2024 Jun 1;14(2):470–9.
- Borba et al., 2020: Borba M, Val F, Sampaio V, Alexandre M, Melo G, Brito M, et al. Effect of High vs Low Doses of Chloroquine Diphosphate as Adjunctive Therapy for Patients Hospitalized With Severe Acute Respiratory Syndrome Coronavirus 2 (SARS-CoV-2) Infection: A Randomized Clinical Trial. JAMA Network Open. 2020;3:e208857. <https://doi.org/10.1001/jamanetworkopen.2020.8857>.
- Bosa et al., 2021: Bosa I, Castelli A, Castelli M, Ciani O, Compagni A, Galizzi MM, et al. Corona-regionalism? Differences in regional responses to COVID-19 in Italy. Health Policy. 2021;125:1179-1187. <https://doi.org/10.1016/j.healthpol.2021.07.012>.

Böttcher et al., 2021: Böttcher L, D'Orsogna MR, Chou T. Using excess deaths and testing statistics to determine COVID-19 mortalities. *Eur J Epidemiol.* 2021;36:545–558.

<https://doi.org/10.1007/s10654-021-00748-2>.

Bottiroli et al., 2021: Bottiroli M, Calini A, Pinciroli R, Mueller A, Siragusa A, Anelli C, et al. The repurposed use of anesthesia machines to ventilate critically ill patients with coronavirus disease 2019 (COVID-19). *BMC Anesthesiology.* 2021;21:155. <https://doi.org/10.1186/s12871-021-01376-9>.

<https://doi.org/10.1186/s12871-021-01376-9>.

Bouadma et al., 2015: Bouadma L, Sonnevile R, Garrouste-Orgeas M, Darmon M, Souweine B, Voiriot G, et al. Ventilator-Associated Events: Prevalence, Outcome, and Relationship With Ventilator-Associated Pneumonia. *Critical Care Medicine.* 2015;43:1798-1806.

<https://doi.org/10.1097/CCM.0000000000001091>.

Brockmann & Helbing, 2013: Brockmann D, Helbing D. The Hidden Geometry of Complex, Network-Driven Contagion Phenomena. *Science.* 2013;342:1337.

<https://doi.org/10.1126/science.1245200>.

Burton et al., 2010: Burton DC, Flannery B, Bennett NM, Farley MM, Gershman K, Harrison LH, et al. Socioeconomic and Racial/Ethnic Disparities in the Incidence of Bacteremic Pneumonia Among US Adults. *American Journal of Public Health.* 2010;100:1904-1911.

<https://doi.org/10.2105/AJPH.2009.181313>.

Bustos Sierra et al., 2020: Bustos Sierra N, Bossuyt N, Braeye T, Leroy M, Moyersoen I, Peeters I, et al. All-cause mortality supports the COVID-19 mortality in Belgium and comparison with major fatal events of the last century. *Arch Public Health.* 2020;78:117.

<https://doi.org/10.1186/s13690-020-00496-x>.

Caballero et al., 2024: Caballero J, García-Sánchez M, Vich JG-E. Current role of midazolam in the sedation of the ventilated critically ill patient: against. *Medicina Intensiva.* 2024;48:177-179.

<https://doi.org/10.1016/j.medin.2023.10.004>.

Campitelli et al., 2021: Campitelli MA, Bronskill SE, Maclagan LC. Comparison of Medication Prescribing Before and After the COVID-19 Pandemic Among Nursing Home Residents in Ontario, Canada. *JAMA Network Open.* 2021;4:e2118441.

<https://doi.org/10.1001/jamanetworkopen.2021.18441>.

Capano & Lippi, 2021: Capano G, Lippi A. Decentralization, policy capacities, and varieties of first health response to the COVID-19 outbreak: evidence from three regions in Italy. *Journal of European Public Policy.* 2021;28:1197-1218. <https://doi.org/10.1080/13501763.2021.1942156>.

Casas-Rojo et al., 2020: Casas-Rojo JM, Antón-Santos JM, Millán-Núñez-Cortés J, Lumbreras-Bermejo C, Ramos-Rincón JM, Roy-Vallejo E, et al. Clinical characteristics of patients hospitalized with COVID-19 in Spain: results from the SEMI-COVID-19 Registry. *Rev Clin Esp.* 2020;220:480-494. <https://doi.org/10.1016/j.rceng.2020.07.003>.

<https://doi.org/10.1016/j.rceng.2020.07.003>.

Cassidy, 2022: Cassidy RE. Pharmacy. In: Shabsigh R, editor. Health crisis management in acute care hospitals: Lessons learned from COVID-19 and beyond. Cham: Springer; 2022. pp. 183-200. <https://link.springer.com/book/10.1007/978-3-030-95806-0>.

CDC, 2024a: Centers for Disease Control and Prevention. Weekly Counts of Deaths by Jurisdiction and Age. Accessed on 2024-02-13 from: https://data.cdc.gov/NCHS/Weekly-Counts-of-Deaths-by-Jurisdiction-and-Age/y5bj-9g5w/about_data.

CDC, 2024b: Centers for Disease Control and Prevention. National Center for Health Statistics Mortality Data on CDC WONDER. Accessed on 2024-02-15 from: <https://wonder.cdc.gov/mcd.html>.

CDC, 2024c: Centers for Disease Control and Prevention. US Diabetes Surveillance System Application. Accessed on 2024-10-29 from: <https://gis.cdc.gov/grasp/diabetes/diabetesatlas-surveillance.html>.

CDC, 2025. Centers for Disease Control and Prevention. COVID-19 Vaccinations in the United States, County. Accessed on 2025-01-05 from: https://data.cdc.gov/Vaccinations/COVID-19-Vaccinations-in-the-United-States-County/8xkx-amqh/about_data.

Cereda et al., 2021: Cereda D, Manica M, Tirani M, Rovida F, Demicheli V, Ajelli M, et al. The early phase of the COVID-19 epidemic in Lombardy, Italy. *Epidemics*. 2021;37:100528. <https://doi.org/10.1016/j.epidem.2021.100528>.

Chaillot, 2024: Chaillot P. Covid 19: Decoding Official Data: Mortality, tests, vaccines, hospitals. The truth emerges. Paris: L'Artilleur; 2024. ISBN-10: 2810012393, ISBN-13: 978-2810012398.

Chan et al., 2021: Chan EYS, Cheng D, Martin J. Impact of COVID-19 on excess mortality, life expectancy, and years of life lost in the United States. *PLOS ONE*. 2021;16(9):e0256835. <https://doi.org/10.1371/journal.pone.0256835>.

Chastre & Fagon, 2002: Chastre J, Fagon J-Y. Ventilator-associated Pneumonia. *Am J Respir Crit Care Med*. 2002;165:867-903. <https://doi.org/10.1164/rccm.2105078>.

Chinazzi et al., 2020: Chinazzi M, Davis JT, Ajelli M, Gioannini C, Litvinova M, Merler S, et al. The effect of travel restrictions on the spread of the 2019 novel coronavirus (COVID-19) outbreak. *Science*. 2020;368:395-400. <https://doi.org/10.1126/science.aba9757>.

Clark & Shabsigh, 2022: Clark S, Shabsigh R. Background, the hospital system, the patient community, and the Bronx. In: Shabsigh R, editor. Health crisis management in acute care hospitals: Lessons learned from COVID-19 and beyond. Cham: Springer; 2022. pp. 1-7. <https://link.springer.com/book/10.1007/978-3-030-95806-0>.

Coker et al., 2020: Coker ES, Cavalli L, Fabrizi E, Guastella G, Lippo E, Parisi ML, et al. The Effects of Air Pollution on COVID-19 Related Mortality in Northern Italy. *Environmental and Resource Economics*. 2020;76:611–634. <https://doi.org/10.1007/s10640-020-00486-1>.

Colizza et al., 2007: Colizza V, Barrat A, Barthelemy M, Valleron A-J, Vespignani A. Modeling the Worldwide Spread of Pandemic Influenza: Baseline Case and Containment Interventions. *PLOS Med.* 2007;4:e13. <https://doi.org/10.1371/journal.pmed.0040013>.

Cook, 2020: Cook DC. Implementing shared ventilation must be scientific and ethical, or it risks harm. *British Journal of Anesthesiology.* 2020;125:E181-E183. <https://doi.org/10.1016/j.bja.2020.04.061>.

Cooper et al., 2006: Cooper BS, Pitman RJ, Edmunds WJ, Gay NJ. Delaying the International Spread of Pandemic Influenza. *PLOS Med.* 2006;3:e212. <https://doi.org/10.1371/journal.pmed.0030212>.

Dahal et al., 2021: Dahal S, Banda JM, Bento AI, Mizumoto K, Chowell G. Characterizing all-cause excess mortality patterns during COVID-19 pandemic in Mexico. *BMC Infect Dis.* 2021;21:432. <https://doi.org/10.1186/s12879-021-06122-7>.

Das-Munshi et al., 2021: Das-Munshi J, Kuo Chang C, Bakolis I, Broadbent M, Dregan A, Hotopf M, et al. All-cause and cause-specific mortality in people with mental disorders and intellectual disabilities, before and during the COVID-19 pandemic: cohort study. *Lancet Reg Health Eur.* 2021;11:100228. <https://doi.org/10.1016/j.lanepe.2021.100228>.

Davis, 2006: Davis KA. Ventilator-Associated Pneumonia: A Review. *J Intensive Care Med.* 2006;21:211-226. <https://doi.org/10.1177/0885066606288837>.

Davis et al., 2021: Davis JT, Chinazzi M, Perra N, Mu K, Pastore y Piontti A, Ajelli M, et al. Cryptic transmission of SARS-CoV-2 and the first COVID-19 wave. *Nature.* 2021;600:127-132. <https://doi.org/10.1038/s41586-021-04130-w>.

de Boer et al., 2023: de Boer PT, van de Kasstele J, Vos ERA, van Asten L, Dongelmans DA, van Gageldonk-Lafeber AB, et al. Age-specific severity of SARS-CoV-2 in February 2020 – June 2021 in the Netherlands. *medRxiv.* 2023.02.09.23285703. <https://doi.org/10.1101/2023.02.09.23285703>.

de Freytas-Tamura et al., 2020: de Freytas-Tamura K, Hu W, Cook LR. “It’s the death towers”: How the Bronx became New York’s virus hot spot. *New York Times.* 26 May 2020. Accessed on 2025-02-04 from: <https://www.nytimes.com/2020/05/26/nyregion/bronx-coronavirus-outbreak.html>.

de Gier et al., 2023: de Gier B, van Asten L, Boere TM, van Roon A, van Roekl C, Pijpers J, et al. Effect of COVID-19 vaccination on mortality by COVID-19 and on mortality by other causes, the Netherlands, January 2021–January 2022. *Vaccine.* 2023;41:4488-4496. <https://doi.org/10.1016/j.vaccine.2023.06.005>.

de Terwangne et al., 2021: de Terwangne C, Sorgente A, Tortora R, Cheung D, Duprez F, Place S, et al. Mortality Rate and Predictors among Patients with COVID-19 Related Acute Respiratory Failure Requiring Mechanical Ventilation: A Retrospective Single Centre Study. *The Journal of Critical Care Medicine*. 2021;7:21-27. <https://doi.org/10.2478/jccm-2020-0043>.

Demetriou et al., 2023: Demetriou CA, Achilleos S, Qattrocchi A, Gabel J, Critselis E, Constantinou C, et al. Impact of the COVID-19 pandemic on total, sex- and age-specific all-cause mortality in 20 countries worldwide during 2020: results from the C-MOR project. *Int J Epidemiol*. 2023;52:664–676. <https://doi.org/10.1093/ije/dyac170>.

Department of Transportation, 2024: Department of Transportation. U.S. International Air Passenger and Freight Statistics. December 2020. Accessed on 2024-11-25 from: <https://www.transportation.gov/sites/dot.gov/files/2020-12/US%20International%20Air%20Passenger%20and%20Freight%20Statistics%20for%20December%202019.pdf>.

Deshmukh et al., 2021: Deshmukh Y, Suraweera W, Tumbe C, et al. Excess mortality in India from July 2020 to July 2021 during the COVID pandemic: death registration, health facility deaths, and survey data. *medRxiv* 2021.07.20.21260872. <https://doi.org/10.1101/2021.07.20.21260872>.

Docquier et al., 2022: Docquier F, Golenvaux N, Nijssen S, Schaus P, Stips F. Cross-border mobility responses to COVID-19 in Europe: new evidence from facebook data. *Globalization and Health*. 2022;18:41. <https://doi.org/10.1186/s12992-022-00832-6>.

Doyno et al., 2020: Doyno C, Sobieraj DM, Baker WL. Toxicity of chloroquine and hydroxychloroquine following therapeutic use or overdose. *Clinical Toxicology*. 2021;59:12-23. <https://doi.org/10.1080/15563650.2020.1817479>.

Eder et al., 2020: Eder S, Fountain H, Keller MH, Xiao M, Stevenson A. 430,000 people have traveled from China to U.S. since coronavirus surfaced. *New York Times*. 4 April 2020. Accessed on 2024-11-25 from: <https://www.nytimes.com/2020/04/04/us/coronavirus-china-travel-restrictions.html> [Archived at: <https://archive.is/8pjlN>].

ENAC, 2017: Ente Nazionale per l'Aviazione Civile. Traffic Data 2017. Sapia P, Di Agostino M, editors. Accessed on 2024-10-11 from: https://www.enac.gov.it/app/uploads/2024/04/ENAC_Traffic_data_2017_en.pdf.

ENAC, 2018: Ente Nazionale per l'Aviazione Civile. Traffic Data 2018. Sapia P, Di Agostino M, editors. Accessed on 2024-10-11 from: https://www.enac.gov.it/app/uploads/2019/06/ENAC_Traffic-data_2018.pdf.

ENAC, 2019: Ente Nazionale per l'Aviazione Civile. Dati di Traffico 2019. Dolci S, Sgrelli E, Petrini R, editors. Accessed on 2024-10-11 from: <http://web.unibas.it/donatociampa/wp-content/uploads/2020/09/ENAC-Dati-di-traffico-2019.pdf>.

Engler, 2022: Engler J. Were the unprecedented excess deaths curves in Northern Italy in spring 2020 caused by the spread of a novel deadly virus? A reassessment of the available evidence suggests another factor was involved. BizNews. 14 September 2022. Accessed on 2025-03-14 from: <https://www.biznews.com/health/2022/09/14/excess-deaths-healthcare-panic>. [See also: The Lombardy Analysis: Lombardy deaths in March 2020 reveal a pattern which seems difficult to explain by viral spread. *PANDA Uncut*, 22 August 2022. Accessed on 2025-03-12 from: <https://pandauncut.substack.com/p/the-lombardy-analysis>].

Epstein et al., 2007: Epstein JM, Goedecke DM, Yu F, Morris RJ, Wagener DK, Bobashev GV. Controlling Pandemic Flu: The Value of International Air Travel Restrictions. *PLOS One*. 2007;2:e401. <https://doi.org/10.1371/journal.pone.0000401>.

European Environment Agency, 2018: European Environment Agency. PM2.5 annual mean in 2018. Published 2020-09-09, Modified 2024-09-20. Accessed on 2024-10-11 from: <https://www.eea.europa.eu/en/analysis/maps-and-charts/pm2-5-annual-mean-in-2> [Archived at: <https://archive.is/OOuck>].

Eurostat, 2021: Eurostat. Commuting between regions. 10 June 2021. Accessed on 2024-10-01 from: <https://ec.europa.eu/eurostat/web/products-eurostat-news/-/ddn-20210610-1>.

Eurostat, 2024a: Eurostat. Deaths by week, sex and NUTS 3 region. Accessed on 2024-02-10 from: https://ec.europa.eu/eurostat/databrowser/view/DEMO_R_MWK3_TS/default/table?lang=en&category=demo.demomwk.

Eurostat, 2024b: Eurostat. Population on 1 January by NUTS 2 region. Accessed on 2024-10-07 from: <https://ec.europa.eu/eurostat/databrowser/view/tgs00096/default/table?lang=en>.

Eurostat, 2024c: Eurostat. Population density by NUTS 2 region. Accessed on 2024-02-26 from: <https://ec.europa.eu/eurostat/databrowser/view/tgs00024/default/table?lang=en>.

Eurostat, 2024d: Eurostat. At-risk-of-poverty rate by NUTS 2 region. Accessed on 2024-03-22 from: <https://ec.europa.eu/eurostat/databrowser/view/tgs00103/default/table?lang=en>.

Eurostat, 2024e: Eurostat. International road freight transport - loaded goods in reporting country by country of unloading and type of transport (t, tkm) - quarterly data. Accessed on 2024-10-02 from: https://ec.europa.eu/eurostat/databrowser/view/road_go_iq_ltt_custom_13116607/default/table?lang=en.

Eurostat, 2024f: Eurostat. International road freight transport - unloaded goods in reporting country by country of loading and type of transport (t, tkm) - quarterly data. Accessed on 2024-10-02 from:

https://ec.europa.eu/eurostat/databrowser/view/road_go_iq_utt/default/table?lang=en&category=road.road_go.road_go_int.

Eurostat, 2024g: Eurostat. Available beds in hospitals by NUTS 2 region. Accessed on 2024-10-11 from:

https://ec.europa.eu/eurostat/databrowser/view/hlth_rs_bdsrg2/default/table?lang=en&category=hlth.hlth_care.hlth_res.hlth_facil.

Eurostat, 2025: Eurostat. NUTS – NOMENCLATURE OF TERRITORIAL UNITS FOR STATISTICS. Accessed on 2025-01-17 from: <https://ec.europa.eu/eurostat/web/nuts>.

Fagioli et al., 2020: Fagioli S, Lorini FL, Remuzzi G. Adaptations and Lessons in the Province of Bergamo. *New England Journal of Medicine*. 2020;382:e71.

<https://doi.org/10.1056/NEJMc2011599>.

Faisant et al., 2024: Faisant M, Vincent N, Hubert B, le Tertre A. Regional excess mortality in France during COVID-19 pandemic: the first three epidemic periods (March 2020–June 2021). *European Journal of Public Health*. 2024 Jun 1;34(3):606–12.

Faust et al., 2021. Faust JS, Krumholz HM, Du C. All-Cause Excess Mortality and COVID-19–Related Mortality Among US Adults Aged 25–44 Years, March–July 2020. *JAMA*. 2020;325:785–787. <https://doi.org/10.1001/jama.2020.24243>.

Faust et al., 2022: Faust JS, Renton B, Chen AJ, Du C, Liang C, Li S-X, et al. Uncoupling of all-cause excess mortality from COVID-19 cases in a highly vaccinated state. *The Lancet*. 2022;22:1419–1420. [https://doi.org/10.1016/S1473-3099\(22\)00547-3](https://doi.org/10.1016/S1473-3099(22)00547-3).

Félix-Cardoso et al., 2020: Félix-Cardoso F, Vasconcelos H, Pereira Rodrigues P, Cruz-Correia R. Excess mortality during COVID-19 in five European countries and a critique of mortality data analysis. *medRxiv* 2020.04.28.20083147. <https://doi.org/10.1101/2020.04.28.20083147>.

Ferguson et al., 2006: Ferguson NM, Cummings DAT, Fraser C, Cajka JC, Cooley PC, Burke DS. Strategies for mitigating an influenza pandemic. *Nature*. 2006;442:448–452. <https://doi.org/10.1038/nature04795>.

Ferguson et al., 2020: Ferguson NM, Laydon D, Nedjati-Gilani G, Imai N, Ainslie K, Baguelin M, et al. Report 9: Impact of non-pharmaceutical interventions (NPIs) to reduce COVID-19 mortality and healthcare demand. MRC Centre for Global Infectious Disease Analysis, Imperial College London. 16 March 2020. Accessed 2025-04-30 from: <https://www.imperial.ac.uk/mrc-global-infectious-disease-analysis/disease-areas/covid-19/report-9-impact-of-npis-on-covid-19/>.

Fiolet et al., 2021: Fiolet T, Guihur A, Rebeaud ME, Mulot M, Peiffer-Smadja N, Mahamat-Saleh Y. Effect of hydroxychloroquine with or without azithromycin on the mortality of coronavirus disease 2019 (COVID-19) patients: a systematic review and meta-analysis. *Clin Microbiol Inf.* 2021;27:19-27. <https://doi.org/10.1016/j.cmi.2020.08.022>.

Financial Mirror, 2020: Financial Mirror. Cyprus melted under hottest May on record. *Financial Mirror*. 4 June 2020. Accessed 2025-04-17 from: <https://www.financialmirror.com/2020/06/04/cyprus-melted-under-hottest-may-on-record/>.

Flory et al., 2009: Flory JH, Joffe M, Fishman NO, Edelstein PH, Metlay JP. Socioeconomic risk factors for bacteraemic pneumococcal pneumonia in adults. *Epidemiol Infect.* 2009;137:717-726. <https://doi.org/10.1017/S0950268808001489>.

Foster et al., 2024: Foster TB, Fernandez L, Porter SR, Pharris-Ciurej N. Racial and Ethnic Disparities in Excess All-Cause Mortality in the First Year of the COVID-19 Pandemic. *Demography*. 2024 Feb 1;61(1):59–85.

Fouillet et al., 2020: Fouillet A, Pontais I, Caserio-Schönemann C. Excess all-cause mortality during the first wave of the COVID-19 epidemic in France, March to May 2020. *Euro Surveill.* 2020;25:2001485. <https://doi.org/10.2807/1560-7917.ES.2020.25.34.2001485>.

Gallo et al., 2021: Gallo E, Prosepe I, Lorenzoni G, Akar AS, Lanera C, Berchiolla P, et al. Excess of all-cause mortality is only partially explained by COVID-19 in Veneto (Italy) during spring outbreak. *BMC Public Health.* 2021;21:797. <https://doi.org/10.1186/s12889-021-10832-7>.

Gattinoni et al., 2017: Gattinoni L, Marini JJ, Collino F, Maiolo G, Rapetti F, Tonetti T, et al. The future of mechanical ventilation: lessons from the present and the past. *Critical Care.* 2017;21:183. <https://doi.org/10.1186/s13054-017-1750-x>.

Gautret et al., 2020: Gautret P, Lagier J-C, Parola P, Hoang VT, Meddeb L, Mailhe M, et al. Hydroxychloroquine and azithromycin as a treatment of COVID-19: results of an open-label non-randomized clinical trial. *Int J Antimicrob Agents.* 2020;56:105949. <https://doi.org/10.1016/j.ijantimicag.2020.105949>.

Gautret et al., 2025: Gautret P, Lagier J-C, Parola P, Hoang VT, Meddeb L, Mailhe M, et al. Retraction notice to “Hydroxychloroquine and azithromycin as a treatment of COVID-19: results of an open-label non-randomized clinical trial” [International Journal of Antimicrobial Agents 56 (2020), 105949]. *Int J Antimicrob Agents.* 2025;65:107416. <https://doi.org/10.1016/j.ijantimicag.2024.107416>.

Ghaznavi et al., 2022: Ghaznavi C, Eguchi A, Tanoue Y, Yoneoka D, Kawashima T, Suzuki M, et al. Pre- and post-COVID-19 all-cause mortality of Japanese citizens versus foreign residents living in Japan, 2015–2021. *SSM - Population Health.* 2022;18:101114. <https://doi.org/10.1016/j.ssmph.2022.101114>.

Gil-Rodrigo et al., 2020: Gil-Rodrigo A, Miró Ò, Piñera P, Burillo-Putze G, Jiménez S, Martín A, et al. Analysis of clinical characteristics and outcomes in patients with COVID-19 based on a series of 1000 patients treated in Spanish emergency departments. *Emergencias*. 2020;32:233-241.

Gilbertoni et al., 2021: Gilbertoni D, Adja KYC, Golinelli D, Reno C, Regazzi L, Lenzi J, et al. Patterns of COVID-19 related excess mortality in the municipalities of Northern Italy during the first wave of the pandemic. *Health and Place*. 2021;67:102508.
<https://doi.org/10.1016/j.healthplace.2021.102508>.

Gobiņa et al., 2022: Gobiņa I, Avotiņš A, Kojalo U, Strēle I, Pildava S, Villeruša A, et al. Excess mortality associated with the COVID-19 pandemic in Latvia: a population-level analysis of all-cause and noncommunicable disease deaths in 2020. *BMC Public Health*. 2022;22:1109.
<https://doi.org/10.1186/s12889-022-13491-4>.

Gonzalez-Zorn, 2021: Gonzalez-Zorn B. Antibiotic use in the COVID-19 crisis in Spain. *Clin Microbiol Inf*. 2021;27:646-647. <https://doi.org/10.1016/j.cmi.2020.09.055>.

Goodall et al., 2020: Goodall JW, Reed TAN, Ardissino M, Bassett P, Whittington AM, Cohen DL, et al. Risk factors for severe disease in patients admitted with COVID-19 to a hospital in London, England: a retrospective cohort study. *Epidemiol Infect*. 2020;148:e251.
<https://doi.org/10.1017/S0950268820002472>.

Grasselli et al., 2020a: Grasselli G, Pesenti A, Cecconi M. Critical Care Utilization for the COVID-19 Outbreak in Lombardy, Italy: Early Experience and Forecast During an Emergency Response. *JAMA*. 2020;323(16):1545–1546. <https://doi.org/10.1001/jama.2020.4031>.

Grasselli et al., 2020b: Grasselli G, Zangrillo A, Zanella A, Antonelli M, Cabrini L, Castelli A. Baseline Characteristics and Outcomes of 1591 Patients Infected With SARS-CoV-2 Admitted to ICUs of the Lombardy Region, Italy. *JAMA*. 2020;323(16):1574–1581.
<https://doi.org/10.1001/jama.2020.5394>.

Grasselli et al., 2020c: Grasselli G, Greco M, Zanella A, Albano G, Antonelli M, Bellani G, et al. Risk Factors Associated With Mortality Among Patients With COVID-19 in Intensive Care Units in Lombardy, Italy. *JAMA Internal Medicine*. 2020;180(10):1345–1355.
<https://doi.org/10.1001/jamainternmed.2020.3539>.

Greater London Authority, 2023: Greater London Authority. Land Area and Population Density, Ward and Borough. 17 August 2023. Accessed on 2024-12-05 from:
<https://www.data.gov.uk/dataset/a76f46f9-c10b-4fe7-82f6-aa928471fcd1/land-area-and-population-density-ward-and-borough>.

Grenfell et al. 2001: Grenfell BT, Bjørnstad, Kappey J. Travelling waves and spatial hierarchies in measles epidemics. *Nature*. 2001;414:716-723. <https://doi.org/10.1038/414716a>.

Gutiérrez-Abejón et al., 2020: Gutiérrez-Abejón E, Tamayo E, Martín-García D, Álvarez FJ, Herrera-Gómez F. Clinical Profile, Treatment and Predictors during the First COVID-19 Wave: A Population-Based Registry Analysis from Castile and Leon Hospitals. *Int J Environ Res Public Health*. 2020;17:9360. <https://doi.org/10.3390/ijerph17249360>.

Haugen, 2023: Haugen M. Excess mortality compared to vaccination in the covid era. *Substack*. 20 January 2023. Accessed on 2025-03-12 from: <https://electricgerms.substack.com/p/excess-mortality-compared-to-vaccination>.

He et al., 2022: He G, Xiao J, Lin Z, Ma W. Excess mortality, rather than case fatality rate, is a superior indicator to assess the impact of COVID-19 pandemic. *The Innovation*. 2022;3:100298. <https://doi.org/10.1016/j.xinn.2022.100298>.

Henry et al., 2022: Henry NJ, Elagali A, Nguyen M, Chipeta MG, Moore CE. Variation in excess all-cause mortality by age, sex, and province during the first wave of the COVID-19 pandemic in Italy. *Sci Rep*. 2022;12:1077. <https://doi.org/10.1038/s41598-022-04993-7>.

Hentschke-Lopes et al., 2022: Hentschke-Lopes M, Botton MR, Borges P, Freitas M, Mancuso ACB, Matte U. *Cad Saúde Pública*. 2022;38:e00001022. <https://doi.org/10.1590/0102-311XEN001022>.

Hess et al., 2020: Hess DR, Kallet RH, Beitler JR. Ventilator Sharing: The Good, the Bad, and the Ugly. *Resp Care*. 2020;65:1059-1062. <https://doi.org/10.4187/respcare.08140>.

HHS, 2024: US Department of Health and Human Services. Part D Prescriber Data CY 2017. Accessed on 2024-11-13 from: <https://www.hhs.gov/guidance/document/part-d-prescriber-data-cy-2017-0>. [Alternative link: <https://www.hhs.gov/guidance/document/part-d-prescriber-data-cy-2017>].

Hickey & Rancourt, 2023a: Hickey J, Rancourt DG. Predictions from standard epidemiological models of consequences of segregating and isolating vulnerable people into care facilities. *PLOS ONE*. 2023;18:e0293556. <https://doi.org/10.1371/journal.pone.0293556>.

Hickey & Rancourt, 2023b: Hickey J, Rancourt DG. Viral Respiratory Epidemic Modeling of Societal Segregation Based on Vaccination Status. *Cureus*. 2023;15:e50520. <https://doi.org/10.7759/cureus.50520>.

Institute for Government Analysis, 2022: Institute for Government Analysis. Timeline of UK government coronavirus lockdowns and measures, March 2020 to December 2021. 9 December 2022. Accessed on 2025-01-27 from: <https://www.instituteforgovernment.org.uk/sites/default/files/2022-12/timeline-coronavirus-lockdown-december-2021.pdf>.

Ioannidis et al., 2023: Ioannidis JPA, Zonta F, Levitt M. Variability in excess deaths across countries with different vulnerability during 2020–2023. PNAS. 2023;120:e2309557120. <https://doi.org/10.1073/pnas.2309557120>.

Islam, et al., 2021a: Islam N, Jdanov DA, Shkolnikov VM, Khunti K, Kawachi I, White M, et al. Effects of covid-19 pandemic on life expectancy and premature mortality in 2020: time series analysis in 37 countries. BMJ. 2021;375:e066768. <https://doi.org/10.1136/bmj-2021-066768>.

Islam, et al., 2021b: Islam N, Shkolnikov VM, Acosta RJ, Klimkin I, Kawachi I, Irizarry RA, et al. Excess deaths associated with covid-19 pandemic in 2020: age and sex disaggregated time series analysis in 29 high income countries. BMJ. 2021;373:n1137. <https://doi.org/10.1136/bmj.n1137>.

Jacobson & Jokela, 2021: Jacobson SH, Jokela JA. Beyond COVID-19 deaths during the COVID-19 pandemic in the United States. Health Care Management Science. 2021;24:661–665. <https://doi.org/10.1007/s10729-021-09570-4>.

Jdanov et al., 2021: Jdanov DA, Galarza AA, Shkolnikov VM, Jasilionis D, Németh L, Leon DA, et al. The short-term mortality fluctuation data series, monitoring mortality shocks across time and space. Scientific Data. 2021;8:235. <https://doi.org/10.1038/s41597-021-01019-1>.

Jha et al., 2022: Jha P, Deshmukh Y, Tumbe C, Suraweera W, Bhowmick A, Sharma S, et al. COVID mortality in India: National survey data and health facility deaths. Science. 2022;375:667–671. <https://www.science.org/doi/10.1126/science.abm5154>.

Joffe, 2021: Joffe AR. COVID-19: Rethinking the Lockdown Groupthink. Front Public Health. 2021;9: 625778. <https://doi.org/10.3389/fpubh.2021.625778>.

Johnson & Rancourt, 2022: Johnson JA, Rancourt DG. Evaluating the Effect of Lockdowns On All-Cause Mortality During the COVID Era: Lockdowns Did Not Save Lives. ResearchGate. 9 July 2022. Accessed on 2025-03-12 from: <http://dx.doi.org/10.13140/RG.2.2.34191.46242>. Also available at: <https://correlation-canada.org/effect-of-lockdowns-in-usa/>.

Jones & Ponomarenko, 2023: Jones RP, Ponomarenko A. Effect of Age, Sex, and COVID-19 Vaccination History on All-Cause Mortality: Unexpected Outcomes in a Complex Biological and Social System. Preprints. 2023; 2023040248. <https://www.preprints.org/manuscript/202304.0248/v1>.

Joseph et al., 2010: Joseph NM, Sistla S, Dutta TK, Badhar AS, Parija SC. Ventilator-associated pneumonia: A review. European Journal of Internal Medicine. 2010;21:360–388. <https://doi.org/10.1016/j.ejim.2010.07.006>.

Juul et al., 2022: Juul FE, Jodal HC, Barua I, Refsum E, Olsvik Ø, Helsingen LM, et al. Mortality in Norway and Sweden during the COVID-19 pandemic. *Scandinavian Journal of Public Health*. 2022;50:38-45. <https://doi.org/10.1177/14034948211047137>.

Juurlink, 2020: Juurlink DN. Safety considerations with chloroquine, hydroxychloroquine and azithromycin in the management of SARS-CoV-2 infection. *CMAJ*. 2020;192:E450. <https://doi.org/10.1503/cmaj.200528>.

Karlinsky & Kobak, 2021: Karlinsky A, Kobak D. Tracking excess mortality across countries during the COVID-19 pandemic with the World Mortality Dataset. *eLife*. 2021;10:e69336. <https://doi.org/10.7554/eLife.69336>.

Keane, 2023: Keane D. One of London's busiest A&Es needs urgent funding for more beds. *The Standard*. 20 February 2023. Accessed on 2025-02-04 from: <https://www.standard.co.uk/news/health/northwick-park-hospital-funding-accident-and-emergency-beds-b1061659.html>.

Kobak, 2021: Kobak D. Excess mortality reveals Covid's true toll in Russia. *Significance*. 2021;18:16-19. . <https://doi.org/10.1111/1740-9713.01486>.

Kontis et al., 2020: Kontis V, Bennett JE, Rashid T, Parks RM, Pearson-Stuttard J, Guillot M, et al. Magnitude, demographics and dynamics of the effect of the first wave of the COVID-19 pandemic on all-cause mortality in 21 industrialized countries. *Nature Med*. 2020;26:1919–1928. <https://doi.org/10.1038/s41591-020-1112-0>.

Kontis et al., 2022: Kontis V, Bennett JE, Parks RM, Rashid T, Pearson-Stuttard J, Asaria P, et al. Lessons learned and lessons missed: impact of the coronavirus disease 2019 (COVID-19) pandemic on all-cause mortality in 40 industrialised countries and US states prior to mass vaccination. [version 2; peer review: 2 approved]. *Wellcome Open Res*. 2022;6:279. <https://doi.org/10.12688/wellcomeopenres.17253.2>.

Kontopantelis et al., 2021a. Kontopantelis E, Mamas MA, Webb RI, Castro A, Rutter MK, Gale CP, et al. Excess deaths from COVID-19 and other causes by region, neighbourhood deprivation level and place of death during the first 30 weeks of the pandemic in England and Wales: A retrospective registry study. *Lancet Reg Health Eur*. 2021;7:100144. <https://doi.org/10.1016/j.lanepe.2021.100144>

Kontopantelis et al., 2021b. Kontopantelis E, Mamas MA, Deanfield J, Asaria M, Doran T. Excess mortality in England and Wales during the first wave of the COVID-19 pandemic. *J Epidemiol Community Health*. 2021;75:213–223. <https://jech.bmj.com/content/75/3/213>.

Kontopantelis et al., 2022. Kontopantelis E, Mamas MA, Webb RT, Castro A, Rutter MK, Gale CP, et al. Excess years of life lost to COVID-19 and other causes of death by sex, neighbourhood

deprivation, and region in England and Wales during 2020: A registry-based study. *PLOS Medicine*. 2022;19:e1003904. <https://doi.org/10.1371/journal.pmed.1003904>.

Korosec, 2020: Korosec M. Extreme Heatwave with up to +43C in Turkey, 41.5C in Cyprus, +40C in Greece, and South Italy today, May 16th. 16 May 2020. Accessed 2025-04-17 from: <https://www.severe-weather.eu/mcd/heatwave-above-40-degrees-turkey-mk/>.

Korsgaard, 2024: Korsgaard SR. All-cause mortality and Japan's early countermeasures. *Health Science Reports*. 2024;7:e1905. <https://doi.org/10.1002/hsr2.1905>.

Kotfis et al., 2020: Kotfis K, Williams Roberson S, Wilson JE, Dabrowski W, Pun BT, Ely EW. COVID-19: ICU delirium management during SARS-CoV-2 pandemic. *Critical Care*. 2020;24:176. <https://doi.org/10.1186/s13054-020-02882-x>.

Kuhbandner & Reitzner, 2023: Kuhbandner C, Reitzner M. Excess mortality in Germany 2020-2022. *Cureus*. 2023;15:e39371. <https://doi.org/10.7759/cureus.39371>

Kung et al., 2021a: Kung S, Doppen M, Black M, Brathwaite I, Kearns C, Weatherall M, et al. Underestimation of COVID-19 mortality during the pandemic. *ERJ Open Res*. 2021;7:00766-2020. <https://doi.org/10.1183/23120541.00766-2020>.

Kung et al., 2021b: Kung S, Doppen M, Black M, Hills T, Kearns N. Reduced mortality in New Zealand during the COVID-19 pandemic. *The Lancet*. 2020;397:25. [https://doi.org/10.1016/S0140-6736\(20\)32647-7](https://doi.org/10.1016/S0140-6736(20)32647-7).

Lacout et al., 2021: Lacout A, Perronne C, Lounnas V. Hydroxychloroquine in Hospitalized Patients with Covid-19. *New England Journal of Medicine*. 2021;389:881-882. <https://doi.org/10.1056/NEJMc2035374>.

LaHue et al., 2020: LaHue SC, James TC, Newman JC, Esmaili AM, Ormseth CH, Ely EW. Collaborative Delirium Prevention in the Age of COVID-19. *Journal of the American Geriatrics Society*. 2020;68:947-949. <https://doi.org/10.1111/jgs.16480>.

La Maestra et al., 2020: La Maestra S, Abbondandolo A, De Flora S. Epidemiological trends of COVID-19 epidemic in Italy over March 2020: From 1000 to 100 000 cases. *Journal of Medical Virology*. 2020;92:1956-1961. <https://doi.org/10.1002/jmv.25908>.

Lane et al., 2020: Lane JCE, Weaver J, Kostka K, Duarte-Salles T, Abrahao MTF, Alghoul H, et al. Risk of hydroxychloroquine alone and in combination with azithromycin in the treatment of rheumatoid arthritis: a multinational, retrospective study. *Lancet Rheumatol*. 2020;2:e698-711. [https://doi.org/10.1016/S2665-9913\(20\)30276-9](https://doi.org/10.1016/S2665-9913(20)30276-9).

Lee et al., 2022: Lee W-E, Park SW, Weinberger DM, Olson D, Simonsen L, Grenfell BT, et al. Direct and indirect mortality impacts of the COVID-19 pandemic in the US, March 2020-April 2021. *medRxiv*. 2022.02.10.22270721. <https://doi.org/10.1101/2022.02.10.22270721>.

Leffler et al., 2022: Leffler CT, Lykins V JD, Das S, Yang E, Konda S. Preliminary Analysis of Excess Mortality in India During the COVID-19 Pandemic. *Am J Trop Med Hyg.* 2022;106:1507-1510. <https://doi.org/10.4269/ajtmh.21-0864>.

Léger & Rizzi, 2024: Léger AE, Rizzi S. Month-to-month all-cause mortality forecasting: a method allowing for changes in seasonal patterns. *American Journal of Epidemiology.* 2024;193:898–907. <https://doi.org/10.1093/aje/kwae004>.

Lewnard et al., 2022: Lewnard JA, Mahmud A, Narayan T, Wahl B, Selvavinayagam TS, Mohan C, et al. All-cause mortality during the COVID-19 pandemic in Chennai, India: an observational study. *Lancet Infect Dis.* 2022;22:463-472. [https://doi.org/10.1016/S1473-3099\(21\)00746-5](https://doi.org/10.1016/S1473-3099(21)00746-5).

Liu et al., 2021: Liu J, Zhang L, Yan Y, Zhou Y, Yin P, Qi J et al. Excess mortality in Wuhan city and other parts of China during the three months of the covid-19 outbreak: findings from nationwide mortality registries. *BMJ.* 2021;372:n415. <https://doi.org/10.1136/bmj.n415>.

Locatelli & Rousson, 2021: Locatelli I, Rousson V. A first analysis of excess mortality in Switzerland in 2020. *PLOS ONE.* 2021;16:e0253505. <https://doi.org/10.1371/journal.pone.0253505>.

Maantay, 2007: Maantay J. Asthma and air pollution in the Bronx: Methodological and data considerations in using GIS for environmental justice and health research. *Health & Place.* 2007;13:32-56. <https://doi.org/10.1016/j.healthplace.2005.09.009>.

Machado-Duque et al., 2022: Machado-Duque ME, Gaviria-Mendoza A, Valladales-Restrepo LF, Albanés-Beltrán JP, Machado-Alba JE. Trends in the Use of Sedative-Hypnotics, Opioids, and Neuromuscular Blockers in Hospitalized Patients During the COVID-19 Pandemic: Observational Retrospective Study. *Drugs – Real World Outcomes.* 2022;9:629-638. <https://doi.org/10.1007/s40801-022-00337-z>.

Mackenzie, 1983: Mackenzie AH. Dose Refinements in Long-Term Therapy of Rheumatoid Arthritis with Antimalarials. *Am J Med.* 1983;75:40-45. [https://doi.org/10.1016/0002-9343\(83\)91269-x](https://doi.org/10.1016/0002-9343(83)91269-x).

Mahase, 2020: Mahase E. Covid-19: most patients require mechanical ventilation in first 24 hours of critical care. *BMJ.* 2020;368:m1201 <https://doi.org/10.1136/bmj.m1201>.

Mannucci et al., 2020: Mannucci E, Besmir N, Monami M. Factors associated with increased all-cause mortality during the COVID-19 pandemic in Italy. *Int J Infect Dis.* 2020;98:121–124. <https://doi.org/10.1016/j.ijid.2020.06.077>.

Marinella, 1997: Marinella MA. Propofol for sedation in the intensive care unit: essentials for the clinician. *Respir med.* 1997;91:505-510. [https://doi.org/10.1016/S0954-6111\(97\)90082-2](https://doi.org/10.1016/S0954-6111(97)90082-2).

Marliot et al., 2020: Marliot G, Penel N, Gamblin V. Switch in use of midazolam for cancer patients during the COVID-19 pandemic. *J Oncol Pharm Pract.* 2020;26:1817-1818. <https://doi.org/10.1177/1078155220948929>.

Marquardt & Albertson, 2001: Marquardt K, Albertson TE. Treatment of Hydroxychloroquine Overdose. *Therapeutics.* 2001;19:420-424. <https://doi.org/10.1053/ajem.2001.25774>.

Martínez-Sanz et al., 2021. Martínez-Sanz J, Muriel A, Ron R, Herrera S, Pérez-Molina JA, Moreno S, et al. *Clin Microbiol Inf.* 2021;27:238-243. <https://doi.org/10.1016/j.cmi.2020.09.021>.

Masselot et al., 2023: Masselot P, Mistry M, Vanoli J, Schneider R, lungman T, Garcia-Leon D, et al. Excess mortality attributed to heat and cold: a health impact assessment study in 854 cities in Europe. *Lancet Planet Health.* 2023;7:e271-e281. [https://doi.org/10.1016/s2542-5196\(23\)00023-2](https://doi.org/10.1016/s2542-5196(23)00023-2).

Mathews et al., 2021: Mathews KS, Seitz KP, Vranas KC, Druggal A, Valley TS, Zhao B, et al. Variation in Initial U.S. Hospital Responses to the Coronavirus Disease 2019 Pandemic. *Critical Care Medicine.* 2021;49:1038-1048. <https://doi.org/10.1097/CCM.0000000000005013>.

Matthes et al., 2024: Matthes KL, Floris J, Merzouki A, Junker C, Weitkunat R, Rühli F, et al. Spatial pattern of all cause excess mortality in Swiss districts during the pandemic years 1890, 1918 and 2020. *Spatial and Spatio-temporal Epidemiology [Internet].* 2024 Nov;51:100697. Available from: <https://linkinghub.elsevier.com/retrieve/pii/S1877584524000649>.

Matveeva & Shabalina, 2023: Matveeva O, Shabalina SA. Comparison of vaccination and booster rates and their impact on excess mortality during the COVID-19 pandemic in European countries. *Front Immunol.* 2023;14:1151311. <https://doi.org/10.3389/fimmu.2023.1151311>.

Maxwell et al., 2024: Maxwell CJ, Dampf H, Alkabbani W, Cotton CA, Gamble J-M, Hogan DB, et al. Psychotropic, Anticonvulsant, and Opioid Use in Assisted Living Residents Before and During the COVID-19 Pandemic. *Journal of the American Medical Directors Association.* 2024;25:121-129. <https://doi.org/10.1016/j.jamda.2023.09.009>.

McCrae & Watson, 2023: McCrae N, Watson R. The mad rush for ventilators in the Covid killing fields, Part 1. *The Conservative Woman.* 17 April 2023. Accessed on 2024-10-16 from: <https://www.conservativewoman.co.uk/the-mad-rush-for-ventilators-in-the-covid-killing-fields-part-1/> [Archived at: <https://archive.is/YIIGy>].

McDermid et al., 2023: McDermid J, Ballard C, Khan Z, Aarsland D, Fox C, Fossey J, et al. Impact of the Covid-19 pandemic on neuropsychiatric symptoms and antipsychotic prescribing for people with dementia in nursing home settings. *Int J Geriatr Psychiatry.* 2023;38:e5878. <https://doi.org/10.1002/gps.5878>.

McGrail, 2022: McGrail K. Excess mortality, COVID-19 and health care systems in Canada. *CMAJ*. 2022;194:E741-E745. <https://doi.org/10.1503/cmaj.220337>.

Melsen et al., 2011: Melsen WG, Rovers MM, Koeman M, Bonten MJM. Estimating the attributable mortality of ventilator-associated pneumonia from randomized prevention studies. *Crit Care Med*. 2011; 39:2736-2742. <https://doi.org/10.1097/CCM.0b013e3182281f33>.

Merler & Ajelli, 2010: Merler S, Ajelli M. The role of population heterogeneity and human mobility in the spread of pandemic influenza. *Proc R Soc B*. 2010;277:557-565. <https://doi.org/10.1098/rspb.2009.1605>.

Melsen et al., 2013: Melsen WG, Rovers MM, Groenwald RHH, Bergmans DCJJ, Camus C, Bauer TT et al. Attributable mortality of ventilator-associated pneumonia: a meta-analysis of individual patient data from randomised prevention studies. *Lancet Infect Dis*. 2013;13:665-671. [http://dx.doi.org/10.1016/S1473-3099\(13\)70081-1](http://dx.doi.org/10.1016/S1473-3099(13)70081-1).

Miller et al., 2021: Miller S, Wherry LR, Mazumder B. Estimated Mortality Increases During The COVID-19 Pandemic By Socioeconomic Status, Race, And Ethnicity. *Health Affairs*. 2021;40:1252-1260. <https://doi.org/10.1377/hlthaff.2021.00414>.

Mills et al., 2020: Mills EHA., Møller AL, Gnesin F, Zyllyftari N, Broccia M, Schou M, et al. National all-cause mortality during the COVID-19 pandemic: a Danish registry-based study. *Eur J Epidemiol*. 2020;35:1007–1019. <https://doi.org/10.1007/s10654-020-00680-x>.

MIT Election Data Science Lab, 2018: MIT Election Data and Science Lab. County Presidential Election Returns 2000-2020. Accessed on 2024-11-19 from: <https://doi.org/10.7910/DVN/VOQCHQ>.

Mitropoulos et al., 2023: Mitropoulos D, Pytharoulis I, Zanis P, Anagnostopoulou C. Subseasonal-to-Seasonal Predictability Assessment of an Early HeatWave in the Eastern Mediterranean in May 2020. *Environ Sci Proc*. 2023;26:42. <https://doi.org/10.3390/environsciproc2023026042>.

Mostert et al., 2024: Mostert S, Hoogland M, Huibers M, Kaspers G. Excess mortality across countries in the Western World since the COVID-19 pandemic: 'Our World in Data' estimates of January 2020 to December 2022. *BMJ Public Health*. 2024 May;2(1):e000282.

Neil et al., 2022: Neil M, Fenton N, Smalley J, Craig CEH, Guetzkow J, McLachlan S, et al. Official mortality data for England suggest systematic miscategorisation of vaccine status and uncertain effectiveness of Covid-19 vaccination. *ResearchGate*. 12 January 2022. <http://dx.doi.org/10.13140/RG.2.2.28055.09124>.

Neil & Fenton, 2022: Neil M, Fenton N. The Devil's Advocate: An Exploratory Analysis of 2022 Excess Mortality - What is causing excess deaths: Covid, long-covid, lockdowns, healthcare or

the vaccines? Where are the numbers? Substack. 14 December 2022. Accessed on 2025-03-12 from: <https://wherearethenumbers.substack.com/p/the-devils-advocate-an-exploratory>.

Neil & Fenton, 2023: Neil M, Fenton N. The Very Best of Cheap Trick..... How widespread is the (mal)practice of miscategorising vaccination status? Where are the numbers? Substack. 29 July 2023. Accessed on 2025-03-12 from: <https://wherearethenumbers.substack.com/p/the-very-best-of-cheap-trick>.

Nikishimi et al., 2022 : Nikishimi M, Jafari D, Singh N, Shinozaki K, Sison CP, Shoaib M, et al. Mortality of Mechanically Ventilated COVID-19 Patients in Traditional versus Expanded Intensive Care Units in New York. *Ann Am Thorac Soc*. 2022;19:1346-1354. <http://dx.doi.org/10.1513/AnnalsATS.202106-705OC>.

Nørgaard et al., 2021: Nørgaard SK, Vestergaard LS, Nielsen J, Richter L, Schmid D, Bustos N, et al. Real-time monitoring shows substantial excess all-cause mortality during second wave of COVID-19 in Europe, October to December 2020. *Euro Surveill*. 2021;26:2002023. <https://doi.org/10.2807/1560-7917.ES.2021.26.1.2002023>.

Nørgaard et al., 2024: Nørgaard SK, Nielsen J, Nordholm AC, Richter L, Chalupka A, Sierra NB, et al. Excess mortality in Europe coincides with peaks of COVID-19, influenza and respiratory syncytial virus (RSV), November 2023 to February 2024. *Eurosurveillance*. 2024 Apr 11;29(15).

Núñez-Gil et al., 2020: Núñez-Gil IJ, Estrada V, Fernández-Pérez C, Fernández-Rozas I, Martín-Sánchez FJ, Macaya C. Curva pandémica COVID-19, sobrecarga sanitaria y mortalidad. *Emergencias*. 2020;32:290-299.

Olson et al., 2020: Olson DR, Huynh M, Fine A, Baumgartner J, Castro A, Tai Chan H, et al. Preliminary Estimate of Excess Mortality During the COVID-19 Outbreak — New York City, March 11–May 2, 2020. *MMWR Morb Mortal Wkly Rep*. 2020;69:603–605. <http://dx.doi.org/10.15585/mmwr.mm6919e5>.

ONS, 2021: Office for National Statistics. Poverty rate by NUTS 2 region, UK, financial year ending 2018 to financial year ending 2020. Accessed on 2024-12-03 from: <https://www.ons.gov.uk/peoplepopulationandcommunity/personalandhouseholdfinances/incomeandwealth/adhocs/13572povertyratebynuts2regionukfinancialyearending2018tofinancialyearending2020>.

ONS, 2022a: Office for National Statistics. Regional ethnic diversity. 22 December 2022. Accessed on 2024-12-05 from: <https://www.ethnicity-facts-figures.service.gov.uk/uk-population-by-ethnicity/national-and-regional-populations/regional-ethnic-diversity/latest/>.

ONS, 2022b: Office for National Statistics. International migration, England and Wales: Census 2021. 2 November 2022. Accessed on 2024-12-05 from:

<https://www.ons.gov.uk/peoplepopulationandcommunity/populationandmigration/internationalmigration/bulletins/internationalmigrationenglandandwales/census2021>.

ONS, 2024: Office for National Statistics. Regional gross disposable household income: all International Territorial Level (ITL) regions. Accessed on 2024-12-04 from: <https://www.ons.gov.uk/economy/regionalaccounts/grossdisposablehouseholdincome/datasets/regionalgrossdisposablehouseholdincomegdhi>.

Ottaiano et al., 2021: Ottaiano A, Santorsola M, Tamburini M, Corrado F, Scrima M, Bocchetti M, et al. Journal of Epidemiology and Global Health. 2021;11:253-256. <https://doi.org/10.2991/jegh.k.210317.001>.

Paganuzzi et al., 2024: Paganuzzi M, Nattino G, Ghilardi GI, Costantino G, Rossi C, Cortellaro F, et al. Assessing the heterogeneity of the impact of COVID-19 incidence on all-cause excess mortality among healthcare districts in Lombardy, Italy, to evaluate the local response to the pandemic: an ecological study. BMJ Open. 2024;14:e077476. <https://doi.org/10.1136/bmjopen-2023-077476>.

Paglino et al., 2023: Paglino E, Lundberg DJ, Zhou Z, Wasserman JA, Raquib R, Luck AN, et al. Monthly excess mortality across counties in the United States during the COVID-19 pandemic, March 2020 to February 2022. Sci Adv. 2023;9:eadf9742. <https://doi.org/10.1126/sciadv.adf9742>.

Paglino et al., 2024: Paglino E, Lundberg DJ, Wrigley-Field E, Zhou Z, Wasserman JA, Raquib R, et al. Excess natural-cause mortality in US counties and its association with reported COVID-19 deaths. Proceedings of the National Academy of Sciences of the United States of America. 2024;121(6).

Pálinkás & Sándor, 2022: Pálinkás A; Sándor J. Effectiveness of COVID-19 Vaccination in Preventing All-Cause Mortality among Adults during the Third Wave of the Epidemic in Hungary: Nationwide Retrospective Cohort Study. Vaccines. 2022;10:1009. <https://doi.org/10.3390/vaccines10071009>.

Pallari et al., 2024: Pallari CT, Achilleos S, Quattrocchi A, Gabel J, Critselis E, Athanasiadou M, et al. Magnitude and determinants of excess total, age-specific and sex-specific all-cause mortality in 24 countries worldwide during 2020 and 2021: results on the impact of the COVID-19 pandemic from the CMOR project. BMJ Global Health. 2024 Apr 18;9(4).

Panagiotou et al., 2021: Panagiotou OA, Kosar CM, White EM, Bantis LE, Yang X, Santostefano CM, et al. Risk Factors Associated With All-Cause 30-Day Mortality in Nursing Home Residents With COVID-19. JAMA Intern Med. 2021;181(4):439–448. <https://doi.org/10.1001/jamainternmed.2020.7968>.

Pastor-Satorras et al., 2015: Pastor-Satorras R, Castellano C, Van Mieghem P, Vespignani A. Epidemic processes in complex networks. *Rev Mod Phys.* 2015;87:925-979. <http://dx.doi.org/10.1103/RevModPhys.87.925>.

Pecoraro et al., 2020: Pecoraro F, Clemente F, Luzi D. The efficiency in the ordinary hospital bed management in Italy: An in-depth analysis of intensive care unit in the areas affected by COVID-19 before the outbreak. *PLOS One.* 2020;15:e0239249. <https://doi.org/10.1371/journal.pone.0239249>.

Pérez-Belmonte et al., 2020. Pérez-Belmonte LM, Torres-Peña JD, López-Carmona MD, Ayala-Gutiérrez MM, Fuentes-Jiménez F, et al. Mortality and other adverse outcomes inpatients with type 2 diabetes mellitus admitted for COVID-19 in association with glucose-lowering drugs: a nationwide cohort study. *BMC Medicine.* 2020;18:359. <https://doi.org/10.1186/s12916-020-01832-2>.

Piccininni et al., 2020: Piccininni M, Rohmann J L, Foresti L, Lurani C, Kurth T. Use of all cause mortality to quantify the consequences of covid-19 in Nembro, Lombardy: descriptive study. *BMJ.* 2020; 369:m1835. <https://doi.org/10.1136/bmj.m1835>.

Pilkington et al., 2021: Pilkington H, Feuillet T, Rican S, Goupil de Bouillé J, Bouchaud O, Caihol J, et al. Spatial determinants of excess all-cause mortality during the first wave of the COVID-19 epidemic in France. *BMC Public Health.* 2021;21:2157. <https://doi.org/10.1186/s12889-021-12203-8>.

Polyakova et al., 2021: Polyakova M, Udalova V, Kocks G, Genadek K, Finlay K, Finkelstein AN. Racial Disparities In Excess All-Cause Mortality During The Early COVID-19 Pandemic Varied Substantially Across States. *Health Affairs.* 2021;40:307-316. <https://doi.org/10.1377/hlthaff.2020.02142>.

Pradelle et al., 2024a: Pradelle A, Mainbourg S, Provencher S, Massy E, Grenet G, Lega J-C. Deaths induced by compassionate use of hydroxychloroquine during the first COVID-19 wave: an estimate. *Biomed Pharmacother.* 2024;171:116055. <https://doi.org/10.1016/j.biopha.2023.116055>.

Pradelle et al., 2024b. Pradelle A, Mainbourg S, Provencher S, Massy E, Grenet G, Lega J-C. Retraction notice to 'Deaths induced by compassionate use of hydroxychloroquine during the first COVID-19 wave: an estimate' [Biomedicine & Pharmacotherapy, Volume 171 (2024) 116055]. *Biomed Pharmacother.* 2024;179:117353. <https://doi.org/10.1016/j.biopha.2024.117353>.

Prats-Urbe et al., 2021: Prats-Urbe A, Sena AG, Hui Lai LY, Ahmed W-U-R, Alghoul H, Alser O, et al. Use of repurposed and adjuvant drugs in hospital patients with covid-19: multinational network cohort study. *BMJ.* 2021;373:n1038. <http://dx.doi.org/10.1136/bmj.n1038>.

Pulido et al., 2024: Pulido J, Barrio G, Donat M, Politi J, Moreno A, Cea-Soriano L, et al. Excess Mortality During 2020 in Spain: The Most Affected Population, Age, and Educational Group by the COVID-19 Pandemic. *Disaster Medicine and Public Health Preparedness*. 2024 Feb 19;18.

Puliyel, 2020: Puliyel J. Rapid Response: Dose Related Toxicity of Hydroxychloroquine. *BMJ*. 12 July 2020. Accessed 2025-05-07 from: <https://www.bmj.com/content/370/bmj.m2670/rr-1>.

Rancourt, 2020: Rancourt DG. All-cause mortality during COVID-19 — No plague and a likely signature of mass homicide by government response. *ResearchGate*, 2 June 2020. <http://dx.doi.org/10.13140/RG.2.2.24350.77125>. Accessed on 2025-03-12 from: <https://correlation-canada.org/no-plague-mass-homicide-2020/>.

Rancourt, 2021: Rancourt DG. Do Face Masks Reduce COVID-19 Spread in Bangladesh? Are the Abaluck et al. Results Reliable? *denisrancourt.ca*. 20 September 2021. Accessed on 2025-03-12 from: <https://denisrancourt.ca/entries.php?id=106>. Also available at: <https://correlation-canada.org/do-face-masks-work-in-bangladesh/>.

Rancourt, 2022: Rancourt DG. Probable causal association between India's extraordinary April-July 2021 excess-mortality event and the vaccine rollout. *Correlation Research in the Public Interest*. 5 December 2022. Accessed on 2025-03-12 from: <https://correlation-canada.org/report-probable-causal-association-between-indias-extraordinary-april-july-2021-excess-mortality-event-and-the-vaccine-rollout/>.

Rancourt, 2024: Rancourt DG. Medical Hypothesis: Respiratory epidemics and pandemics without viral transmission. *Correlation Research in the Public Interest*. 2 December 2024. Accessed on 2025-03-12 from: <https://correlation-canada.org/respiratory-epidemics-without-viral-transmission/>. [Also available at: <https://doi.org/10.20944/preprints202412.0480.v1>].

Rancourt et al., 2020: Rancourt DG, Baudin M, Mercier J. Evaluation of the virulence of SARS-CoV-2 in France, from all-cause mortality 1946-2020. *ResearchGate*. 20 August 2020. Accessed on 2025-03-12 from: <https://doi.org/10.13140/RG.2.2.16836.65920/1>.

Rancourt et al., 2021a: Rancourt DG, Baudin M, Mercier J. Nature of the COVID-era public health disaster in the USA, from all-cause mortality and socio-geo-economic and climatic data. *ResearchGate*. 25 October 2021. Accessed on 2025-03-12 from: <http://dx.doi.org/10.13140/RG.2.2.11570.32962>. Also available at: <https://correlation-canada.org/Mortality-public-health-disaster-USA/>.

Rancourt et al., 2021b: Rancourt DG, Baudin M, Mercier J. Analysis of all-cause mortality by week in Canada 2010-2021, by province, age and sex: There was no COVID-19 pandemic, and there is strong evidence of response-caused deaths in the most elderly and in young males. *ResearchGate*. 6 August 2021. Accessed on 2025-03-12 from:

<http://dx.doi.org/10.13140/RG.2.2.14929.45921>. Also available at: <https://correlation-canada.org/all-cause-mortality-in-canada-2021/>.

Rancourt et al., 2022a: Rancourt DG, Baudin M, Mercier J. Probable causal association between Australia's new regime of high all-cause mortality and its COVID-19 vaccine rollout. Correlation Research in the Public Interest. 20 December 2022. Accessed on 2025-03-12 from: <https://correlation-canada.org/report-probable-causal-association-between-australias-new-regime-of-high-all-cause-mortality-and-its-covid-19-vaccine-rollout/>.

Rancourt et al., 2022b: Rancourt DG, Baudin M, Mercier J. COVID-Period Mass Vaccination Campaign and Public Health Disaster in the USA: From age/state-resolved all-cause mortality by time, age-resolved vaccine delivery by time, and socio-geo-economic data. ResearchGate. 2 August 2022. Accessed on 2025-03-12 from: <http://dx.doi.org/10.13140/RG.2.2.12688.28164>. Also available at: <https://vixra.org/abs/2208.0023> and archived at: <https://archive.ph/IFNwK>.

Rancourt et al., 2022c: Rancourt DG, Baudin M, Mercier J. Proof that Canada's COVID-19 mortality statistics are incorrect. Correlation Research in the Public Interest. 5 October 2022. Accessed on 2025-03-12 from: <https://correlation-canada.org/report-proof-that-canadas-covid-19-mortality-statistics-are-incorrect/>.

Rancourt et al., 2023a: Rancourt DG, Baudin M, Hickey J, Mercier J. COVID-19 vaccine-associated mortality in the Southern Hemisphere. Correlation Research in the Public Interest. 17 September 2023. Accessed on 2025-03-12 from: <https://correlation-canada.org/covid-19-vaccine-associated-mortality-in-the-Southern-Hemisphere/>.

Rancourt et al., 2023b: Rancourt DG, Baudin M, Hickey J, Mercier J. Age-stratified COVID-19 vaccine-dose fatality rate for Israel and Australia. Correlation Research in the Public Interest. 9 February 2023. Accessed on 2025-03-12 from: <https://correlation-canada.org/report-age-stratified-covid-19-vaccine-dose-fatality-rate-for-israel-and-australia/>.

Rancourt & Hickey, 2023: Rancourt DG, Hickey J. Quantitative evaluation of whether the Nobel-Prize-winning COVID-19 vaccine actually saved millions of lives. Correlation Research in the Public Interest. 08 October 2023. Accessed on 2025-03-12 from: <https://correlation-canada.org/nobel-vaccine-and-all-cause-mortality/>. Also available at: <https://doi.org/10.22541/au.173990833.33272873/v1>.

Rancourt et al., 2024: Rancourt DG, Hickey J, Linard C. Spatiotemporal variation of excess all-cause mortality in the world (125 countries) during the Covid period 2020-2023 regarding socio economic factors and public-health and medical interventions. Correlation Research in the Public Interest. 19 July 2024. Accessed on 2025-03-12 from: <https://correlation-canada.org/covid-excess-mortality-125-countries/>. Also available at: <http://dx.doi.org/10.13140/RG.2.2.23161.48489>.

Rafferty et al., 2018: Rafferty S, Smallman-Raynor MR, Cliff AD. *J Hist Geog.* 2018;59:2-14. <https://doi.org/10.1016/j.jhg.2017.09.006>.

Ramírez-Soto & Ortega-Cáceres, 2022: Ramírez-Soto MC, Ortega-Cáceres G. Analysis of Excess All-Cause Mortality and COVID-19 Mortality in Peru: Observational Study. *Trop Med Infect Dis.* 2022;7:44. <https://doi.org/10.3390/tropicalmed7030044>.

Razak et al., 2022: Razak F, Shin S, Naylor CD, Slutsky AS. Canada's response to the initial 2 years of the COVID-19 pandemic: a comparison with peer countries. *CMAJ.* 2022;194:E870-7. <https://doi.org/10.1503/cmaj.220316>.

RECOVERY Collaborative Group, 2020: The RECOVERY Collaborative Group. Effect of Hydroxychloroquine in Hospitalized Patients with Covid-19. *New England Journal of Medicine.* 2020;383:2030-2040. <https://doi.org/10.1056/NEJMoa2022926>.

Redert, 2022a: Redert A. Short-term Vaccine Fatality Ratio of booster and 4th dose in The Netherlands. ResearchGate. October 2022. Accessed on 2025-03-12 from: <https://doi.org/10.13140/RG.2.2.29841.30568>.

Redert, 2022b. Redert A. Covid-19 vaccinations and all-cause mortality -a long-term differential analysis among municipalities. ResearchGate. July 2022. Accessed on 2025-03-12 from: <https://doi.org/10.13140/RG.2.2.33994.85447>.

Redet, 2023: Redert A. Causal effect of covid vaccination on mortality in Europe. ResearchGate. 24 February 2023. Accessed on 2025-03-12 from: https://www.researchgate.net/publication/368777703_Causal_effect_of_covid_vaccination_on_mortality_in_Europe.

Redondo-Bravo et al., 2020: Redondo-Bravo L, Sierra Moros MJ, Martínez Sánchez EV, Lorusso N, Carmona Ubago A, Gallardo García V, Sánchez Villanueva P, et al. The first wave of the COVID-19 pandemic in Spain: characterisation of cases and risk factors for severe outcomes, as at 27 April 2020. *Euro Surveill.* 2020;25;2004131. <https://doi.org/10.2807/1560-7917.ES.2020.25.50.2001431>.

Rezoagli et al., 2021: Rezoagli E, Magliocca A, Bellani G, Pesenti A, Grasselli G. Development of a Critical Care Response – Experiences from Italy During the Coronavirus Disease 2019 Pandemic. *Anesthesiology Clin.* 2021;39:265-284. <https://doi.org/10.1016/j.anclin.2021.02.003>.

RHIhub, 2024: Rural Health Information Hub. Rural Data Explorer. Accessed on 2024-11-12 from: <https://www.ruralhealthinfo.org/data-explorer>.

Riccardo et al., 2020: Riccardo F, Ajelli M, Andrianou XD, Bella A, Del Manso M, Fabiana M, et al. Epidemiological characteristics of COVID-19 cases and estimates of the reproductive numbers 1

month into the epidemic, Italy, 28 January to 31 March 2020. *Euro Surveill.* 2020;25:2000790. <https://doi.org/10.2807/1560-7917.ES.2020.25.49.2000790>.

Rich, 2020: Rich D. Covid-19: In Cameroon, chloroquine therapy hailed by French expert becomes state protocol. *France 24.* 3 May 2020. Accessed on 2025-01-31 from: <https://www.france24.com/en/20200503-covid-19-in-cameroon-a-chloroquine-therapy-hailed-by-french-expert-becomes-state-protocol>.

Richardson et al., 2020: Richardson S, Hirsch JS, Narasimhan M, Crawford JM, McGinn T, Davidson KW, et al. Presenting Characteristics, Comorbidities, and Outcomes Among 5700 Patients Hospitalized With COVID-19 in the New York City Area. *JAMA.* 2020;323(20):2052–2059. <https://doi.org/10.1001/jama.2020.6775>.

Rossen et al., 2021: Rossen LM, Ahmad FB, Anderson RN, Branum AM, Du C, Krumholz HM, et al. Disparities in Excess Mortality Associated with COVID-19 — United States, 2020. *MMWR Morb Mortal Wkly Rep.* 2021;70:1114–1119. <http://dx.doi.org/10.15585/mmwr.mm7033a2>.

Rossen et al., 2022: Rossen LM, Nørgaard SK, Sutton PD, Krause TG, Ahmad FB, Vestergaard LS, et al. Excess all-cause mortality in the USA and Europe during the COVID-19 pandemic, 2020 and 2021. *Sci Rep.* 2022;12:18559. <https://doi.org/10.1038/s41598-022-21844-7>.

Safavi-Naini et al., 2022: Safavi-Naini SAA, Farsi Y, Alali WQ, Sohlpour A, Pourhoseingholi MA. Excess all-cause mortality and COVID-19 reported fatality in Iran (April 2013–September 2021): age and sex disaggregated time series analysis. *BMC Res Notes.* 2022;15:130. <https://doi.org/10.1186/s13104-022-06018-y>.

Sanmarchi et al., 2021: Sanmarchi F, Golinelli D, Lenzi J, Capodici A, Reno C, Gibertoni D. Exploring the Gap Between Excess Mortality and COVID-19 Deaths in 67 Countries. *JAMA Network Open.* 2021;4:e2117359. <https://doi.org/10.1001/jamanetworkopen.2021.17359>.

Sattenspiel & Dietz, 1995: Sattenspiel L, Dietz K. A Structured Epidemic Model Incorporating Geographic Mobility Among Regions. *Math Biosci.* 1995;128:71-91. [https://doi.org/10.1016/0025-5564\(94\)00068-B](https://doi.org/10.1016/0025-5564(94)00068-B).

Schellekens, 2023: Schellekens P. Excess mortality and vaccination: How front-runners in the vaccination space compare across countries on excess mortality. *pandem-ic.* Updated 6 April 2024. Accessed on 2025-03-12 from: <https://pandem-ic.com/excess-mortality-and-vaccination/>.

Scherb & Hayashi, 2023: Scherb H, Hayashi K. Annual All-Cause Mortality Rate in Germany and Japan (2005 to 2022) With Focus on The Covid-19 Pandemic: Hypotheses And Trend Analyses. *Med Clin Sci.* 2023;5:1-7. Accessed on 2025-03-12 from: <https://www.sciencexcel.com/articles/RZ2ZUhxYkEj0DhgjZAtR9kZitZyJDfKaVQhO3JP.pdf>.

Schöley et al., 2022: Schöley J, Aburto JM, Kashnitsky I, Kniffka MS, Zhang L, Jaadia H, et al. Life expectancy changes since COVID-19. *Nat Hum Behav.* 2022;6:1649–1659.

<https://doi.org/10.1038/s41562-022-01450-3>.

Schulte et al., 2020: Schulte F, Lucas E, Rau J, Szabo L, Hancock J. Millions Of Older Americans Live In Counties With No ICU Beds As Pandemic Intensifies. 20 March 2020. Accessed on 2024-10-25 from: <https://kffhealthnews.org/news/as-coronavirus-spreads-widely-millions-of-older-americans-live-in-counties-with-no-icu-beds/>. [Archived at: <https://archive.is/OrUTD>].

Sempé et al., 2021: Sempé L, Lloyd-Sherlock P, Martínez R, Ebrahim S, McKee M, Acosta E. Estimation of all-cause excess mortality by age-specific mortality patterns for countries with incomplete vital statistics: a population-based study of the case of Peru during the first wave of the COVID-19 pandemic. *Lancet Reg Health Am.* 2021;2:100039.

<https://doi.org/10.1016/j.lana.2021.100039>.

Shabsigh, 2022: Shabsigh R. Prologue. In: Shabsigh R, editor. *Health crisis management in acute care hospitals: Lessons learned from COVID-19 and beyond*. Cham: Springer; 2022. pp. ix-x.

<https://link.springer.com/book/10.1007/978-3-030-95806-0>.

Sheppard et al., 2023. Sheppard N, Carroll M, Gao C, Lane T. Particulate matter air pollution and COVID-19 infection, severity, and mortality: A systematic review and meta-analysis. *Science of the Total Environment.* 2023;880:163272. <http://dx.doi.org/10.1016/j.scitotenv.2023.163272>.

Silverio et al., 2020. Silverio A, Di Maio M, Ciccarelli M, Carrizzo A, Vecchione C, Galasso G. Timing of national lockdown and mortality in COVID-19: The Italian experience. *Int J Infect Dis.* 2020;100:193-195. <https://doi.org/10.1016/j.ijid.2020.09.006>.

Simon & Ebbs, 2020: Simon E, Ebbs S. Poverty, pollution and neglect: How the Bronx became a coronavirus “formula for disaster”. *ABC News.* 11 April 2020. Accessed on 2025-02-04 from:

<https://abcnews.go.com/Health/poverty-pollution-neglect-bronx-coronavirus-formula-disaster/>.

Sinnathamby et al., 2020: Sinnathamby MA, Whitaker H, Coughlan L, Lopez Bernal J, Ramsay M, Andrews N. All-cause excess mortality observed by age group and regions in the first wave of the COVID-19 pandemic in England. *Euro Surveill.* 2020;25:2001239.

<https://doi.org/10.2807/1560-7917.ES.2020.25.28.2001239>.

Slutsky & Ranieri, 2013: Slutsky AS, Ranieri VM. Ventilator-Induced Lung Injury. *New England Journal of Medicine.* 2013;369:2126-2136. <https://doi.org/10.1056/NEJMra1208707>.

Soneji et al., 2021: Soneji S, Beltrán-Sánchez H, Yang JW, Mann C. Population-level mortality burden from novel coronavirus (COVID-19) in Europe and North America. *Genus.* 2021;77:7.

<https://doi.org/10.1186/s41118-021-00115-9>.

Šorli et al., 2023: Šorli AS, Makovec T, Krevel Z, Gorjup R. Forgotten “Primum Non Nocere” and Increased Mortality after COVID-19 Vaccination. *Qual Prim Care*. 2023;31:006. Accessed on 2025-03-12 from: <https://www.primescholars.com/articles/forgotten-primum-non-nocere-and-increased-mortality-after--covid19-vaccination.pdf>.

Spiteri et al., 2020: Spiteri G, Fielding J, Diercke M, Campese C, Enouf V, Gaymard A, et al. First cases of coronavirus disease 2019 (COVID-19) in the WHO European Region, 24 January to 21 February 2020. *Euro Surveill*. 2020;25(9):pii=2000178. <https://doi.org/10.2807/1560-7917.ES.2020.25.9.2000178>.

Stein et al., 2021: Stein RE, Corcoran KE, Colyer CJ, Mackay AM, Guthrie SK. Closed but Not Protected: Excess Deaths Among the Amish and Mennonites During the COVID-19 Pandemic. *J Relig Health*. 2021;60:3230–3244. <https://doi.org/10.1007/s10943-021-01307-5>.

Stokes et al., 2021: Stokes AC, Lundberg DJ, Elo IT, Hempstead K, Bor J, Preston SH. COVID-19 and excess mortality in the United States: A county-level analysis. *PLoS Med*. 2021;18:e1003571. <https://doi.org/10.1371/journal.pmed.1003571>.

Sy, 2024: Sy W. Excess Deaths in the United Kingdom: Midazolam and Euthanasia in the COVID-19 Pandemic. *Med Clin Res*. 2024;9:1-21. <https://www.medclinrese.org/open-access/excess-deaths-in-the-united-kingdom-midazolam-and-euthanasia-in-the-covid19-pandemic.pdf>.

Tadbiri et al., 2020: Tadbiri H, Moradi-Lakeh M, Naghavi M. All-cause excess mortality and COVID-19-related deaths in Iran. *Med J Islam Repub Iran*. 2020;34:8. <https://www.ncbi.nlm.nih.gov/pmc/articles/PMC7711045/>.

Tarazi et al., 2022: Tarazi W, Welch P, Nguyen N, Bosworth A, Sheingold S, De Lew N, et al. Medicare Beneficiary Enrollment Trends and Demographic Characteristics. Assistant Secretary for Planning and Evaluation, Office of Health Policy. 2 March 2022. Accessed on 2024-12-07 from: <https://aspe.hhs.gov/sites/default/files/documents/b9ac26a13b4fdf30c16c24e79df0c99c/medicare-beneficiary-enrollment-ib.pdf>.

Taccone et al., 2021: Taccone FS, Van Goethem N, De Pauw R, Wittebole X, Blot K, Van Oyen H, et al. The role of organizational characteristics on the outcome of COVID-19 patients admitted to the ICU in Belgium. *The Lancet Regional Health – Europe*. 2021;2:100019. <https://doi.org/10.1016/j.lanepe.2020.100019>.

Thoma & Declercq, 2022: Thoma ME, Declercq ER. All-Cause Maternal Mortality in the US Before vs During the COVID-19 Pandemic. *JAMA Netw Open*. 2022;5:e2219133. <https://doi.org/10.1001%2Fjamanetworkopen.2022.19133>

Thomas et al., 2020: Thomas LJ, Huang P, Yin F, Lui XI, Almquist ZW, Hipp JR, et al. Spatial heterogeneity can lead to substantial local variations in COVID-19 timing and severity. PNAS. 2020;117:24180-24187. <https://doi.org/10.1073/pnas.2011656117>.

Torjesen, 2021: Torjesen I. Covid-19: When to start invasive ventilation is “the million dollar question”. BMJ. 2021;372:n121. <http://dx.doi.org/10.1136/bmj.n121>.

Trust for London, 2024: Trust for London. Poverty rates by London borough. Last updated September 2024. Accessed on 2024-12-04 from: <https://trustforlondon.org.uk/data/poverty-borough/>.

US Census Bureau, 2023: United States Census Bureau. American Community Survey 1-year estimates. Accessed on 2025-04-17 from: <http://censusreporter.org/profiles/31000US35620-new-york-newark-jersey-city-ny-nj-metro-area/>.

US Census Bureau, 2024a: United States Census Bureau. County Intercensal Population Totals: 2010-2020. Accessed on 2024-11-14 from: <https://www.census.gov/data/tables/time-series/demo/popest/intercensal-2010-2020-counties.html>.

US Census Bureau, 2024b: United States Census Bureau. COVID-19 Demographic and Economic Resources (V3). Accessed on 2024-03-13 from: <https://covid19.census.gov/datasets/21843f238cbb46b08615fc53e19e0daf/explore?location=3.618777%2C0.315550%2C0.51>. Alternative link: <https://covid19.census.gov/>.

US Census Bureau, 2024c: United States Census Bureau. 2020 Census Urban Areas Facts. Accessed on 2024-11-25 from: <https://www.census.gov/programs-surveys/geography/guidance/geo-areas/urban-rural/2020-ua-facts.html>.

van der Velde et al., 2021: van der Velde M, Sijtsma D, Goossens M, Maartense B. The Dutch–German Border: Open in Times of Coronavirus Lockdowns. Borders in Globalization Review. 2021;2:149-155. <https://doi.org/10.18357/bigr22202120205>.

Vestergaard et al., 2020: Vestergaard LS, Nielsen J, Richter L, Schmid D, Bustos N, Braeye T, et al. Excess all-cause mortality during the COVID-19 pandemic in Europe – preliminary pooled estimates from the EuroMOMO network, March to April 2020. Euro Surveill. 2020;25:2001214. <https://doi.org/10.2807/1560-7917.ES.2020.25.26.2001214>.

Vila-Corcoles et al., 2021: Vila-Corcoles A, Satue-Gracia E, Vila-Rovira A, de Diego-Cabanes, C, Forcadell-Peris MJ, Hospital-Guardiola I, et al. COVID19-related and all-cause mortality risk among middle-aged and older adults across the first epidemic wave of SARS-COV-2 infection: a population-based cohort study in Southern Catalonia, Spain, March–June 2020. BMC Public Health. 2021;21:1795. <https://doi.org/10.1186/s12889-021-11879-2>.

Villani, L. et al., 2020: Villani L, McKee M, Cascini F, Ricciardi W, Boccia S. Comparison of Deaths Rates for COVID-19 across Europe During the First Wave of the COVID-19 Pandemic. *Front Public Health*. 2020;8:620416. <https://doi.org/10.3389/fpubh.2020.620416>.

Wang et al., 2022: Wang H, Paulson KR, Pease SA, Watson S, Comfort H, Zheng P, et al. Estimating excess mortality due to the COVID-19 pandemic: a systematic analysis of COVID-19-related mortality, 2020–21. *The Lancet*. 2022;399:1513–1536. [https://doi.org/10.1016/S0140-6736\(21\)02796-3](https://doi.org/10.1016/S0140-6736(21)02796-3).

Watson et al., 2020: Watson JA, Tarning J, Hoglund RM, Baud FJ, Megarbane B, Clemessy J-L, et al. Concentration-dependent mortality of chloroquine in overdose. *eLife*. 2020;9:e58631. <https://doi.org/10.7554/eLife.58631>.

WHO, 2020: World Health Organization. WHO Director-General's opening remarks at the media briefing on COVID-19 - 11 March 2020. 11 March 2020. Accessed on 2025-05-13 from: <https://www.who.int/director-general/speeches/detail/who-director-general-s-opening-remarks-at-the-media-briefing-on-covid-19---11-march-2020>.

WHO, 2023: World Health Organization. WHO chief declares end to COVID-19 as a global health emergency. 5 May 2023. Accessed on 2025-05-13 from: <https://news.un.org/en/story/2023/05/1136367>.

Wilcox et al., 2021: Wilcox CR, Islam N, Dambha-Miller H. Association between influenza vaccination and hospitalisation or all-cause mortality in people with COVID-19: a retrospective cohort study. *BMJ Open Resp Res*. 2021;8:e000857. <https://doi.org/10.1136/bmjresp-2020-000857>.

Williams, 2024: Williams G. New acute unit to cut A&E waits at Northwick Park Hospital. *Brent & Kilburn Times*. 2 August 2024. Accessed on 2025-02-04 from: <https://www.kilburntimes.co.uk/news/24494062.new-acute-unit-cut-e-waits-northwick-park-hospital/>.

Wise & Coombes, 2020: Wise J, Coombes R. Covid-19: The inside story of the RECOVERY trial. *BMJ*. 2020;370:m2670. <http://dx.doi.org/10.1136/bmj.m2670>.

Woolf et al., 2021a. Woolf SH, Chapman DA, Sabo RT, Zimmerman EB. Excess Deaths From COVID-19 and Other Causes in the US, March 1, 2020, to January 2, 2021. *JAMA*. 2021;325:1786–1789. <https://doi.org/10.1001/jama.2021.5199>.

Woolf et al., 2021b: Woolf SH, Masters RK, Aron LY. Effect of the covid-19 pandemic in 2020 on life expectancy across populations in the USA and other high income countries: simulations of provisional mortality data. *BMJ*. 2021;373:n1343. <https://doi.org/10.1136/bmj.n1343>.

Woolf et al., 2023: Woolf SH, Wolf ER, Rivara FP. The New Crisis of Increasing All-Cause Mortality in US Children and Adolescents. *JAMA*. 2023;329:975–976. <https://doi.org/10.1001/jama.2023.3517>.

Wunsch, 2020. Wunsch H. Mechanical Ventilation in COVID-19: Interpreting the Current Epidemiology. *American Journal of Respiratory and Critical Care Medicine*. 2020;202:1-21. <https://doi.org/10.1164/rccm.202004-1385ED>.

Yorifuji et al., 2021: Yorifuji T, Matsumoto N, Takao S. Excess All-Cause Mortality During the COVID-19 Outbreak in Japan. *Journal of Epidemiology*. 2021;31:90-92. <https://doi.org/10.2188/jea.JE20200492>.

Zawisza et al., 2024: Zawisza K, Sekuła P, Gajdzica M, Tobiasz-Adamczyk B. Social capital and all-cause mortality before and during the COVID-19 pandemic among middle-aged and older people: Prospective cohort study in Poland. *Social Science and Medicine*. 2024;343:116573. <https://doi.org/10.1016/j.socscimed.2024.116573>.

Zehender et al., 2020: Zehender G, Lai A, Bergna A, Meroni L, Riva A, Balotta C, et al. Genomic characterization and phylogenetic analysis of SARS-COV-2 in Italy. *Journal of Medical Virology*. 2020;92:1637-1640. <https://doi.org/10.1002/jmv.25794>.

Zou et al., 2024: Zou F, Xiao J, Jin Y, Jian R, Hu Y, Liang X, et al. Multilayer factors associated with excess all-cause mortality during the omicron and non-omicron waves of the COVID-19 pandemic: time series analysis in 29 countries. *BMC Public Health*. 2024;24:350. <https://doi.org/10.1186/s12889-024-17803-8>.

A. Additional graphs pertaining to section 3.3

A.1 Europe, weekly P-scores for national-level (NUTS0) jurisdictions, all countries, geographic subsets

The figures in this appendix subsection show weekly P-scores (top panels) for groups of European countries organized geographically, from west to east.

The bottom panel in each figure shows the same data as the top panel, with each curve scaled by its maximum weekly P-score.

In all figures, Italy (black) is included as a reference curve.

European countries PT, ES, FR, UK, IE, IT

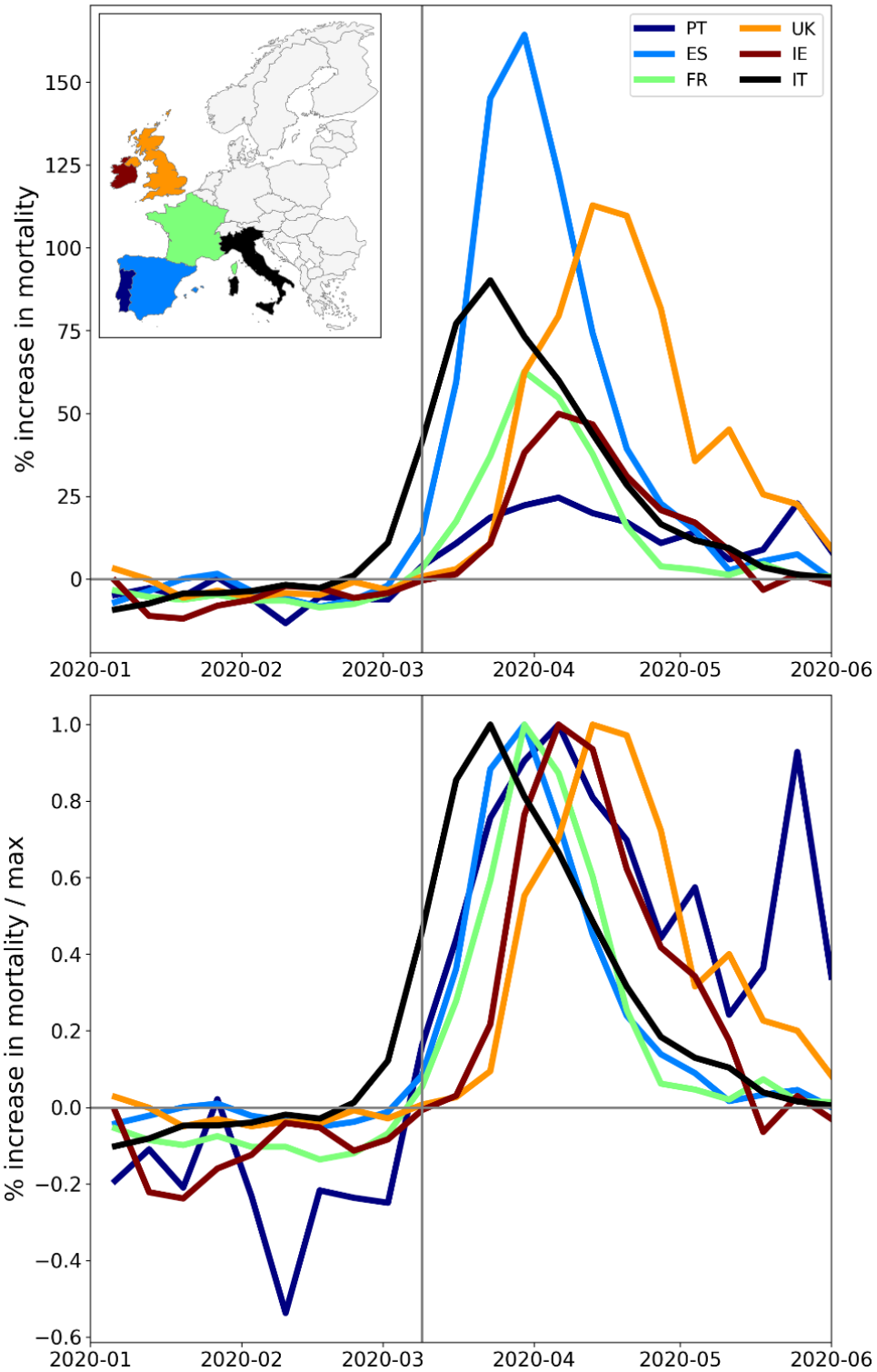


Figure 170: Upper panel: weekly P-scores during the first-peak period for European countries Portugal, Spain, France, UK, Ireland (plus Italy, in black). Lower panel: same as upper panel, with each curve scaled by its maximum.

European countries BE, NL, LU, DE, CH, AT, IT

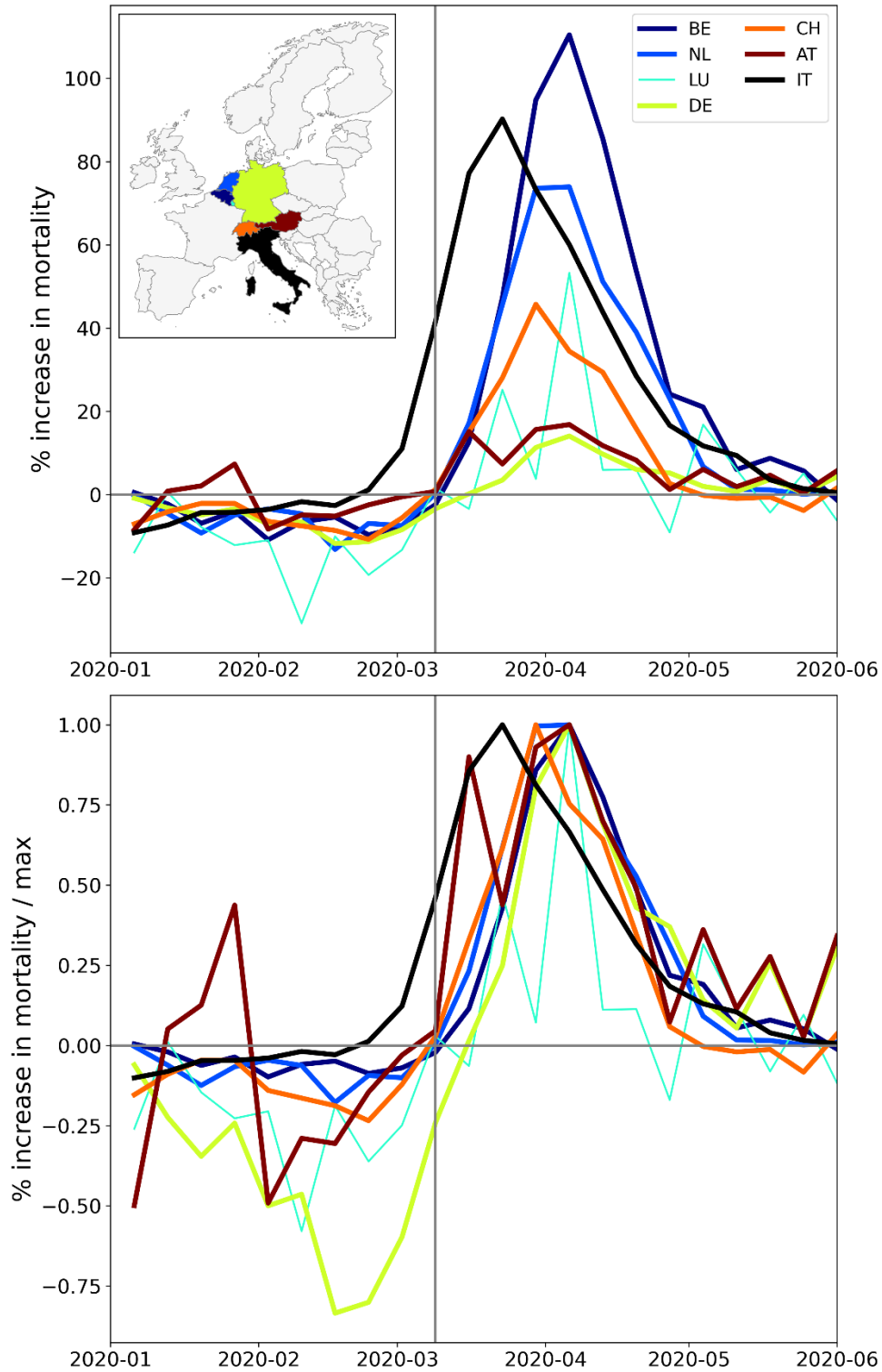


Figure 171: Upper panel: weekly P-scores during the first-peak period for European countries Belgium, Netherlands, Luxembourg, Germany, Switzerland, Austria (plus Italy, in black). Lower panel: same as upper panel, with each curve scaled by its maximum.

European countries DK, NO, SE, FI, IS, IT

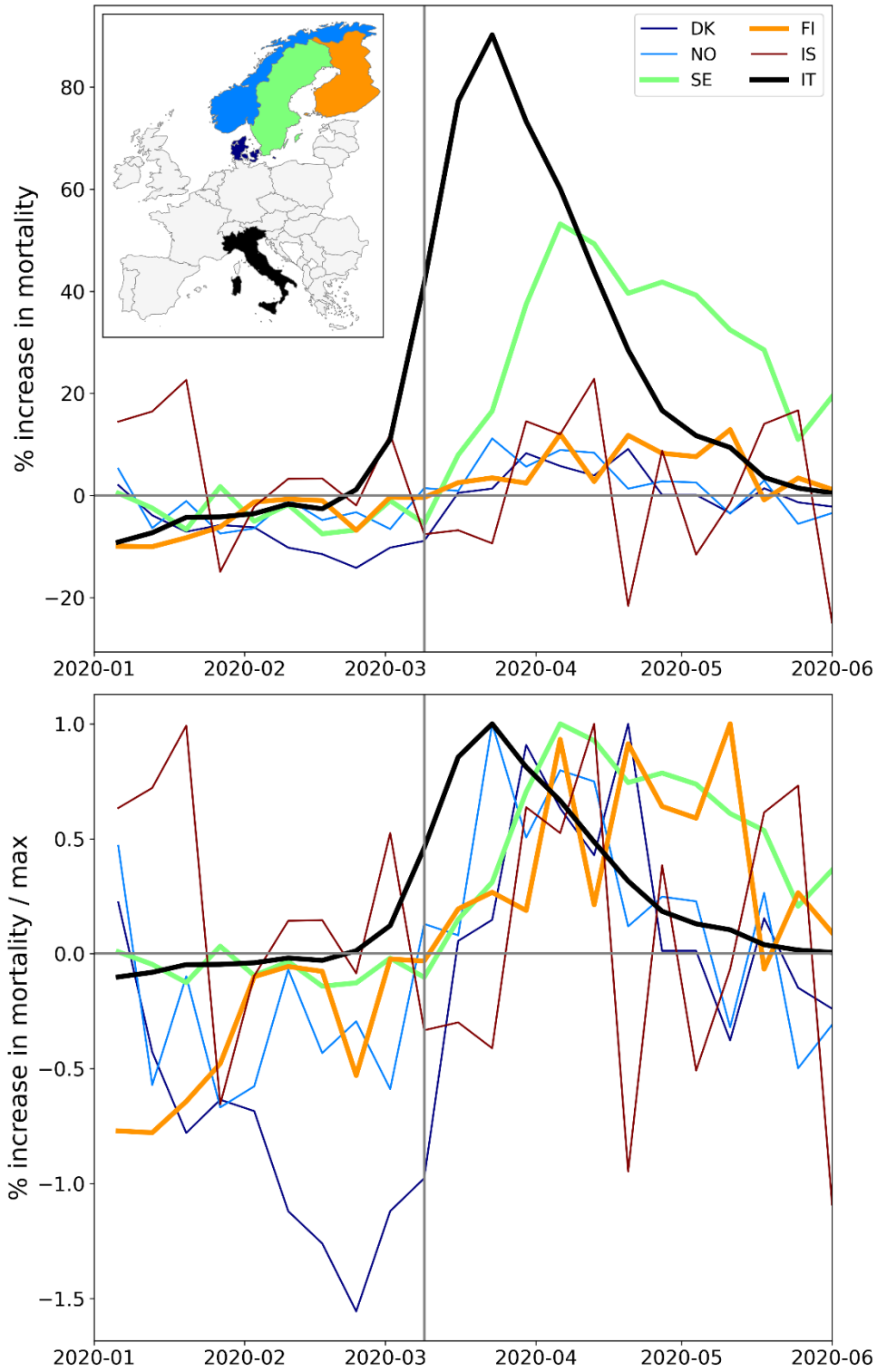


Figure 172: Upper panel: weekly P-scores during the first-peak period for European countries Denmark, Norway, Sweden, Finland, Iceland (plus Italy, in black). Lower panel: same as upper panel, with each curve scaled by its maximum.

European countries EE, LV, LT, IT

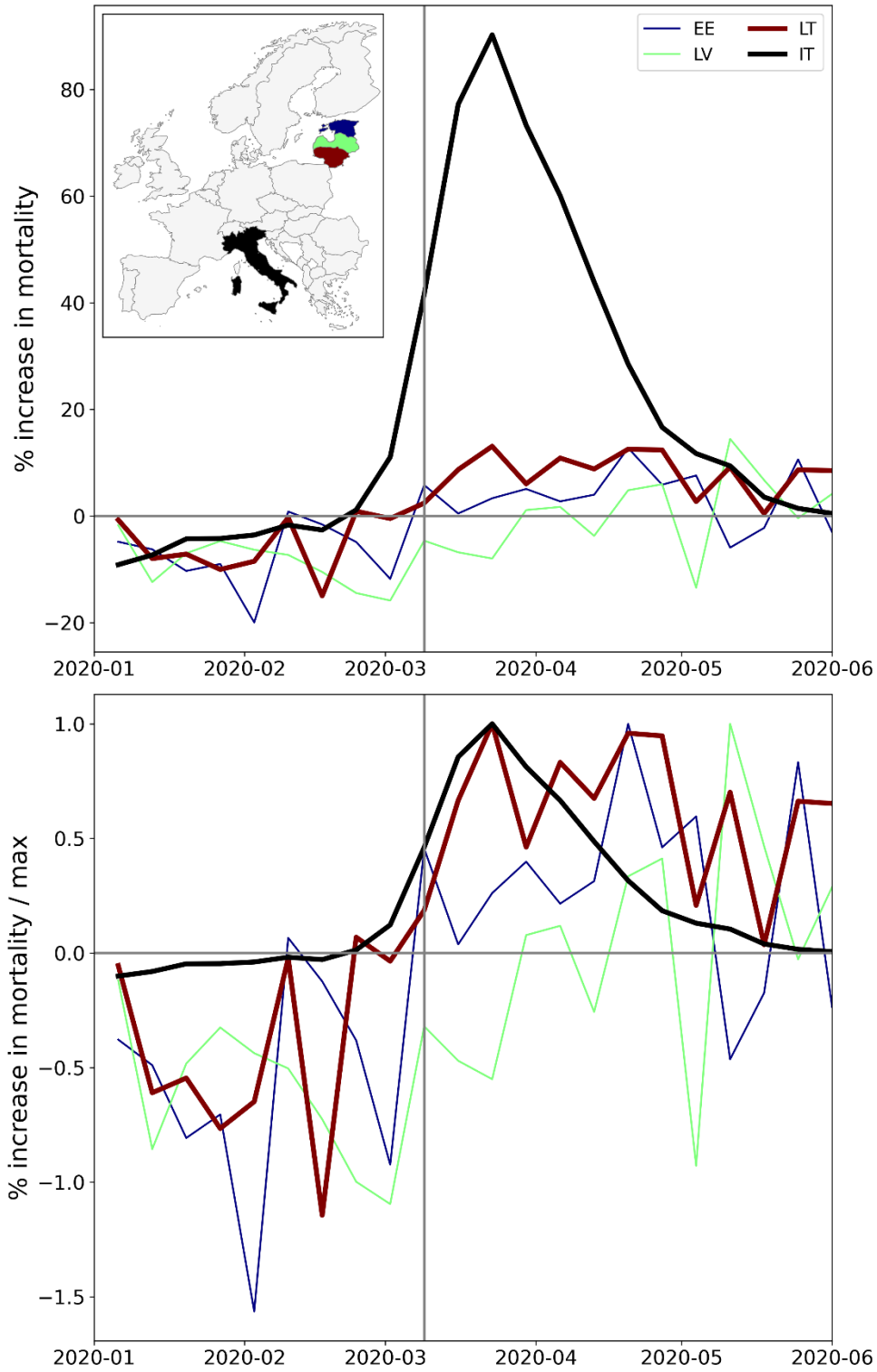


Figure 173: Upper panel: weekly P-scores during the first-peak period for European countries Estonia, Latvia, Lithuania (plus Italy, in black). Lower panel: same as upper panel, with each curve scaled by its maximum.

European countries PL, SK, CZ, HU, IT

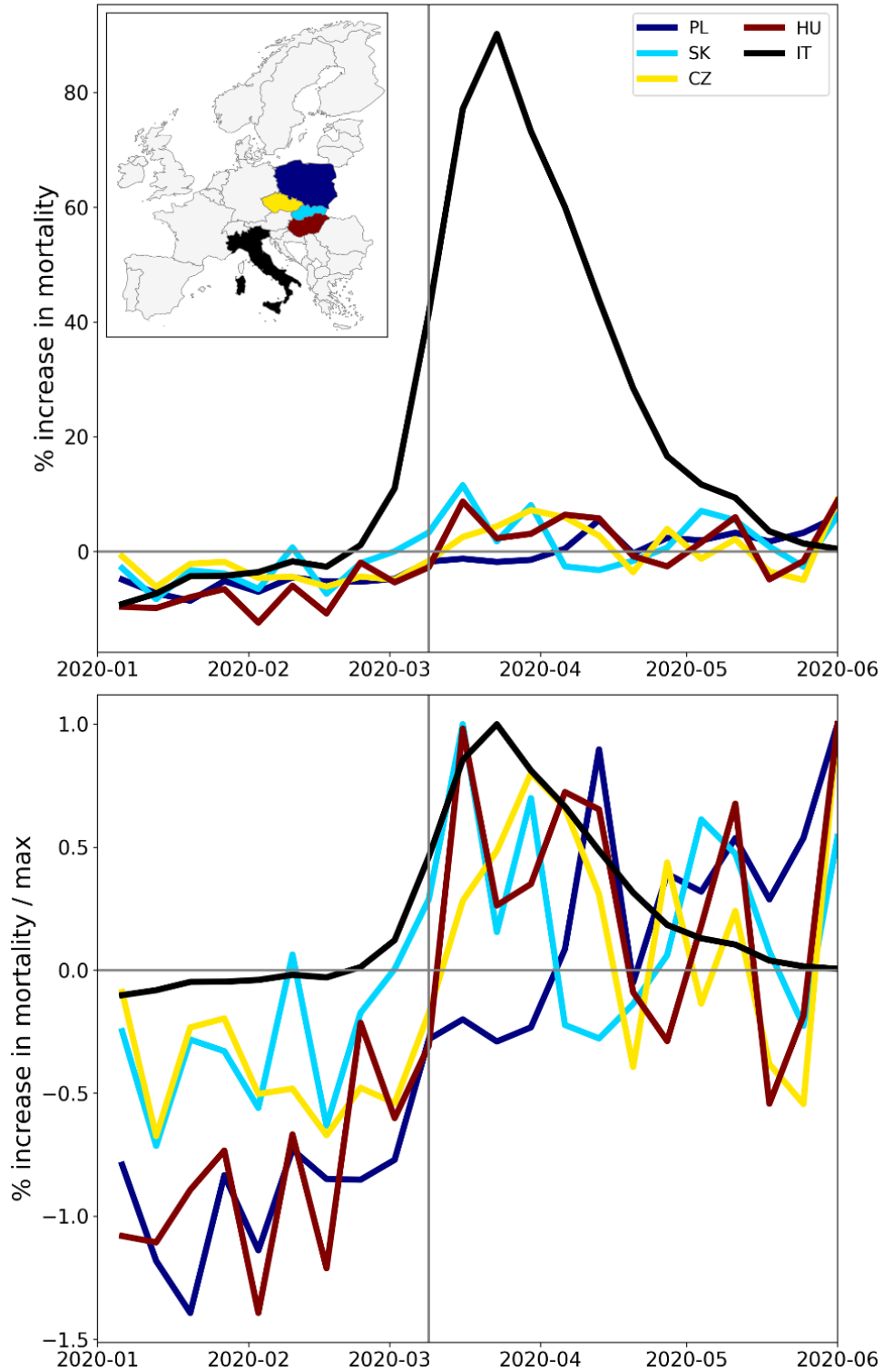


Figure 174: Upper panel: weekly P-scores during the first-peak period for European countries Poland, Slovakia, Czechia, Hungary (plus Italy, in black). Lower panel: same as upper panel, with each curve scaled by its maximum.

European countries SI, HR, RS, AL, ME, IT

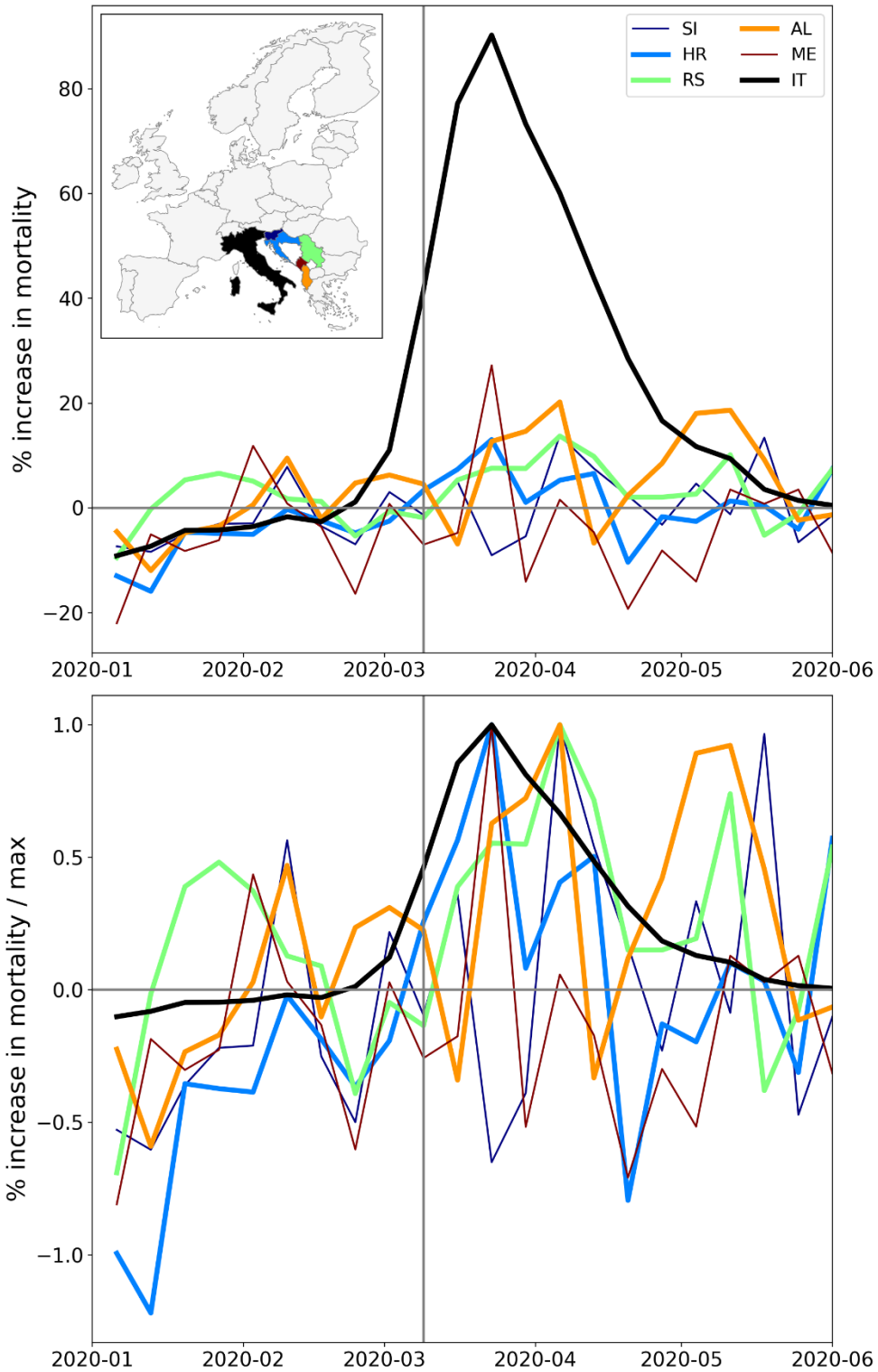


Figure 175: Upper panel: weekly P-scores during the first-peak period for European countries Slovenia, Croatia, Serbia, Albania, Montenegro (plus Italy, in black). Lower panel: same as upper panel, with each curve scaled by its maximum.

European countries EL, RO, BG, CY, IT

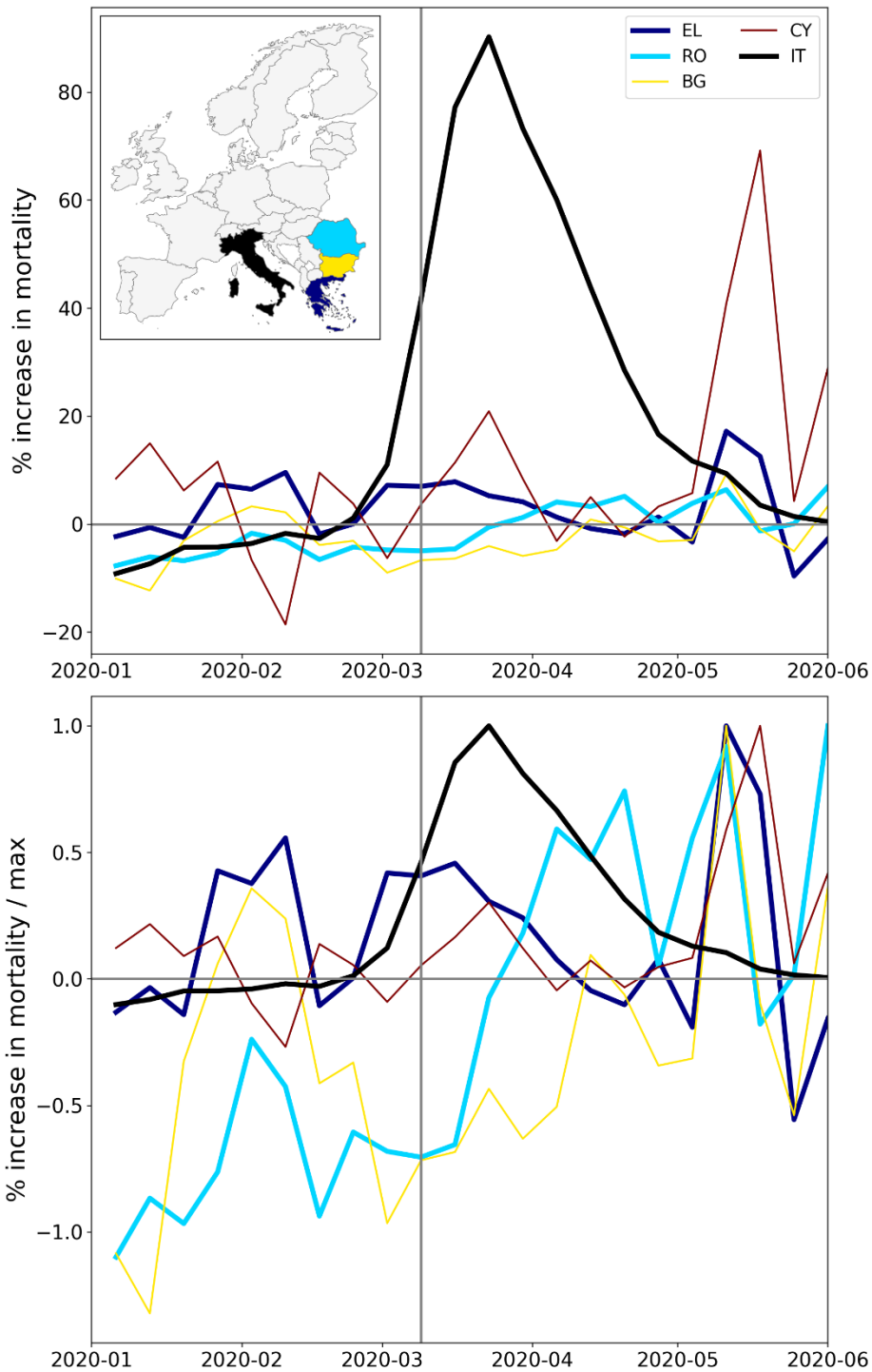


Figure 176: Upper panel: weekly P-scores during the first-peak period for European countries Greece, Romania, Bulgaria, Cyprus (plus Italy, in black). Lower panel: same as upper panel, with each curve scaled by its maximum. The sharp peak in mid-May for Cyprus (also seen to a lesser extent for Greece and Bulgaria) is due to a heatwave affecting the eastern Mediterranean region (Financial Mirror, 2020; Korosec, 2020; Mitropoulos et al., 2023).

A.2 USA, weekly P-scores for all states, organized geographically by census division

The figures in this appendix subsection show weekly P-scores (top panels) for groups of USA states organized geographically, by census division.

The bottom panel in each figure shows the same data as the top panel, with each curve scaled by its maximum weekly P-score.

In all figures, New York State (black) is included as a reference curve.

Census Division = New England

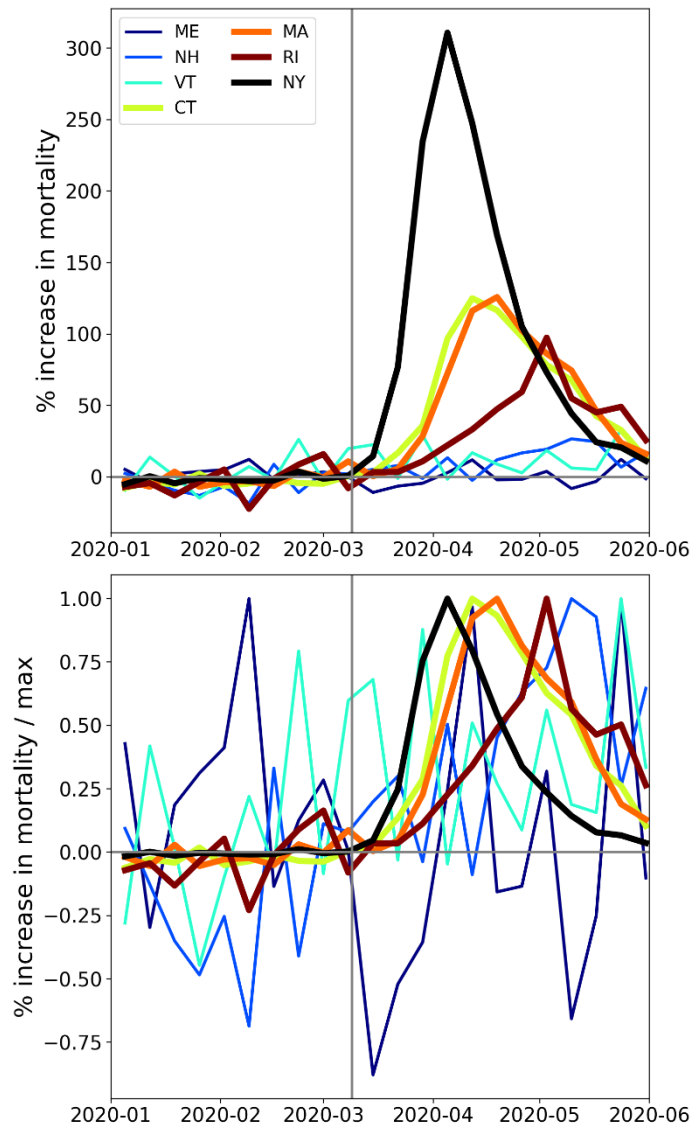


Figure 177: Top panel: states in the New England census division (plus New York State, in black). Middle panel: weekly P-scores during the first-peak period. Lower panel: same as middle panel, with each curve scaled by its maximum.

Census Division = Middle Atlantic

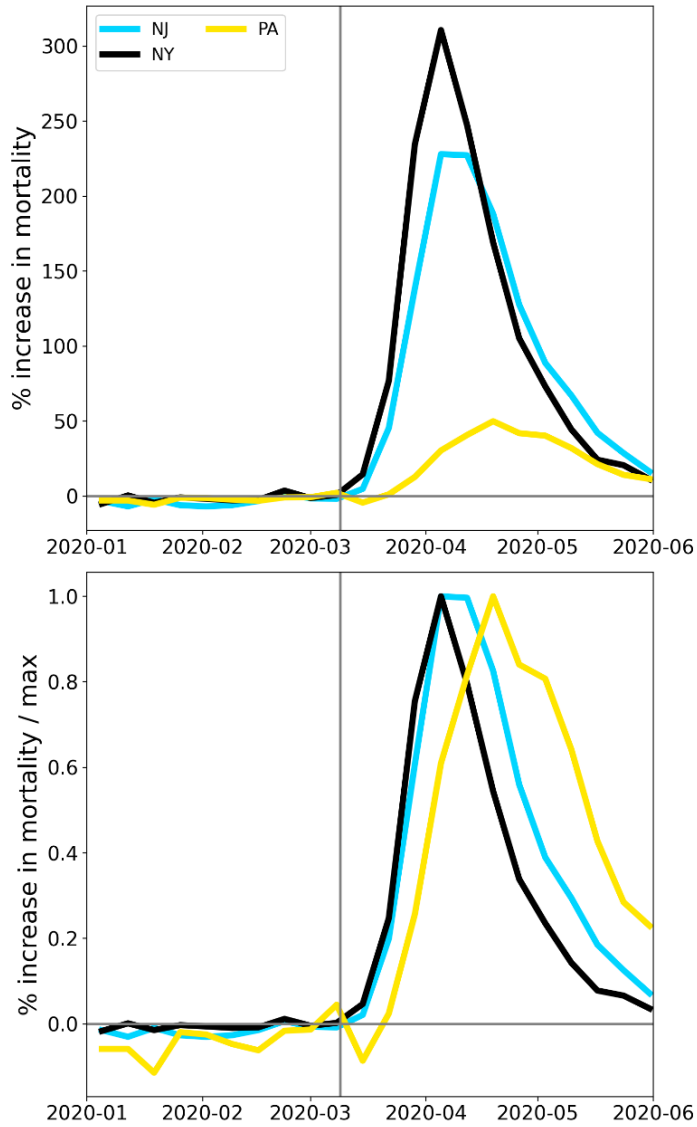


Figure 178: Top panel: states in the Middle Atlantic census division. Middle panel: weekly P-scores during the first-peak period. Lower panel: same as middle panel, with each curve scaled by its maximum.

Census Division = South Atlantic (part 1)

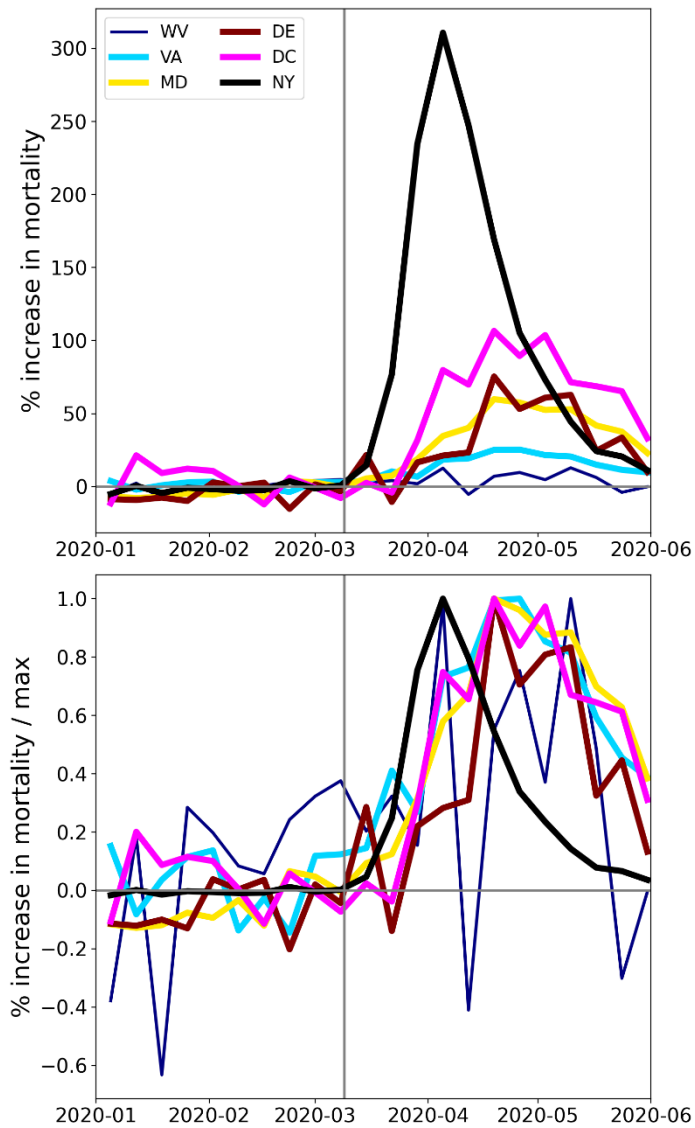
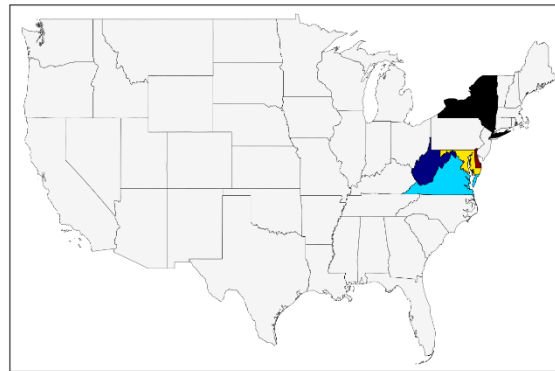


Figure 179: Top panel: states in the northern half of the South Atlantic census division (plus NY, black). Middle panel: weekly P-scores during the first-peak period. Lower panel: same as middle panel, with each curve scaled by its maximum.

Census Division = South Atlantic (part 2)

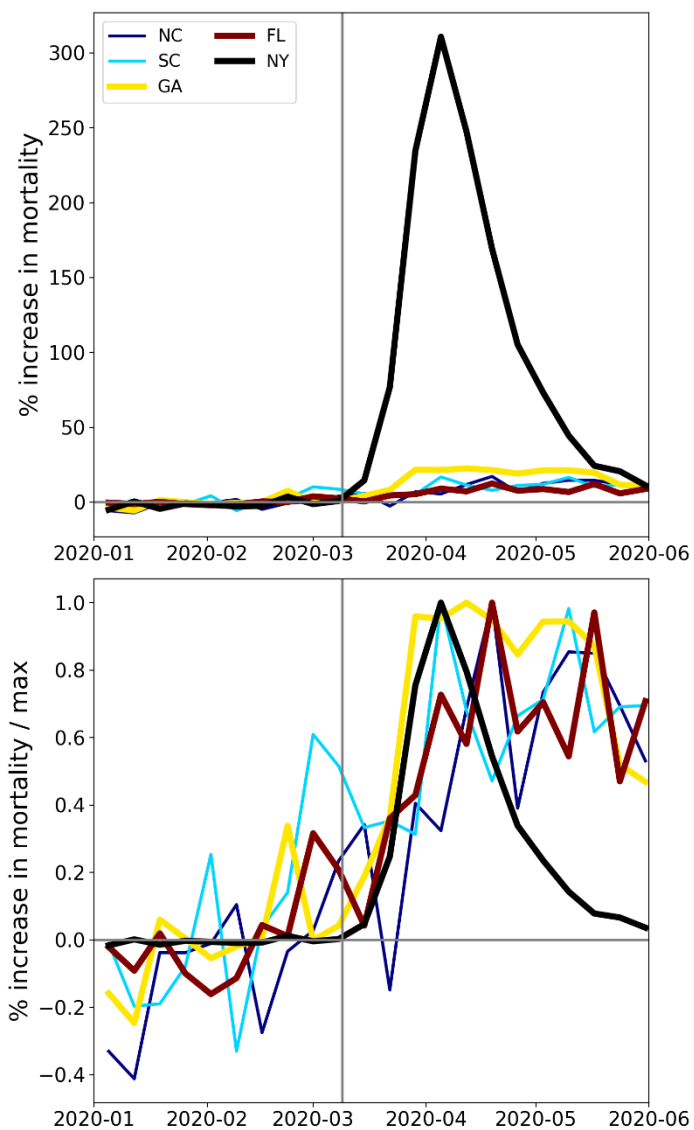
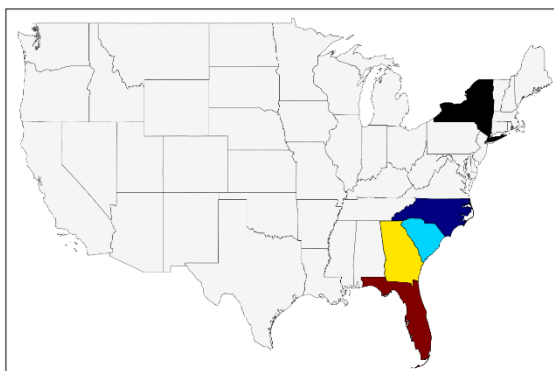


Figure 180: Top panel: states in the southern half of the South Atlantic census division (plus NY, black). Middle panel: weekly P-scores during the first-peak period. Lower panel: same as middle panel, with each curve scaled by its maximum.

Census Division = East North Central

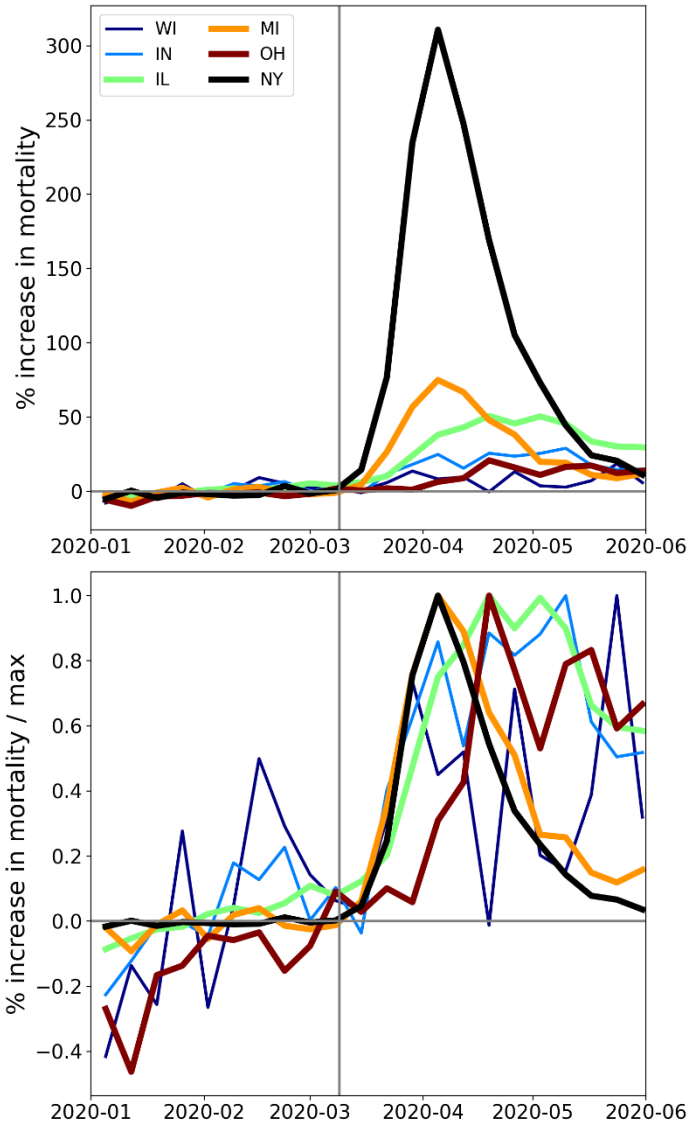
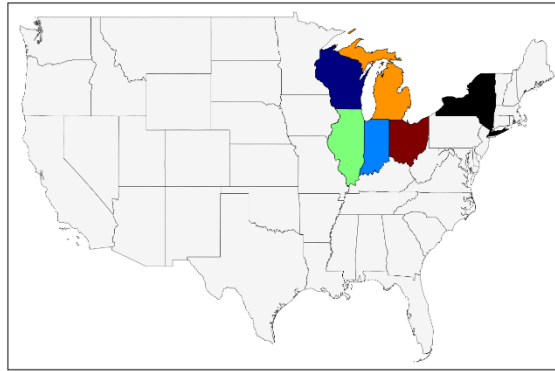


Figure 181: Top panel: states in the East North Central census division (plus NY, in black). Middle panel: weekly P-scores during the first-peak period. Lower panel: same as middle panel, with each curve scaled by its maximum.

Census Division = East South Central

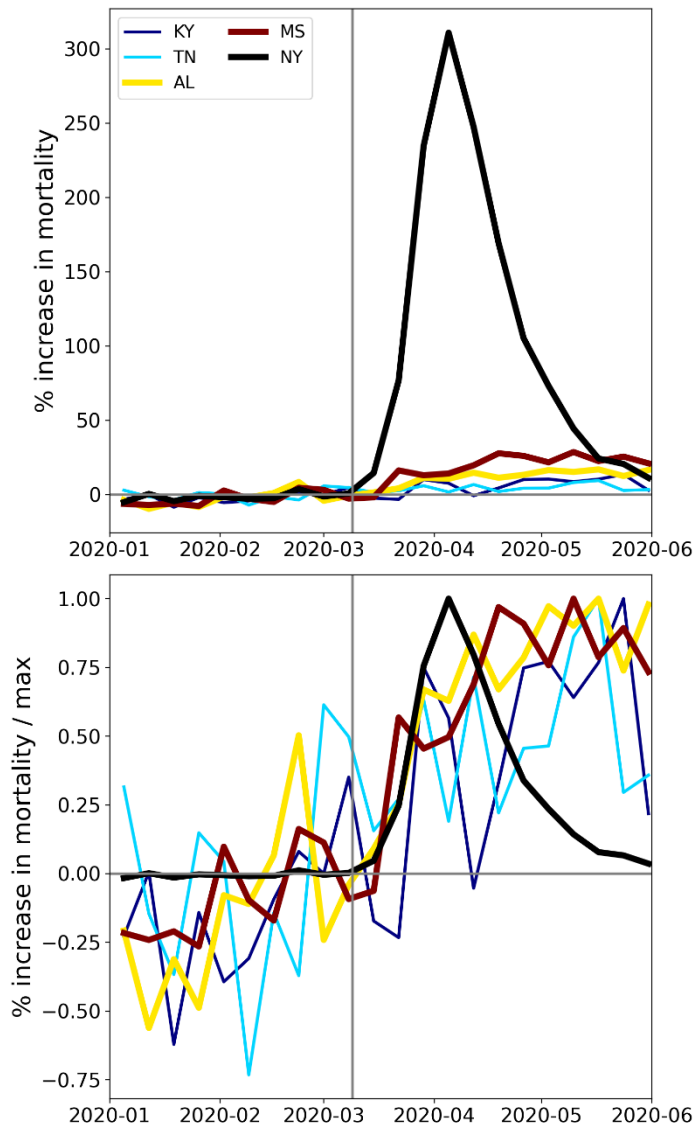


Figure 182: Top panel: states in the East South Central census division (plus NY, in black). Middle panel: weekly P-scores during the first-peak period. Lower panel: same as middle panel, with each curve scaled by its maximum.

Census Division = West North Central (part 1)

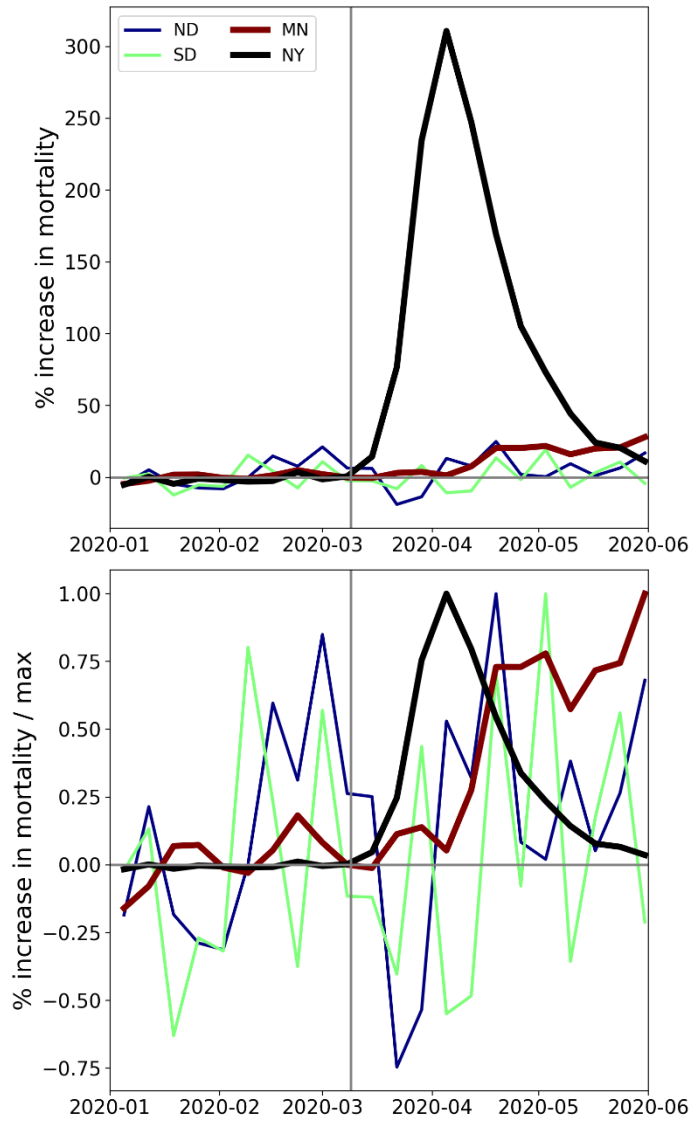
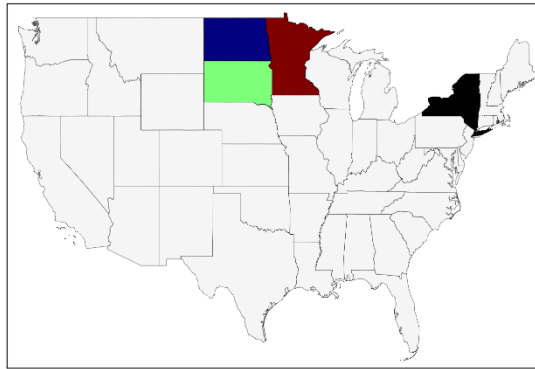


Figure 183: Top panel: states in the northern half of the West North Central census division (plus New York State, in black). Middle panel: weekly P-scores during the first-peak period. Lower panel: same as middle panel, with each curve scaled by its maximum.

Census Division = West North Central (part 2)

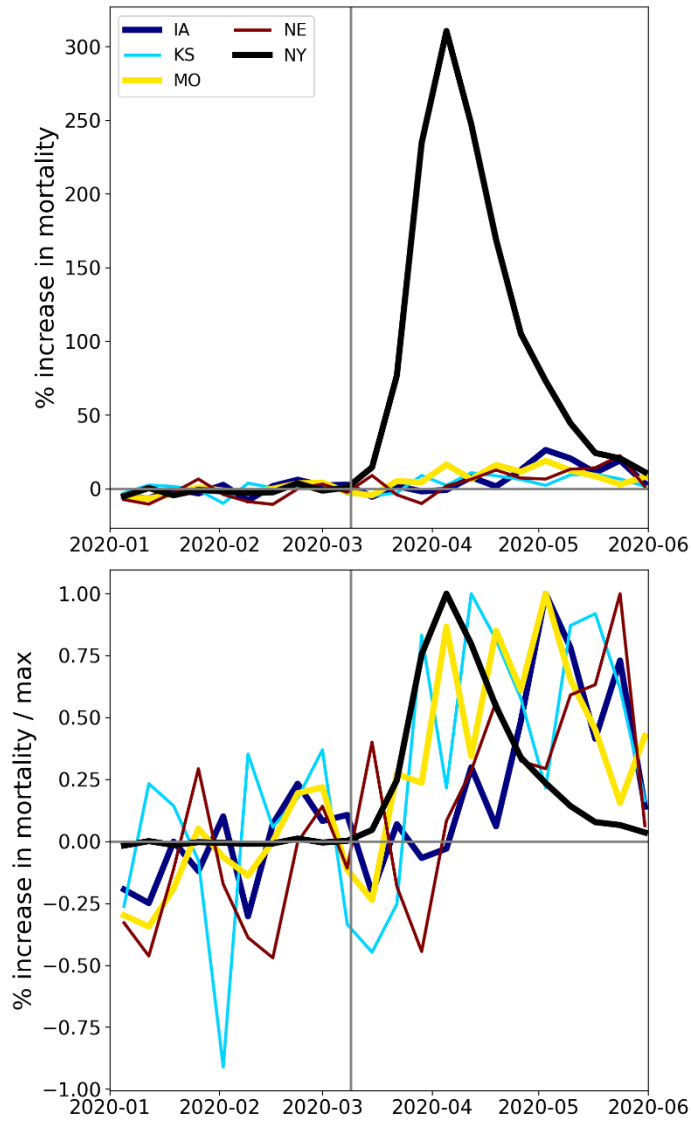
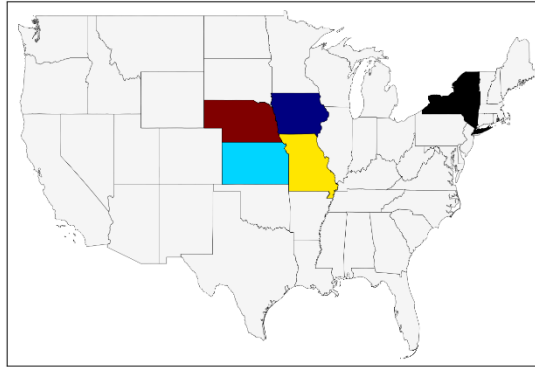


Figure 184: Top panel: states in the southern half of the West North Central census division (plus New York State, in black). Middle panel: weekly P-scores during the first-peak period. Lower panel: same as middle panel, with each curve scaled by its maximum.

Census Division = West South Central

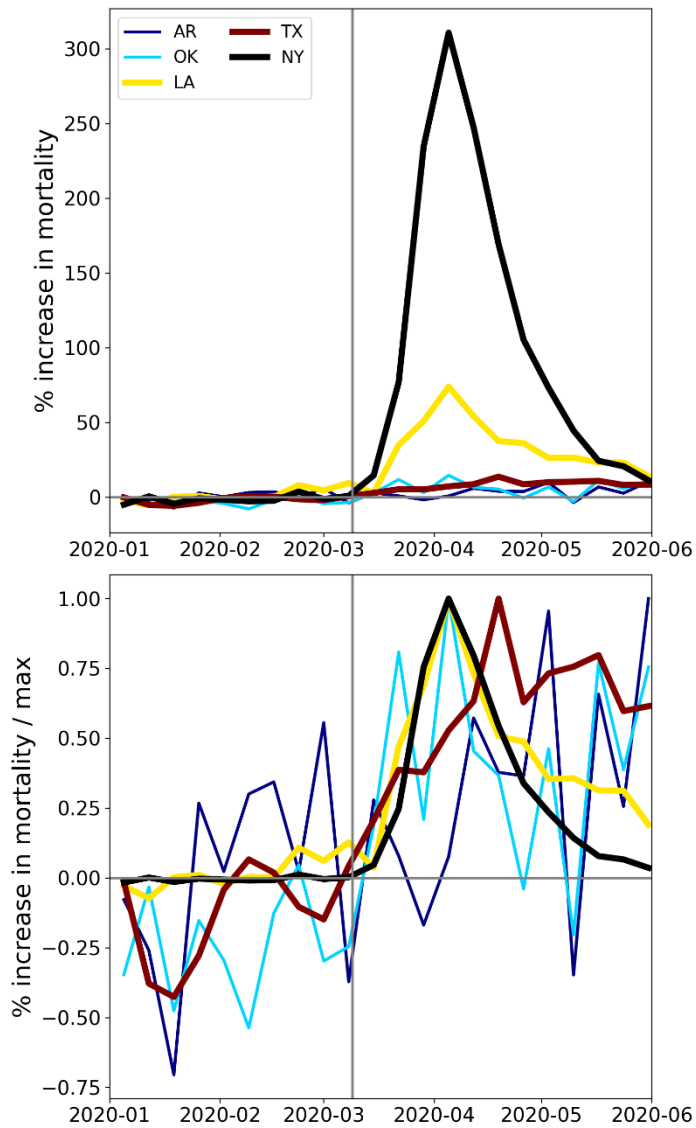
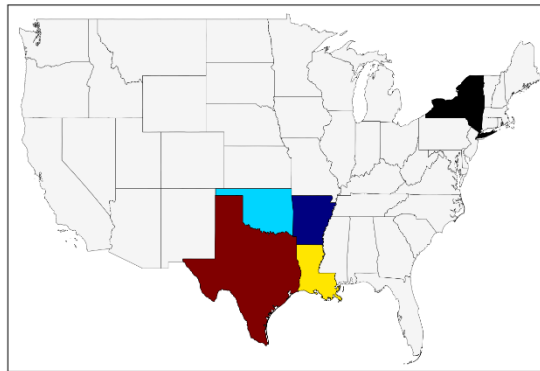


Figure 185: Top panel: states in the West South Central census division (plus NY, in black). Middle panel: weekly P-scores during the first-peak period. Lower panel: same as middle panel, with each curve scaled by its maximum.

Census Division = Mountain (part 1)

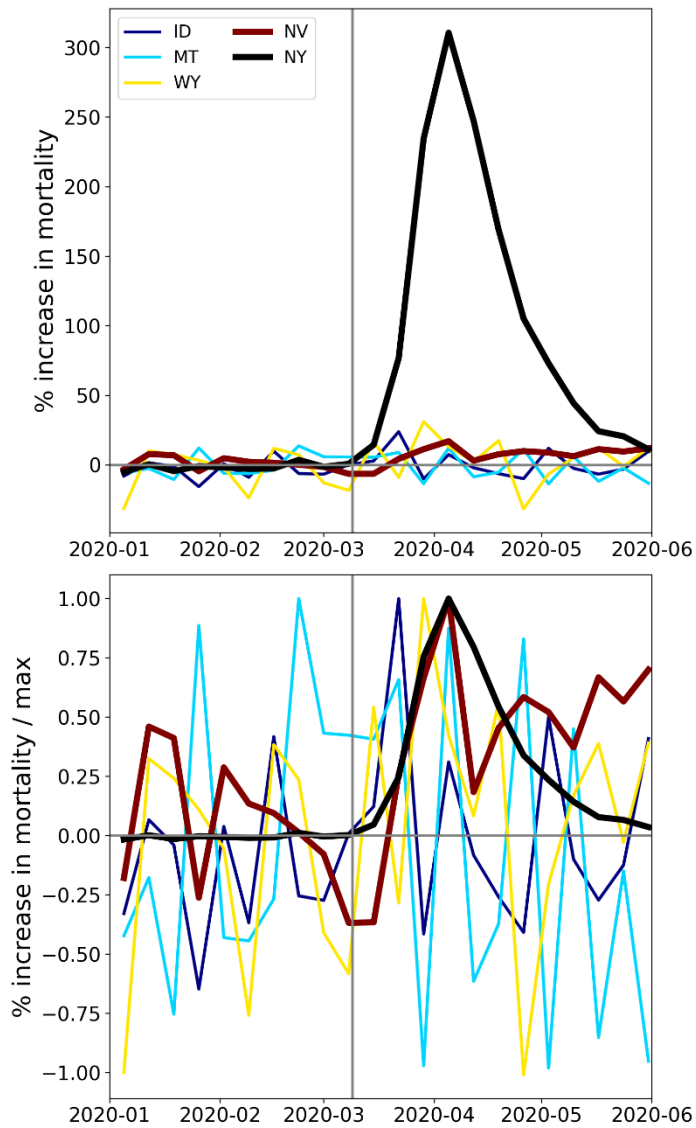
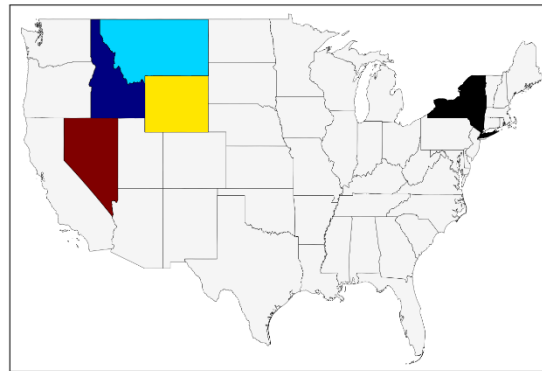


Figure 186: Top panel: states in the northern part of the Mountain census division (plus NY, in black). Middle panel: weekly P-scores during the first-peak period. Lower panel: same as middle panel, with each curve scaled by its maximum.

Census Division = Mountain (part 2)

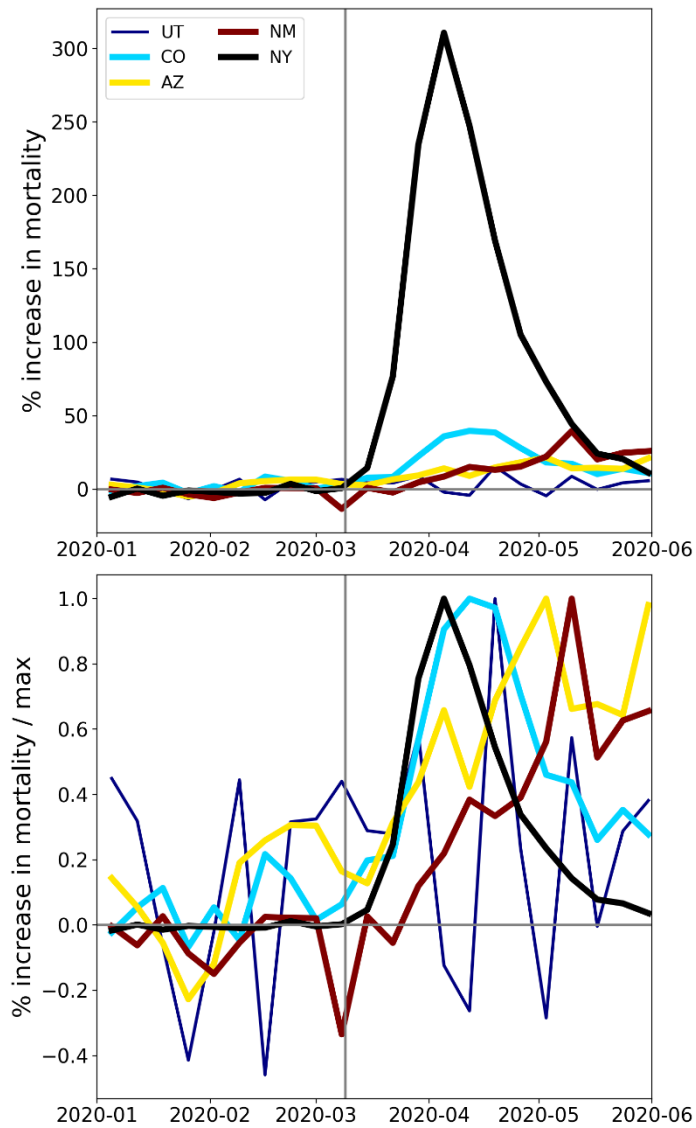
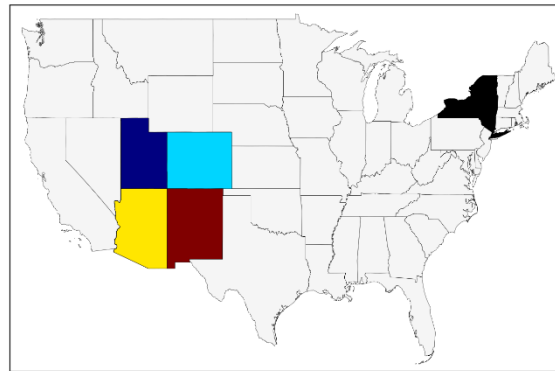


Figure 187: Top panel: states in the southern part of the Mountain census division (plus NY, in black). Middle panel: weekly P-scores during the first-peak period. Lower panel: same as middle panel, with each curve scaled by its maximum.

Census Division = Pacific

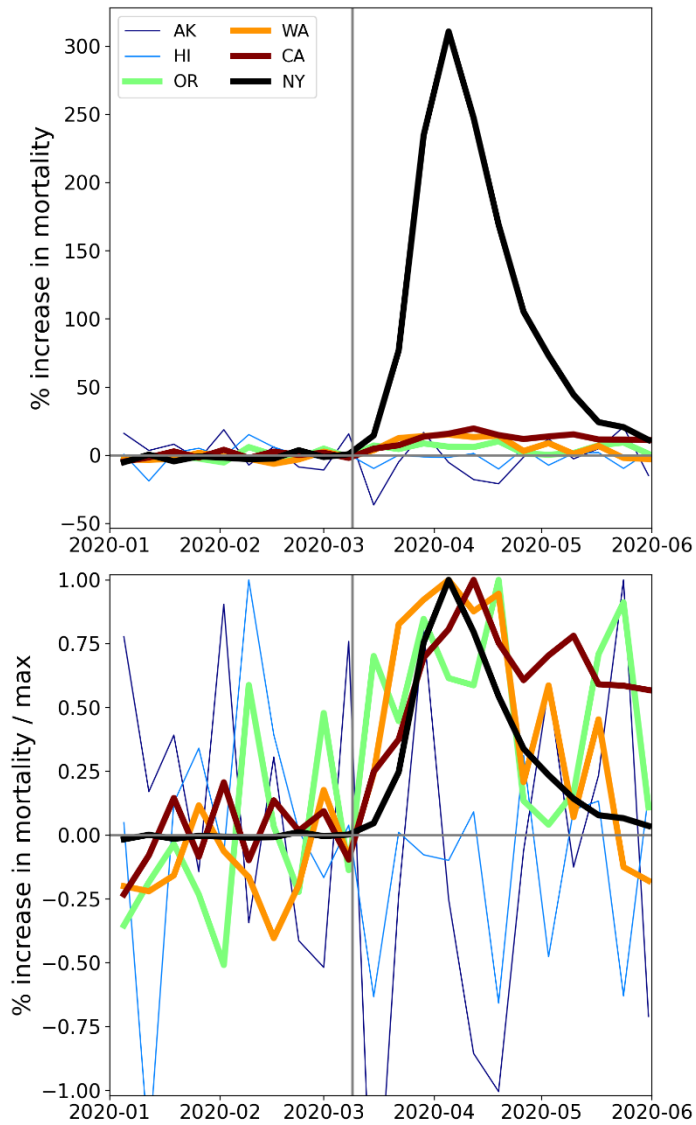
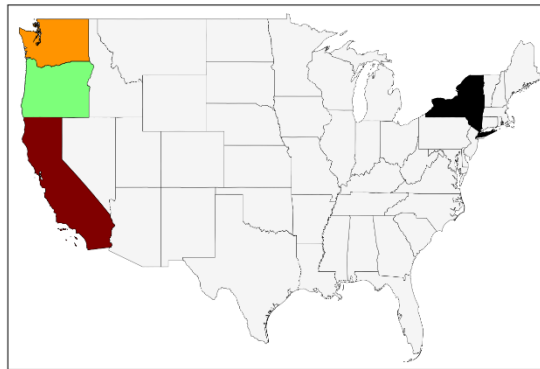
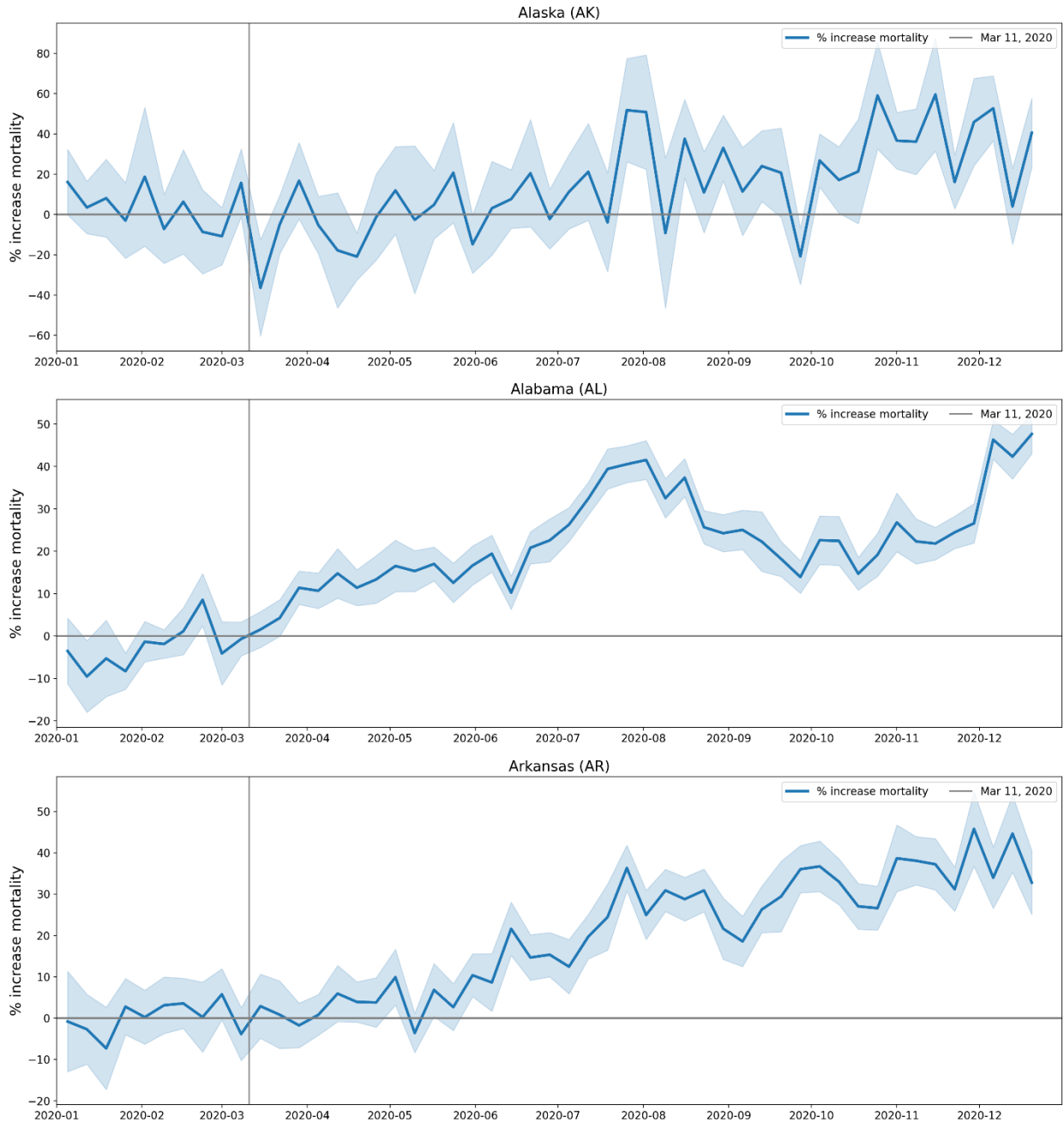
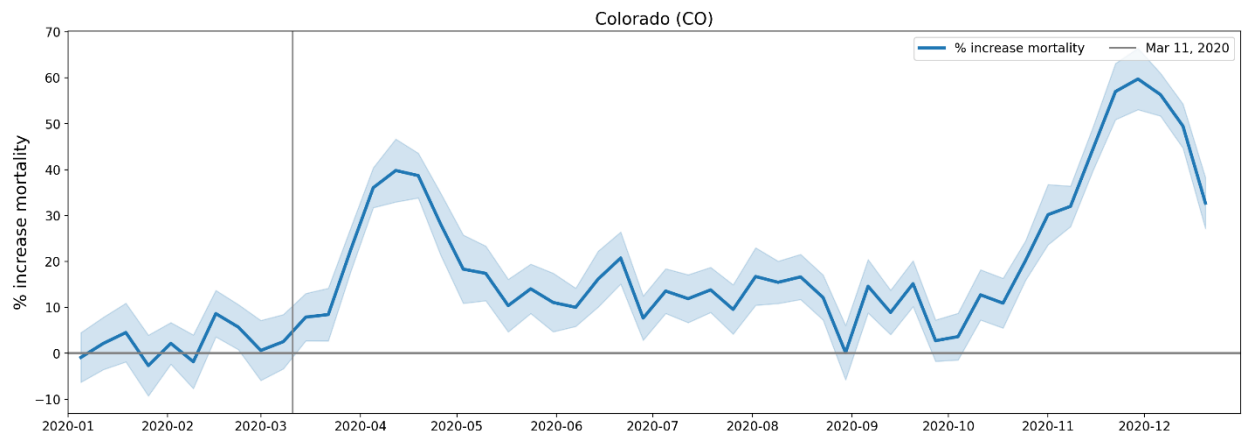
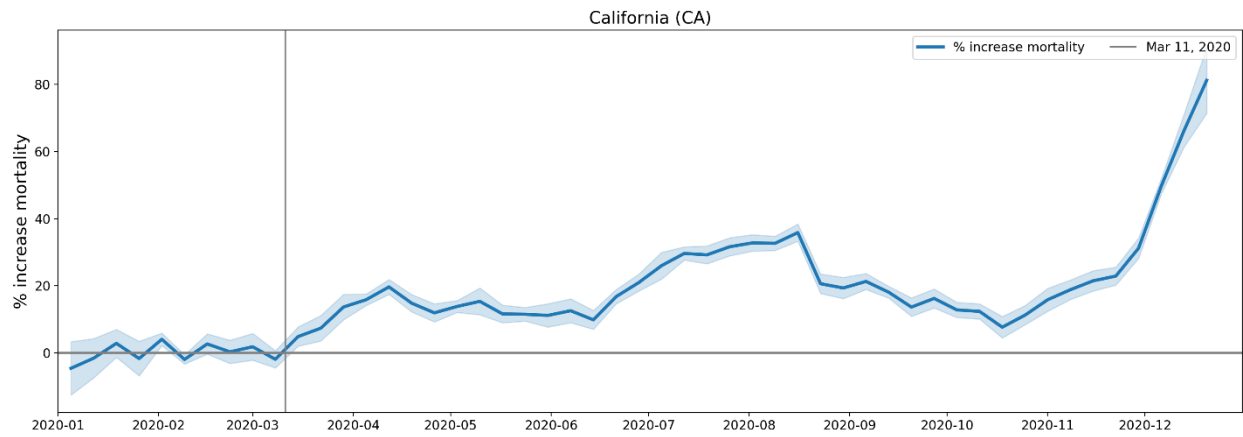
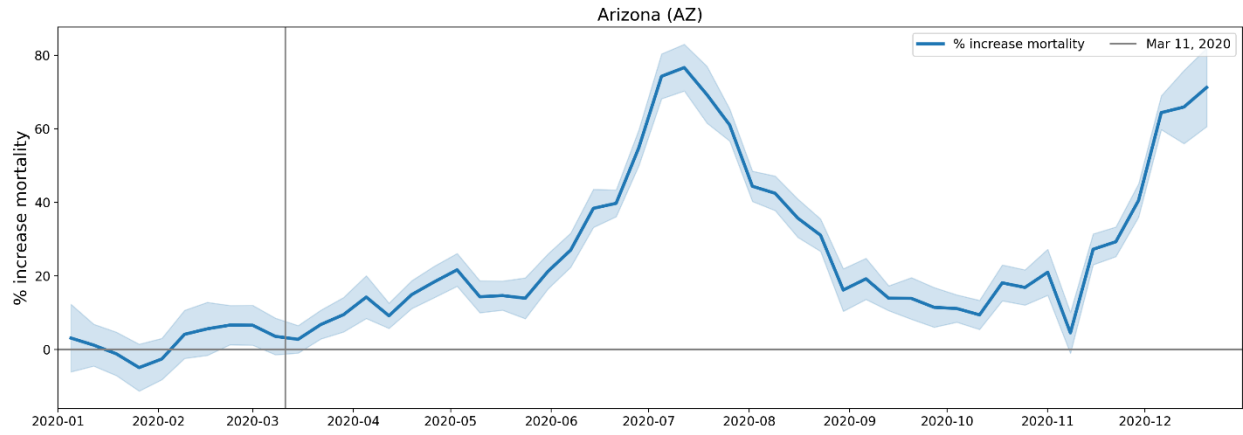


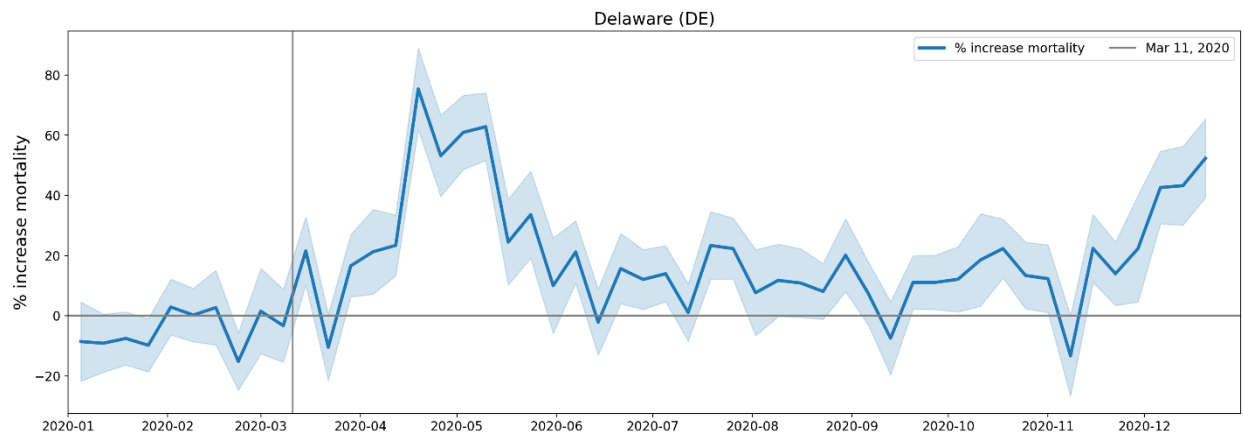
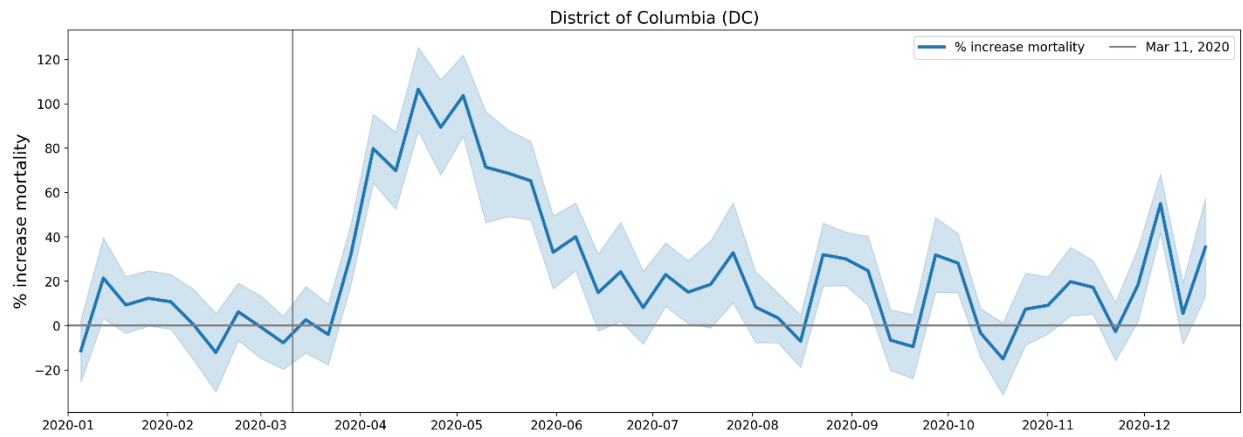
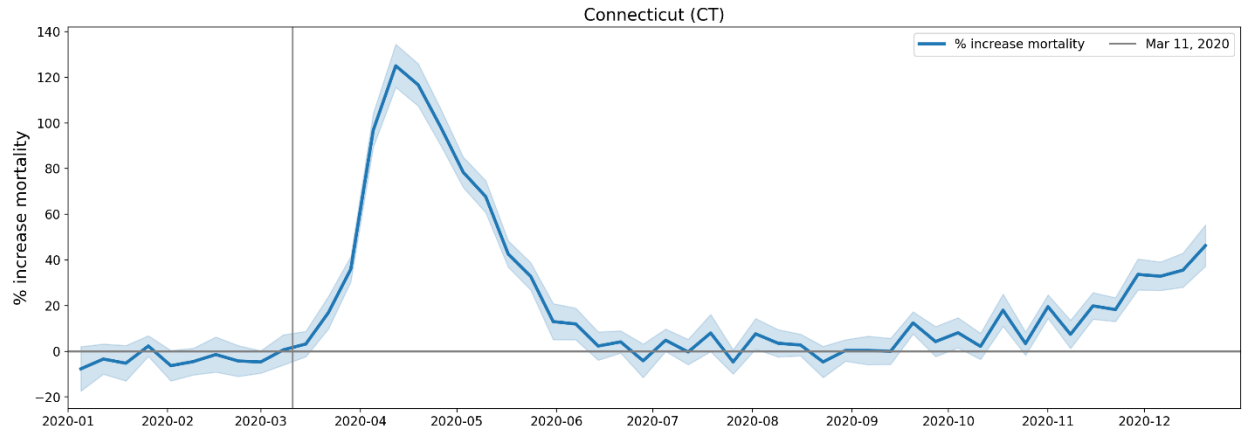
Figure 188: Top panel: states in the Pacific census division (plus NY, black; Hawaii and Alaska not shown). Middle panel: weekly P-scores during the first-peak period. Lower panel: same as middle panel, with each curve scaled by its maximum.

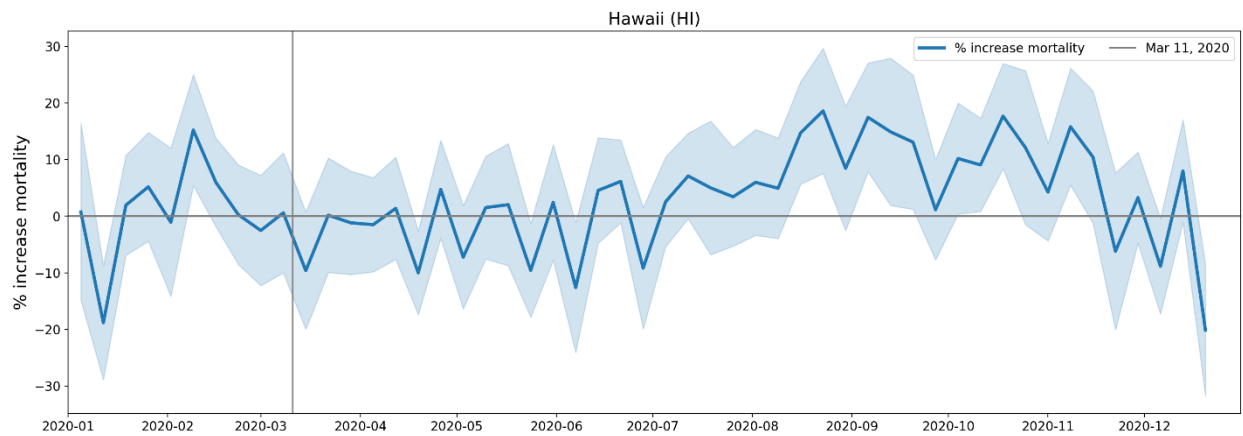
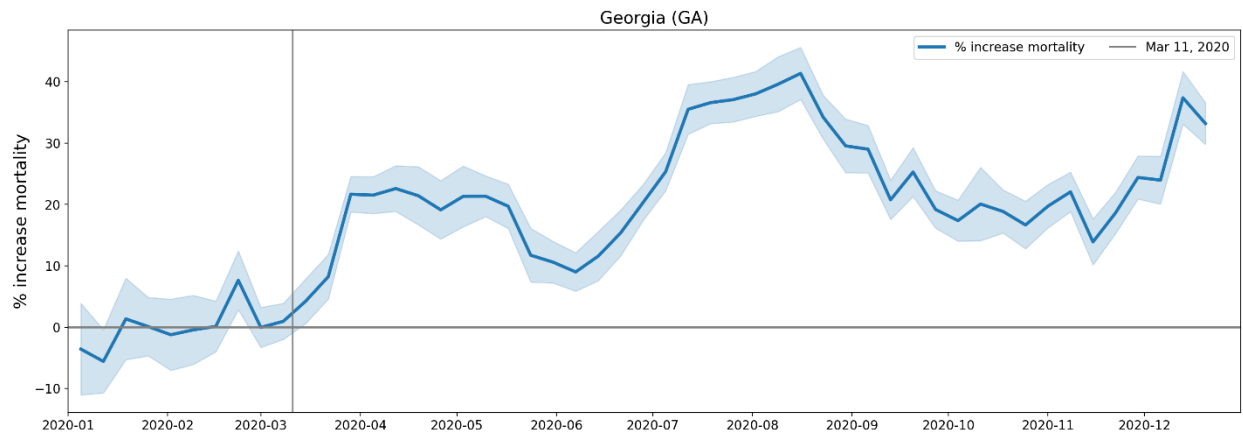
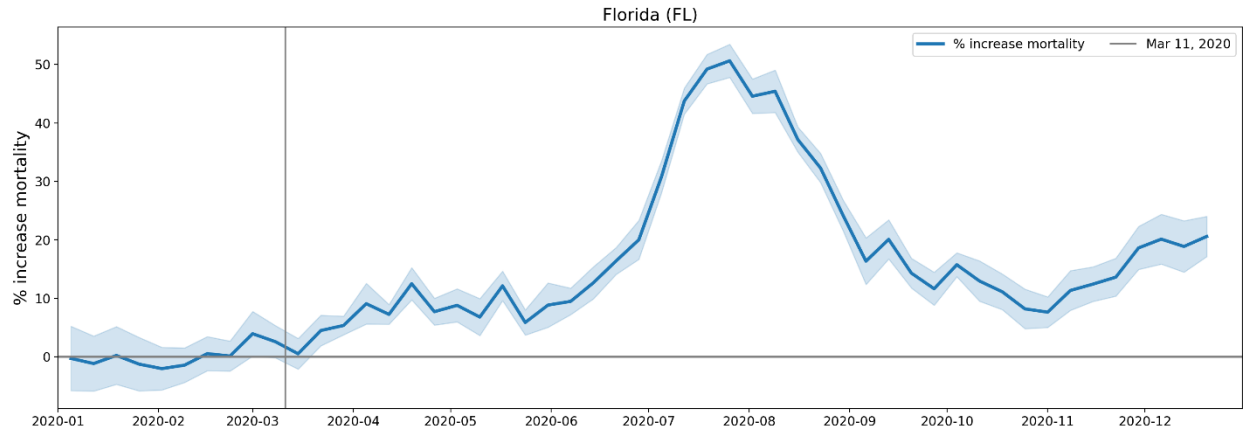
A.3 USA, weekly P-scores for each state, for the year 2020

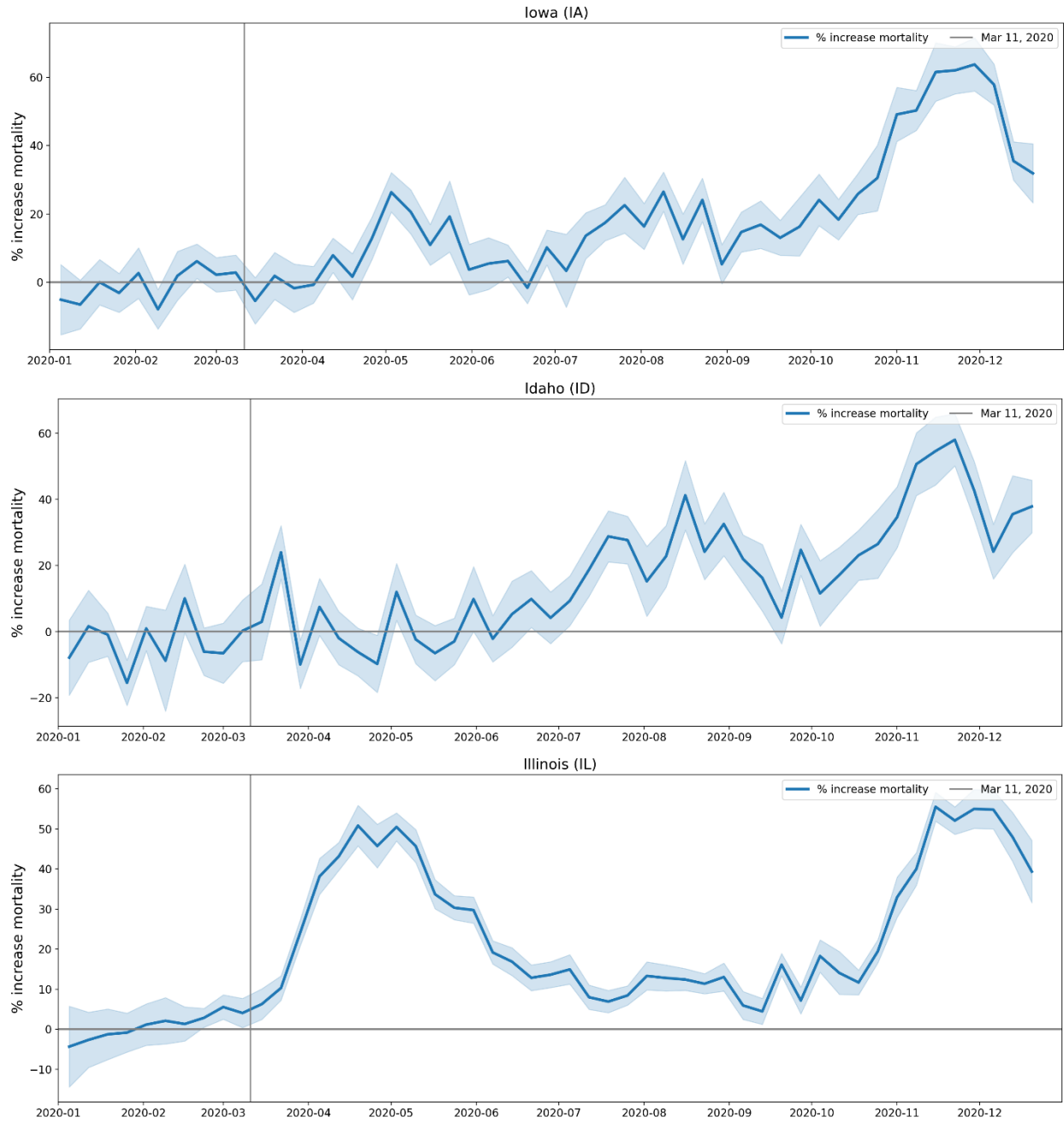
The figures in this appendix subsection show weekly P-scores for USA states (solid blue lines) with 1σ error ranges shown as shaded blue areas.

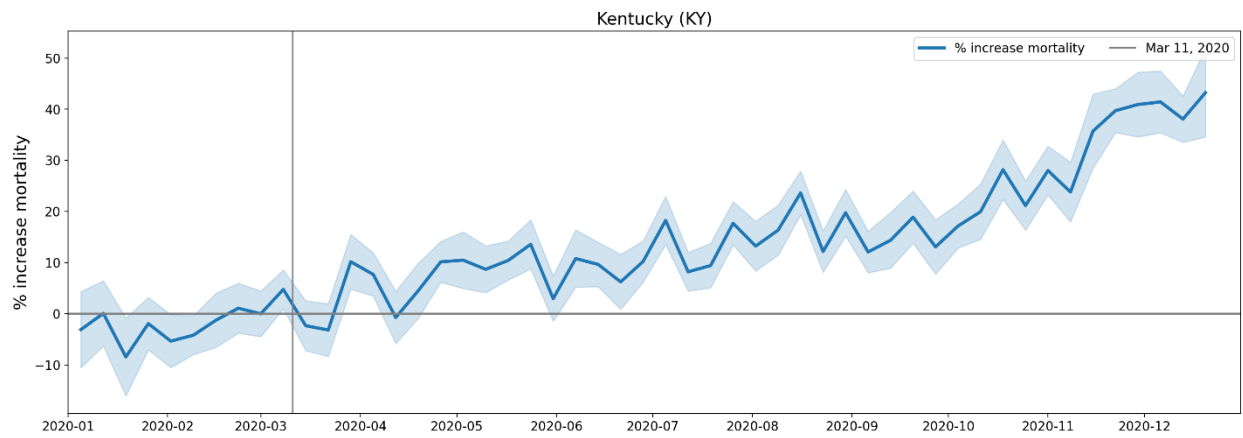
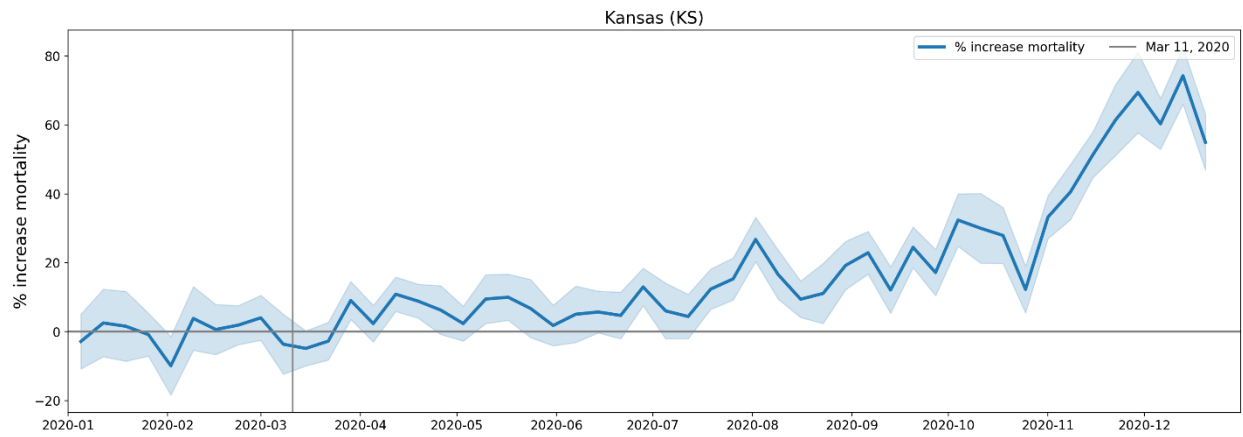
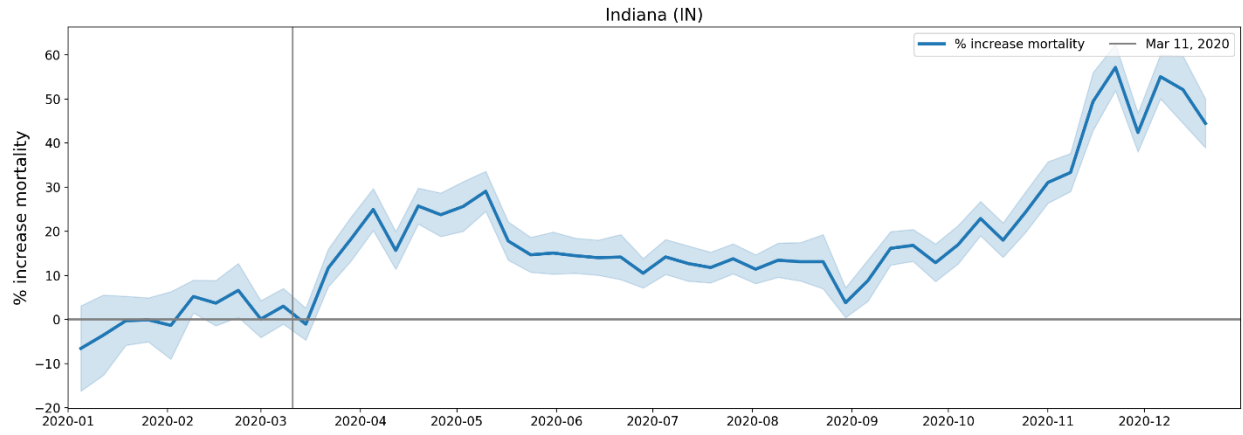


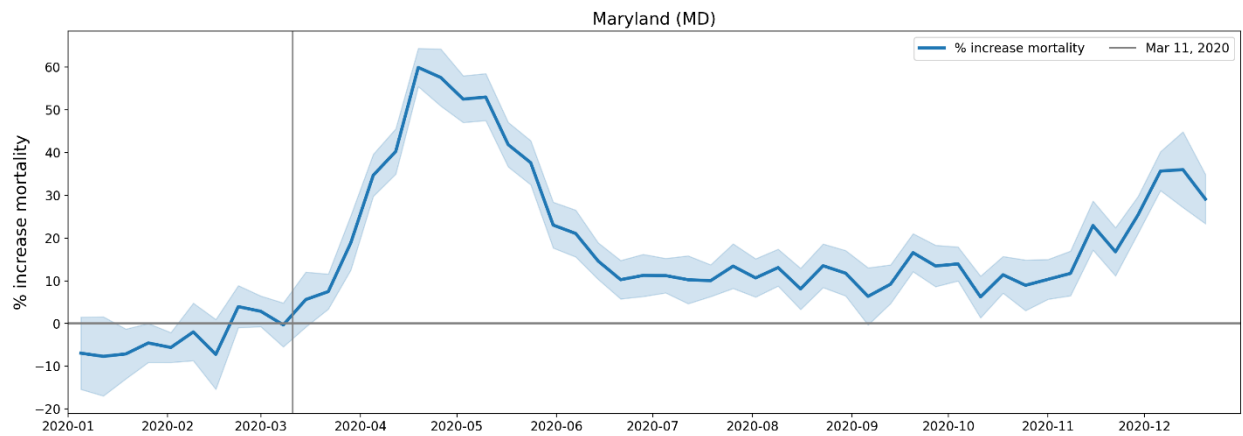
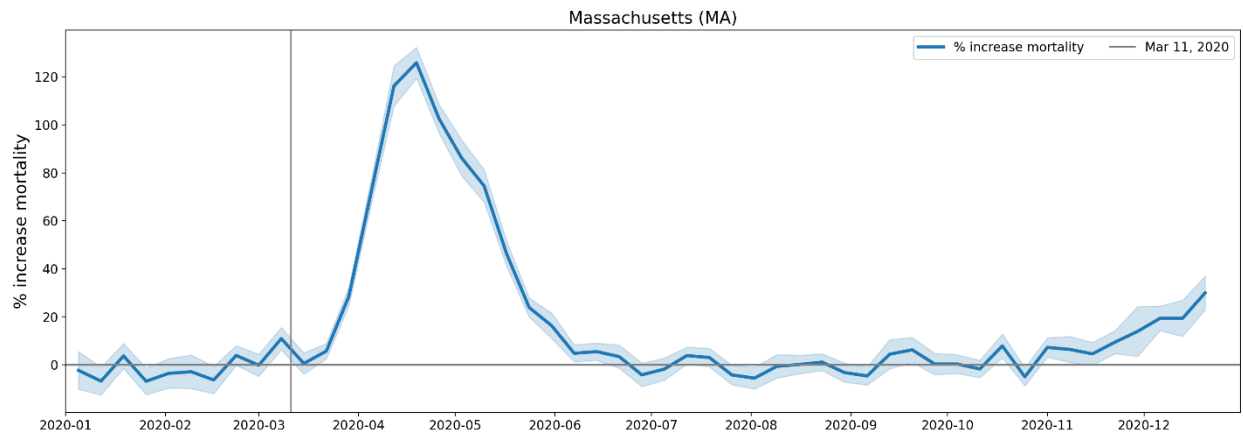
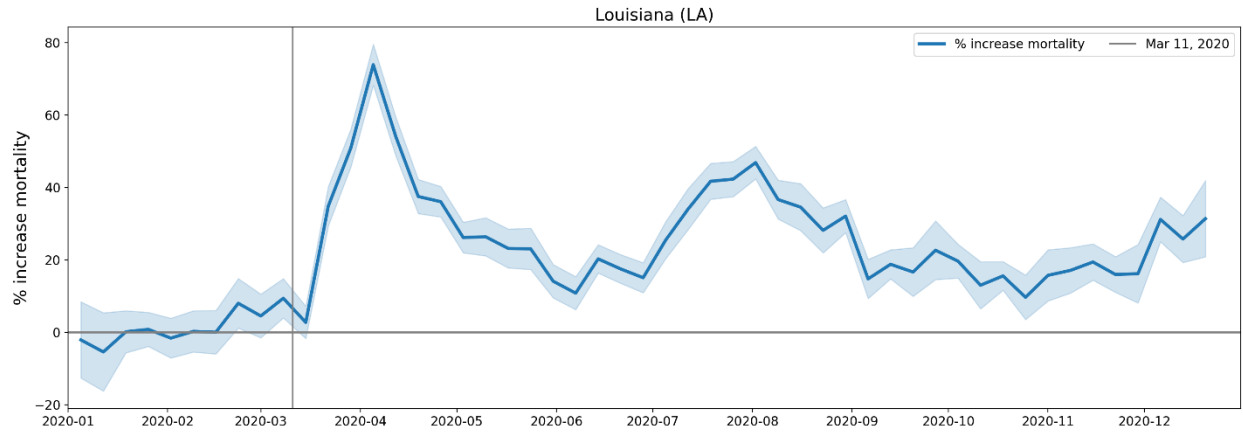


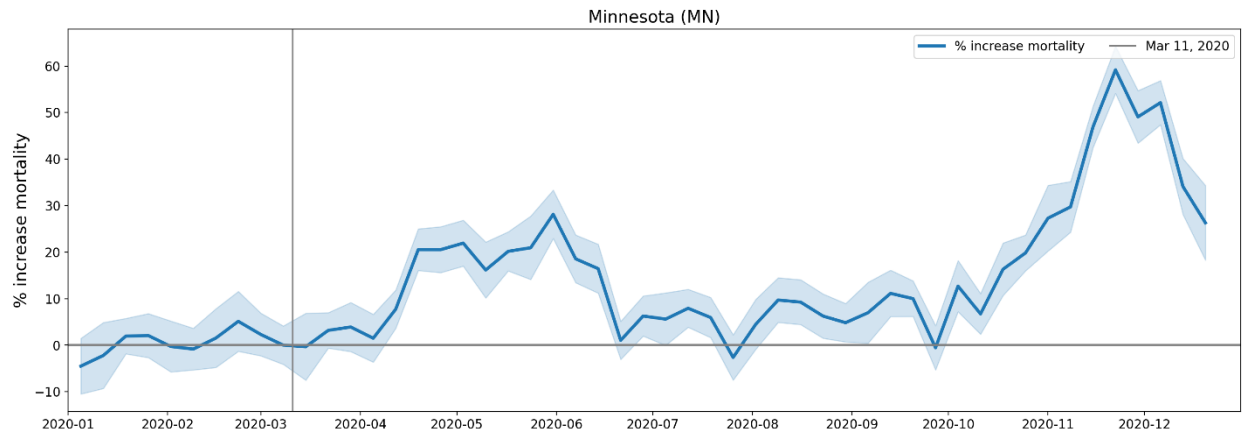
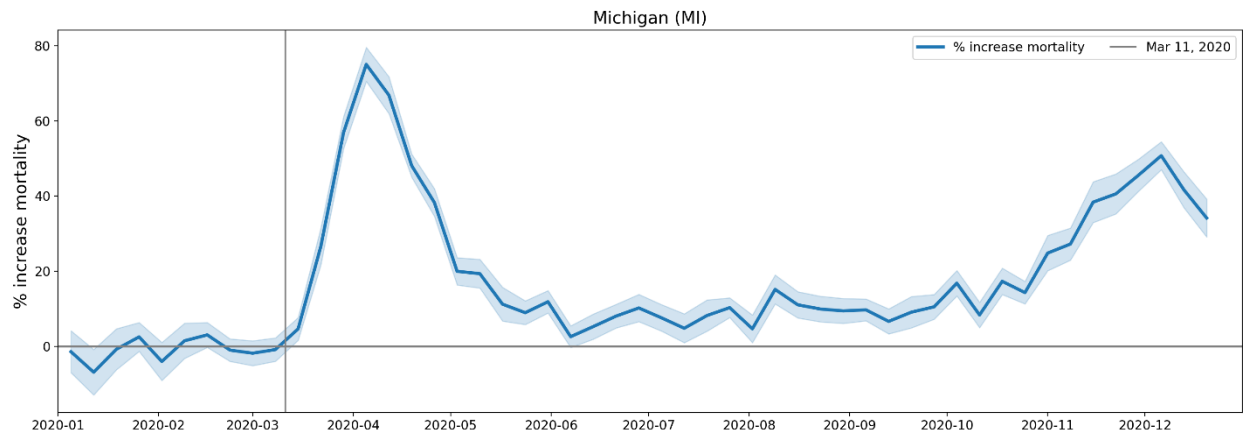
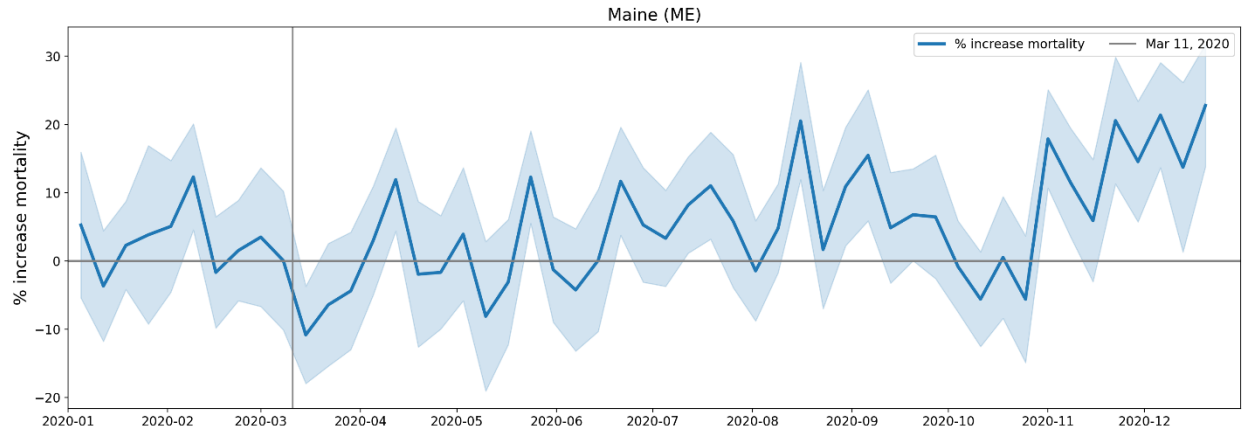


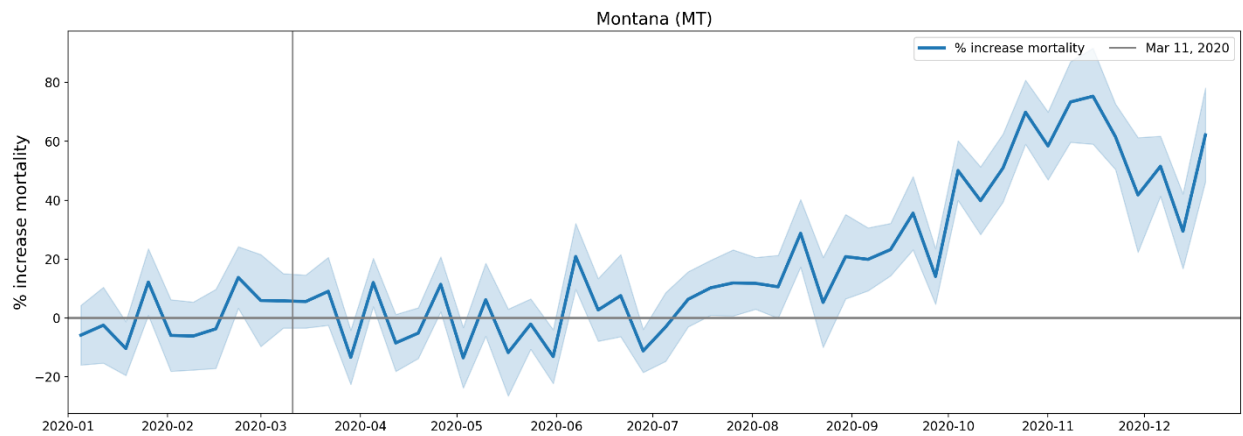
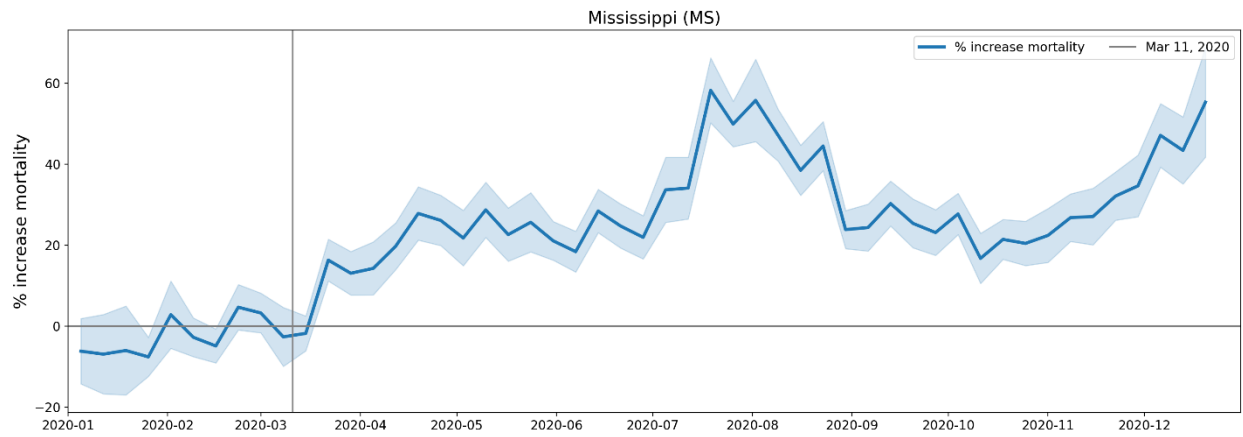
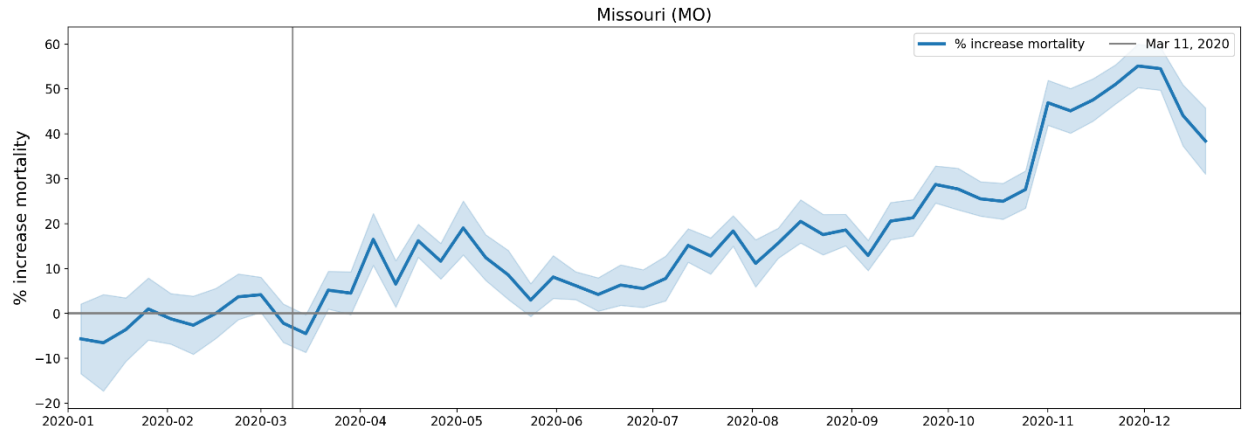


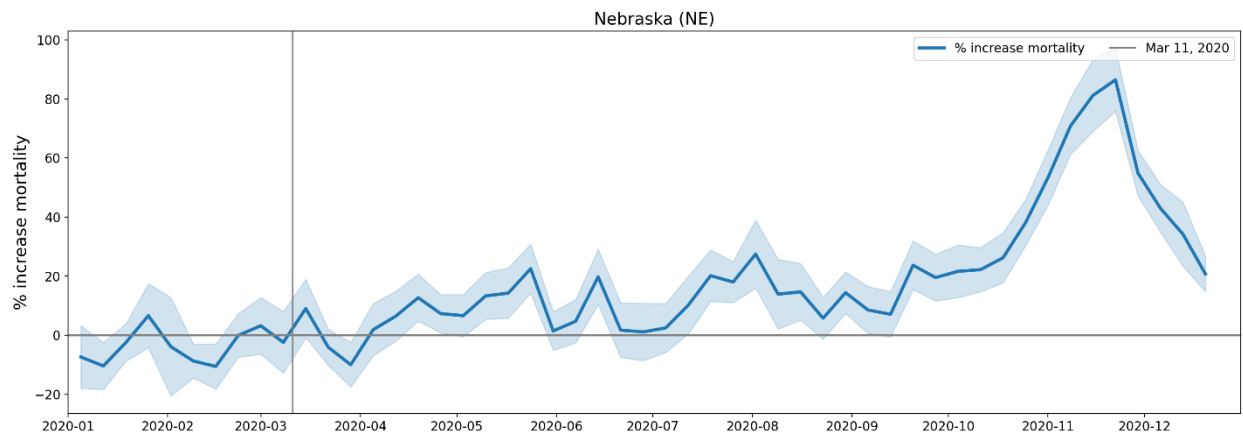
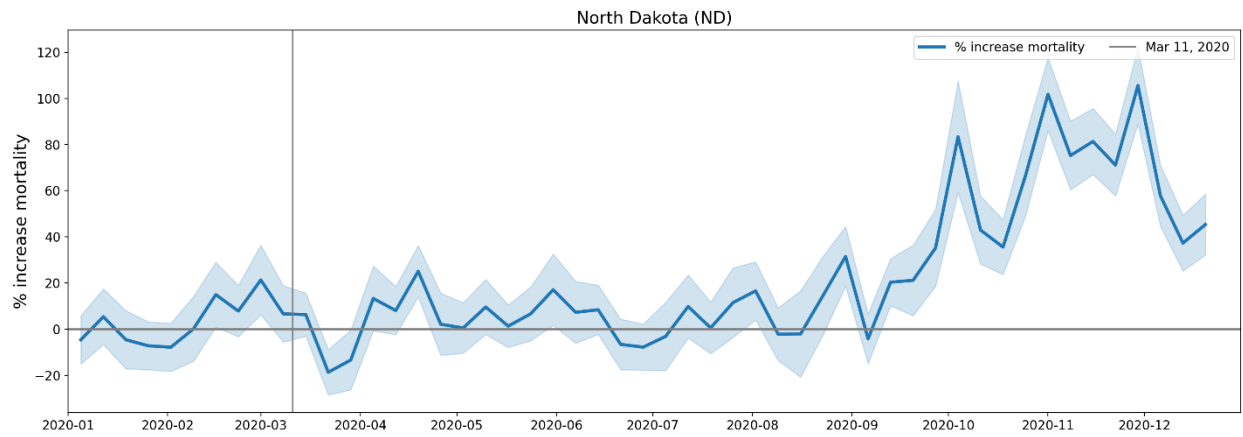
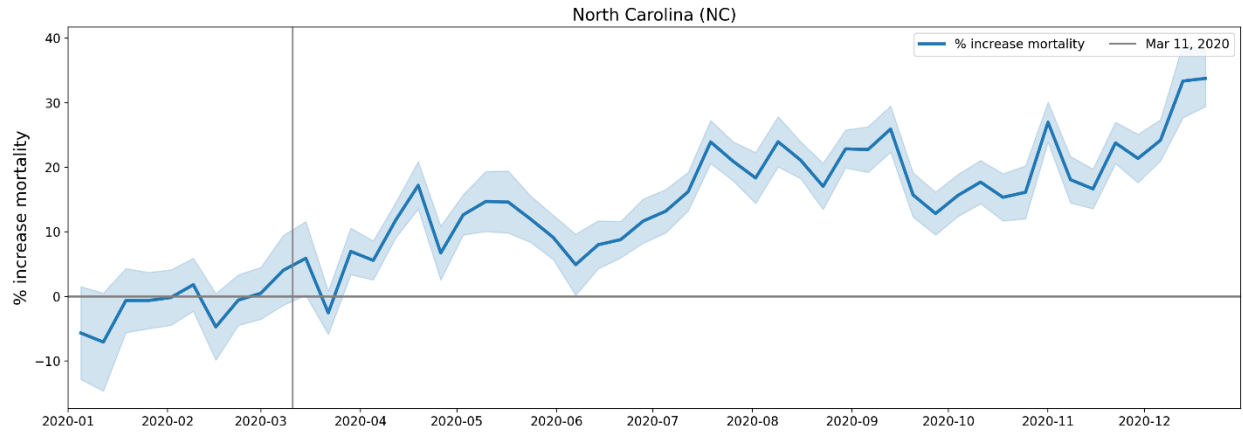


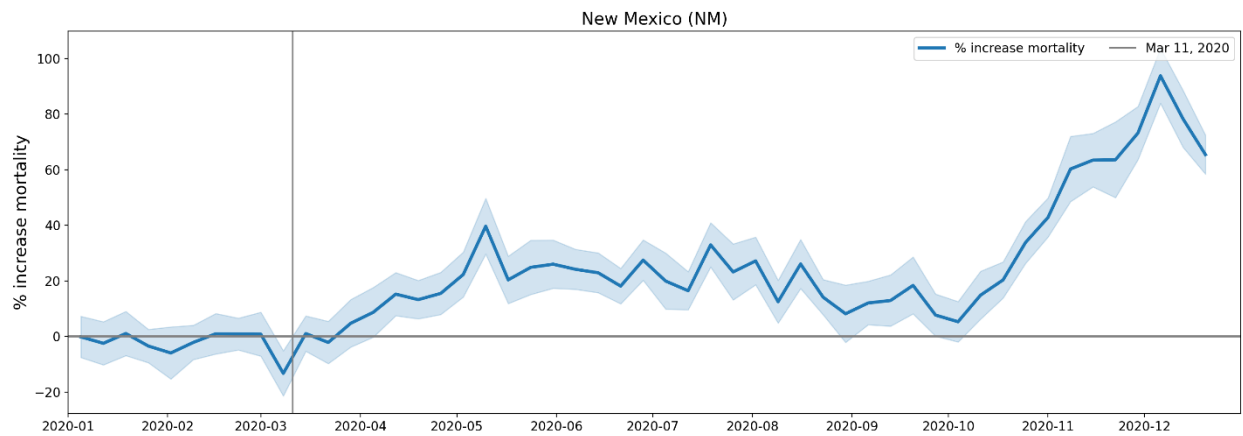
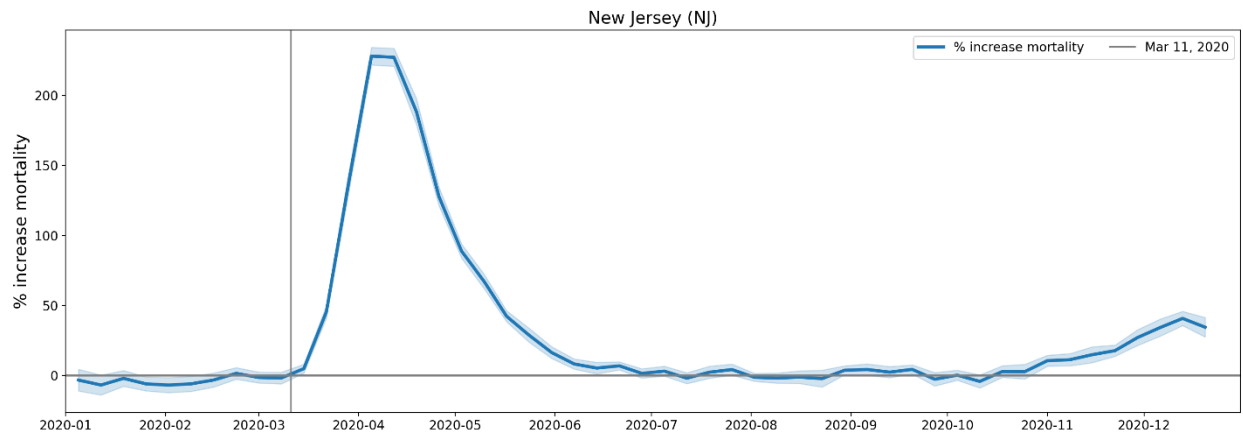
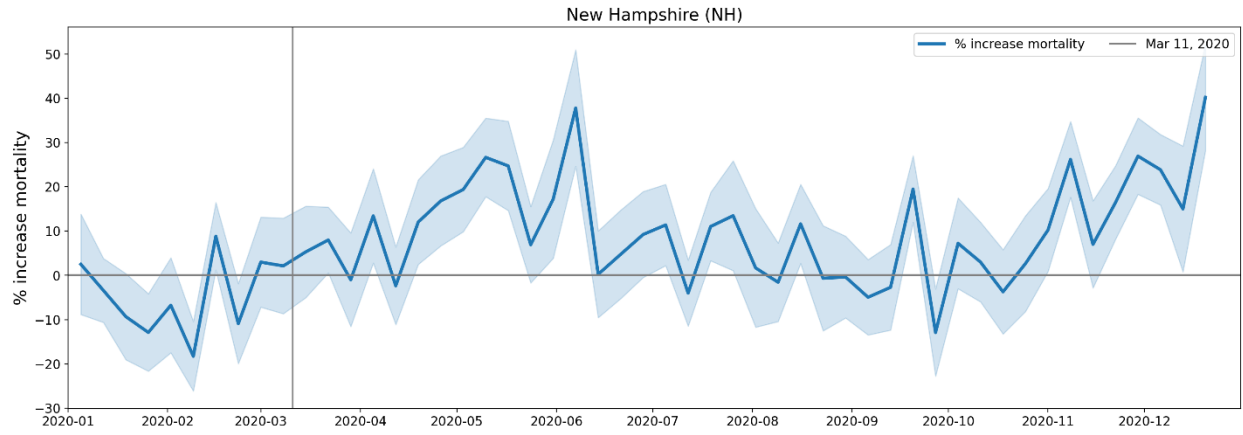


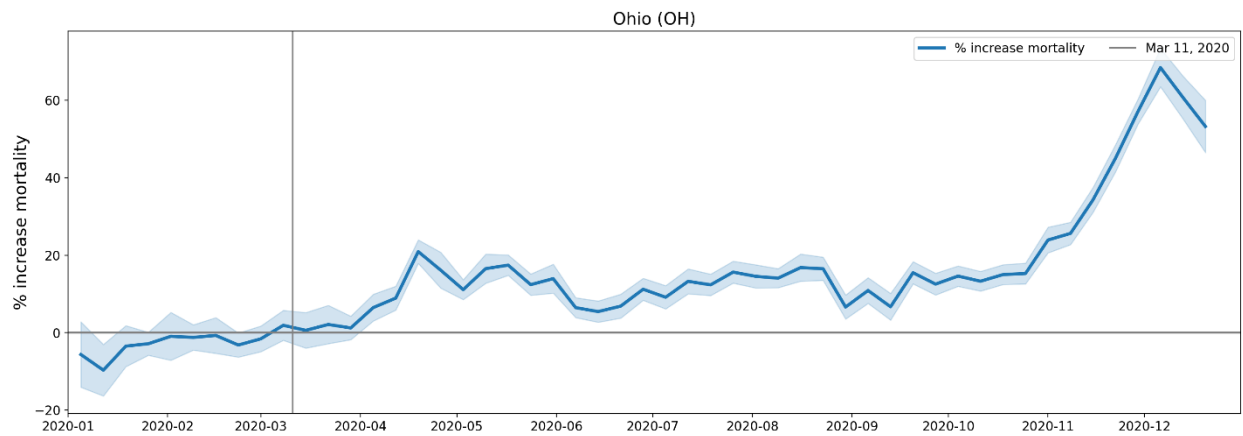
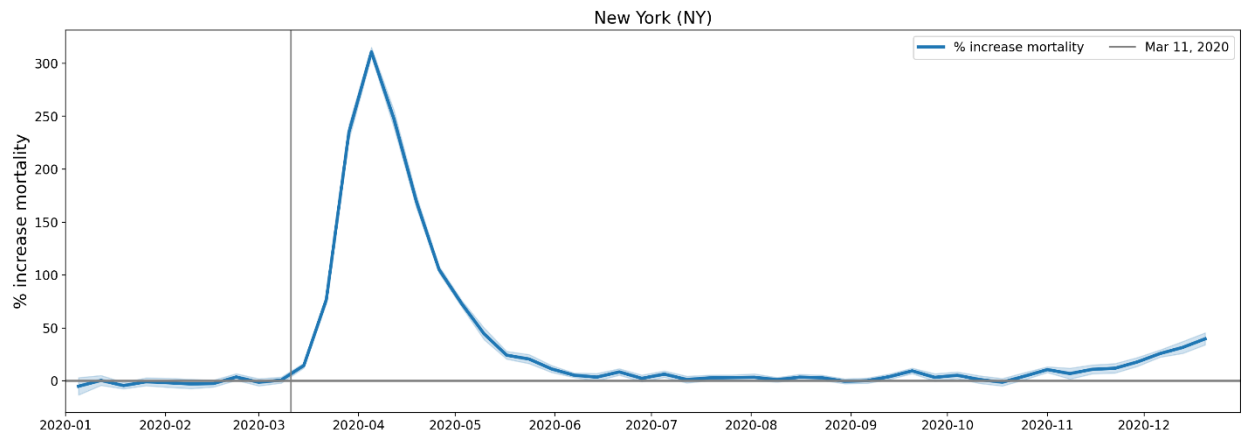
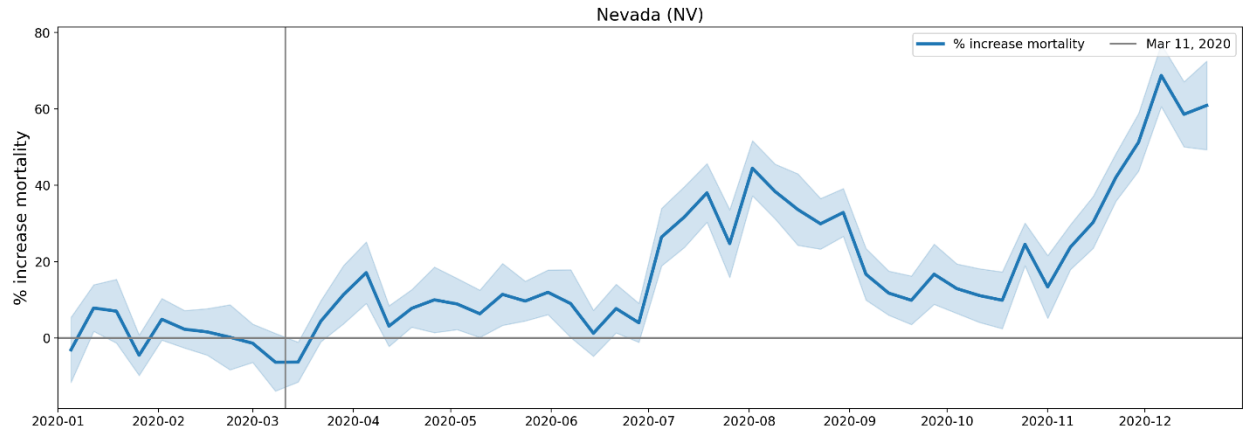


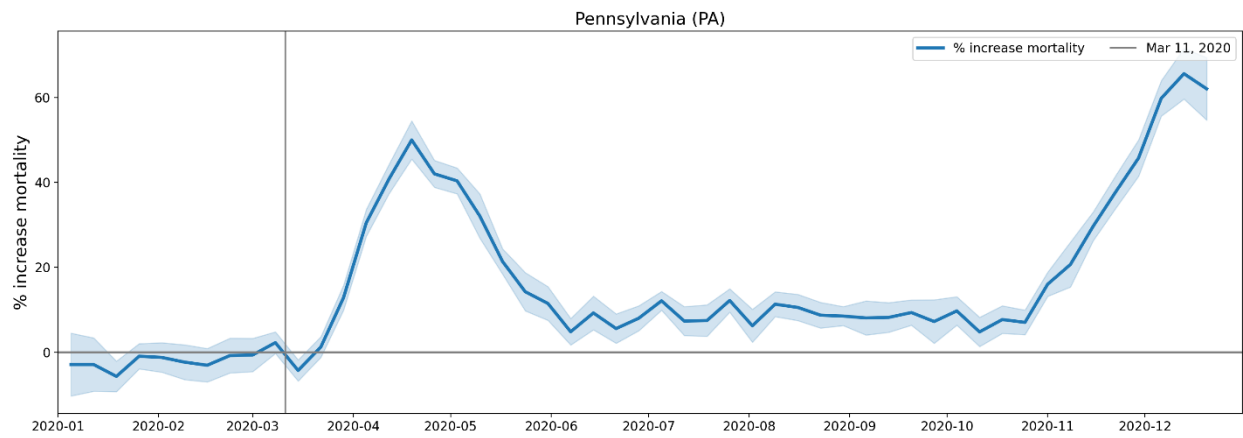
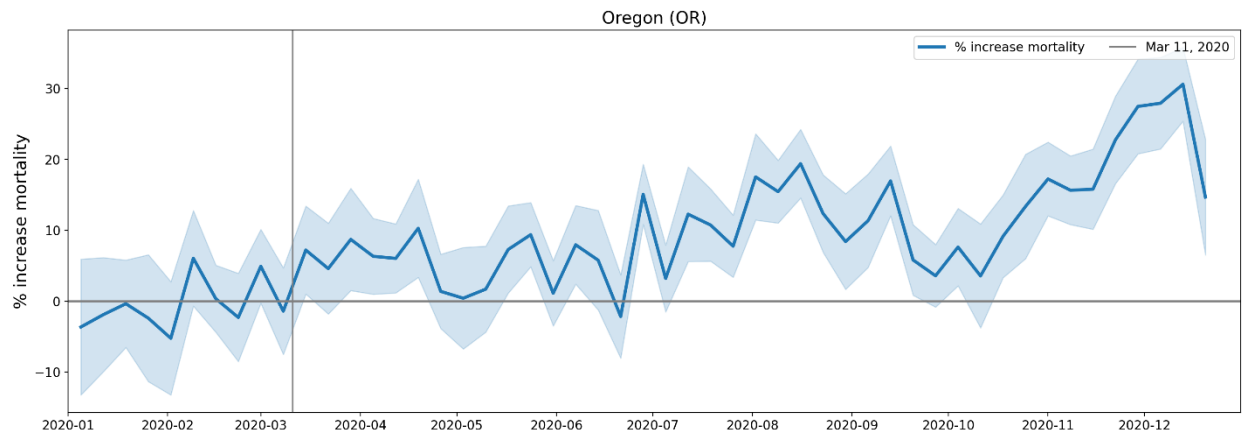
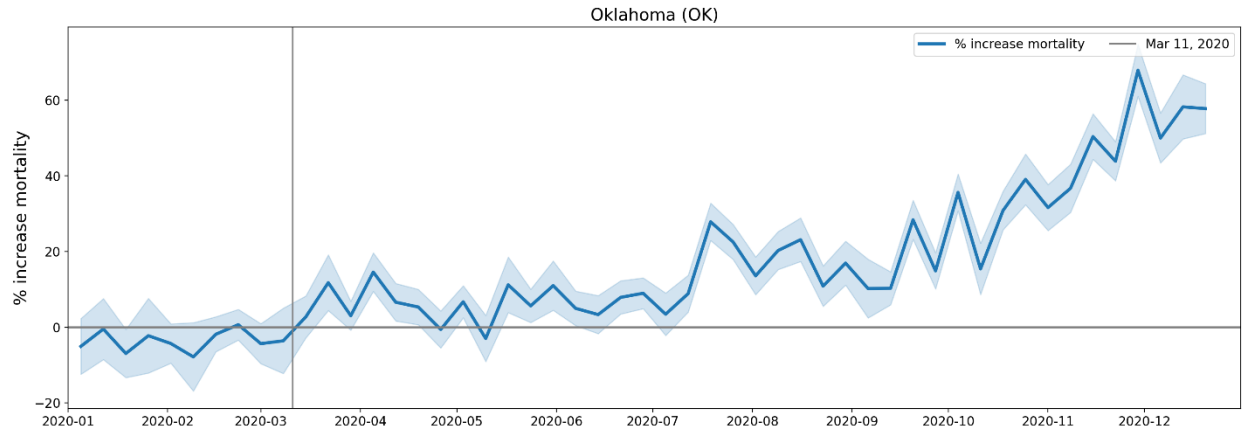


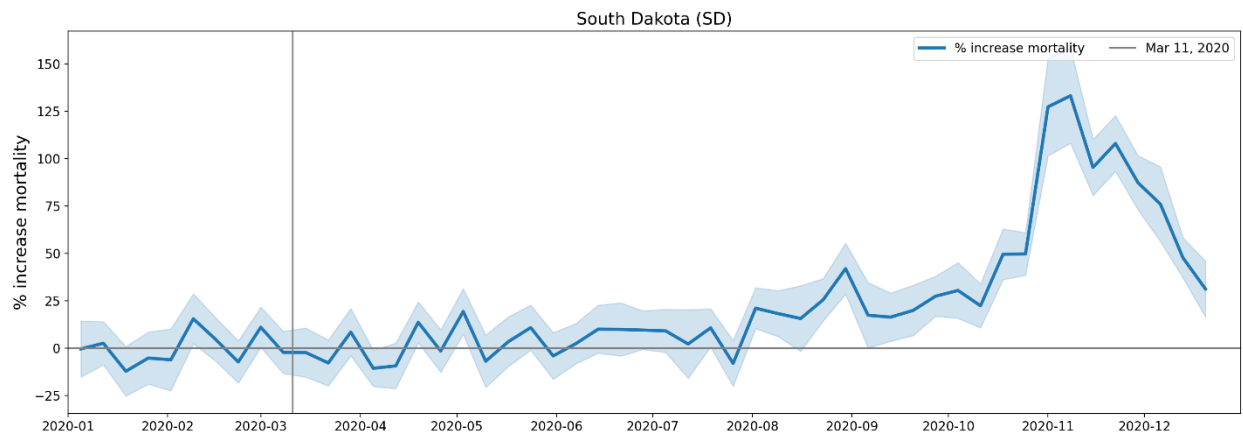
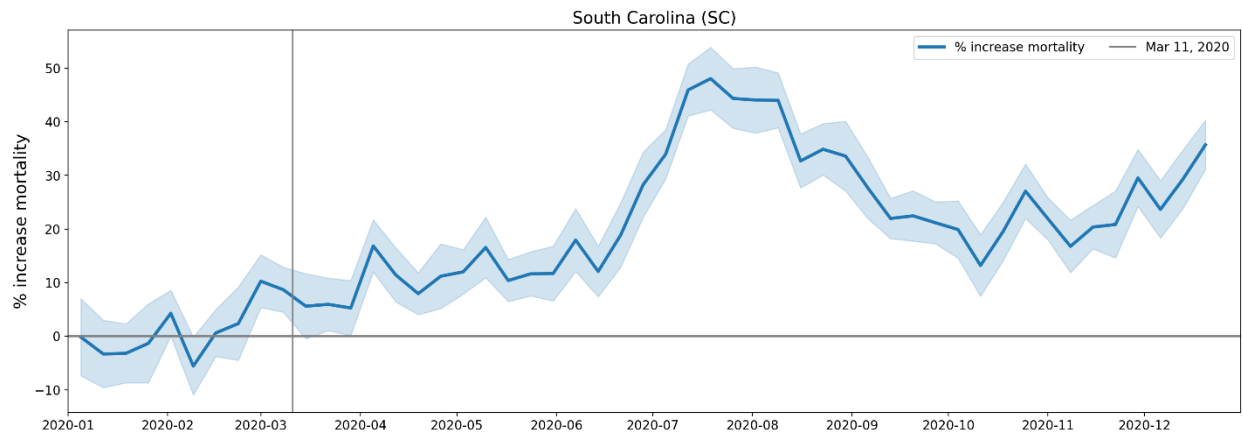
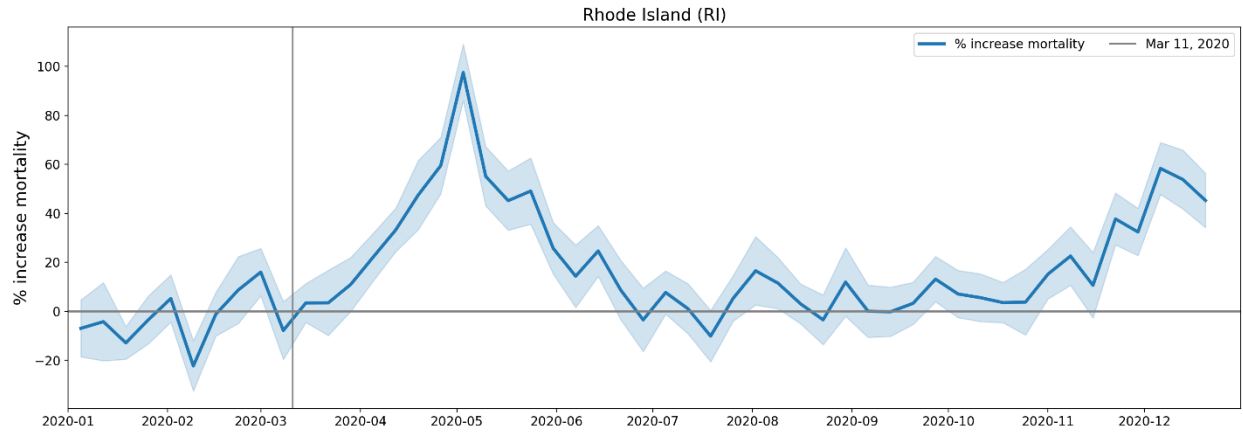


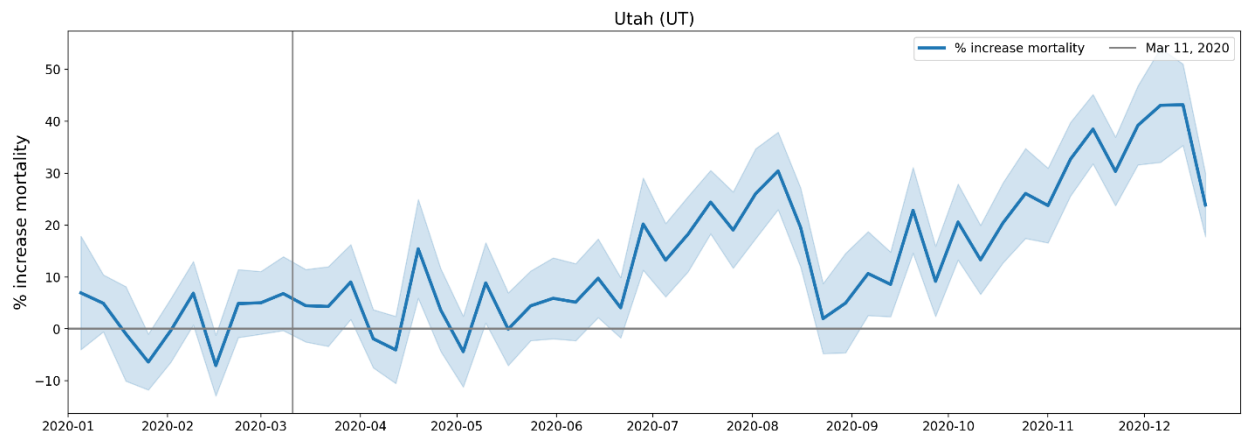
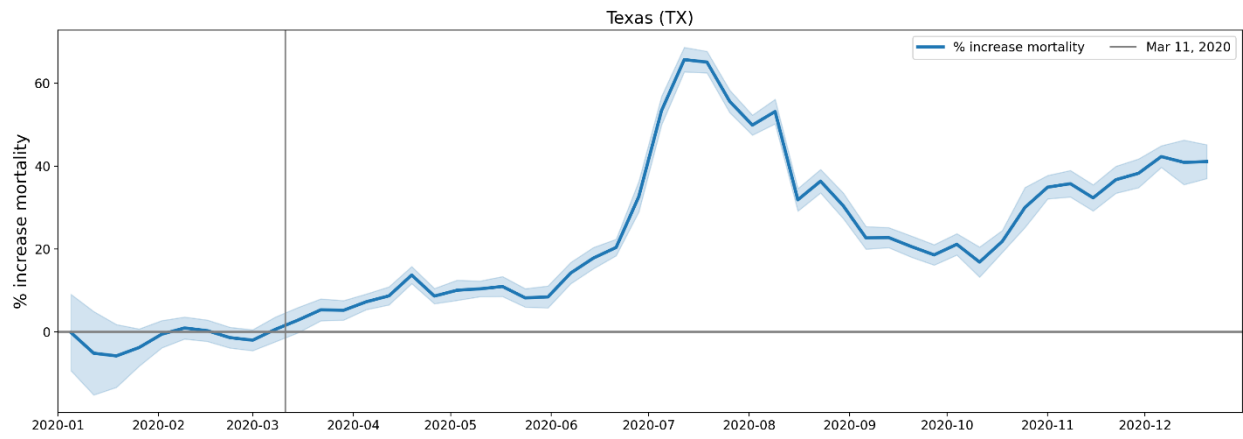
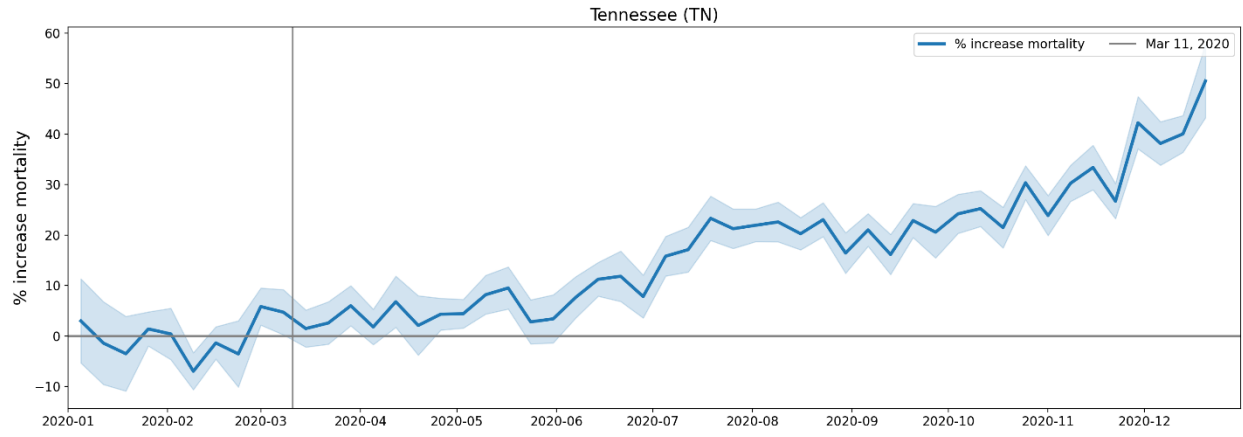


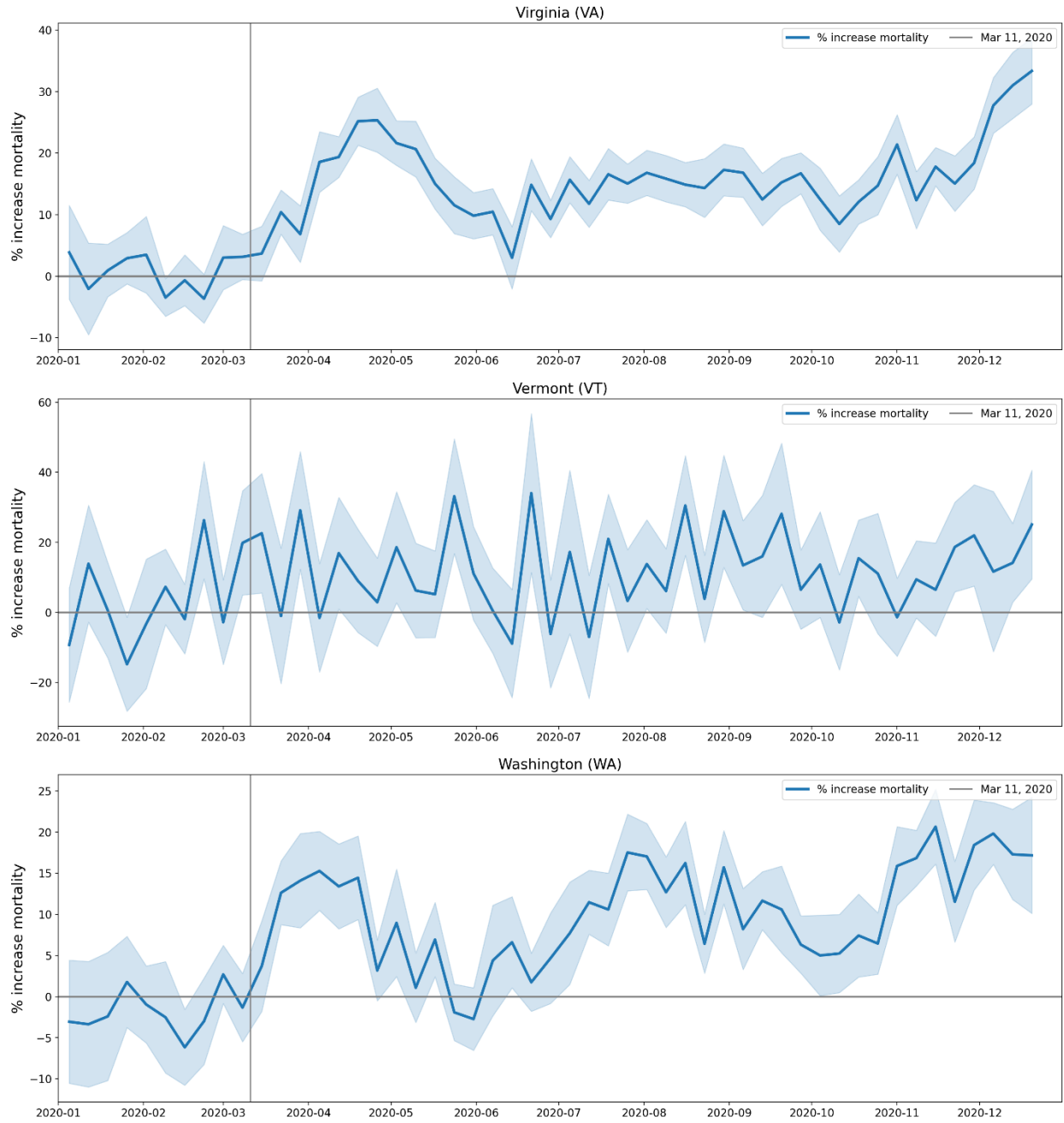


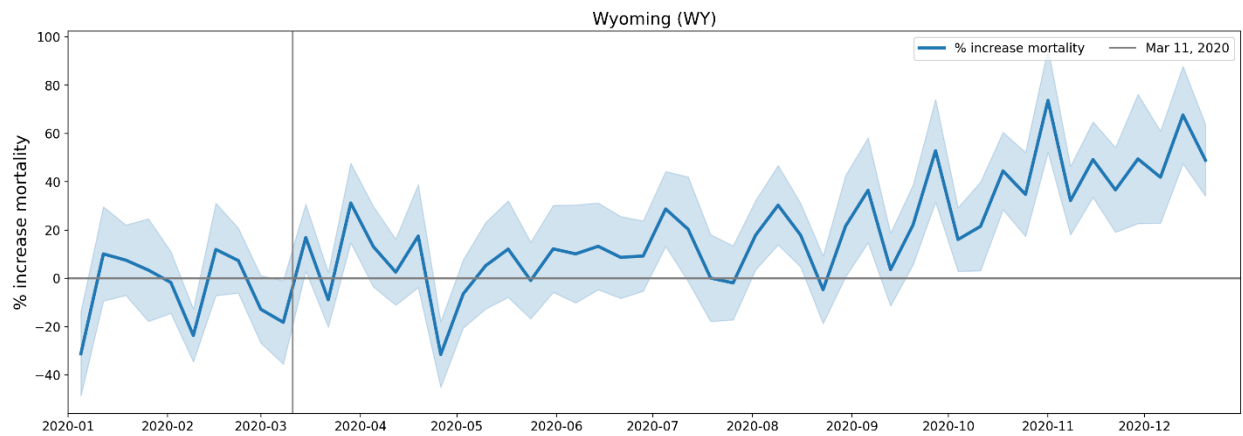
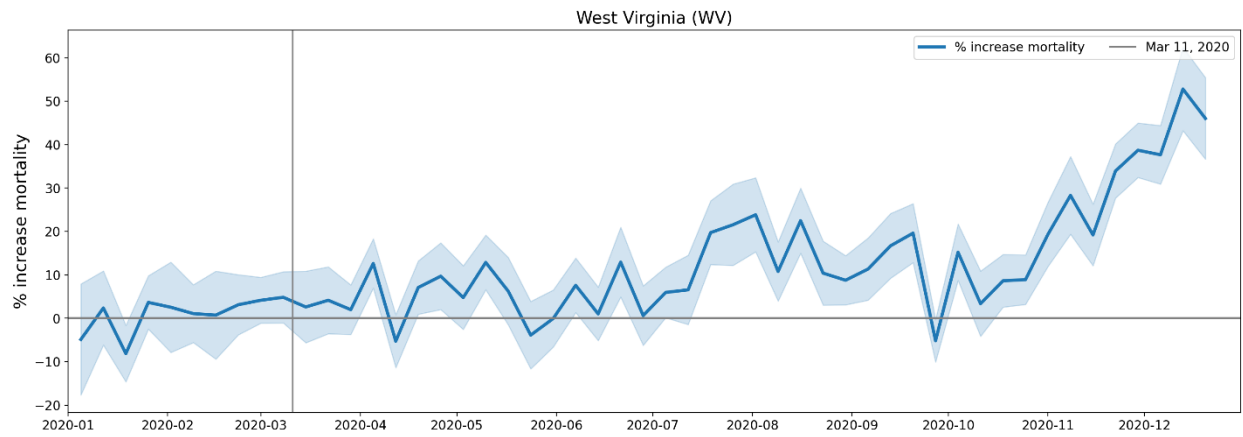
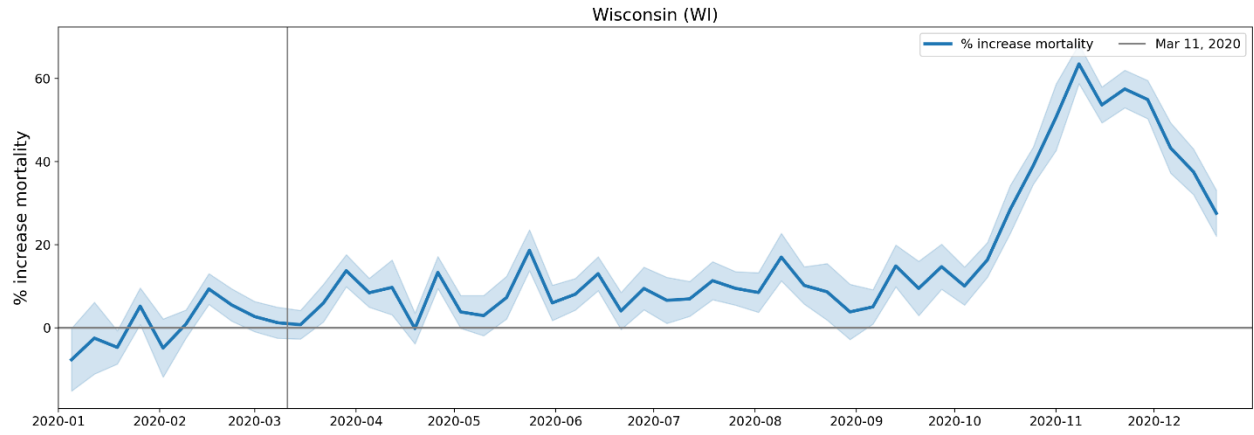








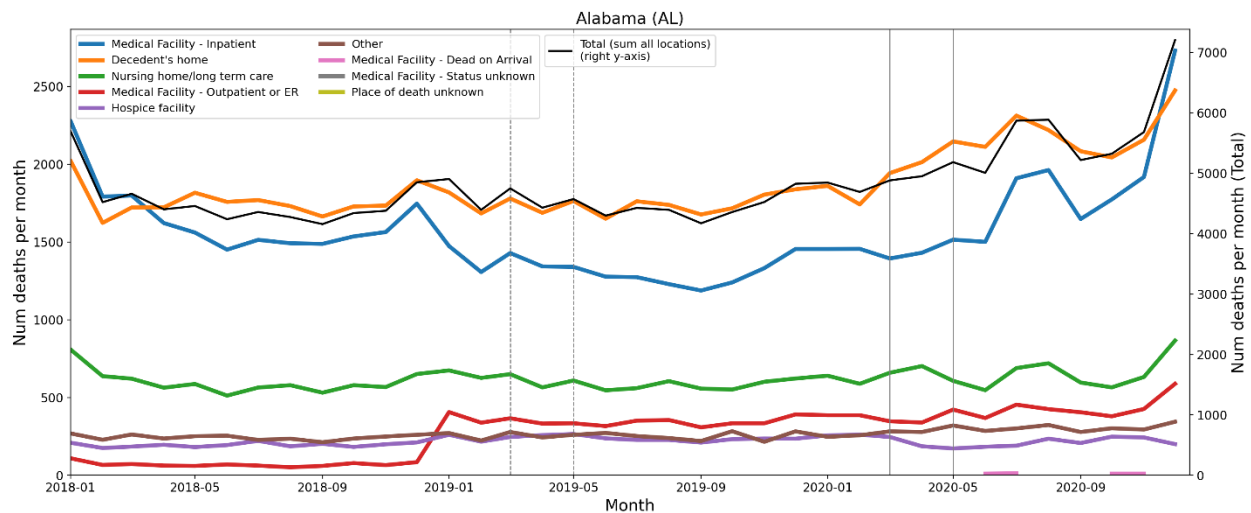
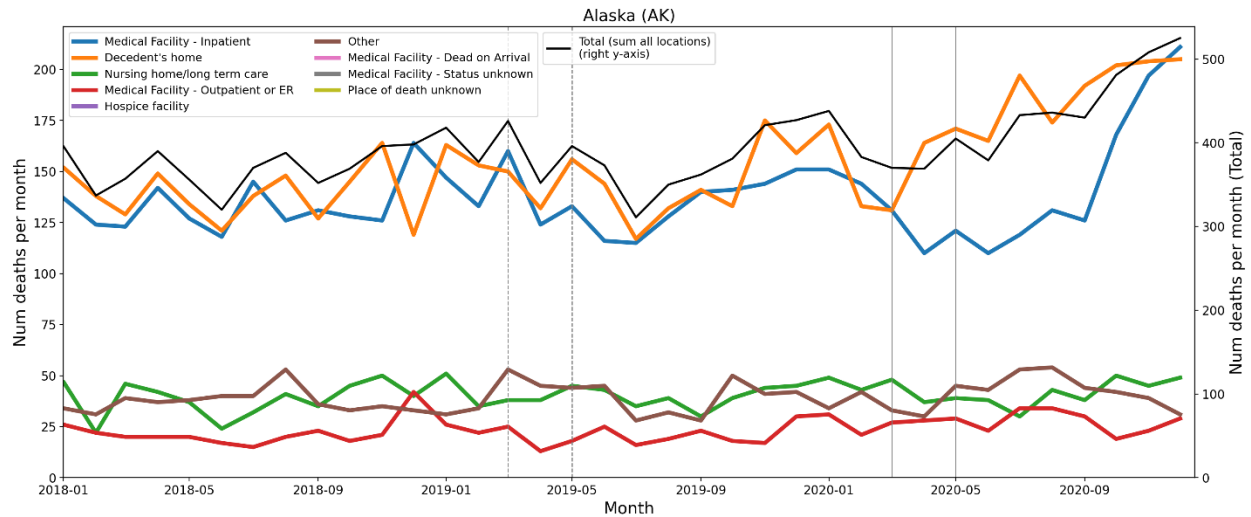


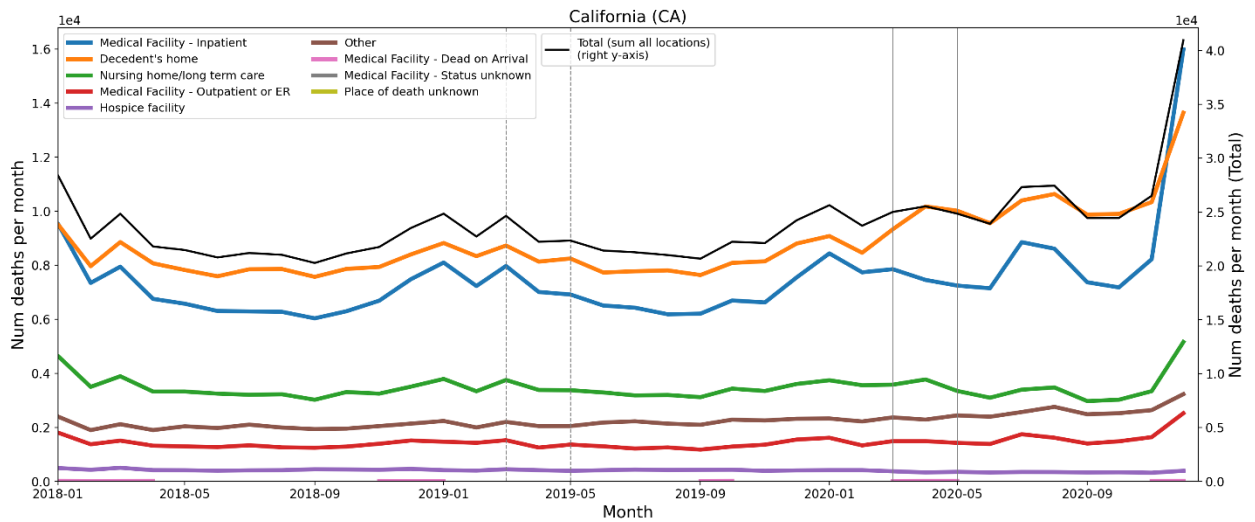
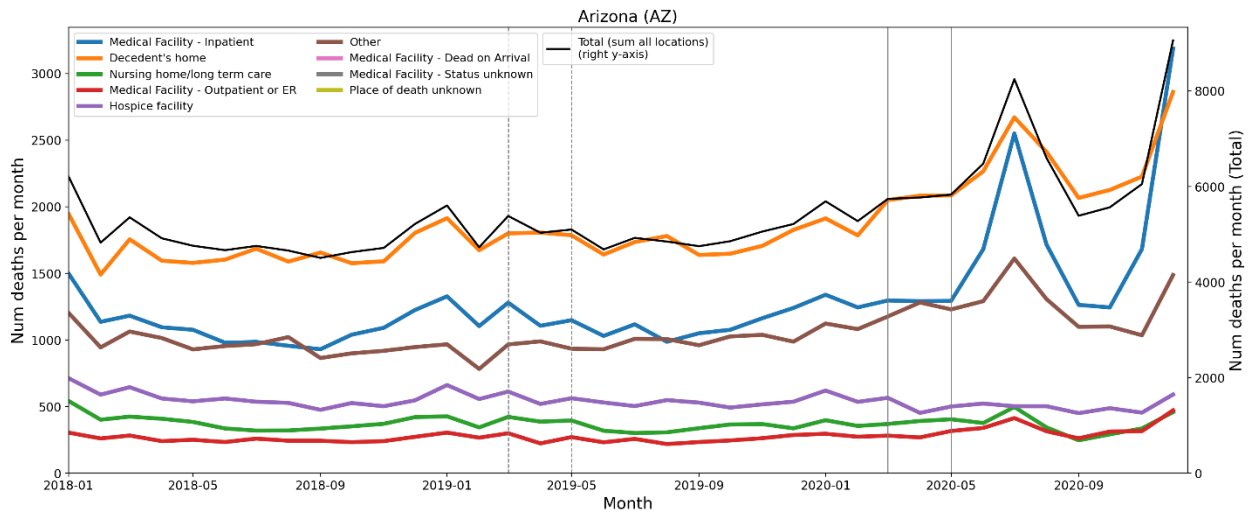
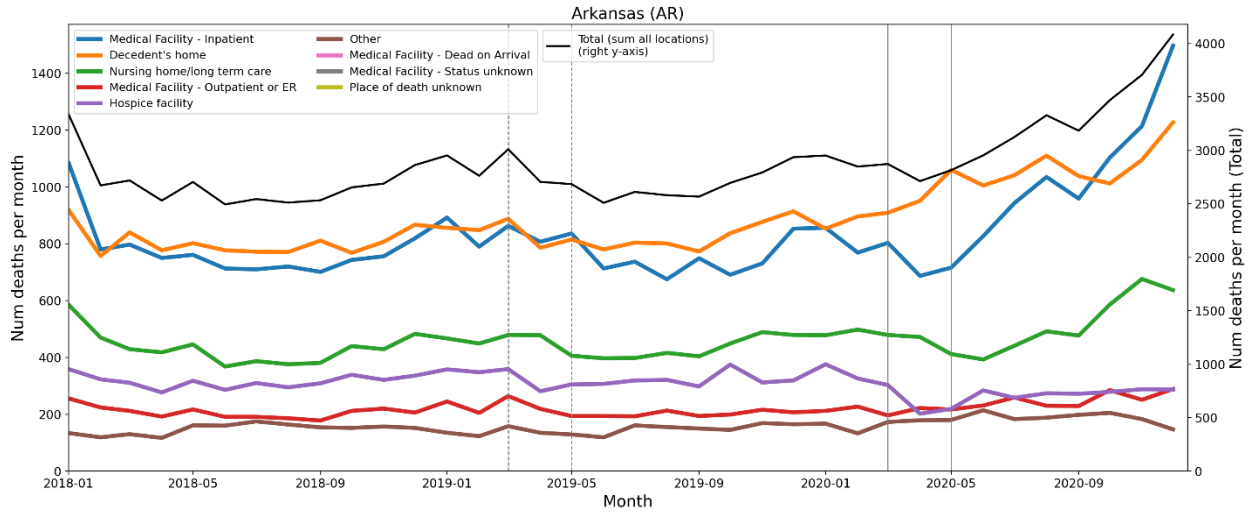


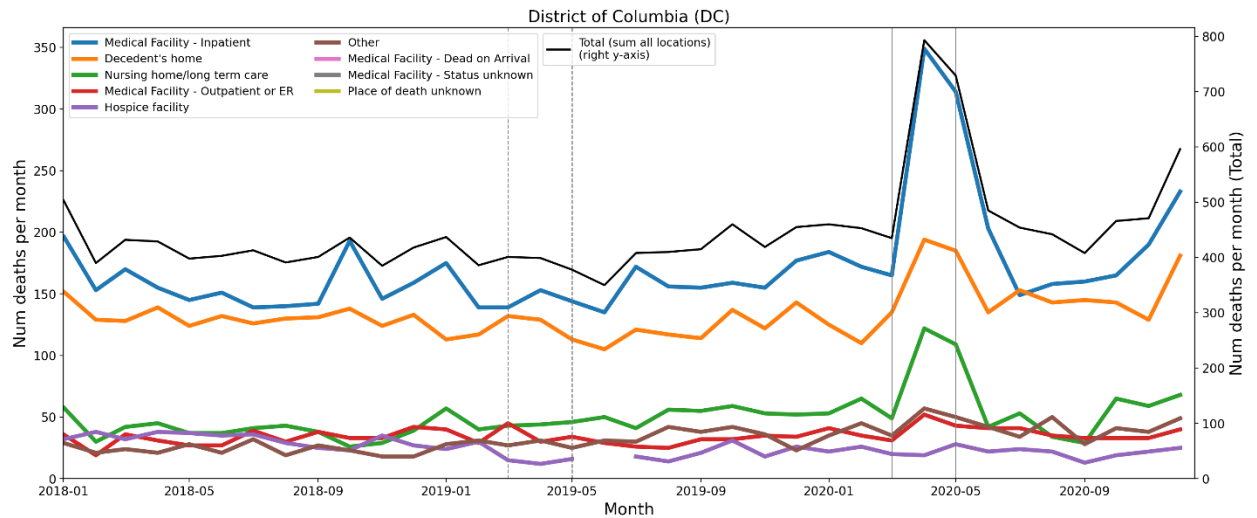
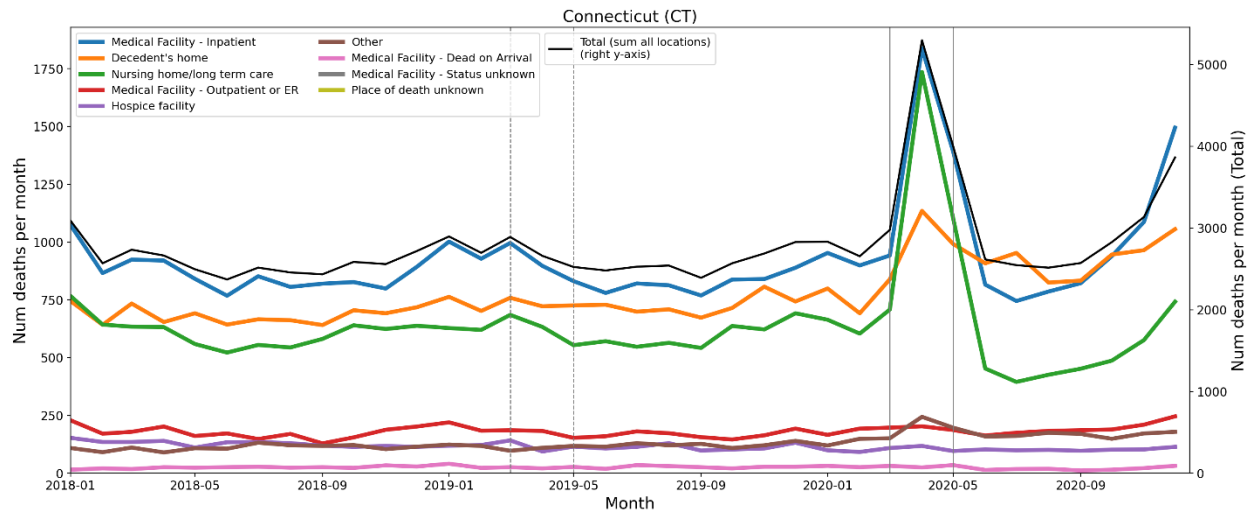
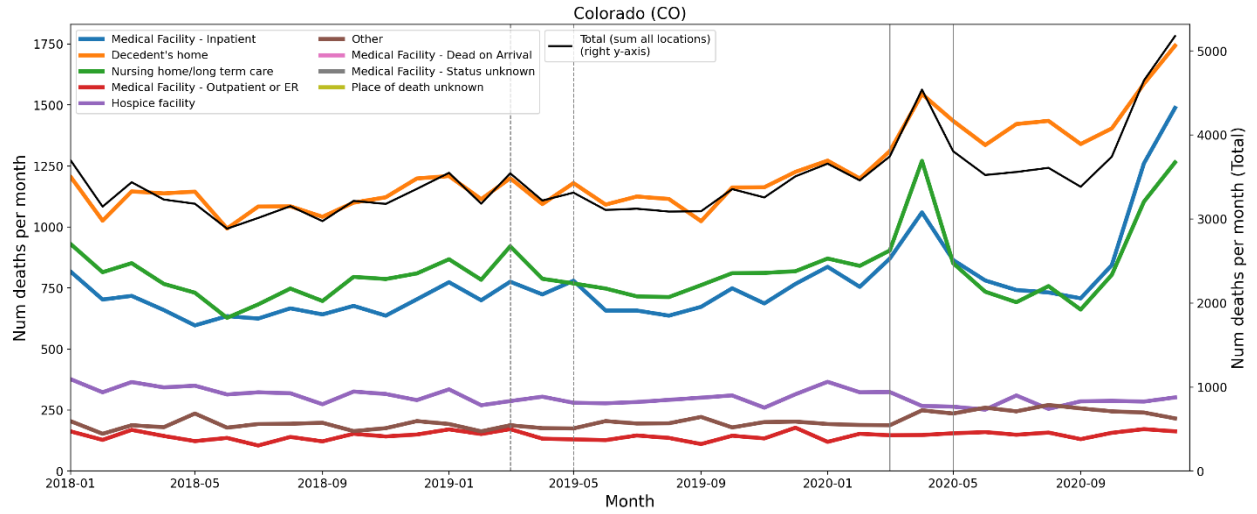
B. Additional graphs pertaining to section 3.5

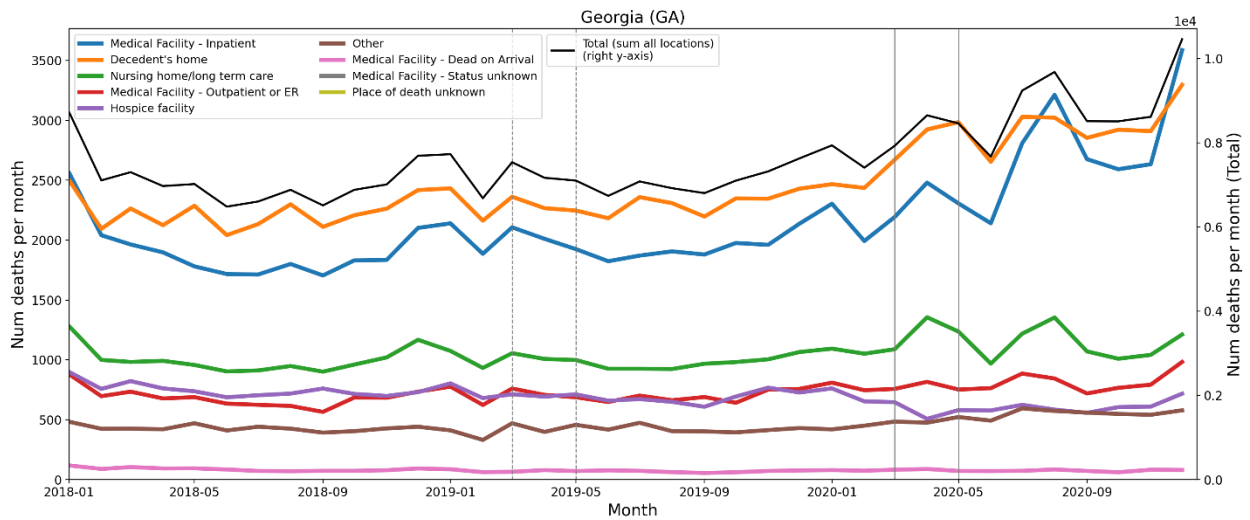
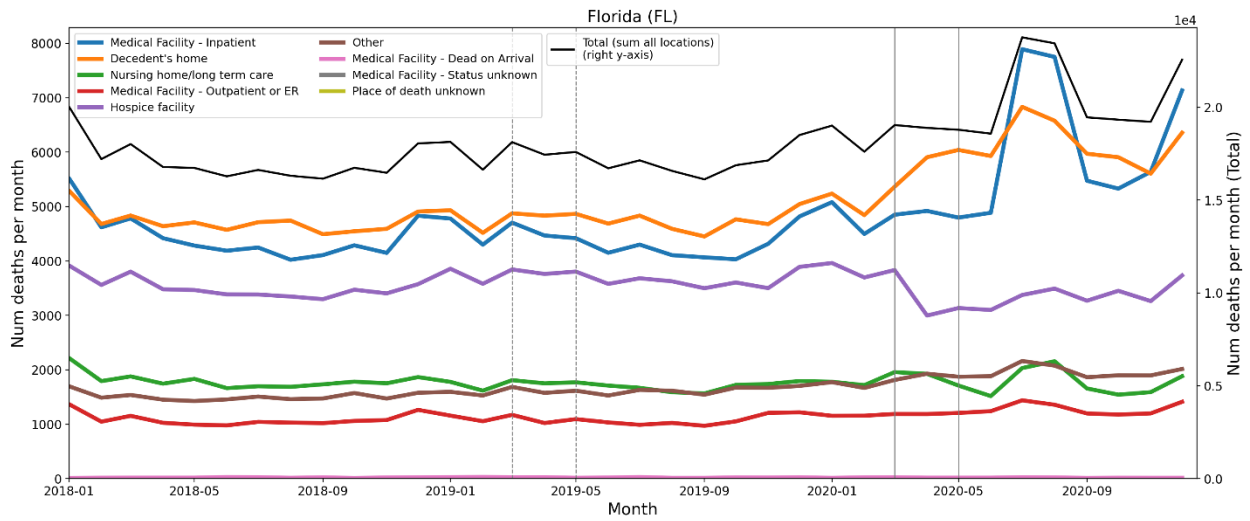
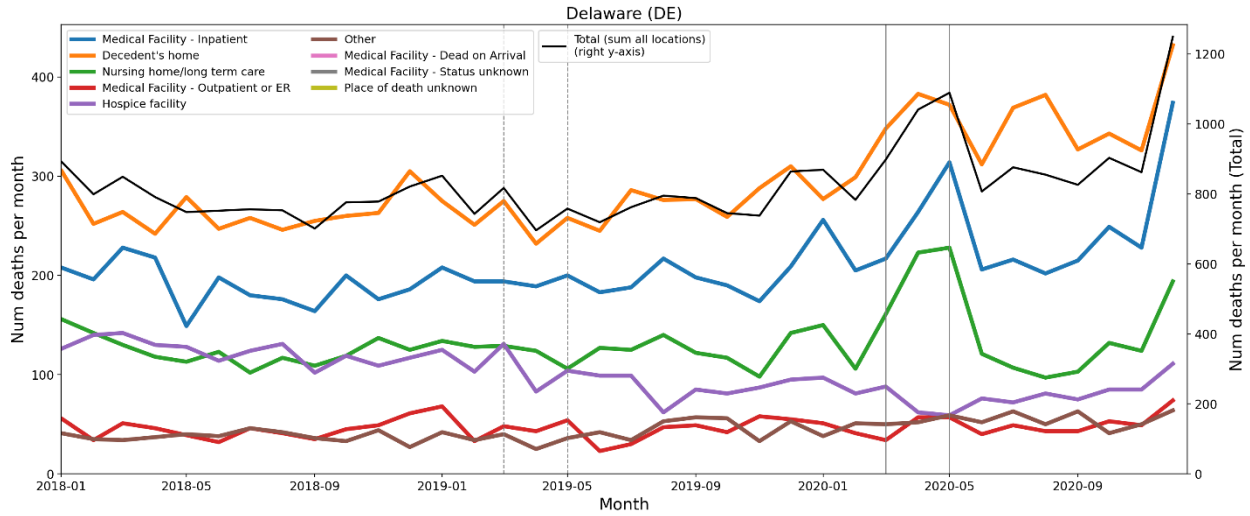
The graphs in this appendix show the number of deaths per month for different institutional locations of death (left y-axes), for each USA state. The right y-axes show the total number of deaths (sum over all institutional locations of death) per month.

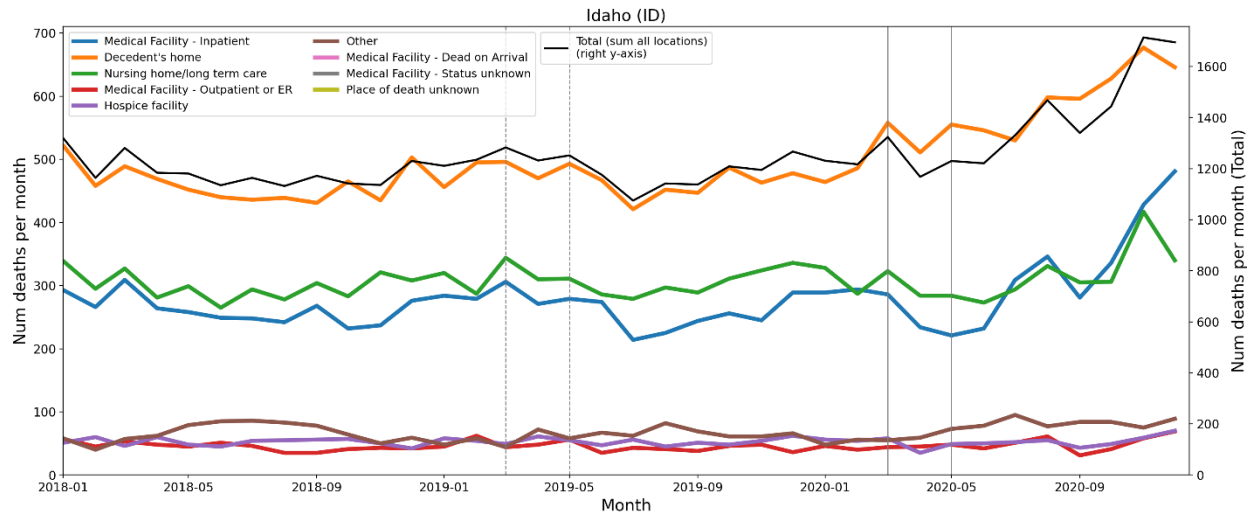
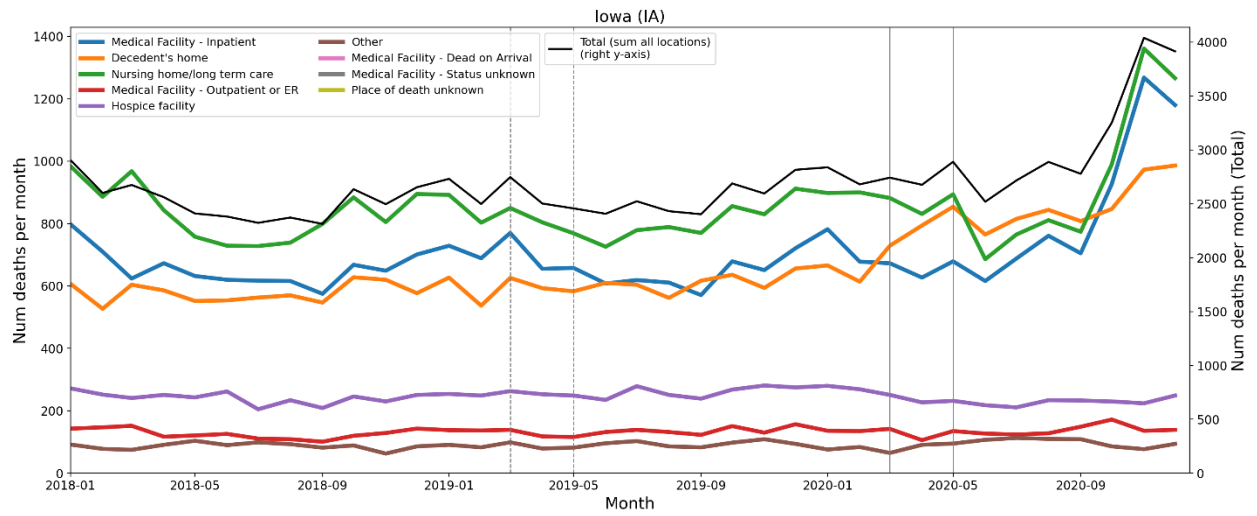
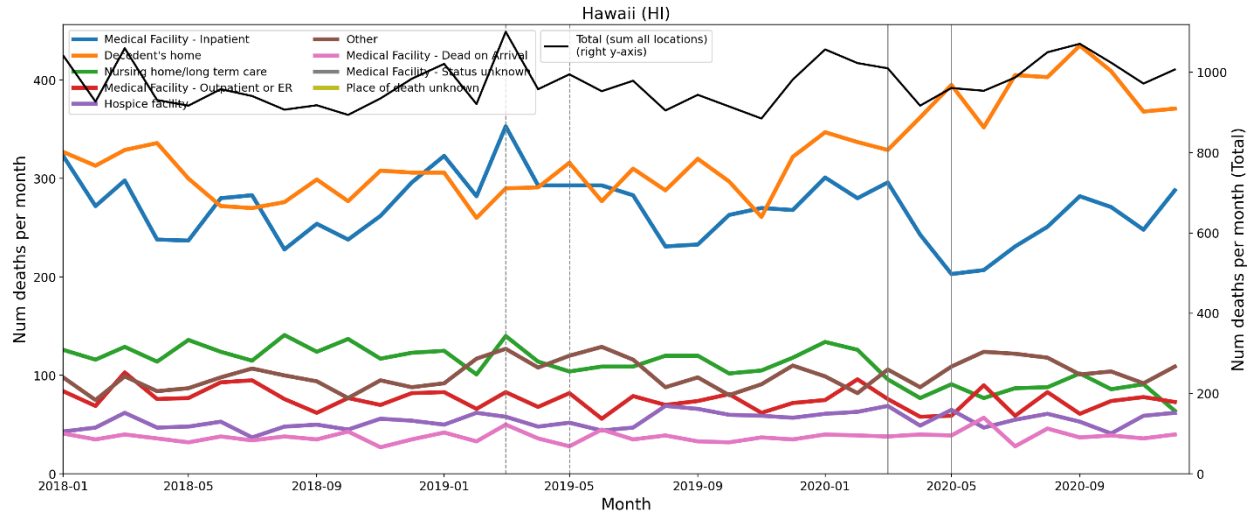
The solid vertical lines are placed at March 1, 2020 and May 1, 2020, and the dashed vertical lines are placed at March 1, 2019 and May 1, 2019.

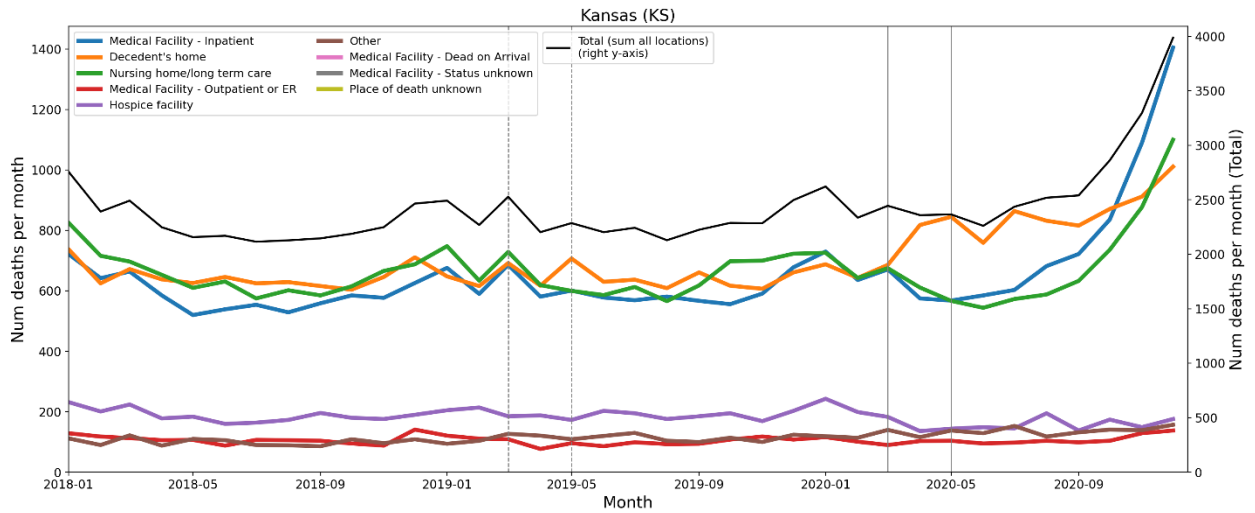
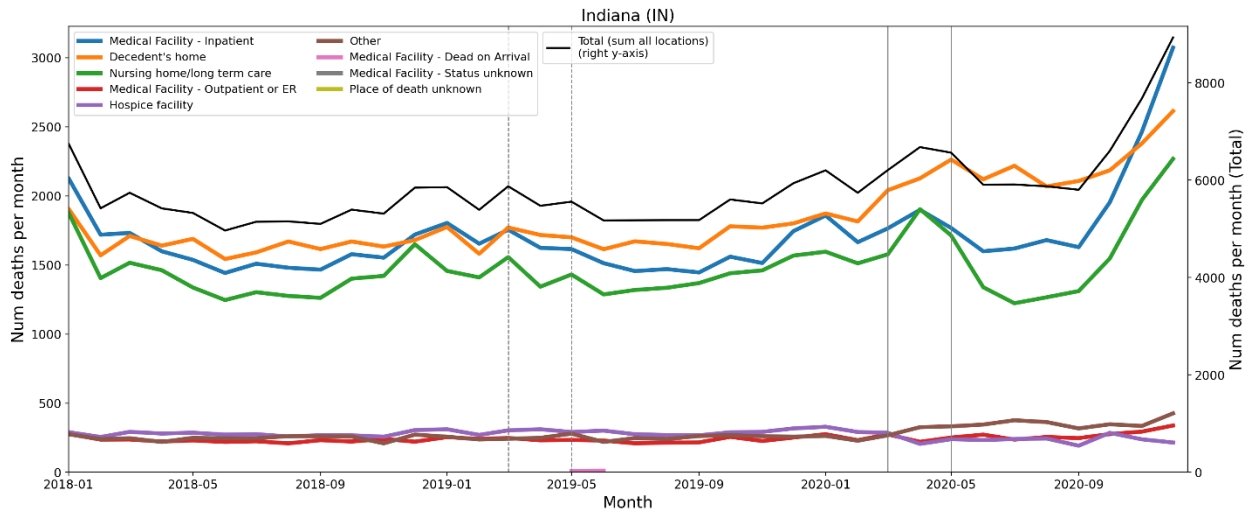
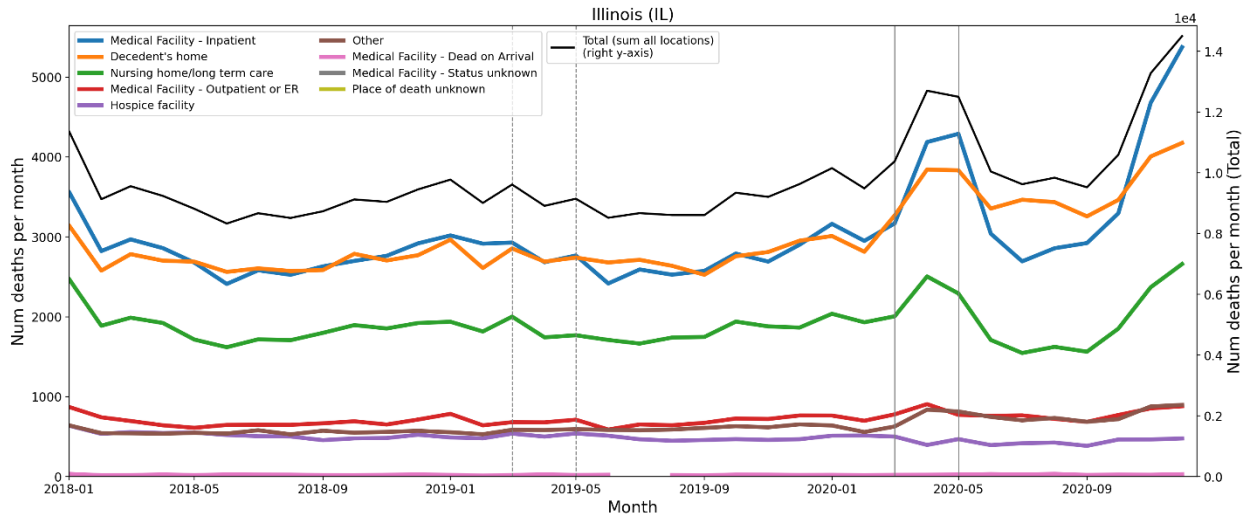


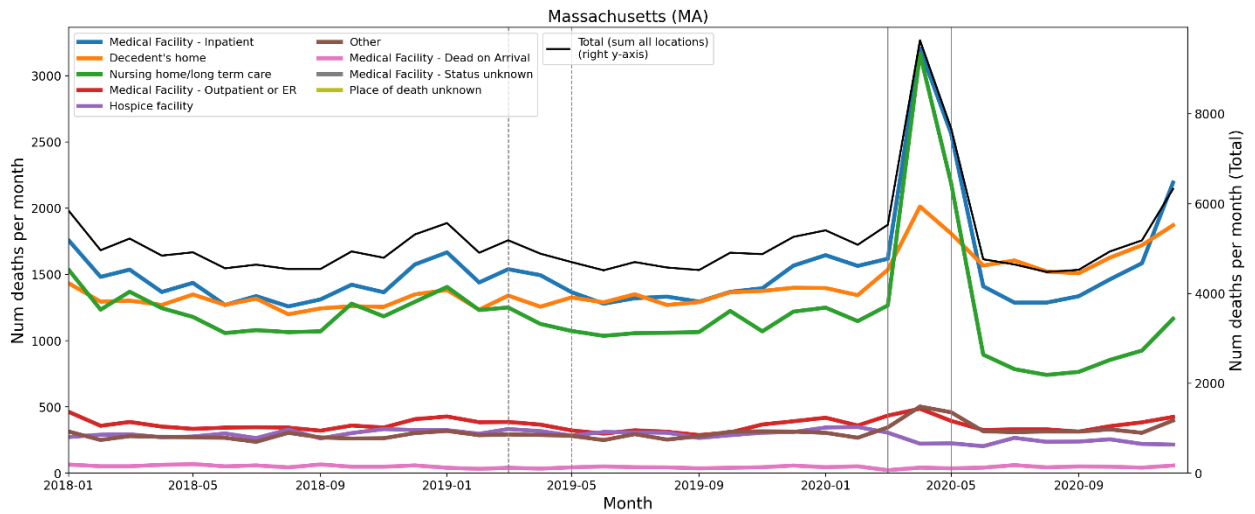
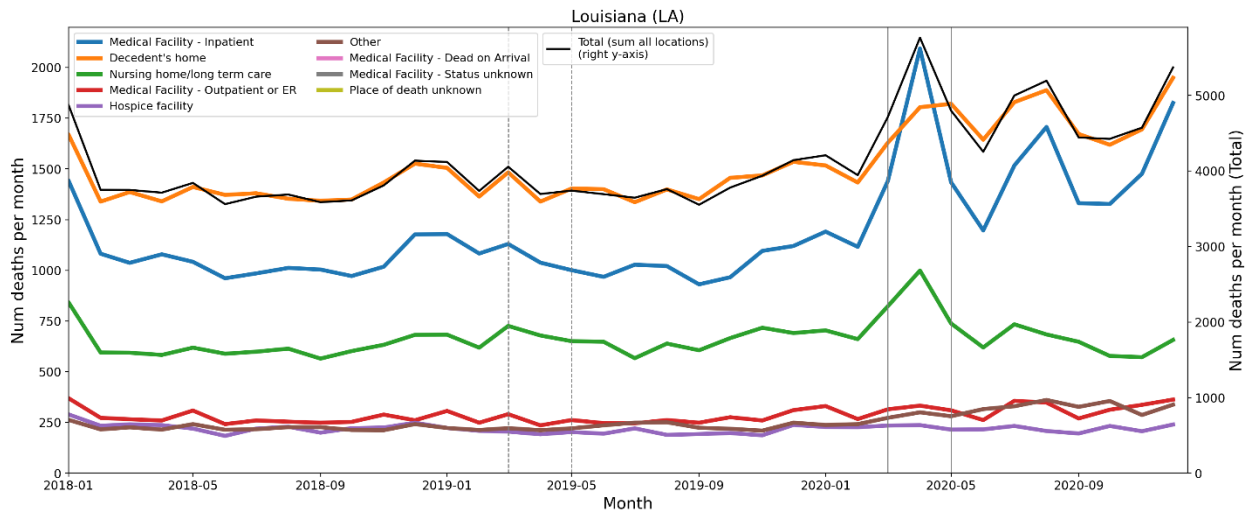
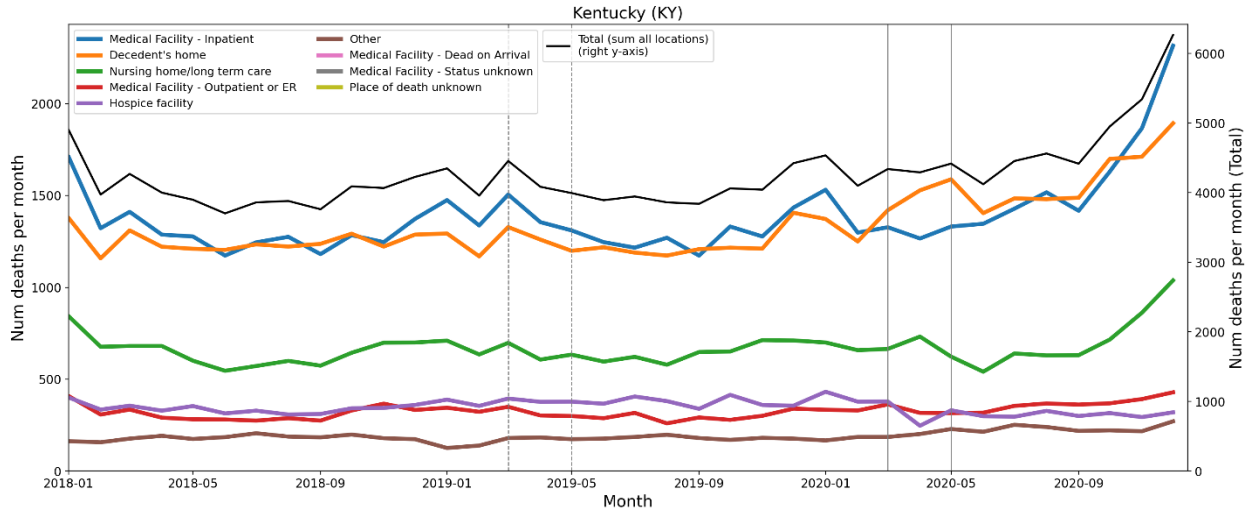


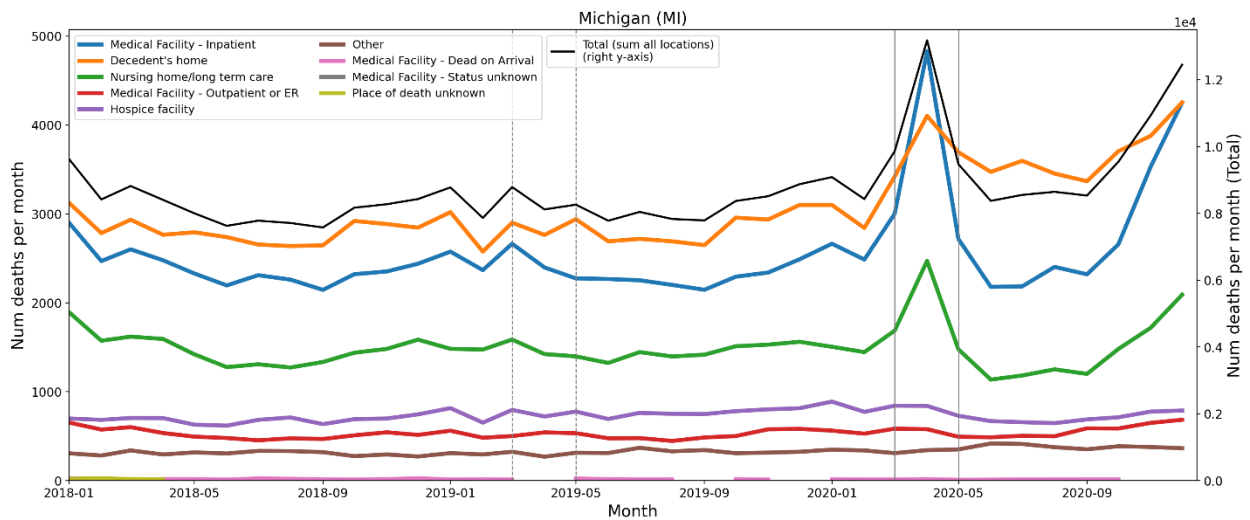
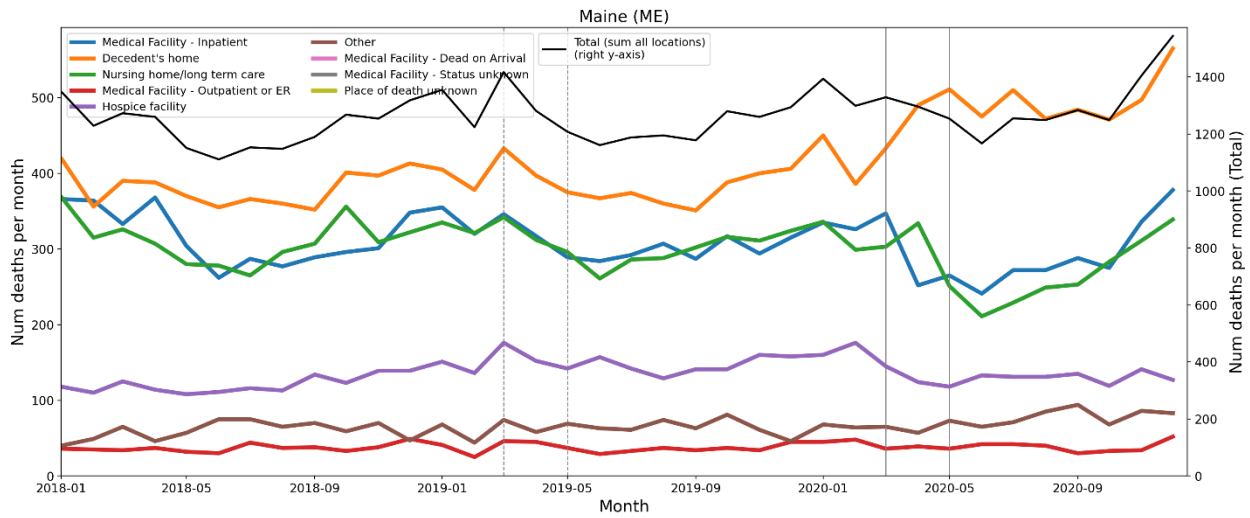
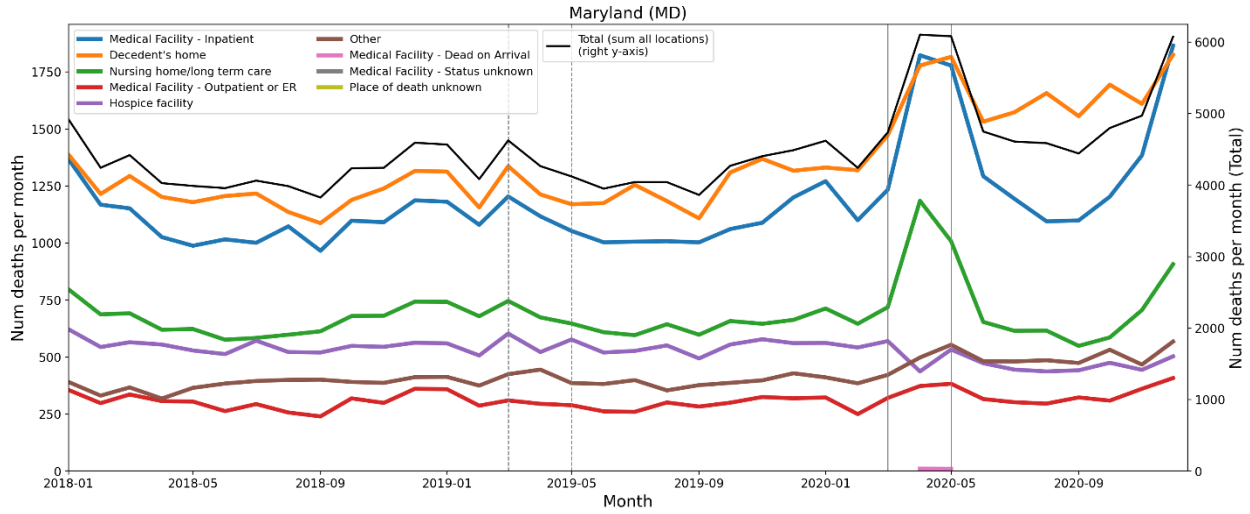


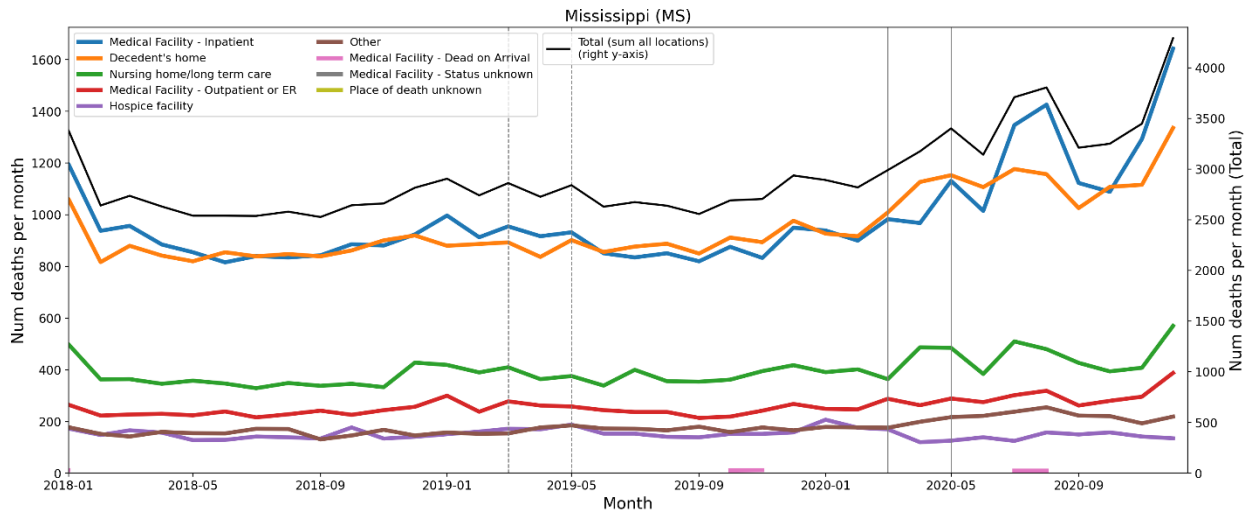
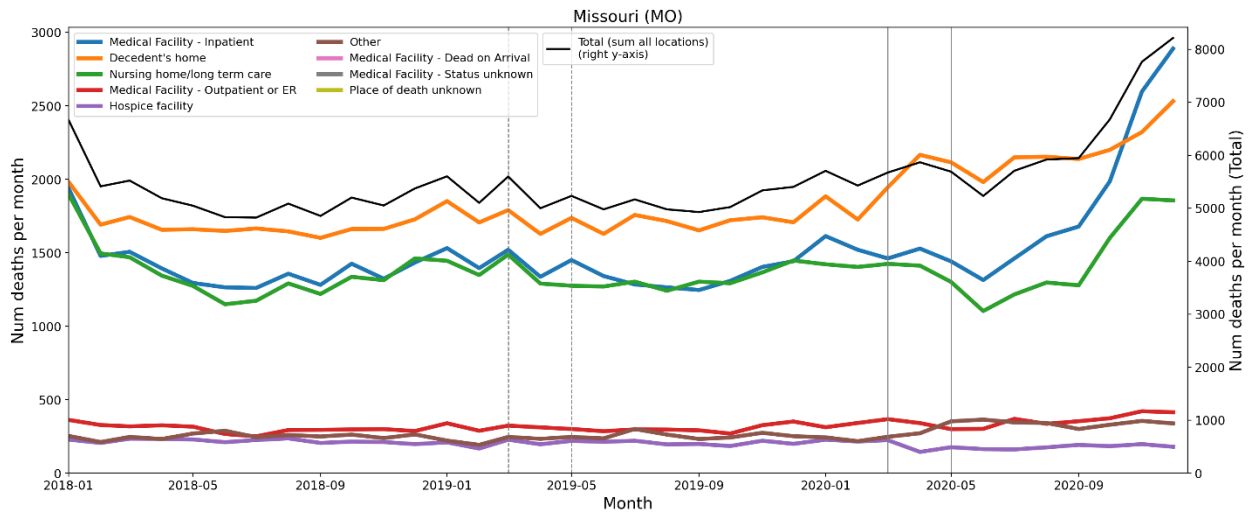
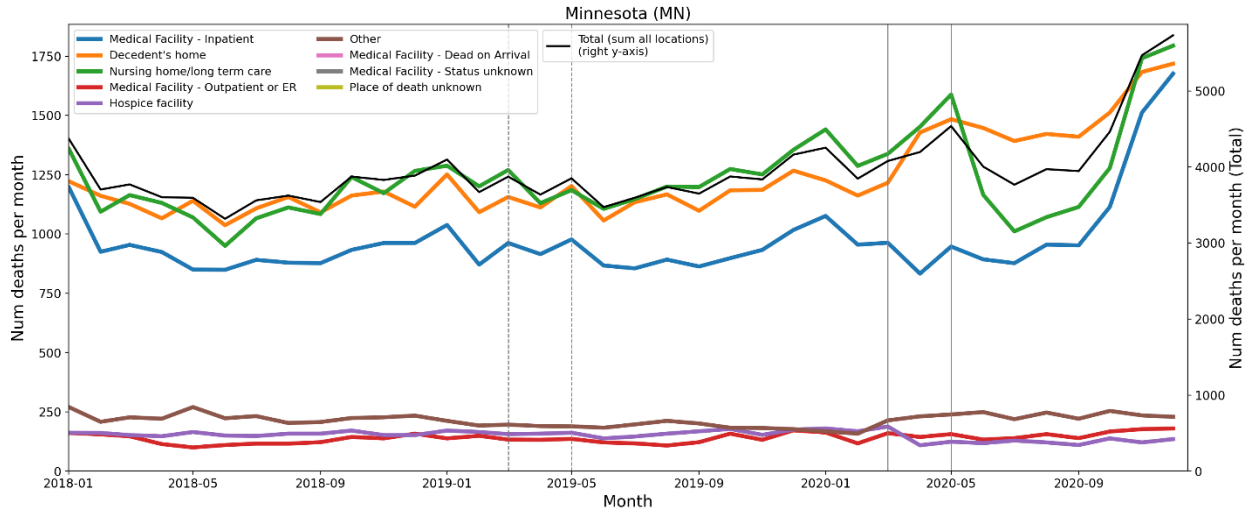


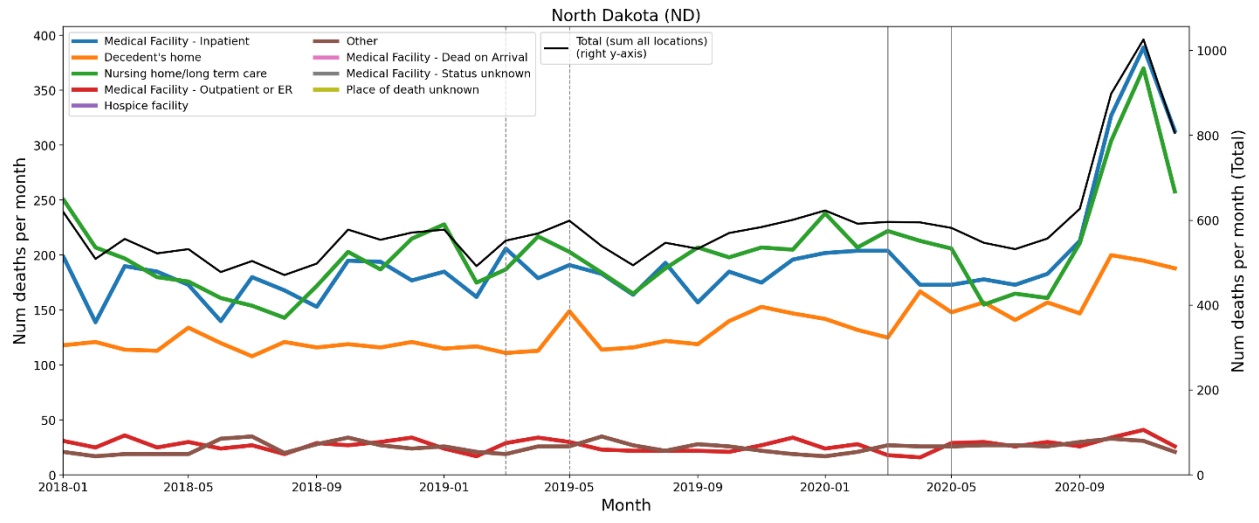
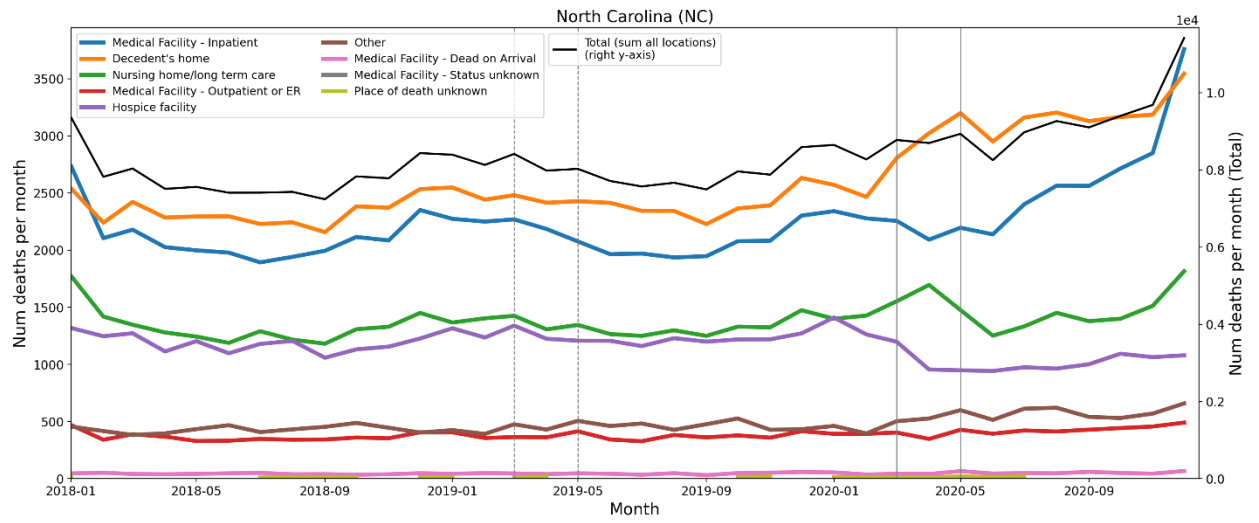
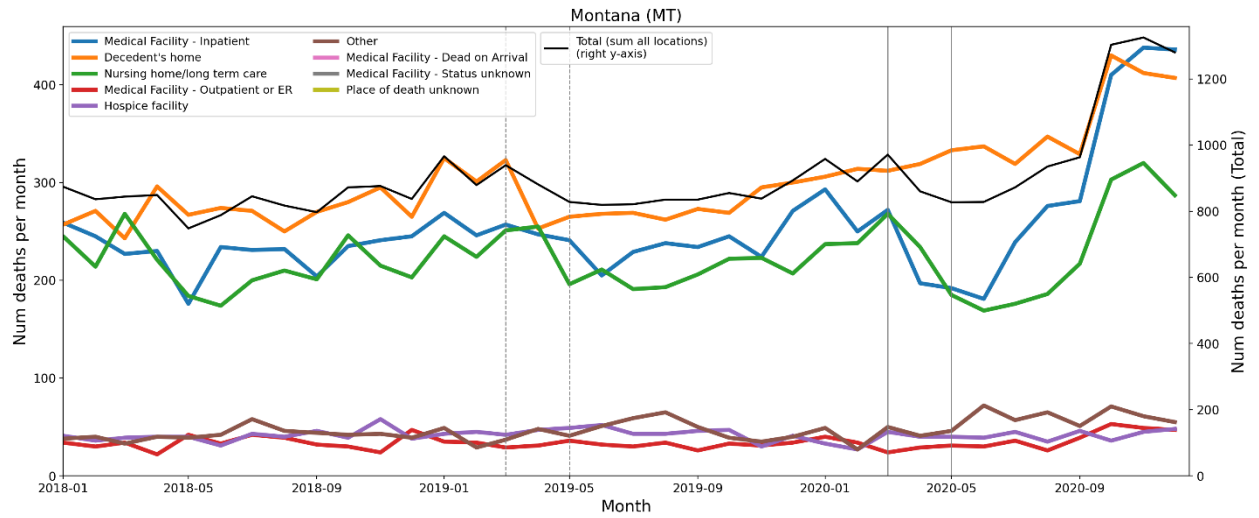


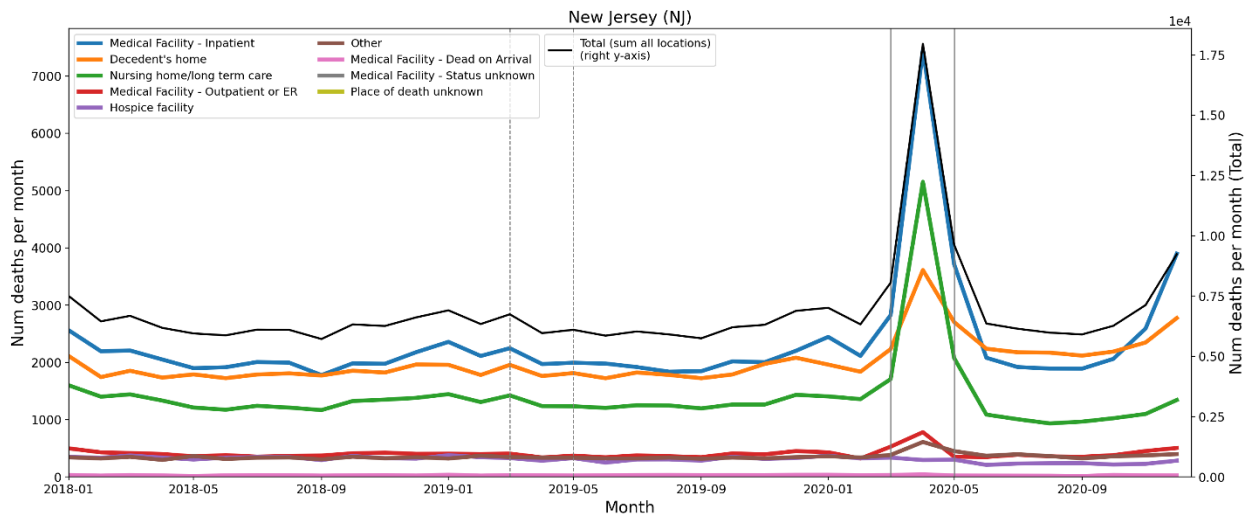
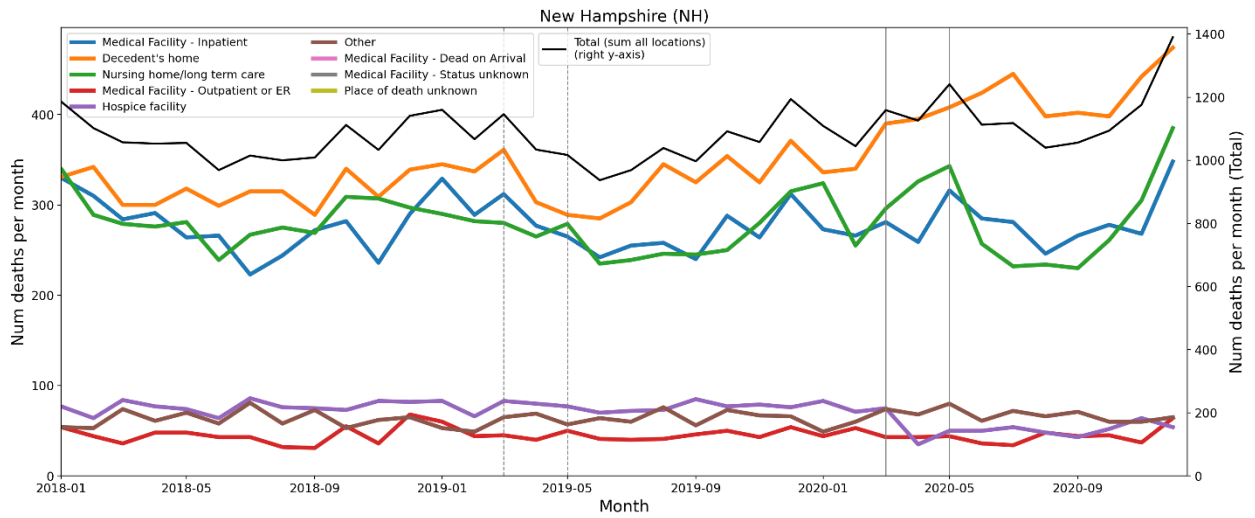
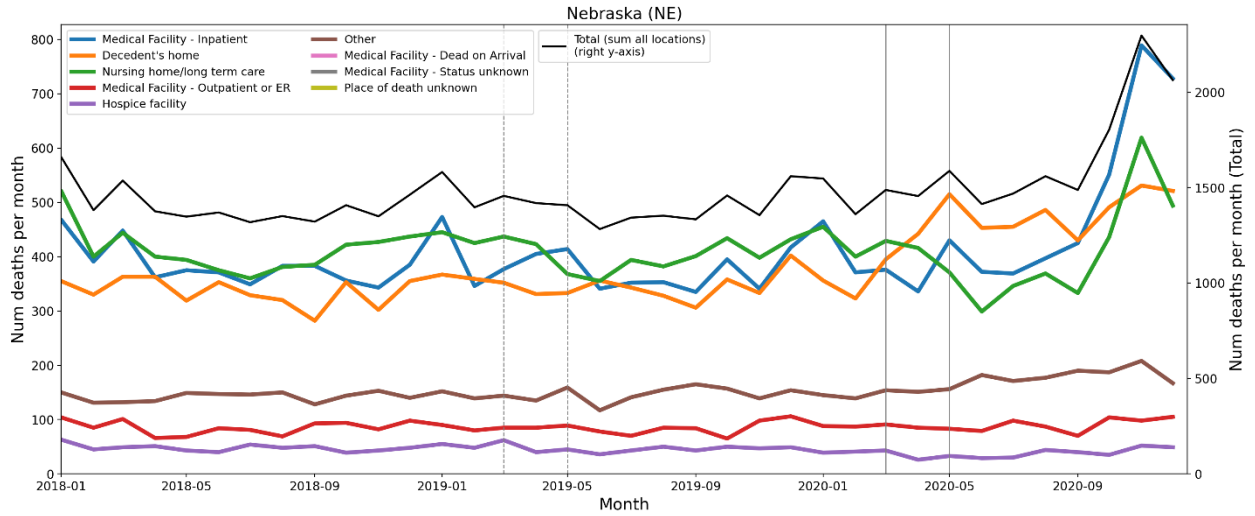


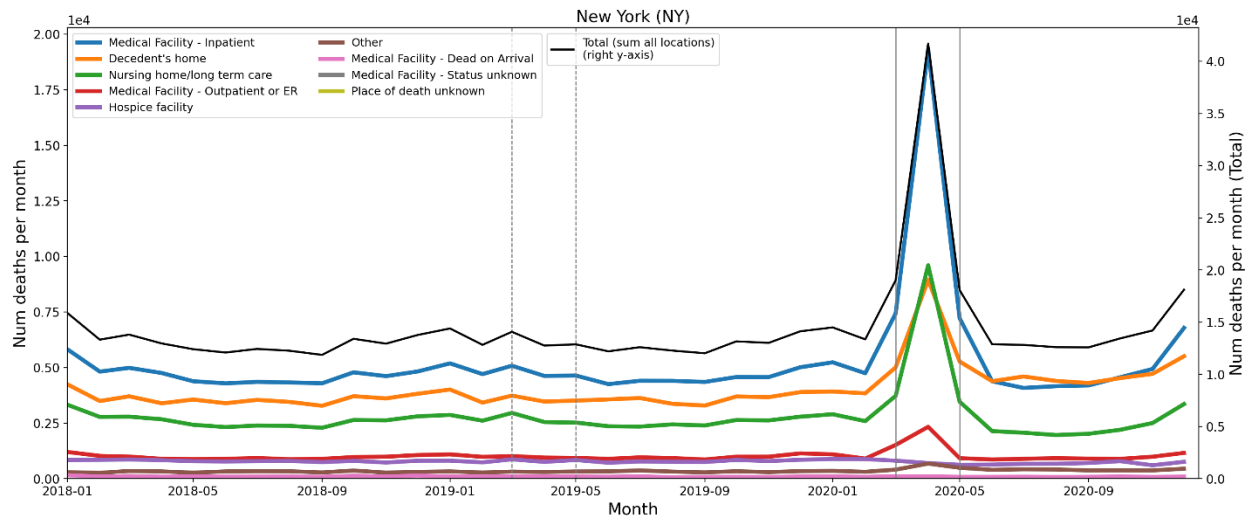
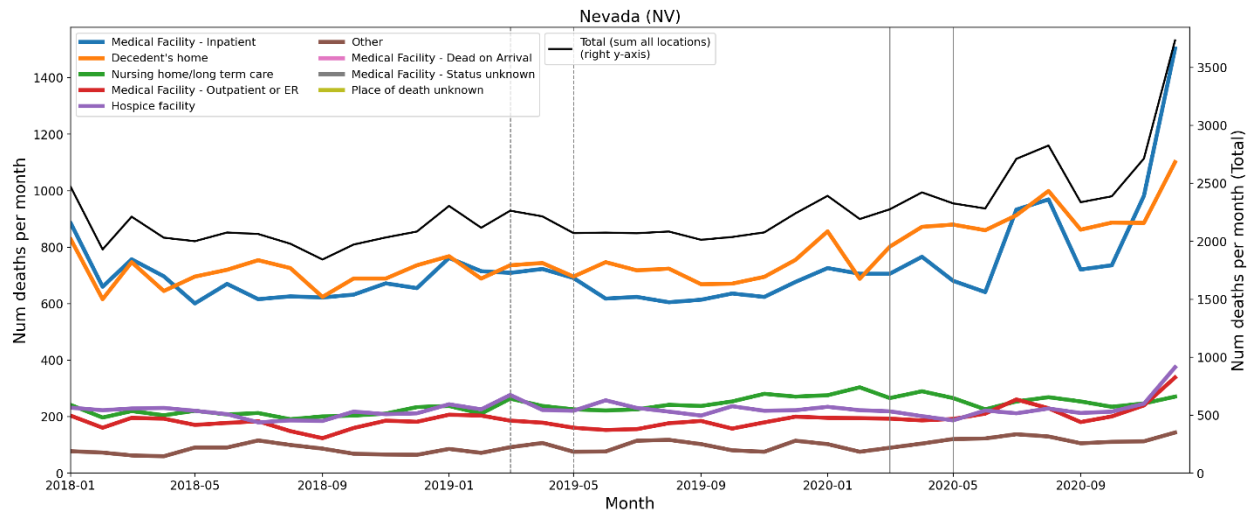
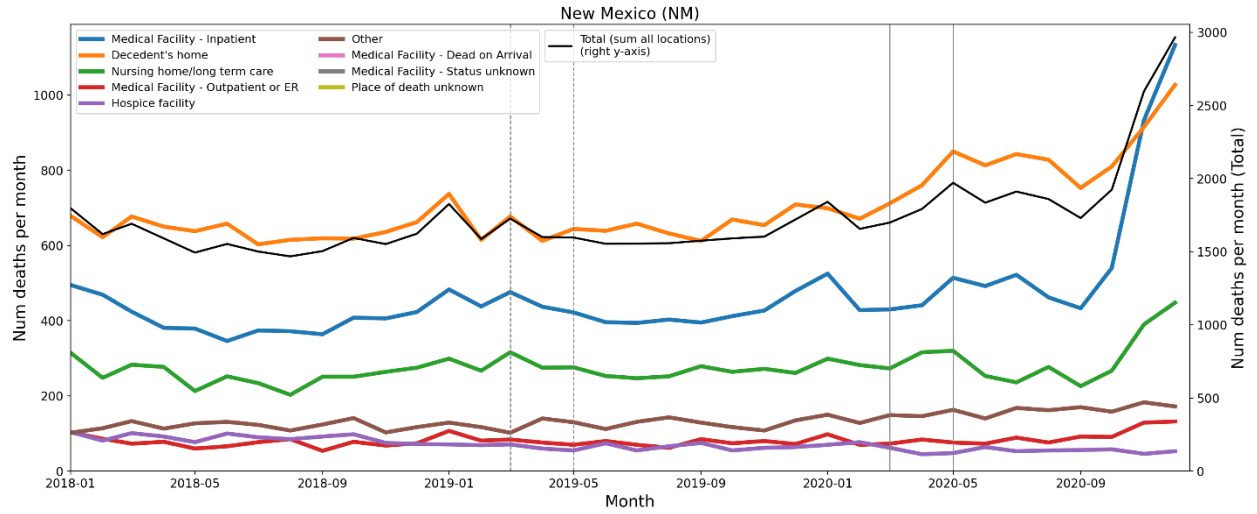


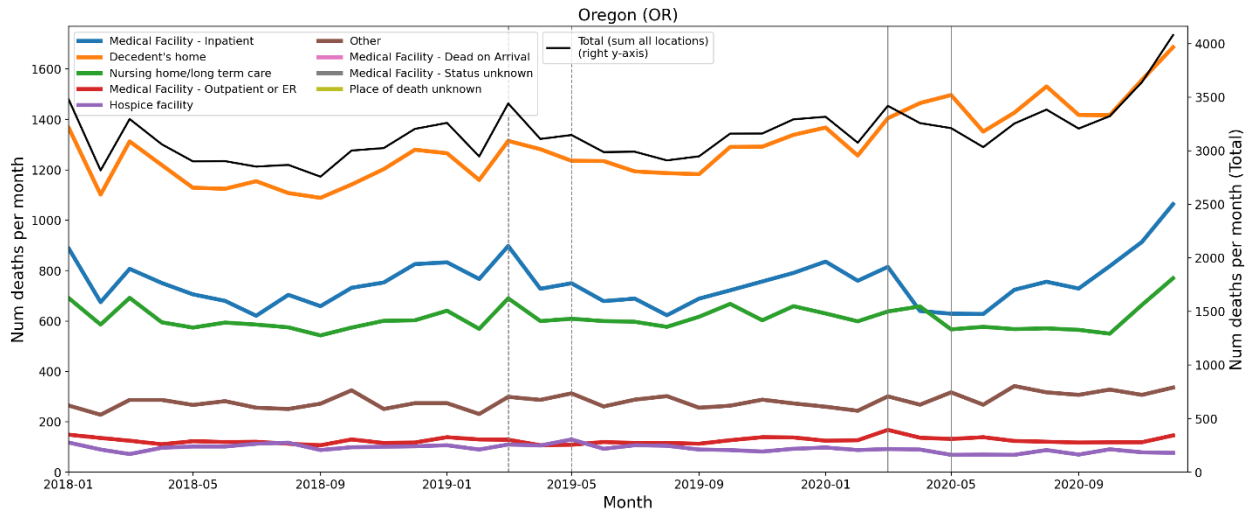
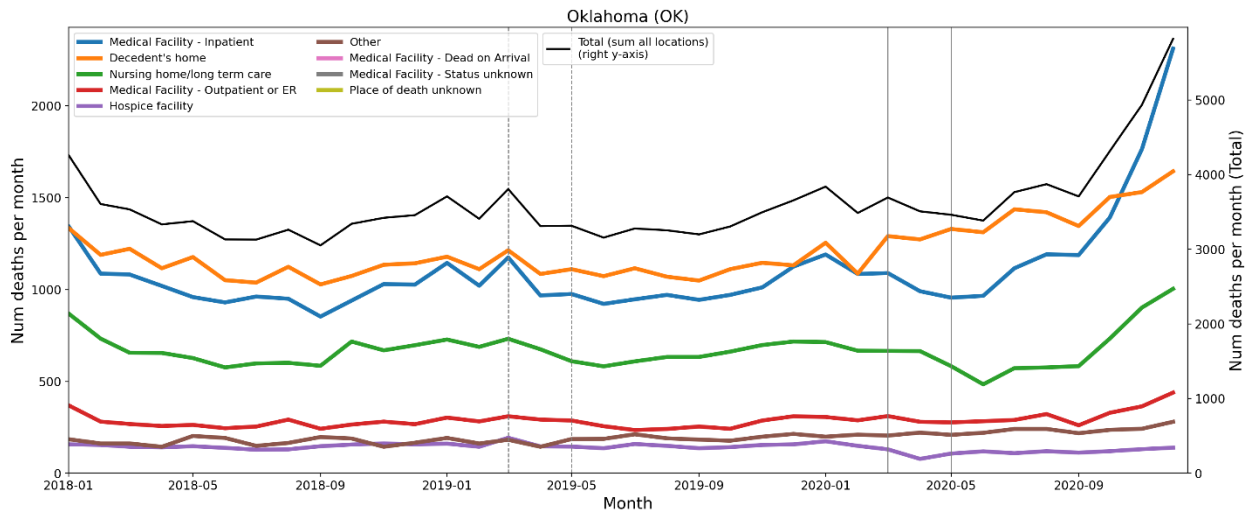
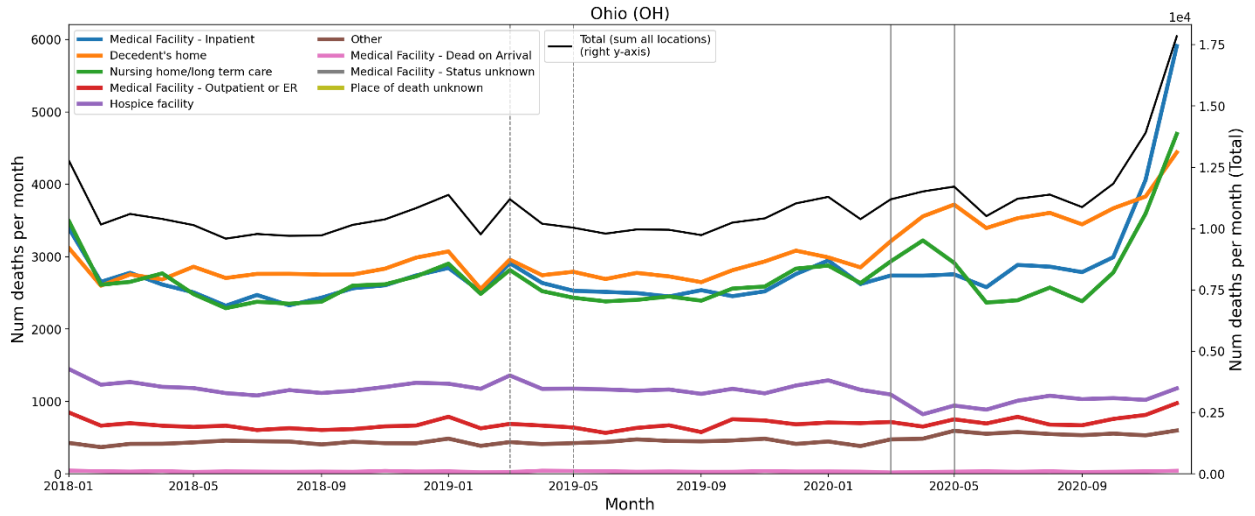


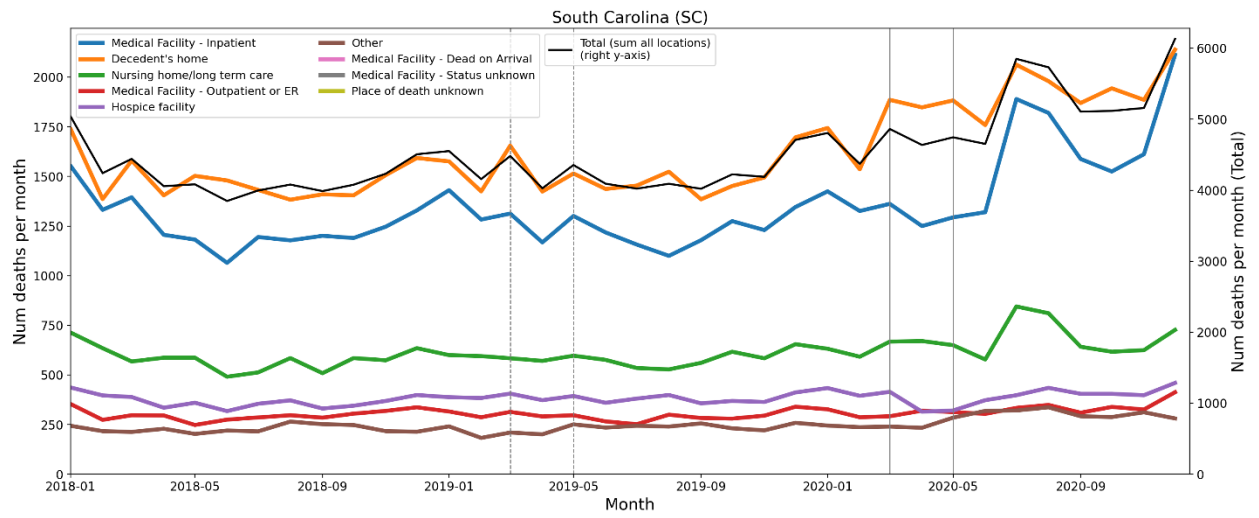
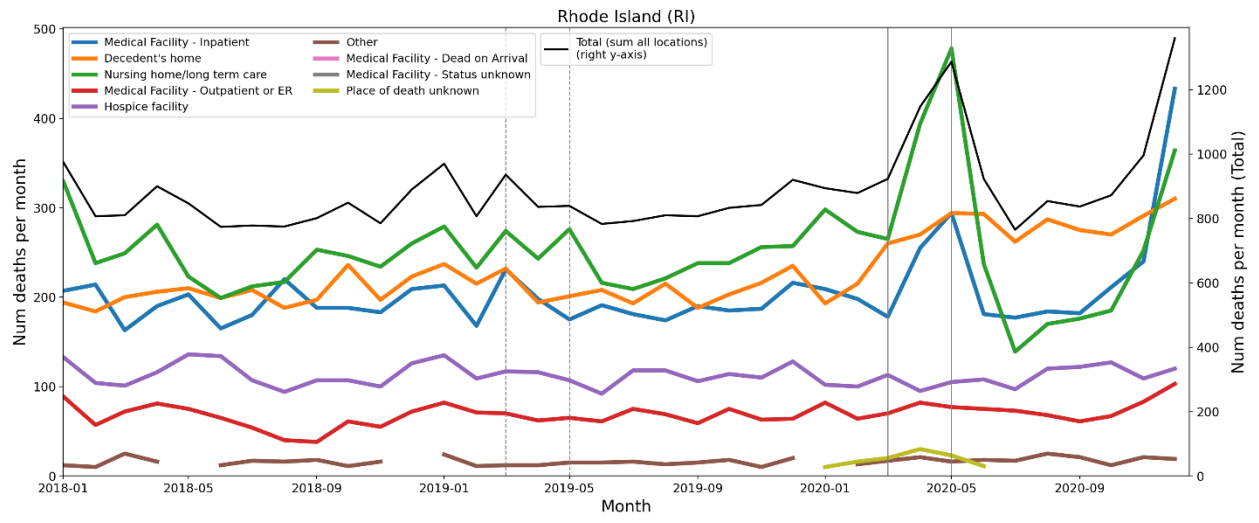
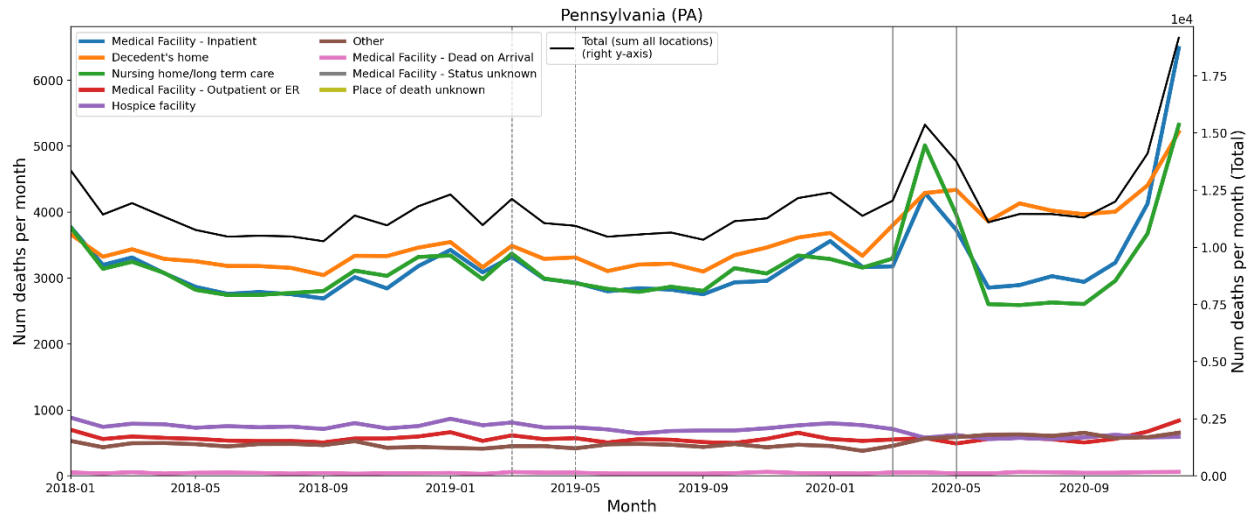


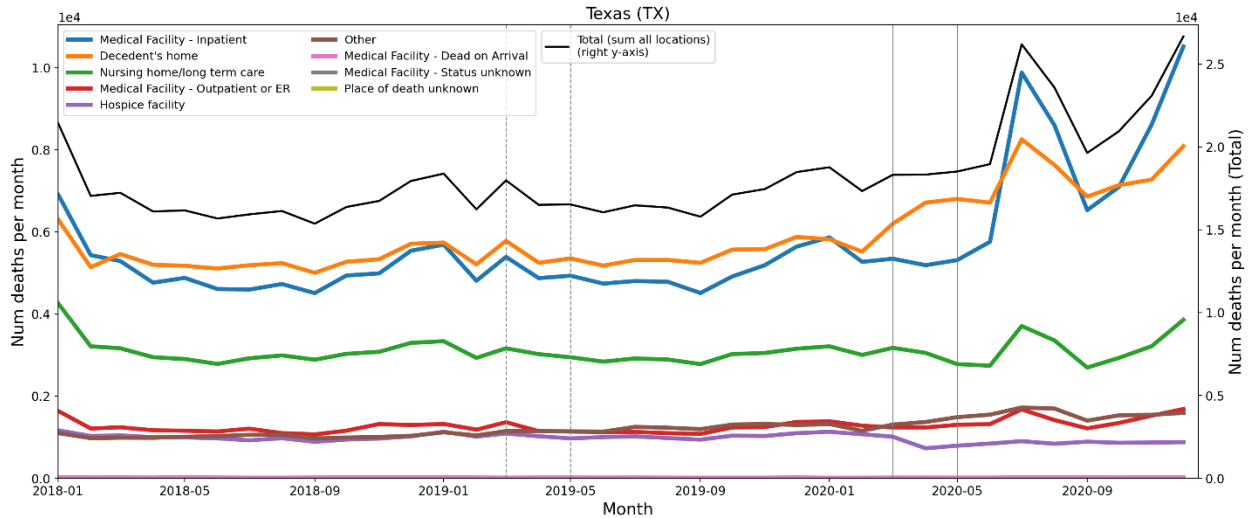
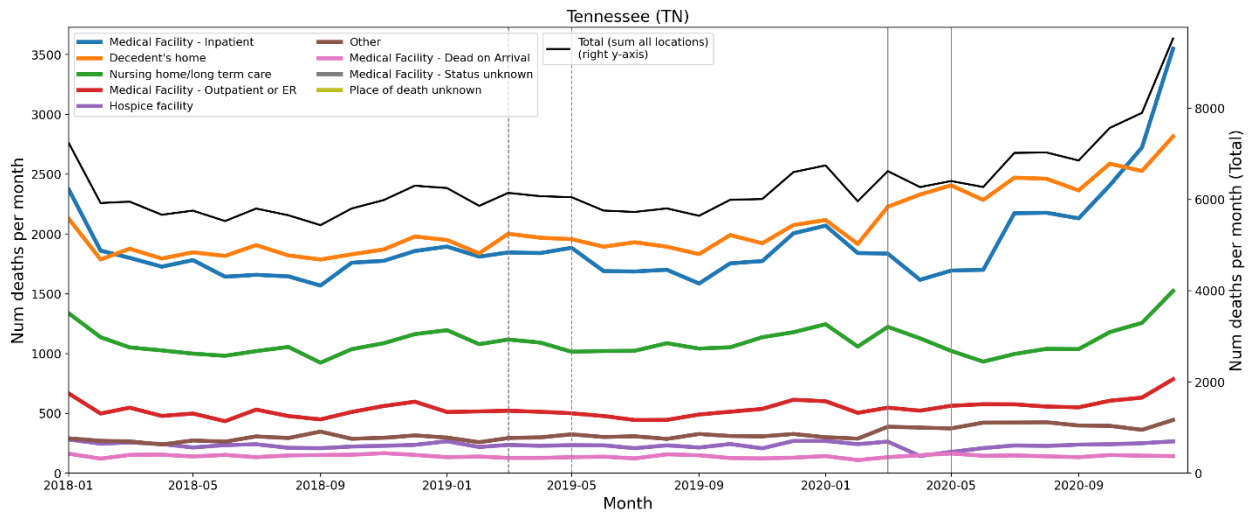
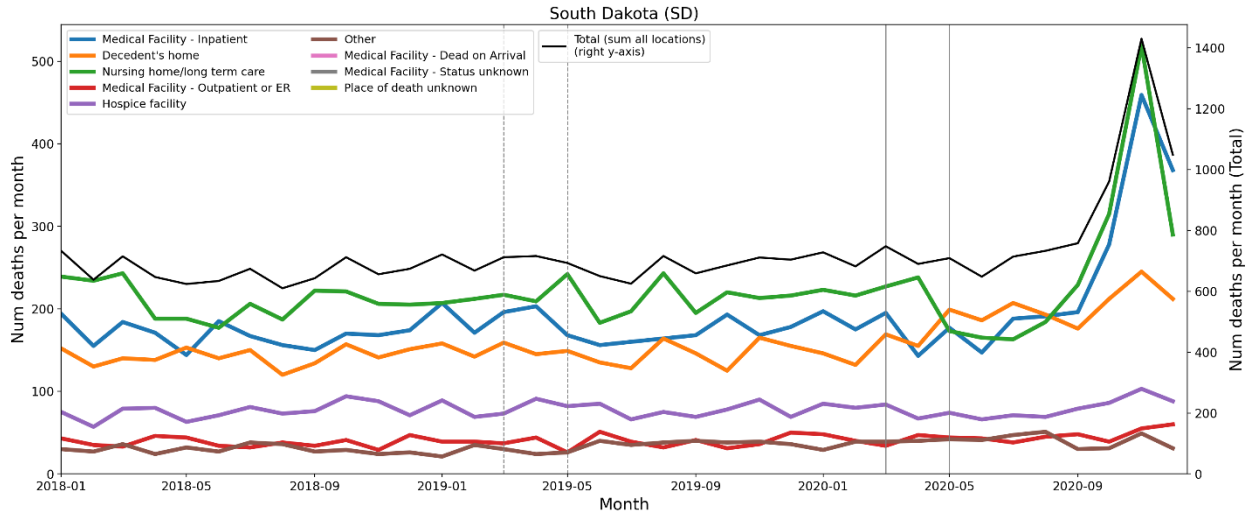


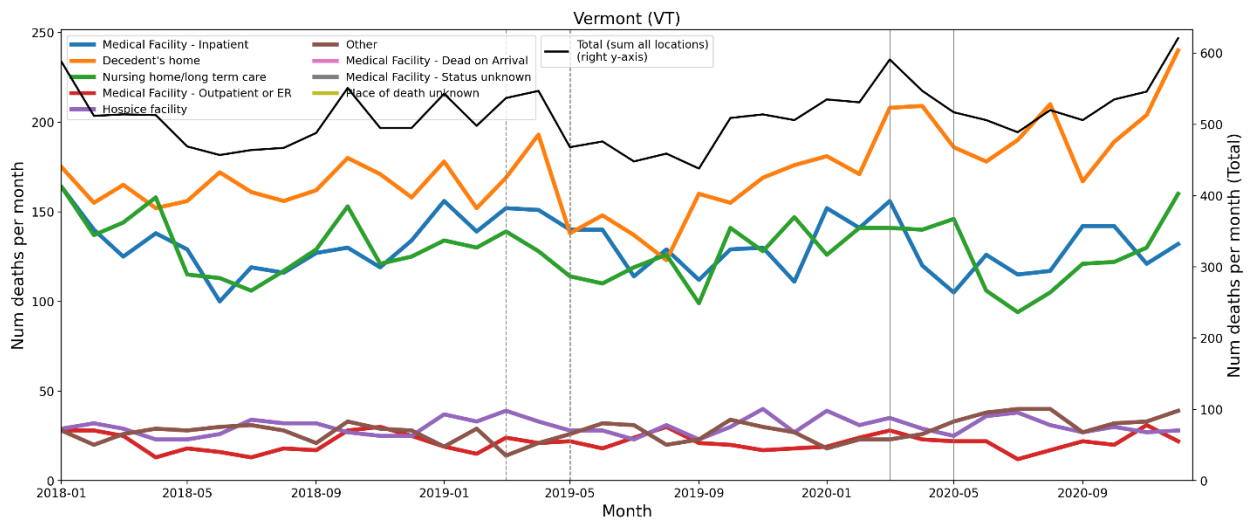
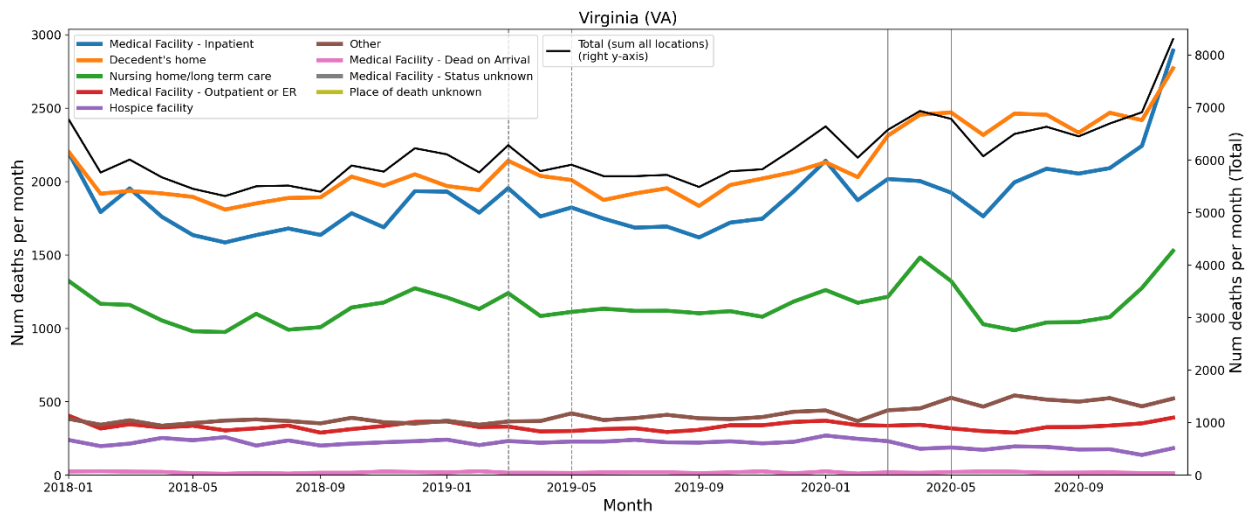
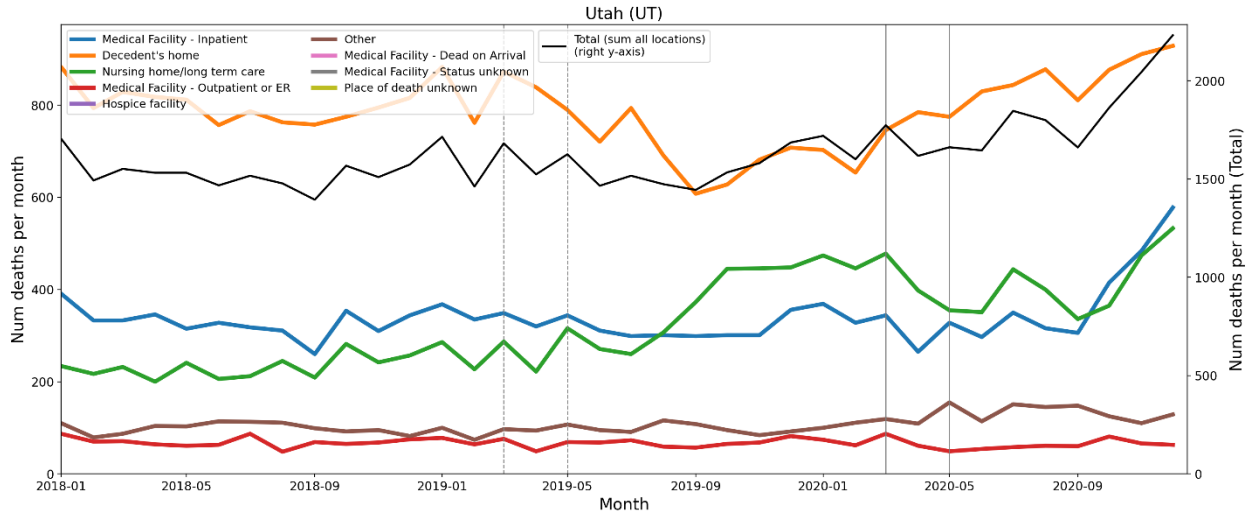


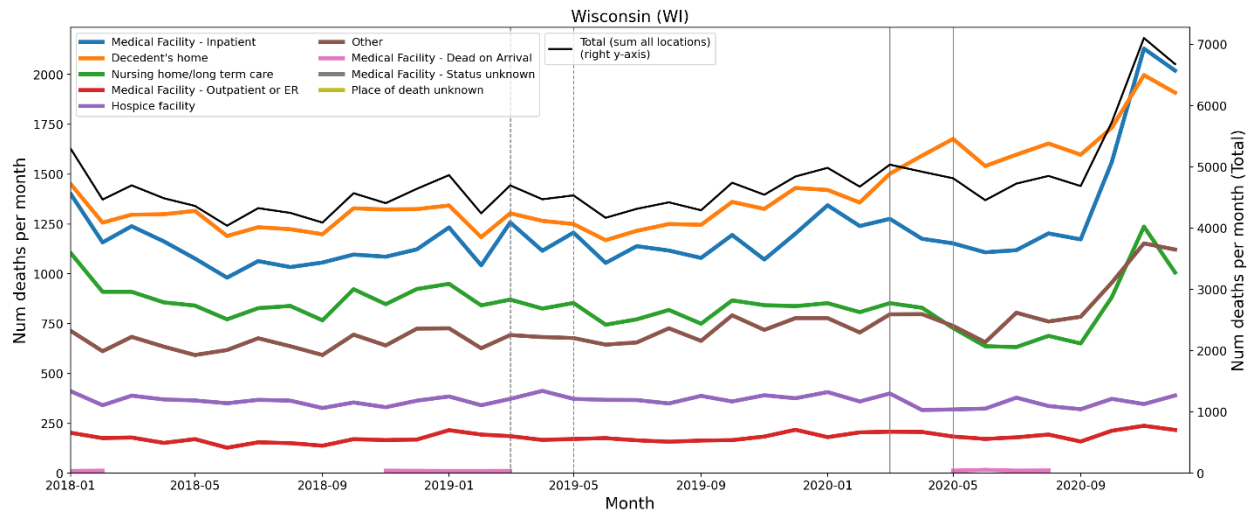
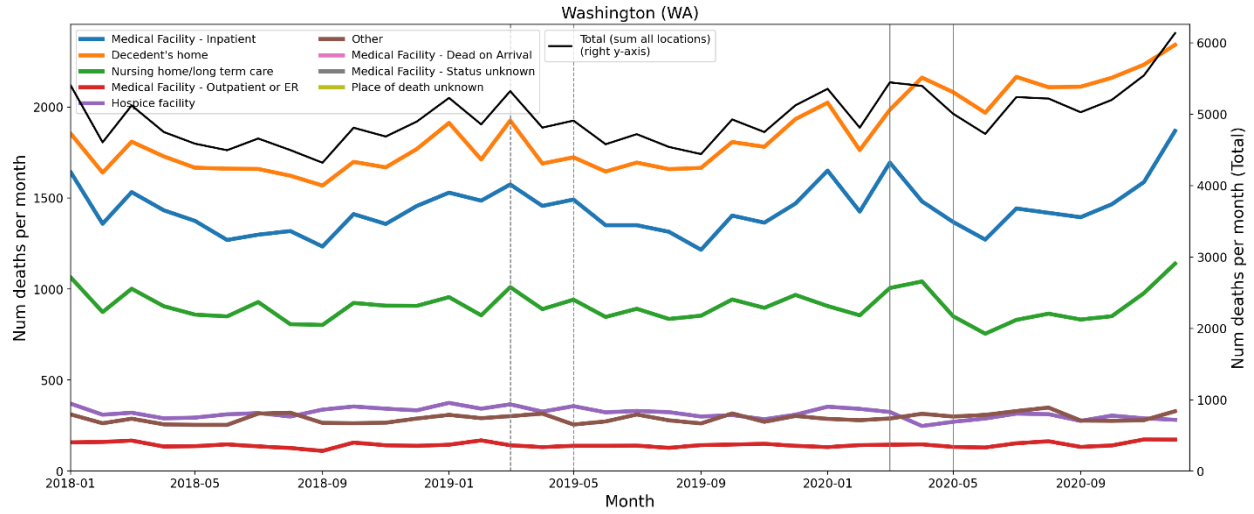


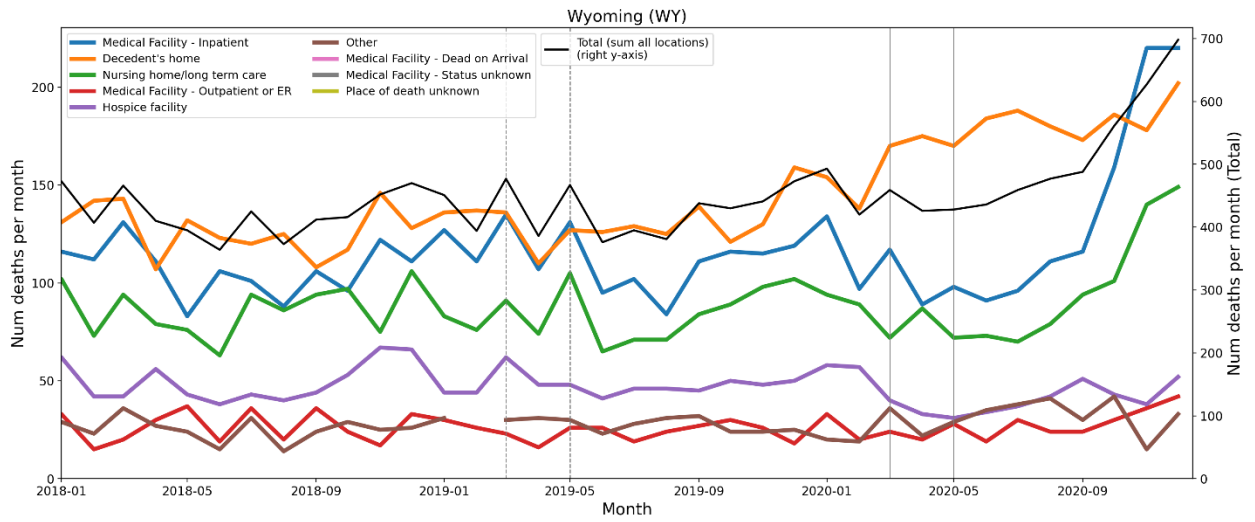
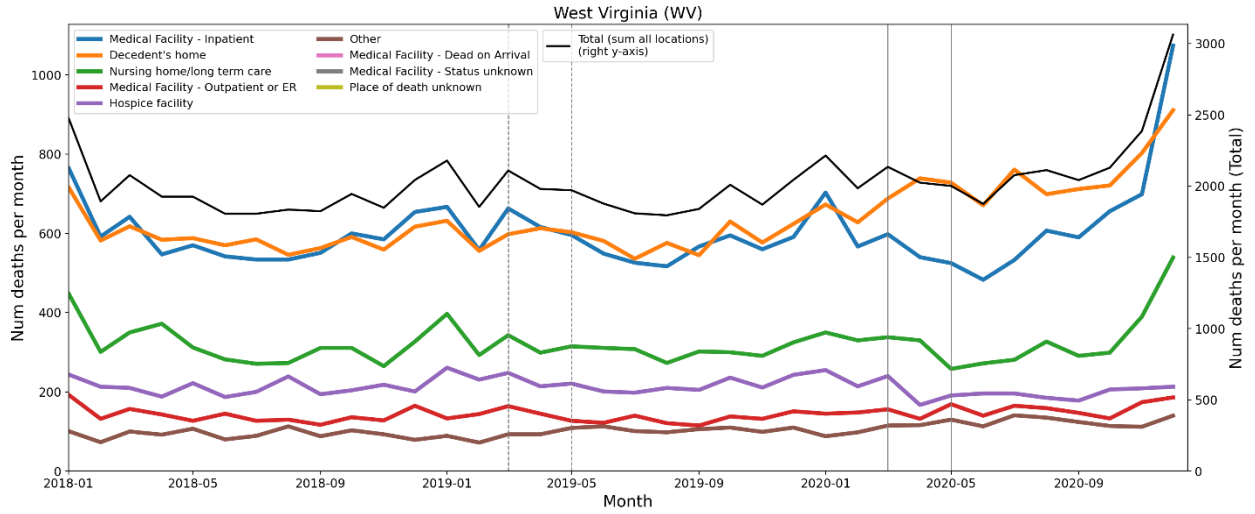












C. Tables of European regions by NUTS level, ordered by integrated first-peak period P-score

C.1 NUTS0 level (countries)

Rank	NUTS Code	NUTS Level	Country	P-score (%)	(1 σ) Err (%)	P-score / Err	Rise-side half-maximum (weeks after Mar 9-15, 2020)*
1	ES	0	Spain	47.6	1.7	28	1
2	UK	0	United Kingdom	41.3	2.7	15	3
3	IT	0	Italy	34	1.5	23	0
4	BE	0	Belgium	31	2.6	12	2
5	SE	0	Sweden	23.7	2.1	11	3
6	NL	0	Netherlands	22.2	2	11	2
7	FR	0	France	16.4	1.5	11	2
8	IE	0	Ireland	14.9	2.1	7.1	3
9	PT	0	Portugal	11.6	1.7	6.8	1
10	CY	0	Cyprus	11	4.2	2.6	-
11	CH	0	Switzerland	10.5	2	5.3	2
12	AL	0	Albania	7.1	2.6	2.7	-
13	MT	0	Malta	6.8	5.1	1.3	-
14	LT	0	Lithuania	6.7	1.9	3.5	1
15	AT	0	Austria	6.1	1.9	3.2	1
16	LU	0	Luxembourg	4.5	4.6	0.98	-
17	FI	0	Finland	4.1	1.8	2.3	-
18	EL	0	Greece	3.4	1.5	2.3	-
19	RS	0	Serbia	3.3	1.8	1.8	-
20	IS	0	Iceland	3	5.4	0.56	-
21	EE	0	Estonia	2.1	2.6	0.81	-
22	DE	0	Germany	2	2	1.0	-
24	NO	0	Norway	1.9	1.7	1.0	-
23	SK	0	Slovakia	1.9	1.9	1.0	-
25	HU	0	Hungary	1	1.8	0.56	-
27	HR	0	Croatia	0.9	2	0.45	-
26	SI	0	Slovenia	0.9	2.2	0.41	-
28	CZ	0	Czechia	0.3	1.8	0.17	-
29	RO	0	Romania	0.1	1.6	0.06	-
30	PL	0	Poland	0	1.7	0	-

31	LI	0	Liechtenstein	0	17	0	-
32	DK	0	Denmark	-0.8	1.6	-0.50	-
33	LV	0	Latvia	-2.7	2.1	-1.3	-
34	BG	0	Bulgaria	-3.1	1.5	-2.1	-
35	ME	0	Montenegro	-4	3.4	-1.2	-

* F-peaks were considered to have discernible rise-side half-maximum dates if the ratio of P-score / Err(P-score) ≥ 3 .

C.2 NUTS1 level

Rank	NUTS Code	NUTS Level	Region Name	Country	P-score (%)	(1 σ) Err (%)
1	ES3	1	COMUNIDAD DE MADRID	Spain	145.6	3.2
2	ITC	1	NORD-OVEST	Italy	80.6	2
3	UKI	1	LONDON	United Kingdom	80.5	4
4	ES4	1	CENTRO (ES)	Spain	73.8	2.7
5	BE1	1	RÉGION DE BRUXELLES-CAPITALE/BRUSSELS HOOFDSTEDELIJK GEWEST	Belgium	60.9	5.2
6	FR1	1	ILE-DE-FRANCE	France	58	2.4
7	UKG	1	WEST MIDLANDS (ENGLAND)	United Kingdom	49.5	3.7
8	UKD	1	NORTH WEST (ENGLAND)	United Kingdom	46.4	2.8
9	UKC	1	NORTH EAST (ENGLAND)	United Kingdom	43.2	3.1
10	SE1	1	ÖSTRA SVERIGE	Sweden	42.5	2.8
11	UKJ	1	SOUTH EAST (ENGLAND)	United Kingdom	40.6	3.3
12	NL4	1	ZUID-NEDERLAND	Netherlands	40.6	2.9
13	UKH	1	EAST OF ENGLAND	United Kingdom	40.3	3.5
14	ES5	1	ESTE	Spain	39.4	2.1
15	UKE	1	YORKSHIRE AND THE HUMBER	United Kingdom	39	2.9
16	ES2	1	NORESTE	Spain	37	2.5
17	FRF	1	ALSACE-CHAMPAGNE-ARDENNE-LORRAINE	France	35.4	2.8
18	UKF	1	EAST MIDLANDS (ENGLAND)	United Kingdom	35	3.2
19	BE3	1	RÉGION WALLONNE	Belgium	33.2	3.1
20	ITH	1	NORD-EST	Italy	32.6	1.5
21	UKM	1	SCOTLAND	United Kingdom	31.7	2.4
22	UKK	1	SOUTH WEST (ENGLAND)	United Kingdom	26.6	3.6
23	BE2	1	VLAAMS GEWEST	Belgium	25.6	2.7

24	UKL	1	WALES	United Kingdom	24.8	3.2
25	UKN	1	NORTHERN IRELAND	United Kingdom	23	3.8
26	NL2	1	OOST-NEDERLAND	Netherlands	19.7	2.8
27	FRC	1	BOURGOGNE-FRANCHE-COMTÉ	France	18.8	2.4
28	NL3	1	WEST-NEDERLAND	Netherlands	18.8	2
29	FRE	1	NORD-PAS DE CALAIS-PICARDIE	France	17.9	2.3
30	IE0	1	IRELAND	Ireland	14.9	2.1
31	FRK	1	AUVERGNE-RHÔNE-ALPES	France	14	1.8
32	SE3	1	NORRA SVERIGE	Sweden	13.7	2.7
33	SE2	1	SÖDRA SVERIGE	Sweden	13.7	2.3
34	ITI	1	CENTRO (IT)	Italy	12.1	1.6
35	ES1	1	NOROESTE	Spain	11.9	1.7
36	PT1	1	CONTINENTE	Portugal	11.8	1.8
37	ES6	1	SUR	Spain	11.5	1.6
38	CY0	1	Kypros	Cyprus	11	4.2
39	ITF	1	SUD	Italy	10.9	1.5
40	FRB	1	CENTRE - VAL DE LOIRE	France	10.6	2.1
41	CH0	1	SCHWEIZ/SUISSE/SVIZZERA	Switzerland	10.5	2
42	PT2	1	REGIÃO AUTÓNOMA DOS AÇORES	Portugal	9.9	6.4
43	AT2	1	SÜDÖSTERREICH	Austria	8.6	2.7
44	DE2	1	BAYERN	Germany	8	2.1
45	FRM	1	CORSE	France	7.2	5.4
46	FRL	1	PROVENCE-ALPES-CÔTE D'AZUR	France	6.9	1.5
47	MT0	1	MALTA	Malta	6.8	5.1
48	LTO	1	LIETUVA	Lithuania	6.7	1.9
49	AT1	1	OSTÖSTERREICH	Austria	6.5	2.1
50	ITG	1	ISOLE	Italy	6.4	1.7
51	FRD	1	NORMANDIE	France	6.3	2.1
52	DE1	1	BADEN-WÜRTTEMBERG	Germany	5.6	2.2
53	FRG	1	PAYS DE LA LOIRE	France	5	1.9
54	HU1	1	KÖZÉP-MAGYARORSZÁG	Hungary	4.9	2.1
55	EL6	1	KENTRIKI ELLADA	Greece	4.6	2.2
56	PT3	1	REGIÃO AUTÓNOMA DA MADEIRA	Portugal	4.6	5.4
57	LU0	1	LUXEMBOURG	Luxembourg	4.5	4.6
58	EL4	1	NISIA AIGAIUOY, KRITI	Greece	4.2	2.7
59	FI1	1	MANNER-SUOMI	Finland	4.1	1.8
60	RS2	1	Srbija - jug	Serbia	4.1	2
61	AT3	1	WESTÖSTERREICH	Austria	3.9	2.4
62	DE6	1	HAMBURG	Germany	3.6	2.6
63	EL5	1	VOREIA ELLADA	Greece	3.6	2
64	DE5	1	BREMEN	Germany	3.4	4.4

65	RO4	1	MACROREGIUNEA PATRU	Romania	3.1	2.1
66	ES7	1	CANARIAS	Spain	3.1	2.6
67	IS0	1	ÍSLAND	Iceland	3	5.4
68	NL1	1	NOORD-NEDERLAND	Netherlands	2.9	2.7
69	FRJ	1	LANGUEDOC-ROUSSILLON-MIDI-PYRÉNÉES	France	2.7	1.5
70	RS1	1	Srbija - sever	Serbia	2.3	2
71	EL3	1	ATTIKI	Greece	2.2	1.9
72	PL2	1	MAKROREGION POŁUDNIOWY	Poland	2.1	1.8
73	EE0	1	EESTI	Estonia	2	2.6
74	SK0	1	SLOVENSKO	Slovakia	1.9	1.9
75	NO0	1	NORGE	Norway	1.9	1.7
76	DE7	1	HESSEN	Germany	1.8	2.1
77	DE3	1	BERLIN	Germany	1.6	2.2
78	DE9	1	NIEDERSACHSEN	Germany	1.3	2.1
79	DEA	1	NORDRHEIN-WESTFALEN	Germany	1.2	2.2
80	HU2	1	DUNÁNTÚL	Hungary	1.1	2.1
81	DEC	1	SAARLAND	Germany	1.1	3.5
82	PL9	1	MAKROREGION WOJEWÓDZTWO MAZOWIECKIE	Poland	1	1.7
83	SI0	1	SLOVENIJA	Slovenia	0.9	2.2
84	PL8	1	MAKROREGION WSCHODNI	Poland	0.9	1.8
85	HR0	1	HRVATSKA	Croatia	0.9	2
86	RO3	1	MACROREGIUNEA TREI	Romania	0.6	1.7
87	PL7	1	MAKROREGION CENTRALNY	Poland	0.5	2.3
88	FRY	1	RUP FR - RÉGIONS ULTRAPÉRIPHÉRIQUES FRANÇAISES	France	0.4	2.4
89	CZ0	1	ČESKÁ REPUBLIKA	Czechia	0.3	1.8
90	RO1	1	MACROREGIUNEA UNU	Romania	0.3	1.8
91	DEB	1	RHEINLAND-PFALZ	Germany	-0.2	2.4
92	LI0	1	LIECHTENSTEIN	Liechtenstein	0	17
93	FRH	1	BRETAGNE	France	-0.3	1.9
94	PL5	1	MAKROREGION POŁUDNIOWO-ZACHODNI	Poland	-0.8	2.5
95	FRI	1	AQUITAINE-LIMOUSIN-POITOU-CHARENTES	France	-0.8	1.7
96	DK0	1	DANMARK	Denmark	-0.8	1.6
97	DED	1	SACHSEN	Germany	-0.8	2.7
98	DE4	1	BRANDENBURG	Germany	-1.1	2.5
99	HU3	1	ALFÖLD ÉS ÉSZAK	Hungary	-1.6	2.1
100	DE8	1	MECKLENBURG-VORPOMMERN	Germany	-2.1	2.5

101	PL6	1	MAKROREGION PÓŁNOCNY	Poland	-2.2	1.7
102	RO2	1	MACROREGIUNEA DOI	Romania	-2.2	1.8
103	PL4	1	MAKROREGION PÓŁNOCNO-ZACHODNI	Poland	-2.3	2
104	BG4	1	YUGOZAPADNA I YUZHNA TSENTRALNA BULGARIA	Bulgaria	-2.4	1.9
105	DEG	1	THÜRINGEN	Germany	-2.7	3
106	LV0	1	LATVIJA	Latvia	-2.7	2.1
107	DEF	1	SCHLESWIG-HOLSTEIN	Germany	-3	2.4
108	BG3	1	SEVERNA I YUGOIZTOCHNA BULGARIA	Bulgaria	-3.7	1.7
109	ME0	1	CRNA GORA	Montenegro	-4	3.4
110	DEE	1	SACHSEN-ANHALT	Germany	-4.1	2.6
111	FI2	1	ÅLAND	Finland	-15	16

C.3 NUTS2 level

Rank	NUTS Code	NUTS Level	Region Name	Country	P-score (%)	(1 σ) Err (%)
1	ES30	2	Comunidad de Madrid	Spain	145.6	3.2
2	ES42	2	Castilla-La Mancha	Spain	108.7	4.4
3	ITC4	2	Lombardia	Italy	106.2	2.5
4	UKI4	2	Inner London - East	United Kingdom	87.3	6
5	UKI7	2	Outer London - West and North West	United Kingdom	86.4	5
6	UKI5	2	Outer London - East and North East	United Kingdom	80.2	5.5
7	UKI3	2	Inner London - West	United Kingdom	77.2	6.2
8	ES51	2	Cataluña	Spain	72.4	2.8
9	UKI6	2	Outer London - South	United Kingdom	67.2	5.8
10	ES41	2	Castilla y León	Spain	66.3	3.3
11	UKG3	2	West Midlands	United Kingdom	61.3	4.6
12	BE10	2	Région de Bruxelles-Capitale/ Brussels Hoofdstedelijk Gewest	Belgium	60.9	5.2
13	SE11	2	Stockholm	Sweden	59.4	3.6
14	FR10	2	Ile-de-France	France	56.2	2.4
15	UKH2	2	Bedfordshire and Hertfordshire	United Kingdom	55.5	4.3
16	FRF1	2	Alsace	France	53.7	3.6
17	ITH2	2	Provincia Autonoma di Trento	Italy	53.5	5.6

18	UKD3	2	Greater Manchester	United Kingdom	53.1	3.5
19	UKD7	2	Merseyside	United Kingdom	51.2	4
20	ES22	2	Comunidad Foral de Navarra	Spain	49.5	5
21	ITC2	2	Valle d'Aosta/Vallée d'Aoste	Italy	48.1	9.4
22	ITC1	2	Piemonte	Italy	47.9	2.1
23	ES23	2	La Rioja	Spain	47.8	7.2
24	CH07	2	Ticino	Switzerland	47.8	6.7
25	UKJ1	2	Berkshire, Buckinghamshire and Oxfordshire	United Kingdom	47.3	3.4
26	BE22	2	Prov. Limburg (BE)	Belgium	46.2	5.2
27	UKC1	2	Tees Valley and Durham	United Kingdom	46.2	4.2
28	ITH5	2	Emilia-Romagna	Italy	45.9	2.3
29	UKD1	2	Cumbria	United Kingdom	45.4	5.2
30	UKM8	2	West Central Scotland	United Kingdom	45.4	3.7
31	ITH1	2	Provincia Autonoma di Bolzano/Bozen	Italy	44.7	6.2
32	ITC3	2	Liguria	Italy	44.6	3.2
33	NL42	2	Limburg (NL)	Netherlands	44.6	4.2
34	UKE3	2	South Yorkshire	United Kingdom	44.2	4
35	UKJ2	2	Surrey, East and West Sussex	United Kingdom	44	4.5
36	UKD6	2	Cheshire	United Kingdom	43.9	4.5
37	UKF2	2	Leicestershire, Rutland and Northamptonshire	United Kingdom	43	3.8
38	UKH3	2	Essex	United Kingdom	41.9	4.8
39	UKE4	2	West Yorkshire	United Kingdom	41.8	3.2
40	UKG1	2	Herefordshire, Worcestershire and Warwickshire	United Kingdom	41.3	4.2
41	UKC2	2	Northumberland and Tyne and Wear	United Kingdom	40.6	3.7
42	BE33	2	Prov. Liège	Belgium	39.8	3.6
43	UKK1	2	Gloucestershire, Wiltshire and Bristol/Bath area	United Kingdom	39.6	4.4
44	UKE2	2	North Yorkshire	United Kingdom	39.4	4.9
45	UKG2	2	Shropshire and Staffordshire	United Kingdom	38.8	4.2
46	NL41	2	Noord-Brabant	Netherlands	38.5	3
47	ES24	2	Aragón	Spain	37.4	3.1
48	UKF1	2	Derbyshire and Nottinghamshire	United Kingdom	36.7	4.1
49	UKJ4	2	Kent	United Kingdom	35.7	3.8
50	UKJ3	2	Hampshire and Isle of Wight	United Kingdom	33.6	3.8
51	BE32	2	Prov. Hainaut	Belgium	33.6	4.3
52	ES43	2	Extremadura	Spain	33.4	3.3
53	UKD4	2	Lancashire	United Kingdom	33.4	3.4

54	ITI3	2	Marche	Italy	33.1	2.8
55	UKM7	2	Eastern Scotland	United Kingdom	32.9	3.1
56	UKL2	2	East Wales	United Kingdom	32.4	4.2
57	ES21	2	País Vasco	Spain	31.8	3
58	UKH1	2	East Anglia	United Kingdom	30.3	3.9
59	FRF3	2	Lorraine	France	30	3.3
60	FRE2	2	Picardie	France	29.9	3
61	UKM9	2	Southern Scotland	United Kingdom	29.3	3.6
62	BE35	2	Prov. Namur	Belgium	27.8	5.1
63	FRC2	2	Franche-Comté	France	27	3.9
64	BE24	2	Prov. Vlaams-Brabant	Belgium	27	4.1
65	UKK2	2	Dorset and Somerset	United Kingdom	26.5	4.4
66	UKE1	2	East Yorkshire and Northern Lincolnshire	United Kingdom	25.8	4.2
67	CH01	2	Région lémanique	Switzerland	25.8	3.7
68	SE12	2	Östra Mellansverige	Sweden	25.5	3.2
69	BE34	2	Prov. Luxembourg (BE)	Belgium	24.9	6.3
70	BE31	2	Prov. Brabant Wallon	Belgium	24	6.1
71	UKM5	2	North Eastern Scotland	United Kingdom	23.1	5
72	UKN0	2	Northern Ireland	United Kingdom	23	3.8
73	BE25	2	Prov. West-Vlaanderen	Belgium	21.9	3
74	BE23	2	Prov. Oost-Vlaanderen	Belgium	21.7	3.4
75	BE21	2	Prov. Antwerpen	Belgium	21.5	3.5
76	ES13	2	Cantabria	Spain	21.2	4.1
77	UKL1	2	West Wales and The Valleys	United Kingdom	21.1	3.4
78	NL32	2	Noord-Holland	Netherlands	21	2.6
79	ITH3	2	Veneto	Italy	21	1.7
80	NL22	2	Gelderland	Netherlands	20.9	3.1
81	SE21	2	Småland med öarna	Sweden	19.5	4.3
82	NL21	2	Overijssel	Netherlands	19.1	4
83	NL33	2	Zuid-Holland	Netherlands	18.4	2.4
84	ITF1	2	Abruzzo	Italy	18.2	3
85	UKM6	2	Highlands and Islands	United Kingdom	18.2	4.8
86	ES12	2	Principado de Asturias	Spain	18	2.8
87	NL31	2	Utrecht	Netherlands	17.9	3.4
88	SE31	2	Norra Mellansverige	Sweden	17.8	3.8
89	FRF2	2	Champagne-Ardenne	France	17.5	3.3
90	SE32	2	Mellersta Norrland	Sweden	17.2	5
91	ES52	2	Comunidad Valenciana	Spain	17	2.1
92	FRK2	2	Rhône-Alpes	France	16.7	1.8
93	PT11	2	Norte	Portugal	16.5	2.2

94	UKF3	2	Lincolnshire	United Kingdom	16.5	4
95	ES63	2	Ciudad Autónoma de Ceuta	Spain	16	13
96	ITF4	2	Puglia	Italy	15.1	2.2
97	ITH4	2	Friuli-Venezia Giulia	Italy	14.8	3
98	SE23	2	Västsverige	Sweden	14.6	2.7
99	UKK4	2	Devon	United Kingdom	13.4	3.8
100	ITI1	2	Toscana	Italy	13.4	2
101	FI1B	2	Helsinki-Uusimaa	Finland	13.2	3
102	NL23	2	Flevoland	Netherlands	12.5	6.4
103	ES61	2	Andalucía	Spain	12	1.7
104	FRC1	2	Bourgogne	France	11.9	2.5
105	NL34	2	Zeeland	Netherlands	11.7	5
106	ITF2	2	Molise	Italy	11.4	4.6
107	CY00	2	Kypros	Cyprus	11	4.2
108	PT18	2	Alentejo	Portugal	10.9	3.7
109	PT16	2	Centro (PT)	Portugal	10.3	2.5
110	AT22	2	Steiermark	Austria	10.2	3.2
111	FRE1	2	Nord-Pas de Calais	France	10.2	2.4
112	LT01	2	Sostinės regionas	Lithuania	10.1	3.4
113	PT20	2	Região Autónoma dos Açores	Portugal	9.9	6.4
114	ES53	2	Illes Balears	Spain	9.8	3.5
115	FRB0	2	Centre - Val de Loire	France	9.7	2.1
116	ITF6	2	Calabria	Italy	9.7	2.5
117	UKK3	2	Cornwall and Isles of Scilly	United Kingdom	9.7	4.6
118	EL53	2	Dytiki Makedonia	Greece	9.3	4.9
119	PT17	2	Área Metropolitana de Lisboa	Portugal	9.2	2.2
120	ITG2	2	Sardegna	Italy	8.8	3
121	RS22	2	Region Južne i Istočne Srbije	Serbia	8.7	2.7
122	SE22	2	Sydsverige	Sweden	8.7	3.3
123	AT13	2	Wien	Austria	8.5	2.9
124	ITF5	2	Basilicata	Italy	8.1	4
125	ES62	2	Región de Murcia	Spain	8	3.1
126	FRD2	2	Haute-Normandie	France	7.8	2.5
127	ES11	2	Galicia	Spain	7.8	1.9
128	ITI2	2	Umbria	Italy	7.6	3.5
129	CH03	2	Nordwestschweiz	Switzerland	7.5	3.3
130	EL61	2	Thessalia	Greece	7.4	3.4
131	AT33	2	Tirol	Austria	7.2	4
132	RS11	2	Beogradski region	Serbia	7.1	2.4
133	EL63	2	Dytiki Ellada	Greece	7	3.9
134	HU11	2	Budapest	Hungary	7	2.6

135	MT00	2	Malta	Malta	6.8	5.1
136	ITF3	2	Campania	Italy	6.6	1.8
137	FRL0	2	Provence-Alpes-Côte d'Azur	France	6.2	1.5
138	EL42	2	Notio Aigaio	Greece	6.1	5.4
139	AT34	2	Vorarlberg	Austria	6.1	6
140	CH02	2	Espace Mittelland	Switzerland	5.9	2.7
141	RO42	2	Vest	Romania	5.8	2.3
142	AT11	2	Burgenland	Austria	5.8	5
143	ITI4	2	Lazio	Italy	5.8	1.7
144	LT02	2	Vidurio ir vakarų Lietuvos regionas	Lithuania	5.7	2
145	ITG1	2	Sicilia	Italy	5.7	1.7
146	SK04	2	Východné Slovensko	Slovakia	5.7	3.1
147	FRM0	2	Corse	France	5.5	5.3
148	EL51	2	Anatoliki Makedonia, Thraki	Greece	5.4	3.4
149	NO01	2	Oslo og Akershus	Norway	5.3	3.3
150	AT21	2	Kärnten	Austria	5	4
151	AT12	2	Niederösterreich	Austria	5	2.5
152	NO03	2	Sør-Østlandet	Norway	4.9	3.1
153	FRJ1	2	Languedoc-Roussillon	France	4.6	2
154	EL41	2	Voreio Aigaio	Greece	4.6	6.2
155	PT30	2	Região Autónoma da Madeira	Portugal	4.6	5.4
156	LU00	2	Luxembourg	Luxembourg	4.5	4.6
157	SE33	2	Övre Norrland	Sweden	4.4	3.9
158	CH06	2	Zentralschweiz	Switzerland	4.4	4
159	PT15	2	Algarve	Portugal	4.4	4.2
160	FRG0	2	Pays de la Loire	France	4.3	1.9
161	EL62	2	Ionia Nisia	Greece	4.3	5.8
162	AT32	2	Salzburg	Austria	4	4
163	PL72	2	Świętokrzyskie	Poland	3.7	3.1
164	NL12	2	Friesland (NL)	Netherlands	3.7	3.8
165	DK01	2	Hovedstaden	Denmark	3.6	2.4
166	NL13	2	Drenthe	Netherlands	3.4	4.1
167	EL65	2	Peloponnisos	Greece	3.4	3.5
168	CZ01	2	Praha	Czechia	3.3	3
169	CZ08	2	Moravskoslezsko	Czechia	3.2	2.9
170	SK02	2	Západné Slovensko	Slovakia	3.2	2.7
171	EL43	2	Kriti	Greece	3.2	3.6
172	ES70	2	Canarias	Spain	3.1	2.6
173	CH05	2	Ostschweiz	Switzerland	3	3.1
174	IS00	2	Ísland	Iceland	3	5.4

175	EL52	2	Kentriki Makedonia	Greece	2.9	2.2
176	CZ04	2	Severozápad	Czechia	2.8	2.8
177	PL22	2	Śląskie	Poland	2.8	2
178	HU22	2	Nyugat-Dunántúl	Hungary	2.7	3.1
179	CH04	2	Zürich	Switzerland	2.6	3
180	RO32	2	București - Ilfov	Romania	2.5	1.9
181	CZ03	2	Jihozápad	Czechia	2.5	3.3
182	CZ07	2	Střední Morava	Czechia	2.3	2.9
183	FI19	2	Länsi-Suomi	Finland	2.2	2.7
184	EL30	2	Attiki	Greece	2.2	1.9
185	FI1D	2	Pohjois- ja Itä-Suomi	Finland	2.2	2.7
186	HU12	2	Pest	Hungary	2	2.5
187	EE00	2	Eesti	Estonia	2	2.6
188	AT31	2	Oberösterreich	Austria	2	3.1
189	PL81	2	Lubelskie	Poland	1.7	2.2
190	HU23	2	Dél-Dunántúl	Hungary	1.7	2.8
191	FRD1	2	Basse-Normandie	France	1.5	2.6
192	NL11	2	Groningen	Netherlands	1.4	4.2
193	PL21	2	Małopolskie	Poland	1.1	1.9
194	PL92	2	Mazowiecki regionalny	Poland	1	2.1
195	PL91	2	Warszawski stołeczny	Poland	1	1.9
196	RO11	2	Nord-Vest	Romania	0.9	2.2
197	NO06	2	Trøndelag	Norway	0.8	4.3
198	RO41	2	Sud-Vest Oltenia	Romania	0.8	2.6
199	NO02	2	Hedmark og Oppland	Norway	0.6	4.5
200	NO05	2	Vestlandet	Norway	0.6	3.6
201	HU33	2	Dél-Alföld	Hungary	0.5	2.3
202	PL84	2	Podlaskie	Poland	0.5	2.9
203	PL82	2	Podkarpackie	Poland	0.3	2.6
204	RS21	2	Region Šumadije i Zapadne Srbije	Serbia	0.2	2.2
205	EL64	2	Sτέρα Ellada	Greece	0	3.8
206	HU32	2	Észak-Alföld	Hungary	0	2.9
207	NO04	2	Agder og Rogaland	Norway	0	3.7
208	FI1C	2	Etelä-Suomi	Finland	-0.1	2.8
209	PL52	2	Opolskie	Poland	-0.1	3.1
210	LI00	2	Liechtenstein	Liechtenstein	0	17
211	RO12	2	Centru	Romania	-0.4	2.1
212	DK02	2	Sjælland	Denmark	-0.4	2.9
213	RO21	2	Nord-Est	Romania	-0.4	2.2
214	RO31	2	Sud - Muntenia	Romania	-0.5	2
215	HU21	2	Közép-Dunántúl	Hungary	-0.9	2.8

216	PL51	2	Dolnośląskie	Poland	-1	2.6
217	FRI2	2	Limousin	France	-1	3.1
218	PL71	2	Łódzkie	Poland	-1	2.5
219	SK03	2	Stredné Slovensko	Slovakia	-1.2	2.2
220	EL54	2	Ipeiros	Greece	-1.2	4.8
221	FRH0	2	Bretagne	France	-1.2	1.9
222	FRI3	2	Poitou-Charentes	France	-1.3	2.4
223	PL63	2	Pomorskie	Poland	-1.4	2.2
224	BG42	2	Yuzhen tsentralen	Bulgaria	-1.4	2.5
225	BG32	2	Severen tsentralen	Bulgaria	-1.4	2.7
226	PL61	2	Kujawsko-pomorskie	Poland	-1.4	2.2
227	FRJ2	2	Midi-Pyrénées	France	-1.4	1.7
228	DK04	2	Midtjylland	Denmark	-1.5	2.8
229	RS12	2	Region Vojvodine	Serbia	-1.5	2.3
230	PL41	2	Wielkopolskie	Poland	-1.5	2.3
231	CZ06	2	Jihovýchod	Czechia	-2	2.5
232	FRK1	2	Auvergne	France	-2	2.6
233	PL42	2	Zachodniopomorskie	Poland	-2.3	2.4
234	LV00	2	Latvija	Latvia	-2.7	2.1
235	FRI1	2	Aquitaine	France	-2.8	1.9
236	CZ05	2	Severovýchod	Czechia	-3	2.8
237	BG41	2	Yugozapaden	Bulgaria	-3.1	2
238	NO07	2	Nord-Norge	Norway	-3.1	4
239	BG34	2	Yugoiztochen	Bulgaria	-3.8	2.3
240	SK01	2	Bratislavský kraj	Slovakia	-3.9	3.4
241	ME00	2	Crna Gora	Montenegro	-4	3.4
242	DK03	2	Syddanmark	Denmark	-4.1	2.5
243	PL62	2	Warmińsko-mazurskie	Poland	-4.5	2.8
244	BG31	2	Severozapaden	Bulgaria	-4.5	2.4
245	RO22	2	Sud-Est	Romania	-4.5	1.9
246	DK05	2	Nordjylland	Denmark	-4.7	4
247	PL43	2	Lubuskie	Poland	-4.7	3.3
248	CZ02	2	Střední Čechy	Czechia	-4.8	2.8
249	BG33	2	Severoiztochen	Bulgaria	-5.2	2.8
250	HU31	2	Észak-Magyarország	Hungary	-5.5	2.6
251	FI20	2	Åland	Finland	-15	16

C.4 NUTS3 level

Rank	NUTS Code	NUTS Level	Region Name	Country	P-score (%)	(1 σ) Err (%)
1	ITC46	3	Bergamo	Italy	241	8.6
2	ITC4A	3	Cremona	Italy	210	11
3	ITC49	3	Lodi	Italy	170	14
4	ES416	3	Segovia	Spain	167	15
5	ITH51	3	Piacenza	Italy	146.9	9.9
6	ES300	3	Madrid	Spain	145.6	3.2
7	ITC47	3	Brescia	Italy	145.5	6
8	ES424	3	Guadalajara	Spain	136	12
9	ES422	3	Ciudad Real	Spain	135.1	8.3
10	UKI72	3	Brent	United Kingdom	120	12
11	ES417	3	Soria	Spain	119	17
12	UKI54	3	Enfield	United Kingdom	118	12
13	ITH52	3	Parma	Italy	113.3	7.2
14	ITC43	3	Lecco	Italy	111.6	8.8
15	UKI32	3	Westminster	United Kingdom	110	18
16	ES423	3	Cuenca	Spain	109.3	9.9
17	ES421	3	Albacete	Spain	105.9	8.6
18	ITC48	3	Pavia	Italy	104.3	6.4
19	UKI41	3	Hackney and Newham	United Kingdom	102	11
20	UKI53	3	Redbridge and Waltham Forest	United Kingdom	98.3	8.5
21	UKI71	3	Barnet	United Kingdom	98	11
22	UKI45	3	Lambeth	United Kingdom	93	14
23	ES415	3	Salamanca	Spain	89.5	7
24	ES511	3	Barcelona	Spain	87.9	2.9
25	UKI73	3	Ealing	United Kingdom	87	11
26	UKI62	3	Croydon	United Kingdom	84	9.4
27	UKI43	3	Haringey and Islington	United Kingdom	83	11

28	UKI74	3	Harrow and Hillingdon	United Kingdom	82.4	7.9
29	UKJ26	3	East Surrey	United Kingdom	81	9.9
30	ES425	3	Toledo	Spain	80.4	6.5
31	UKI44	3	Lewisham and Southwark	United Kingdom	80	9.6
32	ES411	3	Ávila	Spain	78.8	9.6
33	ITC4C	3	Milano	Italy	78.6	3.4
34	FR106	3	Seine-Saint-Denis	France	77.7	5.1
35	UKI33	3	Kensington & Chelsea and Hammersmith & Fulham	United Kingdom	77	10
36	UKI42	3	Tower Hamlets	United Kingdom	76	13
37	FRF12	3	Haut-Rhin	France	75.1	5.3
38	ITC4B	3	Mantova	Italy	75.1	6.8
39	UKG31	3	Birmingham	United Kingdom	73.7	6.7
40	UKI34	3	Wandsworth	United Kingdom	73	11
41	ITI31	3	Pesaro e Urbino	Italy	73.3	6.2
42	UKH32	3	Thurrock	United Kingdom	73	13
43	FR105	3	Hauts-de-Seine	France	72.4	5.1
44	ITC13	3	Biella	Italy	71.6	8.7
45	UKI63	3	Merton, Kingston upon Thames and Sutton	United Kingdom	67.9	7.7
46	UKG32	3	Solihull	United Kingdom	67.1	9.9
47	UKD33	3	Manchester	United Kingdom	66.9	8.9
48	ITC18	3	Alessandria	Italy	66.4	5.5
49	BE323	3	Arr. Mons	Belgium	66	7.9
50	ITC4D	3	Monza e della Brianza	Italy	65.8	4.5
51	FR108	3	Val-d'Oise	France	65.6	4.6
52	UKF21	3	Leicester	United Kingdom	64.8	8.4
53	UKI52	3	Barking & Dagenham and Havering	United Kingdom	63.5	7.4
54	UKH21	3	Luton	United Kingdom	63.2	9.8
55	ES432	3	Cáceres	Spain	63	6.2

56	FR107	3	Val-de-Marne	France	62.2	4.3
57	UKI51	3	Bexley and Greenwich	United Kingdom	62.1	7.1
58	UKG38	3	Walsall	United Kingdom	62	8.4
59	UKG39	3	Wolverhampton	United Kingdom	62	8.7
60	NL413	3	Noordoost-Noord-Brabant	Netherlands	61.9	6
61	ES418	3	Valladolid	Spain	61.9	5.9
62	BE100	3	Arr. de Bruxelles-Capitale/Arr. van Brussel-Hoofdstad	Belgium	60.9	5.2
63	UKI75	3	Hounslow and Richmond upon Thames	United Kingdom	60.3	7.7
64	UKJ25	3	West Surrey	United Kingdom	60.1	6.9
65	ES211	3	Araba/Álava	Spain	59.6	7.2
66	SE110	3	Stockholms län	Sweden	59.4	3.6
67	UKD34	3	Greater Manchester South West	United Kingdom	59.1	6.2
68	UKD72	3	Liverpool	United Kingdom	58.9	5.9
69	ITC12	3	Vercelli	Italy	57.7	8.6
70	ITC15	3	Novara	Italy	57.3	5.9
71	FR104	3	Essonne	France	56.3	5
72	UKJ12	3	Milton Keynes	United Kingdom	56.2	9.5
73	UKH23	3	Hertfordshire	United Kingdom	55.9	4.9
74	UKK14	3	Swindon	United Kingdom	55.7	9.8
75	UKG37	3	Sandwell	United Kingdom	55.4	7.9
76	UKH25	3	Central Bedfordshire	United Kingdom	54.9	8.6
77	UKI31	3	Camden and City of London	United Kingdom	55	11
78	ITC44	3	Sondrio	Italy	54.2	8.6
79	UKC14	3	Durham CC	United Kingdom	53.5	6
80	ITH20	3	Trento	Italy	53.5	5.6
81	UKD74	3	Wirral	United Kingdom	53.4	7.9

82	UKJ28	3	West Sussex (North East)	United Kingdom	53.3	7.8
83	UKH35	3	West Essex	United Kingdom	53.2	8.9
84	ES413	3	León	Spain	53.2	5.1
85	UKD12	3	East Cumbria	United Kingdom	52.7	7.2
86	ITC42	3	Como	Italy	52.2	5.5
87	UKD35	3	Greater Manchester South East	United Kingdom	51.7	6
88	UKJ11	3	Berkshire	United Kingdom	51.1	5.6
89	ITC33	3	Genova	Italy	51	4
90	UKD37	3	Greater Manchester North East	United Kingdom	50.9	5.6
91	UKM83	3	Inverclyde, East Renfrewshire and Renfrewshire	United Kingdom	50.5	6.5
92	UKD73	3	Sefton	United Kingdom	50.3	7.6
93	UKM75	3	Edinburgh, City of	United Kingdom	50.2	5.6
94	UKE21	3	York	United Kingdom	50.2	9.7
95	UKI61	3	Bromley	United Kingdom	50.2	8.2
96	ITH53	3	Reggio nell'Emilia	Italy	50.1	4.9
97	BE221	3	Arr. Hasselt	Belgium	50.1	6.6
98	FR102	3	Seine-et-Marne	France	50	4.6
99	UKJ43	3	Kent Thames Gateway	United Kingdom	49.9	6.9
100	UKE41	3	Bradford	United Kingdom	49.9	5.4
101	UKD62	3	Cheshire East	United Kingdom	49.9	6.8
102	ES220	3	Navarra	Spain	49.5	5
103	UKM81	3	East Dunbartonshire, West Dunbartonshire and Helensburgh & Lomond	United Kingdom	49	7.7
104	UKE32	3	Sheffield	United Kingdom	48.7	6.5
105	ITC20	3	Valle d'Aosta/Vallée d'Aoste	Italy	48.1	9.4
106	NL421	3	Noord-Limburg	Netherlands	48	7.1
107	ES230	3	La Rioja	Spain	47.8	7.2

108	CH070	3	Ticino	Switzerland	47.8	6.7
109	UKC23	3	Sunderland	United Kingdom	47.3	6.7
110	UKC12	3	South Teesside	United Kingdom	47.1	6.4
111	UKM82	3	Glasgow City	United Kingdom	46.7	5.6
112	FR103	3	Yvelines	France	46.7	3.9
113	UKG13	3	Warwickshire	United Kingdom	46.6	5.5
114	UKH24	3	Bedford	United Kingdom	46	10
115	UKF14	3	Nottingham	United Kingdom	45.9	9
116	FR101	3	Paris	France	45.6	3.1
117	UKG24	3	Staffordshire CC	United Kingdom	45.6	5.1
118	UKF13	3	South and West Derbyshire	United Kingdom	45.4	6.7
119	ITC11	3	Torino	Italy	45.1	2.5
120	ITC17	3	Asti	Italy	45.1	6.6
121	NL422	3	Midden-Limburg	Netherlands	45	7.4
122	BE335	3	Arr. Verviers - communes francophones	Belgium	44.8	8.1
123	UKG36	3	Dudley	United Kingdom	44.8	6.4
124	ITH10	3	Bolzano-Bozen	Italy	44.7	6.2
125	UKD36	3	Greater Manchester North West	United Kingdom	44.5	4.7
126	UKK15	3	Wiltshire CC	United Kingdom	44.4	6.6
127	ES412	3	Burgos	Spain	44.3	5.6
128	UKG33	3	Coventry	United Kingdom	44.3	8
129	FRE22	3	Oise	France	43.9	4.8
130	UKJ13	3	Buckinghamshire CC	United Kingdom	43.6	6
131	BE332	3	Arr. Liège	Belgium	43.5	4.8
132	ITC14	3	Verbano-Cusio-Ossola	Italy	43.3	9
133	NL423	3	Zuid-Limburg	Netherlands	43.2	4.9
134	UKJ14	3	Oxfordshire	United Kingdom	43	5.6
135	BE222	3	Arr. Maaseik	Belgium	42.9	9.2

136	UKD61	3	Warrington	United Kingdom	42.9	7.5
137	UKJ37	3	North Hampshire	United Kingdom	42.9	8.7
138	UKD71	3	East Merseyside	United Kingdom	42.8	5.3
139	UKC22	3	Tyneside	United Kingdom	42.7	4.7
140	UKF11	3	Derby	United Kingdom	42.7	7.9
141	ITC31	3	Imperia	Italy	42.5	6.8
142	FRF34	3	Vosges	France	42.3	7.5
143	UKL22	3	Cardiff and Vale of Glamorgan	United Kingdom	42.2	6.8
144	UKH36	3	Heart of Essex	United Kingdom	42.2	7.6
145	UKM95	3	South Lanarkshire	United Kingdom	41.6	6.3
146	UKE31	3	Barnsley, Doncaster and Rotherham	United Kingdom	41.5	4.5
147	UKC13	3	Darlington	United Kingdom	41	10
148	BE223	3	Arr. Tongeren	Belgium	40.7	8.8
149	ITH59	3	Rimini	Italy	40.4	5.4
150	UKM66	3	Shetland Islands	United Kingdom	40	28
151	UKH37	3	Essex Thames Gateway	United Kingdom	40.3	7
152	ES243	3	Zaragoza	Spain	40.2	3.9
153	FRF11	3	Bas-Rhin	France	40	4
154	UKE44	3	Calderdale and Kirklees	United Kingdom	40	5.3
155	UKE42	3	Leeds	United Kingdom	40	5.2
156	ITC41	3	Varese	Italy	40	3.6
157	UKF22	3	Leicestershire CC and Rutland	United Kingdom	39.6	5
158	UKG12	3	Worcestershire	United Kingdom	38.9	5.3
159	NL212	3	Zuidwest-Overijssel	Netherlands	38.9	9.9
160	UKF25	3	North Northamptonshire	United Kingdom	38.7	5.6
161	NL412	3	Midden-Noord-Brabant	Netherlands	38.7	5.5

162	UKL15	3	Central Valleys	United Kingdom	38.6	6.8
163	UKN06	3	Belfast	United Kingdom	38.5	6.7
164	UKF24	3	West Northamptonshire	United Kingdom	38.4	6.5
165	UKJ35	3	South Hampshire	United Kingdom	38.4	5.9
166	UKE45	3	Wakefield	United Kingdom	38.4	5.4
167	FRC21	3	Doubs	France	38.4	6.3
168	UKK13	3	Gloucestershire	United Kingdom	38.3	6.3
169	UKD47	3	Chorley and West Lancashire	United Kingdom	38.2	7.3
170	BE342	3	Arr. Bastogne	Belgium	38	15
171	BE336	3	Bezirk Verviers - Deutschsprachige Gemeinschaft	Belgium	38	13
172	UKD63	3	Cheshire West and Chester	United Kingdom	37.7	6
173	UKM71	3	Angus and Dundee City	United Kingdom	37.5	6.6
174	UKK12	3	Bath and North East Somerset, North Somerset and South Gloucestershire	United Kingdom	37.5	5.5
175	UKD11	3	West Cumbria	United Kingdom	37.5	7.5
176	UKH14	3	Suffolk	United Kingdom	37.4	4.7
177	UKM73	3	East Lothian and Midlothian	United Kingdom	37.2	7.3
178	UKJ32	3	Southampton	United Kingdom	37.1	7.8
179	UKD46	3	East Lancashire	United Kingdom	37	6.1
180	NL414	3	Zuidoost-Noord-Brabant	Netherlands	36.9	5
181	UKD41	3	Blackburn with Darwen	United Kingdom	36.6	9.8
182	ES242	3	Teruel	Spain	36.6	8.9
183	UKE22	3	North Yorkshire CC	United Kingdom	36.5	5.3
184	BE334	3	Arr. Wareme	Belgium	36	13
185	UKJ36	3	Central Hampshire	United Kingdom	36.3	5.3

186	UKH31	3	Southend-on-Sea	United Kingdom	36.2	9.1
187	UKE12	3	East Riding of Yorkshire	United Kingdom	36.1	6
188	BE343	3	Arr. Marche-en-Famenne	Belgium	36	14
189	UKD42	3	Blackpool	United Kingdom	35.8	8.4
190	EL532	3	Kastoria	Greece	36	14
191	ES414	3	Palencia	Spain	35.6	7.9
192	ITC32	3	Savona	Italy	35.4	5.8
193	UKJ44	3	East Kent	United Kingdom	35.1	5.5
194	BE352	3	Arr. Namur	Belgium	35	6.2
195	UKM84	3	North Lanarkshire	United Kingdom	34.9	5.7
196	NL224	3	Zuidwest-Gelderland	Netherlands	34.8	8.5
197	UKJ27	3	West Sussex (South West)	United Kingdom	34.7	6.2
198	FRE21	3	Aisne	France	34.6	5.5
199	ITI11	3	Massa-Carrara	Italy	34.6	6.7
200	BE321	3	Arr. Ath	Belgium	35	11
201	ES512	3	Girona	Spain	34.1	4.9
202	FRF33	3	Moselle	France	34	3.6
203	CH013	3	Genève	Switzerland	34	5.6
204	ITC34	3	La Spezia	Italy	33.9	6.5
205	UKG11	3	Herefordshire, County of	United Kingdom	33.8	7.9
206	UKM76	3	Falkirk	United Kingdom	33.7	8.9
207	UKG21	3	Telford and Wrekin	United Kingdom	33.4	9.2
208	UKG23	3	Stoke-on-Trent	United Kingdom	33.2	7.9
209	ES419	3	Zamora	Spain	32.9	6.6
210	UKJ41	3	Medway	United Kingdom	32.9	8
211	UKC11	3	Hartlepool and Stockton-on-Tees	United Kingdom	32.9	7.4
212	BE242	3	Arr. Leuven	Belgium	32.8	6.1
213	UKH12	3	Cambridgeshire CC	United Kingdom	32.8	5.8

214	UKN13	3	Antrim and Newtownabbey	United Kingdom	32.7	9.3
215	UKL21	3	Monmouthshire and Newport	United Kingdom	32.6	8.1
216	SE214	3	Gotlands län	Sweden	33	15
217	ITH31	3	Verona	Italy	32.5	3.8
218	UKD45	3	Mid Lancashire	United Kingdom	32.4	6
219	UKM78	3	West Lothian	United Kingdom	32.3	9
220	SE122	3	Södermanlands län	Sweden	31.9	6.1
221	UKH34	3	Essex Haven Gateway	United Kingdom	31.8	6.1
222	BE353	3	Arr. Philippeville	Belgium	32	13
223	UKK11	3	Bristol, City of	United Kingdom	31.6	6.7
224	SE312	3	Dalarnas län	Sweden	31.5	6.7
225	UKJ45	3	Mid Kent	United Kingdom	31.5	6.4
226	ES213	3	Bizkaia	Spain	31.5	3.5
227	UKF12	3	East Derbyshire	United Kingdom	31.5	6.5
228	BE324	3	Arr. Mouscron	Belgium	31	12
229	UKM93	3	East Ayrshire and North Ayrshire mainland	United Kingdom	31.4	6.1
230	NL211	3	Noord-Overijssel	Netherlands	31.3	6.5
231	UKK21	3	Bournemouth and Poole	United Kingdom	31.3	7.1
232	ITH55	3	Bologna	Italy	31.3	3.3
233	ITF13	3	Pescara	Italy	31.2	6.3
234	UKL16	3	Gwent Valleys	United Kingdom	31.2	6.3
235	BE322	3	Arr. Charleroi	Belgium	30.9	6.4
236	BE231	3	Arr. Aalst	Belgium	30.8	6.8
237	UKF16	3	South Nottinghamshire	United Kingdom	30.8	6.3
238	BE254	3	Arr. Kortrijk	Belgium	30.7	6
239	ITH54	3	Modena	Italy	30.6	4.1
240	UKC21	3	Northumberland	United Kingdom	30.3	6.6
241	UKK22	3	Dorset CC	United Kingdom	30.3	6.2

242	RS225	3	Nišavska oblast	Serbia	30.3	5.5
243	UKH16	3	North and West Norfolk	United Kingdom	30.2	6.8
244	UKJ21	3	Brighton and Hove	United Kingdom	29.9	8.1
245	PT16D	3	Região de Aveiro	Portugal	29.8	5.6
246	SE125	3	Västmanlands län	Sweden	29.6	6.2
247	UKL18	3	Swansea	United Kingdom	29.5	7.4
248	ES514	3	Tarragona	Spain	29.5	4.3
249	UKE11	3	Kingston upon Hull, City of	United Kingdom	29.5	8
250	BE344	3	Arr. Neufchâteau	Belgium	29	13
251	BE257	3	Arr. Tielt	Belgium	29	11
252	UKM65	3	Orkney Islands	United Kingdom	29	19
253	NL221	3	Veluwe	Netherlands	28.9	4.8
254	UKG22	3	Shropshire CC	United Kingdom	28.8	5.9
255	UKF15	3	North Nottinghamshire	United Kingdom	28.7	5.8
256	ES513	3	Lleida	Spain	28.6	5.5
257	UKJ46	3	West Kent	United Kingdom	28.6	5.9
258	BE232	3	Arr. Dendermonde	Belgium	28.5	7.9
259	ITI33	3	Macerata	Italy	28.5	5.7
260	UKM94	3	South Ayrshire	United Kingdom	28.4	8
261	FRF32	3	Meuse	France	28.4	8
262	UKM61	3	Caithness & Sutherland and Ross & Cromarty	United Kingdom	28	11
263	UKH11	3	Peterborough	United Kingdom	28.1	8.6
264	ITC16	3	Cuneo	Italy	27.6	4.7
265	ITH44	3	Trieste	Italy	27.6	5.6
266	BE325	3	Arr. Soignies	Belgium	27.4	8.6
267	FRK26	3	Rhône	France	27.4	3.2
268	FRC23	3	Haute-Saône	France	27.1	7.1
269	NL329	3	Groot-Amsterdam	Netherlands	27	3.7
270	ES241	3	Huesca	Spain	26.5	6.6
271	UKM77	3	Perth & Kinross and Stirling	United Kingdom	26.3	5.9

272	BE258	3	Arr. Veurne	Belgium	26	11
273	NL328	3	Alkmaar en omgeving	Netherlands	26	6.9
274	FRB03	3	Indre	France	25.5	5.4
275	AT334	3	Tiroler Oberland	Austria	25	12
276	BE213	3	Arr. Turnhout	Belgium	25.1	5.3
277	FRF24	3	Haute-Marne	France	25.1	8.1
278	CH011	3	Vaud	Switzerland	25	4.8
279	SE123	3	Östergötlands län	Sweden	24.7	5.1
280	PT112	3	Cávado	Portugal	24.7	5.9
281	ITH58	3	Forli-Cesena	Italy	24.7	5.1
282	PT11D	3	Douro	Portugal	24.7	7.5
283	NL323	3	IJmond	Netherlands	24.4	7.5
284	SE121	3	Uppsala län	Sweden	24	6.7
285	FRK28	3	Haute-Savoie	France	24	4.4
286	BE310	3	Arr. Nivelles	Belgium	24	6.1
287	ITG16	3	Enna	Italy	23.9	7.5
288	BE253	3	Arr. Ieper	Belgium	23.8	9.6
289	SE211	3	Jönköpings län	Sweden	23.8	6.4
290	UKL23	3	Flintshire and Wrexham	United Kingdom	23.8	5.7
291	UKD44	3	Lancaster and Wyre	United Kingdom	23.7	6.1
292	BE251	3	Arr. Brugge	Belgium	23.7	6.2
293	UKN12	3	Causeway Coast and Glens	United Kingdom	23.7	8.8
294	FRB02	3	Eure-et-Loir	France	23.7	4.9
295	FRF23	3	Marne	France	23.5	4.9
296	ES614	3	Granada	Spain	23.4	4.3
297	UKH17	3	Breckland and South Norfolk	United Kingdom	23.1	7
298	ES522	3	Castellón / Castelló	Spain	23.1	4.9
299	UKM50	3	Aberdeen City and Aberdeenshire	United Kingdom	23.1	5
300	UKN09	3	Ards and North Down	United Kingdom	23	7.6
301	UKL24	3	Powys	United Kingdom	22.9	8.2
302	ITI32	3	Ancona	Italy	22.6	4.1
303	NL324	3	Agglomeratie Haarlem	Netherlands	22.5	6.4
304	FRC22	3	Jura	France	22.4	7.1
305	UKN16	3	Fermanagh and Omagh	United Kingdom	22	11

306	NL325	3	Zaanstreek	Netherlands	22.1	8.3
307	BE241	3	Arr. Halle-Vilvoorde	Belgium	22.1	4.7
308	BE256	3	Arr. Roeselare	Belgium	21.9	8
309	ITF46	3	Foggia	Italy	21.7	3.9
310	CH063	3	Schwyz	Switzerland	22	10
311	CH064	3	Obwalden	Switzerland	22	19
312	UKM63	3	Lochaber, Skye & Lochalsh, Arran & Cumbrae and Argyll & Bute	United Kingdom	21.5	9.7
313	ITH34	3	Treviso	Italy	21.5	3.8
314	ES212	3	Gipuzkoa	Spain	21.5	4
315	AL014	3	Lezhë	Albania	21.5	9.5
316	ES130	3	Cantabria	Spain	21.2	4.1
317	ITH32	3	Vicenza	Italy	21.2	3.5
318	BE211	3	Arr. Antwerpen	Belgium	21.1	4.1
319	FRF31	3	Meurthe-et-Moselle	France	21	4.2
320	ITF12	3	Teramo	Italy	21	5.9
321	UKL17	3	Bridgend and Neath Port Talbot	United Kingdom	21	6.6
322	UKK23	3	Somerset	United Kingdom	20.7	4.9
323	UKN14	3	Lisburn and Castlereagh	United Kingdom	20.7	9.6
324	BE236	3	Arr. Sint-Niklaas	Belgium	20.6	6.6
325	NL33C	3	Groot-Rijnmond	Netherlands	20.3	3.2
326	BE233	3	Arr. Eeklo	Belgium	20	11
327	NL332	3	Agglomeratie's-Gravenhage	Netherlands	20.2	3.8
328	RS229	3	Toplička oblast	Serbia	20.1	8.3
329	UKJ31	3	Portsmouth	United Kingdom	19.2	8.6
330	ITH35	3	Venezia	Italy	19.2	3.3
331	ITI14	3	Firenze	Italy	19.1	3.4
332	UKM91	3	Scottish Borders	United Kingdom	18.9	8.1
333	UKN07	3	Armagh City, Banbridge and Craigavon	United Kingdom	18.8	8.6
334	PT11A	3	Área Metropolitana do Porto	Portugal	18.7	2.9
335	ITH41	3	Pordenone	Italy	18.5	6.4
336	ITF44	3	Brindisi	Italy	18.5	5.6
337	UKH15	3	Norwich and East Norfolk	United Kingdom	18.4	6.3
338	ITF62	3	Crotone	Italy	18.4	9.4
339	BE212	3	Arr. Mechelen	Belgium	18.3	5.5

340	ITF34	3	Avellino	Italy	18.2	5.1
341	FRC24	3	Territoire de Belfort	France	18.1	6.2
342	FRE23	3	Somme	France	18	4.1
343	FI1D5	3	Keski-Pohjanmaa	Finland	18	12
344	ES120	3	Asturias	Spain	18	2.8
345	CH012	3	Valais	Switzerland	17.9	7.2
346	NL310	3	Utrecht	Netherlands	17.9	3.4
347	UKN08	3	Newry, Mourne and Down	United Kingdom	17.8	8.5
348	SE124	3	Örebro län	Sweden	17.8	6
349	ITG25	3	Sassari	Italy	17.7	5.4
350	PT11E	3	Terras de Trás-os-Montes	Portugal	17.7	7.8
351	ITI35	3	Fermo	Italy	17.7	6.6
352	NL33B	3	Oost-Zuid-Holland	Netherlands	17.5	6.2
353	SE321	3	Västernorrlands län	Sweden	17.3	6.2
354	FRK25	3	Loire	France	17.3	3.6
355	FRC11	3	Côte-d'Or	France	17.3	4
356	UKJ22	3	East Sussex CC	United Kingdom	17.2	5
357	NL411	3	West-Noord-Brabant	Netherlands	17.2	4.2
358	SE322	3	Jämtlands län	Sweden	17	8.3
359	BE326	3	Arr. Thuin	Belgium	16.8	7.9
360	NL226	3	Arnhem/Nijmegen	Netherlands	16.8	4.2
361	UKN11	3	Mid Ulster	United Kingdom	16.8	9.9
362	CH054	3	Appenzell Innerrhoden	Switzerland	17	25
363	ITH33	3	Belluno	Italy	16.6	6.5
364	BE235	3	Arr. Oudenaarde	Belgium	16.5	9.5
365	UKF30	3	Lincolnshire	United Kingdom	16.5	4
366	ITF14	3	Chieti	Italy	16.5	4.7
367	SE232	3	Västra Götalands län	Sweden	16.4	3
368	RO215	3	Suceava	Romania	16.4	3.8
369	ES521	3	Alicante / Alacant	Spain	16.3	2.9
370	CH025	3	Jura	Switzerland	16	12
371	FRK22	3	Ardèche	France	16.2	5
372	ES617	3	Málaga	Spain	16.2	2.8
373	ES523	3	Valencia / València	Spain	16.1	2.3
374	NL33A	3	Zuidoost-Zuid-Holland	Netherlands	16.1	5.4
375	UKM72	3	Clackmannanshire and Fife	United Kingdom	16	4.8
376	FRD21	3	Eure	France	16	4.4

377	UKN15	3	Mid and East Antrim	United Kingdom	16	8.5
378	PT16E	3	Região de Coimbra	Portugal	16	4.5
379	ITI42	3	Rieti	Italy	15.9	7.5
380	AT221	3	Graz	Austria	15.9	4.9
381	BE234	3	Arr. Gent	Belgium	15.7	4.4
382	UKK42	3	Torbay	United Kingdom	15.7	7.6
383	ITH37	3	Rovigo	Italy	15.7	5.2
384	ES630	3	Ceuta	Spain	16	13
385	BE345	3	Arr. Virton	Belgium	16	14
386	SE213	3	Kalmar län	Sweden	15.6	6.9
387	FRF22	3	Aube	France	15.4	5.9
388	ITF45	3	Lecce	Italy	15.1	3.5
389	EL624	3	Lefkada	Greece	15	17
390	FRC13	3	Saône-et-Loire	France	14.9	3.9
391	UKK41	3	Plymouth	United Kingdom	14.9	6.4
392	ITI16	3	Livorno	Italy	14.7	5.2
393	NL333	3	Delft en Westland	Netherlands	14.7	7.6
394	ITF47	3	Bari	Italy	14.6	3.2
395	EL621	3	Zakynthos	Greece	15	15
396	NL341	3	Zeeuwsch-Vlaanderen	Netherlands	14.6	8.6
397	AT113	3	Südburgenland	Austria	14.6	8.6
398	CH022	3	Freiburg	Switzerland	14.5	7.2
399	PT185	3	Lezíria do Tejo	Portugal	14.5	5.6
400	ITH56	3	Ferrara	Italy	14.4	4.6
401	PT184	3	Baixo Alentejo	Portugal	14.2	7.4
402	FRM01	3	Corse-du-Sud	France	14	8.6
403	ES431	3	Badajoz	Spain	13.9	3.6
404	AL032	3	Fier	Albania	13.9	6.6
405	ITH36	3	Padova	Italy	13.9	3.2
406	UKL11	3	Isle of Anglesey	United Kingdom	14	11
407	ITG2B	3	Medio Campidano	Italy	13.8	9.3
408	FI1D8	3	Kainuu	Finland	13.7	9.5
409	FRB05	3	Loir-et-Cher	France	13.7	5
410	ES616	3	Jaén	Spain	13.7	3.9
411	BE331	3	Arr. Huy	Belgium	13.7	8.8
412	AT224	3	Oststeiermark	Austria	13.6	6.5
413	SE313	3	Gävleborgs län	Sweden	13.4	5.8
414	SE212	3	Kronobergs län	Sweden	13.3	7.5

415	EL512	3	Xanthi	Greece	13.3	8.5
416	ITI13	3	Pistoia	Italy	13.3	4.9
417	FRL04	3	Bouches-du-Rhône	France	13.3	2.4
418	FI1B1	3	Helsinki-Uusimaa	Finland	13.2	3
419	FRE11	3	Nord	France	13.2	2.8
420	CH024	3	Neuchâtel	Switzerland	13.1	7.6
421	FRK23	3	Drôme	France	13.1	4.1
422	CH023	3	Solothurn	Switzerland	13	6.4
423	NL337	3	Agglomeratie Leiden en Bollenstreek	Netherlands	13	4.8
424	ITF22	3	Campobasso	Italy	12.9	6.2
425	AL015	3	Shkodër	Albania	12.8	7.3
426	UKM64	3	Na h-Eileanan Siar (Western Isles)	United Kingdom	13	19
427	ITI17	3	Pisa	Italy	12.7	4.4
428	CH032	3	Basel-Landschaft	Switzerland	12.6	6.4
429	UKK43	3	Devon CC	United Kingdom	12.6	4.2
430	SE332	3	Norrbottnens län	Sweden	12.6	5.6
431	NL230	3	Flevoland	Netherlands	12.5	6.4
432	ES113	3	Ourense	Spain	12.5	4.5
433	EL526	3	Serres	Greece	12.4	6.4
434	FRK27	3	Savoie	France	12.4	5
435	UKE13	3	North and North East Lincolnshire	United Kingdom	12.4	5.3
436	ITF65	3	Reggio di Calabria	Italy	12.3	4.5
437	PT181	3	Alentejo Litoral	Portugal	12.2	8.8
438	ITF48	3	Barletta-Andria-Trani	Italy	12.2	5.3
439	PT11C	3	Tâmega e Sousa	Portugal	12	5.5
440	EE004	3	Lääne-Eesti	Estonia	11.9	7.4
441	ES532	3	Mallorca	Spain	11.8	3.7
442	UKM92	3	Dumfries & Galloway	United Kingdom	11.6	6.7
443	EL434	3	Chania	Greece	11.5	7.4
444	NO032	3	Buskerud	Norway	11.4	6.4
445	EL633	3	Ileia	Greece	11.2	7.2
446	UKL14	3	South West Wales	United Kingdom	11.2	4.5
447	ITI12	3	Lucca	Italy	11.2	4.2
448	RO421	3	Arad	Romania	11.1	3.9
449	AT126	3	Wiener Umland/Nordteil	Austria	11	5.3
450	CY000	3	Kypros	Cyprus	11	4.2
451	NO011	3	Oslo	Norway	11	4.6

452	ITG2C	3	Carbonia-Iglesias	Italy	10.8	7.9
453	FRK24	3	Isère	France	10.7	2.9
454	UKJ34	3	Isle of Wight	United Kingdom	10.5	7.3
455	NL342	3	Overig Zeeland	Netherlands	10.5	5.9
456	ITG19	3	Siracusa	Italy	10.5	4.5
457	PT16H	3	Beira Baixa	Portugal	10.4	8.1
458	BE327	3	Arr. Tournai	Belgium	10.3	7
459	FRK21	3	Ain	France	10.2	4.4
460	AT213	3	Unterkärnten	Austria	10.2	6.6
461	LT011	3	Vilniaus apskritis	Lithuania	10.1	3.4
462	LT022	3	Kauno apskritis	Lithuania	10	3.7
463	RS215	3	Pomoravska oblast	Serbia	9.9	5.5
464	AT335	3	Tiroler Unterland	Austria	9.9	6.6
465	PT200	3	Região Autónoma dos Açores	Portugal	9.9	6.4
466	PT187	3	Alentejo Central	Portugal	9.9	6.5
467	UKL12	3	Gwynedd	United Kingdom	9.9	7.6
468	EL632	3	Achaia	Greece	9.8	5.8
469	CH031	3	Basel-Stadt	Switzerland	9.7	6.2
470	EL613	3	Magnisia, Sporades	Greece	9.7	6.1
471	UKK30	3	Cornwall and Isles of Scilly	United Kingdom	9.7	4.6
472	PT16G	3	Viseu Dão Lafões	Portugal	9.7	5.8
473	NL225	3	Achterhoek	Netherlands	9.6	4.7
474	FRJ12	3	Gard	France	9.6	3.9
475	FRC14	3	Yonne	France	9.5	4.6
476	BG311	3	Vidin	Bulgaria	9.5	7.3
477	PT16I	3	Médio Tejo	Portugal	9.5	5.6
478	EL305	3	Anatoliki Attiki	Greece	9.5	4.5
479	PT119	3	Ave	Portugal	9.4	5
480	ITG28	3	Oristano	Italy	9.3	5.8
481	FRF21	3	Ardennes	France	9.3	6
482	AL022	3	Tiranë	Albania	9.3	4.6
483	PT170	3	Área Metropolitana de Lisboa	Portugal	9.2	2.2
484	SE224	3	Skåne län	Sweden	9.1	3.4
485	ES111	3	A Coruña	Spain	9	2.8
486	ITI1A	3	Grosseto	Italy	9	5.8
487	ITH57	3	Ravenna	Italy	9	4.6
488	FRD12	3	Manche	France	9	4
489	ITG13	3	Messina	Italy	9	4.1
490	ITF52	3	Matera	Italy	8.9	6.8

491	NL321	3	Kop van Noord-Holland	Netherlands	8.9	5.3
492	ITF61	3	Cosenza	Italy	8.9	3.7
493	HU233	3	Tolna	Hungary	8.8	5.2
494	ES618	3	Sevilla	Spain	8.8	2.6
495	EL515	3	Thasos, Kavala	Greece	8.8	6.8
496	ES612	3	Cádiz	Spain	8.8	3.4
497	ITI22	3	Terni	Italy	8.7	5.4
498	RO423	3	Hunedoara	Romania	8.7	3.8
499	FI1C5	3	Etelä-Karjala	Finland	8.7	6.9
500	ITI34	3	Ascoli Piceno	Italy	8.7	6.4
501	FRG04	3	Sarthe	France	8.7	4.1
502	UKM62	3	Inverness & Nairn and Moray, Badenoch & Strathspey	United Kingdom	8.7	6.5
503	EL514	3	Drama	Greece	8.6	8
504	ITH42	3	Udine	Italy	8.6	3.8
505	AT130	3	Wien	Austria	8.5	2.9
506	RO415	3	Vâlcea	Romania	8.4	6
507	SE311	3	Värmlands län	Sweden	8.4	5.7
508	EL612	3	Larisa	Greece	8.4	5.8
509	NL213	3	Twente	Netherlands	8.3	4.3
510	ES613	3	Córdoba	Spain	8.3	3.7
511	RS224	3	Jablanička oblast	Serbia	8.2	5.6
512	EL411	3	Lesvos, Limnos	Greece	8.2	8.5
513	AL021	3	Elbasan	Albania	8.1	6.3
514	AT222	3	Liezen	Austria	8.1	9.1
515	LT023	3	Klaipėdos apskritis	Lithuania	8.1	4.4
516	AT124	3	Waldviertel	Austria	8.1	5.8
517	ES620	3	Murcia	Spain	8	3.1
518	FRE12	3	Pas-de-Calais	France	8	3
519	ITF43	3	Taranto	Italy	8	4
520	NL327	3	Het Gooi en Vechtstreek	Netherlands	8	5.5
521	ITF21	3	Isernia	Italy	7.9	8.4
522	DK012	3	Københavns omegn	Denmark	7.9	4.1
523	ES615	3	Huelva	Spain	7.8	4.8
524	BE255	3	Arr. Oostende	Belgium	7.8	6
525	EL521	3	Imathia	Greece	7.8	7.1
526	BG343	3	Yambol	Bulgaria	7.8	6.1
527	AT121	3	Mostviertel-Eisenwurzen	Austria	7.7	5.4
528	ITF51	3	Potenza	Italy	7.7	4.9
529	FRB01	3	Cher	France	7.7	4.7
530	PT111	3	Alto Minho	Portugal	7.7	5.6

531	NL126	3	Zuidoost-Friesland	Netherlands	7.7	7.2
532	ITF33	3	Napoli	Italy	7.6	2.3
533	AT122	3	Niederösterreich-Süd	Austria	7.6	5.6
534	EL531	3	Grevena, Kozani	Greece	7.5	5.9
535	SK021	3	Trnavský kraj	Slovakia	7.5	4.3
536	ITI44	3	Latina	Italy	7.4	4.1
537	CH055	3	St. Gallen	Switzerland	7.4	4.7
538	ITH43	3	Gorizia	Italy	7.3	7.3
539	FRL03	3	Alpes-Maritimes	France	7.3	2.6
540	FRG02	3	Maine-et-Loire	France	7.3	3.5
541	ITI45	3	Frosinone	Italy	7.2	3.8
542	SK042	3	Košický kraj	Slovakia	7.2	3.8
543	FRD22	3	Seine-Maritime	France	7.2	2.8
544	ITI21	3	Perugia	Italy	7.1	4
545	RS110	3	Beogradska oblast	Serbia	7.1	2.4
546	HU110	3	Budapest	Hungary	7	2.6
547	EL421	3	Kalymnos, Karpathos, Kos, Rodos	Greece	7	7.1
548	EL527	3	Chalkidiki	Greece	6.9	8.4
549	AT342	3	Rheintal-Bodenseegebiet	Austria	6.9	6.4
550	RS216	3	Rasinska oblast	Serbia	6.8	4.8
551	FRJ25	3	Lot	France	6.8	6
552	BE341	3	Arr. Arlon	Belgium	7	11
553	FRI22	3	Creuse	France	6.7	7.6
554	ES611	3	Almería	Spain	6.7	4
555	LT025	3	Panevėžio apskritis	Lithuania	6.6	5.1
556	BE351	3	Arr. Dinant	Belgium	6.5	8.2
557	FRC12	3	Nièvre	France	6.5	5.2
558	ITG27	3	Cagliari	Italy	6.5	4.4
559	PT11B	3	Alto Tâmega	Portugal	6.4	8.1
560	RS228	3	Pčinjaška oblast	Serbia	6.4	6
561	SE221	3	Blekinge län	Sweden	6.4	6.8
562	FRJ24	3	Gers	France	6.4	6.2
563	RO412	3	Gorj	Romania	6.3	4.7
564	AT314	3	Steyr-Kirchdorf	Austria	6.2	7.5
565	RO125	3	Mureș	Romania	6.2	3.8
566	FRI14	3	Lot-et-Garonne	France	6.2	4.6
567	AT225	3	West- und Südsteiermark	Austria	6.2	6.5
568	PL815	3	Puławski	Poland	6.1	4
569	EL644	3	Fthiotida	Greece	6.1	7.2
570	PL22A	3	Katowicki	Poland	6.1	3.4
571	AT322	3	Pinzgau-Pongau	Austria	6.1	7.3

572	FRG03	3	Mayenne	France	6.1	5.3
573	FRJ26	3	Hautes-Pyrénées	France	6	5.7
574	RS122	3	Južnobanatska oblast	Serbia	6	4.6
575	FI1D2	3	Pohjois-Savo	Finland	5.9	5.5
576	AT111	3	Mittelburgenland	Austria	6	13
577	PL721	3	Kielecki	Poland	5.8	3.8
578	SE231	3	Hallands län	Sweden	5.7	5.4
579	ITF63	3	Catanzaro	Italy	5.7	4.3
580	ITI43	3	Roma	Italy	5.6	1.9
581	ITG15	3	Caltanissetta	Italy	5.6	4.6
582	FRJ11	3	Aude	France	5.5	4.6
583	PL415	3	Miasto Poznań	Poland	5.4	3.9
584	RO322	3	Ilfov	Romania	5.4	4.5
585	PL228	3	Bytomski	Poland	5.4	4.2
586	ES114	3	Pontevedra	Spain	5.4	3.1
587	ITF11	3	L'Aquila	Italy	5.4	4.7
588	BG324	3	Razgrad	Bulgaria	5.4	6.6
589	ITI18	3	Arezzo	Italy	5.3	4.5
590	PL22B	3	Sosnowiecki	Poland	5.3	3.3
591	ITI15	3	Prato	Italy	5.2	5.6
592	FRJ13	3	Hérault	France	5.2	2.7
593	DK041	3	Vestjylland	Denmark	5.2	4.5
594	EL301	3	Voreios Tomeas Athinon	Greece	5.1	3.8
595	FI197	3	Pirkanmaa	Finland	5.1	4.8
596	NO051	3	Hordaland	Norway	5.1	4.9
597	LT026	3	Šiaulių apskritis	Lithuania	5	4.6
598	ES705	3	Gran Canaria	Spain	5	3.5
599	EL611	3	Karditsa, Trikala	Greece	5	5
600	NL113	3	Overig Groningen	Netherlands	4.9	5.1
601	LT027	3	Tauragės apskritis	Lithuania	4.9	7
602	FRI33	3	Deux-Sèvres	France	4.9	5.2
603	EL422	3	Andros, Thira, Kea, Milos, Mykonos, Naxos, Paros, Syros, Tinos	Greece	4.9	8
604	PL224	3	Częstochowski	Poland	4.9	3.7
605	EL651	3	Argolida, Arkadia	Greece	4.8	5.6
606	FRG01	3	Loire-Atlantique	France	4.8	2.8
607	PL926	3	Żyrardowski	Poland	4.7	4.9
608	ITF64	3	Vibo Valentia	Italy	4.7	6.7
609	AT211	3	Klagenfurt-Villach	Austria	4.7	5.6
610	ES112	3	Lugo	Spain	4.7	4.1
611	PL911	3	Miasto Warszawa	Poland	4.6	2.3

612	AT332	3	Innsbruck	Austria	4.6	6.1
613	AT313	3	Mühlviertel	Austria	4.6	6.9
614	PT300	3	Região Autónoma da Madeira	Portugal	4.6	5.4
615	DK011	3	Byen København	Denmark	4.6	3.8
616	FRB06	3	Loiret	France	4.6	3.9
617	NL132	3	Zuidoost-Drenthe	Netherlands	4.5	6.4
618	LU000	3	Luxembourg	Luxembourg	4.5	4.6
619	ES709	3	Tenerife	Spain	4.5	3.7
620	EL413	3	Chios	Greece	4	12
621	AL034	3	Korcë	Albania	4.5	6.4
622	AT223	3	Östliche Obersteiermark	Austria	4.5	6.8
623	ES533	3	Menorca	Spain	4	12
624	NL131	3	Noord-Drenthe	Netherlands	4.4	6.6
625	PT150	3	Algarve	Portugal	4.4	4.2
626	ITG26	3	Nuoro	Italy	4.3	6.3
627	FRD13	3	Orne	France	4.3	5.7
628	RO113	3	Cluj	Romania	4.2	3.5
629	LT024	3	Marijampolės apskritis	Lithuania	4.1	5.8
630	RO126	3	Sibiu	Romania	4.1	4.1
631	ITG18	3	Ragusa	Italy	4.1	5.2
632	UKL13	3	Conwy and Denbighshire	United Kingdom	4.1	5.6
633	SK041	3	Prešovský kraj	Slovakia	4	3.7
634	HU222	3	Vas	Hungary	4	5.1
635	RS212	3	Kolubarska oblast	Serbia	4	5.4
636	ITF31	3	Caserta	Italy	4	3.6
637	EL653	3	Lakonia, Messinia	Greece	4	5.4
638	PL921	3	Radomski	Poland	4	3.8
639	FI193	3	Keski-Suomi	Finland	4	5.2
640	RO112	3	Bistrița-Năsăud	Romania	4	4.6
641	NL125	3	Zuidwest-Friesland	Netherlands	3.9	7.8
642	HU331	3	Bács-Kiskun	Hungary	3.9	3.6
643	CZ031	3	Jihočeský kraj	Czechia	3.9	3.8
644	CH033	3	Aargau	Switzerland	3.9	4.2
645	FI1C2	3	Kanta-Häme	Finland	3.9	6.8
646	BG325	3	Silistra	Bulgaria	3.8	6.5
647	FI1C3	3	Päijät-Häme	Finland	3.8	6.1
648	AT226	3	Westliche Obersteiermark	Austria	3.8	8.2
649	ITG12	3	Palermo	Italy	3.8	2.7
650	PL924	3	Ostrołęcki	Poland	3.8	4.8
651	ITF32	3	Benevento	Italy	3.7	5.1

652	ITG17	3	Catania	Italy	3.6	2.8
653	ITG11	3	Trapani	Italy	3.6	4.1
654	BG415	3	Kyustendil	Bulgaria	3.6	5.4
655	AT341	3	Bludenz-Bregenz Wald	Austria	3	11
656	IS002	3	Landsbyggð	Iceland	3.4	9
657	PT16J	3	Beiras e Serra da Estrela	Portugal	3.4	5.1
658	CZ041	3	Karlovarský kraj	Czechia	3.4	5.4
659	HU221	3	Győr-Moson-Sopron	Hungary	3.4	4.5
660	NO031	3	Østfold	Norway	3.3	5.5
661	CZ010	3	Hlavní město Praha	Czechia	3.3	3
662	CZ080	3	Moravskoslezský kraj	Czechia	3.2	2.9
663	RO424	3	Timiș	Romania	3.2	3.7
664	FRJ15	3	Pyrénées-Orientales	France	3.2	3.9
665	PL214	3	Krakowski	Poland	3.2	3.7
666	RO212	3	Botoșani	Romania	3.2	4
667	CZ072	3	Zlínský kraj	Czechia	3.2	3.8
668	AT323	3	Salzburg und Umgebung	Austria	3.1	5
669	DK021	3	Østsjælland	Denmark	3.1	6
670	EE001	3	Põhja-Eesti	Estonia	3	3.9
671	FRH04	3	Morbihan	France	2.9	3.1
672	BG422	3	Haskovo	Bulgaria	2.9	5
673	EL302	3	Dytikos Tomeas Athinon	Greece	2.9	4.4
674	FRJ14	3	Lozère	France	2.7	9.4
675	NO033	3	Vestfold	Norway	2.7	6.1
676	EL306	3	Dytiki Attiki	Greece	2.7	7.6
677	IS001	3	Höfuðborgarsvæði	Iceland	2.7	6.9
678	PL517	3	Wałbrzyski	Poland	2.6	3.9
679	AT125	3	Weinviertel	Austria	2.6	6.6
680	CZ042	3	Ústecký kraj	Czechia	2.6	3
681	AT312	3	Linz-Wels	Austria	2.6	4.4
682	CH040	3	Zürich	Switzerland	2.6	3
683	PL518	3	Wrocławski	Poland	2.6	3.7
684	EL431	3	Irakleio	Greece	2.5	4.9
685	AL011	3	Dibër	Albania	2.5	9.5
686	SK022	3	Trenčiansky kraj	Slovakia	2.5	4.2
687	HU231	3	Baranya	Hungary	2.5	4.6
688	FRK13	3	Haute-Loire	France	2.5	5.8
689	BG424	3	Smolyan	Bulgaria	2.5	6.4
690	AT321	3	Lungau	Austria	2	20
691	FRL05	3	Var	France	2.4	3
692	HU323	3	Szabolcs-Szatmár-Bereg	Hungary	2.4	4.2

693	ITG14	3	Agrigento	Italy	2.4	3.7
694	EL522	3	Thessaloniki	Greece	2.3	2.8
695	PL225	3	Bielski	Poland	2.3	3.2
696	PT186	3	Alto Alentejo	Portugal	2.3	6.7
697	AL031	3	Berat	Albania	2.3	8
698	PL841	3	Białostocki	Poland	2.2	4.1
699	CH061	3	Luzern	Switzerland	2.2	5.5
700	HU213	3	Veszprém	Hungary	2.1	4.3
701	EL524	3	Pella	Greece	2.1	6.7
702	PL814	3	Lubelski	Poland	2.1	3.4
703	HU120	3	Pest	Hungary	2	2.5
704	PL218	3	Nowosądecki	Poland	2	4
705	RS227	3	Podunavska oblast	Serbia	2	5.7
706	ITF35	3	Salerno	Italy	2	2.9
707	RO321	3	București	Romania	2	2.1
708	EL541	3	Arta, Preveza	Greece	2	7
709	RS123	3	Južnobačka oblast	Serbia	1.9	3.9
710	LT021	3	Alytaus apskritis	Lithuania	1.8	6.1
711	EL622	3	Kerkyra	Greece	1.7	7.5
712	PL638	3	Starogardzki	Poland	1.7	4.6
713	RO311	3	Argeș	Romania	1.7	3.3
714	HU212	3	Komárom-Esztergom	Hungary	1.6	4.8
715	CZ071	3	Olomoucký kraj	Czechia	1.5	3.9
716	NO021	3	Hedmark	Norway	1.5	6.1
717	PL416	3	Kaliski	Poland	1.4	4
718	RS125	3	Severnobačka oblast	Serbia	1.4	5.6
719	PL524	3	Opolski	Poland	1.3	3.7
720	PL217	3	Tarnowski	Poland	1.3	4.5
721	FRI32	3	Charente-Maritime	France	1.3	3.1
722	AL012	3	Durrës	Albania	1.3	6.1
723	AL033	3	Gjirokastër	Albania	1.3	9.9
724	EL307	3	Peiraias, Nisoi	Greece	1.3	4
725	FRB04	3	Indre-et-Loire	France	1.3	3.5
726	NL124	3	Noord-Friesland	Netherlands	1.2	5
727	PL823	3	Rzeszowski	Poland	1.1	4
728	PL812	3	Chełmsko-zamojski	Poland	1.1	3.3
729	FRM02	3	Haute-Corse	France	1.1	6.2
730	FRH02	3	Finistère	France	1.1	3
731	NO042	3	Vest-Agder	Norway	1.1	7.2
732	PL824	3	Tarnobrzieski	Poland	1.1	4.1
733	FRK11	3	Allier	France	1	4.6

734	FI1D9	3	Pohjois-Pohjanmaa	Finland	1	4.4
735	CZ032	3	Plzeňský kraj	Czechia	1	4.3
736	CH056	3	Graubünden	Switzerland	1	6.5
737	NO034	3	Telemark	Norway	0.9	7
738	RO114	3	Maramureș	Romania	0.9	3.5
739	PT16B	3	Oeste	Portugal	0.9	4.2
740	LV006	3	Rīga	Latvia	0.9	3.4
741	IT119	3	Siena	Italy	0.9	4.9
742	FRJ22	3	Aveyron	France	0.9	4.6
743	RS213	3	Mačvanska oblast	Serbia	0.8	4.8
744	NO043	3	Rogaland	Norway	0.8	5
745	NO060	3	Trøndelag	Norway	0.8	4.3
746	RO314	3	Giurgiu	Romania	0.8	4.2
747	PL617	3	Inowrocławski	Poland	0.8	4.5
748	SK023	3	Nitriansky kraj	Slovakia	0.7	3.6
749	PL715	3	Skierniewicki	Poland	0.7	4.4
750	NO022	3	Oppland	Norway	0.7	7
751	HU223	3	Zala	Hungary	0.6	4.8
752	BG322	3	Gabrovo	Bulgaria	0.6	6.4
753	PT16F	3	Região de Leiria	Portugal	0.6	5.3
754	NL133	3	Zuidwest-Drenthe	Netherlands	0.5	7.7
755	PL722	3	Sandomiersko-jędrzejowski	Poland	0.5	4.1
756	EL652	3	Korinthia	Greece	0.5	6.6
757	PL713	3	Piotrkowski	Poland	0.4	3.9
758	FI194	3	Etelä-Pohjanmaa	Finland	0.4	6.1
759	CH052	3	Schaffhausen	Switzerland	0.4	8.8
760	PL21A	3	Oświęcimski	Poland	0.4	3.7
761	PL843	3	Suwalski	Poland	0.4	5.3
762	EL631	3	Aitolokarnania	Greece	0.4	5.5
763	LT028	3	Telšių apskritis	Lithuania	0.4	6.8
764	FRK14	3	Puy-de-Dôme	France	0.4	3.5
765	CH053	3	Appenzell Ausserrhoden	Switzerland	0	12
766	RO315	3	Ialomița	Romania	0.4	4.7
767	PL619	3	Włocławski	Poland	0.4	4.2
768	CH021	3	Bern	Switzerland	0.3	3.2
769	PL925	3	Siedlecki	Poland	0.3	4.1
770	EL304	3	Notios Tomeas Athinon	Greece	0.3	3.8
771	RO121	3	Alba	Romania	0.3	4.2
772	RS126	3	Srednjobanatska oblast	Serbia	0.2	5.5
773	EL513	3	Rodopi	Greece	0.1	6.9
774	NO012	3	Akershus	Norway	0	4.2

775	FI195	3	Pohjanmaa	Finland	0	5.9
776	RO317	3	Teleorman	Romania	0	3.7
777	RO312	3	Călărași	Romania	-0.1	4.6
778	PL213	3	Miasto Kraków	Poland	-0.1	3.6
779	SK031	3	Žilinský kraj	Slovakia	-0.1	3.5
780	FI1D1	3	Etelä-Savo	Finland	-0.1	6.2
781	RO413	3	Mehedinți	Romania	-0.2	5
782	RS222	3	Braničevska oblast	Serbia	-0.2	5.3
783	BG313	3	Vratsa	Bulgaria	-0.2	5
784	RO111	3	Bihor	Romania	-0.2	3.5
785	HU321	3	Hajdú-Bihar	Hungary	-0.3	4.2
786	NL112	3	Delfzijl en omgeving	Netherlands	0	11
787	LI000	3	Liechtenstein	Liechtenstein	0	17
788	PL822	3	Przemyski	Poland	-0.3	4.8
789	FRG05	3	Vendée	France	-0.3	3.3
790	AT112	3	Nordburgenland	Austria	-0.4	6.6
791	HU332	3	Békés	Hungary	-0.4	3.9
792	PL227	3	Rybnicki	Poland	-0.4	4
793	NO071	3	Nordland	Norway	-0.4	6.1
794	FRL06	3	Vaucluse	France	-0.5	3.8
795	PL229	3	Gliwicki	Poland	-0.5	4.3
796	EL511	3	Evros	Greece	-0.5	6.1
797	PL427	3	Szczecinecko-pyrzycki	Poland	-0.5	3.9
798	CZ053	3	Pardubický kraj	Czechia	-0.6	3.9
799	AT212	3	Oberkärnten	Austria	-0.7	7.2
800	FRI31	3	Charente	France	-0.7	4.7
801	EL303	3	Kentrikos Tomeas Athinon	Greece	-0.7	2.8
802	RO316	3	Prahova	Romania	-0.8	2.9
803	EL645	3	Fokida	Greece	-1	12
804	CZ063	3	Kraj Vysočina	Czechia	-0.8	4
805	DK013	3	Nordsjælland	Denmark	-0.9	4.1
806	PL219	3	Nowotarski	Poland	-0.9	5.2
807	PL613	3	Bydgosko-toruński	Poland	-0.9	3.1
808	AT315	3	Traunviertel	Austria	-0.9	5.9
809	AT127	3	Wiener Umland/Südteil	Austria	-1	5.1
810	AT311	3	Innviertel	Austria	-1	5.2
811	RO422	3	Caraș-Severin	Romania	-1	4.5
812	BE252	3	Arr. Diksmuide	Belgium	-1	11
813	PL821	3	Krośnieński	Poland	-1.2	4.3
814	PL711	3	Miasto Łódź	Poland	-1.2	3.2
815	FRI21	3	Corrèze	France	-1.3	4.9

816	EE008	3	Lõuna-Eesti	Estonia	-1.3	4.6
817	FRJ23	3	Haute-Garonne	France	-1.3	2.5
818	PL842	3	Łomżyński	Poland	-1.3	4.1
819	UKN10	3	Derry City and Strabane	United Kingdom	-1.4	7.4
820	FI1C4	3	Kymenlaakso	Finland	-1.4	5.8
821	DK022	3	Vest- og Sydsjælland	Denmark	-1.5	3.3
822	FI1D3	3	Pohjois-Karjala	Finland	-1.5	6
823	AL013	3	Kukës	Albania	-2	12
824	FRI13	3	Landes	France	-1.6	4.6
825	FI196	3	Satakunta	Finland	-1.6	5.2
826	PL424	3	Miasto Szczecin	Poland	-1.6	4.2
827	PL634	3	Gdański	Poland	-1.6	3.8
828	RO414	3	Olt	Romania	-1.7	3.5
829	CH057	3	Thurgau	Switzerland	-1.7	6.3
830	PL633	3	Trójmiejski	Poland	-1.7	3.3
831	AL035	3	Vlorë	Albania	-1.8	7
832	CH051	3	Glarus	Switzerland	-2	13
833	PL637	3	Chojnicki	Poland	-1.9	5.9
834	FRD11	3	Calvados	France	-1.9	3.1
835	RO214	3	Neamț	Romania	-1.9	3.8
836	FRL02	3	Hautes-Alpes	France	-1.9	6.9
837	ES531	3	Eivissa y Formentera	Spain	-2	9.9
838	RS214	3	Moravička oblast	Serbia	-2	5.3
839	RO115	3	Satu Mare	Romania	-2	4.7
840	ITI41	3	Viterbo	Italy	-2	4.7
841	FRI34	3	Vienne	France	-2.1	3.9
842	EL543	3	Ioannina	Greece	-2.1	6.6
843	EL642	3	Evvoia	Greece	-2.2	5.2
844	PL618	3	Świecki	Poland	-2.2	6.8
845	SK032	3	Banskobystrický kraj	Slovakia	-2.2	3
846	RO411	3	Dolj	Romania	-2.2	3.8
847	RS217	3	Raška oblast	Serbia	-2.2	4.5
848	PL523	3	Nyski	Poland	-2.3	4.7
849	BG423	3	Pazardzhik	Bulgaria	-2.3	4.6
850	RO223	3	Constanța	Romania	-2.4	2.9
851	BG342	3	Sliven	Bulgaria	-2.4	5.3
852	FRI12	3	Gironde	France	-2.4	2.4
853	FRI23	3	Haute-Vienne	France	-2.4	4.3
854	PL712	3	Łódzki	Poland	-2.4	4.7
855	FRH03	3	Ille-et-Vilaine	France	-2.4	3.2

856	LT029	3	Utenos apskritis	Lithuania	-2.5	5.5
857	PL418	3	Poznański	Poland	-2.5	4
858	CZ064	3	Jihomoravský kraj	Czechia	-2.6	2.8
859	ES708	3	Lanzarote	Spain	-2.6	9
860	HU322	3	Jász-Nagykun-Szolnok	Hungary	-2.6	3.8
861	EL641	3	Voiotia	Greece	-2.6	6.7
862	FRI15	3	Pyrénées-Atlantiques	France	-2.6	3.4
863	BG331	3	Varna	Bulgaria	-2.7	4
864	ES707	3	La Palma	Spain	-2.8	8.7
865	BG421	3	Plovdiv	Bulgaria	-2.8	3.1
866	DK032	3	Syddjylland	Denmark	-2.9	3.1
867	HU333	3	Csongrád	Hungary	-2.9	3.6
868	BG413	3	Blagoevgrad	Bulgaria	-2.9	4.3
869	BG323	3	Ruse	Bulgaria	-2.9	4.6
870	PL714	3	Sieradzki	Poland	-2.9	4
871	BG333	3	Shumen	Bulgaria	-2.9	5
872	LV003	3	Kurzeme	Latvia	-2.9	4.7
873	NO073	3	Finnmark	Norway	-3	9.4
874	EL433	3	Rethymni	Greece	-3	8.7
875	PL514	3	Miasto Wrocław	Poland	-3	4
876	RO226	3	Vrancea	Romania	-3	3.9
877	BG414	3	Pernik	Bulgaria	-3.1	5.7
878	FRL01	3	Alpes-de-Haute-Provence	France	-3	13
879	FRH01	3	Côtes-d'Armor	France	-3.2	3.3
880	EL412	3	Ikaria, Samos	Greece	-3	13
881	PL922	3	Ciechanowski	Poland	-3.3	4.2
882	RS124	3	Severnobanatska oblast	Serbia	-3.3	6.2
883	LV005	3	Latgale	Latvia	-3.3	4
884	HU311	3	Borsod-Abaúj-Zemplén	Hungary	-3.3	3.3
885	PL623	3	Etcki	Poland	-3.4	5.4
886	BG411	3	Sofia (stolitsa)	Bulgaria	-3.4	2.6
887	PL426	3	Koszaliński	Poland	-3.4	4.5
888	RO122	3	Braşov	Romania	-3.4	3.4
889	RO124	3	Harghita	Romania	-3.4	4.8
890	LV009	3	Zemgale	Latvia	-3.4	4.7
891	PL636	3	Słupski	Poland	-3.5	4.1
892	EL432	3	Lasithi	Greece	-3.5	9
893	PL411	3	Pilski	Poland	-3.5	4.2
894	PL912	3	Warszawski wschodni	Poland	-3.5	3.4
895	RO224	3	Galaţi	Romania	-3.5	3.3
896	FRJ27	3	Tarn	France	-3.5	4

897	NO053	3	Møre og Romsdal	Norway	-3.5	5.8
898	PL621	3	Elbląski	Poland	-3.7	4.2
899	PL432	3	Zielonogórski	Poland	-3.7	3.9
900	PL428	3	Szczeciński	Poland	-3.8	3.7
901	SK010	3	Bratislavský kraj	Slovakia	-3.9	3.4
902	PL515	3	Jeleniogórski	Poland	-4	3.8
903	ME000	3	Crna Gora	Montenegro	-4	3.4
904	BG425	3	Kardzhali	Bulgaria	-4	5.9
905	CZ052	3	Královéhradecký kraj	Czechia	-4.1	3.7
906	RS211	3	Zlatiborska oblast	Serbia	-4.1	4.2
907	NO041	3	Aust-Agder	Norway	-4.2	8.7
908	CH062	3	Uri	Switzerland	-4	15
909	HU232	3	Somogy	Hungary	-4.2	4.4
910	PL414	3	Koniński	Poland	-4.4	3.7
911	PL516	3	Legnicko-głogowski	Poland	-4.4	4.5
912	SE331	3	Västerbottens län	Sweden	-4.4	5
913	PL811	3	Bialski	Poland	-4.4	4.7
914	CZ051	3	Liberecký kraj	Czechia	-4.4	4.4
915	FI1D7	3	Lappi	Finland	-4.6	5.6
916	RO116	3	Sălaj	Romania	-4.6	4.8
917	FRJ21	3	Ariège	France	-4.6	5.7
918	RO313	3	Dâmbovița	Romania	-4.6	3.5
919	DK050	3	Nordjylland	Denmark	-4.7	4
920	RS226	3	Pirotska oblast	Serbia	-4.8	8
921	FRI11	3	Dordogne	France	-4.8	3.8
922	CZ020	3	Středočeský kraj	Czechia	-4.8	2.8
923	RO221	3	Brăila	Romania	-4.9	4.1
924	PL923	3	Płocki	Poland	-4.9	4.2
925	HU211	3	Fejér	Hungary	-5	3.7
926	DK042	3	Østjylland	Denmark	-5.1	3.2
927	ITG2A	3	Ogliastra	Italy	-5	10
928	NL111	3	Oost-Groningen	Netherlands	-5.3	6.4
929	AT333	3	Osttirol	Austria	-5	13
930	PL913	3	Warszawski zachodni	Poland	-5.5	3.1
931	RO211	3	Bacău	Romania	-5.5	3.1
932	FI1C1	3	Varsinais-Suomi	Finland	-5.7	4.3
933	PL622	3	Olsztyński	Poland	-5.7	3.6
934	LV007	3	Pierīga	Latvia	-5.8	4
935	PL22C	3	Tyski	Poland	-5.9	3.9
936	DK031	3	Fyn	Denmark	-5.9	3.4
937	RO213	3	Iași	Romania	-5.9	3.1

938	BG341	3	Burgas	Bulgaria	-6	3.3
939	PL616	3	Grudziądzki	Poland	-6	4
940	PL431	3	Gorzowski	Poland	-6.2	4.2
941	DK014	3	Bornholm	Denmark	-6.3	9.9
942	BG412	3	Sofia	Bulgaria	-6.3	3.8
943	PL417	3	Leszczyński	Poland	-6.3	3.7
944	LV008	3	Vidzeme	Latvia	-6.5	4.8
945	AT123	3	Sankt Pölten	Austria	-6.5	6.6
946	FRJ28	3	Tarn-et-Garonne	France	-6.6	4.6
947	BG321	3	Veliko Tarnovo	Bulgaria	-6.6	4.2
948	CH066	3	Zug	Switzerland	-6.7	8.1
949	NO052	3	Sogn og Fjordane	Norway	-6.7	8.9
950	EL623	3	Ithaki, Kefallinia	Greece	-7	13
951	BG344	3	Stara Zagora	Bulgaria	-6.9	4
952	RS127	3	Sremska oblast	Serbia	-7.1	3.9
953	EL525	3	Pieria	Greece	-7.2	6
954	RO222	3	Buzău	Romania	-7.3	3
955	NO072	3	Troms	Norway	-7.5	7
956	EL533	3	Florina	Greece	-8	10
957	EL523	3	Kilkis	Greece	-7.6	8
958	BG314	3	Pleven	Bulgaria	-7.8	3.8
959	BG315	3	Lovech	Bulgaria	-7.9	4.9
960	HU312	3	Heves	Hungary	-8	4
961	BG332	3	Dobrich	Bulgaria	-8.2	5
962	EL542	3	Thesprotia	Greece	-8	11
963	RO216	3	Vaslui	Romania	-8.5	4
964	HU313	3	Nógrád	Hungary	-8.5	4.5
965	FRK12	3	Cantal	France	-8.6	5.9
966	RS218	3	Šumadijska oblast	Serbia	-8.6	4.7
967	RO225	3	Tulcea	Romania	-8.6	5.1
968	ITG29	3	Olbia-Tempio	Italy	-8.8	6.7
969	EL643	3	Evrytania	Greece	-9	16
970	CH065	3	Nidwalden	Switzerland	-9	14
971	BG312	3	Montana	Bulgaria	-10.6	4.8
972	BG334	3	Targovishte	Bulgaria	-11.9	5.5
973	ES704	3	Fuerteventura	Spain	-12	11
974	RS121	3	Zapadnobačka oblast	Serbia	-14.2	4.8
975	RO123	3	Covasna	Romania	-14.8	4.7
976	FI200	3	Åland	Finland	-15	16
977	AT331	3	Außerfern	Austria	-17	13

D. Tables of USA regions (states and counties), ordered by integrated first-peak period P-score

D.1 USA states

Rank (by P-score)	State Name	State Abbrev.	P-score (%)	(1 σ) Err (%)	P-score / Err	Rise-side half-maximum (weeks after March 8-14, 2020)*
1	New York	NY	101.9	1.6	63.7	2
2	New Jersey	NJ	90.3	1.8	50.2	2
3	Connecticut	CT	54	2.2	24.6	3
4	Massachusetts	MA	52.5	1.7	30.9	3
5	District of Columbia	DC	51.1	5.5	9.3	3
6	Rhode Island	RI	32.9	3.5	9.4	5
7	Maryland	MD	31.1	1.7	18.3	3
8	Louisiana	LA	30.9	1.6	19.3	2
9	Illinois	IL	29.4	1.2	24.5	3
10	Michigan	MI	28.7	1.2	23.9	2
11	Delaware	DE	27.9	3.9	7.2	5
12	Pennsylvania	PA	21.2	1.1	19.3	3
13	Colorado	CO	18.8	1.8	10.4	2
14	Mississippi	MS	16.2	1.8	9.0	2
15	Indiana	IN	15.8	1.3	12.2	2
16	Georgia	GA	14.7	1.1	13.4	2
17	Virginia	VA	14	1.3	10.8	3
18	Vermont	VT	11.9	4.5	2.6	-
19	Arizona	AZ	11.4	1.3	8.8	3
20	New Mexico	NM	11.1	2.4	4.6	7
21	California	CA	10.63	0.88	12.1	2
22	Minnesota	MN	10.4	1.5	6.9	5
23	South Carolina	SC	10.2	1.4	7.3	3
24	New Hampshire	NH	10.1	2.8	3.6	5
25	Alabama	AL	9.3	1.5	6.2	2
26	Ohio	OH	8.5	1.1	7.7	5
27	North Carolina	NC	8.3	1.2	6.9	4
28	Missouri	MO	7.6	1.4	5.4	3
29	Iowa	IA	7.2	1.9	3.8	6

30	Washington	WA	7.1	1.4	5.1	1
31	Texas	TX	6.77	0.69	9.8	3
32	Wisconsin	WI	6.7	1.2	5.6	2
33	Florida	FL	6.61	0.78	8.5	3
34	Nebraska	NE	5.9	2.4	2.5	-
35	Nevada	NV	5.7	1.9	3.0	2
36	Kentucky	KY	5.5	1.3	4.2	2
37	Oregon	OR	5.1	1.7	3.0	1
38	North Dakota	ND	5	3.4	1.5	-
39	West Virginia	WV	4.8	1.9	2.5	-
40	Tennessee	TN	4.6	1.2	3.8	2
41	Kansas	KS	4.3	1.8	2.4	-
42	Oklahoma	OK	4.2	1.6	2.6	-
43	Utah	UT	3.9	2	2.0	-
44	Arkansas	AR	2.6	1.8	1.4	-
45	South Dakota	SD	1.8	3.3	0.6	-
46	Wyoming	WY	1.4	4.4	0.3	-
47	Montana	MT	0.1	3	0.03	-
48	Idaho	ID	-0.1	2.4	-0.04	-
49	Maine	ME	-0.2	2.5	-0.08	-
50	Alaska	AK	-2.1	5.9	-0.4	-
51	Hawaii	HI	-2.4	2.6	-0.9	-

* F-peaks were considered to have discernible rise-side half-maximum dates if the ratio of P-score / Err(P-score) ≥ 3 .

D.2 USA counties

Rank	County Name	State Abbrev.	P-score (%)	(1 σ) Err (%)
1	Bronx County	NY	232.5	7.4
2	Queens County	NY	223.9	5.6
3	Kings County	NY	213.6	6
4	Hudson County	NJ	187.8	8.6
5	Essex County	NJ	160	7.1
6	Rockland County	NY	150.2	9.1
7	New York County	NY	143.5	6.4
8	Union County	NJ	142.4	7.4
9	Passaic County	NJ	137.9	9.7
10	Richmond County	NY	122.6	9.3
11	Nassau County	NY	122.4	5
12	Westchester County	NY	121.8	6.2

13	Bergen County	NJ	108.1	6.2
14	Morris County	NJ	93.9	7.9
15	Middlesex County	NJ	93.7	7
16	Somerset County	NJ	93.7	9.2
17	Chambers County	AL	94	23
18	Suffolk County	NY	87.8	4.4
19	Suffolk County	MA	85.6	6.2
20	Fairfield County	CT	81.4	4.8
21	Mercer County	NJ	81	7.2
22	Orleans Parish	LA	78.6	8.1
23	Iberville Parish	LA	76	30
24	Hunterdon County	NJ	74	14
25	Morgan County	CO	73	25
26	Orange County	NY	71.3	6.7
27	Putnam County	NY	71	13
28	McKinley County	NM	70	13
29	Sussex County	NJ	70	10
30	Warren County	NJ	69	13
31	Assumption Parish	LA	68	30
32	Wayne County	MI	67	2.8
33	Apache County	AZ	66	14
34	Neshoba County	MS	65	20
35	Arlington County	VA	65	11
36	Norfolk County	MA	64.3	5.3
37	Dougherty County	GA	64	11
38	Holmes County	MS	63	28
39	Middlesex County	MA	61.4	3.5
40	Monmouth County	NJ	61.1	5.1
41	Hartford County	CT	59.3	4.1
42	Prince George's County	MD	59.2	6.1
43	Franklin County	MA	58	12
44	Copiah County	MS	58	23
45	Union Parish	LA	58	22
46	District of Columbia	DC	57.6	6
47	Philadelphia County	PA	57.4	2.8
48	Essex County	MA	55.7	5.3
49	Pointe Coupee Parish	LA	55	22
50	Plymouth County	MA	54.6	6.2
51	Kent County	MD	55	21
52	New Haven County	CT	54.4	5.8
53	Panola County	TX	54	21

54	Montgomery County	MD	53.4	4.9
55	Leflore County	MS	52	16
56	Ocean County	NJ	51.5	5.1
57	Cook County	IL	51.3	1.9
58	Hampden County	MA	51.3	6
59	St. Charles Parish	LA	51	15
60	Dodge County	GA	50	23
61	Decatur County	IN	50	22
62	Delaware County	PA	50.1	5.4
63	Tippah County	MS	49	22
64	Jefferson Parish	LA	49	6
65	Macomb County	MI	48.3	3.7
66	St. John the Baptist Parish	LA	48	14
67	Butts County	GA	47	18
68	Worcester County	MA	46.9	4.6
69	Denver County	CO	46.6	5.3
70	Washington County	TX	45	16
71	Clarendon County	SC	45	14
72	Choctaw County	OK	45	30
73	Oakland County	MI	44.7	2.8
74	Broomfield County	CO	44	20
75	Burlington County	NJ	43.8	5.4
76	San Juan County	NM	44	10
77	Coconino County	AZ	43	12
78	Juniata County	PA	42	25
79	Marion County	IN	42.3	3.4
80	Providence County	RI	41.9	5.2
81	Arapahoe County	CO	41.3	5.5
82	Mahoning County	OH	41.3	6
83	Toombs County	GA	41	21
84	Carbon County	PA	41	14
85	Frederick County	MD	41	7.1
86	Poweshiek County	IA	41	26
87	Clarke County	MS	41	25
88	Drew County	AR	41	28
89	Jefferson County	OR	40	21
90	Montgomery County	PA	40.3	4
91	Vance County	NC	40	19
92	Lauderdale County	MS	40	13
93	Pike County	PA	40	16
94	Litchfield County	CT	39.1	7.9

95	Columbia County	AR	39	19
96	Columbus County	NC	38	15
97	Howard County	TX	38	20
98	Orange County	IN	38	18
99	Fairfax County	VA	37.4	4.6
100	Washington Parish	LA	37	14
101	East Baton Rouge Parish	LA	37.1	5.1
102	Palo Pinto County	TX	37	21
103	McLeod County	MN	37	15
104	Iberia Parish	LA	36	14
105	Hampshire County	MA	36	10
106	Pasquotank County	NC	36	13
107	Fayette County	IN	36	19
108	Imperial County	CA	35	13
109	St. Louis city	MO	34.9	7.3
110	Orleans County	NY	35	15
111	Lackawanna County	PA	34.6	7.9
112	Prince William County	VA	34.5	6.8
113	Bucks County	PA	34.5	4.7
114	Lyon County	KS	34	21
115	Carroll County	TN	34	18
116	Alexandria city	VA	34	13
117	Union County	SC	34	16
118	Lehigh County	PA	34.1	5.2
119	Lincoln County	MS	34	20
120	Rockingham County	VA	34	13
121	Manassas city	VA	34	24
122	Jackson County	GA	34	13
123	Caddo Parish	LA	33.6	8.8
124	Middlesex County	CT	33.5	8.6
125	Attala County	MS	33	23
126	Camden County	NJ	33.4	4.6
127	Morgan County	MO	33	23
128	Lee County	SC	33	19
129	Sussex County	DE	33	5.9
130	Northampton County	PA	33	5.5
131	Northampton County	NC	33	32
132	Berks County	PA	32.7	5.7
133	Page County	VA	33	20
134	Williamsburg County	SC	33	17
135	Clay County	MN	33	15

136	Benton County	WA	32.5	8.6
137	De Soto Parish	LA	32	18
138	Columbia County	NY	32	13
139	Bristol County	MA	32.2	4.5
140	Hennepin County	MN	32.1	3.9
141	Hopkins County	KY	32	13
142	Clinton County	IN	32	15
143	Upson County	GA	32	16
144	Benton County	MO	32	19
145	Sullivan County	NY	32	14
146	Charles County	MD	31.7	7.5
147	Putnam County	TN	31	12
148	Hillsdale County	MI	31	13
149	Lake County	IL	31.3	5.3
150	Montgomery County	AL	31.1	7.6
151	Wapello County	IA	31	13
152	Mitchell County	GA	31	21
153	Pontotoc County	MS	31	18
154	Carroll County	MD	30.7	10
155	Burke County	GA	31	25
156	Waller County	TX	31	18
157	Livingston Parish	LA	30.4	8.3
158	Allen Parish	LA	30	17
159	Lafourche Parish	LA	30	10
160	Coahoma County	MS	30	17
161	Sabine Parish	LA	30	19
162	Henry County	IN	30	17
163	Douglas County	CO	29.6	8.3
164	Duplin County	NC	29	13
165	Cass County	NE	29	22
166	Lucas County	OH	29.3	5.6
167	St. Mary Parish	LA	29	13
168	Covington County	MS	29	20
169	Henderson County	TN	29	18
170	Harrisonburg city	VA	29	14
171	Lancaster County	PA	29.1	4.5
172	Bremer County	IA	29	23
173	Carroll County	VA	29	14
174	Franklin County	AL	29	17
175	Jefferson County	AR	29	11
176	Baltimore city	MD	29	4.4

177	Geauga County	OH	29	12
178	Fairfield County	SC	29	21
179	Portsmouth city	VA	29	11
180	Bartow County	GA	28.7	9.9
181	DuPage County	IL	28.7	4.7
182	Washington County	IA	29	19
183	Rabun County	GA	28	22
184	Salem County	NJ	28	11
185	Gloucester County	NJ	28.3	6
186	Lincoln County	NC	28	10
187	Johnson County	MO	28	15
188	Monroe County	PA	28.1	7.5
189	Brown County	SD	28	16
190	St. Clair County	IL	27.5	7.8
191	Spalding County	GA	27	13
192	Baltimore County	MD	27.4	4.3
193	Atlantic County	NJ	27.4	5.5
194	Chester County	PA	27.3	5.1
195	Fluvanna County	VA	27	21
196	Box Elder County	UT	27	16
197	Union County	GA	27	15
198	Bolivar County	MS	27	15
199	Lamar County	MS	27	16
200	Cape Girardeau County	MO	27	12
201	Caroline County	MD	27	17
202	Susquehanna County	PA	27	19
203	Lincoln County	KY	26	24
204	Colonial Heights city	VA	26	20
205	Fauquier County	VA	26	12
206	Ascension Parish	LA	26	11
207	Kane County	IL	26.3	7.1
208	Delaware County	OK	26	16
209	Hickman County	TN	26	23
210	Henrico County	VA	25.9	6.6
211	Livingston County	MI	25.8	7.2
212	Wyandotte County	KS	25.6	7.6
213	Monroe County	FL	26	13
214	Fillmore County	MN	26	19
215	McHenry County	IL	25.5	7.4
216	Oktibbeha County	MS	26	20
217	Marion County	MS	26	23

218	Russell County	AL	25	15
219	Berkeley County	WV	25	11
220	Staunton city	VA	25	15
221	Grant County	KY	25	20
222	Miami County	IN	25	18
223	Erie County	NY	25.1	3.5
224	Will County	IL	24.9	4.7
225	Warren County	MO	25	21
226	Loudoun County	VA	24.8	8.5
227	Milwaukee County	WI	24.7	4.6
228	Habersham County	GA	25	16
229	Yakima County	WA	24.6	9.1
230	Marengo County	AL	25	19
231	Dallas County	IA	24	14
232	New Castle County	DE	24.3	4.8
233	Marion County	AL	24	14
234	Robertson County	TN	24	11
235	Niagara County	NY	24.2	5.8
236	Dutchess County	NY	24.1	6.3
237	Sumter County	GA	24	15
238	Shenandoah County	VA	24	14
239	Suffolk city	VA	24	11
240	Los Angeles County	CA	23.9	2.1
241	Bryan County	GA	24	17
242	Buchanan County	VA	24	21
243	Navajo County	AZ	23.7	8
244	Van Wert County	OH	24	21
245	Macon County	NC	24	15
246	Escambia County	AL	24	16
247	Dearborn County	IN	23	16
248	Johnson County	IN	23.4	8.3
249	Monroe County	MS	23	13
250	Custer County	OK	23	20
251	Chenango County	NY	23	13
252	Ulster County	NY	23.2	7.5
253	St. Tammany Parish	LA	23.1	5.8
254	Haralson County	GA	23	18
255	St. Bernard Parish	LA	23	16
256	Henry County	AL	23	21
257	Clay County	MS	23	23
258	Franklin County	GA	23	16

259	Gage County	NE	23	24
260	Harnett County	NC	22.7	9.2
261	Adams County	PA	23	11
262	Genesee County	MI	22.7	4
263	Clark County	IN	22.7	9.7
264	Caldwell County	TX	23	16
265	Finney County	KS	23	22
266	Alleghany County	MD	22.5	8.6
267	Rowan County	KY	23	20
268	St. Louis County	MO	22.5	4.1
269	LaPorte County	IN	22.5	8
270	Schenectady County	NY	22.4	8.8
271	Jackson County	NC	22	15
272	Scott County	MN	22	13
273	Douglas County	GA	22.4	9.5
274	Fayette County	TN	22	15
275	Cherokee County	AL	22	14
276	Walker County	GA	22	13
277	Tioga County	NY	22	15
278	Davie County	NC	22	17
279	Sequoyah County	OK	22	13
280	Stark County	ND	22	21
281	Pike County	MS	22	12
282	Lincoln County	WI	22	16
283	Clay County	IN	22	17
284	Baldwin County	GA	22	12
285	Martin County	NC	22	15
286	Clayton County	GA	21.8	8.2
287	Dinwiddie County	VA	22	17
288	St. Martin Parish	LA	22	14
289	Saginaw County	MI	21.7	5.7
290	Kent County	DE	21.7	6.9
291	Curry County	OR	22	14
292	Branch County	MI	22	16
293	Elmore County	AL	22	11
294	Monroe County	IN	21	12
295	Williamson County	IL	21	10
296	DeKalb County	IL	21	11
297	Fulton County	GA	20.9	3.4
298	Macon County	AL	21	22
299	Jennings County	IN	21	17

300	Somerset County	MD	21	18
301	Salem city	VA	21	18
302	Hancock County	IN	21	16
303	Calcasieu Parish	LA	20.6	6.6
304	Union County	AR	21	13
305	St. Landry Parish	LA	20.6	8.4
306	Lavaca County	TX	21	20
307	Taylor County	KY	20	17
308	Wood County	OH	20.5	7.8
309	Lincoln County	NE	20	18
310	Lincoln County	MT	20	21
311	Marshall County	IA	20	15
312	Delaware County	IN	20.4	8.9
313	Fayette County	GA	20	13
314	Hamilton County	IN	20.1	6.7
315	Weld County	CO	20.1	7.6
316	Bristol County	RI	20	15
317	Houston County	AL	20	8.2
318	Decatur County	GA	20	15
319	Miami-Dade County	FL	19.8	2.8
320	Hart County	GA	20	20
321	Pinal County	AZ	19.8	5
322	Pearl River County	MS	20	10
323	Mercer County	OH	20	16
324	Muscatine County	IA	20	13
325	Carroll County	GA	19.5	8.8
326	Sweetwater County	WY	20	19
327	Monroe County	GA	19	23
328	Albany County	NY	19.5	4.8
329	Coffee County	TN	19	12
330	Natchitoches Parish	LA	19	14
331	Perry County	OH	19	16
332	Indiana County	PA	19	12
333	Cobb County	GA	19.3	4
334	Jefferson County	CO	19.3	4.3
335	Madison County	IN	19.3	7.8
336	Gratiot County	MI	19	16
337	Fayette County	IA	19	19
338	Tillamook County	OR	19	17
339	Morehouse Parish	LA	19	15
340	Marion County	IL	19	13

341	Dauphin County	PA	19.2	5.3
342	Kershaw County	SC	19	12
343	Webster County	IA	19	13
344	Woodbury County	IA	19	12
345	Whitley County	KY	19	18
346	Owen County	IN	19	22
347	Hertford County	NC	19	15
348	Montgomery County	NC	19	14
349	Fremont County	WY	19	14
350	Gwinnett County	GA	18.7	4
351	Grundy County	IL	19	15
352	Washtenaw County	MI	18.6	6.3
353	Lake County	IN	18.6	4.6
354	Onondaga County	NY	18.6	5.1
355	Tate County	MS	19	15
356	Howard County	MD	18.6	10
357	Clinton County	IL	19	20
358	Olmsted County	MN	19	11
359	Washington County	RI	18.4	9
360	DeKalb County	GA	18.4	3.5
361	Lincoln Parish	LA	18	16
362	Hall County	GA	18.3	7.2
363	Wayne County	NC	18.3	7.6
364	Levy County	FL	18	12
365	Otero County	NM	18	14
366	Accomack County	VA	18	13
367	Jo Daviess County	IL	18	21
368	Madison County	OH	18	15
369	Pemiscot County	MO	18	24
370	Linn County	IA	17.9	7.2
371	Auglaize County	OH	18	14
372	Dixie County	FL	18	22
373	DeSoto County	FL	18	17
374	Tangipahoa Parish	LA	17.9	8.8
375	Albemarle County	VA	18	11
376	Henry County	IL	18	13
377	Jackson County	AL	18	10
378	Vernon County	MO	18	19
379	Dickinson County	MI	18	17
380	Summit County	OH	17.7	4.5
381	Centre County	PA	17.7	9.6

382	Terrebonne Parish	LA	18	10
383	Crisp County	GA	18	16
384	Wyandot County	OH	18	19
385	Muskegon County	MI	17.6	8.2
386	Hillsborough County	NH	17.5	4.8
387	Lawrence County	SD	17	21
388	Fentress County	TN	17	18
389	Rockingham County	NH	17.4	5.3
390	Webb County	TX	17.4	7.7
391	Isabella County	MI	17	14
392	Jackson County	WV	17	18
393	Bullitt County	KY	17	12
394	Richland County	SC	17.3	6.1
395	Hendricks County	IN	17.3	7.6
396	Wayne County	KY	17	22
397	Ogle County	IL	17	12
398	Cumberland County	NJ	17.2	9.1
399	Pitt County	NC	17.2	6.9
400	Hall County	NE	17	15
401	Stoddard County	MO	17	16
402	Bedford County	VA	17	10
403	Linn County	OR	17	6.9
404	Porter County	IN	17	7.9
405	Peach County	GA	17	19
406	Coryell County	TX	17	14
407	Franklin County	OH	16.9	3.6
408	Victoria County	TX	17	12
409	Highland County	OH	17	17
410	Brown County	TX	17	15
411	Barnstable County	MA	16.7	4.8
412	Madison County	TN	17	13
413	Wayne County	WV	17	17
414	Cass County	ND	16.5	8.2
415	Knox County	KY	16	15
416	Merced County	CA	16.5	7.8
417	Henry County	GA	16.5	7.7
418	Henderson County	NC	16.4	8.6
419	Manistee County	MI	16	15
420	McDonald County	MO	16	18
421	Adams County	CO	16.3	5.4
422	Wilson County	NC	16.3	9.6

423	Greene County	IN	16	16
424	Beaver County	PA	16.3	6.7
425	Colleton County	SC	16	13
426	Charlotte County	FL	16.1	4.8
427	Mobile County	AL	16.1	5
428	Lyon County	NV	16	10
429	Montrose County	CO	16	16
430	Union County	PA	16	14
431	Okmulgee County	OK	16	17
432	Mendocino County	CA	16	11
433	Sutter County	CA	15.9	9.9
434	Allen County	KY	16	19
435	Columbiana County	OH	15.9	8.1
436	Dallas County	TX	15.8	2
437	Troup County	GA	16	13
438	Newberry County	SC	16	15
439	Erie County	OH	16	11
440	Georgetown County	SC	15.7	9.6
441	Ingham County	MI	15.7	6.4
442	Whitman County	WA	16	20
443	Colquitt County	GA	16	16
444	Paulding County	GA	15.7	8.1
445	Elbert County	GA	16	20
446	Vernon County	WI	16	19
447	Sunflower County	MS	16	15
448	Dorchester County	MD	16	15
449	Beauregard Parish	LA	15	16
450	Luzerne County	PA	15.5	5.6
451	Goodhue County	MN	15	14
452	Chilton County	AL	15	15
453	Cleburne County	AR	15	14
454	Webster Parish	LA	15	13
455	Kendall County	IL	15	11
456	Lafayette Parish	LA	15.3	7.2
457	Ray County	MO	15	22
458	Harrison County	TX	15	13
459	Coles County	IL	15	13
460	Shiawassee County	MI	15	12
461	Steuben County	IN	15	17
462	Alamance County	NC	15.2	7
463	Jasper County	IA	15	22

464	Yazoo County	MS	15	17
465	Ellis County	TX	15.2	9.3
466	Franklin County	VA	15	13
467	Simpson County	MS	15	17
468	Tuolumne County	CA	15	12
469	Sumter County	SC	15	9.4
470	Otsego County	NY	15	14
471	Weakley County	TN	15	16
472	Douglas County	OR	14.9	7.3
473	Kankakee County	IL	14.9	8.3
474	Campbell County	VA	15	12
475	Wagoner County	OK	15	12
476	Craven County	NC	14.7	8.7
477	Putnam County	GA	15	21
478	Fayette County	KY	14.7	5.7
479	Newport News city	VA	14.7	8.1
480	Tulare County	CA	14.6	5.5
481	Winnebago County	IL	14.6	4.9
482	Sarpy County	NE	14.6	8.3
483	Mecklenburg County	NC	14.6	4.2
484	Lebanon County	PA	14.6	8.3
485	Dakota County	MN	14.6	5.6
486	Clarke County	GA	15	10
487	Rockingham County	NC	14.5	8.1
488	Rankin County	MS	14.5	7.5
489	Graves County	KY	15	12
490	Meriwether County	GA	15	17
491	Washington County	ME	14	16
492	Brown County	OH	14	14
493	Walton County	GA	14	13
494	Lafayette County	MS	14	15
495	Fannin County	GA	14	15
496	Morton County	ND	14	15
497	Carson City	NV	14	11
498	Giles County	TN	14	18
499	Ross County	OH	14.2	9.3
500	Washington County	VT	14	13
501	Rogers County	OK	14.2	8.4
502	Iredell County	NC	14.1	7.5
503	Colorado County	TX	14	17
504	Anne Arundel County	MD	14	4.7

505	Franklin County	NY	14	12
506	Calvert County	MD	14	12
507	Warren County	NC	14	17
508	Delaware County	OH	14	8.8
509	Cortland County	NY	14	15
510	Macoupin County	IL	14	12
511	Burleigh County	ND	14	11
512	Talbot County	MD	14	17
513	Warren County	NY	13.8	9.7
514	Grant County	IN	14	11
515	Davidson County	NC	13.8	9.2
516	Buncombe County	NC	13.8	6.6
517	Clarke County	AL	14	14
518	Carlton County	MN	14	18
519	Wicomico County	MD	13.7	8.2
520	Jackson County	MO	13.7	3.8
521	Roanoke city	VA	13.7	7.9
522	Green County	WI	14	16
523	Allegan County	MI	13.6	8.6
524	Monroe County	IL	14	16
525	Laurel County	KY	13.6	9.1
526	Hardin County	TN	14	15
527	Warren County	MS	14	14
528	Shawano County	WI	14	13
529	Nez Perce County	ID	14	15
530	McDowell County	NC	14	11
531	Lawrence County	TN	14	13
532	Durham County	NC	13.5	7.1
533	Mason County	MI	13	16
534	Douglas County	WA	13	22
535	Hockley County	TX	13	19
536	Shelby County	IN	13	12
537	Portage County	OH	13.4	8.3
538	Jefferson County	TX	13.4	5.9
539	DeKalb County	TN	13	18
540	Windham County	VT	13	13
541	Gadsden County	FL	13	14
542	Berrien County	MI	13.3	7.5
543	Texas County	MO	13	16
544	Ozaukee County	WI	13	11
545	Hood County	TX	13	13

546	James City County	VA	13.3	9.7
547	Pickaway County	OH	13	12
548	Pine County	MN	13	17
549	Rutherford County	TN	13.2	7.2
550	Morgan County	IN	13	12
551	Rapides Parish	LA	13.2	6.8
552	Cumberland County	NC	13.2	4.8
553	Yolo County	CA	13.2	9.4
554	Malheur County	OR	13	26
555	Winston County	AL	13	15
556	White County	IN	13	17
557	Pima County	AZ	13.1	4.1
558	Boone County	WV	13	19
559	Van Buren County	MI	13	13
560	Worcester County	MD	13	13
561	Franklin County	PA	13	7.2
562	Greenville County	SC	13	4.5
563	Elko County	NV	13	15
564	Oneida County	NY	12.9	6.9
565	Montgomery County	KS	13	18
566	Lee County	AL	12.9	9.1
567	Dillon County	SC	13	13
568	Robeson County	NC	12.9	6.8
569	Cecil County	MD	12.8	8.1
570	Acadia Parish	LA	12.8	9.3
571	Marshall County	AL	12.8	8.4
572	Ionia County	MI	13	11
573	Monroe County	NY	12.7	3.4
574	Hunt County	TX	12.7	9.8
575	Caroline County	VA	13	16
576	Rensselaer County	NY	12.7	8
577	Anoka County	MN	12.7	6.3
578	Anderson County	SC	12.7	6.4
579	Potter County	TX	12.6	8.8
580	San Miguel County	NM	13	19
581	Guernsey County	OH	13	15
582	Kent County	RI	12.6	8.4
583	Fayette County	TX	13	17
584	Bartholomew County	IN	13	12
585	Cayuga County	NY	13	13
586	Tipton County	TN	13	13

587	Tishomingo County	MS	12	19
588	Jefferson County	KY	12.3	3.6
589	Thomas County	GA	12	13
590	Spotsylvania County	VA	12.3	8.7
591	Bertie County	NC	12	16
592	Adams County	NE	12	15
593	Polk County	TX	12	13
594	Cass County	MI	12	12
595	Jones County	MS	12	13
596	Meigs County	OH	12	16
597	Iroquois County	IL	12	15
598	Freeborn County	MN	12	14
599	Pike County	AL	12	14
600	Valencia County	NM	12	11
601	Washington County	NY	12	11
602	Ramsey County	MN	11.9	5.8
603	Pettis County	MO	12	15
604	Muscogee County	GA	11.9	8.7
605	Cape May County	NJ	11.9	6.9
606	Cabarrus County	NC	11.8	7.8
607	Lapeer County	MI	11.8	8.5
608	Forrest County	MS	11.8	9.3
609	Hinds County	MS	11.8	6.4
610	Blue Earth County	MN	12	12
611	Monroe County	MI	11.7	6.6
612	Putnam County	IN	12	14
613	Nicollet County	MN	12	17
614	Laurens County	GA	12	12
615	Cass County	TX	12	15
616	Snohomish County	WA	11.6	4.2
617	Rock County	WI	11.6	6.4
618	Grand Traverse County	MI	12	12
619	Montgomery County	NY	12	12
620	Montgomery County	VA	12	12
621	Pulaski County	AR	11.5	4.5
622	Bedford County	PA	11	15
623	Wyoming County	WV	11	16
624	Fayette County	OH	11	19
625	Grant County	WA	11	11
626	Jackson County	IL	11	12
627	Boone County	KY	11	10

628	Pickens County	GA	11	14
629	Scotland County	NC	11	15
630	Broward County	FL	11.4	2.4
631	Warrick County	IN	11	11
632	Boulder County	CO	11.4	5.9
633	Kalamazoo County	MI	11.3	6.6
634	Howard County	IN	11.3	7.6
635	Jasper County	IN	11	15
636	Citrus County	FL	11.3	5.3
637	Bastrop County	TX	11	11
638	Lawrence County	PA	11.2	8.1
639	Clarion County	PA	11	15
640	Dyer County	TN	11	13
641	Calhoun County	MI	11.2	7.8
642	Antrim County	MI	11	20
643	Adams County	MS	11	14
644	Wilson County	TN	11.1	9.2
645	Sedgwick County	KS	11.1	4.1
646	Sawyer County	WI	11	18
647	Ohio County	WV	11	12
648	Ouachita Parish	LA	11	8.1
649	Sanilac County	MI	11	12
650	Ottawa County	MI	11	5.3
651	Harris County	TX	11	1.5
652	Bell County	KY	11	16
653	Belmont County	OH	11	10
654	Columbia County	GA	10.8	7.9
655	Marion County	SC	11	12
656	Mecklenburg County	VA	11	12
657	Stark County	OH	10.8	3.9
658	Covington County	AL	11	12
659	Polk County	IA	10.8	4.9
660	King County	WA	10.7	2.6
661	San Bernardino County	CA	10.7	2.4
662	Champaign County	OH	11	15
663	St. Lucie County	FL	10.7	4.4
664	Sumner County	TN	10.7	6
665	Cleveland County	OK	10.7	6.2
666	Scott County	IA	10.7	7.7
667	Phelps County	MO	11	15
668	Racine County	WI	10.7	7.2

669	Brazos County	TX	10.6	9
670	St. Clair County	MI	10.6	6.3
671	Spartanburg County	SC	10.6	4.5
672	Davis County	UT	10.6	5.8
673	Washington County	OK	11	10
674	Comanche County	OK	11	10
675	Shelby County	TX	11	17
676	Carter County	TN	10.6	9.1
677	Peoria County	IL	10.6	6.1
678	Lancaster County	SC	10.5	8.8
679	Churchill County	NV	10	17
680	Shelby County	TN	10.5	3.9
681	Lenoir County	NC	10	11
682	Fulton County	NY	10	12
683	Washington County	OR	10.5	4.9
684	Somerset County	ME	10	11
685	Montgomery County	KY	10	17
686	Seminole County	OK	10	14
687	Palm Beach County	FL	10.3	2.8
688	Bell County	TX	10.3	7.7
689	St. Louis County	MN	10.3	7
690	Newton County	GA	10.2	8.8
691	Barnwell County	SC	10	18
692	Coffee County	GA	10	13
693	St. Francis County	AR	10	21
694	Catoosa County	GA	10	11
695	Dallas County	AL	10	15
696	Franklin County	TN	10	11
697	Nacogdoches County	TX	10	12
698	Alameda County	CA	10.1	2.9
699	Cuyahoga County	OH	10.1	2.6
700	Howell County	MO	10	13
701	Overton County	TN	10	14
702	Windsor County	VT	10	15
703	Smith County	TX	10	6.6
704	Manatee County	FL	10	4.3
705	New Madrid County	MO	10	17
706	Pontotoc County	OK	10	14
707	Knox County	OH	10	14
708	Chatham County	NC	10	11
709	Ripley County	IN	10	18

710	Aransas County	TX	10	24
711	Travis County	TX	9.9	3.1
712	Cheatham County	TN	10	21
713	Worth County	GA	10	17
714	Jefferson County	MO	9.9	5.6
715	San Francisco County	CA	9.8	3.3
716	Marion County	OR	9.8	5.3
717	York County	SC	9.8	6.2
718	Jefferson County	WV	10	11
719	Greenwood County	SC	9.8	8.4
720	Franklin County	WA	10	12
721	Scott County	TN	10	17
722	Madison County	MS	9.7	9.1
723	Yuma County	AZ	9.7	6.2
724	DeSoto County	MS	9.6	8
725	Chittenden County	VT	9.6	7.9
726	Belknap County	NH	10	10
727	Walworth County	WI	10	11
728	Grays Harbor County	WA	9.5	9.6
729	Jessamine County	KY	10	13
730	Sarasota County	FL	9.5	4.1
731	Riverside County	CA	9.5	2.5
732	Otsego County	MI	9	16
733	Chesterfield County	VA	9.5	5.7
734	Waynesboro city	VA	9	18
735	Umatilla County	OR	9.5	9.4
736	Clackamas County	OR	9.5	5.5
737	Gregg County	TX	9.4	7.1
738	Lexington County	SC	9.4	5.1
739	Independence County	AR	9	14
740	Ward County	ND	9	11
741	Rowan County	NC	9.3	6.3
742	Wayne County	IN	9.3	9.2
743	Houston County	TX	9	15
744	Jackson County	MI	9.3	8.2
745	Brown County	WI	9.3	6.2
746	Boone County	IL	9	17
747	Floyd County	IN	9	11
748	Calloway County	KY	9	13
749	Dorchester County	SC	9.3	8.8
750	Tazewell County	IL	9.3	9.9

751	Sauk County	WI	9	13
752	Florence County	SC	9.2	6.5
753	Hamilton County	OH	9.2	4.4
754	Hamblen County	TN	9	11
755	Santa Clara County	CA	9.2	2.7
756	Montgomery County	TX	9.2	5.1
757	Orange County	TX	9	10
758	Petersburg city	VA	9	12
759	Lubbock County	TX	9.2	5.9
760	Lee County	MS	9.1	9.4
761	Chaves County	NM	9	11
762	Putnam County	FL	9.1	8.3
763	Butler County	KS	9.1	9.7
764	Fulton County	OH	9	16
765	Maricopa County	AZ	9.1	2.1
766	Jefferson County	IL	9	13
767	Macon County	TN	9	17
768	Crawford County	KS	9	16
769	Kanawha County	WV	9	6.8
770	Harris County	GA	9	18
771	Garrett County	MD	9	15
772	Tarrant County	TX	9	2.4
773	Bibb County	GA	9	7.9
774	Amador County	CA	9	12
775	Iron County	UT	9	15
776	Coffee County	AL	9	12
777	Floyd County	KY	9	12
778	Armstrong County	PA	9	10
779	Merrimack County	NH	8.9	6.7
780	Johnston County	NC	8.9	6.9
781	Dawson County	GA	9	17
782	Oconee County	GA	9	14
783	Starke County	IN	9	18
784	Catawba County	NC	8.9	7.3
785	Stokes County	NC	9	10
786	Cumberland County	ME	8.9	6.4
787	Bradley County	TN	8.8	8.2
788	Tolland County	CT	8.8	8.3
789	Burke County	NC	8.8	8.4
790	Chatham County	GA	8.8	7.6
791	Minnehaha County	SD	8.8	7.1

792	Shelby County	KY	9	14
793	Madison County	NY	9	12
794	Allegany County	NY	9	15
795	Leavenworth County	KS	9	14
796	Martin County	FL	8.7	6.3
797	Washington County	MS	9	13
798	San Joaquin County	CA	8.7	4.7
799	Greenup County	KY	9	12
800	San Mateo County	CA	8.7	4.9
801	Buffalo County	NE	9	14
802	Stanly County	NC	9	11
803	Tuscola County	MI	9	12
804	Butler County	OH	8.6	4.6
805	Orange County	NC	8.6	9.4
806	Rutland County	VT	8.6	9.4
807	Randolph County	NC	8.6	6.4
808	LaSalle County	IL	8.6	8.9
809	Cheboygan County	MI	9	14
810	Grant County	WI	9	13
811	Kendall County	TX	8	16
812	Itasca County	MN	8	14
813	Brooke County	WV	8	15
814	Davidson County	TN	8.4	3.9
815	Christian County	IL	8	13
816	Pope County	AR	8	13
817	Jackson County	MS	8.4	6.6
818	Aiken County	SC	8.4	5.8
819	Lake County	MT	8	17
820	Berkeley County	SC	8.4	7.6
821	Hanover County	VA	8.3	9.2
822	Warren County	KY	8.2	8.8
823	Harford County	MD	8.2	6
824	Lowndes County	MS	8	12
825	Franklin County	VT	8	13
826	Prentiss County	MS	8	14
827	Beaufort County	SC	8.2	6.8
828	Cass County	IN	8	13
829	Perry County	PA	8	12
830	Doña Ana County	NM	8.1	7.1
831	Caledonia County	VT	8	18
832	Cameron County	TX	8.1	6.6

833	Logan County	KY	8	14
834	Granville County	NC	8	12
835	Grimes County	TX	8	14
836	Greene County	OH	7.9	7.6
837	Weber County	UT	7.9	7.9
838	Gilmer County	GA	8	14
839	Schuylkill County	PA	7.9	5.9
840	New London County	CT	7.9	5.2
841	Otter Tail County	MN	8	11
842	Sullivan County	TN	7.9	6.2
843	Bulloch County	GA	8	11
844	Jefferson County	AL	7.8	3.3
845	Spokane County	WA	7.8	4.7
846	Clark County	WA	7.8	4.6
847	Rusk County	TX	8	16
848	Tulsa County	OK	7.7	3.5
849	Barry County	MI	8	13
850	Clark County	NV	7.7	2.5
851	Hillsborough County	FL	7.7	3.1
852	Meade County	KY	8	19
853	Washington County	VA	7.7	9.7
854	Oneida County	WI	8	14
855	Richmond County	NC	8	11
856	Coweta County	GA	7.6	9.8
857	Columbia County	PA	7.6	9.7
858	Gloucester County	VA	8	12
859	Leelanau County	MI	8	17
860	Franklin County	AR	8	19
861	Mille Lacs County	MN	8	16
862	Marshall County	MS	8	15
863	Ottawa County	OH	8	10
864	Casey County	KY	8	19
865	Murray County	GA	8	13
866	St. Clair County	AL	7.5	8.9
867	Austin County	TX	8	16
868	Bristol city	VA	8	22
869	Darlington County	SC	7.5	8.5
870	Knox County	TN	7.4	4.1
871	Cleveland County	NC	7.4	7.6
872	Fort Bend County	TX	7.4	5.5
873	Tuscaloosa County	AL	7.4	8.7

874	McLean County	IL	7	11
875	Madison County	IL	7.3	4.9
876	San Diego County	CA	7.3	1.9
877	Edgefield County	SC	7	17
878	Dane County	WI	7.3	5
879	Contra Costa County	CA	7.2	3.6
880	Northumberland County	PA	7.2	8.8
881	Hardeman County	TN	7	17
882	Sumter County	FL	7.2	7.1
883	Oceana County	MI	7	16
884	Lycoming County	PA	7.2	7.4
885	Bradford County	FL	7	14
886	Inyo County	CA	7	19
887	Glynn County	GA	7.1	9
888	Mifflin County	PA	7	13
889	Broome County	NY	7.1	6.8
890	Montgomery County	IL	7	18
891	Whatcom County	WA	7.1	6.7
892	Moore County	NC	7	7.8
893	Van Zandt County	TX	7	11
894	Wyoming County	NY	7	17
895	Limestone County	AL	7	11
896	Ware County	GA	7	11
897	White County	GA	7	17
898	Horry County	SC	7	4.9
899	Mohave County	AZ	6.9	4.8
900	Berkshire County	MA	6.9	7.6
901	Brazoria County	TX	6.9	6
902	Sioux County	IA	7	18
903	Allegheny County	PA	6.9	2.8
904	Mercer County	WV	6.9	9.4
905	Windham County	CT	6.9	7.5
906	Wilkes County	NC	7	11
907	Beaufort County	NC	7	11
908	Walla Walla County	WA	7	14
909	El Paso County	CO	6.7	3.9
910	Sandoval County	NM	6.7	7.8
911	Kalkaska County	MI	7	18
912	Stevens County	WA	7	13
913	Jackson County	OR	6.7	5.4
914	Bladen County	NC	7	14

915	Scott County	MO	7	13
916	Fresno County	CA	6.6	3.3
917	Boone County	IA	7	16
918	Chesapeake city	VA	6.5	6.4
919	Spencer County	IN	7	22
920	Upshur County	TX	7	14
921	Beltrami County	MN	7	15
922	Barrow County	GA	7	11
923	Washburn County	WI	7	20
924	Vilas County	WI	7	14
925	Washington County	MD	6.5	6.7
926	Callaway County	MO	6	18
927	Hill County	TX	6	14
928	Calumet County	WI	6	18
929	Henderson County	KY	6	13
930	Wayne County	OH	6.4	7.2
931	Ontario County	NY	6.4	8.1
932	Taney County	MO	6	12
933	Angelina County	TX	6.3	8.2
934	Johnson County	IA	6	11
935	Trumbull County	OH	6.3	5.9
936	Yankton County	SD	6	19
937	Talladega County	AL	6.3	8.2
938	Wayne County	PA	6	11
939	Sanpete County	UT	6	19
940	Salt Lake County	UT	6.2	3.5
941	St. Francois County	MO	6.2	8.8
942	Ector County	TX	6.2	7.7
943	Franklin County	KY	6	12
944	Walker County	AL	6.2	10
945	Athens County	OH	6	12
946	Lee County	FL	6.2	4.8
947	Jefferson County	WA	6	15
948	Carroll County	AR	6	18
949	Forsyth County	GA	6.2	8.3
950	Yamhill County	OR	6.1	8.8
951	Stephenson County	IL	6	10
952	Suwannee County	FL	6	12
953	El Dorado County	CA	6	7.1
954	Chesterfield County	SC	6	11
955	Carver County	MN	6	14

956	Cherokee County	OK	6	11
957	Rock Island County	IL	6	6.7
958	Forsyth County	NC	5.9	5.1
959	El Paso County	TX	5.9	3.9
960	Washington County	TN	5.9	6.4
961	Allen County	IN	5.9	4.4
962	Grenada County	MS	6	16
963	Hardin County	KY	5.9	9
964	Clinton County	MI	6	14
965	Madison County	KY	5.7	9.8
966	St. Charles County	MO	5.7	5.4
967	Gem County	ID	6	21
968	Grainger County	TN	6	16
969	Waukesha County	WI	5.7	4.4
970	Houston County	GA	5.7	8.3
971	Indian River County	FL	5.6	6.3
972	Craighead County	AR	5.6	9.1
973	Newport County	RI	6	11
974	Randolph County	AL	6	17
975	Caddo County	OK	6	15
976	Sangamon County	IL	5.6	6
977	Kern County	CA	5.6	3.6
978	Berrien County	GA	6	17
979	Scioto County	OH	5.5	8.1
980	Bernalillo County	NM	5.5	3.9
981	Lee County	NC	5	11
982	Baker County	OR	5	19
983	Caswell County	NC	5	18
984	Scott County	IN	5	16
985	Kings County	CA	5.4	9.4
986	Halifax County	NC	5	10
987	Kent County	MI	5.4	3.9
988	Tuscarawas County	OH	5.3	7.5
989	Roane County	TN	5.3	9.8
990	Orangeburg County	SC	5.3	8
991	Twin Falls County	ID	5	11
992	Ouachita County	AR	5	17
993	Autauga County	AL	5	12
994	Bosque County	TX	5	17
995	Medina County	OH	5.2	8.1
996	Alexander County	NC	5	14

997	Santa Cruz County	AZ	5	15
998	Cerro Gordo County	IA	5	13
999	Frederick County	VA	5.1	9.9
1000	McCracken County	KY	5.1	9.8
1001	Lancaster County	NE	5.1	5.4
1002	Sheboygan County	WI	5.1	7.5
1003	Lee County	IA	5	14
1004	Gaston County	NC	5.1	5.9
1005	Hardin County	OH	5	19
1006	Collin County	TX	5.1	3.7
1007	Washoe County	NV	5.1	6
1008	Nevada County	CA	5.1	8.7
1009	Williamson County	TX	5	4.8
1010	Ashe County	NC	5	12
1011	Washington County	UT	5	6.1
1012	McMinn County	TN	5	11
1013	Winona County	MN	5	18
1014	Blair County	PA	4.9	6.3
1015	Hopkins County	TX	5	13
1016	Galveston County	TX	4.9	5.7
1017	Polk County	GA	5	13
1018	Lyon County	MN	5	23
1019	Jackson County	OK	5	19
1020	Guilford County	NC	4.7	4.6
1021	Midland County	MI	5	11
1022	Roscommon County	MI	5	14
1023	Henderson County	TX	4.6	7.2
1024	Virginia Beach city	VA	4.6	4.7
1025	Douglas County	NE	4.6	3.7
1026	Huntington County	IN	5	16
1027	Charlottesville city	VA	5	23
1028	St. Joseph County	IN	4.5	5.2
1029	Randolph County	IL	5	16
1030	Duval County	FL	4.5	3.1
1031	Taylor County	FL	4	22
1032	Hancock County	MS	4	15
1033	Flathead County	MT	4.4	8
1034	McCurtain County	OK	4	16
1035	Whitfield County	GA	4	10
1036	Marlboro County	SC	4	17
1037	St. Mary's County	MD	4.4	8.9

1038	Volusia County	FL	4.4	3.6
1039	Panola County	MS	4	15
1040	Lynchburg city	VA	4	11
1041	Clark County	OH	4.3	7.3
1042	Baxter County	AR	4.3	9.6
1043	Vernon Parish	LA	4	13
1044	Gillespie County	TX	4	14
1045	Etowah County	AL	4.3	7.1
1046	York County	PA	4.2	5.1
1047	Ventura County	CA	4.2	4.2
1048	Jones County	GA	4	16
1049	Campbell County	KY	4.1	9.7
1050	Cumberland County	PA	4.1	5.3
1051	Evangeline Parish	LA	4	17
1052	Black Hawk County	IA	4.1	7.9
1053	Sebastian County	AR	4	6.5
1054	Erath County	TX	4	18
1055	Chester County	SC	4	12
1056	Fond du Lac County	WI	3.9	8.2
1057	Kerr County	TX	4	11
1058	Plymouth County	IA	4	17
1059	Jasper County	TX	4	14
1060	Somerset County	PA	3.8	7.8
1061	Pottawattamie County	IA	3.8	9.8
1062	Lewis and Clark County	MT	4	12
1063	DeKalb County	IN	4	12
1064	Island County	WA	3.8	9.8
1065	Washington County	OH	3.8	9.6
1066	Gila County	AZ	3.7	9.9
1067	Raleigh County	WV	3.7	8.2
1068	Humphreys County	TN	4	17
1069	Lenawee County	MI	3.7	7
1070	Hopewell city	VA	4	16
1071	Oconto County	WI	4	13
1072	Jackson County	FL	4	12
1073	Elkhart County	IN	3.6	6.9
1074	Vanderburgh County	IN	3.6	6
1075	Wayne County	GA	4	14
1076	Ada County	ID	3.5	4.8
1077	Westmoreland County	VA	3	15
1078	Delaware County	NY	3	10

1079	Montgomery County	IN	3	16
1080	Franklin County	IL	3	14
1081	New Hanover County	NC	3.4	7.6
1082	Charleston County	SC	3.4	4.9
1083	Logan County	OH	3	11
1084	Pueblo County	CO	3.4	5.8
1085	Huron County	OH	3	10
1086	Washington County	MN	3.4	6.1
1087	Lincoln County	OK	3	14
1088	Kaufman County	TX	3.3	9.3
1089	Augusta County	VA	3.3	8.6
1090	Montgomery County	TN	3.3	5.7
1091	DeKalb County	AL	3.3	9.2
1092	Pulaski County	KY	3.3	8.7
1093	Gladwin County	MI	3	14
1094	Solano County	CA	3.3	4.6
1095	Klamath County	OR	3	10
1096	Mesa County	CO	3.3	6.4
1097	Camden County	MO	3	13
1098	Wood County	TX	3.2	9.5
1099	Steuben County	NY	3	10
1100	Arkansas County	AR	3	19
1101	Richmond County	GA	3.2	6.6
1102	Columbia County	WI	3	12
1103	Miller County	MO	3	18
1104	Norfolk city	VA	3.1	5.6
1105	Kennebec County	ME	3	6.9
1106	Skagit County	WA	3	7.5
1107	Vermilion Parish	LA	3	12
1108	Noble County	IN	3	12
1109	Del Norte County	CA	3	16
1110	Johnson County	TX	3	6.6
1111	Marathon County	WI	3	9.3
1112	Hot Spring County	AR	3	13
1113	Multnomah County	OR	2.9	3.9
1114	Osceola County	MI	3	16
1115	Avoyelles Parish	LA	3	11
1116	Maverick County	TX	3	13
1117	Douglas County	WI	3	12
1118	Utah County	UT	2.9	5.5
1119	Bennington County	VT	3	11

1120	Shelby County	AL	2.9	8
1121	McNairy County	TN	3	13
1122	Whiteside County	IL	3	11
1123	Crook County	OR	3	16
1124	Anderson County	TX	3	12
1125	Audrain County	MO	3	18
1126	Monroe County	AL	3	17
1127	Grayson County	KY	3	15
1128	Pasco County	FL	2.8	3.3
1129	Boyd County	KY	3	12
1130	Stearns County	MN	2.7	7.6
1131	Harrison County	MS	2.7	5.2
1132	Larimer County	CO	2.7	5.4
1133	Polk County	FL	2.7	2.6
1134	Marion County	FL	2.6	5.2
1135	Escambia County	FL	2.6	4.7
1136	Boone County	IN	3	11
1137	Bingham County	ID	3	11
1138	Cooke County	TX	3	13
1139	Calhoun County	AL	2.6	7.9
1140	Oklahoma County	OK	2.6	3
1141	Matanuska-Susitna Borough	AK	3	10
1142	Platte County	MO	3	11
1143	Crawford County	MO	3	16
1144	Monongalia County	WV	3	10
1145	Iosco County	MI	2	15
1146	Atascosa County	TX	2	12
1147	Danville city	VA	2	10
1148	Mason County	WA	2	10
1149	Newton County	MO	2	10
1150	Jefferson County	WI	2.4	9.8
1151	Claiborne County	TN	2	14
1152	Burnet County	TX	2	11
1153	Pittsburg County	OK	2	10
1154	Knox County	IN	2	11
1155	York County	VA	2	13
1156	McLennan County	TX	2.3	5.2
1157	Clinton County	PA	2	14
1158	Fairbanks North Star Borough	AK	2	13
1159	Orange County	CA	2.3	1.9
1160	Clay County	FL	2.3	5.7

1161	Tippecanoe County	IN	2.3	7.4
1162	Stafford County	VA	2.3	8.9
1163	Williamson County	TN	2.2	8
1164	Portage County	WI	2	12
1165	Napa County	CA	2.2	7.8
1166	Morgan County	WV	2	23
1167	Matagorda County	TX	2	14
1168	Morgan County	IL	2	13
1169	Fairfield County	OH	2.2	6
1170	Bowie County	TX	2.1	8.4
1171	Pottawatomie County	OK	2.1	9.5
1172	Baker County	FL	2	17
1173	Trempealeau County	WI	2	17
1174	Edgecombe County	NC	2.1	9.2
1175	Aroostook County	ME	2.1	9.6
1176	Walker County	TX	2	13
1177	Santa Fe County	NM	2.1	7.7
1178	Lawrence County	AL	2	14
1179	Carroll County	OH	2	15
1180	Flagler County	FL	2	6.2
1181	Concordia Parish	LA	2	19
1182	Warren County	PA	2	13
1183	Union County	OH	2	12
1184	La Plata County	CO	2	14
1185	Rockdale County	GA	1.9	9.9
1186	Outagamie County	WI	1.9	6.9
1187	Door County	WI	2	15
1188	Roanoke County	VA	1.8	8.7
1189	Putnam County	WV	2	12
1190	Dubois County	IN	2	12
1191	Monterey County	CA	1.8	5.3
1192	Highlands County	FL	1.8	6.8
1193	Logan County	AR	2	15
1194	Siskiyou County	CA	2	11
1195	Pierce County	WA	1.7	3.1
1196	Sheridan County	WY	2	14
1197	Cibola County	NM	2	15
1198	Osceola County	FL	1.7	5
1199	Sacramento County	CA	1.7	2.7
1200	Codington County	SD	2	17
1201	Vigo County	IN	1.7	8.1

1202	Rice County	MN	2	13
1203	Benton County	MN	2	13
1204	Macon County	IL	1.6	6.9
1205	Henry County	TN	2	12
1206	Huntingdon County	PA	2	13
1207	Franklin County	MO	1.6	9
1208	Daviess County	IN	2	14
1209	Jasper County	SC	2	15
1210	Baldwin County	AL	1.6	5.1
1211	Ford County	KS	2	17
1212	Yavapai County	AZ	1.5	5.4
1213	Clay County	MO	1.5	7.1
1214	Saratoga County	NY	1.5	6
1215	Riley County	KS	1	15
1216	Hawkins County	TN	1.5	9.6
1217	Caldwell County	NC	1.4	8.3
1218	Dickson County	TN	1	12
1219	Lincoln County	TN	1	15
1220	Nueces County	TX	1.3	5.6
1221	McDowell County	WV	1	15
1222	Yates County	NY	1	14
1223	Barbour County	AL	1	14
1224	Gallia County	OH	1	12
1225	Alpena County	MI	1	14
1226	Midland County	TX	1.2	7.7
1227	Wakulla County	FL	1	14
1228	Parker County	TX	1.1	7.6
1229	Pickens County	SC	1.1	7
1230	Pike County	OH	1	12
1231	Walton County	FL	1	8.5
1232	Yellowstone County	MT	1	6.5
1233	Wake County	NC	1	4.5
1234	Pulaski County	MO	1	14
1235	Dunklin County	MO	1	15
1236	Langlade County	WI	1	17
1237	Waupaca County	WI	1	12
1238	Carroll County	IA	1	17
1239	Washington County	IN	1	19
1240	Geneva County	AL	1	14
1241	Patrick County	VA	1	17
1242	Montgomery County	OH	0.8	4.4

1243	Graham County	AZ	1	14
1244	Lorain County	OH	0.8	4.5
1245	Morgan County	AL	0.8	7.6
1246	Butler County	MO	1	13
1247	Marshall County	IN	1	13
1248	Jefferson County	TN	0.7	9.6
1249	Pittsylvania County	VA	0.7	10
1250	Lawrence County	IN	1	11
1251	Orange County	FL	0.7	3.2
1252	Campbell County	TN	1	12
1253	Clearfield County	PA	0.6	7.9
1254	Tazewell County	VA	0.6	9.4
1255	Lake County	FL	0.6	3.4
1256	Woodford County	IL	1	14
1257	Pennington County	SD	0.6	7.9
1258	Boone County	AR	1	11
1259	Grayson County	TX	0.6	7.4
1260	Ben Hill County	GA	1	17
1261	Clermont County	OH	0.5	7.3
1262	Kenosha County	WI	0.4	6.9
1263	Shelby County	OH	0	15
1264	Carroll County	NH	0.4	9.5
1265	Sherburne County	MN	0	11
1266	Hampton city	VA	0.4	7.8
1267	Taos County	NM	0	18
1268	Randolph County	AR	0	14
1269	Vermilion County	IL	0.4	7.9
1270	Hancock County	ME	0	12
1271	Denton County	TX	0.3	4
1272	Genesee County	NY	0.3	9.4
1273	Marinette County	WI	0	10
1274	Muskogee County	OK	0	11
1275	Strafford County	NH	0.2	9.9
1276	Putnam County	OH	0	13
1277	Reno County	KS	0.1	9.7
1278	Adams County	IL	0	10
1279	Washington County	MO	0	15
1280	Clay County	KY	0	18
1281	Holmes County	OH	0	14
1282	Crawford County	AR	0	12
1283	Starr County	TX	0	12

1284	Bexar County	TX	0	2
1285	Mecosta County	MI	0	11
1286	Sonoma County	CA	-0.1	4.3
1287	Brunswick County	NC	-0.1	6.2
1288	Coshocton County	OH	0	14
1289	Union County	TN	0	15
1290	Missoula County	MT	0	10
1291	Snyder County	PA	0	12
1292	Lauderdale County	AL	-0.2	7.3
1293	Randolph County	IN	0	14
1294	Chautauqua County	NY	-0.2	7.5
1295	Chelan County	WA	0	11
1296	Laurens County	SC	0	11
1297	Orleans County	VT	0	16
1298	Kenton County	KY	-0.2	6.9
1299	Becker County	MN	0	14
1300	Rutherford County	NC	0	11
1301	Wythe County	VA	0	15
1302	Adams County	IN	0	15
1303	Greene County	MO	-0.3	5.4
1304	Wise County	VA	0	12
1305	Harvey County	KS	0	12
1306	Cass County	MN	0	16
1307	Buchanan County	MO	-0.4	8.7
1308	Floyd County	GA	-0.4	7.8
1309	Hidalgo County	TX	-0.5	3.8
1310	Marshall County	TN	-1	14
1311	Gibson County	TN	-0.5	9.5
1312	Luna County	NM	-1	13
1313	Randall County	TX	-0.6	8.3
1314	Erie County	PA	-0.6	4.7
1315	Marin County	CA	-0.6	6.8
1316	Okeechobee County	FL	-1	12
1317	San Benito County	CA	-1	13
1318	Hamilton County	TN	-0.6	4.9
1319	Dodge County	WI	-0.7	7.9
1320	Honolulu County	HI	-0.8	3.6
1321	Rhea County	TN	-1	16
1322	Union County	FL	-1	17
1323	Crittenden County	AR	-0.8	9.5
1324	Emmet County	MI	-1	17

1325	Rockbridge County	VA	-1	16
1326	Jasper County	MO	-0.8	6.9
1327	Osage County	OK	-1	11
1328	Deschutes County	OR	-0.9	6
1329	Lamar County	TX	-0.9	9.7
1330	Fayette County	WV	-1	13
1331	Clinton County	IA	-1	13
1332	Lonoke County	AR	-1	11
1333	Herkimer County	NY	-1	10
1334	Hernando County	FL	-1	5.2
1335	Brevard County	FL	-1	2.9
1336	Jackson County	AR	-1	18
1337	Richmond city	VA	-1	6
1338	Bonneville County	ID	-1	7.5
1339	Carter County	OK	-1	9.5
1340	Clinton County	NY	-1	10
1341	Seminole County	FL	-1	5
1342	Guadalupe County	TX	-1	7.5
1343	Harrison County	IN	-1	14
1344	Le Flore County	OK	-1	10
1345	St. Johns County	FL	-1.2	5.3
1346	Halifax County	VA	-1	14
1347	Liberty County	GA	-1	12
1348	Gray County	TX	-1	18
1349	Polk County	NC	-1	15
1350	Bay County	MI	-1.3	7.1
1351	Warren County	IA	-1	13
1352	Seneca County	NY	-1	15
1353	Marion County	AR	-1	17
1354	Humboldt County	CA	-1.3	7
1355	Leon County	FL	-1.3	5.5
1356	Calaveras County	CA	-1	10
1357	Dubuque County	IA	-1.3	9
1358	Mayes County	OK	-1	12
1359	Upshur County	WV	-1	18
1360	Stanislaus County	CA	-1.5	4.4
1361	Mercer County	PA	-1.5	6.6
1362	Mineral County	WV	-1	15
1363	Lincoln County	ME	-1	14
1364	Lee County	IL	-1	13
1365	Morgan County	TN	-1	14

1366	Miami County	OH	-1.5	7.5
1367	Winnebago County	WI	-1.6	7.6
1368	Transylvania County	NC	-2	12
1369	Cherokee County	GA	-1.6	7.1
1370	Union County	NC	-1.6	5.7
1371	Cabell County	WV	-1.6	7.1
1372	Jefferson County	NY	-1.6	8.8
1373	Mingo County	WV	-2	14
1374	Santa Cruz County	CA	-1.7	6.4
1375	Phillips County	AR	-2	17
1376	Tioga County	PA	-2	13
1377	Nicholas County	WV	-2	13
1378	Dodge County	NE	-2	12
1379	Shasta County	CA	-1.8	5.9
1380	Bedford County	TN	-2	14
1381	Person County	NC	-2	11
1382	Garland County	AR	-1.8	6.7
1383	Clark County	WI	-2	12
1384	Clare County	MI	-2	12
1385	Pinellas County	FL	-1.8	2.5
1386	Chattooga County	GA	-2	13
1387	Huron County	MI	-2	13
1388	Shawnee County	KS	-1.9	7.1
1389	Grand Forks County	ND	-2	11
1390	Jay County	IN	-2	16
1391	Fayette County	PA	-1.9	6.2
1392	Labette County	KS	-2	17
1393	Ashtabula County	OH	-1.9	7.5
1394	Tom Green County	TX	-1.9	9.6
1395	Cumberland County	TN	-2	7.9
1396	Hawaii County	HI	-2	6.1
1397	Lawrence County	AR	-2	15
1398	Holmes County	FL	-2	15
1399	Lane County	OR	-2	3.9
1400	McPherson County	KS	-2	14
1401	McDonough County	IL	-2	13
1402	Anchorage Muni	AK	-2.1	5.6
1403	Cowlitz County	WA	-2.1	7.3
1404	Wood County	WV	-2.1	8.5
1405	Madison County	AL	-2.1	4.6
1406	Placer County	CA	-2.1	4.3

1407	Smyth County	VA	-2	11
1408	Eau Claire County	WI	-2	10
1409	Cherokee County	SC	-2.2	9.8
1410	Monroe County	TN	-2	10
1411	Lincoln County	OR	-2	12
1412	Preston County	WV	-2	13
1413	Lake County	OH	-2.2	4.5
1414	Haywood County	NC	-2	11
1415	Fairfax city	VA	-2	17
1416	Collier County	FL	-2.3	4.7
1417	Logan County	WV	-2	10
1418	Greenbrier County	WV	-2	12
1419	Botetourt County	VA	-2	16
1420	Grady County	OK	-2	11
1421	Westmoreland County	PA	-2.4	3.7
1422	Newaygo County	MI	-2	11
1423	Madera County	CA	-2.4	8.9
1424	Cowley County	KS	-2	13
1425	Houghton County	MI	-2	14
1426	Val Verde County	TX	-2	14
1427	Story County	IA	-2	12
1428	Blount County	TN	-2.4	6.1
1429	Alachua County	FL	-2.4	5.4
1430	Randolph County	MO	-2	15
1431	Johnson County	KS	-2.5	4.9
1432	Stephens County	GA	-2	14
1433	Randolph County	WV	-3	12
1434	Pike County	KY	-2.5	8.7
1435	Hart County	KY	-3	21
1436	Alleghany County	VA	-3	18
1437	Wells County	IN	-3	14
1438	Butler County	PA	-2.6	6.2
1439	Young County	TX	-3	17
1440	Seneca County	OH	-3	13
1441	Fremont County	CO	-2.7	9.4
1442	Douglas County	KS	-3	11
1443	Lawrence County	KY	-3	19
1444	Allen County	OH	-2.7	8.5
1445	Hoke County	NC	-3	14
1446	Sandusky County	OH	-2.9	9.1
1447	Benton County	TN	-3	15

1448	Licking County	OH	-2.9	6.7
1449	Green Lake County	WI	-3	14
1450	Knox County	ME	-3	9.6
1451	Greene County	NY	-3	11
1452	Clatsop County	OR	-3	13
1453	Monroe County	WI	-3	11
1454	Tallapoosa County	AL	-3	10
1455	Hays County	TX	-3.1	8.6
1456	Lowndes County	GA	-3.1	7.6
1457	Kitsap County	WA	-3.2	5
1458	Garfield County	CO	-3	13
1459	Fannin County	TX	-3	14
1460	Anderson County	TN	-3.2	7.9
1461	Washington County	WI	-3.3	7.5
1462	Grant County	NM	-3	12
1463	Manitowoc County	WI	-3	10
1464	Miller County	AR	-3	12
1465	York County	ME	-3.4	6.1
1466	Camden County	GA	-3	11
1467	Steele County	MN	-3	16
1468	Oswego County	NY	-3.4	8.2
1469	Christian County	KY	-3	11
1470	Lewis County	WA	-3.4	9
1471	Loudon County	TN	-3.4	9.5
1472	Perry County	KY	-3	11
1473	Gibson County	IN	-4	16
1474	Polk County	MN	-4	13
1475	Hampton County	SC	-4	15
1476	Wichita County	TX	-3.5	7.4
1477	Gallatin County	MT	-4	10
1478	Faulkner County	AR	-3.6	8.7
1479	Wasco County	OR	-4	15
1480	Adams County	OH	-4	13
1481	Waldo County	ME	-4	11
1482	Darke County	OH	-3.6	9.7
1483	Daviess County	KY	-3.7	6.9
1484	Cocke County	TN	-4	11
1485	Bossier Parish	LA	-3.7	7.3
1486	Henry County	OH	-4	15
1487	Cattaraugus County	NY	-3.8	9.1
1488	Wayne County	NY	-4	11

1489	Navarro County	TX	-4	14
1490	Wise County	TX	-4	11
1491	Boone County	MO	-3.8	7.8
1492	Garfield County	OK	-3.9	9.5
1493	Warren County	OH	-3.9	6
1494	San Patricio County	TX	-3.9	9.8
1495	Sharp County	AR	-4	15
1496	Obion County	TN	-4	12
1497	Park County	WY	-4	13
1498	Shelby County	IL	-4	19
1499	Christian County	MO	-4	12
1500	Posey County	IN	-4	17
1501	Columbia County	OR	-4	11
1502	Leon County	TX	-4	17
1503	Jackson County	OH	-4	14
1504	Prince Edward County	VA	-4	16
1505	Cherokee County	TX	-4.2	9.8
1506	Eaton County	MI	-4.3	7.9
1507	Kay County	OK	-4.3	8.7
1508	Kandiyohi County	MN	-4	15
1509	Ravalli County	MT	-4	12
1510	Hendry County	FL	-4	12
1511	Lewis County	WV	-5	19
1512	Isle of Wight County	VA	-5	13
1513	Brown County	MN	-5	13
1514	La Crosse County	WI	-4.7	7.1
1515	Des Moines County	IA	-5	13
1516	Essex County	NY	-5	14
1517	Russell County	VA	-5	16
1518	Oldham County	KY	-5	12
1519	Effingham County	GA	-5	12
1520	Lassen County	CA	-5	18
1521	Anson County	NC	-5	19
1522	Juneau County	WI	-5	14
1523	Rio Arriba County	NM	-5	11
1524	Santa Barbara County	CA	-5	4.6
1525	Wood County	WI	-5	8
1526	Sampson County	NC	-5	8.9
1527	Delta County	CO	-5	11
1528	Harlan County	KY	-5	12
1529	Benton County	AR	-5.2	5.8

1530	Comal County	TX	-5.2	7.1
1531	Madison County	NE	-5	11
1532	Douglas County	MN	-5	12
1533	Scott County	VA	-5	14
1534	Lauderdale County	TN	-5	15
1535	Columbia County	FL	-5.3	8.2
1536	Madison County	GA	-5	18
1537	Marion County	MO	-5	14
1538	Nassau County	FL	-5.4	7.9
1539	Carteret County	NC	-5.4	8
1540	Henry County	VA	-5.5	9.1
1541	Knox County	IL	-5	12
1542	Bannock County	ID	-5.5	9.8
1543	Franklin County	KS	-5	14
1544	Logan County	IL	-6	14
1545	Blount County	AL	-5.5	8.5
1546	Nye County	NV	-5.5	8.4
1547	Canyon County	ID	-5.6	5.3
1548	Saline County	MO	-6	17
1549	Bee County	TX	-6	15
1550	Maui County	HI	-5.6	7
1551	Medina County	TX	-6	13
1552	Jackson County	IN	-6	12
1553	White County	AR	-6	11
1554	St. Lawrence County	NY	-5.7	8.3
1555	Nash County	NC	-5.7	7.2
1556	Preble County	OH	-6	13
1557	Polk County	OR	-5.8	9.4
1558	Taylor County	TX	-5.8	6.5
1559	Nelson County	KY	-6	11
1560	Tift County	GA	-6	12
1561	Penobscot County	ME	-6	6.2
1562	Tompkins County	NY	-6	9.3
1563	Alcorn County	MS	-6	13
1564	Barry County	MO	-6	13
1565	San Jacinto County	TX	-6	14
1566	Pacific County	WA	-6	15
1567	Cascade County	MT	-6.1	7.8
1568	Livingston County	IL	-6	14
1569	Union County	OR	-6	14
1570	Polk County	AR	-6	16

1571	White County	TN	-6	13
1572	Jefferson County	OH	-6	10
1573	Culpeper County	VA	-6	12
1574	Richland Parish	LA	-6	16
1575	Okaloosa County	FL	-6.5	5.4
1576	Okanogan County	WA	-6	13
1577	Lawrence County	OH	-6	11
1578	St. Croix County	WI	-6.5	9.8
1579	Grafton County	NH	-6.5	7.5
1580	Mason County	WV	-7	13
1581	Mississippi County	AR	-6.5	9.5
1582	Dale County	AL	-7	11
1583	Hardin County	TX	-7	10
1584	Jersey County	IL	-7	17
1585	Josephine County	OR	-6.7	6.6
1586	Scott County	MS	-7	14
1587	Saline County	KS	-6.7	9.7
1588	Wexford County	MI	-7	13
1589	Orange County	VA	-7	12
1590	Ottawa County	OK	-7	15
1591	Wright County	MN	-6.9	8.3
1592	Androscoggin County	ME	-6.9	6.5
1593	Tehama County	CA	-7	11
1594	Itawamba County	MS	-7	16
1595	Marshall County	KY	-7	14
1596	Laramie County	WY	-7	8.2
1597	Marshall County	WV	-7	12
1598	Bay County	FL	-7.1	6.1
1599	Oxford County	ME	-7.2	9.8
1600	Thurston County	WA	-7.2	4.9
1601	Unicoi County	TN	-7	15
1602	Ashley County	AR	-7	17
1603	Champaign County	IL	-7.3	7.1
1604	Cass County	MO	-7.3	7.5
1605	Ohio County	KY	-7	13
1606	Woodford County	KY	-7	15
1607	Webster County	MO	-7	14
1608	Muskingum County	OH	-7.4	9.2
1609	Venango County	PA	-7	11
1610	Limestone County	TX	-7	14
1611	Logan County	OK	-7	12

1612	Butte County	CA	-7.4	6.1
1613	Surry County	NC	-7.4	8.1
1614	Sevier County	TN	-7.5	8.1
1615	Effingham County	IL	-8	16
1616	Greene County	AR	-8	10
1617	Grant Parish	LA	-8	16
1618	Lincoln County	NM	-8	16
1619	Elk County	PA	-8	14
1620	Union County	MS	-8	15
1621	Cambria County	PA	-7.8	7.2
1622	Asotin County	WA	-8	15
1623	Washington County	AR	-7.9	6.8
1624	Garvin County	OK	-8	12
1625	Jefferson County	IN	-8	13
1626	Prince George County	VA	-8	15
1627	Cole County	MO	-8	9.7
1628	McKean County	PA	-8	11
1629	Rockwall County	TX	-8	12
1630	Payne County	OK	-8.1	9.2
1631	Onslow County	NC	-8.2	7.3
1632	Cheshire County	NH	-8	10
1633	Sullivan County	NH	-8	10
1634	Winchester city	VA	-8	17
1635	Cullman County	AL	-8.3	7.5
1636	Yadkin County	NC	-8	13
1637	St. Joseph County	MI	-8.5	9.8
1638	Washington County	PA	-8.5	4.7
1639	Pender County	NC	-8	10
1640	Waushara County	WI	-9	14
1641	McClain County	OK	-9	15
1642	Curry County	NM	-9	12
1643	San Luis Obispo County	CA	-8.7	5.1
1644	Amherst County	VA	-9	12
1645	Meeker County	MN	-9	13
1646	Morrow County	OH	-9	14
1647	Hancock County	WV	-9	13
1648	Lafayette County	MO	-9	11
1649	Johnson County	KY	-9	13
1650	Orange County	VT	-9	13
1651	Kittitas County	WA	-9	16
1652	Ashland County	OH	-9	11

1653	Addison County	VT	-9	15
1654	Cache County	UT	-9.2	9.9
1655	Charlevoix County	MI	-9	13
1656	Fulton County	IL	-9	11
1657	Polk County	MO	-9	12
1658	Trinity County	TX	-10	14
1659	Polk County	WI	-10	12
1660	Tooele County	UT	-10	11
1661	Clinton County	OH	-10	11
1662	Fayette County	IL	-10	18
1663	Abbeville County	SC	-10	14
1664	Jefferson Davis Parish	LA	-10	10
1665	Louisa County	VA	-10	13
1666	Wadena County	MN	-10	17
1667	Natrona County	WY	-10	10
1668	Ogemaw County	MI	-10	15
1669	Canadian County	OK	-10	7.4
1670	Warren County	VA	-10	12
1671	Cherokee County	NC	-10	13
1672	Livingston County	NY	-10.1	9.8
1673	Yuba County	CA	-10.1	9.9
1674	Mower County	MN	-10	12
1675	Marion County	OH	-10.2	7.8
1676	Adams County	WI	-10	13
1677	Jefferson County	PA	-10	11
1678	Cochise County	AZ	-10.4	6.5
1679	Lincoln County	WV	-10	14
1680	Hancock County	OH	-10.5	8.5
1681	Marion County	TN	-11	12
1682	Lincoln County	MO	-11	12
1683	Marion County	WV	-10.6	9.2
1684	Wyoming County	PA	-11	13
1685	Clallam County	WA	-10.7	7.4
1686	Edgar County	IL	-11	17
1687	Saline County	AR	-11	7.4
1688	Gordon County	GA	-11	9.2
1689	Scotts Bluff County	NE	-11	12
1690	Santa Rosa County	FL	-11.3	6.1
1691	Greene County	PA	-11	11
1692	Martin County	MN	-11	17
1693	Pulaski County	VA	-11.5	9.9

1694	Harrison County	KY	-11	18
1695	Muhlenberg County	KY	-12	14
1696	Richland County	OH	-11.6	7.1
1697	Lumpkin County	GA	-12	13
1698	Jim Wells County	TX	-12	15
1699	Kauai County	HI	-12	11
1700	Johnson County	TN	-12	13
1701	Grady County	GA	-12	17
1702	McIntosh County	OK	-12	13
1703	Wharton County	TX	-12	12
1704	Kenai Peninsula Borough	AK	-12	13
1705	Stephens County	OK	-12	11
1706	Winston County	MS	-12	16
1707	Kootenai County	ID	-12.4	5.7
1708	Saline County	IL	-12	13
1709	Lee County	VA	-12	16
1710	Chisago County	MN	-13	11
1711	Liberty County	TX	-12.6	8.5
1712	Franklin County	NC	-13	12
1713	Hale County	TX	-13	13
1714	Queen Anne's County	MD	-13	10
1715	Defiance County	OH	-13	13
1716	Bonner County	ID	-13	11
1717	Platte County	NE	-13	15
1718	Crawford County	OH	-13.1	9.7
1719	Chemung County	NY	-13.1	8.1
1720	Lincoln County	SD	-13	12
1721	Scott County	KY	-13	11
1722	Harrison County	WV	-13.2	7.3
1723	Lake County	CA	-13.2	8.2
1724	Arenac County	MI	-13	15
1725	LaGrange County	IN	-13	17
1726	Llano County	TX	-13	12
1727	Barron County	WI	-13.5	9.2
1728	Letcher County	KY	-13	13
1729	Rockcastle County	KY	-14	16
1730	Creek County	OK	-13.7	9.1
1731	Whitley County	IN	-14	16
1732	Lawrence County	MO	-14	12
1733	Emanuel County	GA	-14	11
1734	Warren County	TN	-14	12

1735	Clark County	KY	-14	12
1736	Franklin County	ME	-14	13
1737	Chippewa County	WI	-14.1	9.2
1738	Bryan County	OK	-14.2	9.5
1739	Marquette County	MI	-14	10
1740	Colbert County	AL	-14.3	9.9
1741	Dare County	NC	-15	12
1742	Kosciusko County	IN	-14.8	8.7
1743	Crow Wing County	MN	-14.8	8.5
1744	Silver Bow County	MT	-15	12
1745	Yell County	AR	-15	15
1746	Mercer County	KY	-15	13
1747	Marion County	IA	-15	11
1748	Wabash County	IN	-15	11
1749	Wilson County	TX	-15	11
1750	Watauga County	NC	-15	12
1751	DeWitt County	TX	-15	16
1752	Benton County	OR	-15	10
1753	Sumner County	KS	-15	14
1754	Washington County	FL	-16	13
1755	Pierce County	WI	-16	15
1756	Delta County	MI	-16	12
1757	Oconee County	SC	-15.9	7.4
1758	Morrison County	MN	-16	14
1759	Barren County	KY	-16.3	9.5
1760	George County	MS	-16	15
1761	Bibb County	AL	-16	13
1762	Chowan County	NC	-16	16
1763	Titus County	TX	-16	12
1764	Chippewa County	MI	-17	12
1765	Milam County	TX	-17	15
1766	Burleson County	TX	-17	14
1767	Hempstead County	AR	-17	13
1768	Martinsville city	VA	-17	16
1769	Williams County	OH	-17	12
1770	Bradford County	PA	-17.5	7.7
1771	Montcalm County	MI	-17.6	9.5
1772	Eddy County	NM	-17.8	8.8
1773	Perry County	IL	-18	15
1774	Lea County	NM	-18	9.6
1775	Maury County	TN	-18.3	6.9

1776	Coos County	NH	-18	11
1777	Adair County	MO	-18	14
1778	Sagadahoc County	ME	-19	12
1779	Greene County	TN	-18.6	7.7
1780	Coos County	OR	-18.7	7.2
1781	Beckham County	OK	-19	15
1782	Crawford County	PA	-18.7	7.9
1783	Boyle County	KY	-19	12
1784	Johnson County	AR	-19	12
1785	Hocking County	OH	-19	12
1786	Miami County	KS	-19	16
1787	Cross County	AR	-19	13
1788	Carter County	KY	-20	12
1789	Glenn County	CA	-21	14
1790	Clay County	AR	-21	13
1791	Henry County	MO	-21	14
1792	Cherokee County	KS	-22	13
1793	Isanti County	MN	-22	11
1794	Bureau County	IL	-23	11
1795	Eastland County	TX	-23	12
1796	Conway County	AR	-23	12
1797	Menominee County	MI	-24	11
1798	Stutsman County	ND	-25	13
1799	Hubbard County	MN	-25	14
1800	Kleberg County	TX	-25	14
1801	Nottoway County	VA	-25	16
1802	Stone County	MO	-25.7	9.5
1803	Poinsett County	AR	-26	12
1804	Schoharie County	NY	-29	11
1805	Laclede County	MO	-29.7	8.1
1806	Dunn County	WI	-30	11